Università degli Studi di Napoli *Federico II*

DOTTORATO DI RICERCA IN

FISICA

Ciclo XXXIII

Coordinatore: prof. Salvatore Capozziello

Classical Cepheids: an updated theoretical scenario in the *Gaia* Era

Settore Scientifico Disciplinare FIS/05

Dottoranda
Giulia De Somma

Tutori
Prof.ssa Marcella Marconi
Prof. Salvatore Capozziello

Anni 2018/2021

In memory of my lovely parents

Acknowledgements

This is the third time I am writing the acknowledgements for my thesis; but this time I am on the one-yard-line from my dream, from seeing all my sacrifices pay off.
I started my academic career a long time ago and when I wrote the acknowledgements for my bachelor's thesis, I was still a young girl with many dreams in my heart and much to do. Writing now, is a woman whose life forced her to grow up early and for this reason, feels more mature than the other people who will graduate with her. Despite this, she still has the same dreams in her heart. I have gritted my teeth so hard to get to this point that for a while I didn't believe it was really going to happen.
I'm very happy that I am finally here.
There are people who I sincerely feel thankful to, for their help during my PhD.
I'd like to say thank you,
To Marcella, my advisor,
Our meeting completely changed my perspectives and allowed me to be calm again. I thank you because despite many commitments, you always supported me with your enormous scientific competence and dedication. I really hope this is just the first of many successes together.
To her group, Vincenzo, Ilaria, Roberto and Silvio,
because I feel lucky to have colleagues like you all.
To Professor Capozziello,
You represent everything that any student would like to become. I thank you because you chose to listen to me and support me when I realized it was essential for me to change direction. I thank you because I felt your happiness at each of my little achievements and this was really important.
To Professor Capaccioli,
Because you believed in me before anyone else.
To Santi, who I met during my PhD,
I feel lucky to have met you. Despite our short time together, I was enriched by your advice not just within my field of study but also outside it. I really hope our collaboration can continue even after the thesis.
To Enzo who I also met during my Phd,
I thank you for your advice and peace of mind which reassured me.
To my husband Gianluca, who has lived with me every moment of my academic career and life,
I thank you because I feel lucky to have you close to me in life. You are always understanding and you always try to make me smile. I thank you because I never stopped feeling your love for me.
To my parents-in-law who represent a great example of strength for me,
Your closeness is of inestimable value to me.
To my brother Enzo,
Life has challenged us with a very hard test but referring to one of my favorite De Gregori songs 'true love can hide, be confused but it can never get lost'.
To Andrea,
because your computer advice were often fundamental and because it is always a good time for a new friend.
To Ciro, my best friend, my important person, my safety,
I neglected our relationship during my busy PhD years but I know you understood everything and that you know we will have time to recover.

To Silvio,
Because I know I can count on you.
To my aunts and Angela,
Despite panicking, you all found a way to offer me your help. I thank you because even just trying to make me feel protected again was fundamental.
To my doctor, Doctor Florio,
You probably know me better than anyone else. I thank you because although the time for your well-deserved retirement had arrived, you understood I could not lose another point of reference and you have never stopped being close to me.
To the M.S. with which I have to forcibly share this goal as well,
I thank her because her strength made me understand how much strength I can have and how great my passion for science is. In this continuous struggle, I try to keep ignoring her every day, just like John Nash with his hallucinations; and in this eternal fight, I'll also win this other battle.
To Sara, Cate, Lina, Valeria, Ottavia, Matteo, Luca B., Marco, Luca T., Mauro, Edu, Alessia, Rosa, Lidia, Ugo, Ila, Orny, Enzo, Ida and all my friends,
I am happy to grow and share every moment with you all.
To Princess,
Your fundamental advice, patience and kindness allow us to go beyond our English lessons and become friends.

Give me now a journey that takes me beyond the clouds and beyond this Universe and leave me to imagination,
Imagination that allows me to look my parents and my brother-in-law Antonio in the eye and to feel all their pride.
I really thank my parents for their love. Their efforts were not in vain because I did my PhD despite missing them very much. Achieving my dream of becoming a scientist is thanks everything they taught me and their immense love that I never stopped feeling, and which makes me feel protected every day.

Thanks to all of you, your every smile has made these last few years better.

Finally, I'd like to thank myself,
This is just the beginning ...

List of publications

The present Phd thesis is based on the following works:

- An Extended Theoretical Scenario for Classical Cepheids. I. Modeling Galactic Cepheids in the Gaia Photometric System.
  De Somma G., Marconi M., Molinaro R., Cignoni M., Musella I., Ripepi V.
  2020, ApJS, 247, 30D, DOI: 10.3847/1538-4365/ab7204

- Updated theoretical period-age and period-age-colour relations for Galactic Classical Cepheids: an application to the Gaia DR2 sample.
  De Somma G., Marconi M., Cassisi S., Ripepi V., Leccia S., Molinaro R., Musella I.
  2020, MNRAS, 496, 5039D, DOI: 10.1093/mnras/staa1834

- Predicted masses of Galactic Cepheids in the Gaia Data Release 2.
  Marconi M., **De Somma G.**, Ripepi V., Molinaro R., Musella I., Leccia S., Moretti M.I.
  2020, ApL, 898L, 7M, DOI: 10.3847/2041-8213/aba12b

Apart from these works that will be presented in Chapters 3, 4, 5, and 6, as part of my Phd project, I have also contributed to the following works listing below:

- V363 Cas: a new lithium rich Galactic Cepheid.
  Catanzaro G., Ripepi V., Clementini G., Cusano F., **De Somma G.**, Leccia S., Marconi M., Molinaro R., Moretti M.I., Musella I.
  2020, A&A, 639L, 4C, DOI: 10.1051/0004-6361/202038486

- On the Period–Luminosity–Metallicity relation of Classical Cepheids.
  Ripepi V., Catanzaro G., Molinaro R., Marconi M., Clementini G., Cusano F., **De Somma G.**, Leccia S., Musella I., Testa V.
  2020, A&A, 642A, 230R, DOI: 10.1051/0004-6361/202038714

- Gaia parallaxes versus updated pulsation model prediction. 53rd ESLAB Symposium: The Gaia Universe conference proceeding.
  De Somma, Giulia; Marconi, Marcella; Capozziello, Salvatore; Molinaro, Roberto; Musella, Ilaria; Ripepi, Vincenzo; 10.5281/zenodo.3402706

- Einstein, Planck and Vera Rubin: relevant encounters between the Cosmological and the Quantum Worlds.
  QGSKY collaboration.
  Frontiers in Physics accepted, arXiv:2011.09278

- New insights into the use of Ultra Long Period Cepheids as cosmological standard candles.
  Musella I., Marconi M., Molinaro R., Fiorentino G., Ripepi V., **De Somma G.**, Moretti M.I.
  2020, MNRAS, 501, 866M, DOI: 10.1093/mnras/staa3678

- A theoretical scenario for Galactic RR Lyrae in the Gaia database: constraints on the parallax offset.

Marconi M., Molinaro R., Ripepi V., Leccia S., Musella I., **De Somma G.**, Gatto M., Moretti M.I.
2021, MNRAS, 500, 5009M, DOI: 10.1093/mnras/staa3558

- HD344787: A True Polaris Analogue?
  Ripepi V., Catanzaro G., Molnar L., Plachy E., Marconi M., Clementini G., Molinaro R., **De Somma G.**, Leccia S., Mancino S., Musella I., Cusano F.
  A&A Accepted, DOI: 10.1051/0004-6361/202040123

- Gaia parallaxes versus updated model predictions, RRL/CEP 2019 conference proceeding.
  De Somma Giulia, Marconi Marcella, Molinaro Roberto, Cignoni Michele, Musella Ilaria, Ripepi Vincenzo, RRL/CEP 2019; Sheridan books

Abstract

Classical Cepheids: an Updated Theoretical Scenario in the Gaia Era

Classical Cepheids are the most important primary distance indicators, and excellent tracers of relatively young and intermediate-age (from a few tens to a few hundreds of Myr) stellar populations.
Indeed, they are well known to obey period-luminosity and period-luminosity-color relations which are traditionally used to calibrate secondary distance indicators and, hence, to estimate the Hubble constant.

Stellar evolution predicts that the evolutionary phase of Classical Cepheids corresponds to the central helium-burning phase of massive and intermediate-mass stars. Stars in this evolutionary phase obey a mass-luminosity relation which is dependent on the chemical composition as well efficiency of some non canonical physical processes such as rotation, core convective overshooting, and mass loss efficiency during (mainly) the red giant branch stage.
The mass-luminosity relation, adopted in the pulsational model computation, affects the shape of light curves and radial velocity curves, the coefficients of PLC and period-Wesenheit relations and, in turn, the Cepheid-based distance scale.

The main focus of this PhD project is the modelling of radially pulsating stars, specifically, Classical Cepheids, through non linear hydrodynamical models.
The primary goal is to constrain the extragalactic distance scale, and test the impact of the various ingredients entering the model computation, on the theoretical calibration of the Classical Cepheid distance scale.

This PhD research was conducted, in the context of one of the most debated issues in current astrophysical literature: the Hubble Constant tension which is the discrepancy (at the level of 4.4 σ) between the value of the Hubble constant derived by Riess et al (2016, 2018) on the basis of Classical Cepheids and the Cosmic Microwave Background results.

Indeed, the first part of this research is devoted to the evaluation of possible residual systematic errors on the cosmic Cepheid-based distance scale calibration and Hubble constant evaluation, in the context of one of the most debated issues in current astrophysical literature: the Hubble constant tension.

The computation of updated and reliable pulsating stellar models for Classical Cepheids is the basis for the derivation of theoretical tools to constrain not only the distance but also intrinsic stellar properties such as the age and the mass of observed pulsators.
Moreover, their comparison with valuable observational datasets, including that provided by the Gaia mission, allows us to test the predictive capability of current pulsation theory, and to trace the properties of Galactic and extra-galactic young and intermediate-age stellar populations.
The pulsational framework developed in this PhD thesis is appropriate not only for typical Galactic Classical Cepheids, but also to chemical patterns characteristic of extra-galactic stellar systems such as the Magellanic Clouds.
The pulsational scenario presented in this work is also important in order to constrain the physical and numerical assumptions adopted in current generation of stellar evolution models for massive and intermediate-mass stars.

In this context, the final part of the PhD thesis is devoted to the use of Classical Cepheids as age indicators. By combining updated stellar evolution models with our updated pulsational scenario, new accurate Classical Cepheid period-age and

the period-age-color relations in the Gaia filters are provided.
The inferred period–age and period–age–color relations are applied to a selected sample of both fundamental and first overtone mode Cepheids observed with the Gaia spacecraft, and individual ages for the various adopted theoretical scenarios are derived.

The thesis will end with a discussion on the first results of the chemical composition effect on the updated and homogeneous theoretical scenario for Classical Cepheids. Accurate metal-dependent relations which represent powerful tools for constraining stellar parameters of Classical Cepheid distances with simultaneous photometric and spectroscopic information in the Local Group of galaxies, are derived.
The development of useful tools for constraining the individual distances and intrinsic stellar parameters in a variety of Galactic and extragalactic environments, involves a direct comparison between observed and predicted light curves.
Therefore, in the era of Gaia astrometric measurements and in view of the next generation of the most advanced observational facilities, the work presented in the PhD thesis paves the way for future applications and comparisons between theory and observations.

Contents

List of Figures

List of Tables

List of Abbreviations

AGB	**A**symptotic **G**iant **B**ranch
AC	**A**nomalous **C**epheid
CC	**C**lassical **C**epheid
CMD	**C**olor **M**agnitude **Diagram**
ELT	**E**xtremely **L**arge **T**elescope
F	**F**undamental (mode)
FO	**F**irst **Overtone** (mode)
FBE	**F**undamental **B**lue **E**dge
FRE	**F**undamental **R**ed **E**dge
FOBE	**F**irst **O**vertone **B**lue **E**dge
FORE	**F**irst **O**vertone **R**ed **E**dge
GC	**G**lobular **C**lusters (GC)
GCC	**G**alactic **G**lobular **C**lusters (GCC)
HR	**H**ertzsprung **R**ussell (diagram)
HST	**H**ubble **S**pace **T**elescope
IS	**I**nstability **S**trip
JWST	**J**ames **W**ebb **S**pace **T**elescope
LAWE	**L**inear **A**diabatic **Wave** **E**quation
LMC	**L**arge **M**agellanic **C**loud
LSST	**L**arge **S**ynoptic **S**urvey **T**elescope
ML	**M**ass **L**uminosity
MS	**M**ain **S**equence
NIR	**N**ear **I**nfra **Red**
PA	**P**eriod **A**ge (relation)
PL	**P**eriod **L**uminosity (relation)
PR	**P**eriod **R**adius (relation)
PW	**P**eriod **W**esenheit (relation)
PAC	**P**eriod **A**ge **C**olor (relation)
PLC	**P**eriod **L**uminosity **C**olor (relation)
PMR	**P**eriod **M**ass **R**adius (relation)
PMLT	**P**eriod **M**ass **L**uminosity **T**emperature
PRZ	**P**eriod **R**adius **M**etallicity (relation)
RGB	**R**ed **G**iant **B**ranch
RRL	**R R L**yrae
SMC	**S**mall **M**agellanic **C**loud
ULP	**U**ltra **L**ong **P**eriod (Cepheids)
W	**W**esenheit function

List of Symbols

$\overline{\rho}_{\odot}$	Mean Solar Density	$1.41\,\mathrm{g/cm^3}$
$L_{\odot}$	Solar Luminosity	$3.828 \times 10^{26}\,\mathrm{W}$
$M_{\odot}$	Solar Mass	$1.988\,47 \times 10^{30}\,\mathrm{kg}$
H_0	Hubble constant	km/s/Mpc
H_P	Pressure Scale Height	m
T_C	Central Temperature	K
T_{eff}	Effective Temperature	K
ρ_C	Central Density	$\mathrm{g/cm^3}$
k	Opacity	$\mathrm{cm^2/g}$

Chapter 1

Introduction

1.1 Historical notes and a general overview on variable stars

For over 2000 years, Aristotelian science, considered untouchable, declared the immutability of the sky that we observe. Celestial objects were considered eternal and invariable.
However, in 1596, the discovery of a star, which regularly changed its luminosity, in the Whale constellation (Omicron Ceti) by the Lutheran pastor, Fabricius, was thus an obvious breaking point from the previous convictions. The relevance of this discovery was such that the star was given the name, Mira Ceti, which means, "wonderful star". In 1638, Johannes Holwarda studied the brightness variation of this star by identifying the regular luminosity variation over a period of time. In an 11 month period, the star reached a maximum of about 2-3 magnitudes and a minimum well below 6 magnitudes, the threshold of visibility to the naked eye. Then, in 1669, the second star found to be variable, Algol, was discovered by Geminiano Montanari. Its brightness variation was correctly understood in 1784 by John Goodricke due to the occurrence of a mutual eclipse between its two components. At the end of the eighteenth century there were about a dozen stars whose variability had been recognized and among them was a star that has a relevant role in the history of astronomy: δ Cephei, the eponymous star for Classical Cepheids.
Until the beginning of the 20th century, Cepheids were considered just as variable as the others. Soon, the fundamental discovery of the correlation between the period and the intrinsic luminosity of Cepheids by Henrietta Leavitt, currently known as Period-Luminosity relation, would make these stars fundamental to determining the distance of astronomical objects from Earth.
In fact, in 1912, she published a work on the Cepheids in the Small Magellanic Cloud (SMC), one of our Milky Way galaxy's closest neighbors. At that time, the distance of that galaxy was a matter of debate. However, Miss Leavitt could ignore the distance effect because the investigated Cepheids were all at the same distance; so, any trend of the intrinsic luminosity with the pulsation period could be revealed from the behaviour of observational apparent magnitudes. Miss Leavitt observed that an increase in the oscillation period corresponded to a brighter apparent magnitude. This correlation between the period and the apparent magnitude implied a correlation between the period and the intrinsic luminosity (absolute magnitude), as the distance was the same for all the investigated SMC Cepheids. The power of this PL relation in the form $M_v = -a \cdot \log P - b$ where, M_v is the absolute V magnitude, P is the oscillation period and, a and b are constants to be properly calibrated, was immediately clear. By measuring the period of a Cepheid, which is an easily measurable quantity that is independent of distance, reddening effects, as well as photometric

errors, one can, in principle, derive the Cepheid absolute magnitude and, in turn, the distance of the star. Thanks to this discovery, towards the middle of the 20th century, Cepheids became the most important primary distance indicators inside the Local Group. They make it possible to calibrate secondary distance indicators and consequently, reach the Hubble Flow at distances of the order of 100 Mpc, and as such measure the Hubble constant H_0 by using the Hubble Law [1].

From the discovery of the first variable stars, many observational efforts have been made, revealing that stellar variability is not a rare phenomenon, with tens of thousands of variable stars having been discovered in our Galaxy alone. At the same time, substantial differences emerged among the various classes of variable stars in terms of both variability characteristics and driving mechanisms. The general variable star classification distinguishes between two big classes of variables depending on the cause of the oscillations: intrinsic variable stars, e.g. with an internal variability cause (like the aforementioned Mira Ceti) and extrinsic variable stars, such as binary systems.
The intrinsic variables are those whose change in brightness is due to some change within the star itself. Among them, the pulsating variables show cyclic or periodic magnitude variation with well-defined amplitudes and periods, while the cataclysmic variables have sudden increases in brightness that are repeated without precise periodicity.
The extrinsic variables are those whose light output changes due to some process external to the star itself. There are two main subgroups of extrinsic variables: the eclipsing binaries, where a binary star system's brightness changes because one orbiting companion passes in front of the other, and the rotating stars, where dark or bright areas on the stellar surface may cause small changes in apparent brightness as the star rotates.

In the rest of my thesis, I will concentrate my attention on radially pulsating stars, that can be investigated through 1D pulsation models and for which the stellar pulsation theory has provided strict relations between pulsational parameters such as periods and amplitudes of the oscillations and evolutionary parameters, such as mass, brightness or effective temperature (T_{eff}). These relations are indeed the basis for the use of radially pulsating stars as distance indicators and stellar population tracers.

In the next sections, I will discuss the different types of pulsating variable stars with a focus on the helium burning ones. Their pulsation properties, corresponding evolutionary phases and relevance in astrophysics will be discussed.

1.2 The pulsating variable stars

Before introducing the main types of radially pulsating stars, let us introduce the fundamental diagram used in stellar astrophysical analysis, i.e. the Hertzprung-Russell (HR) diagram. This is the plot of the intrinsic brightness (bolometric magnitude) of stars against their effective temperature (intrinsic color or stellar spectral classification).

The pulsating variable stars populate a well-defined narrow almost vertical region in the HR diagram. This region is known as the instability strip (IS) and is

[1] Hubble's law affirms a direct correlation between the distance to a galaxy and its recessional velocity as determined by the redshift. It is often expressed by the equation $v = H_0 \cdot D$, where v is the recessional velocity, D the proper distance to a galaxy and H_0 the constant of proportionality between v and D.

shown in Fig. 1.1. From Fig. 1.1 one can notice that various types of radially pulsating stars can be identified in the HR diagram. However these variables stars are associated with distinct evolutionary stages; for instance, δ Scuti and β Cephei stars are associated with the core H-burning stage, δ Cephei and RR Lyrae with the He burning phase, while Mira stars burn hydrogen and helium in two separated shells. Within the strips, all stellar structures show an 'unstable' envelope due to the occurrence of radial pulsations. Radial pulsations are repetitive and correspond to periodic changes in the radius, the brightness and effective temperature.
A list of the main variable stars with their periods, absolute V magnitudes, associated stellar populations and corresponding evolutionary phases is summarized in Table 1.1.

Pulsation is a phenomenon that essentially involves only the outermost layers of the stellar structure. In the so-called classical instability strip marked by dashed lines in Fig. 1.1, the origin of the instability mainly lies in the ionization regions of hydrogen (H) and helium (He) but I will discuss, in detail, the physical mechanisms responsible for stellar pulsation in Chapter 2.

Variable stars can pulsate in one or more pulsation modes. Pulsation at the lowest frequency is known as the fundamental mode (F) and involves oscillation of the whole stellar envelope, while higher modes (first overtone, second overtone and so on) are characterized by longer frequencies (shorter periods) and one or more radial nodes in the envelope. Fig. 1.2 shows a typical light curve for a fundamental Classical Cepheid. The oscillation period and amplitude are indicated. The oscillation period is the time interval between two successive luminosity maximums, while the amplitude is the difference between the maximum and the minimum magnitudes of the curve.

The presence of different classes of variable stars in a galaxy can help to trace the star formation history of the galaxy itself. In fact every class of pulsating stars belongs to a distinct stellar population characterized by a specific age or age range. Therefore, if for example RR Lyrae stars, which trace old (t > 10Gyr) stellar populations, and Classical Cepheids, which trace young (t < 200Myr) stellar populations, are simultaneously observed in the same galaxy, this occurrence is the signature of a complex star formation history, with a very old and a very recent star formation episodes.

In the next sections, I will focus on the pulsating stars typically associated with the central helium burning evolutionary phase, RR Lyrae, Classical Cepheids, Type II Cepheids and Anomalous Cepheids, paying particular attention to Classical Cepheids which have been the main topic of my PhD studies.

1.2.1 Classical Cepheids

Classical Cepheid (CC) variable stars, sometimes called 'delta' or 'type I' Cepheids, have been considered very powerful astrophysical objects since Miss Leavitt, at the beginning of the 20th century, discovered that they obey a period luminosity relation (PL). This relation has made them the current most used primary distance indicators in the Local Group.

Pulsation properties

These variable stars are very bright objects, with intrinsic luminosities ranging from approximately $300 L_{\odot}$ to $25000 L_{\odot}$, which trace young stellar populations (t<200Myr). CCs include both massive and intermediate mass stars with masses from 3 to 13 $M_{\odot}$

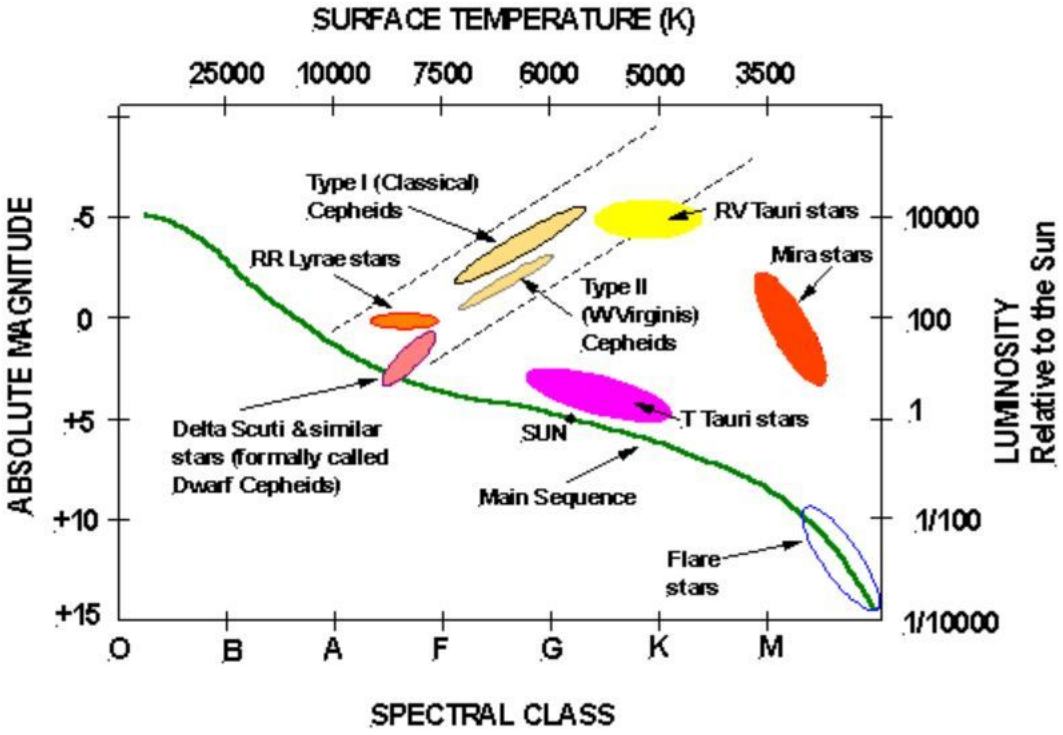

FIGURE 1.1: A schematic distribution of the various types of variable stars in the HR diagram.

(Bono et al., 1999b; Bono et al., 2000b, see Fig. 1.3). These stars cross the instability strip 3 times. The first time is during the sub-giant phase when the star evolves toward the red part of the HR diagram and corresponds to the so-called first crossing. The time-scale of the first crossing is much shorter than the others; as such, the probability of observing stars in this phase is significantly lower than in the central Helium burning phase. The two other crossings, called the second and third crossings, occur during the so-called 'blue loop' phase of the HR diagram, corresponding to the central helium burning phase of massive and intermediate mass stars. Only stars whose blue loop phase crosses the IS will show Cepheid-like behavior.
The IS of CCs depends on the chemical composition of their environment. This effect has been widely debated in literature. According to nonlinear pulsation models (see e.g. Bono et al., 2000b; Fiorentino et al., 2002; Marconi et al., 2005), the strip gets redder as the metallicity (Z) increases at a fixed helium to metal enrichment ratio $\Delta Y/\Delta Z$ [2], and bluer as the helium content (Y) increases at a fixed Z.
Since the blue loop covers a wide range of masses in the HR diagram and consequently, a wide range of mean densities, the well-known pulsation equation also called the period-mean density relation is:

$$P \cdot \sqrt{\bar{\rho}} = Q \tag{1.1}$$

This relation where Q is the pulsational constant (J. P. Cox, 1980) which is slightly dependent on the mass of the variable, suggests that Cepheids cover a wide range of periods too.

[2]The helium to metal enrichment ratio, also called the helium enrichment ratio, indicates the abundance of helium and metals with respect to the primordial chemical composition produced by the Big-Bang nucleosynthesis.

TABLE 1.1: Properties of some types of pulsating stars.

Class	Period[days]	M_V[mag]	Pop	Evolutionary phase
δ Cephei (CC)	1-100	-8÷-2	I	Blue Loop
δ Scuti (δSc)	<0.5	2:3	I	MS-PMS
β Cephei	<0.3	-4.5:-3.5	I	MS
RV Tauri	30-100	-2:-1	I,II	post-AGB
Miras	>100	-2:-1	I,II	AGB
Semiregular (SR)	>50	-3:1	I,II	AGB
RR Lyrae (RRL)	0.2-1	0.5:0.6	II	HB
W Virginis (Type2C)	10-50	-3:-1	II	post-HB
BL Herculis (Type2C)	<10	-1:0	II	poat-HB
SX Phoenicis (SXPhe)	<0.1	2:3	II	MS
Anomalous Cepheids (AC)	0.3-2.5	-2:0	?	HB-Turnover
SP Cepheids (SPC)	<2	$\leq$ 0.0	I	Blue Loop
LL Cepheids (LLC)	0.55-0.65	$\leq$ 0.4	?	?

They have periods between about 1 to 100 days but there are some cases in which this period limits are violated. In the Large Magellanic Cloud (LMC), Ulaczyk et al. (2013) found fundamental mode Cepheids with periods of about 135 days and a first overtone (FO) Cepheid with a period of about 0.5 days. The spectral type of CCs varies with the effective temperature but ranges from F-type, with visual magnitude $M_v = -2mag$, to G or K-type with $M_v = -6\ mag$.

As CCs are associated with intermediate and massive stars, they have relatively short evolutionary timescales when compared with other pulsating stars associated with low-mass stars. In fact, CC ages range from about 10^7 years for massive and bright stars to just 10^8 years for faint ones. CCs are indeed associated with young astrophysical systems where events of star formation are recent or still present. Therefore, we expect and effectively find Cepheids in the disk of the Milky Way but also in other nearby galaxies populated by young stars, like the Andromeda Galaxy (M31) and the Magellanic Clouds. CCs pulsate in the first three radial modes: the fundamental, the first overtone and the second overtone modes. However, second overtone mode CCs do not exist for all chemical compositions.

Light curves

CCs show a typical light curve with the amplitude decreasing from the optical to the near-infrared (NIR) filters (see Fig. 1.4).
The ratios of the amplitudes in different filters are a signature of the Cepheid nature. If the observed amplitudes are the same in all the filters, the investigated object is not pulsating but most likely a binary star.
Another implication of the trend of amplitudes with the wavelength is that, CCs are easy to detect in the optical bands thanks to their large amplitude, whereas towards the NIR filters the amplitude gets very small.
However, optical bands present two problems: the corresponding PL relations are too largely dispersed, as such, in order to have a good light-curve coverage in these bands, more than 10-12 phase points are required and this involves a lot of telescope time.
On the other hand, in the NIR bands, thanks to the small light curve amplitudes, few phase points are needed to get accurate mean magnitudes. However, if the signal to

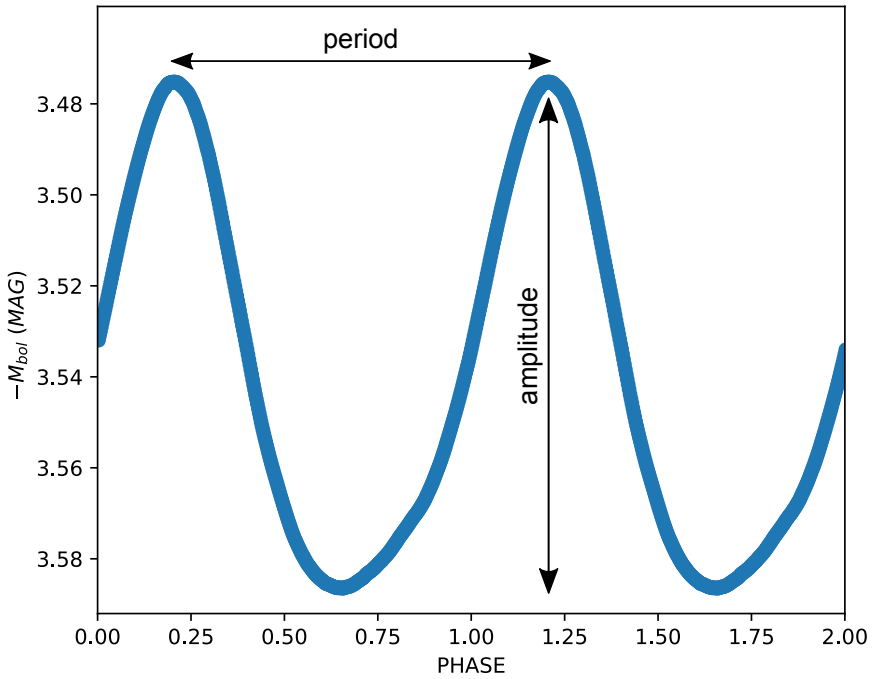

FIGURE 1.2: Fundamental Classical Cepheid light curve showing oscillation period and amplitude.

noise ratio of the observations is not high enough, it is very difficult to detect variables that oscillate with an amplitude of just a few dex of magnitude.
Therefore, to properly study CCs, multiband observations are necessary. In order to detect these variables and obtain accurate periods optical observations are required while NIR observations allow us to obtain accurate magnitudes as well as to be less affected by reddening effects and to produce intrinsically narrower PL relations. On this basis, some current and future facilities such as the Hubble Space Telescope (HST) or the next generation James Webb Space Telescope (JWST) and Large Synoptic Survey Telescope (LSST) plan to observe pulsating stars in a wide range of wavelengths.

Evolutionary properties

As also shown in Fig. 1.3, CCs are associated with the core He burning stage of intermediate-mass or massive stars. Stars within this mass range have structural and evolutionary properties quite different from less massive stellar objects (Bono et al., 2000a).
One of the main differences is associated with the fact that stars with masses larger than about 2.0-2.3$M_{\odot}$ do not develop a significant - if any - level of electronic degeneracy in the helium core in the evolutionary stage, the Red Giant Branch (RGB) that follows the H exhaustion in the core.
Therefore, no electronic degeneracy has to be removed from the core and the helium ignition does not occur with a flash, as in low-mass stars, but quiescently. Due to the absence of electron degeneracy in the core, and the fact that the cooling processes (thermal electron conduction and thermo-neutrino energy losses, (Salaris et al., 2005)) are non efficient in intermediate-mass stars, these objects reach the thermal conditions $T_C \approx 3 \times 10^8 K$ and $\rho \approx 10^4 g\dot{c}m^{-3}$ needed for the He-burning ignition on a much shorter time scale with respect to low-mass stars. This results in a less

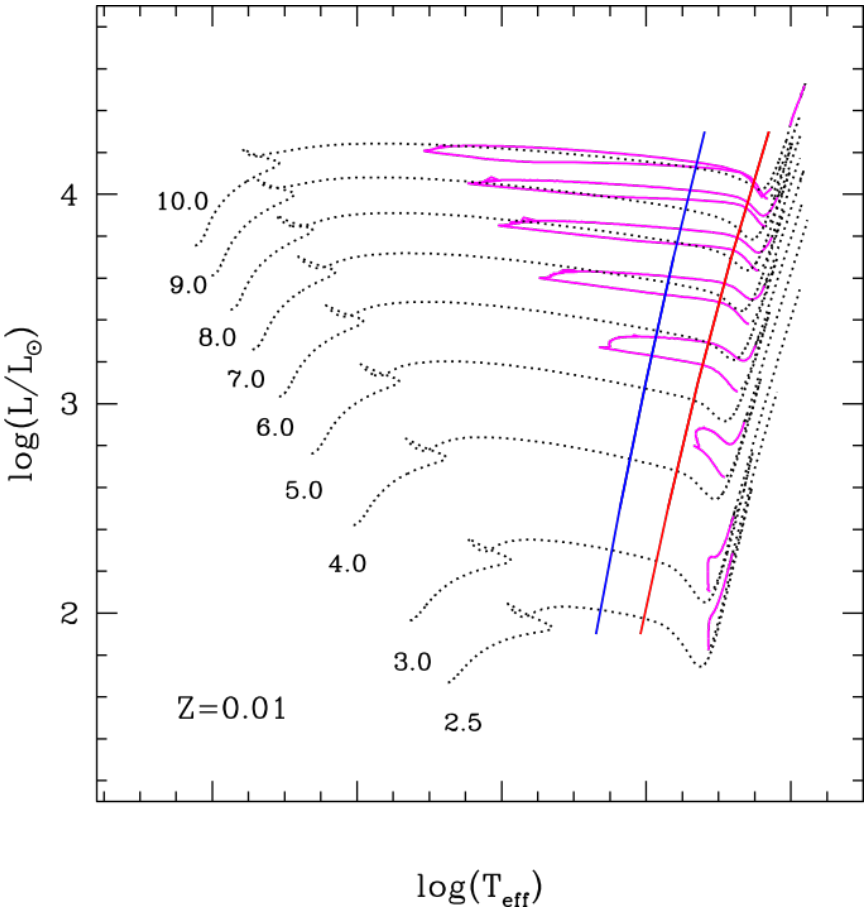

FIGURE 1.3: The evolution in the HR diagram of a selected range of intermediate-mass and massive stars for a given metallicity (see label). The location of the blue and red edges of the IS is shown. The evolutionary stage corresponding to the blue loops is drawn in magenta.

extended RGB in the HR diagram.
At the central Helium ignition, the star needs to find a new stable configuration. First, the star's structure becomes hotter and as such it moves toward the bluer part of the HR diagram, and becomes less luminous because the efficiency of the 3-α process is lower than the efficiency of the CNO-cycle reaction with which the hydrogen is burning in the shell (Catelan et al., 2015b).
The new configuration of the star is a double burning configuration: helium is burning in the core and hydrogen in the shell. During this phase the star performs a loop in the HR diagram, reaching higher effective temperatures and then moving again towards redder colors (blue loop). During the blue loop, the star is two orders of magnitudes brighter than during the Main Sequence (MS) phase due to the presence of a very large He core and as such, can cross the IS.
Fig. 1.5 shows the typical evolutionary track for a solar chemical composition $5M_{\odot}$ star. The core He-burning phase is from E, the tip of the RGB, to I, the point at which the central helium burning is exhausted. From the beginning of the helium burning at point E, the star goes down until point F. At point F, the star moves from the RGB to the blue side of the HR diagram until it reaches the bluest point of the loop, G, where the central helium abundance is about half of the initial central helium abundance. Moving from E to G, the efficiency of the CNO cycle in the shell increases. As soon as the star reaches G, the efficiency of the 3-α reaction in the core supersedes

the efficiency of the CNO cycle in the shell, until the exhaustion of helium at I.
The evolutionary phase that goes from point F to I is called the blue loop phase of the HR diagram.
Along the blue loops an evolving stellar structure can cross the IS. Depending on the extension and morphology of the predicted blue loops, Cepheid variables in a given mass and luminosity range are expected.
In spite of its crucial role, the morphology of the blue loop is very difficult to predict due to its highly non-linear dependence on most physical inputs and assumptions made in the evolutionary computations. It does, however, have a linear dependence on mass; the extension of the blue loop generally increases with the mass of the CCs. Consequently, masses lower than $\sim 3\ M_{\odot}$ do not enter the IS, while more massive stars evolve inside the IS during this evolutionary phase. This happens because the more massive the star is, the higher the effective temperature is.
The dependence of the blue loop on the chemical composition is not simple to describe with an analytical function. Fixing the metallicity and increasing the helium content, produces a slight increase in the blue loop luminosity but a similar effect is also produced when fixing the helium content and decreasing the metal abundance.

The most interesting relation predicted by stellar evolution for the blue loop phase is a logarithmic relation between luminosity and mass:

$$\log(L/L_{\odot}) = a + b \cdot \log(M/M_{\odot}) + c \cdot \log Z + d \cdot \log Y \tag{1.2}$$

This relation, called the mass-luminosity (ML) relation, depends on the chemical composition: the abundance of heavy elements (Z) and the abundance of helium (Y).
This dependence is due to the fact that both the metallicity and the helium content affect the helium core mass at the beginning of the central He-burning stage. Consequently, as noted above, the stellar luminosity during this evolutionary stage is affected, for a given total mass, by the initial chemical composition of the star.
When the ML relation is based on stellar models computed by neglecting core convective overshooting, rotation and mass loss, it is customary to refer to it as a 'canonical ML relation'. When at least one of these non-canonical, physical processes is accounted for in the stellar model computation, the brightness of the stellar model in the blue loop phase, for any given value of the total mass, is increased with respect to the standard (canonical) models. For instance, including some amount of core convective overshooting during the central H-burning stage causes the star to get brighter during the blue loop phase as a consequence of the larger He core (see Fig. 1.6). In passing, we note that empirical constraints seem to suggest that some amount of mild overshooting should be accounted for in stellar modelling in order to better reproduce observational constraints (see e.g. Caputo et al., 2005a; Marconi et al., 2013a; Marconi et al., 2017; Ragosta et al., 2019, and references therein)
The occurrence of efficient mass loss during the red giant phase affects only the mass of the envelope and not the He core mass; therefore, during the blue loop stage the star is characterized by a lower total mass for a given fixed He core mass. Since the luminosity is fixed by the He core mass, we will have a stellar structure with a smaller mass, at a fixed luminosity, with respect to the canonical case, which is equivalent to a brighter luminosity at a fixed mass.
Finally, the occurrence of rotation causes the presence of a larger convective core during the central H-burning stage and hence a larger He core during the blue loop stage; the consequence being that, for a given total mass, the stellar structure is again

brighter than in the canonical case.
Therefore, there is a sort of degeneracy among these three physical phenomena, as it is difficult to disentangle the different contributions to the generally observed and predicted overluminosity of CCs with respect to the canonical assumptions. The impact of the ML relation and, in turn, of these "non-canonical phenomena" on the Cepheid distance scale is discussed below.

CC Period-Luminosity and Period-Luminosity-Color relations

The physical reasons at the basis of the existence of the PL relation possible can be understood from the aforementioned Eq. 1.1 and the Stefan-Boltzmann (SB) law

$$L = 4\pi R^2 \sigma T_{eff}^4 \tag{1.3}$$

Since the mean density ($\overline{\rho}$) is a function of mass and radius,

$$\overline{\rho} = M/[(4\pi/3)R^3] \tag{1.4}$$

substituting the mean density expression in the pulsation equation would provide a period-mass-radius (PMR) relation. By combining the PMR relation with the SB law, a relation connecting the period to the stellar mass, luminosity and effective temperature (PMLT) is derived:

$$\log P = a + b \cdot \log T_{eff} + c \cdot \log(M/M_{\odot}) + d \cdot \log(L/L_{\odot}) \tag{1.5}$$

As an example, for solar chemical composition fundamental pulsators, the relation derived in my PhD work and published in De Somma et al. (2020b), for standard physical assumptions is:

$$\log P = 10.268 - 3.192 \cdot \log T_{eff} - 0.758 \cdot \log(M/M_{\odot}) + 0.919 \cdot \log(L/L_{\odot}) \tag{1.6}$$

This relation is extremely powerful because it allows us to test stellar evolution theory through the investigation of pulsation properties. The left-hand side of the relation, the pulsation period, is a parameter that is very easy to measure from observations. While, the right-hand side, the evolutionary parameters, such as mass, effective temperature and radius, are linked to the age and chemical composition of the star. So, by simply measuring the period and the color, information on other intrinsic stellar parameters can be easily derived.
Stellar metallicity also affects the pulsation period distribution as an increase in the metal content shifts the IS towards lower effective temperatures which means longer periods at a fixed mass and luminosity.
Assuming an evolutionary predicted ML relation for CCs in the form of eq. 1.2 and substituting this relation in eq. 1.5, one obtains a period-luminosity-effective temperature relation and by transforming the temperature into a color index, the following period-luminosity-color (PLC) relation is obtained:

$$M_J = \alpha + \beta \cdot \log P + \gamma[CI] \tag{1.7}$$

.

The PL relation is then derived by averaging the periods over the color extension of the IS at each fixed luminosity level or, in other terms, projecting the PLC relation onto the PL plane.

This implies that the PL relation is a statistical relation that can be inferred only when a statistically significant sample covering the whole extension of the IS is available. Indeed the effect of the finite width of the IS produces an unavoidable intrinsic dispersion of the PL relation (1.7). Therefore, the PL relations should not be applied to individual Cepheids.
The effect of the finite width of the IS on the intrinsic dispersion of the PL relation tends to reduce when one moves from the optical to the NIR bands. This behaviour suggests that NIR PL relations are more accurate and reliable tools to derive Cepheid distances with respect to optical PL relations (Caputo et al., 2000b).

This trend is evident in Fig.1.9 in which Galactic and LMC Cepheid observed PL relations from the optical (BVI) to the near-IR (JHK) filters, are shown; and in Fig. 1.8 in which theoretical synthetic PL relations for Z=0.004, Z=0.008, Z=0.02 and several photometric passbands are shown. The first way of reducing the effects related to the intrinsic dispersion of the PL is to use near or mid infrared filters. Therefore, in NIR or IR filters we can directly use the PL relation to determine distances and the 3D structure of galaxies.
In the optical bands an alternative solution is to introduce a color term and use the so-called period-Wesenheit (PW) relation.
The PW relation in the B-V color is:

$$W(B,V) = M_V - R_V \cdot (B-V) \quad \text{where} \quad R_V = A_V/E(B-V) \tag{1.8}$$

The usefulness of this relation is that it is reddening free by definition because the magnitude is replaced by the Wesenheit function (W) which includes the color term with a coefficient (R_V), and this coefficient is the exact ratio of the total to the selective extension. This definition makes PW relations reddening free. The PW relation can be used to find individual Cepheid distances while the PL can't because of the finite width of the PL. In fact, when using the PW, we find a magnitude for each period and color but when using the PL, we find a range of magnitudes for each period.
A. Riess and collaborators used some combinations of optical and NIR PW relations to estimate the distance of extragalactic CC contained in galaxies hosting Supernovae (SN) Ia. In fact, they used the PW relations to calibrate SNIa extragalactic distance scale (from CCs in the Shoes program), reducing the uncertainty on the estimated Hubble constant (H_0) from 3.3 to 2.4 % (Riess et al., 2016a).
Due to the highly debated 'Hubble constant tension', which is the difference between the value derived by Riess et al. on the basis of Classical Cepheid distances (Riess et al., 2016b; Riess et al., 2018b), and the Cosmic Microwave Background results derived by the Planck collaboration (Planck Collaboration et al., 2016), there are several teams around the world that are trying to reduce the systematic uncertainties on the coefficients of PL and PW relations, as these errors propagate through the various steps of the extra-galactic distance ladder till the estimate of H_0.
As the Cosmic Microwave Background anisotropy measurements are related to the initial phases of the Universe, it is possible that something in the fundamental physics has to be reviewed. However, until the systematic errors on the distance scale calibration are completely removed, it is not possible to check if the tension is real and/or related to underestimated uncertainties.

One of the most debated issues concerning the use of Cepheids as distance indicators is the dependence of PL and PW relations on chemical composition (Macri

et al., 2006; Romaniello et al., 2008; Bono et al., 2010; Freedman et al., 2011; M. Groenewegen, 2013; Ripepi et al., 2020). Indeed, in the past the LMC-based PL relation was used to estimate the distance of CCs in external galaxies with metal abundances often significantly different from the LMC one. Moreover, in recent years A.Riess and coworkers have adopted the CC sample observed in the maser galaxy NGC4258 for which a direct geometric distance modulus is available in literature (Riess et al., 2016b). The metallicity of this galaxy is more similar to the one of external spiral galaxies hosting SNIa, thus significantly reducing the metallicity issue. From the theoretical point of view, nonlinear convective pulsation models predict that the PL depends on chemical composition (Fiorentino et al., 2007; Bono et al., 2010). In particular, the slope of the PL relation is expected to decrease as Z increases at a fixed He enrichment ratio.
On the other hand, the PL slope increases as Y increases at a fixed Z. Both these effects get less important from the optical to the NIR bands (Fiorentino et al., 2007; Bono et al., 2010; Fiorentino et al., 2013; Di Criscienzo et al., 2013). Another debated property of CC PL is its possible nonlinearity over the entire period range. Indeed, the application of a PL relation calibrated on a CC sample with short periods to a galaxy hosting only long period Cepheids can introduce an error in the inferred distances. This aspect was analysed for the first time by Ngeow and Kanbur using MACHO and OGLE data (Ngeow et al., 2005). They found that the cause of the change in the slope of PL at longer periods is the interaction between the ionization front and the stellar photosphere which produces a lower luminosity inferred from the PL than from the ML.
The predicted ML relation for CC is related to the so-called mass discrepancy problem, that is the difference between masses derived with pulsational versus evolutionary methods. The masses derived from the comparison of pulsation models with observations were found to be smaller by 20-40% than masses measured from the comparison with evolutionary models (A. Cox, 1980). With the inclusion of updated physics inputs, including new tables for radiative opacity in the stellar models, the mass discrepancy was reduced to 10-15% (Moskalik et al., 1992b; Moskalik et al., 1992a; Bono et al., 2000c). In any case, an overluminosity with respect to canonical ML relations, due to overshooting and/or mass loss and/or rotation, is needed in order to reconcile evolutionary and pulsational CC mass values (Bono et al., 2001; Caputo et al., 2005b). In conclusion, CCs are important not only as distance indicators but also as benchmarks of stellar evolution theories and stellar physics.

Ultra Long Period Cepheids

In the past few years, another interesting class of variable stars with properties similar to CCs but with longer periods has drawn the attention of astronomers. These are the ultra long period Cepheids (ULPs), identified in nearby star forming galaxies (Ulaczyk et al., 2013).

They have periods longer than 80 days and magnitudes in the I band between -7 mag and -9 mag. Therefore, they are significantly brighter than canonical CCs which, as already mentioned, have magnitudes in the V band between -2 mag and -7 mag.

From their position in the color magnitude diagram (CMD) and in the PL diagrams (Bird et al., 2009; Fiorentino et al., 2012b), ULPs have been suggested to be the extension of CCs at higher masses. If this hypothesis were confirmed from current and future observational and theoretical investigations, these pulsating stars would

represent the most powerful primary distance indicators, able, with the advent of big next generation telescopes like JWST or the Extremely Large Telescope (ELT), to reach the Hubble flow in one step. For example with ELT it might be possible to observe the brightest ULPs at the distance of the Coma cluster (100 Mpc). This, in turn, would allow us to directly estimate H_0, skipping the use of any secondary distance indicators, and providing an independent test of their accuracy.

1.2.2 Other Helium burning variable stars

RR Lyrae

RR Lyrae variable stars are the most abundant class of pulsating stars in the Milky way.
RR Lyrae (RRL) are old, low-mass, radially pulsating stars with periods ranging from 0.2 to 1.0 days and visual magnitudes ranging from $\sim$ 0 to 1 magnitudes (See Fig. 1.12). They are population II variable stars (t>10Gyr) and as such, populate galactic halos, thick disks and globular clusters (GCs) (Marconi et al., 2018). RRL of GCs have historically been and still are of extreme importance due to the existence of samples rich in a few hundred variables, all at the same distance, with the same age and from stars with the same chemical composition. These samples are, therefore, optimal for investigating the intrinsic properties of variability and their connection to evolutionary parameters. The first period-amplitude diagram for RRL in globular clusters was made by Solon Bailey in 1902. From this diagram, now known as the 'Bailey diagram', Bailey divided RR Lyrae into two classes: the 'ab' and 'c' types.

The RRab variable stars show periods ranging from about 0.3 to 1.0 days, with amplitudes decreasing as the period increases and generally asymmetric light curves often characterized by the presence of secondary features, such as bumps or dips. The light variations have steep rising branches and a slow decrease of brightness after the peak brightness has been reached. The amplitude can reach 1.5 mag in the V band and 1 mag in the I band. A typical RRab light curve is shown on the top-left panel of Fig. 1.11. On the other hand, $c-type$ RR Lyrae are concentrated at short periods with a dependence of amplitude on period which explains its characteristic bell-shape. These stars have much more symmetric light curves with the possible presence of a small secondary bump located on the ascending branch, and smaller amplitudes than RRab pulsators (see the top-right panel of Fig. 1.11).

The theory of stellar pulsation has later demonstrated that RRab stars correspond to the fundamental pulsation mode, whereas RRc stars are first overtone pulsators.

A significant number of RRab stars' light curves show a modulation that has a period much longer than that of the primary pulsation cycle. This phenomenon, called 'the Blazhko effect', was discovered by Sergey Blazhko in 1907.
Although the cause of this effect is still highly debated, one possibility is that it is due to the magnetic field of the stars. As such, there are studies on the magnetic field of the stars in both the MS and the more advanced evolutionary phases like the Horizontal Branch (HB). On the bottom-right panel of Fig. 1.11 an RRab star light curve with visible Blazhko effects is shown.
The Blazhko effect is also observed in some RRc stars, but it is much less common than in RRab stars. Less than 10% of first-overtone RR Lyrae stars exhibit Blazhko modulation.

There is also a third group of these variables, the $d-type$ RR Lyrae.
The RRd type variable stars simultaneously pulsate in the fundamental and first overtone modes. The relative number of RRd stars within the whole population of

RRL variables strongly depends on the metallicity of the stellar environment. In the relatively metal-rich Galactic bulge only 0.5% of RR Lyrae stars are double-mode pulsators, while in the more metal-poor Small Magellanic Cloud (SMC), as much as 10% of RR Lyrae variables are of RRd type. The percentage of RRd type variable stars significantly increases in the metal-poor Galactic Halo.

In the vast majority of RRd stars, the first-overtone component has a larger amplitude than the fundamental mode. When the modes are separated in RRd, the first-overtone light curve usually has a similar shape and amplitude as the single-mode RRc stars, while the fundamental mode component visibly differs from the RRab light curves - it has a small amplitude and nearly sinusoidal shape. On the bottom-left panel of Fig. 1.11, a typical RRd star light curve is shown.
The RRd stars are also very important because when plotting the ratio between the two periods as a function of the

fundamental mode period in the Petersen diagram, we notice that the obtained pattern depends on the stellar mass. Thus, by simply measuring the two periods of RRd pulsators, we can directly estimate the stellar mass.
Until now no second-overtone pulsator among RR Lyrae variables has been observed or predicted. The intersection of the HB, that is the location of central Helium burning, with the RR Lyrae IS is sometimes called 'RR Lyrae gap', which may be confusing as it is not really an empty space in the HB star distribution. The RR Lyrae structure is made of a core in which He is burning via the 3-α process and a surrounding shell in which H is burning via the CNO cycle. The longest possible lifetime of an HB star as an RR Lyrae is $t = 10^8$ years as this is the time it takes to fully burn He in the core.

The topology of the RRL IS is shown in Fig.1.10. One can note that the bluest edge, corresponding to the FO blue edge (FOBE), is located at an effective temperature of around T_{eff}=7200K at the Zero-age Horizontal Branch (ZAHB) luminosity level; a value which slightly decreases with increasing stellar luminosity. Moving towards lower effective temperatures you can find the F blue edge (FBE), the FO red edge (FORE) and finally the F-mode red edge (FRE). The region between the FBE and the FORE is called the OR region. In this region a star can pulsate as either a fundamental, first overtone or double pulsator mode variable. The region to the left of the OR region is the "FO zone" as only FO-mode is efficient here, whereas the region to the right of the OR zone is called "F zone" and is bound on the right by the FRE, located around T_{eff}=5900K (Cassisi et al., 2013) at the ZAHB level. The physical reasons for the existence of the blue and red edges of the IS will be largely discussed in Chapter2.

RR Lyrae are population II primary standard candles widely used to measure distances within our own Galaxy and its nearest neighbours up to about 1 Mpc in distance. Over the years different relations from the optical to the mid-infrared (MIR) bands that make RRLs distance indicators have been discovered. The most widely used are: - the $M_V - [Fe/H]$ relation (Caputo et al., 2000a; Di Criscienzo et al., 2004; Catelan et al., 2004; Marconi et al., 2021) which is the relation that links the metallicity to the absolute visual magnitude of RR Lyrae. Its general form is $M_V(RR) = a[Fe/H] + b$ - the PL relation in the K band (Bono et al., 2003; Coppola et al., 2011; Braga et al., 2018). Its general form is:$M_K = a + b \cdot \log P$ A PL relation in the optical bands is not expected as RRL are located on the HB where the luminosity does not vary with the effective temperature and as such it does not vary with the period. In the K band, due to the dependence of V-K on the effective temperature, the K-band magnitude, that is obtained combining V with V-K, is very dependent

on the period.

Both these relations are affected by systematic errors. The MV - [Fe/H] relation is affected by off-ZAHB evolution as well as the metallicity scale and the α element enhancement. Moreover several theoretical studies claim that this relation is not linear over the whole observed metallicity range. On the other hand, the K band PL relation is affected by metallicity variations, so that the true relation is $M_K = \alpha + \log P + c \cdot [Fe/H]$ generally known as the RR Lyrae PLZ relation.

Type II Cepheids

Type II Cepheids, sometimes called Population II Cepheids, are low-mass pulsating stars tracing, like RR Lyrae stars, old stellar populations.
These variable stars can be divided into three subgroups. These subgroups, BL Herculis, W Virginis and RV Tauri stars, are each in a distinct stellar evolutionary phase.
BL Herculis stars are the shortest pulsation period type II Cepheids. Their period ranges from 1 to 10 days.
W Virginis stars are type II Cepheids showing pulsation periods between 10 and 25 days.
RV Tauri stars are the longest pulsation period type II Cepheids with periods between 25 and 150 days. 150 days is the minimum period of another type of variable stars called long period variables (LPV).
Unlike the RR Lyrae or CC, there is no clear distinction between the fundamental or first overtone mode pulsators (if any) among type II Cepheids. Type II Cepheids were discovered and can be observed in the Galactic field but the majority of them are in the Galactic Globular Cluster with a blue HB morphology and average to high metal deficiencies. Like CC and RR variable stars, Type II Cepheids obey a PMLT relation too. The relation for fundamental BL Her pulsators derived by Di Criscienzo et al. (2007) is:

$$\log P = 11.579 + 0.89 \cdot \log(L/L_\odot) - 0.89 \cdot \log(M/M_\odot) - 3.54 \cdot \log T_{eff} \qquad (1.9)$$

Also in this case, establishing a relation between pulsational and evolutionary parameters allows us to probe the evolutionary properties of type II Cepheids observed in stellar clusters once their periodicity is measured.

BL Herculis variables begin their main core HE-burning stage on the blue side of the RRL IS, then crossing the IS while moving from the bluest part of the HB towards the asymptotic giant branch on the red side of the HR diagram. These variable stars cover a wide range of periods because as the total mass decreases, the mean luminosity increases. The typical crossing time is $80 \cdot 10^4$ years, depending on the evolutionary mass.
W Virginis (W Vir) stars are type II Cepheids with pulsation periods in an intermediate range between BL Herculis and RV Tauri variables. The periods and amplitudes of W Virginis stars often vary irregularly from cycle to cycle.
It is widely believed that W Vir variables originate from the post-HB evolution of low-mass stars that enter the asymptotic giant branch (AGB) evolutionary phase with relatively small or intermediate envelopes. After the central helium exhaustion, when there is no fuel in the core, the efficiency of the shell increases because He burning continues in the narrowing shell. The energy released from the He burning shell results in the expansion of its outer layers, depending on the residual mass of the envelope, which in turn starts to reduce the energy released by the H-burning shell.

As a result, the envelope shrinks, the surface luminosity reduces and consequently, the star moves to the bluer part of the HR diagram. This evolutionary path is however stopped and reversed because, as a consequence of the contraction, gravitational energy is released, the stellar envelope is warmed up and this results in the re-ignition of the H-burning shell.
The luminosity of both the He and H burning shells, in this stage, increases concurrently as opposed to the thermal pulsating stage along the AGB. This results in the star performing a blueward nose in the HR diagram and thus reentering the IS. This blueward nose, which typically takes a few Myr, can be repetitive due to the fact that the burning efficiency of one shell affects the other, resulting in the star entering the IS multiple times.
The structural parameters affecting the blueward noses are; the abundance of He in the envelope and the residual mass of the envelope at the end of the He-burning stage. For envelopes with less than $10^{-2}\ M_{\odot}$, after central HE-exhaustion, the star can't reach the AGB thus becoming an AGB manquè. However, for larger envelopes, the star reaches the AGB without performing blueward noses. Stars that experience the blue loop in the HR diagram have envelope masses less than the mass required to perform the blueward noses but more than is required to reach the AGB.
RV Tauri stars are the brightest type II Cepheids. These are stars that experience thermal pulses while burning He in their shell. Although their envelope masses are very small due to both H-burning and efficient mass loss in the AGB stage, they burn H in their external shell. RV Tauri stars include stars that are leaving the AGB towards the white dwarf cooling sequence and thus cross the IS while performing this final blueward motion.

Anomalous Cepheids

Anomalous Cepheid (AC) variable stars are radial and metal poor pulsating stars. They are commonly believed to trace the intermediate age stellar populations (1Gyr < t < 5Gyr) as they are brighter and more massive than RR Lyrae stars. In fact, they enter the IS at absolute magnitudes of about 0.5 to 2.5 magnitudes and their masses ranges from 1 to 2 $M_{\odot}$. See Fig. 1.13.
They belong to the central helium evolutionary phase. ACs pulsate in both fundamental and first overtone modes. Fundamental mode ACs have periods from a few hours to over 2 days while first overtone mode ACs have periods from about 0.3 days to slightly over 1 day. Therefore, as it is shown in Fig.1.14, for Cepheids in the LMC, ACs are located between CCs and population 2 Cepheids in the PL diagram. While the PMLT relation for fundamental mode ACs, according to Fiorentino et al. (2006) is

$$\log P = 10.88 - 3.31 \cdot \log T_{eff} - 0.62 \cdot \log(M/M_{\odot}) + 0.82 \cdot \log(L/L_{\odot}) \qquad (1.10)$$

for a given luminosity, effective temperature and mass, the relation between the first overtone period and the fundamental one, according to the same authors, is $\log P_1 = \log P_0 - 0.13$.

Fundamental mode AC light curves are asymmetric with a rapid rise to the maximum followed by a slow decline, while FO-mode AC light curves are generally smoother than fundamental mode ones.

Due to the fact that ACs are abundant in most Local Group dwarf galaxies but very few in metal-poor, older stellar systems, and their pulsational properties suggest that they are more massive than RR Lyrae stars, two hypotheses for the origin of ACs are possible.
ACs are either intermediate-age stars with astonishingly low metallicity or they are the final result of mass transfers within old binary star systems.
The first hypothesis for the origin of ACs, according to stellar evolution theory, is as follows; once a star with an age equal to or lower than 4-5 Gyr arrives at the RGB tip, He-ignition starts and the He-core mass starts reducing. As a result, for younger stellar systems, the He-core mass at the RGB tip can be viewed as dependent on the mass of the RGB progenitor.
From evolutionary computations, it is clear that for low-mass RGB progenitors, He-core mass and ZAHB brightness are directly correlated. These computations also show that when the He-core mass is fixed and the envelope mass is increasing, T_{eff} of the ZAHB models decrease uniformly but after the minimum T_{eff} is reached, both the brightness and T_{eff} of the ZAHB increase despite the envelope mass increase.
This then creates an 'upper branch' along the ZAHB (HB upturn) for stellar systems ranging from about (1-2) Gyr to about (4-5) Gyr, the exact age depends on the chemical composition. As suggested by Demarque et al. (1975) and Hirshfeld (1980), the 'upper branch' can enter the IS depending on the mass of the RGB progenitor, the mass loss efficiency during the RGB phase and the metallicity. Nevertheless, if the metallicity is larger than approximately $4 \cdot 10^{-4}$, the maximum T_{eff} achieved by the ZAHB locus is too low to push these structures inside the IS (see also Marconi et al., 2004; Caputo et al., 2004). This occurrence justifies why they are only found in metal-poor stellar systems with an intermediate age stellar population. ACs are then brighter and more massive than the RRL stars.
In spite of their larger masses and brightness, ACs are similar to RRL stars with regards to the He-core burning lifetimes (i.e. 10^8 yr) because H shell burning is very efficient.

The second hypothesis for the origin of ACs implies a phenomenon of mass exchange in a binary system. The existence of massive Blue Stragglers in the majority of Galactic globular clusters (GGC) could be the signature of a binary evolution resulting in a progeny whose mass is significantly larger than at the Main Sequence Turn Off (MS TO).

During the He-core burning phase, this progeny would be in the red side of the HB; however, if these stellar structures have masses ranging from $\sim 1 \div \sim 2 M_{\odot}$ and metallicities lower or equal to ~ 0.0004, they then move to the 'upper branch' and become ACs. This hypothesis for the origin of ACs would also provide a possible explanation for their absence in most GGCs. Indeed, a binary system with the required characteristics can survive only in low enough density stellar environments such as Globular Clusters (GC) for a sufficiently long time (Clement et al., 2001; Musella et al., 2012).

However, a problem with this hypothesis is the poor number of ACs observed in the LMC, which has both the right density and metallicity to produce this kind of pulsators (Soszyński et al., 2008; Fiorentino et al., 2012a; Ripepi et al., 2014)

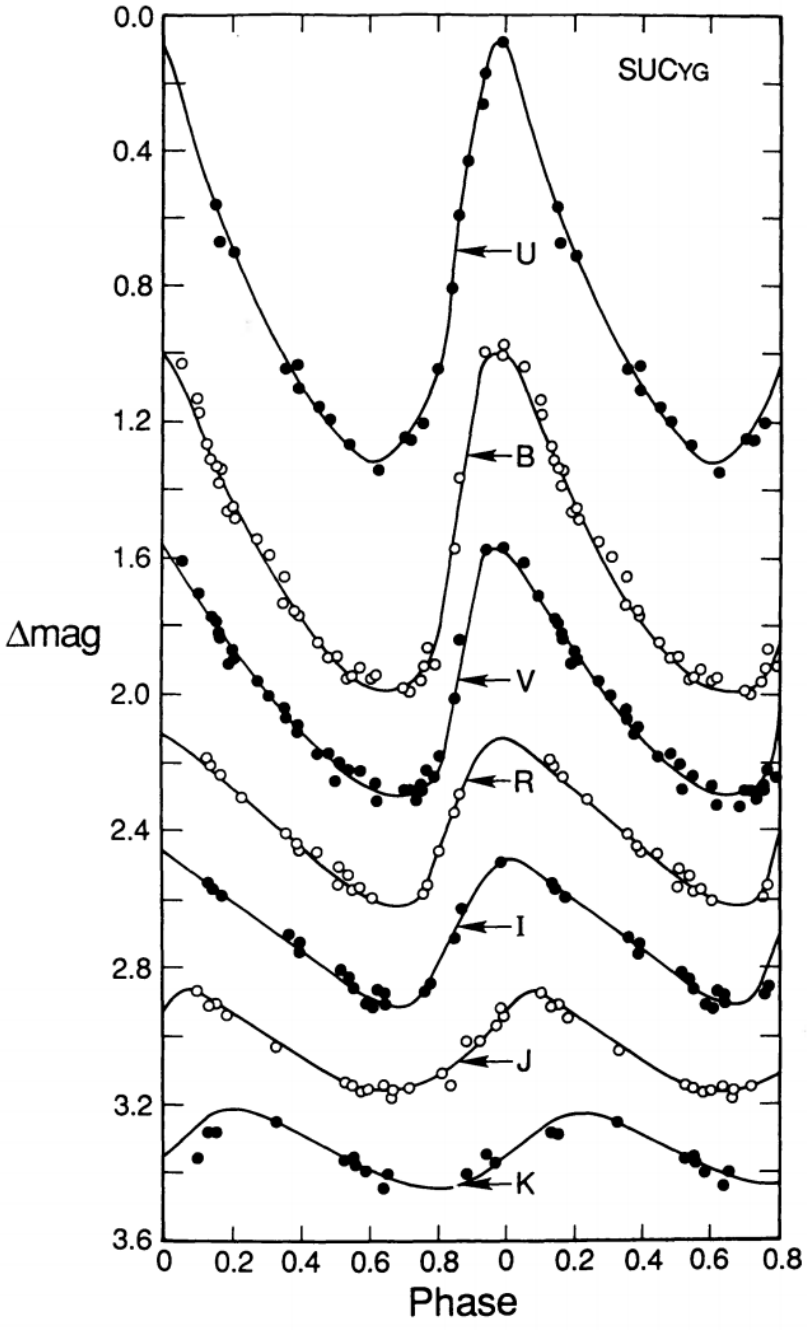

FIGURE 1.4: A map of Classical Cepheid light curves in various photometric bands.

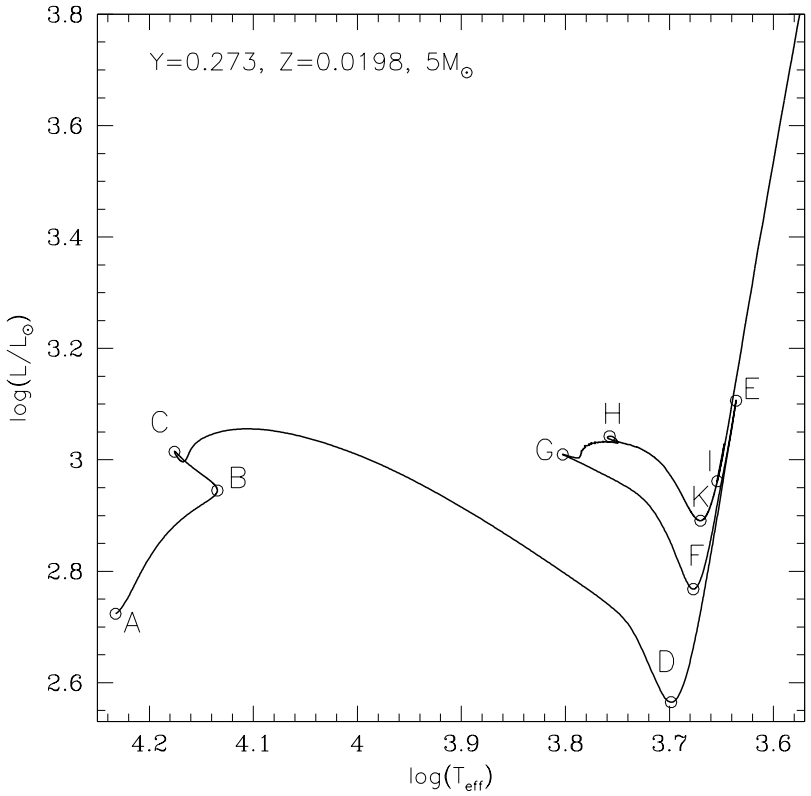

FIGURE 1.5: The evolutionary track of a 5 solar mass star. The labels mark the position of some relevant evolutionary stages, discussed in the text.

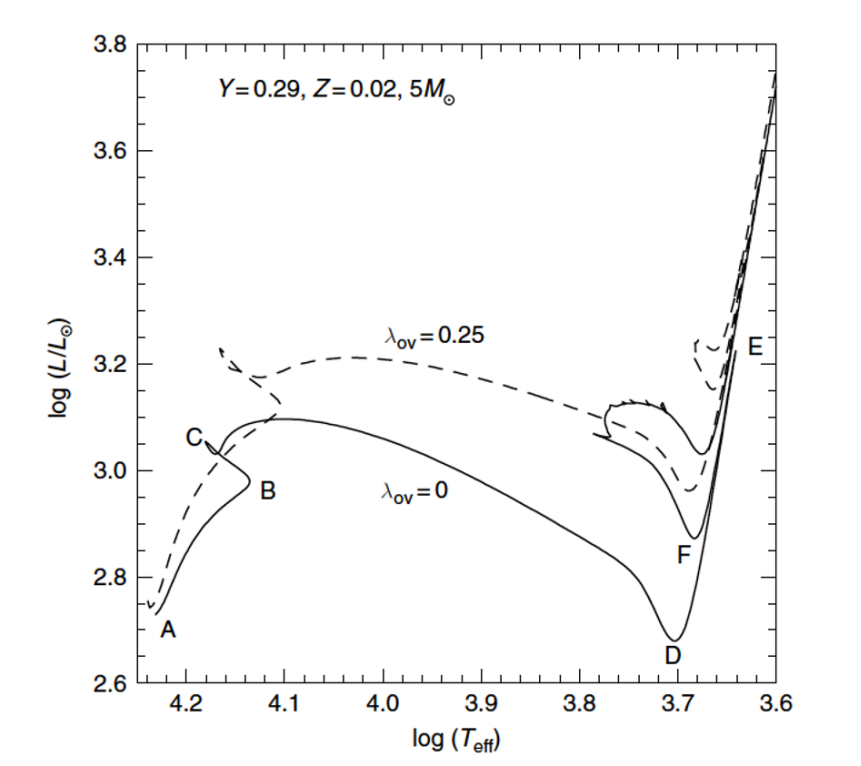

FIGURE 1.6: The Evolutionary tracks of a 5 solar mass star without (solid line) and accounting for (dashed line) a mild overshooting.

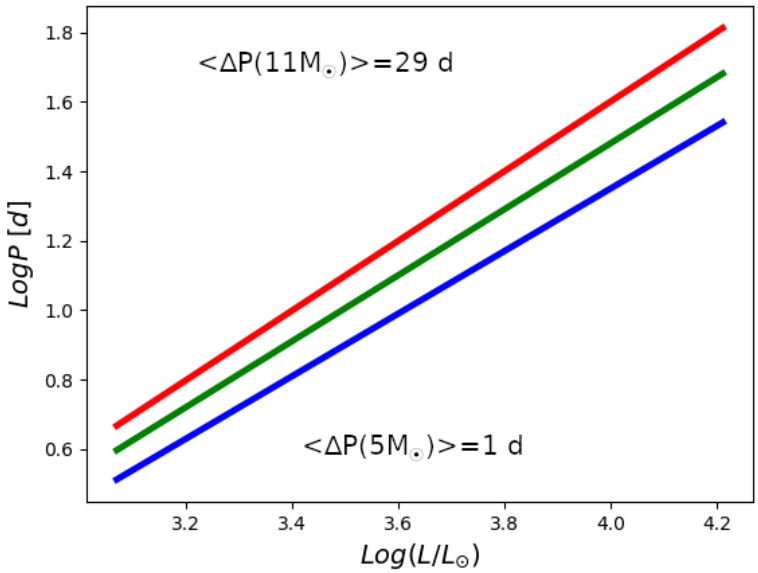

FIGURE 1.7: The period-luminosity relation at different T_{eff} values for masses ranging from 5-11 $M_{\odot}$. The red line corresponds to the T_{eff} of the red edge of the IS, the blue line to the T_{eff} of the Blue Edge of the IS, while the green line represents the average T_{eff} of the IS. The predicted period change when moving within the IS for the cases of the 5 and 11 $M_{\odot}$, is labeled.

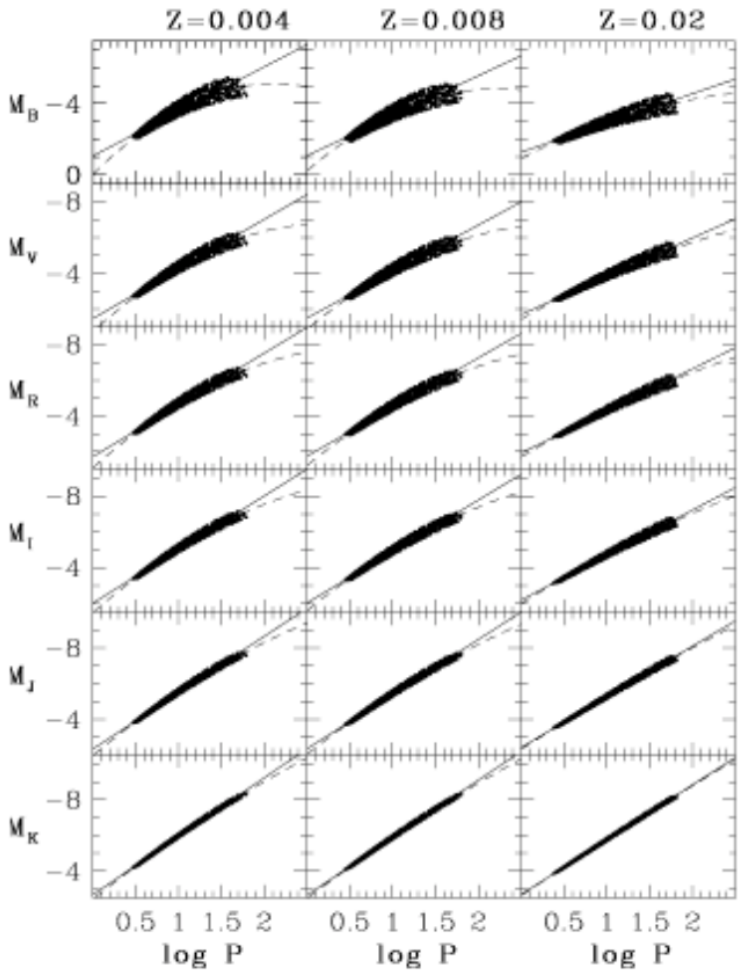

FIGURE 1.8: Period-magnitude distribution of fundamental mode CCs for various assumptions about metallicity and photometric passbands. Dashed and solid lines refer to the quadratic and linear PL relations, respectively.

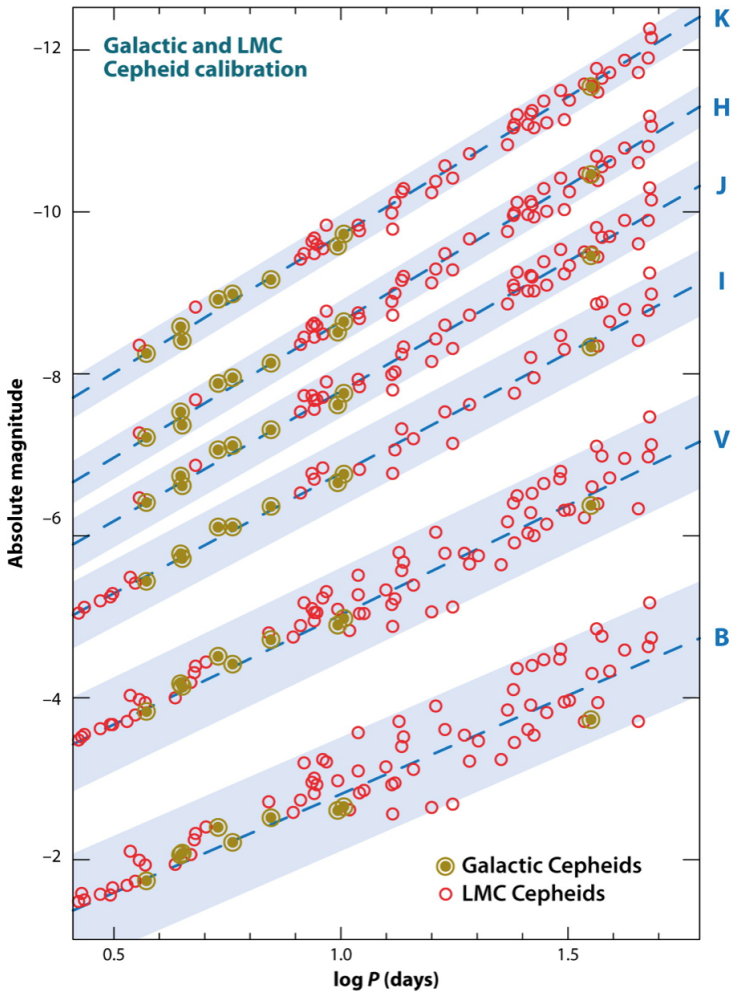

FIGURE 1.9: Multibands period-luminosity relations for Galactic (circled filled yellow dots) and Large Magellanic Cloud (open red circles) Cepheids from the optical (BVI) through the near-IR (JHK) filters. An increase in the slope, coupled with a decrease in total dispersion of the PL relations as longer and longer wavelengths are considered, is evident.

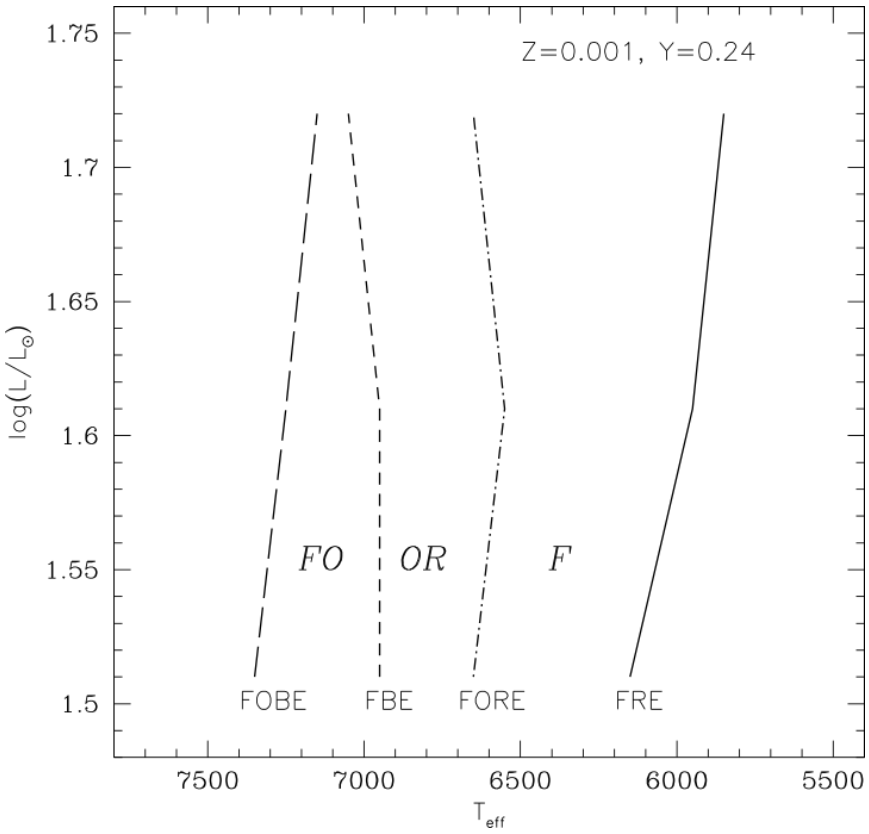

FIGURE 1.10: RR Lyrae instability strip topology: the Fundamental Blue Edge (Dashed line), Fundamental Red Edge (Solid line), First Overtone Blue Edge, (long dash line) and First Overtone Red Edge (dash-dotted line).

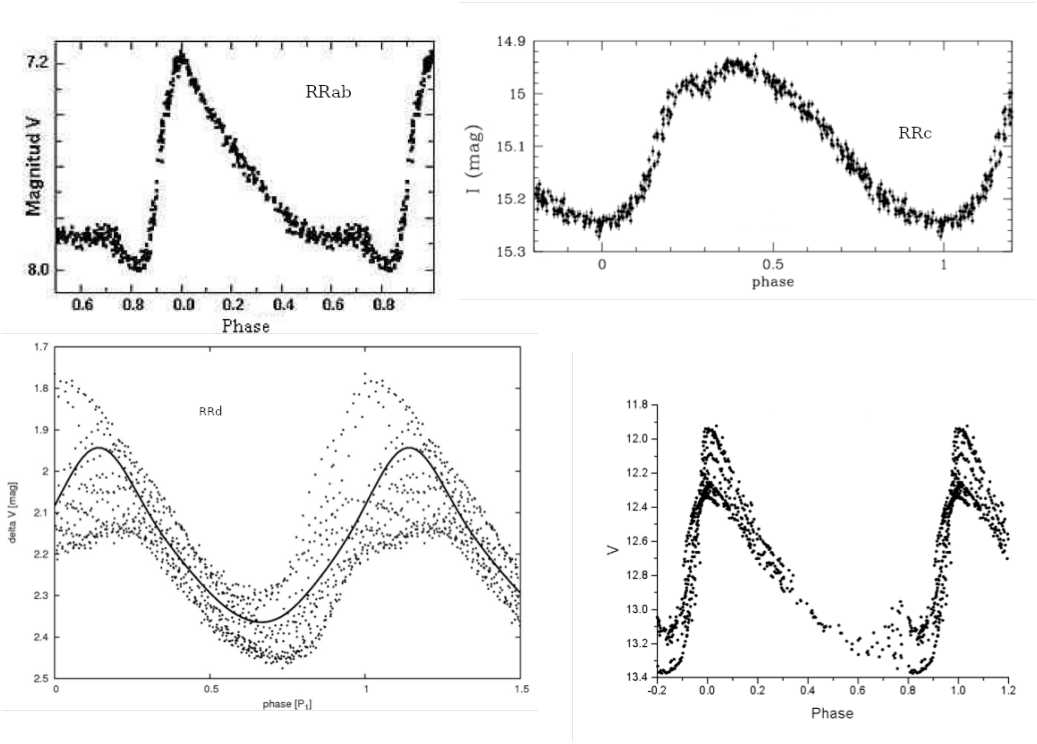

FIGURE 1.11: The typical light curve shape of an RRab variable star (top-left panel); the typical light curve shape of an RRc variable star (top-right panel); the typical light curve shape of an RRd variable star showing a double pulsation mode (bottom-left panel; the Typical light curve of an RRab showing The Blazhko effect (bottom-right panel).

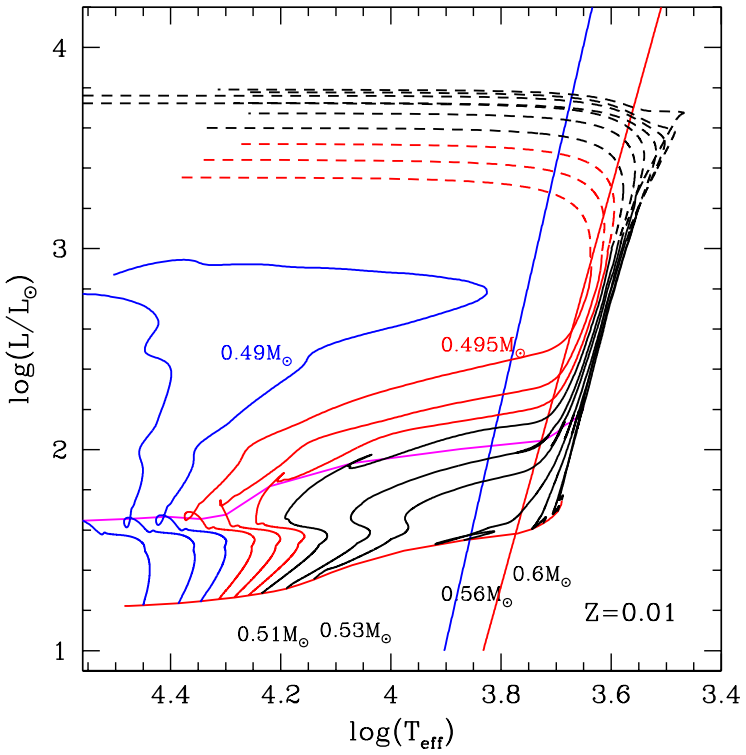

FIGURE 1.12: The evolution in the HR diagram of low mass core and shell helium-burning stellar models.

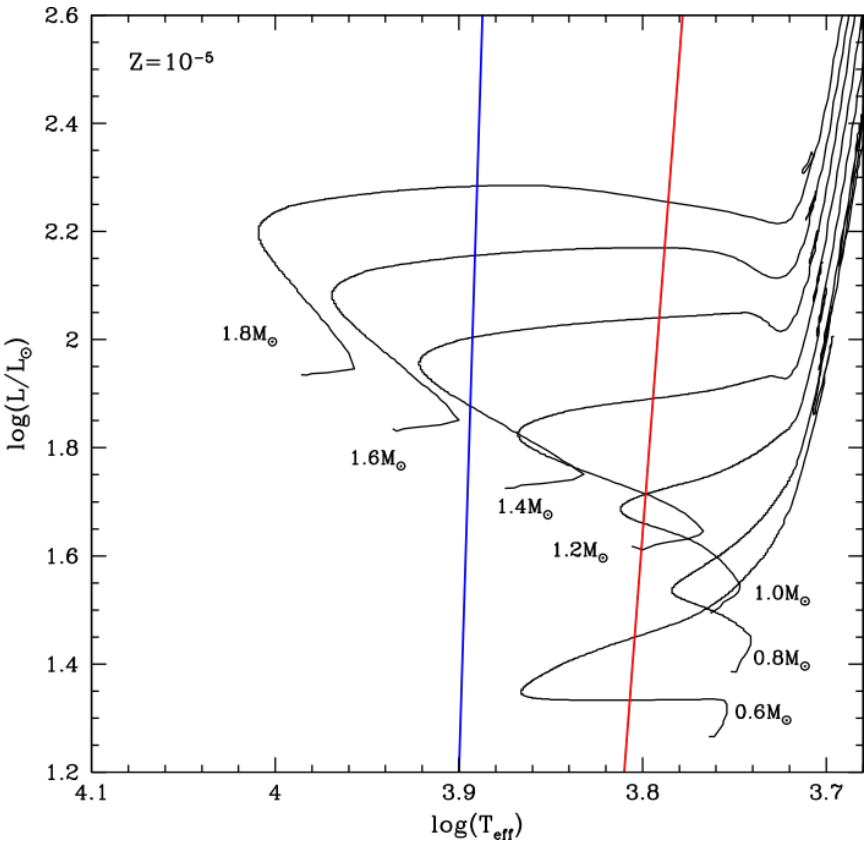

FIGURE 1.13: The location of evolutionary tracks of stellar models corresponding to anomalous Cepheids in the HR diagram.

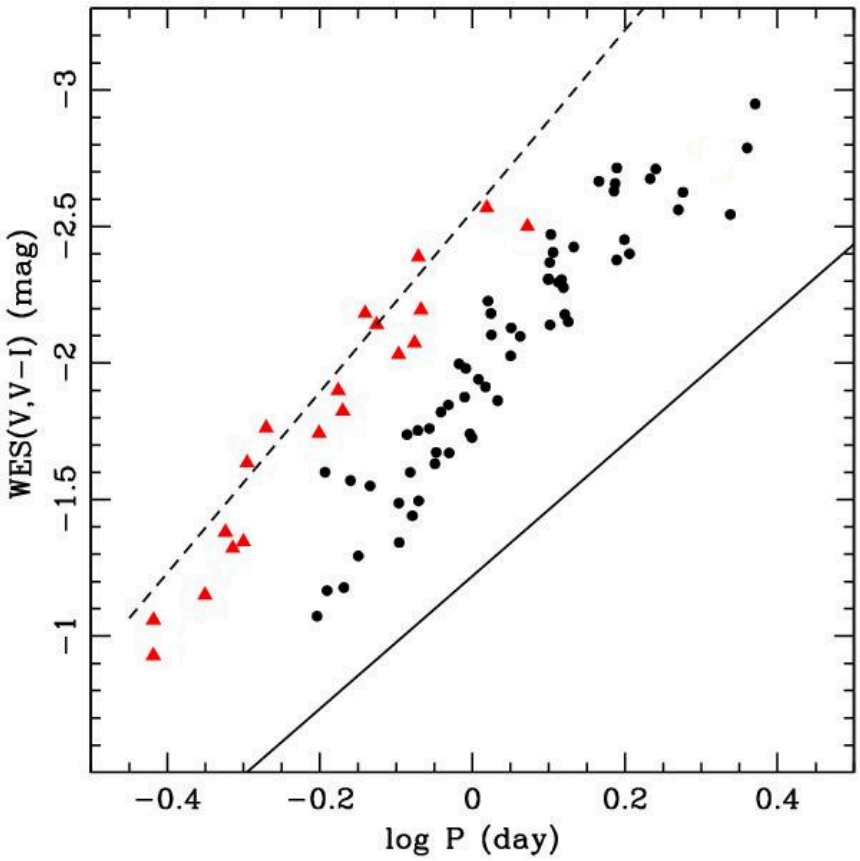

FIGURE 1.14: The Period-Wesenheit diagram for a large sample of LMC anomalous Cepheids. Black circles and red triangles represent fundamental mode and first overtone mode pulsators, respectively. The dashed line represents the theoretical results from CC pulsational models while the same predictions for BL Her variables are represented by the solid line.

Chapter 2

The Physics of Pulsating Stars

2.1 Stellar pulsation theory

Pulsating stars show cyclic or periodic variation on a time scale, of the same order as the free fall time. In fact, the dependence of the oscillation period on density is the same as the free fall time $t_{ff} \simeq \frac{1}{\sqrt{\rho}}$.
This information is very important because this time is much shorter than the nuclear time scale (for typical CCs around 10^6 - 10^7 years). As the oscillations occur in such a short time, nuclear changes can be neglected during the pulsation.
Thanks to the period-mean density relation (see Eq. 1.1) it is possible to provide the stellar pulsation period limits.
During stellar evolution, the average densities of stars vary a lot; giant stars are the lowest mean density astronomical objects with densities $\overline{\rho} \approx 10^{-9}\ \rho_{\odot}$ and white dwarf stars are the highest mean density objects with densities $\overline{\rho} \approx 10^{6}\ \rho_{\odot}$.
Using these values in the period-mean density law, the range for the stellar oscillation period is between 3 seconds (for white dwarfs) to 100 days (for red giants).

The physical-mathematical procedures to investigate the stability of a stellar structure, such as those provided by evolutionary calculations, are conceptually simple. The main procedures are, abandoning the equilibrium condition by writing the equations of motion for the elements of the stellar fluid and perturbing the structure, investigating whether the perturbation tends to dampen (stability) or increase (instability).
Over time, many theoretical efforts have been performed to model stellar pulsation. Starting from the first simplest approaches of small perturbations in linear approximation, which are able to predict the pulsation period but not allowed to follow the evolution to the full amplitude behaviour, to non-linear formulations.
While theoretical predictions of periods are largely reliable, predictions of the temperatures at which instability begins and ends (instability edges) and the amplitude of the pulsation, critically depend on the adequacy of the adopted theoretical scenario.
What is of interest here is that by looking at the location of observed pulsating stars in a color-magnitude diagram, a strip of instability can be identified (See Fig. 1.1). Thus, suggesting the existence of a common phenomenon at the basis of the oscillations in brightness, radius and temperature.

2.1.1 The κ and γ mechanisms

Over the years, several authors have tried to explain the physical mechanism responsible for the stellar oscillations.

The first thing that was understood about stellar pulsation is that it is a phenomenon which essentially involves only the outer layers of the stellar structure. Then, in 1963, S.A.Zhevakin proposed the most accredited explanation about the pulsation mechanisms, the so-called 'Valve effect' (Zhevakin, 1963). According to the valve effect, there are two possible mechanisms responsible for pulsations; the κ and γ mechanisms, related to the effect on luminosity of a variation of opacity (κ) and adiabatic exponent $\Gamma_3 - 1$, respectively. [1]

According to these mechanisms, the origin of the instability lies in the ionization regions of hydrogen, helium and Helium+, and also in their location within the stellar envelope. This means that the 'Valve effect' only activates in a certain range of temperatures and this is also a qualitative reason for the existence of an "instability strip" which is the only region of the HR diagram where the stars pulsate. More details will be discussed at the end of this section.

The IS is bound by two borders which are called the blue and red edges. The stars stop pulsating to the left of the blue and the right of the red edges.

The κ mechanism is due to the opacity variation between completely and partially ionized regions in the star. First of all, it is important to remember that the dependence of radiative opacity on temperature (T) and density (ρ) can be expressed according to the so-called 'Kramer's relation' i.e., $\kappa \propto \rho^n T^{-s}$.

In the stellar interior, n and s, the coefficients of density and temperature, respectively, are positive. Therefore, opacity decreases during contraction of the stellar envelope producing heat loss. However, in the ionization regions, s becomes large and negative which means that small temperature variations cause an increase in opacity during contraction. This implies that the trapped energy released as excess energy during the subsequent expansion is converted to pulsation work. Nevertheless, the pulsation is efficient only in the partially ionized regions of stellar structures.

In order to properly understand why the pulsation occurs only in the partially ionized regions, the physical properties of the star must be analyzed from the surface to the center.

Since the outer stellar layers are cold, the hydrogen is neutral. Entering the star, there is a temperature zone of $T_{eff} \sim 10000 - 13000\ K$ which is the temperature at which hydrogen starts to ionize. In this region, hydrogen is partially ionized.

Further into the star, closer to the core, the hydrogen will be completely ionized. Lower opacity values are expected for regions where hydrogen is completely ionized, as the contribution to opacity of the photoionization phenomenon is not efficient any more. Here, the damping mechanism prevails on the driving one and pulsation is not efficient.

The γ mechanism is due to the temperature variation between complete and partial ionization regions in the star. From the thermodynamic laws it is known that if there is an initial contraction of the star in the partial ionization region, the temperature varies less than in the complete ionization region. This is because in the partial ionization regions a part of the energy is used for the ionization. Therefore, increasing the density during the contraction results in a smaller temperature variation than in the complete ionization. As such, based on the Stefan-Boltzmann law 1.3, a smaller luminosity variation is expected. This means the trapped energy released in the next phase of expansion will be converted to mechanical work and then pulsation as in the κ mechanism.

[1] $\Gamma_1 = \left(\frac{d\ln P}{d\ln \rho}\right)_{\text{ad}}$, $\Gamma_3 - 1 = \left(\frac{d\ln T}{d\ln \rho}\right)_{\text{ad}}$ and $\frac{\Gamma_2 - 1}{\Gamma_2} = \left(\frac{d\, lnT}{d\, lnP}\right)_{\text{ad}} = \frac{\Gamma_3 - 1}{\Gamma_1}$ are the usual adiabatic exponents.

To summarize, the κ and γ mechanisms are two aspects of the same stellar luminosity variation phenomenon. The γ mechanism is the effect caused by temperature variation while the κ mechanism is the effect caused by opacity variation. Both mechanisms are started by a stochastic fluctuation of the external layer's properties which means a contraction is needed to start the driving mechanisms.
If the model effective temperature is too high, the ionization regions of H and He are too superficial (very external), involving a fraction of stellar mass over the ionization regions that is too small (too low density). Therefore, damping prevails and the star cannot oscillate.
Only when the ionization regions are deep enough, does the increase in the opacity in those regions result in a mass sufficient for the pulsation driving mechanism to become efficient.
At this point, the driving mechanisms prevail on the damping mechanisms and the star oscillates.
This is the reason for the existence of the blue edge of the IS. From this, one might deduce that going from the blue to the red part of the HR diagram, since the temperature decreases, the depth of the ionization regions would increase; resulting in a progressively more efficient mechanism for pulsation. This however, is false, as it is known that the red part of the HR diagram is close to the Hayashi track which is the HR diagram zone in which all stellar structures are fully convective.
Indeed as the stellar structure moves towards the red part of the HR diagram, convection becomes progressively more important, thus reducing the efficiency of the κ and γ mechanisms. As a consequence, the quenching effect produced by convection makes the pulsation progressively less efficient until the red edge is achieved and the structure is no longer pulsating.
This is the reason for the existence of the red edge of the IS.

2.1.2 Theory of radial pulsation

My study is focused on core He-burning variable stars, which are radial pulsators.
Several assumptions are necessary in order to approximate pulsation as a radial phenomenon:

- Spherical symmetry is assumed: the luminosity and volume of the star varies on the pulsation time scale but the shape remains spherical.
- Rotations and magnetic fields are neglected.
- The core is excluded from the analysis for two reasons:
  i) the pulsation mechanisms only occur in the H, He and He+ ionization regions that are very close to the star's surface;
  ii) the nuclear time scale associated with the evolution of the core is much longer than the free fall time that is the typical time scale of pulsation.

Then, to study the pulsation properties of the variable stars, hydrodynamic models which solve the hydrodynamic system equations in the stellar envelope, need to be adopted.

The hydrodynamic system of equations is as follows:

$$\frac{\partial r}{\partial m} = \frac{1}{4\pi\rho r^2} \quad \text{Mass conservation equation} \tag{2.1a}$$

$$\frac{\partial^2 r}{\partial t^2} = -4\pi r^2 \frac{\partial P}{\partial m} - \frac{GM}{r^2} \quad \text{Momentum equation} \tag{2.1b}$$

$$\frac{\partial E}{\partial t} - \frac{P}{\rho^2}\frac{\partial \rho}{\partial t} = \epsilon - \frac{\partial H}{\partial m} \quad \text{where } H = 4\pi r^2 F \quad \text{Energy equation} \tag{2.1c}$$

heat transfer equation (2.1d)

The lagrangian description is usually preferred because it gives a better physical interpretation of the equations.

There are two main theoretical approaches to the study of pulsating stars: the linear and nonlinear approaches.
In the linear approach two different kinds of analysis can be done: the linear adiabatic analysis and the linear nonadiabatic analysis.
The linear adiabatic analysis consists of linearizing the system equations (Eq. 2.1) and neglecting heat exchanges.
With this approach, it is possible to derive a unique pulsation observable, the oscillation period, which depends on mass, luminosity and effective temperature.
The linear nonadiabatic approach consists of introducing nonadiabatic effects into the system. Thereby creating opacity gradients which allow for the prediction of the location of the blue IS boundary. Therefore, this treatment results in the prediction of both the oscillation period and the blue IS boundary.
The nonlinear approach, which consists of removing the hypothesis of low amplitude oscillations, allows for two different kinds of analysis: the nonlinear radiative and the nonlinear convective analyses.
The nonlinear radiative analysis allows for the prediction of periods, amplitudes and the blue boundary.
While the nonlinear convective analysis allows us to predict periods, amplitudes, light, radius, radial velocity curves (as well as the variation of any other relevant quantity along the pulsation cycle) and both the blue and red boundaries.

Let's start with the simplest analysis, the linear nonadiabatic analysis; where linear means the treatment of oscillations using the small amplitude approximation and the subsequent linearization of the equations, and adiabatic means that each oscillating mass element does not gain or lose heat.
Adopting a Lagrangian description, let's derive the linearized equations for the lagrangian variation, δf, of the physical variables, f. Assuming for each layer of the envelope a coordinate $x = \frac{r_0}{R_0}$, where r_0 is the average radius of the layer and R_0 the total radius of the star. The relative displacement of the surface of a mass shell is:

$$\xi = \frac{\delta r}{r_0} \tag{2.2}$$

The radial distance out to interior mass m in the perturbed solution is:

$$r = r_0(1 + \xi) \tag{2.3}$$

Since the relative Lagrangian variation ($\frac{\delta f}{f_0}$) of some physical quantity f is often used, in the perturbed solution one gets:

$$f = f_0(1 + \delta f) \tag{2.4}$$

From here, by applying Eq. 2.4 to both sides of the nonlinear form of the conservation mass equation (Eq. 2.1a) and remembering that in the Lagrangian description δ always commutes with $\partial/\partial m$, the linearized mass equation is obtained:

$$\frac{\delta\rho}{\rho} = -3\xi - x\frac{\partial\xi}{\partial x} \tag{2.5}$$

Starting with the nonlinear momentum equation in the form of Eq. 2.1b and remembering $x = \frac{r_0}{R_0}$ and $dm = 4\pi r_0^2\rho_0 dr_0$, solving the equation and dropping the zero manuscript , the momentum equation is derived:

$$\frac{\partial}{\partial x}\frac{\delta P}{P} = \frac{R}{\lambda_P}\left(4\xi - \frac{xR}{g}\ddot{\xi} + \frac{\delta P}{p}\right) \tag{2.6}$$

where

$$\lambda_P = -\frac{dr}{d\ln P} = \frac{P}{\rho g} \tag{2.7}$$

Eq. 2.7 expresses the local pressure scale height in the equilibrium model where g is the local gravitational acceleration.
For the case of complete equilibrium in the unperturbed solution (see Eq. 2.2) and negligible composition changes, due to nuclear reactions, the linearized energy equation may be written in the form:

$$\frac{\partial}{\partial t}\frac{\delta P}{P} = \Gamma_1\frac{\partial}{\partial t}\frac{\delta\rho}{\rho} + \frac{\rho(\Gamma_3 - 1)}{P}\delta\left(\epsilon - \frac{\partial H}{\partial m}\right) \tag{2.8}$$

where H is the interior luminosity. In the diffusion approximations (valid in the deep stellar interior), Eq. $\mathbf{F} = -\frac{4\pi}{3k\rho}\left[\frac{dB(T)}{dT}\right]\nabla T$, for the interior radiative luminosity H, where B(T) is the integrated Planck function, applies.
Taking the logarithmic Lagrangian variation of this equation, the linearized radiative transfer equation is obtained:

$$\left(\frac{\delta H}{H}\right)_{\text{rad}} = 4\xi - \frac{\delta k}{k} + \frac{4\delta T}{T} + \frac{1}{\frac{d\ln T}{d\ln x}}\frac{\partial}{\partial x}\left(\frac{\delta T}{T}\right) \tag{2.9}$$

By combining the time derivative of the momentum equation (Eq. 2.6) with the other two conservation equations (Eq. 2.5 and 2.8) the following equation is derived:

$$\ddot{\xi} - \frac{\dot{\xi}}{r\rho}\frac{d}{dr}\left[\left(3\Gamma_1 - 4\right)P\right] - \frac{1}{\rho r^4}\frac{\partial}{\partial r}\left(\Gamma_1 P r^4\frac{\partial\dot{\xi}}{\partial r}\right) = -\frac{1}{r\rho}\frac{\partial}{\partial r}\left[\rho\left(\Gamma_3 - 1\right)\delta\left(\epsilon - \frac{\partial H}{\partial m}\right)\right] \tag{2.10}$$

For adiabatic oscillations $\delta\left(\epsilon - \frac{\partial H}{\partial m}\right) = 0$.
Assuming the solution of Eq. 2.9 is of the form:

$$\xi(r,t) = \frac{\delta r}{r} = \xi(r)e^{i\sigma t} \tag{2.11}$$

where $\xi(r)$ is a function of r only and σ is a constant. Substituting Eq. 2.11 in Eq. 2.9, writing $\frac{\partial}{\partial m} = (4\pi\rho r^2)^{-1}\frac{\partial}{\partial r}$ and rearranging slightly, results in:

$$-\frac{1}{\rho r^4}\frac{d}{dr}\Big(\Gamma_1 P r^4 \frac{d\xi}{dr}\Big) - \frac{1}{r\rho}\frac{d}{dr}\Big[\Big(3\Gamma_1 - 4\Big)P\Big]\xi = \sigma^2\xi \tag{2.12}$$

This equation is known as the 'linear adiabatic wave equation (LAWE)'.
This is an eigenvalue equation in which ξ is the eigenfunction and σ^2, the eigenvalue.
The solution $\sigma = 0$ is discarded because it corresponds to the perfectly static case that means no time dependence and therefore no oscillations.
If $\sigma \neq 0$, the LAWE equation is an ordinary second order differential equation to resolve and as such the solution contains two integration constants.
Since the LAWE equation is a linear, homogeneous equation in ξ, it means that if ξ is a solution of the Eq. 2.12, then ξ multiplied by a constant is also a solution.
Therefore, the first integration constant is the absolute value of the oscillation amplitudes. The other integration constant is obtained by fixing one of the two boundary conditions, the boundary condition at the center of the star (r=0) or the boundary condition at the surface of the star (r = R stellar radius). The boundary condition that is not fixed is satisfied by varying the other available parameter, the angular frequency of pulsation σ. Only some eigenfrequencies σ_0, σ_1 ... and eigenfunctions ξ_0, ξ_1 satisfy the boundary conditions at both the center and surface.
These eigenfrequencies correspond to the different oscillation modes. σ_0 corresponds to the fundamental mode, σ_1 to the first overtone mode and so on.
The fundamental mode eigenfunction, ξ_0, has no nodes in the range $0 \leq r \leq R$ while k overtone mode, ξ_k, has k nodes in the range $0 \leq r \leq R$. This means that when the stellar structure pulsates in the fundamental mode the whole stellar envelope is involved in the pulsation; while, when the stellar structure pulsates in the first overtone mode only the zone outside its single node pulsates. Therefore, the higher the number of the nodes, the more external the pulsation. In addition, the higher pulsation modes become efficient at high effective temperatures so that the corresponding blue boundaries are hotter than the fundamental one. Similarly, when moving towards the red part of the HR diagram, convection tends to quench the most external, i.e. the highest modes first, and so, the higher the mode, the hotter the corresponding red edge.

There are two possibilities for each k :

1. σ_k is real which means constant amplitude pulsation described by the eigenfunction $\xi_k(r,t) = \xi_k(r)e^{\pm i\sigma k t}$, thus corresponding to sinusoidal oscillations;

2. σ_k is imaginary which means there is a dynamical instability on a free fall time scale.

When σ_k is real it is possible to define the oscillation period $P_k = \frac{2\pi}{\sigma_k}$.
In conclusion, from the LAWE equation, if the eigenfrequency is real the only possible result that can be derived is the oscillation period for each mode.
In the case of nonadiabatic regime, in Eq. 2.9 the term $\delta\Big(\epsilon - \frac{\partial H}{\partial m}\Big) \neq 0$ and the equation is a linear nonadiabatic wave equation.
This assumption implies that the eigenfunctions are not real but complex frequencies $\omega = \sigma + ik$, where σ, like in the adiabatic regime, gives the oscillation period

while ik tells us if the pulsation amplitudes are expected to increase or decrease. In this case we have the possibility to investigate the pulsation stability.

In the linear nonadiabatic regime, if the solution of the Eq. 2.9 is of the form $e^{i\omega t}$ the linearized full energy equation can be written as follows:

$$\frac{\delta P}{P} = \Gamma_1 \frac{\delta \rho}{\rho} - \frac{i}{\omega} \frac{(\Gamma_3 - 1)\rho}{P} \delta\left(\epsilon - \frac{\partial H}{\partial m}\right) \tag{2.13}$$

To better understand the pulsation stability in stars, one can picture the star as if it were made up of a large number of elementary Carnot-type heat engines, with each engine corresponding to one shell of mass dm. There are two possible scenarios that occur at the minimum radius value phase; each shell either gains heat $\left(\int PdV > 0\right)$ or releases heat $\left(\int PdV < 0\right)$.
In the nonadiabatic case, to ensure the κ and γ mechanisms are occuring when the star contracts, each shell must be gaining heat at the minimum radius value phase. Then, if the sum of the closed cycle of all mass shells in the star is positive, the driving regions prevail over the damping ones and the stellar envelope pulsates. As such, finally, pulsation instability occurs.
However, when the aforementioned sum is negative, the damping regions prevail on the driving ones and the stellar envelope does not pulsate.
This means that outside the IS, on the left side of the blue edge, the sum is negative and the envelope does not pulsate. On the other hand, inside the IS, to the right of the blue edge, the sum is positive and the stellar envelope starts to oscillate.
This limit is parametrized through the growth rate of the pulsation parameters, simply called the growth rate parameter, and given by:

$$\eta = \frac{W}{\Psi} = -\frac{4\pi k}{\sigma} \tag{2.14}$$

where W is the work done on the system by the restoring forces around a complete closed cycle and Ψ is the total oscillation energy or equivalently can be written as: $k = -\frac{1}{2}\frac{\langle dW/dt \rangle}{\Psi}$.
The growth rate depends on both the real and the imaginary parts of the eigenfunction. Therefore, the linear nonadiabatic models provide the oscillation period and the blue edge. In fact, the temperature at which the growth rate goes from negative to positive, is the IS blue edge temperature.
The following scheme summarizes what was just explained:

If	$\eta > 0 \Rightarrow W > 0$	and $\Rightarrow k < 0 \Rightarrow$ oscillations are excited
If	$\eta < 0 \Rightarrow W > 0$	and $\Rightarrow k < 0 \Rightarrow$ oscillations are damped

In the linear treatment of pulsation, there are no ways to predict the light curves of variable stars and the red edge of the IS because there is no coupling between convection, a nonlinear phenomenon, and pulsation in the oscillating stellar envelope. The only way to include the convection phenomenon in the linear regime is to include convection by means of the mixing length theory or to make some ad hoc assumptions, e.g. on the expected width of the IS. In most evolutionary codes, the superadiabatic convection is parametrized through a free parameter which is the α_{ml}

parameter. $\alpha_{ml} = \frac{l}{H_P}$ where l is the length of the path covered by the convective elements and H_P is the local pressure scale height.
On this basis, the red edge can be evaluated only by means of some ad hoc assumptions like considering that the super adiabatic convection is efficient when the growth rate is at its maximum. The temperature at which the growth rate is maximum is then the temperature of the red edge of the IS.
Once the star starts to oscillate, the amplitude of the oscillations varies until it reaches an asymptotic value corresponding to a pulsation period and a full amplitude limit cycle, at which the pulsation becomes stable. To predict the asymptotic regime of the oscillations, a nonlinear treatment of the pulsation is needed.
The nonlinear approach can be radiative, if convection is neglected, but in this case it cannot provide a good prediction for the red edge. Otherwise, if the coupling between pulsation and convection is included, we have a nonlinear convective approach. This treatment can predict all the pulsation observables: the periods, the oscillation amplitudes, the complete topology of the IS, e.g. including both the blue and the red edges for each selected pulsation mode.

This complete framework allows us to compare theory to observations.
The crucial property of nonlinear convective code is the modeling of the coupling between convection and pulsation in a stellar oscillating envelope. In fact, by including convection, each shell mass will have dynamic and convective velocity terms as well as a coupling term between these two velocities.
As first suggested by Baker and Kippenhahn (Baker et al., 1965) the increasing efficiency of convection towards lower effective temperatures has a damping effect on the κ and γ mechanisms, thereby restoring stability.
Several efforts to model pulsation through a nonlinear convective treatment are available in literature (Stellingwerf, 1982; Bono et al., 1994; Szabó et al., 2004)
In this thesis the approach originally outlined by Stellingwerf, 1982 and Bono et al., 1994 was adopted.

2.2 The hydrodynamic codes

In this section, guidelines about the hydrodynamic codes used in this PhD project to build-up the new dataset of nonlinear convective models, are described. These codes are fully described by Bono and Stellingwerf in Bono et al. (1992), Bono et al. (1994), and Bono et al. (1999b). The pulsation model calculation is performed in two steps. The first step consists of using a linear hydrodynamic code: this code is a lagrangian hydrodynamic code which analyzes linear nonadiabatic pulsation models, neglecting convection. It linearizes the aforementioned mass, momentum and energy conservation equations. A temporal dependence in the form $e^{i\omega t}$, where w is the complex eigenfrequency, is assumed for all the oscillating quantities. To use the code, several parameters have to be selected e.g. the threshold number of iterations to reach convergence, the number of modes to analyze, the zoning of the envelope, the ratio between core and total radius and the ratio between mass zones both above and below the hydrogen ionization region.
Then, in order to create the model, the code needs several initial inputs about the physical parameters of the model, namely the chemical composition, the mass, the effective temperature and the luminosity. An analytical equation of state and tabular opacities (see De Somma et al., 2020b, and references therein) are also required.
When these values are fixed and once the code reads the initial parameters as well

as the input physics, the eigenfunctions are computed and the static envelope model is provided.
The output data of the linear code include the model number, the effective temperature, the external radius, and for each investigated pulsation mode, the growth rate (see Eq. 2.14), the total kinetic energy, the pulsation constant and the work in both the hydrogen and helium ionization regions. As already explained in the previous section, if the growth rate is positive, the stellar model pulsates in the corresponding mode and the blue edge of the IS for a model with a specific luminosity and effective temperature, is provided. However, if the growth rate is negative the investigated stellar model does not pulsate. As this treatment of the models is completely radiative, this code does not provide the red edge.
For this reason and in order to properly predict the full amplitude behaviour of the pulsation amplitudes, the light curve morphology and the complete IS topology, the second step consisting in the application of a nonlinear pulsation code is needed.
The nonlinear hydrodynamic code is a lagrangian code that uses a nonlocal and time dependent treatment of the convective transport to solve the local conservative equations. Some of the input parameters for the nonlinear code are taken from the output of the linear code. In particular, the predicted radial eigenfunctions are used to modulate the perturbation velocity imposed on the nonlinear model. Moreover, the input file of the nonlinear code includes the number of periods to be calculated, the number of iterations for each period, the convective α_{ml}, the eddy viscosity and the artificial viscosity parameters used in the turbulent convective treatment.
The most important output parameters of this code are, the behaviour of the nonlinear period with the integration time, the bolometric magnitude amplitude, the radius variation, the maximum and minimum radial velocity, the convective quantities and the various total energy and work contributions. Three possible behaviours can be found:

1. The perturbed model has an amplitude that decreases until it is zero and the total work tends to an asymptotic negative value. According to this model, the star does not pulsate.

2. The perturbed model has a stable limit cycle in the mode in which it has been excited. This means that the amplitude increases until it reaches a maximum value corresponding to an almost perfect periodic oscillation and the total work asymptotically tends to 0. This scenario is representative of a star that can pulsate in the corresponding excitation mode of the model.

3. The perturbed model has a stable limit cycle in a different mode from which it has been excited. This means that the amplitude slowly changes from the initial value corresponding to the perturbation mode to another asymptotic value and the work asymptotically tends to 0. This shows a case in which the star does not pulsate in the excitation mode of the model but in a different mode.

Models for which hydrodynamic codes provide the presence of a stable cycle for two modes, e.g. both the fundamental and the first overtone mode, when excited independently, can also be found. These models define the OR region of the HR diagram and represent stars that can pulsate either in one mode or in the other, e.g. either in

the fundamental or in the first overtone mode.
An exception to the three cases enumerated above is represented by the so-called 'mixed mode models', for which multiple pulsation modes are simultaneously active.

Once the nonlinear model has reached the stable full amplitude limit cycle, the variations of all the relevant quantities along a pulsation cycle can be predicted, e.g. the light, radius, temperature, gravity curves as a function of the pulsation phase. Therefore, thanks to the nonlinear convective approach, the detailed study of the morphology of light and radial velocity curves, is possible.
Moreover, once the stable and unstable models are identified, for each mass, luminosity and chemical composition, the effective temperatures corresponding to the blue and red edge, for each pulsation mode, can be obtained.

Chapter 3

An updated theoretical scenario for Galactic Classical Cepheids

The modelling of radial pulsating stars, specifically Classical Cepheids, is fundamental to constraint the extragalactic distance scale. The various ingredients entering the theoretical calibration of the Classical Cepheid distance scale can affect the accuracy and reliability of the inferred distances, as well as the calibration of secondary distance indicators, able to reach the Hubble flow. On this basis, they can cast light on residual uncertainties in the local determination of the Hubble constant and in turn, on the 'Hubble constant tension' debate.
In order to quantify the residual sources of uncertainties still affecting the Cepheid-based extragalactic distance scale and the Hubble constant evaluation, we started a theoretical project devoted to the building of an accurate and updated dataset of nonlinear convective pulsation models. This set extends and complements previously computed models, by homogeneously covering a wide range of stellar parameters, including variations in the assumed Mass-Luminosity relation and super-adiabatic convective efficiency, chemical compositions and helium contents.
This Chapter discusses the first step in building the dataset; computing the model set of pulsation models for Classical Cepheids at solar chemical composition ($Z = 0.02$ $Y = 0.28$).

3.1 The computed set of pulsation models

The hydrodynamic codes as well as the physical and numerical assumptions used to compute the dataset are discussed in Chapter 2 and in great detail in Bono et al. (1999b) and Bono et al. (2000b). However, due to the finely detailed inputs in the parameter grids chosen to compute the dataset, an automated python procedure was developed to allow fast model computations.

The pulsation stability of both fundamental and first overtone mode models with mass values ranging from 3 to 11 solar masses, by steps of 1 solar mass, and effective temperatures from $T_{eff} = 3600K$ to $T_{eff} = 6700K$, by steps of 100 degree, was explored. As a result we were able to predict the IS boundaries, for each selected mode, with an accuracy of $T_{eff} = 50K$.
For each selected pulsation model, the nonlinear equations were integrated until a stable limit cycle was achieved in at least one of the two radial modes.
The models were computed by varying both the ML relation and the assumed efficiency of super adiabatic convection.
For the ML relation, three luminosity levels were considered: a canonical level obtained by Bono et al. (2000b) neglecting rotation, mass loss and core convective overshooting (named A), and two noncanonical luminosity levels obtained by adding

$\Delta \log(L/L_\odot)$= 0.2 *dex* and $\Delta \log(L/L_\odot)$= 0.4 *dex* to the canonical value, named B and C, respectively.

Concerning the nonlocal time dependent treatment of convection, three different values for the mixing length parameter used to close the nonlinear system equations (Bono et al., 1999b), $\alpha_{ml} = l/H_P$ = 1.5, 1.7 and 1.9, were adopted [1]. This choice was suggested by previous investigations by Di Criscienzo et al. (2004), Fiorentino et al. (2007), Natale et al. (2008), and Marconi et al. (2013a). According to these studies hotter variables are well modeled with α_{ml}=1.5–1.6, whereas variables closer to the red edge of the instability strip often require α_{ml}=1.8–2.0 due to the increased importance of efficiency of convection in the redder part of the color–magnitude diagram.

Using these input parameters, around 360 fundamental mode and 40 first overtone mode stable pulsation models were derived.

Tables 3.1 and 3.2 report the intrinsic stellar parameters of the pulsation models that were found to oscillate in the F and FO-modes, respectively. The various columns report the stellar mass, the luminosity level, the effective temperature, the adopted mixing length parameter, the ML identification defined above, the pulsation period and the average radius.

TABLE 3.1: The adopted stellar parameters for computed F mode models. This table is available in its entirety in Section A.1 in Appendix A.

		Z=0.02	Y= 0.28			
$M/M_\odot$	log(L/$L_\odot$)	T_{eff}[K]	α_{ml}	ML	P[d]	log($\overline{R}/R_\odot$)
(1)	(2)	(3)	(4)	(5)	(6)	(7)
3.0	2.32	5900	1.5	A	1.07716	1.142
3.0	2.32	6000	1.5	A	1.03611	1.129
...						
4.0	2.74	5500	1.5	A	2.56311	1.412
4.0	2.74	5600	1.5	A	2.42218	1.399
...						
5.0	3.07	5300	1.5	A	4.73277	1.608
5.0	3.07	5400	1.5	A	4.44069	1.592
...						
6.0	3.33	5000	1.5	A	8.6011	1.789
6.0	3.33	5100	1.5	A	8.0714	1.772
...						
7.0	3.56	4800	1.5	A	14.00799	1.942
7.0	3.56	4900	1.5	A	13.0515	1.928
...						
8.0	3.75	4600	1.5	A	21.7684	2.070
8.0	3.75	4700	1.5	A	20.2235	2.056
...						
9.0	3.92	4400	1.5	A	33.08715	2.190
9.0	3.92	4500	1.5	A	30.575	2.174
...						
10.0	4.08	4200	1.5	A	48.711	2.297
10.0	4.08	4300	1.5	A	45.74965	2.285
...						

[1] See Chapter 2 for the definition of the α_{ml} parameter

TABLE 3.1: continued.

$M/M_\odot$	$\log(L/L_\odot)$	T_{eff}[K]	α_{ml}	ML	P[d]	$\log(\overline{R}/R_\odot)$
(1)	(2)	(3)	(4)	(5)	(6)	(7)
11.0	4.21	4100	1.5	A	66.40289	2.386
11.0	4.21	4200	1.5	A	61.14294	2.371
...						

TABLE 3.2: The adopted stellar parameters for computed FO-mode models. This table is available in its entirety in Section A.1 in Appendix A.

		Z=0.02	Y= 0.28			
$M/M_\odot$	$\log(L/L_\odot)$	T_{eff}[K]	α_{ml}	ML	P[d]	$\log(\overline{R}/R_\odot)$
(1)	(2)	(3)	(4)	(5)	(6)	(7)
3.0	2.32	6200	1.5	A	0.6715	1.103
3.0	2.32	6300	1.5	A	0.6403	1.090
...						
4.0	2.74	5900	1.5	A	1.4240	1.354
4.0	2.74	6000	1.5	A	1.3551	1.341
...						
5.0	3.07	5800	1.5	A	2.3904	1.530
5.0	3.07	5900	1.5	A	2.2912	1.517
...						
6.0	3.33	5800	1.5	A	3.5712	1.664
...						

3.2 The results for solar metallicity models

In this section the theoretical predictions as a function of both the ML relation and α_{ml} parameter, obtained from the new extended dataset at solar chemical composition, are discussed. In particular, the inferred results include:

1. the topology of the IS;
2. the updated period-luminosity-mass-temperature relation;
3. the period-radius and period-mass-radius relations;
4. the updated atlas of both the bolometric light curves and the radial velocity curves.

3.2.1 The topology of the Instability Strip

We predicted new instability strips for both F and FO-mode models by varying the ML relation (cases A, B and C), and the efficiency of super-adiabatic convection (α_{ml} = 1.5, 1.7 and 1.9).
The stability of each of the pulsation modes were investigated in order to predict the hottest and the coolest model for each combination of M, L, and α_{ml}. The blue and red boundaries of the F and FO strips were then evaluated by increasing and decreasing the effective temperature by $T_{eff} = 50K$ for the bluest and reddest model,

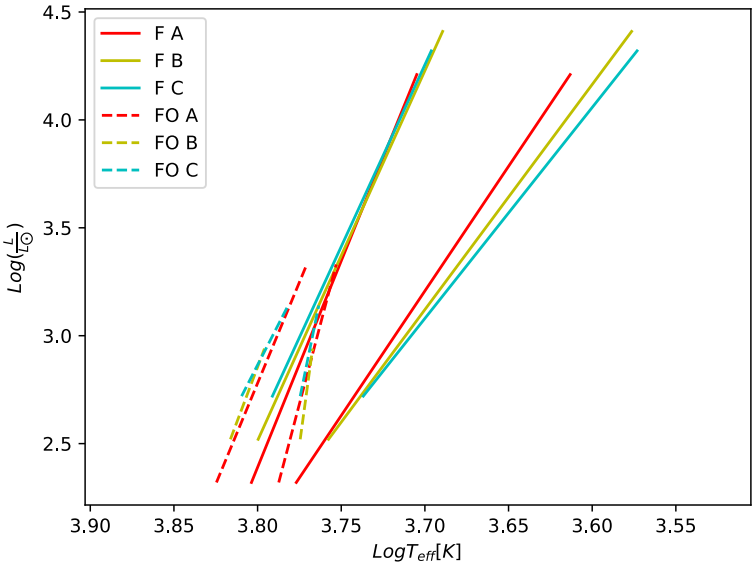

FIGURE 3.1: The F and FO instability strips at a fixed mixing length parameter $\alpha_{ml} = 1.5$ for the assumed A, B, C ML relations.

respectively.
The inferred F and FO boundary values are reported in Table 3.3. The columns show the mass, the luminosity level, the adopted mixing length parameter, the ML label and the effective temperatures for the FOBE, FBE, FORE and FRE. We noticed that the FO pulsation is found only for masses lower than 6 solar masses; in agreement with results based on previous model computations ((see e.g. Bono et al., 2000a, and references therein)).
The linear fit of the inferred boundary effective temperature values, as a function of the luminosity level, varying the α_{ml} parameter, allows us to derive the relations reported in Tables 3.4 and 3.5, for F and FO pulsators, respectively. The quadratic fit coefficients of the boundary values are instead listed in 3.6. In the case of the FO-mode, only the linear fit was taken into account due to the smaller number of pulsating models and the well-known linear behaviour of the predicted edges (Bono et al., 2000b).
We note that while the majority of the R^2 values of these regressions are above 0.9, the FRE relations seem to be less accurate for the brightest ML (case C) relation. This occurrence reflects the trend, as already discussed in some previous papers (Bono et al., 2000b), of the FRE getting hotter when the brightest luminosity levels are achieved as a consequence of the decreased density in the driving regions.
The linear relations are plotted by varying in Fig. 3.1 the ML relation, and in Fig. 3.2, the superadiabatic convection efficiency. An inspection of these plots shows that, in agreement with previous theoretical investigations (Bono et al., 2000b; Fiorentino et al., 2007), a variation in the ML relation (see Fig. 3.1) does not significantly affect the topology of the instability strip.
On the other hand, increasing the efficiency of superadiabatic convection (see Fig. 3.2) results in a more important quenching effect on pulsation and, in turn, in a narrowing of the instability strip; in agreement with previous studies (see e.g. Fiorentino et al., 2007). In particular, increasing the α_{ml} parameter from $\alpha_{ml} = 1.5$ to α_{ml} =1.9

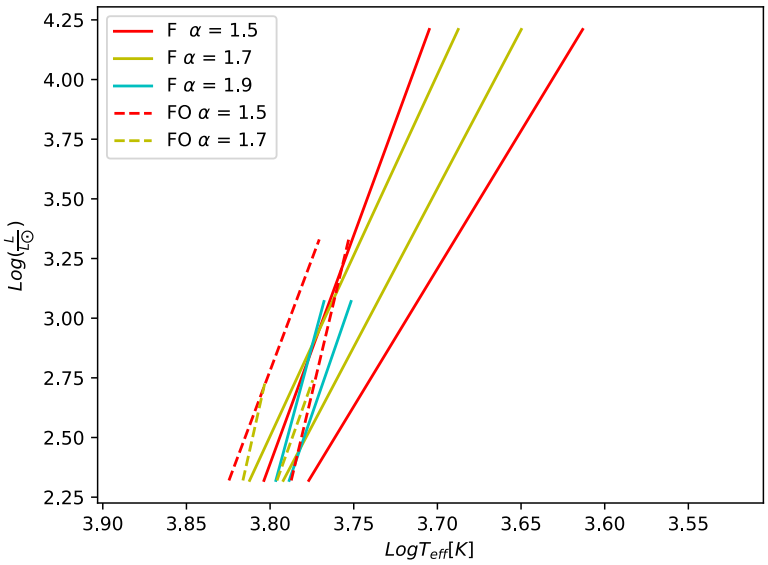

FIGURE 3.2: The canonical F and FO instability strips for the various assumptions about the superadiabatic convective efficiency.

made the FOBE redder by about $T_{eff} = 100K$ and the FRE bluer by about $T_{eff} = 300K$, confirming that the quenching effect due to superadiabatic convection is especially efficient in the red part of the instability strip.

TABLE 3.3: Predicted Effective Temperatures of the Instability Strip Boundaries. The assumed uncertainties of these boundaries is of $T_{eff} = \pm$ 50 K, estimated on the basis of the T_{eff} grid used in the model computations

$M/M_\odot$	log(L/$L_\odot$)	α_{ml}	ML	FOBE	FBE	FORE	FRE
(1)	(2)	(3)	(4)	(5)	(6)	(7)	(8)
3.0	2.32	1.5	A	6550	6150	6150	5850
3.0	2.32	1.7	A	6550	6250	6250	6050
3.0	2.32	1.9	A		6250		6150
3.0	2.52	1.5	B	6550	6050	5950	5550
3.0	2.52	1.7	B	6550	6150	6150	5750
3.0	2.52	1.9	B		6150		5950
3.0	2.72	1.5	C	6450	6050	5950	5350
3.0	2.72	1.7	C	6250	6150	6150	5550
3.0	2.72	1.9	C		6150		5750
4.0	2.74	1.5	A	6450	5950	5850	5450
4.0	2.74	1.7	A	6350	6050	5850	5750
4.0	2.74	1.9	A		6050		5850
4.0	2.94	1.5	B	6250	5950	5850	5250
4.0	2.94	1.7	B		5950		5450
4.0	2.94	1.9	B		5950		5650
4.0	3.14	1.5	C	6050	5850	5950	4950
4.0	3.14	1.7	C		5850		5150
4.0	3.14	1.9	C		5750		5450
5.0	3.07	1.5	A	6150	5850	5750	5250

TABLE 3.3: continued.

$M/M_{\odot}$	$\log(L/L_{\odot})$	α_{ml}	ML	FOBE	FBE	FORE	FRE
(1)	(2)	(3)	(4)	(5)	(6)	(7)	(8)
5.0	3.07	1.7	A		5950		5450
5.0	3.07	1.9	A		5850		5650
5.0	3.27	1.5	B		5850		4950
5.0	3.27	1.7	B		5750		5150
5.0	3.47	1.5	C		5750		4550
5.0	3.47	1.7	C		5550		4850
5.0	3.47	1.9	C		5350		5250
6.0	3.33	1.5	A	5850	5850	5750	4950
6.0	3.33	1.7	A		5650		5250
6.0	3.53	1.5	B		5650		4650
6.0	3.53	1.7	B		5450		4950
6.0	3.73	1.5	C		5350		4250
6.0	3.73	1.7	C		5250		4550
7.0	3.56	1.5	A		5550		4750
7.0	3.56	1.7	A		5450		5150
7.0	3.76	1.5	B		5350		4350
7.0	3.76	1.7	B		5250		4750
7.0	3.96	1.5	C		5150		3950
7.0	3.96	1.7	C		5050		4350
8.0	3.75	1.5	A		5450		4550
8.0	3.75	1.7	A		5250		4850
8.0	3.95	1.5	B		5250		4150
8.0	3.95	1.7	B		5050		4450
8.0	4.15	1.5	C		5150		3750
8.0	4.15	1.7	C		4950		4050
9.0	3.92	1.5	A		5250		4350
9.0	3.92	1.7	A		5150		4750
9.0	4.12	1.5	B		5050		3950
9.0	4.12	1.7	B		4850		4250
9.0	4.32	1.5	C		4950		4150
9.0	4.32	1.7	C		4750		4250
10.0	4.08	1.5	A		5150		4150
10.0	4.08	1.7	A		4950		4550
10.0	4.28	1.5	B		4950		3750
10.0	4.28	1.7	B		4750		4050
10.0	4.48	1.5	C		4850		4450
10.0	4.48	1.7	C		4750		4450
11.0	4.21	1.5	A		4950		4050
11.0	4.21	1.7	A		4750		4350
11.0	4.41	1.5	B		4850		3950
11.0	4.41	1.7	B		4750		3850
11.0	4.61	1.5	C		4850		4550
11.0	4.61	1.7	C		4650		4550

TABLE 3.4: The coefficient of the linear relation $\log T_{eff}$ = a +blog(L/$L_\odot$) for the boundaries of the F-mode IS, varying both the ML relation and the mixing length parameter.

α_{ml}	ML	a	b	σ_a	σ_b	R^2
FBE						
1.5	A	3.91	-0.05	0.02	0.005	0.917
1.5	B	3.93	-0.05	0.02	0.005	0.944
1.5	C	3.94	-0.05	0.01	0.004	0.967
1.7	A	3.95	-0.06	0.02	0.005	0.954
1.7	B	3.96	-0.06	0.01	0.003	0.976
1.7	C	3.97	-0.07	0.009	0.002	0.991
1.9	A	3.88	-0.04	0.008	0.003	0.994
FRE						
1.5	A	3.97	-0.08	0.01	0.004	0.985
1.5	B	3.99	-0.09	0.02	0.006	0.966
1.5	C	3.83	-0.05	0.08	0.02	0.434
1.7	A	3.96	-0.07	0.015	0.004	0.975
1.7	B	4.00	-0.09	0.02	0.006	0.965
1.7	C	3.88	-0.06	0.05	0.01	0.707
1.9	A	3.90	-0.05	0.004	0.002	0.998

TABLE 3.5: The coefficient of the linear relation $\log T_{eff}$ = a +blog(L/$L_\odot$) for the boundaries of the FO-mode IS, varying both the ML relation and the mixing length parameter.

α_{ml}	ML	a	b	σ_a	σ_b	R^2
1.5	A	3.94	-0.05	0.03	0.01	0.9045
FORE						
1.5	A	3.85	-0.03	0.02	0.008	0.8690

TABLE 3.6: The coefficients of the quadratic relation $\log T_{eff}$ = a + b log(L/$L_\odot$) +c (log(L/$L_\odot$))^2 for the boundaries of the F-mode IS, varying both the ML relation and the mixing length parameter.

α_{ml}	ML	a	b	c	σ_a	σ_b	σ_c	R^2
FBE								
1.5	A	3.667	0.104	-0.023	0.054	0.033	0.005	0.981
1.5	B	3.675	0.098	-0.022	0.053	0.031	0.004	0.988
1.5	C	3.874	-0.019	-0.005	0.099	0.055	0.007	0.970
1.7	A	3.708	0.092	-0.023	0.037	0.023	0.003	0.994
1.7	B	3.820	0.019	-0.012	0.069	0.040	0.005	0.986
1.7	C	4.005	-0.084	0.002	0.064	0.035	0.005	0.990
FRE								
1.5	A	3.788	0.030	-0.018	0.031	0.019	0.003	0.998
1.5	B	3.901	-0.042	-0.007	0.150	0.087	0.012	0.968
1.5	C	4.915	-0.651	0.081	0.342	0.189	0.0255	0.790
1.7	A	3.773	0.044	-0.018	0.050	0.031	0.005	0.993
1.7	B	3.645	0.121	-0.030	0.042	0.025	0.003	0.997
1.7	C	4.534	-0.420	0.050	0.243	0.134	0.018	0.869

TABLE 3.7: The coefficients of the PMLT relations log P = a +blog T_{eff} + c log $(M/M_{\odot})$ + d log(L/$L_{\odot}$) for both F and FO pulsators as a function of the assumed α_{ml} parameter.

α_{ml}	a	b	c	d	σ_a	σ_b	σ_c	σ_d	R^2
F									
1.5	10.268	-3.192	-0.758	0.919	0.001	0.025	0.015	0.005	0.9995
1.7	10.538	-3.258	-0.749	0.911	0.002	0.050	0.019	0.007	0.9996
1.9	11.488	-3.469	-0.695	0.847	0.003	0.089	0.012	0.006	0.9999
FO									
1.5	10.595	-3.253	-0.621	0.804	0.002	0.067	0.014	0.005	0.9996
1.7	10.359	-3.186	-0.576	0.788	0.002	0.056	0.009	0.003	0.9999

3.2.2 The pulsation relation between the period and intrinsic stellar parameters

In order to obtain the pulsation relation connecting the period to the luminosity, mass, and effective temperature (PLMT relation) for both the F and FO-mode models as a function of the assumed mixing length parameter, a linear regression analysis of the values reported in Tables 3.1 and 3.2 was carried out. The coefficients for the F and FO pulsators are reported in Table 3.7.
These relations, which update previous relations published in the literature for solar metallicity models (Bono et al., 2000b), are consistent with them, and validate the use of pulsation models to establish good relations between pulsation and evolutionary parameters. Indeed, we remember that the PMLT relation is directly derived from the combination of the period–mean density relation (see Eq. 1.1) and the Stefan–Boltzmann law (see Eq. 1.3), and holds for each individual pulsator, independent of its position in the HR diagram. Therefore, it is not surprising that the coefficients of the PMLT relation reported in Table 3.7 are not significantly affected by varying the mixing length parameter except for the α_{ml}=1.9 case. In this last case, the number of pulsation models significantly decreases and pulsation is limited to the lowest masses, and these occurrences affect the derived relations.

3.2.3 The Period-Radius and Period-Mass-Radius relations

An important aspect of Cepheid research concerns the use of CCs to infer stellar radii. CCs are known to obey both period-radius (PR) and period-mass-radius (PMR) relations, the former involving an averaging operation over the mass distribution (Bono et al., 2001).
The PR relations are used to derive the stellar radii directly from the pulsation periods, whereas PMR relations can be used to infer an independent value of the stellar mass, once the period and the radius are known, which would then be compared with the evolutionary mass estimates.
The coefficients for the F and FO-mode models of the PR and PMR relations derived from current nonlinear model sets are reported in Tables 3.8 and 3.9, respectively.
Fig. 3.3 shows the PR relations assuming the canonical ML relation for the three values of α_{ml} for F and FO-mode models, and Fig. 3.4 shows the PR relations, at a fixed α_{ml}=1.5, for ML relation, cases A, B and C, for F-mode models.
We confirm previous results by Bono et al. (1998) that the PR relation does not vary considerably with the different assumptions of the ML relation, even if we notice that the relation gets flatter as the ML relation gets brighter. Moreover, varying the

TABLE 3.8: The coefficients of the relation $\log R = a + b \log P$, for both F and FO Galactic Cepheids derived by adopting A, B , C ML relations.

α_{ml}	ML	a	b	σ_a	σ_b	R^2
1.5	A	1.142	0.702	0.004	0.003	0.998
1.5	B	1.128	0.685	0.005	0.003	0.998
1.5	C	1.104	0.680	0.005	0.003	0.998
1.7	A	1.140	0.705	0.004	0.003	0.999
1.7	B	1.126	0.685	0.005	0.003	0.999
1.7	C	1.105	0.678	0.005	0.003	0.999
1.9	A	1.124	0.743	0.003	0.007	0.999
1.9	B	1.101	0.729	0.003	0.008	0.999
1.9	C	1.077	0.715	0.003	0.005	0.999
FO						
1.5	A	1.242	0.768	0.001	0.005	0.999
1.5	B	1.216	0.762	0.003	0.015	0.997
1.5	C	1.193	0.742	0.003	0.009	0.997
1.7	A	1.243	0.773	0.002	0.009	0.840

efficiency of superadiabatic convection has a mild effect on the PR coefficients (see Table 3.8).
Furthermore, we performed a comparison of our PR with that of the literature (see Fig. 3.4), confirming a generally good agreement with the PR relations from both Molinaro et al. (2011) and Gallenne et al. (2017). While we had a better agreement with the Molinaro et al. (2011) relation at shorter periods, the Gallenne et al. (2017) relation had a better agreement at longer periods.

3.2.4 An updated theoretical atlas of light and radial velocity curves

In this subsection, we present the new theoretical atlas of light and radial velocity curves for both F and FO-modes resulting from the nonlinear computation of full amplitude models.
The predicted bolometric light curves (left panels) and radial velocity variations (right panels) are shown in Fig. 3.5 for the sequence of canonical models. The curves are plotted over two consecutive pulsation cycles, as a function of the pulsation phase. In each plot, dashed lines refer to FO-mode models, whereas solid lines represent F-mode models. The period in days and the effective temperature in kelvin of each model are labelled in the corresponding light curve and radial velocity curve panels, respectively.
Positive values of radial velocity along the curves indicate an expansion phase for the stellar envelope, while negative values of the velocity correspond to a contraction phase.
The complete atlas of the bolometric light curves for the various assumptions about the ML relation and the superadiabatic convection efficiency are available in De Somma et al. (2020b).
Focusing on canonical models (luminosity level A) with α_{ml}=1.5, we notice that for masses lower than or equal to 5 $M_{\odot}$, the curve amplitudes steadily decrease as the effective temperature decreases, moving from the FBE to the FRE. Above $\sim$ 5 solar mass, this trend is less evident because the FO pulsation is no longer efficient. In particular, in the period range from $\sim$ 7 to $\sim$ 12 days, a secondary maximum (bump) is

TABLE 3.9: The coefficients of the relation $\log P = a + b \log M + c \log R$, for both F and FO Galactic Cepheids derived by adopting A, B , C ML relations.

α_{ml}	ML	a	b	c	σ_a	σ_b	σ_c	R^2
F								
1.5	A	-1.641	-0.890	1.830	0.007	0.06	0.03	0.999
1.5	B	-1.709	-0.920	1.874	0.01	0.072	0.03	0.998
1.5	C	-1.721	-0.687	1.784	0.01	0.06	0.03	0.998
1.7	A	-1.642	-1.144	1.948	0.008	0.14	0.06	0.999
1.7	B	-1.725	-1.194	2.001	0.01	0.13	0.06	0.999
1.7	C	-1.687	-0.583	1.728	0.02	0.11	0.05	0.999
1.9	A	-1.570	-0.778	1.737	0.02	0.3	0.1	0.999
1.9	B	-1.573	-0.720	1.709	0.01	0.09	0.05	0.999
1.9	C	-1.587	-0.547	1.654	0.01	0.06	0.03	0.999
FO								
1.5	A	-1.659	-0.564	1.590	0.005	0.06	0.03	0.999
1.5	B	-1.695	-0.779	1.707	0.02	0.1007	0.05	0.999
1.5	C	-1.738	-0.698	1.704	0.01	0.06	0.03	0.999
1.7	A	-1.644	-0.589	1.591	0.01	0.1	0.05	0.902

present in the light and radial velocity curves.
For this reason, Cepheids in this period range are called "bump Cepheids." The evolution of the bump pulsation phase from the descending to the ascending branch of the curve is the Hertzprung progression (HP) (Bono et al., 2000c, and references therein). At the center of the HP, the principal and secondary maximum are very close in magnitude and the pulsation amplitude often reaches its minimum.

The effect of the adopted ML relation

To show the effect of a variation of the ML relation on the predicted light and radial velocity curves, we chose two models whose trends are representative of all other models.

In the panels of Fig. 3.6, we show the light (left) and radial velocity (right) curves of an F-mode model, at a fixed $\frac{M}{M_\odot} = 9.0$, $T_{eff} = 4600K$ and $\alpha_{ml} = 1.5$ for three different levels of luminosity (cases A, B, and C). Fig. 3.7 is the same as Fig. 3.6 but for an FO-mode model with $\frac{M}{M_\odot} = 3.0$, $T_{eff} = 6300K$ and $\alpha_{ml} = 1.5$.
These plots confirm that both the morphology and amplitude of light and radial velocity curves depend on the assumed ML relation. This effect is evident in particular for the FO-mode model. Moreover, as expected, longer periods are found for the B and C cases, at a fixed mass, due to the increased luminosity levels.
As a consequence, "bump Cepheids" are found at lower masses, and the center of the HP is found at slightly shorter periods. This trend, once the metallicity is known, makes the HP phenomenon a useful tracer of the Cepheid ML relation.

The effect of the superadiabatic convective efficiency

As discussed above, the main effect of superadiabatic convection is to quench pulsation; and so, lower pulsation amplitudes are expected as α_{ml} increases from 1.5 to 1.7 and 1.9.

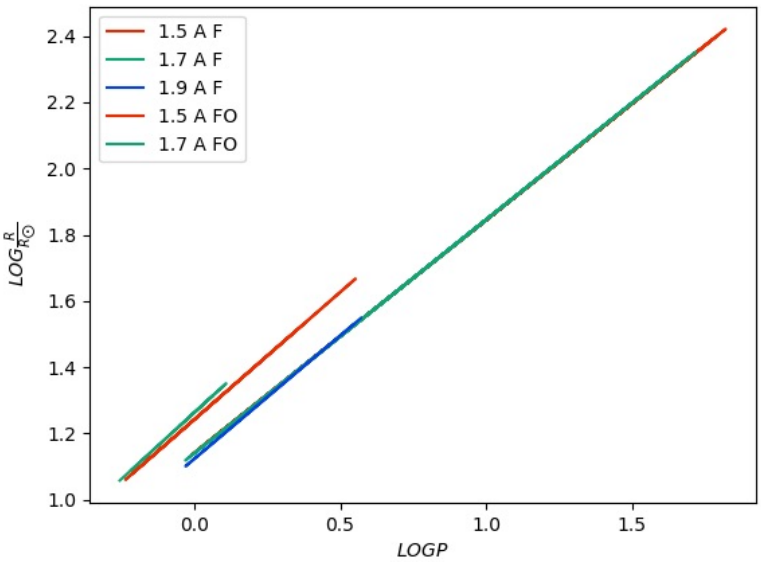

FIGURE 3.3: The canonical F and FO period-radius relations for the various assumptions of the superadiabatic convective efficiency, $\alpha_{ml} = 1.5$, $\alpha_{ml} = 1.7$, $\alpha_{ml} = 1.9$.

Assuming a canonical ML relation, Fig. 3.8 and 3.9 corresponding to the F-mode model with $\frac{M}{M_\odot} = 4.0$, $T_{eff} = 5900K$ and the FO-mode model with $\frac{M}{M_\odot} = 4.0$, $T_{eff} = 6200K$, respectively, show the comparison between the light and radial velocity curves obtained for the three values of α_{ml}.
The morphology of the curves gets smoother and the pulsation amplitude decreases as α_{ml} increases. In particular, the FO pulsation disappears for α_{ml}=1.9 because, at this value of α_{ml}, the quenching effect is very efficient and the pulsation disappears. The same trend is followed by all other models.

In the next three Chapters, we will apply this extended theoretical scenario to the data for Galactic Cepheids with Gaia Data Release 2 (DR2) parallaxes. In particular, the implications of our models for the use of CCs as distance indicators (Chapter 4) as well as the implications of our models for the individual mass estimates (Chapter 5) and age indicators (Chapter 6) of CC will be discussed.

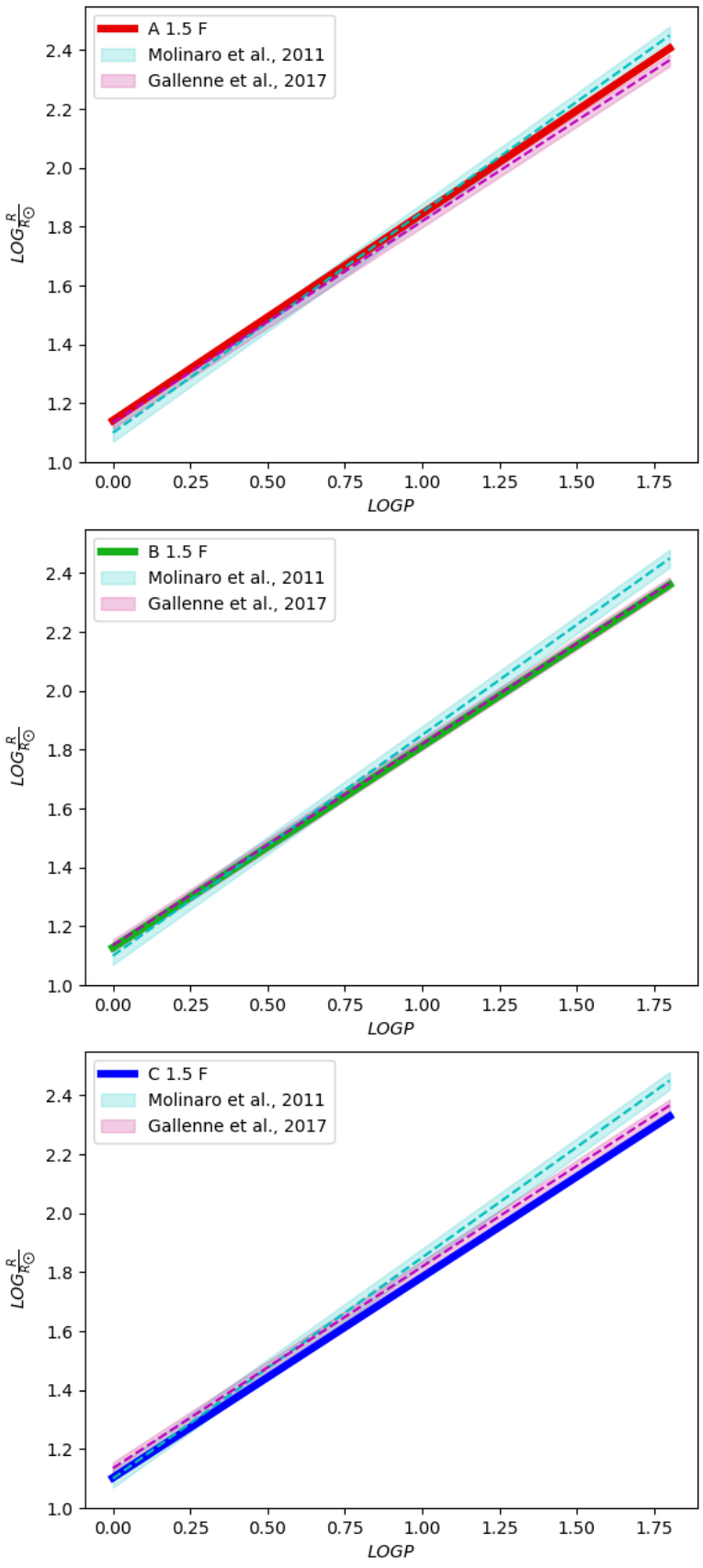

FIGURE 3.4: The PR relations for F-mode GCCs derived by adopting $\alpha_{ml} = 1.5$ and A, B, C ML relations compared with available results in literature.

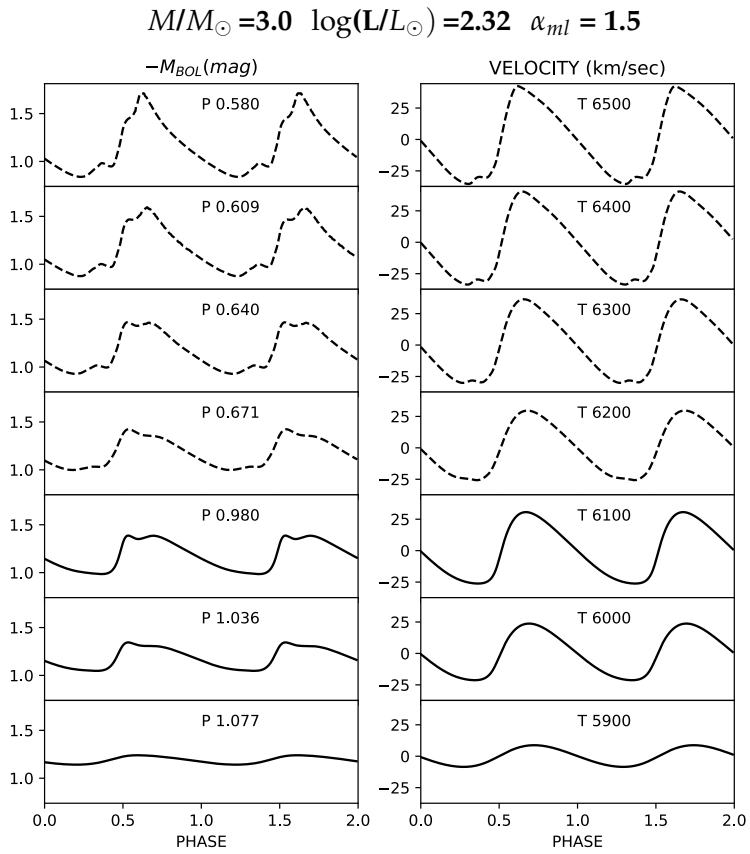

FIGURE 3.5: Bolometric light curves (left panel) and radial velocity curves (right panel) for a sequence of nonlinear F (solid line) and FO-mode models (dashed lines) derived at a fixed mass, luminosity, α_{ml} parameter (see labeled values on the top of the plot) adopting the canonical ML relation. On each left and right panel the period in days and the effective temperature in kelvin are labeled, respectively.

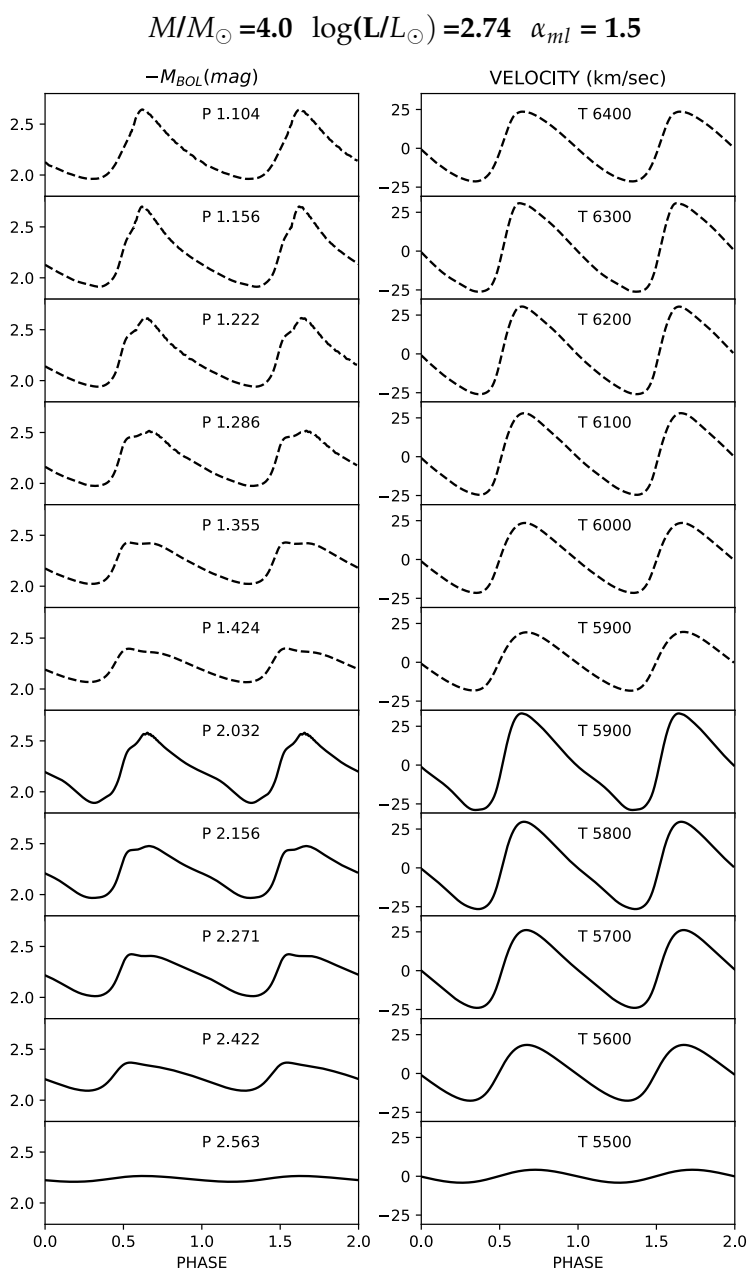

FIG.3.5-Continued.

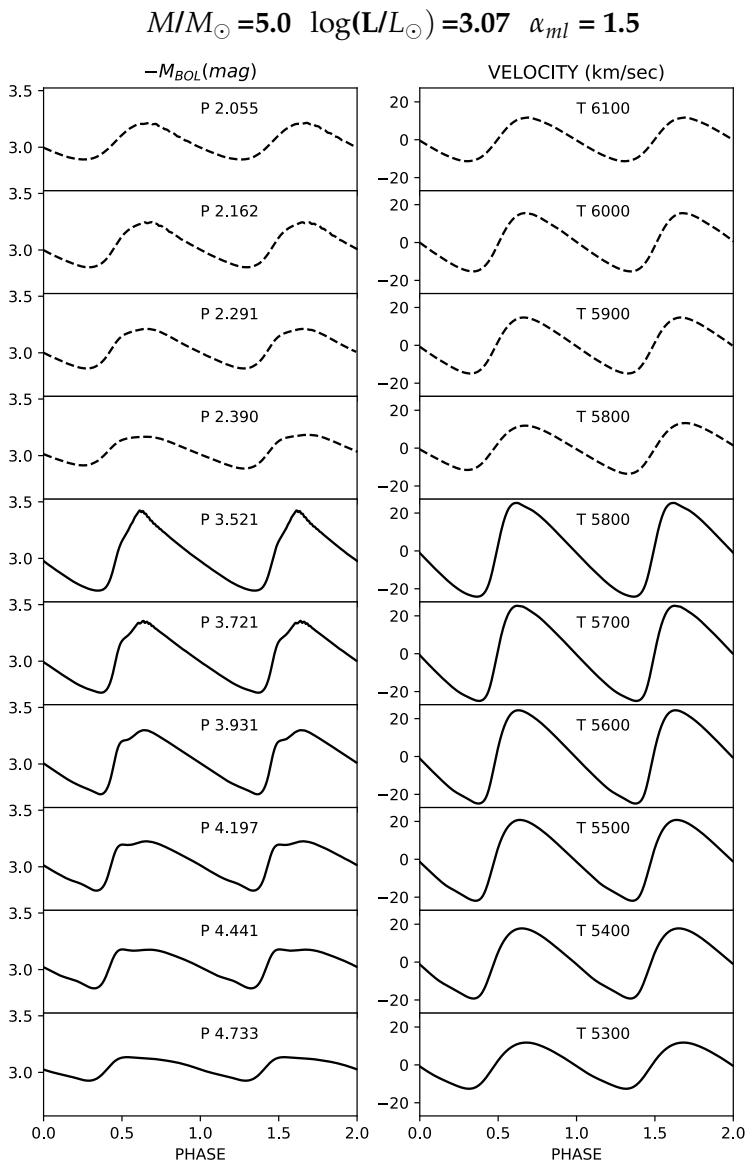

FIG.3.5-Continued.

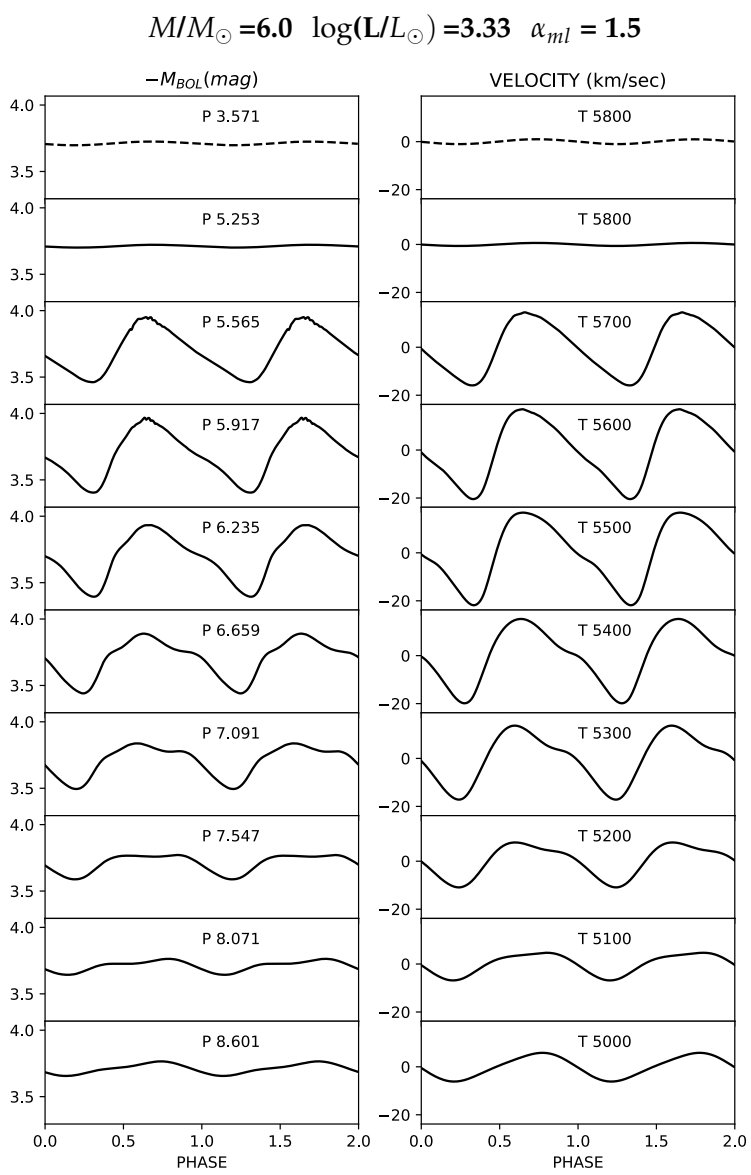

FIG.3.5-Continued.

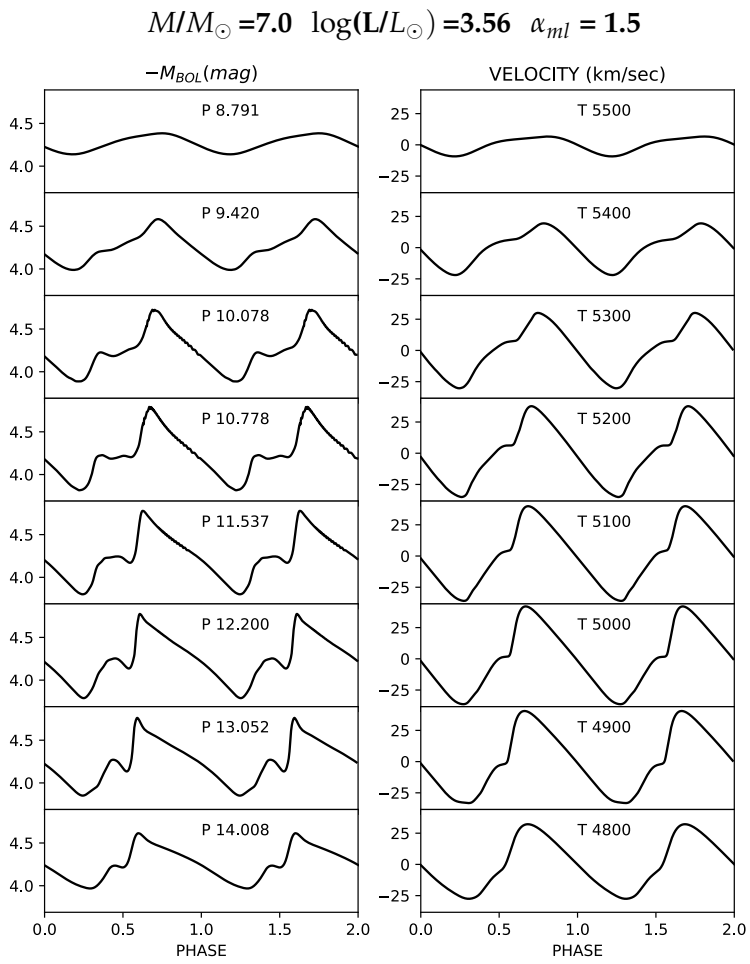

FIG.3.5-Continued.

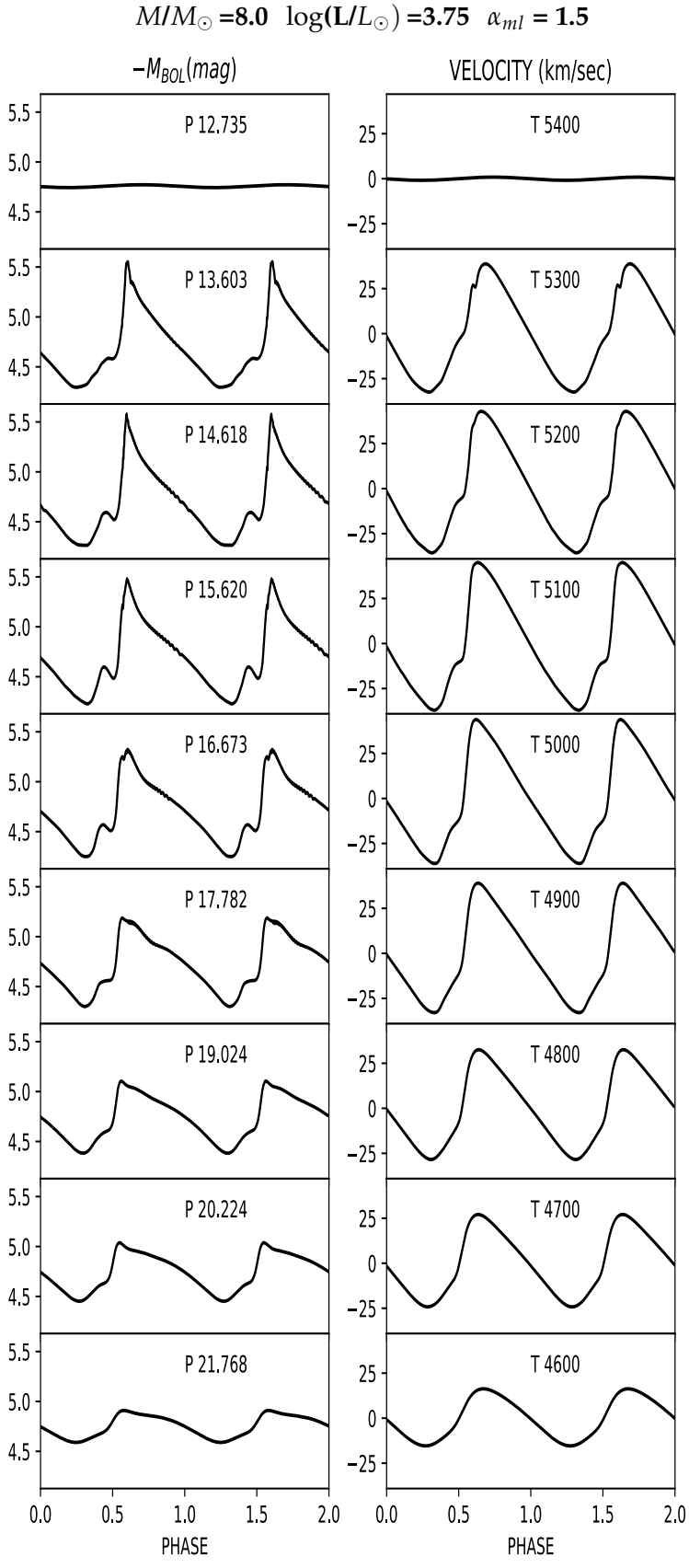

FIG.3.5-Continued.

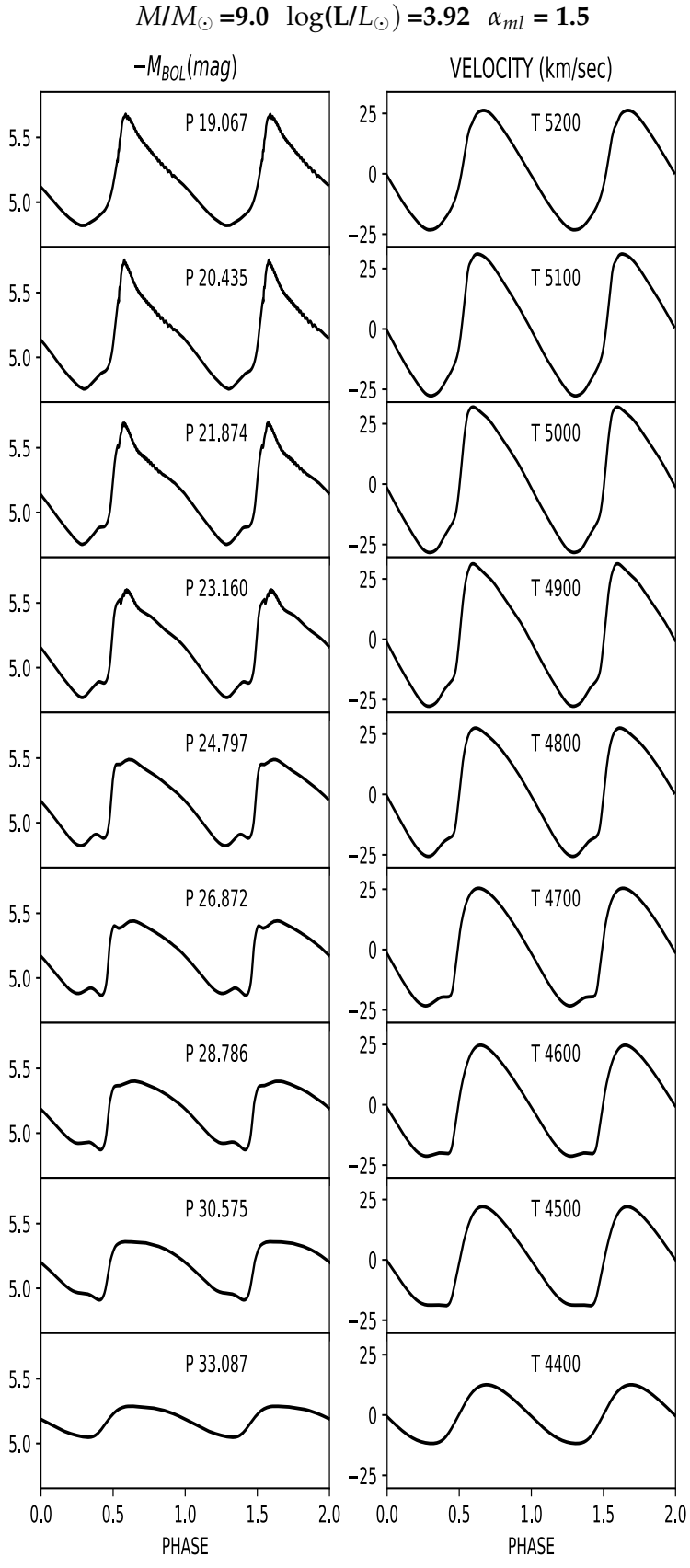

FIG.3.5-Continued.

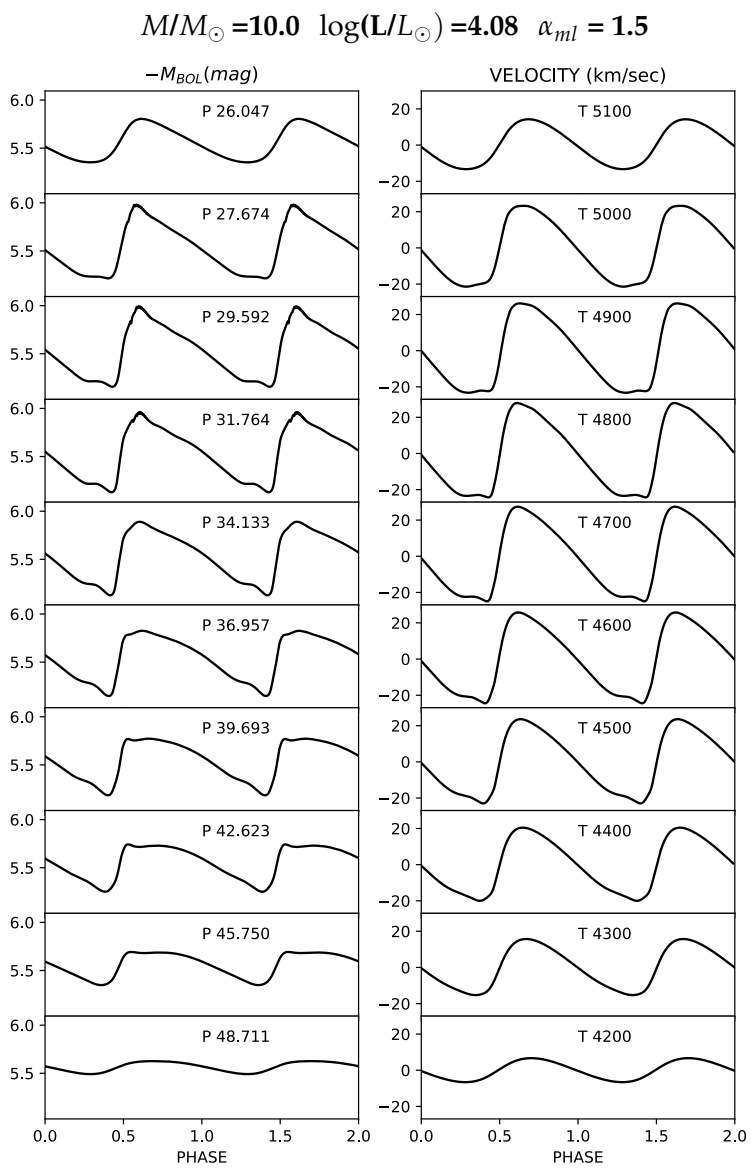

FIG.3.5-Continued.

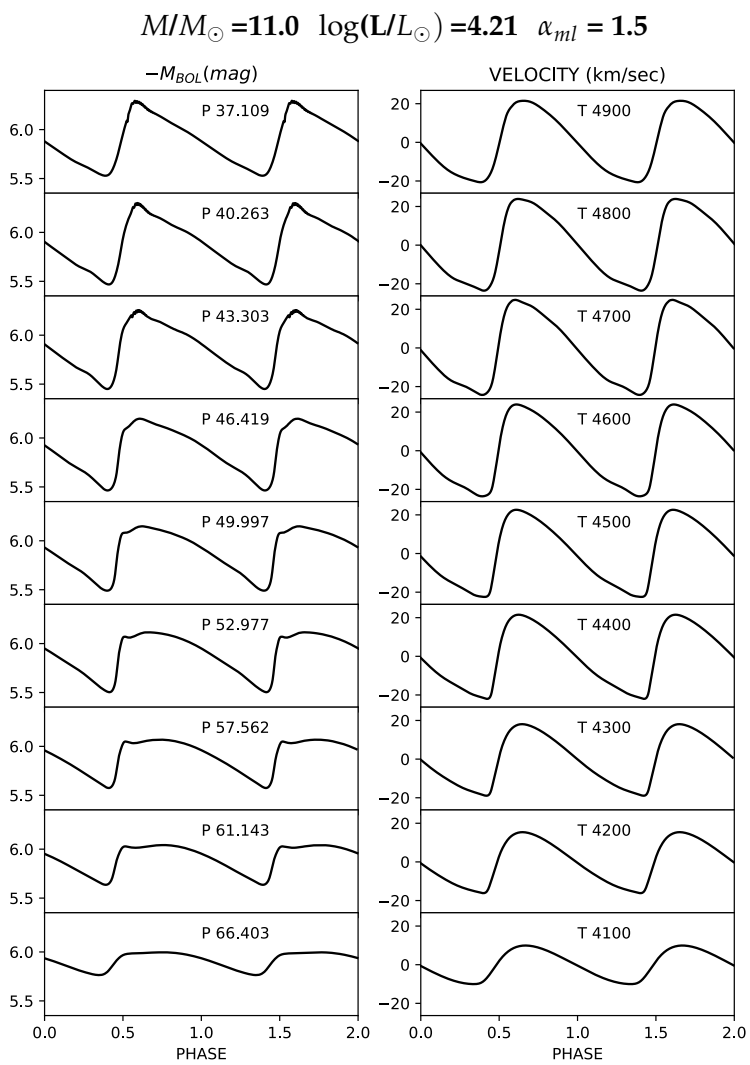

FIG.3.5-Continued.

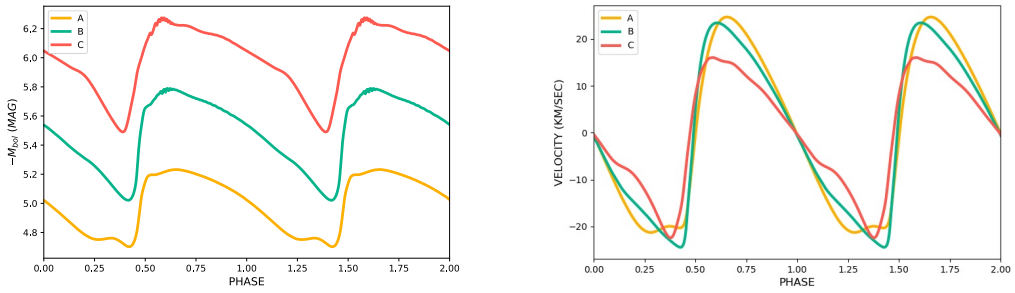

FIGURE 3.6: Light curve (*left panel*) and radial velocity curve (*right panel*) of $T_{eff} = 4600K$, $M/M_{\odot}$ =9.0, α_{ml} = 1.5 F model for the three assumed ML relations.

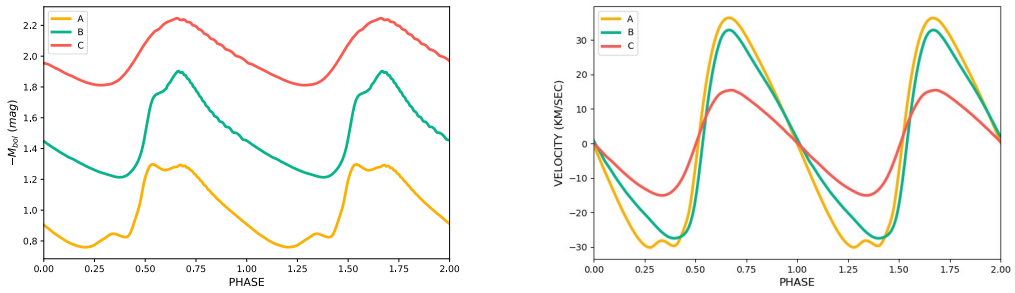

FIGURE 3.7: Light curve (*left panel*) and radial velocity curve (*right panel*) of $T_{eff} = 6300K$, $M/M_{\odot}$ =3.0, α_{ml} = 1.5 FO-mode model for the three assumed ML relations.

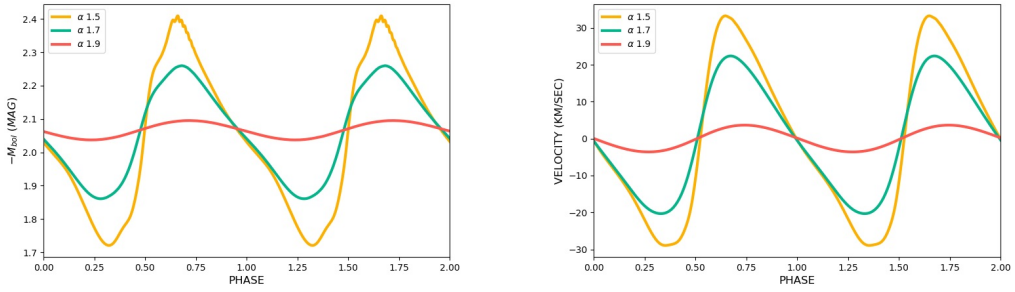

FIGURE 3.8: Light curve (*left panel*) and radial velocity curve (*right panel*) for $M/M_{\odot}$ =4.0, $T_{eff} = 5900K$ canonical F-mode model for the three adopted valued of α_{ml}.

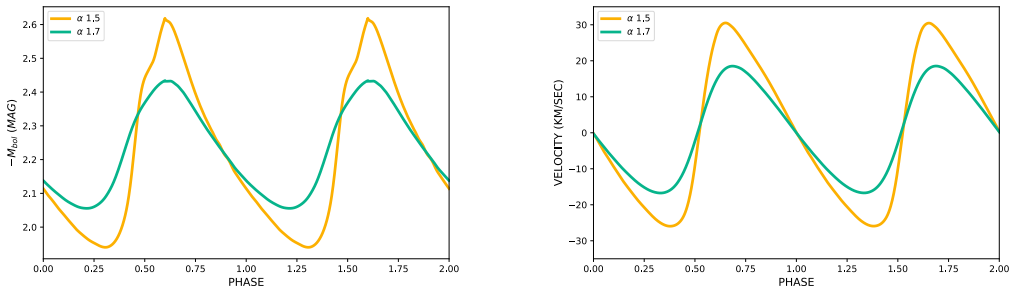

FIGURE 3.9: Light curve (*left panel*) and radial velocity curve (*right panel*) for $M/M_{\odot}$ =4.0, $T_{eff} = 6200K$ canonical FO-mode model for the two $\alpha_{ml} = 1.5$ and 1.7 assumptions.

Chapter 4

The comparison between updated pulsation model predictions and Gaia DR2 parallaxes

In the context of this PhD project, the comparison of the updated pulsating stellar models to valuable observational datasets is extremely important. In order to test the physical and numerical assumptions used in the model computations and also to trace the properties of Galactic and extra-Galactic stellar populations, it is important to transfer the models from the theoretical plane to the observational ones. In particular, for this project, to compare the theoretical models to the observational dataset provided by the Gaia Space mission (Gaia Collaboration et al., 2016a; Gaia Collaboration et al., 2016b), the theoretical models were converted from the theoretical plane to the Gaia photometric passbands. Indeed, recently, the Gaia DR2 (Gaia Collaboration et al., 2018) provided, to the scientific community, accurate parallaxes and proper motions for a large sample of Cepheids observed in the three Gaia photometric passbands, namely G, G_{BP} and G_{RP} (Clementini et al., 2019; Ripepi et al., 2019).
In order to perform the comparison with Gaia data, we transformed the bolometric light curves presented in 3 into the Gaia filters and derived the Gaia mean magnitudes and colors as detailed below.

4.1 From bolometric to Gaia DR2 light curves

In order to provide the first theoretical catalog of CC light curves in the Gaia photometric system passbands, the bolometric light curves shown in Chapter 3 were converted in the Gaia filters using the ATLAS9 non-overshooting model atmospheres (Castelli et al., 2003).
The convolution between the Gaia passbands and the synthetic spectra provided by these model atmospheres, with the chemical composition, the effective temperature and the surface gravity given as input quantities. provides us with the bolometric corrections, i.e. the differences between the bolometric magnitude and the magnitude in each specified photometric passband, The predicted light curves for a sequence of canonical models with $\alpha_{ml} = 1.5$ and masses ranging from 3 to 11 solar masses are shown in Fig. 4.1. In each plot, dashed and solid lines represent the FO and F-mode models, respectively; while in each panel, the green line indicates the G_{BP} band, the blue line the G band, and the orange line the G_{RP} band light curve. The model effective temperature and period are labeled for each model. As usual the effective temperature is in kelvin, while the pulsational period is in days.

From the analysis of the curves, it is evident that the morphology of each predicted Gaia light curve follows the trends of the corresponding bolometric curve, for temperature, mass, luminosity and wavelength.
The complete atlas of the light curves in the Gaia photometric system for the various assumptions of the ML relation and the superadiabatic convection efficiency is available in De Somma et al. (2020b)

$M/M_{\odot}$ **=3.0** $\log(\mathbf{L}/L_{\odot})$ **=2.32** α_{ml} **= 1.5**

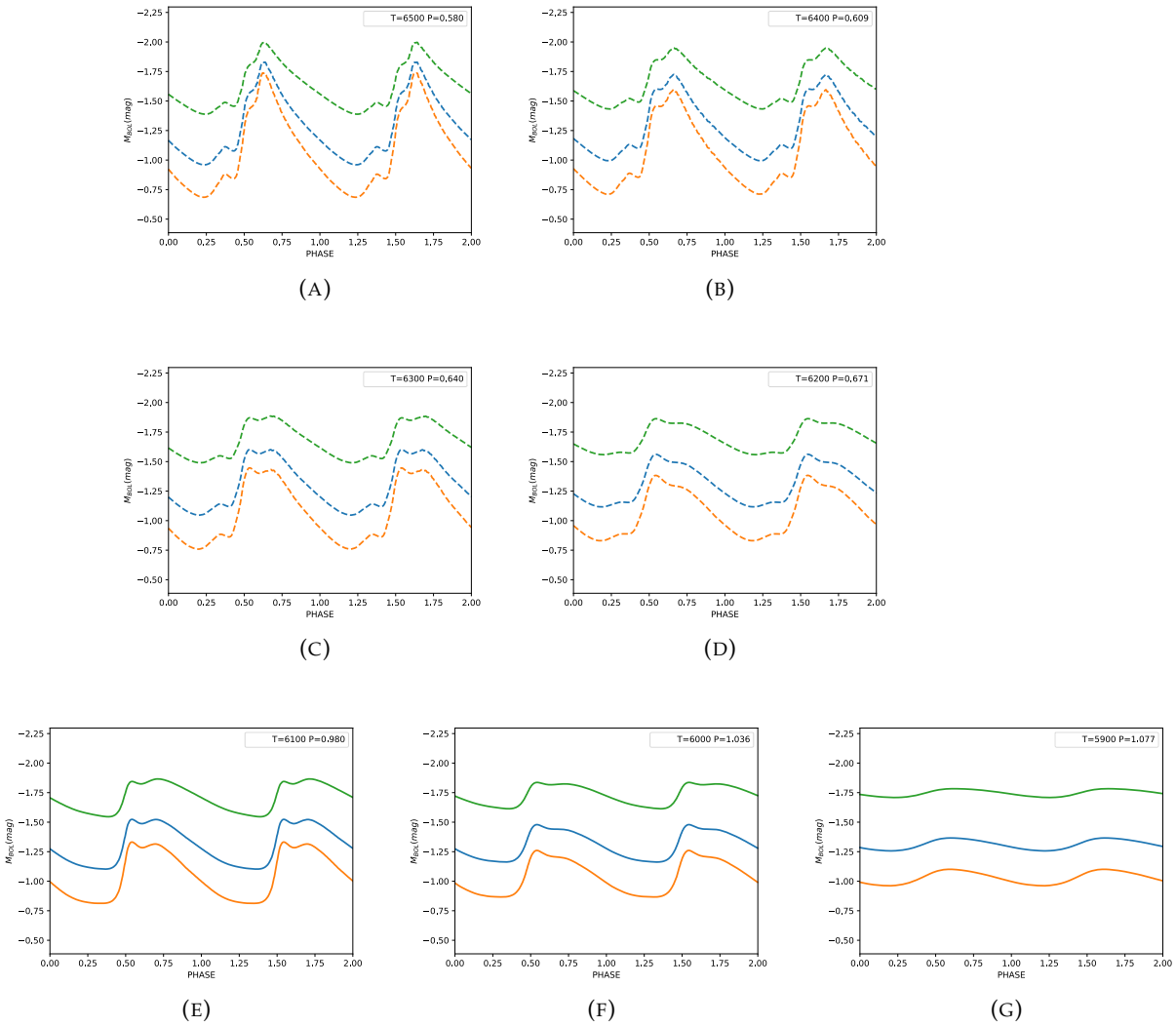

FIGURE 4.1: Theoretical *Gaia* light curves for a sequence of non linear F (solid line) and FO-mode models (dashed line) derived at fixed mass, luminosity, α_{ml} parameter (see labeled values on the top of the plot) adopting the canonical ML relation.

$M/M_{\odot}$ **=4.0** $\log(\mathbf{L}/L_{\odot})$ **=2.74** $\alpha_{ml} = 1.5$

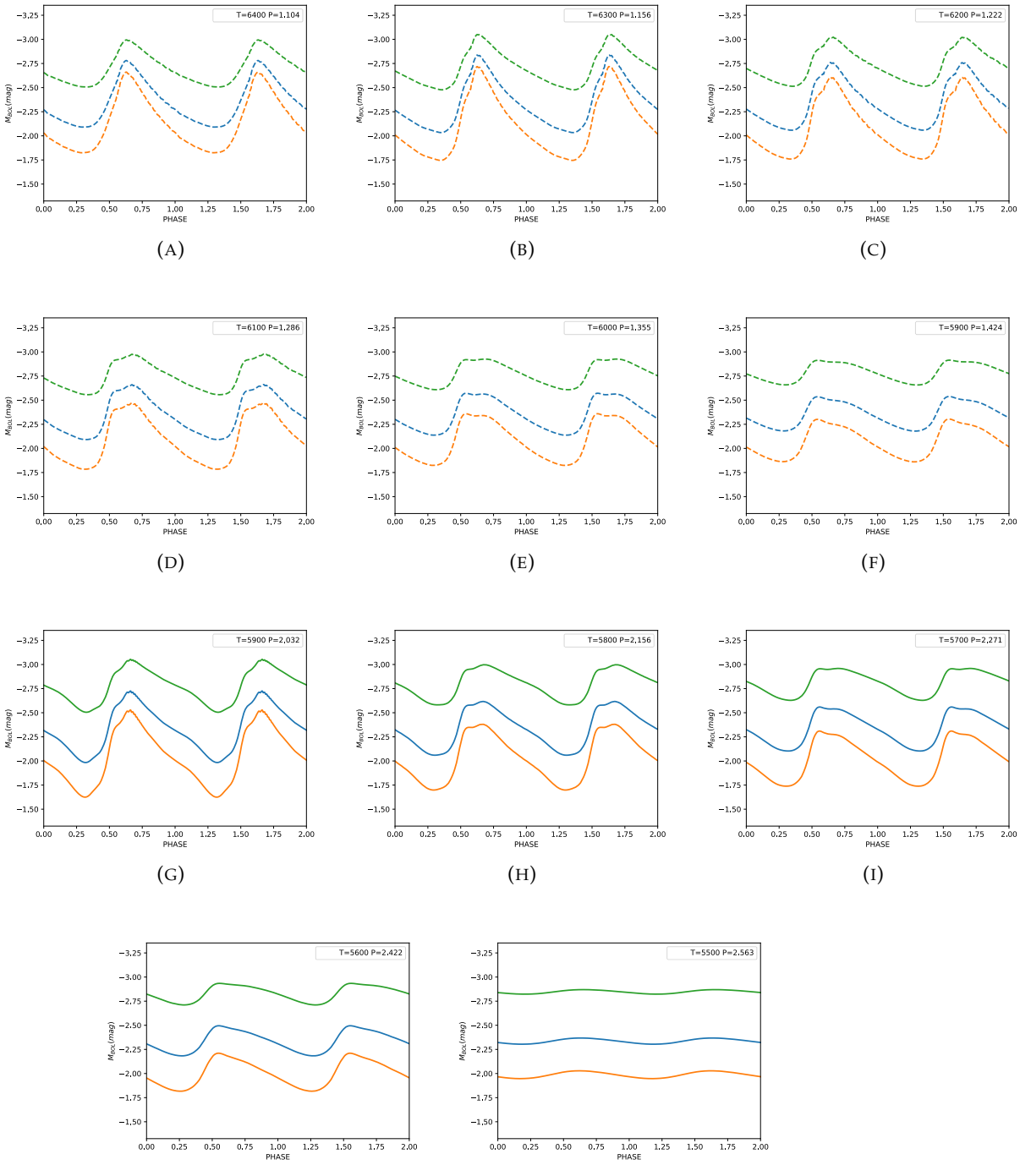

(A) (B) (C)

(D) (E) (F)

(G) (H) (I)

(J) (K)

FIG.4.1-Continued.

$M/M_{\odot}$ **=5.0** $\log(\mathbf{L}/L_{\odot})$ **=3.07** α_{ml} **= 1.5**

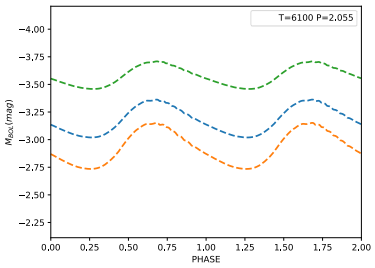

(A)

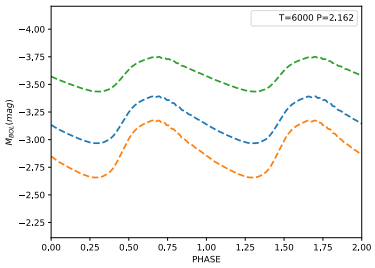

(B)

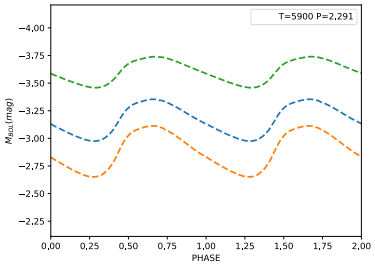

(C)

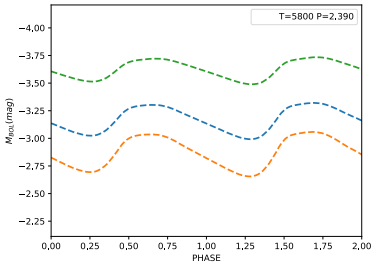

(D)

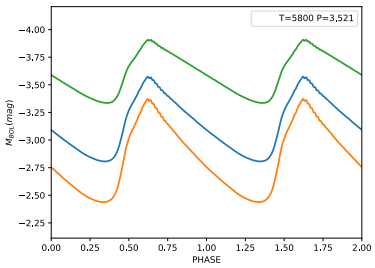

(E)

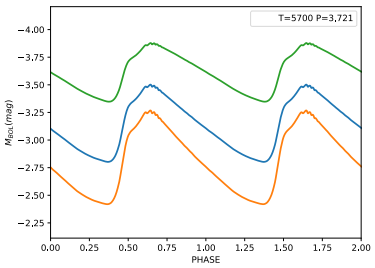

(F)

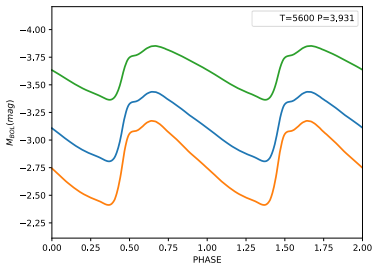

(G)

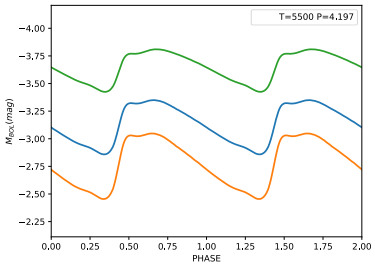

(H)

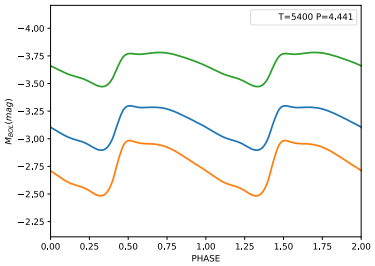

(I)

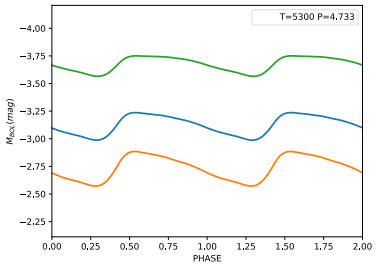

(J)

FIG.4.1-Continued.

$M/M_{\odot}$ **=6.0** $\log(\mathbf{L}/L_{\odot})$ **=3.33** α_{ml} **= 1.5**

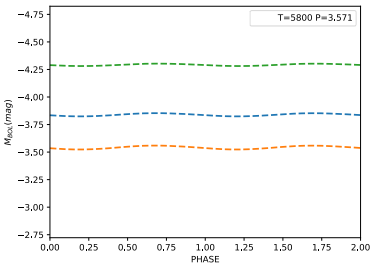

(A)

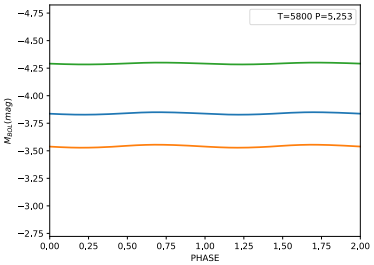

(B)

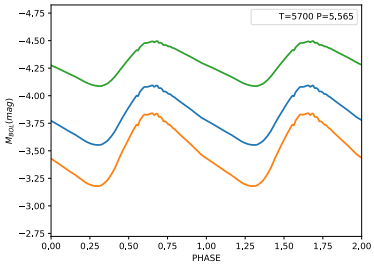

(C)

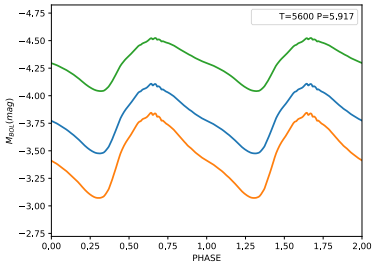

(D)

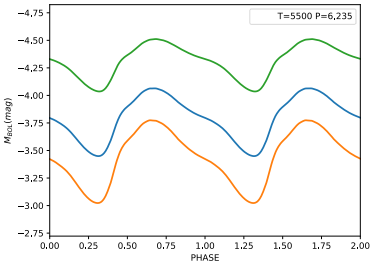

(E)

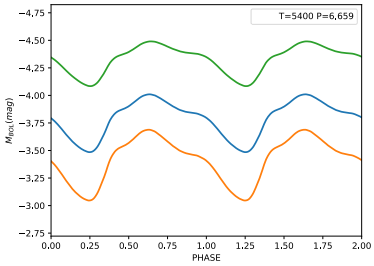

(F)

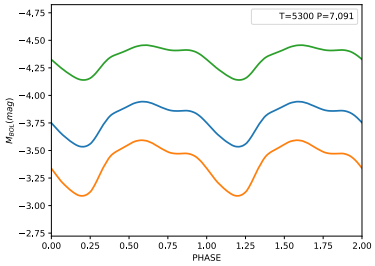

(G)

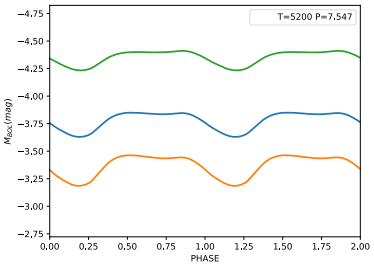

(H)

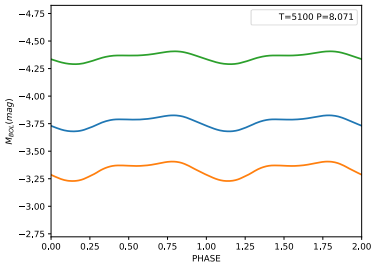

(I)

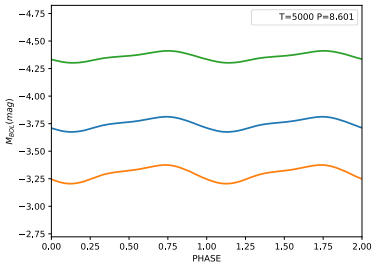

(J)

FIG.4.1-Continued.

$M/M_{\odot}$ **=7.0** $\log(\mathbf{L}/L_{\odot})$ **=3.56** α_{ml} **= 1.5**

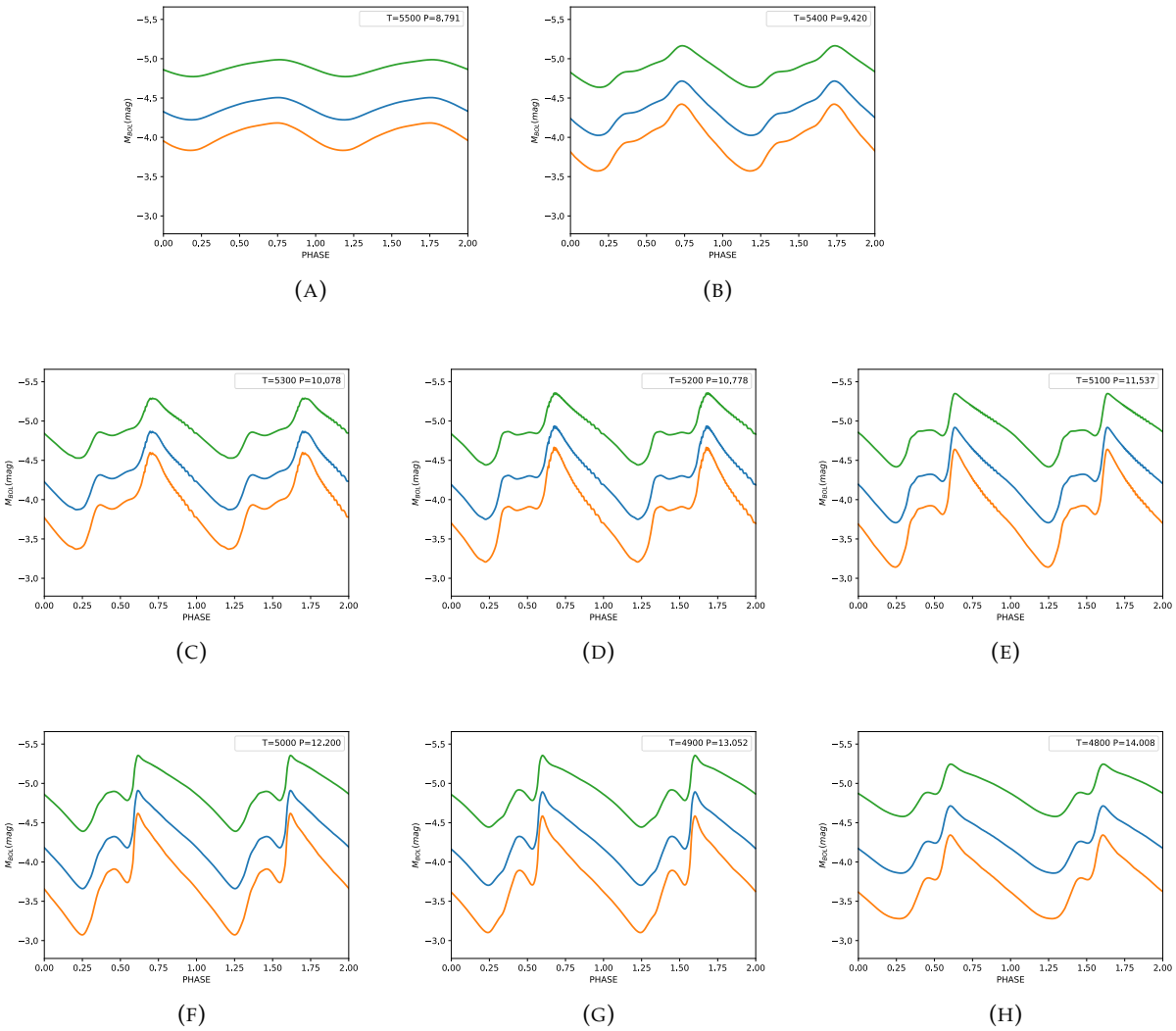

(A) (B)

(C) (D) (E)

(F) (G) (H)

FIG.4.1-Continued.

$M/M_{\odot}$ **=8.0** $\log(\mathbf{L}/L_{\odot})$ **=3.75** α_{ml} **= 1.5**

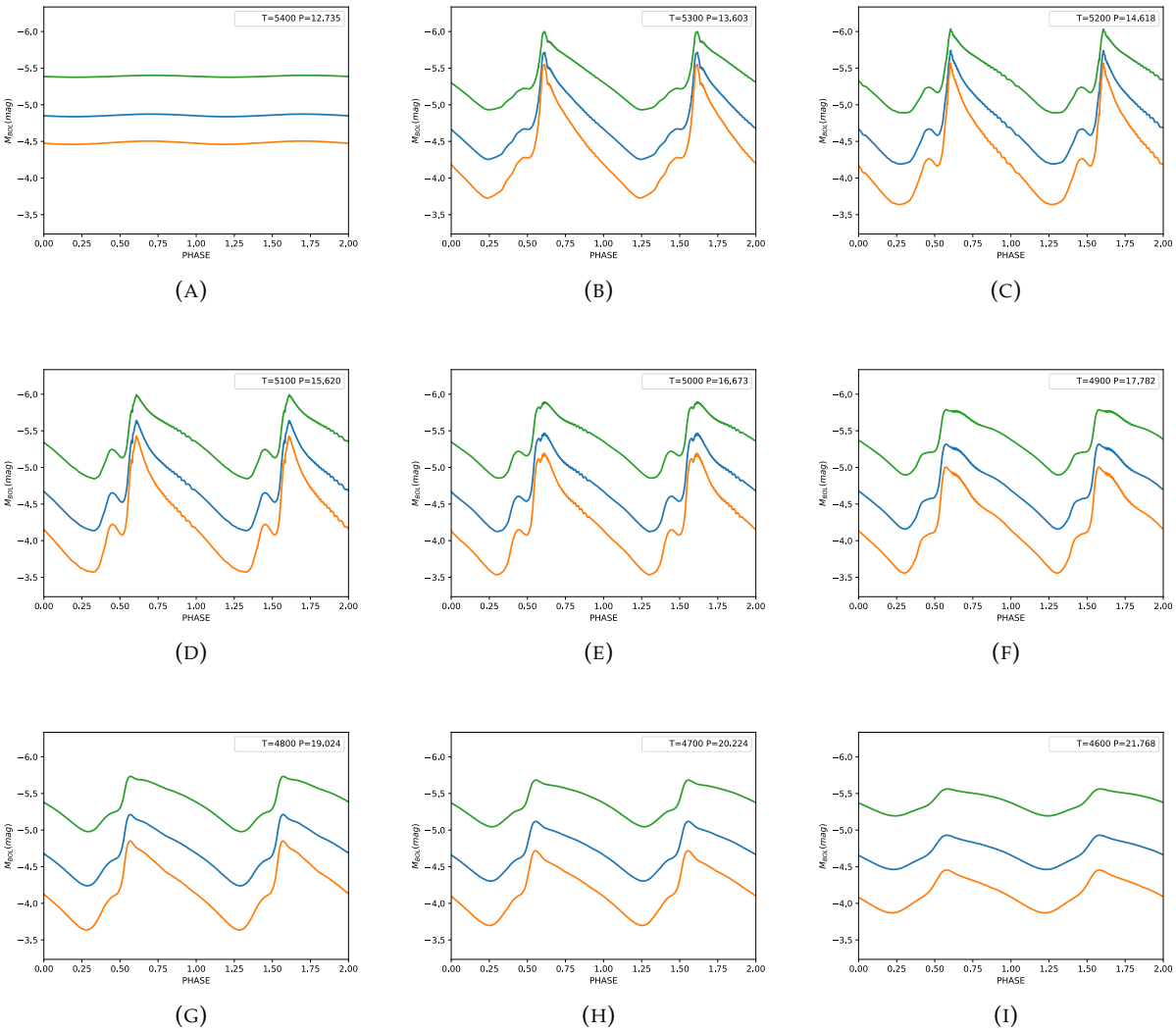

(A) (B) (C)

(D) (E) (F)

(G) (H) (I)

FIG.4.1-Continued.

$M/M_{\odot}$ **=9.0** $\log(\mathbf{L}/L_{\odot})$ **=3.92** α_{ml} **= 1.5**

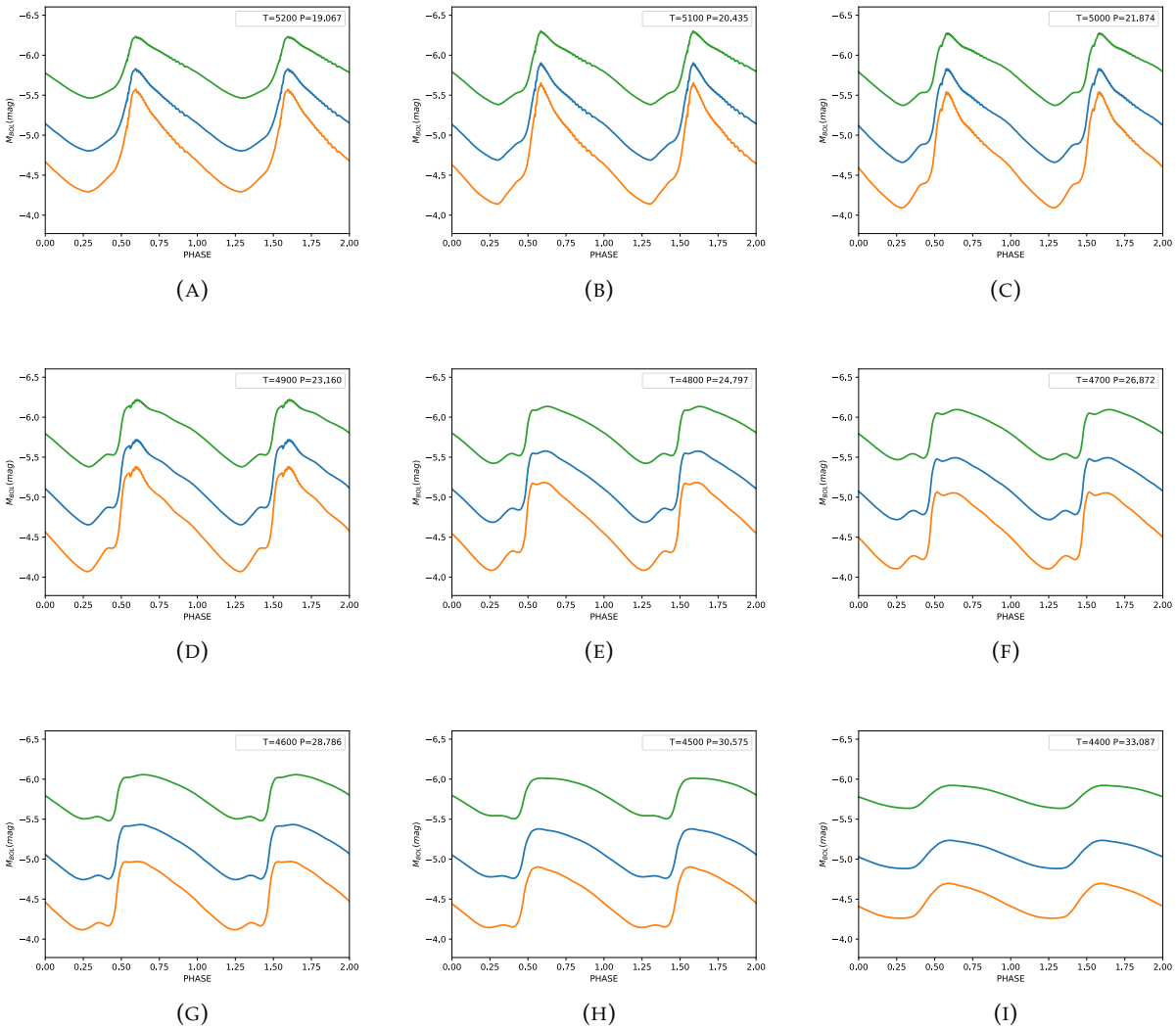

(A) (B) (C)

(D) (E) (F)

(G) (H) (I)

FIG.4.1-Continued.

$M/M_{\odot}$ **=10.0** $\log(\mathbf{L}/L_{\odot})$ **=4.08** α_{ml} **= 1.5**

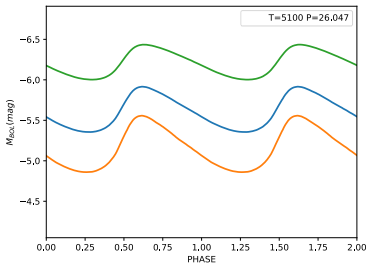

(A)

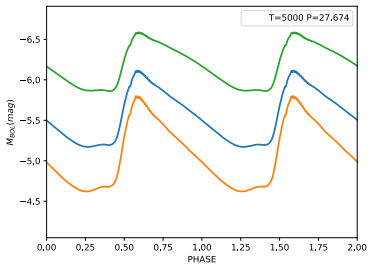

(B)

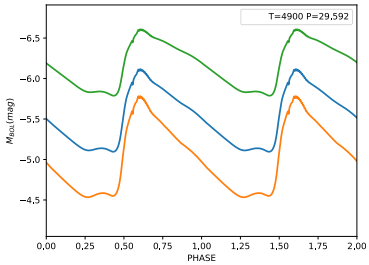

(C)

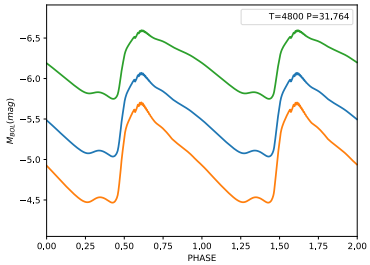

(D)

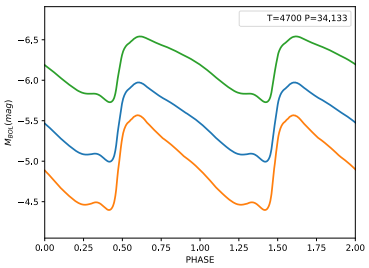

(E)

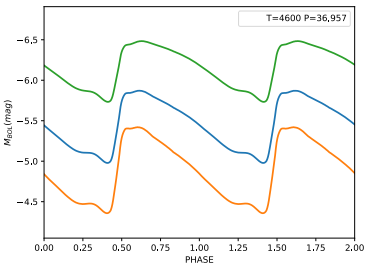

(F)

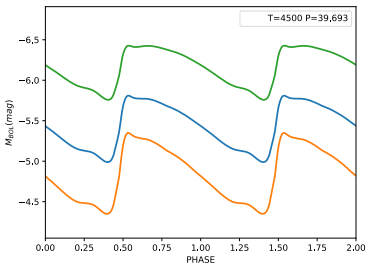

(G)

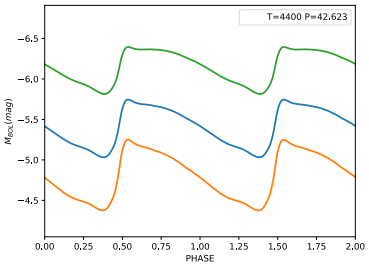

(H)

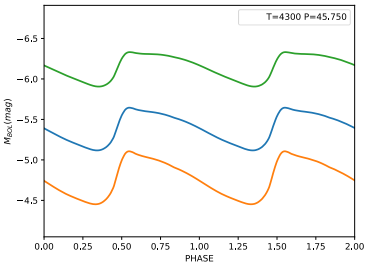

(I)

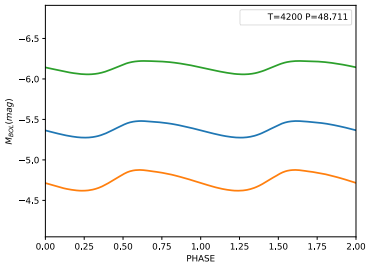

(J)

FIG.4.1-Continued.

$M/M_{\odot}$ **=11.0** $\log(\mathbf{L}/L_{\odot})$ **=4.21** α_{ml} **= 1.5**

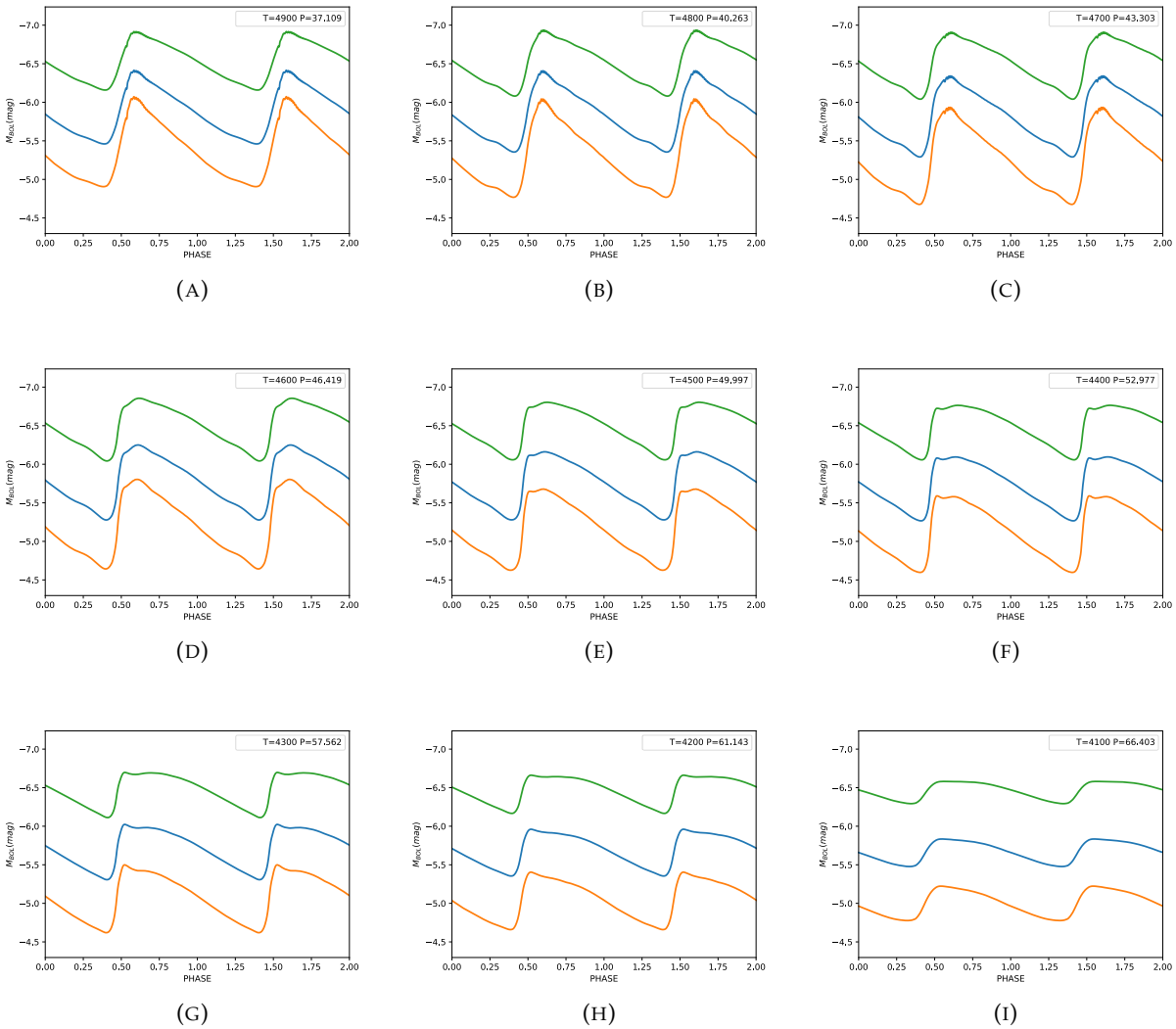

(A) (B) (C)

(D) (E) (F)

(G) (H) (I)

FIG.4.1-Continued.

4.1.1 The inferred mean magnitudes and colors in the Gaia filters

The light curves transferred in the Gaia photometric plane allow us to derive intensity-averaged mean magnitudes and colors in the Gaia filters, $< G >$, $< G_{BP} >$ and $< G_{RP} >$ magnitudes and the $< G_{BP} >$ - $< G_{RP} >$ color.
The three mean magnitudes for each computed stable pulsation model, are reported in Tables 4.1 and 4.2 for F and FO-mode models, respectively. The columns show the stellar mass, the logarithmic luminosity, the effective temperature, the adopted mixing length parameter, the adopted ML relation, and the intensity-weighted mean magnitudes in the Gaia passbands.

TABLE 4.1: Mean magnitudes in the *Gaia* filters for F-mode models at varying ML relation and α_{ml} parameters. This table is available in its entirety in A.2 in A.

		Z=0.02	Y= 0.28				
$M/M_{\odot}$	$\log(L/L_{\odot})$	T_{eff}[K]	α_{ml}	ML	G	G_{BP}	G_{RP}
(1)	(2)	(3)	(4)	(5)	(6)	(7)	(8)
3.0	2.32	5900	1.5	A	1.31	-1.03	-1.75
3.0	2.32	6000	1.5	A	1.31	-1.05	-1.73
...							
4.0	2.74	5500	1.5	A	2.34	-1.99	-2.85
4.0	2.74	5600	1.5	A	2.34	-2.01	-2.83
...							
5.0	3.07	5300	1.5	A	3.13	-2.74	-3.68
5.0	3.07	5400	1.5	A	3.14	-2.77	-3.67
...							
6.0	3.33	5000	1.5	A	3.75	-3.30	-4.36
6.0	3.33	5100	1.5	A	3.76	-3.33	-4.36
...							
7.0	3.56	4800	1.5	A	4.26	-3.77	-4.91
7.0	3.56	4900	1.5	A	4.28	-3.81	-4.90
...							
8.0	3.75	4600	1.5	A	4.70	-4.16	-5.39
8.0	3.75	4700	1.5	A	4.72	-4.21	-5.39
...							
9.0	3.92	4400	1.5	A	5.07	-4.48	-5.79
9.0	3.92	4500	1.5	A	5.09	-4.53	-5.80
...							
10.0	4.08	4200	1.5	A	5.38	-4.75	-6.15
10.0	4.08	4300	1.5	A	5.41	-4.80	-6.16
...							
11.0	4.21	4100	1.5	A	5.68	-5.02	-6.47
11.0	4.21	4200	1.5	A	5.72	-5.08	-6.49
...							

TABLE 4.2: The same as in Table 4.1 but for FO-mode models.This table is available in its entirety in A.2 in A.

		Z=0.02	Y= 0.28				
$M/M_\odot$	$\log(L/L_\odot)$	T_{eff}[K]	α_{ml}	ML	G	G_{BP}	G_{RP}
(1)	(2)	(3)	(4)	(5)	(6)	(7)	(8)
3.0	2.32	6200	1.5	A	-1.32	-1.08	-1.70
3.0	2.32	6300	1.5	A	-1.32	-1.10	-1.68
...							
4.0	2.74	5900	1.5	A	-2.36	-2.08	-2.80
4.0	2.74	6000	1.5	A	-2.37	-2.10	-2.78
...							
5.0	3.07	5800	1.5	A	-3.17	-2.88	-3.63
5.0	3.07	5900	1.5	A	-3.18	-2.90	-3.61
...							
6.0	3.33	5800	1.5	A	-3.84	-3.54	-4.29

4.2 The first theoretical PLC and PW relations in the Gaia filters for Galactic Classical Cepheids

The mean magnitudes and colors derived in the previous subsection can be used to derive the first theoretical GCC PLC and PW relations in the Gaia filters.
The coefficients of PLC and PW relations with varying ML relations and efficiencies of superadiabatic convection, for F and FO-mode models, are reported in Tables 4.3 and 4.4, respectively.
To derive the Wesenheit magnitude, the relation provided by Ripepi et al. (2019), $W = G - 1.9\,(G_{BP} - G_{RP})$, was adopted.
Both the PLC and the PW relations are valid for each individual pulsator thus allowing us to derive individual distances of observed Cepheids in the Gaia database.
We noticed that the PLC and PW relations, and, in turn, the individual distances derived by applying them to the observed pulsators, depend on the assumed ML relation but are almost insensitive to the value of the mixing length parameter.

In particular, assuming $\alpha_{ml} = 1.5$, if we consider a F-mode Cepheid pulsator with $P = 10$ days and $< G_{BP} >$ - $< G_{RP} >$ = 1.0 mag, the G magnitude obtained from the theoretical PLC relation varies from $< G >= -4.11$ mag at the canonical ML (case A) to $< G >= -3.94$ mag for an ML relation brighter by $\Delta \log(L/L_\odot)$=0.2 *dex* (case B) and to $< G > = -3.79$ mag for an ML relation brighter by $\Delta \log(L/L_\odot)$=0.4 *dex* (case C). Consequently, assuming $P = 10$ days and $< G_{BP} >$ - $< G_{RP} >$ = 1.0 mag, the difference in the predicted G magnitude amounts to 0.1 mag and 0.3 mag as the ML relation goes from case A to C. On the other hand, assuming the canonical case A, the G magnitude obtained from the PLC relation can then change up to 0.1 mag when moving from $\alpha_{ml} = 1.5$ to $\alpha_{ml} = 1.9$.
In order to better show what could occur in typical extra-galactic distance scale applications, we performed the same kind of test with F-mode PLC relations at fixed periods of $P = 30$ and $P = 100$ days and $< G_{BP} >$ - $< G_{RP} >$ = 1.0 mag.
We found that, assuming $\alpha_{ml} = 1.5$ and $P = 30$ days, $< G >$ varies from -5.91 (case A) to -5.73 (case B) and -5.57 (case C), whereas for a longer period ($P = 100$ days), G varies from -7.89 (case A) to -7.7 (case B) and -7.51 (case C). In addition, we

find very small variations due to the efficiency of super-adiabatic convection, with the predicted G magnitude that changes by about 0.15 mag and 0.20 mag for $P = 30$ days and $P = 100$ days, respectively, moving from $\alpha_{ml} = 1.5$ to $\alpha_{ml} = 1.9$. Similar considerations hold for the predicted F-mode PW relations. For FO pulsators, both PLC and PW relations are insensitive to variations in the efficiency of superadiabatic convection.

TABLE 4.3: PLC coefficients ($< G >$=a+blog P +c($< G_{BP} >$ - $< G_{RP} >$) for F and FO Galactic Cepheids derived by adopting A, B , C ML relations and $\alpha_{ml} = 1.5$, $\alpha_{ml} = 1.7$ and $\alpha_{ml} = 1.9$ in the *Gaia* filters.

α_{ml}	ML	a	b	c	σ_a	σ_b	σ_c	R^2
F								
1.5	A	-3.52	-3.78	3.19	0.04	0.03	0.06	0.998
1.5	B	-3.45	-3.76	3.27	0.03	0.03	0.06	0.998
1.5	C	-3.27	-3.71	3.18	0.03	0.02	0.05	0.998
1.7	A	-3.61	-3.94	3.42	0.09	0.06	0.15	0.999
1.7	B	-3.65	-3.91	3.62	0.08	0.06	0.14	0.998
1.7	C	-3.21	-3.69	3.09	0.06	0.04	0.11	0.998
1.9	A	-3.33	-3.92	3.05	0.12	0.05	0.19	0.999
1.9	B	-3.24	-3.93	3.14	0.07	0.01	0.12	0.999
1.9	C	-2.89	-3.81	2.81	0.03	0.02	0.06	0.999
FO								
1.5	A	-3.53	-3.95	2.48	0.04	0.02	0.06	0.999
1.5	B	-3.49	-3.96	2.63	0.06	0.04	0.11	0.999
1.5	C	-3.45	-3.97	2.80	0.08	0.07	0.16	0.999
1.7	A	-3.49	-3.90	2.38	0.06	0.03	0.11	0.999

TABLE 4.4: PW coefficients ($< W >=< G > -1.9 < G_{BP} - G_{RP} >= a + b \log P$) for F and FO Galactic Cepheids derived by adopting A, B , C ML relations and , $\alpha_{ml} = 1.5$, $\alpha_{ml} = 1.7$ and $\alpha_{ml} = 1.9$ in the *Gaia* filters.

α_{ml}	ML	a	b	σ_a	σ_b	R^2
F						
1.5	A	-2.73	-3.26	0.04	0.03	0.995
1.5	B	-2.68	-3.18	0.05	0.03	0.994
1.5	C	-2.56	-3.16	0.07	0.05	0.992
1.7	A	-2.75	-3.37	0.06	0.05	0.998
1.7	B	-2.68	-3.20	0.03	0.04	0.996
1.7	C	-2.54	-3.23	0.08	0.06	0.997
1.9	A	-2.64	-3.52	0.05	0.11	0.999
1.9	B	-2.55	-3.44	0.09	0.21	0.999
1.9	C	-2.51	-3.11	0.08	0.11	0.999
FO						
1.5	A	-3.17	-3.80	0.02	0.07	0.999
1.5	B	-3.02	-3.85	0.02	0.13	0.996
1.7	A	-3.24	-3.96	0.05	0.28	0.999

4.3 The comparison between theoretical and Gaia DR2 parallaxes

In this section, we perform a comparison between the individual theoretical parallaxes based on the PW relations[1] in the Gaia filters derived in the previous section and the observed classical F and FO Cepheid parallaxes taken from the recent catalog made by Ripepi et al. (2019) and based on Gaia DR2 results.
In their work, Ripepi et al. (2019) reclassify the DR2 Galactic Cepheids and provide accurate observable PL and PW relations in the Gaia passbands. To ensure a good astrometry, we chose from the sample, the classical F and FO Cepheids for which the G magnitude is brighter than 6 mag and the renormalized unit weight error values defined by Lindegren et al. (2018) is less than 1.4.
The theoretical PW relations derived in the previous section are applied to the observed periods, the Gaia magnitudes and colors reported in the quoted catalog, to derive reddening-free individual distances and, in turn, theoretical estimates of individual parallaxes.
The comparison between our theoretical parallax estimates and the Gaia DR2 ones is shown in Fig. 4.2. These plots show the predicted and Gaia DR2 parallax differences versus the Gaia DR2 parallaxes for the adopted assumptions concerning both the ML relation and the α_{ml} parameter (See labels in the plot). In each panel, the computed mean offset (solid line) is compared with the mean offset derived by Riess et al. (2018a) (dashed line) from the HST space astrometric technique, corresponding to $< \Delta\varpi >$=0.046$\pm$0.013 mas. This offset value is consistent, within the errors, with the value derived from our models, apart from a few cases at the brightest luminosity levels (See plot for F-mode case C in Fig. 4.2).
Quantifying such an offset and its dependence on the physical and numerical assumptions is crucial to understanding and trying to reduce the Hubble constant tension. In particular, we found that a systematic shift in the parallax of the order of $< \Delta\varpi > \pm 0.02$ mas at a typical parallax of the order of 0.5 mas implies a relative parallax error and, in turn, a relative distance error of 4%. This consequently affects the H_0 estimates; In fact, parallaxes which are 4% smaller imply longer distances and, in turn, smaller values of H_0 by 4%. A similar effect would be enough to significantly reduce, if not completely remove, the H_0 tension.

[1]The theoretical PLC relations are not adopted because they require a correction for the individual reddening of the observed Cepheid.

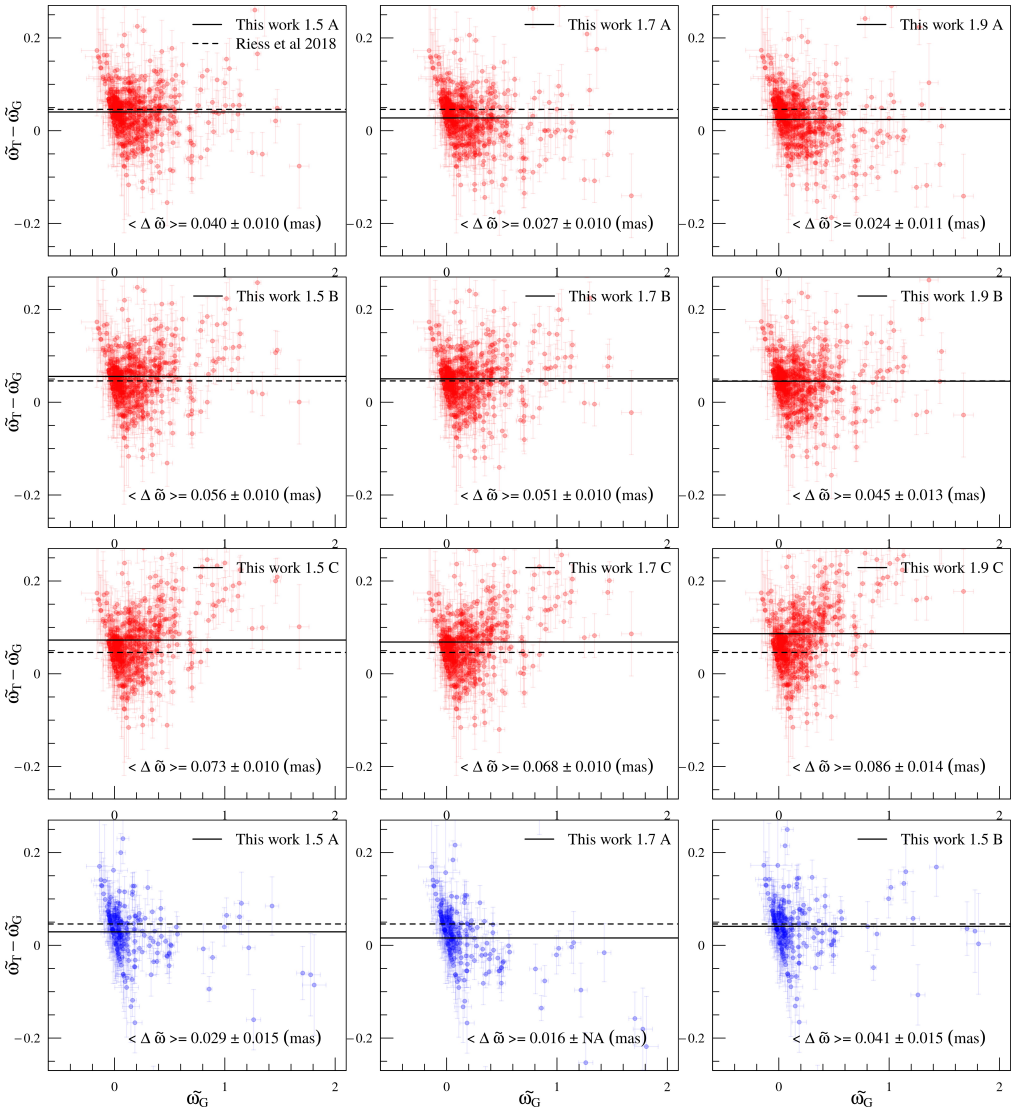

FIGURE 4.2: Parallax difference ϖ_T - ϖ_G for F (red points) and FO (blue points) Galactic Cepheids as a function of *Gaia DR2* parallax ϖ_G.

Chapter 5

The impact of the updated models for CC mass determinations

Deriving PL and PLC relations for CCs relies on the existence of the period-mean density relation (See Eq. 1.1) coupled with the Stefan-Boltzmann law (See Eq. 1.3) and the Mass-Luminosity relation predicted by stellar evolution models for central helium burning massive and intermediate-mass stars (see e.g. Bono et al., 1999a; Bono et al., 2000a; Chiosi et al., 1993).
This implies that any phenomenon affecting the CC ML relation also affects the coefficients of the resulting PL and PLC relations and, in turn, the associated distance scale.

Theoretical predictions about the ML relation as provided by stellar models are affected by both the physical inputs and assumptions adopted in stellar modeling. Any change in the adopted inputs, such as radiative opacity (see, e.g, the new study by Bailey et al., 2015, suggesting that opacity might be underestimated) and equation of state, impacts the size of the convective core during the core H-burning stage and, hence, the ML relation during the Cepheid stage. At the same time, different assumptions about, for instance, the amount of convective core overshooting and/or the rotational rate during the central H-burning stage, and/or mass loss during the RGB stage, do affect the CC ML relation.

As already discussed in Chapter 1, several theoretical investigations to derive Cepheid masses from stellar pulsation (see, e.g. Bono et al., 2001; Caputo et al., 2005a; Keller et al., 2006; Marconi et al., 2013b; Marconi et al., 2013a; Marconi et al., 2017; Ragosta et al., 2019, and references therein) suggest that noncanonical models do provide systematically lower masses than canonical ones. However, as the ML relation is brighter for noncanonical models, it also allows us to match dynamical stellar mass derivations for Cepheids in eclipsing binary systems (see e.g. Marconi et al., 2013b; Neilson et al., 2012; G. Pietrzyński et al., 2010; Grzegorz Pietrzyński et al., 2011; Prada Moroni et al., 2012).

Using our updated nonlinear convective pulsation models of Galactic Cepheids (see Chapter 3), in Chapter 4 we derived the PW relations varying both the ML relation and the efficiency of super-adiabatic convection. Then, we applied these relations to a selected sample of Gaia DR2 to constrain their individual distances and parallaxes and found that the results depend on the assumed mass luminosity relation.
In Marconi et al. (2020), we reversed the perspective and relied on Gaia DR2 (Gaia Collaboration et al., 2018; Gaia Collaboration et al., 2016b) parallaxes to constrain GCC individual masses through the inversion of predicted mass-dependent PW relations. To explain the approach adopted in Marconi et al. (2020), in this Chapter

TABLE 5.1: The coefficients of the PWM relation ($W = a + b \log P + c \log M/M_{\odot}$) predicted for the F and FO-mode GCC, varying the mixing length parameter. The last column represents the root-mean-square deviation (σ) coefficient.

α_{ml}	a	b	c	σ_a	σ_b	σ_c	σ
F							
1.5	-1.654	-2.419	-2.423	0.036	0.021	0.067	0.064
1.7	-1.686	-2.496	-2.285	0.040	0.026	0.082	0.058
FO							
1.5	-2.162	-3.068	-1.819	0.023	0.020	0.044	0.013
1.7	-2.205	-3.093	-1.765	0.032	0.027	0.062	0.008

we discuss the procedure to derive mass-dependent PW relations and the application of these relations to the sub-sample of Gaia Data Release 2 Galactic Cepheids investigated in Chapter 4.

5.1 The derived mass-dependent PW relations

In order to derive the individual masses for the sample of GCC with Gaia DR2 distances investigated in Chapter 4, we derived the mass-dependent Period-Wesenheit (hereinafter PWM) relations for the fundamental and first overtone mode models, by including models with different ML relations in the regression. The coefficients of the predicted relations for both F and FO-mode models are reported in Table 5.1 for the two assumptions of the efficiency of super-adiabatic convection, $\alpha_{ml} = 1.5$ and $\alpha_{ml} = 1.7$.
We noticed that a variation in the α_{ml} parameter does not significantly affect the coefficients of the PWM relations, in spite of significant effects on the amplitude and morphology of light curves (see Bhardwaj et al., 2017; De Somma et al., 2020b, for details). For this reason, to conduct our research we only considered model predictions for $\alpha_{ml} = 1.5$.

We notice that, for Cepheid samples at the same distance, such relations allow us to constrain the stellar mass distribution, whereas in the case of available individual distances, as with the Gaia database, the absolute individual mass values are directly determined.
In Fig 5.1 we plotted the derived F (green symbols) and FO (red symbols) model distribution in the $W - c \log M$ *vs* $\log P$ plane, superimposed on the projection of the inferred PWM relations.

5.2 Application to Gaia DR2 GCC sample

We decided to apply the PWM relations to the Gaia Cepheid sample compiled by Ripepi et al. (2019), just used in Chapter 4, and in turn, derive the individual mass estimates. The PWM relations were derived using the same period range as for the observed GCC selected from the sample by Ripepi et al. (2019).
In order to convert the observed Gaia parallaxes into distance moduli μ_{Gaia}, and then to correct apparent Wesenheit magnitudes, we selected only Cepheids in the Ripepi et al. (2019) sample with a relative error on Gaia DR2 parallax lower than 10% and positive mean parallax values.

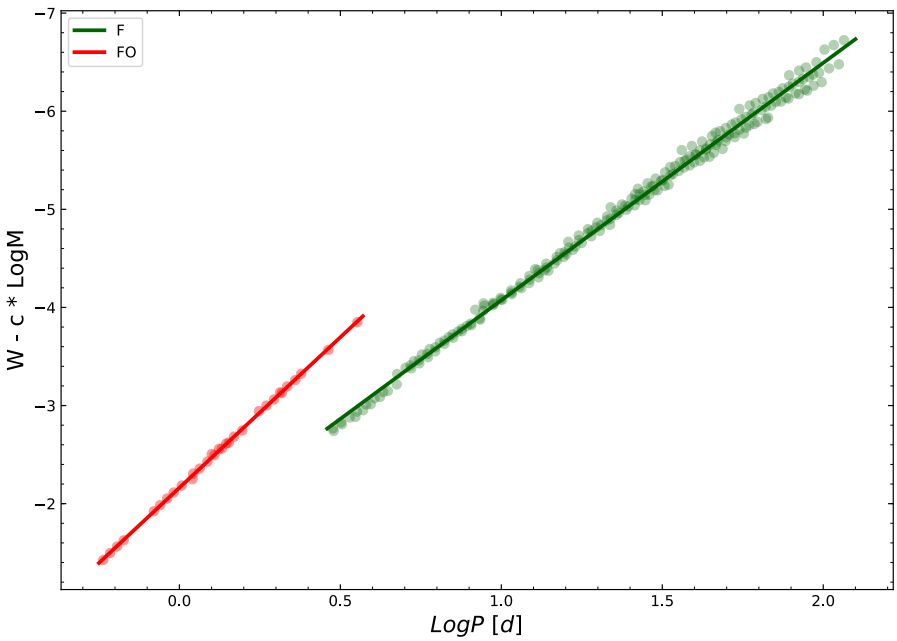

FIGURE 5.1: Projection of the inferred PWM relations for the F (green symbols) and FO (red symbols) model distributions in the $W - c \log M$ *vs* $\log P$ plane.

Table 5.2, from column 1 to 8 reports the Gaia source identification, the pulsation mode, the pulsation period, the mean apparent magnitudes in the Gaia filters, the measured parallax and the associated uncertainty of the selected GCC.
We used these observed properties to constrain the individual stellar masses, through the application of theoretical PWM relations.

5.2.1 The individual Cepheid mass estimate procedure

From the equation

$$W_{oss} - \mu_{Gaia} = W_{teo} = a + b \log P + c \log M/M_{\odot}$$

where W_{oss} is defined as

$$W_{oss} =< G > -1.9(< G_{BP} > - < G_{BR} >)$$

we were able to derive the stellar mass for each individual F and FO-mode pulsator. The inferred stellar masses with the associated errors[1], for the F and FO-mode models, are reported in columns 9 and 10 of Table 5.2.
The upper panel of Fig. 5.2 shows the derived mass distribution histograms for the selected F (green bars) and FO (red bars) Gaia DR2 GCC.
We notice that the selected GCC sample covers a relatively wide range of masses and

[1]The estimated errors take into account the uncertainty in the individual Gaia parallaxes, the intrinsic dispersion of the predicted PWM relations and the error of the estimated W_{oss} considering a mean photometric error of the Gaia mean magnitudes of the order of 0.02 mag.

TABLE 5.2: The individual masses estimated from the theoretical PWM relations combined with Gaia DR2 parallaxes, for the F and FO-mode GCCs in the selected sample. This table is available in its entirety in Section A.3 in Appendix A.

Gaia DR2 Source Id	Mode	P[d]	G[mag]	G_{BP}[mag]	G_{RP}[mag]	ϖ[mas]	$\sigma\,\varpi$[mas]	$M/M_{\odot}$	$\sigma M/M_{\odot}$	$M/M_{\odot}$ corr	$\sigma M/M_{\odot}$ corr
(1)	(2)	(3)	(4)	(5)	(6)	(7)	(8)	(9)	(10)	(11)	
1857884212378132096	F	4.43546	5.46	5.77	5.07	1.674	0.089	4.2	0.5	4.0	0.5
4066429066901946368	F	5.05787	6.82	7.37	6.23	1.119	0.053	5.2	0.6	4.8	0.5
5235910694044165760	F	3.08613	8.70	9.22	8.06	0.681	0.032	4.1	0.5	3.6	0.4
...	...	...	...	...	...	...	...	...	...		
5351436724362450304	FO	1.11936	11.09	11.62	10.41	0.389	0.030	3.3	0.7	2.4	0.5
2164475809937299584	FO	1.76585	10.18	10.74	9.49	0.343	0.027	7.6	1.7	5.4	1.2
5245796334347122944	FO	2.06344	8.09	8.53	7.54	0.858	0.026	3.5	0.4	3.0	0.3
...	...	...	...	...	...	...	...	...	...		

it peaks around $5.6 M_{\odot}$ and $5.4 M_{\odot}$ for the F and FO-mode pulsators, respectively. Interestingly enough, if the error on the measured parallaxes decreases, as expected in the next Gaia Data Releases, we would obtain a corresponding improvement in the precision of our mass determinations. In particular, a precision on parallaxes of the order of 1% would imply an error on the inferred stellar mass of the order of 2% and 3% in the case of the F and FO pulsators, respectively.

To take into account the Gaia DR2 Cepheid parallax offset corresponding to $< \Delta\varpi >$=0.046$\pm$ 0.013 mas and derived by Riess et al. (2018a) through a comparison with HST space scan astrometric determinations (see Riess et al., 2018a, for details), we performed our mass derivation procedure for the F and FO GCC again, by increasing the parallax values reported in Table 5.2 by $< \Delta\varpi >$=0.046 mas. The new estimated masses and the relative errors for the F and FO-mode pulsators are reported in the last two columns of the aforementioned Table. The obtained results are shown in the bottom panel of Fig. 5.2.

We notice that the parallax offset effect moves the peak of the distribution to lower masses, around 5.2 $M_{\odot}$ and 5.1 $M_{\odot}$, for the F and FO-mode, respectively. This occurrence is expected on the basis of the coefficients of the PWM relations. Indeed, an increase of the parallax implies a decrease in the distance modulus and, in turn, a fainter Wesenheit function, which implies a lower mass at a fixed period. For the same reason, if the applied offset were $< \Delta\varpi > = 0.046 + 0.013 = 0.059$ mas, the inferred masses would be, on average, smaller than the literature ones (see below), while if an offset $< \Delta\varpi > = 0.046 - 0.013 = 0.033$ mas were assumed, the inferred masses would become more discrepant from the literature ones with respect to Fig. 5.3

5.3 Comparison with independent results for Cepheids in binary systems

In the upper panel of Fig. 5.3 we show the behaviour of the theoretical masses derived with the PWM relations. The relations include the DR2 parallax offset, as a function of the pulsation period, for the F (filled circles) and FO-mode (open circles) GCCs. The plot also includes a comparison of our mass estimates with the position of the Cepheids in binary systems for which independent mass estimates are available in Kervella et al. (2019, red symbols) and Evans et al. (2011, and references therein, cyan symbols).

The general trend predicted by our theoretical scenario is in good agreement with the plotted data and with the more recent determination of V350 Sgr mass (5.2 $\pm$ 0.3 $M_{\odot}$) by Evans et al. (2018).

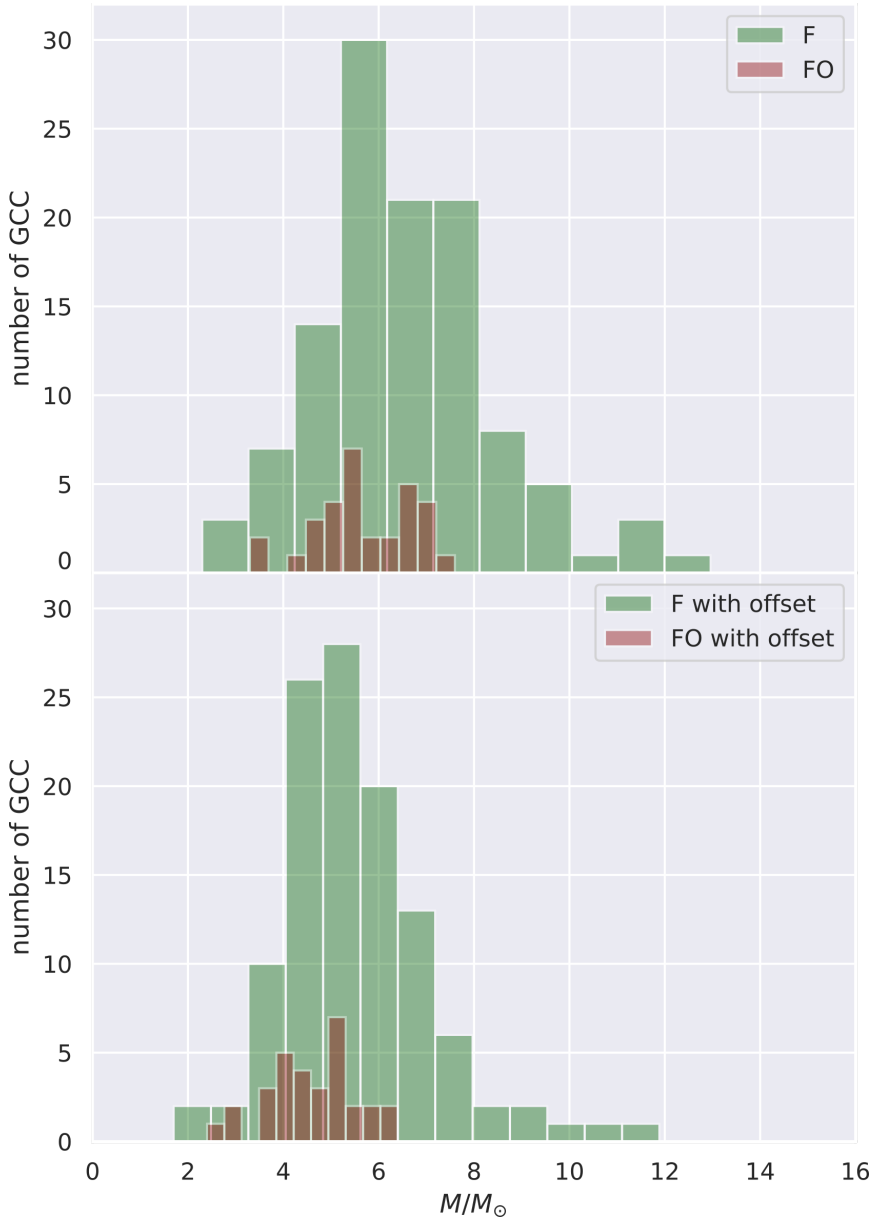

FIGURE 5.2: *Top panel: The predicted mass distribution of the F (green bars) and FO-mode (red bars) pulsators. Bottom panel: The same distribution as in the upper panel but obtained including the Gaia DR2 Cepheid parallax offset.*

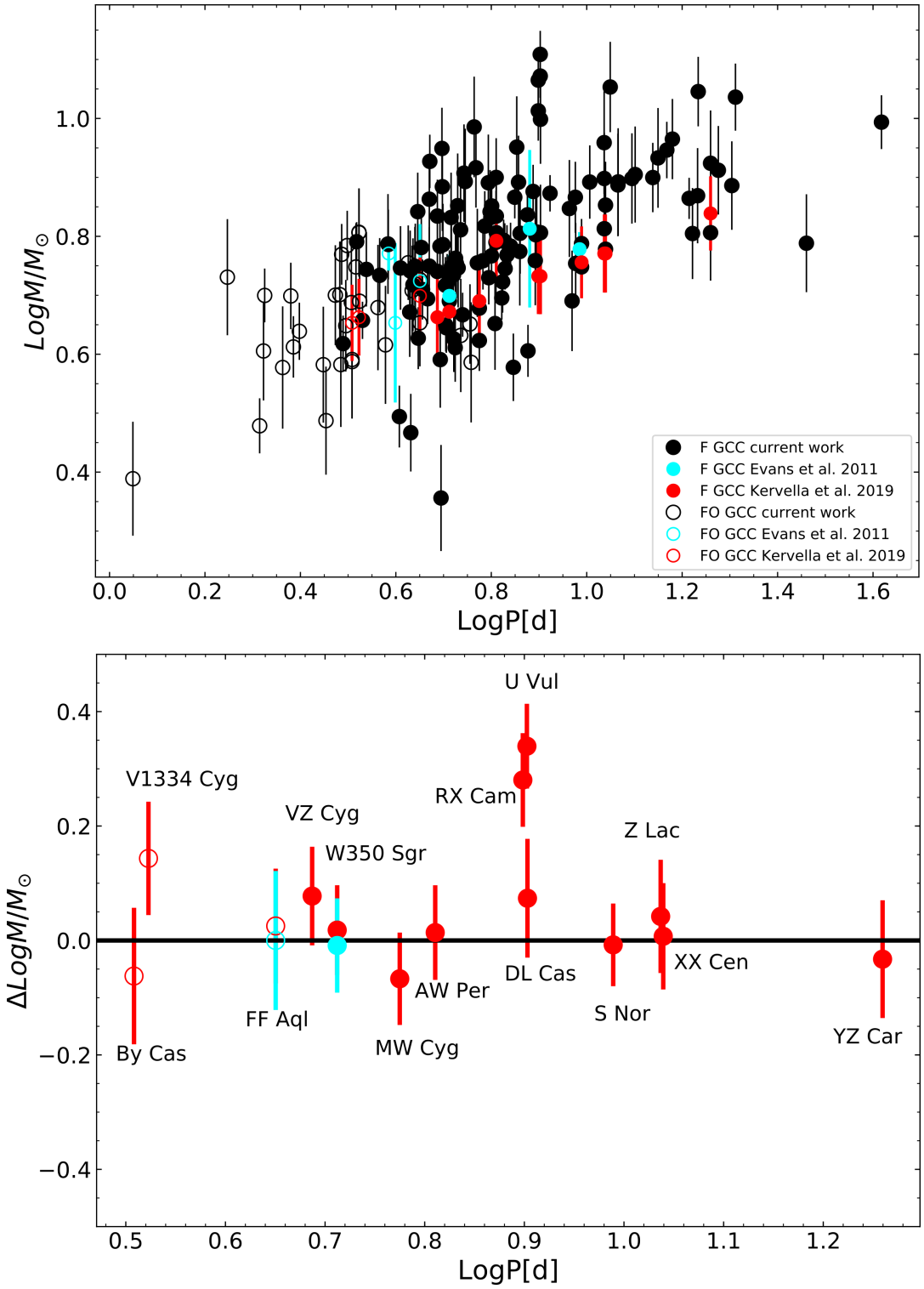

FIGURE 5.3: *Top panel:The predicted mass distribution of the F (filled circles) and FO (open circles) pulsators as a function of the pulsation period. Bottom panel: The difference between our results and the ones by Kervella et al. (2019, red symbols) and Evans et al. (2011, cyan symbols) for the Cepheids in common with the two data sets.*

To better quantify this agreement, in the lower panel we show the difference between our results and the ones by Kervella et al. (2019, red symbols) and Evans et al. (2011, cyan symbols) for the Cepheids in common with the two data sets. This plot confirms that we find a good agreement with the literature, for most of the stars with the exception of RX Cam and U Vul for the F-mode. We notice that these two stars also deviate by more than 1 σ from the empirical PW relation derived by Ripepi et al. (2019). For the FO V1334 Cyg, our estimate with the assumed offset and the result by Kervella et al. (2019) are quite different but still consistent within the errors. The same occurs when the more recent determination of V1334 Cyg ($4.288 \pm 0.133\ M_{\odot}$) by Gallenne et al. (2018) is taken into account.
We also verified that a worse agreement with literature mass values is obtained when no offset is applied to Gaia parallaxes.
Moreover, by forcing the coincidence, within the errors, of our "uncorrected" mass evaluations as reported in columns 9 and 10 of Table 5.2, with the literature determinations by Kervella et al. and Evans et al., reported in Fig. 5.3, we can derive an independent estimate of the offset that should be applied to Gaia DR2 parallaxes. In particular, by excluding RX Cam, U Vul and DL Cas, as well as V1334 Cyg, that deviate by more than 1 σ from the PW relations by Ripepi et al. (2019), we obtain a mean offset $< \Delta\varpi >= 0.053 \pm 0.029$ mas, where the uncertainty is the standard error of the mean. This result is slightly higher, but consistent within the errors, than the value obtained by Riess et al. (2018a).

The results shown in this Chapter suggest that a generally good agreement can be found between our mass determinations based on Gaia DR2 parallaxes combined with new derived theoretical PWM relations and the independent mass values obtained for Cepheids in binary systems in the literature. This occurrence supports the accuracy of the current theoretical scenario and at the same time paves the way for future applications. In particular, we plan to apply the same theoretical tool to the next, more accurate, Gaia Data Releases in order to reduce the percentage error in mass determinations with relevant implications for our knowledge of both the present mass function and the ML relation of intermediate-massive He-burning stars in the Milky Way. Moreover, by extending the PWM relation to other bands (including LSST Vera Rubin filters) and chemical compositions, we will be able to: i) infer the mass distributions of Cepheid samples in the Local Group for which accurate distances e.g. LSST astrometric distances, will become available; ii) to constrain the coefficients of chemical abundances in theoretical Cepheid ML relations; iii) to predict the implications for the dependence of Cepheid properties and distance scale on the chemical composition. Our results were consistent with our expectations that the PWM relation would depend on metallicity because as metallicity decreases, the theoretical quantity Mag-1.9*color is expected to get slightly fainter than in the solar case, according to previous results (see e.g. Fig. 9 in Caputo et al., 2000c). Moreover, preliminary tests in the optical bands, based on the previously quoted computed models, suggest that the mass dependence of the PWM relation is reduced in lower metallicity model sets, with the effect of predicting systematically higher masses at a fixed distance and period.

Chapter 6

Galactic Classical Cepheids as age indicators in the Gaia Era

Classical Cepheids are excellent tracers of relatively young (from a few tens to a few hundreds of Myr) stellar populations.
As already mentioned in the previous Chapters, according to stellar evolution, CCs obey a ML relation that is dependent on chemical composition and the efficiency of a number of noncanonical physical processes, such as rotation and core convective overshooting during the core hydrogen burning-phase, and mass-loss efficiency during (mainly) the red giant branch stage (see, e.g. Catelan et al., 2015a; Salaris et al., 2006, and references therein).
By combining the existence of the ML relation for CCs with the well known PL relation and the anti-correlation between mass and age, we can easily conclude that if CCs obey a PL relation, they also have to obey a period-age (PA) relation.
In particular, if the period increases, the luminosity and the mass also increase according to the PL and ML relations, while the Cepheid age decreases (See Fig. 6.1).

The existence of a PA relation has been extensively investigated in the literature from both the observational and theoretical point of view (see, e.g. Anderson et al., 2016; I. N. Efremov, 1978; Y. N. Efremov et al., 1998; Yu. N. Efremov, 2003; Grebel et al., 1998; Inno et al., 2015; Magnier et al., 1997; Senchyna et al., 2015), with most of the applications related to cluster pulsators both in the Milky Way and in other Local Group galaxies, such as M31 and the Magellanic Clouds, for which independent age estimates were available (see Bono et al., 2005; Yu. N. Efremov, 2003; Marconi et al., 2006, and references therein).
However, Cepheid-based ages are more promising than age estimates based on, for instance, isochrone fitting on the cluster CMD. This is because they only rely on the pulsation period, which can be measured with a high accuracy and is not affected by uncertainties in reddening, distance, and photometric calibration.
In addition, the PA relation is also suitable for application to field pulsators and, hence, accurate relative[1] age estimates, based on this method, can provide strong constraints on the existence of population age gradients in the various Galactic fields[2].

In this Chapter we will discuss the combination of the most updated evolutionary predictions with our pulsation model predictions for a solar chemical abundance pattern ($Z = 0.02$, $Y = 0.28$), described in Chapter 3, to interpret the properties of GCCs in the Gaia Data Release 2.

[1] It is worth noting that relative age estimates are more robust than absolute age determinations, being less affected by systematic uncertainties affecting stellar models.

[2] In this context, we emphasized that the number of CCs in the Galactic field is quite larger than in star clusters.

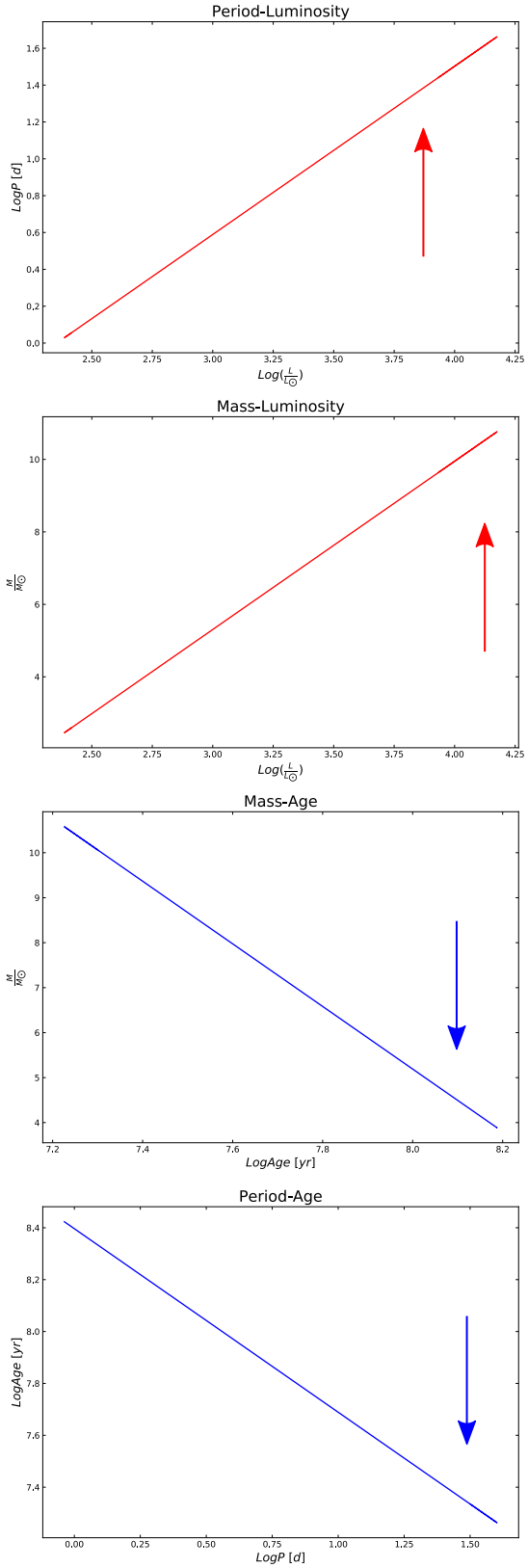

FIGURE 6.1: From the top panel to the bottom panel, the period luminosity, mass-luminosity, mass-age and period age relations are shown, highlighting a correlation in the period-luminosity and mass-luminosity plots as well as an anticorrelation in the mass-age and period-age plots.

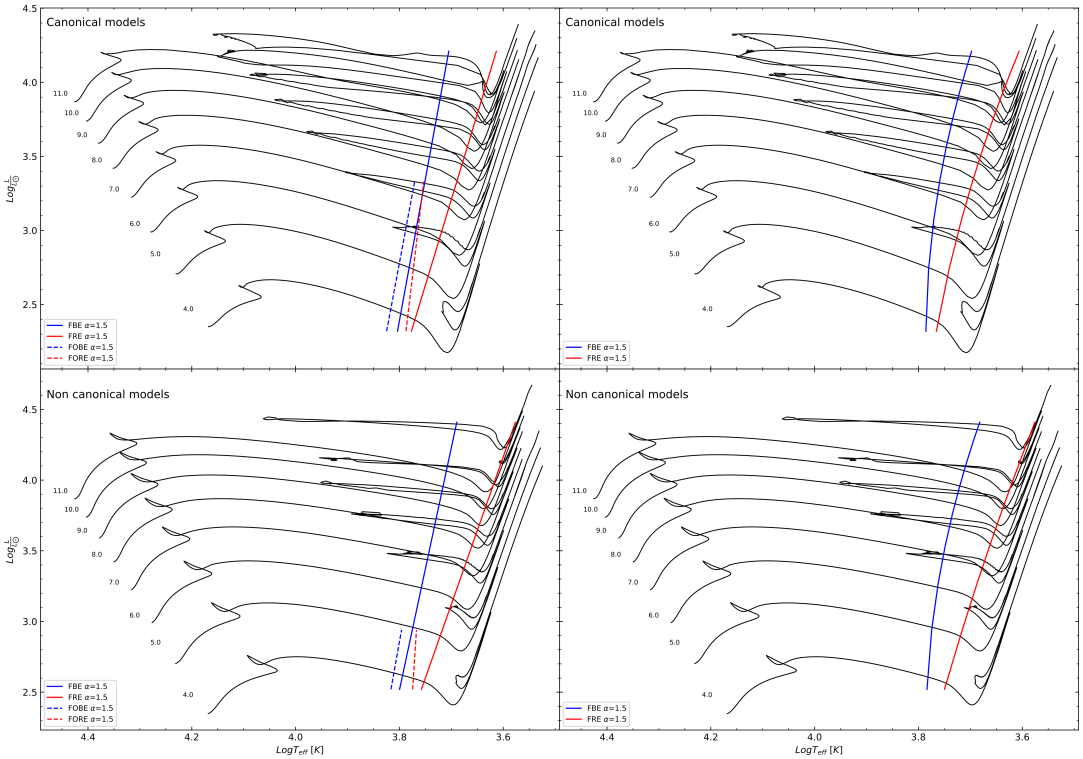

FIGURE 6.2: The location in the HR diagram of selected massive and intermediate-mass stellar models for the adopted solar chemical composition, compared with the predicted linear IS boundaries (*left panels*) and quadratic IS boundaries (*right panels*) of radial F (solid lines) and FO-mode pulsators (dashed lines) obtained for the canonical *(top panels)* and noncanonical ML relations *(bottom panels)*, assuming α_{ml} = 1.5.

6.1 The adopted theoretical framework for Galactic Classical Cepheids

In this section we will discuss the GCC theoretical scenario adopted to derive reliable and accurate period–age and the first theoretical period–age–color relations in the Gaia bands.

6.1.1 The evolutionary framework

Our previous works on the theoretical PA relationship (see, Bono et al., 2005; Marconi et al., 2006) were based on the theoretical evolutionary framework developed by Pietrinferni et al., 2004, named the BaSTI library.
However, since the first release of the BaSTI library, several improvements to the stellar physics inputs, some revisions of the solar metal distribution, and corresponding revisions of the solar metallicity (we refer to, e.g. Bergemann et al., 2014, and references therein for a detailed discussion on this issue) have become available.
Therefore, the BaSTI library has been recently updated. This version, known as the BaSTI-IAC version,[3], takes into account all the presently available updates and improvements in the input physics.
The new complete library for a scaled solar chemical mixture has been provided in Hidalgo et al., 2018. It is important to briefly discuss the main differences between the BaSTI-IAC models adopted in our work and BaSTI predictions accounted for in Bono et al., 2005 and Marconi et al., 2006.

One of the main differences is associated with the use of different reference solar heavy element distributions. The previous BaSTI models were based on the solar mixture provided by Grevesse et al., 1998. The new ones take into account the recent, significant revisions of the solar metal distributions, and rely on measurements provided by Caffau et al., 2011, supplemented when necessary by the abundance estimates provided by Lodders, 2010.

The treatment of overshooting beyond the Schwarzschild boundary of convective cores during the H-burning stage, is included as an instantaneous mixing between the formal convective border and layers at a distance $\lambda_{ov} H_P$ from this boundary – keeping the radiative temperature gradient in this overshooting region. H_P is the pressure scale height at the Schwarzschild boundary, and λ_{ov} is a free parameter that is set to 0.2 in the BaSTI-IAC model computations and decreased to zero when the mass decreases below a certain value[4] (typically, equal to $\sim 1.5 M_{\odot}$). Like the previous BaSTI library, the new BaSTI-IAC library provides two complete sets of evolutionary models alternately accounting (noncanonical models) or not accounting at all (canonical models) for core convective overshooting.

The mass loss phenomenon is accounted for by using the Reimers, 1975 formula, with the free parameter η - present in this mass loss prescription - set to zero when neglecting mass loss, or to η=0.3 when mass loss is accounted for (see Hidalgo et al., 2018, for the discussion about this choice).

The treatment of superadiabatic convection is based on the Böhm-Vitense, 1958 flavor of the mixing length theory, using the formalism by J. P. Cox et al., 1968. The value of the mixing length free parameter, fixed via the standard solar model (SSM)

[3]The whole BaSTI-IAC library is available at the following URL: http://basti-iac.oa-abruzzo.inaf.it

[4]See Hidalgo et al., 2018 for a discussion about the need to decrease the core convective overshooting with the mass as well as the procedure adopted for reducing the value of λ_{ov} below a given critical mass.

calibration[5], to α_{ml} = 2.006, was kept constant for all stellar masses, initial chemical compositions and evolutionary phases.

As mentioned, the calibration of the SSM sets the value of α_{ml}, and the initial solar He abundance $Y_{\odot}$ and metallicity $Z_{\odot}$. The BaSTI-IAC SSM, properly accounting for atomic diffusion of both He and metals, matches the empirical solar constraints with the following initial abundances $Z_{\odot}$=0.01721 and $Y_{\odot}$=0.2695.

To conduct our analysis, we selected the stellar models with a solar chemical composition and mass range between $4M_{\odot}$ and $11M_{\odot}$, with a step of $0.5M_{\odot}$.

6.1.2 The pulsation framework

For the purpose of our work, we considered some of the pulsation models included in the updated data set of nonlinear and convective pulsation models described in detail in Chapter 3.
In particular, we considered only models with both an ML relation corresponding to either *case A* and *B*, and an efficiency of convection in the outer layers of either α_{ml} =1.5 or α_{ml} =1.7. The reasons for not considering the brightest models and the highest α_{ml} value were related to the need for consistency with the adopted evolutionary scenario which does not predict overluminosities as high as +0.4 dex with respect to the canonical ML, and the small number of pulsating models we obtained for α_{ml} =1.9 (see De Somma et al., 2020b, for detail).

We noted that, despite the improvements in the physical framework adopted for the BaSTI-IAC stellar model computation, the ML relationship predicted by the solar chemical composition, canonical (no overshooting) models were in quite good agreement with the the canonical ML relation adopted to build the Cepheid pulsation models (Bono et al., 2000a). At the same time, the increase of the brightness in the ML relation by $\Delta \log(L/L_{\odot})$= 0.2 at a given stellar mass to simulate the effect of noncanonical processes was consistent with the brightness increase of the ML relation predicted by the noncanonical, BaSTI-IAC models with respect to the corresponding canonical ones (See Hidalgo et al., 2018, for a detailed comparison between the various model libraries). These considerations allowed us to safely rely on the ML prescriptions created for developing the pulsational scenario adopted for our aim.

Fig. 6.2 shows the location in the HR diagram of the linear (left panels) and quadratic (right panels) fits of the IS boundaries with respect to the already discussed evolutionary tracks. For clarity, only a subsample of stellar evolutionary tracks was plotted. Inspection of this figure suggested that stellar models with masses lower than about $5M_{\odot}$, cross the predicted IS only once (first crossing) while evolving towards the Red Giant Branch. However, stars with masses higher than $\sim 5M_{\odot}$ show three crossings with the second and the third crossings corresponding to the blue-ward and red-ward evolution along the blue loop, respectively.

As expected on the basis of evolutionary considerations, the time spent during the first crossing is significantly shorter than the second and the third ones. For example, in the case of a $6M_{\odot}$ star, the time spent inside the instability strip varies from $7.41 \cdot 10^3 yr$ for the 1^{th} crossing to $3.73 \cdot 10^5 yr$ for the 2^{nd} and $1.80 \cdot 10^5 yr$ for the 3^{rd} one; while for a $11M_{\odot}$ model the corresponding evolutionary lifetimes are $2.87 \cdot 10^3$ yr for the 1^{th} crossing, and $3.16 \cdot 10^4 yr$ and $1.41 \cdot 10^4 yr$ for the 2^{nd} and 3^{rd} crossings, respectively.

[5]The adopted procedure and the properties of the BaSTI-IAC SSM are fully described in Hidalgo et al., 2018.

To discuss the reliability of evolutionary predictions about the blue loop morphology (and extension), it is worth mentioning that the physics behind the existence of blue loops challenged our understanding of stellar evolution for long time. As such, it is still a difficult task to predict the response of an intermediate-mass stellar model, during this phase, to changes in the physical parameters and/or the physical assumptions adopted in the evolutionary computations. Indeed, both the morphology, and the actual occurrence of the blue loops have a highly non-linear dependence on the physical inputs and assumptions adopted in the stellar evolution models. Even minor changes, for example, in the chemical composition, the initial mass and the efficiency of the mixing processes - such as convective core and envelope overshooting - can have a huge impact on the blue loop properties (see, e.g., Renzini et al., 1992; Salaris et al., 2006, and references therein for a detailed discussion on this topic).

6.2 The updated theoretical period-age and period-age-color relations

In order to derive theoretical PA relations, we combined the evolutionary tracks with the predicted instability strips and pulsation periods inferred from the pulsation models computed in De Somma et al. (2020b).

At first, we adopted two different sub-samples: one including all the crossings and the other including only the second and third crossings. However, since we verified that the resulting PA relations are not significantly affected by the choice of sub-sample, we only considered the relations obtained including all the crossings[6]. Incidentally, we noted that this choice is also consistent with the methodological approach adopted by Bono et al. (2005) and Marconi et al. (2006) to derive the PA relationship.

Adopting the PMLT relation, $\log P = \mathrm{a} + \mathrm{b}\log T_{eff} + \mathrm{c}\log M/M_{\odot} + \mathrm{d}\log(\mathrm{L}/L_{\odot})$, derived by our team (De Somma et al., 2020b) and described in subsection 3.2.2 of Chapter 3, we were able to predict the period for each combination of mass, luminosity and effective temperature along the selected portions of the evolutionary tracks. By combining the period estimate with the age predicted by the evolutionary models, we derived the theoretical PA relations through a linear regression procedure. The coefficients obtained for each combination of ML and convective efficiency, assuming both linear and quadratic fits to the F boundaries, are reported in Tables 6.1 and 6.2, respectively. We noticed that, in the FO-mode case, due to the limited number of models, only the PA relations based on linear boundaries were obtained.

Fig. 6.3 shows a comparison between the predicted PA relations for F pulsators with α_{ml} =1.5 and α_{ml} =1.7, in *case A* (canonical ML relation) using both the quadratic (right panel) and the linear (left panel) boundary analytical relations.

The data shown in this figure reveals that the PA relation is largely unaffected by the exact value of the mixing length parameter adopted in the pulsation model computations; therefore, one can safely assume that the predicted Cepheid ages are barely affected by the lingering uncertainties in the adopted mixing length parameter.

[6] As discussed at the end of the previous section, this occurrence is due to the fact that the time spent in the IS during the first crossing is a small fraction of the time spent inside the IS during the blue loop evolutionary stage.

Fig. 6.4 shows the same kind of comparison but varying the ML relation at a fixed α_{ml} =1.5. In this case, we noticed that brighter ML relations provide systematically older ages. This result is consistent with the theoretical prediction of a longer core hydrogen burning stage for stellar models, accounting for core convective overshooting being the ones that have been combined with our *case B* pulsation models; an occurrence obviously due to the larger amount of fuel available during the central H-burning stage. In particular, the age difference between *case B* and *A* ranges from $\sim$ 36 % at log P=0.4 to $\sim$ 60 % at log P=1.8. We noticed that the period range in these figures is the same as that estimated by De Somma et al. (2020b) (refer to the quoted reference for more detail) for *cases A* and *B* models. Since we found that the relations obtained using linear and quadratic F boundaries were perfectly consistent within the errors, we continued our work only relying on the relations obtained assuming the IS boundaries are linear.

Moreover, we compared our theoretical PA relations (dashed blue line) obtained for both case A ML (left-hand panels) and case B ML (right-hand panels), assuming α_{ml} = 1.5 for both cases, with other theoretical relations available in the literature. We selected a common period range for both *case A* (from log P = 0.4 to log P = 1.8) and *B* (from log P = 0.4 to log P = 1.6).

For the canonical case (left panels), we compared our *case A* relations with: i) the theoretical PA relation published by Bono et al. (2005) (dotted yellow line) and ii) the semi-empirical PA relations derived by Tsvetkov (1980) for the second (dashed red line) and third crossings (dash-dotted green line), respectively.
For the noncanonical case (right panels), we compared our *case B* relations with: i) the theoretical PA relations derived by Anderson et al. (2016) assuming a mild rotation efficiency, for the second (cyan star marker) and third crossings (green square marker), respectively; ii) the semi-empirical PA relations by Senchyna et al. (2015) based on both M31 Cepheids (dash-dotted orange line) and M31 cluster isochrone fitting (solid magenta line); iii) the semi-empirical relation provided by Magnier et al. (1997) (brown triangle marker) and iv) the empirical relationship by Yu. N. Efremov (2003) (red dot marker).

Fig. 6.6 shows the same kind of comparison but for *case A* FO-mode models with α_{ml} =1.5 and the FO relation by Bono et al. (2005).

The coefficients of the various PA relations used for the comparison are summarized in Table 6.3.

Inspection of the bottom panels of Fig. 6.5 and 6.6 suggests a very good agreement, within the errors, between our canonical PA relations and the one previously derived by Bono et al. (2005) on the basis of a less extended and updated set of models and a slightly different ML relation. No error estimate was provided by Anderson et al. (2016), Yu. N. Efremov (2003) and Magnier et al. (1997) but we found a good agreement between their (noncanonical) relations and our case B.

In order to better quantify the level of agreement among the various PA relationships, the two upper panels in Fig. 6.5 show the relative age difference between the relations obtained in the present work and the ones selected from the literature for both the canonical and noncanonical ML cases. For the canonical case, the present PA relation predicts ages systematically larger than the other relations with a maximum difference of the order of $\sim 15-20\%$. The smallest difference is found when considering the PA relation provided by Bono et al. (2005), while the maximum discrepancy is obtained when comparing the present result with the relation obtained by Tsvetkov (1980) for the third crossing. In this case the percentage difference can

TABLE 6.1: The coefficients of the F and FO-mode PA relations in the form $\log t = a + b \log P$, assuming linear IS boundaries and adopting both *case A* and *B* ML relations and α_{ml} =1.5 and α_{ml} =1.7. The last two columns represent the R-squared (R^2) and the root-mean-square deviation (σ) coefficients.

Fundamental mode							
α_{ml}	ML	a	b	σ_a	σ_b	R^2	σ
1.5	A	8.393	-0.704	0.008	0.009	0.916	0.084
1.7	A	8.369	-0.680	0.015	0.017	0.908	0.080
1.5	B	8.480	-0.626	0.010	0.009	0.866	0.080
1.7	B	8.460	-0.618	0.013	0.010	0.852	0.090
First overtone mode							
1.5	A	8.120	-0.396	0.020	0.057	0.506	0.052

also reach a value as large as $\sim$ 50% and it is likely related to the difference in luminosity between the second and the third crossings in spite of the quite similar evolutionary times.

For the noncanonical case, apart from the case of the PA relation, the relative age differences are within $\sim 15 - 20\%$, based on Cepheids in M31 provided by Senchyna et al. (2015), who predicts ages about 25% smaller than those provided by our relation. However, we wish to emphasize the large uncertainty associated with the Senchyna et al. (2015) Cepheid-based PA relationship. For the case of FO PA relations, the agreement is remarkably good; there is a difference of about 5% between present predictions and those obtained using the Bono et al. (2005) relation, but this is well within the errors.

The general good agreement among the various PA relations based on similar ML relations, as well as the age difference obtained when comparing the results based on canonical and noncanonical stellar models support the idea that different assumptions about noncanonical physical processes, e.g., moderate rotation as in Anderson et al. (2016), and mild overshooting as in the other semi-empirical relations, have the same effect of producing a brighter luminosity at a fixed mass, and in turn, an older age at a fixed period.

PA relations have the advantage of allowing a direct evaluation of CC ages when only the pulsation periods are known, however they suffer from the limitation related to the finite color width of the IS, which causes, mostly in the optical photometric passband, an inherent dispersion of PL relations. This occurrence implies that PA relations are also affected by an intrinsic scatter within a range for both colors and periods for each fixed age; an effect that can be removed if a color term is included in the linear regression procedure.

As our main goal was to derive the individual ages of GCCs with Gaia DR2 parallaxes, we used the Gaia band model light curves and the resulting mean magnitudes $< G_{BP} >$ and $< G_{RP} >$ discussed in chapter 4, to compute the first period-age-color (PAC) relations in the Gaia filters. The coefficients of the derived PAC relations, for the F and FO-mode models and the discussed assumptions concerning ML and α_{ml}, are presented in Table 6.4 .

In Fig. 6.7, we compare the projections onto a plane of the PAC relations varying the assumptions on α_{ml} and the ML relations. As already found for the PA relations, a change in the super adiabatic convection efficiency does not affect the ages predicted from the new derived theoretical PAC relations. As a consequence, we only adopt the PAC relation obtained for α_{ml} =1.5.

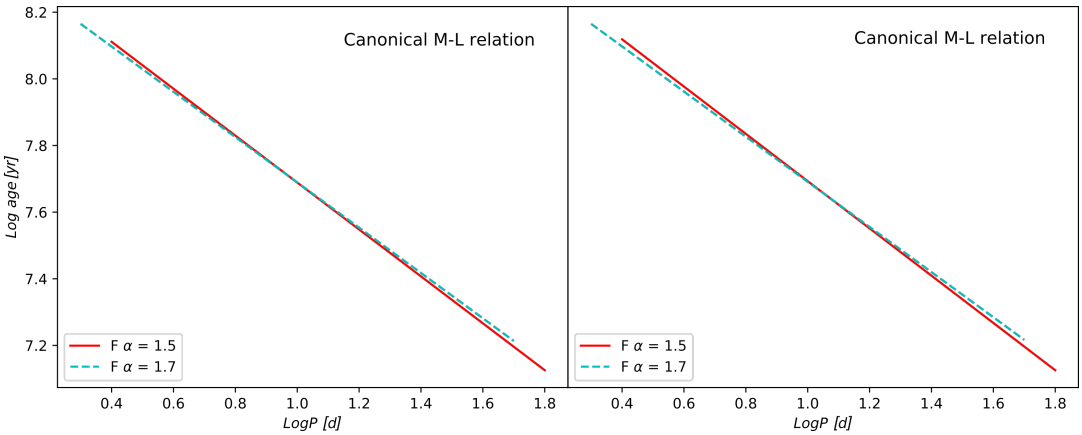

FIGURE 6.3: Canonical PA relations for various assumptions about superadiabatic convective efficiency, assuming linear *(left panel) and quadratic (right panel)* analytical relations for the IS boundaries.

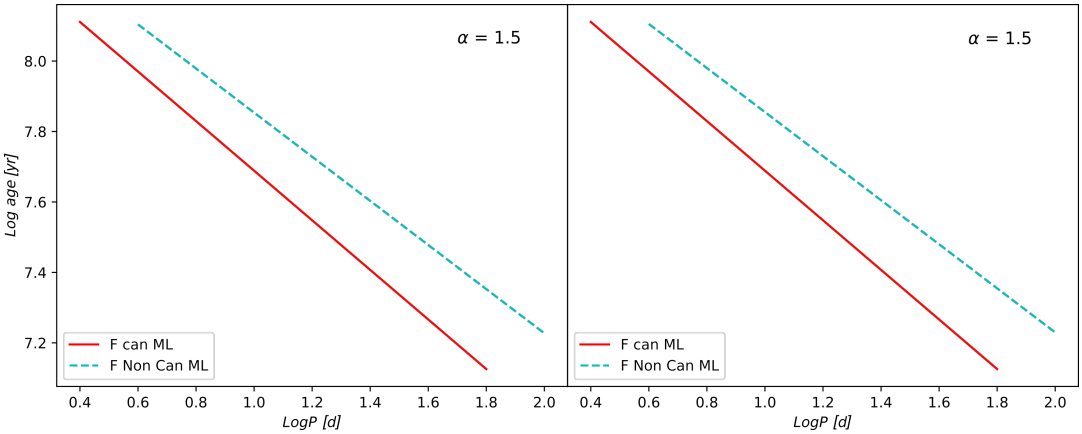

FIGURE 6.4: Fundamental PA relations at a fixed mixing length parameter α_{ml} =1.5 for the two assumed ML relations, using linear *(left panel)* and quadratic *(right panel)* IS boundary analytical relations.

TABLE 6.2: The coefficients of the F-mode PA relation $\log t = a + b \log P$, assuming quadratic IS boundaries and adopting both *case A* and *B* ML relations and α_{ml} =1.5 and α_{ml} =1.7. The last two columns represent the R-squared (R^2) and the root-mean-square deviation (σ) coefficients.

Fundamental mode							
α_{ml}	ML	a	b	σ_a	σ_b	R^2	σ
1.5	A	8.396	-0.708	0.007	0.009	0.910	0.083
1.7	A	8.362	-0.676	0.014	0.017	0.898	0.084
1.5	B	8.511	-0.660	0.010	0.009	0.856	0.090
1.7	B	8.477	-0.639	0.013	0.010	0.847	0.099

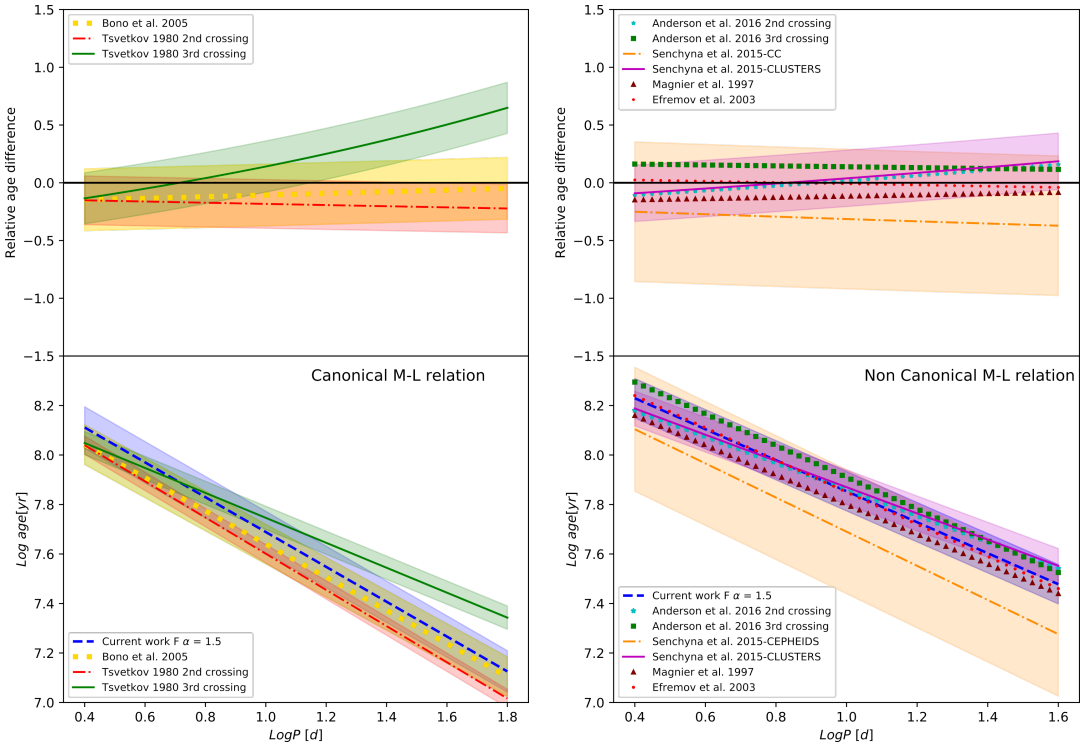

FIGURE 6.5: *Bottom panels*: comparison between present F-mode PA relations (dashed blue line), obtained by varying the adopted ML relation (see labels) at a fixed value of the mixing length (α_{ml}), and similar predictions from the literature. The dashed red line and dash-dotted green line show the PA relations by Tsvetkov (1980), for the second and third crossings, respectively. The dotted yellow line shows the PA relation obtained by Bono et al. (2005). The relations marked with stars and squares represent the PA relations by Anderson et al. (2016), for the second and third crossings, respectively. The dash-dotted orange line refers to the PA relation by Senchyna et al. (2015) for M31 CCs. The solid magenta line is the PA relation by Senchyna et al. (2015) for M31 clusters. Filled circles and triangles correspond to the PA relations by Yu. N. Efremov (2003) and Magnier et al. (1997), respectively. The colored shaded areas represent the 1σ errors in these relationships as provided by the authors. *Upper panels*: the relative age difference between the age predictions obtained by present PA relations for the canonical case *(left panel)* and the noncanonical one *(right panel)* and those obtained with the mentioned PA relationships taken from literature.

TABLE 6.3: The PA relations $\log t = a + b \log P$ derived by various authors for different CC samples. σ is the predicted root-mean-square deviation coefficient.

Authors	Source	a	b	σ
Anderson et al. (2016)	F GCC 2nd crossing	8.393	- 0.532	
Anderson et al. (2016)	F GCC 3rd crossing	8.551	-0.641	
Bono et al. (2005)	F GCC	8.31	-0.67	0.08
Bono et al. (2005)	FO GCC	8.08	-0.39	0.04
Yu. N. Efremov (2003)	LMC bar CC	8.50	-0.65	
Magnier et al. (1997)	M31 CC	8.4	-0.6	
Senchyna et al. (2015)	M31 CLUSTERS	8.40	-0.53	0.07
Senchyna et al. (2015)	M31 CC	8.38	-0.69	0.25
Tsvetkov (1980)	F GCC 2nd crossing	8.332	-0.731	0.037
Tsvetkov (1980)	F GCC 3rd crossing	8.250	-0.504	0.047

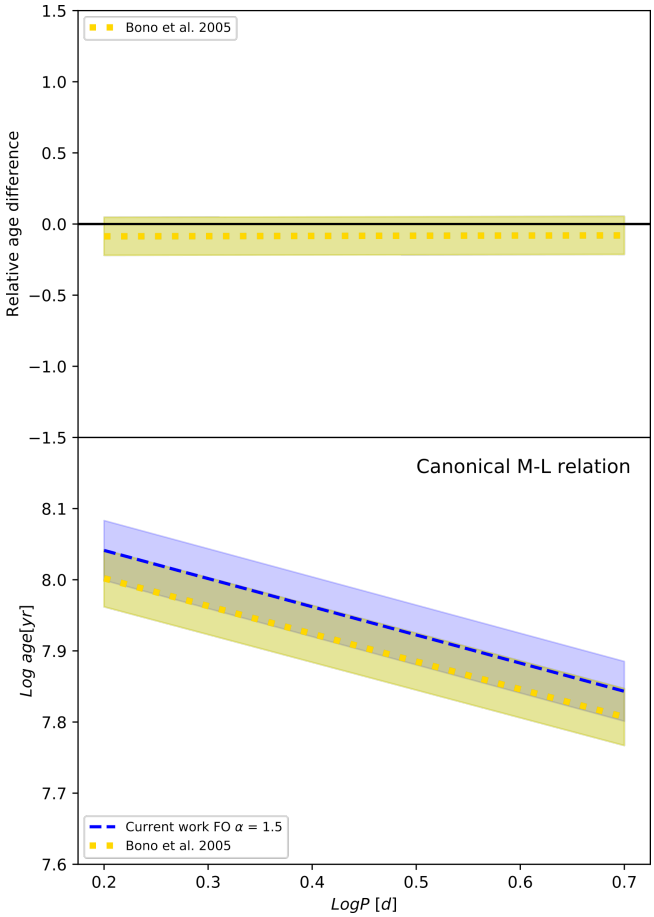

FIGURE 6.6: *Bottom panel*: comparison between present FO-mode PA relation (dashed blue line) obtained for ML case A and α_{ml} =1.5, with the theoretical FO-mode GCC PA relation obtained by Bono et al. (2005) (dotted yellow line). *Upper panel*: the relative difference between the age estimates provided by these PA relations.

TABLE 6.4: The coefficients of the PAC relation: $\log t = a + b \log P + c$ ($< G_{BP} >$ - $< G_{RP} >$) for F and FO pulsators, derived by varying both the ML relation and mixing length value.

Fundamental mode									
α_{ml}	ML	a	b	c	σ_a	σ_b	σ_c	R^2	σ
1.5	A	8.303	-0.751	0.121	0.045	0.025	0.060	0.916	0.083
1.7	A	8.346	-0.720	0.077	0.109	0.062	0.156	0.934	0.046
1.5	B	8.275	-0.734	0.278	0.029	0.017	0.037	0.876	0.077
1.7	B	8.453	-0.624	0.012	0.030	0.026	0.047	0.852	0.090
First overtone mode									
1.5	A	7.961	-0.508	0.255	0.137	0.064	0.204	0.603	0.046

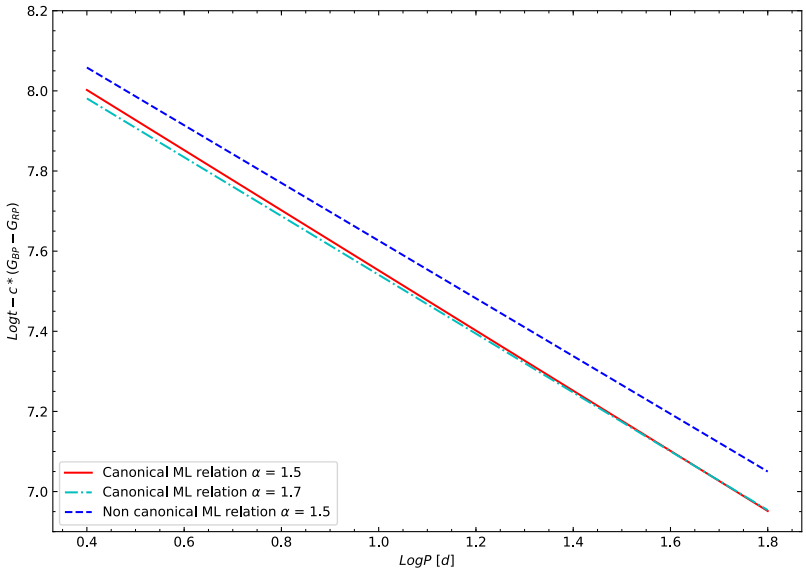

FIGURE 6.7: Projection onto a plane of the new Gaia band PAC relation (red solid line) for F-mode models obtained by adopting case A ML and α_{ml} =1.5; for comparison with either the same relation obtained by varying the super adiabatic convective efficiency (dash-dotted cyan line) or the ML relation (dashed blue line), is also shown.

6.3 Application to Gaia DR2 GCC sample

In this section we apply the theoretical PA and *Gaia*-band PAC relations derived above to a sample of GCCs published in *Gaia* DR2 (Gaia Collaboration et al., 2018) and reclassified by Ripepi et al. (2019).

The selected sample consists of 568 F-mode and 198 FO-mode pulsators. Using the period and color values reported by Ripepi et al. (2019) and both the PA and PAC relations, we derived the individual ages for each adopted assumption of the ML relation. Before applying the PAC relation, it is mandatory to obtain dereddened $(G_{BP} - G_{RP})$ colors for the selected GCC sample. For 320 objects in our sample we adopted the E(B-V) estimates available in the compilation by M. A. T. Groenewegen (2018). For all other stars, the CC period-$(V-I)_0$ color relation obtained by Ripepi et al. (in preparation) was used to derive the intrinsic unreddened color.

The (V-I) color estimate, averaged over the pulsation cycle, was obtained for 89 objects from the catalog of the OGLE Galactic Disk survey (Udalski et al., 2018). While for all other stars,[7] the averaged *Gaia* DR2 $(G_{BP} - G_{RP})$ color was transformed into the corresponding (V-I) one by using a conversion formula, suitable for the color range spanned by GCC, derived by Ripepi et al. (in preparation). These E(V-I) values were initially converted into E(B-V) by adopting the relation E(B-V)=1.283·E(V-I) (Tammann et al., 2003), and then into E$(G_{BP} - G_{RP})$ by means of Eq. 9-10 in Ripepi et al. (2019). The average errors of the E(B-V) estimates are ∼0.08 mag and ∼ 0.11 mag, for the (V-I) color estimated from the OGLE survey and the *Gaia* magnitude conversion, respectively.

[7]For 11 multi-mode GCCs the PC was not used because the results are less reliable.

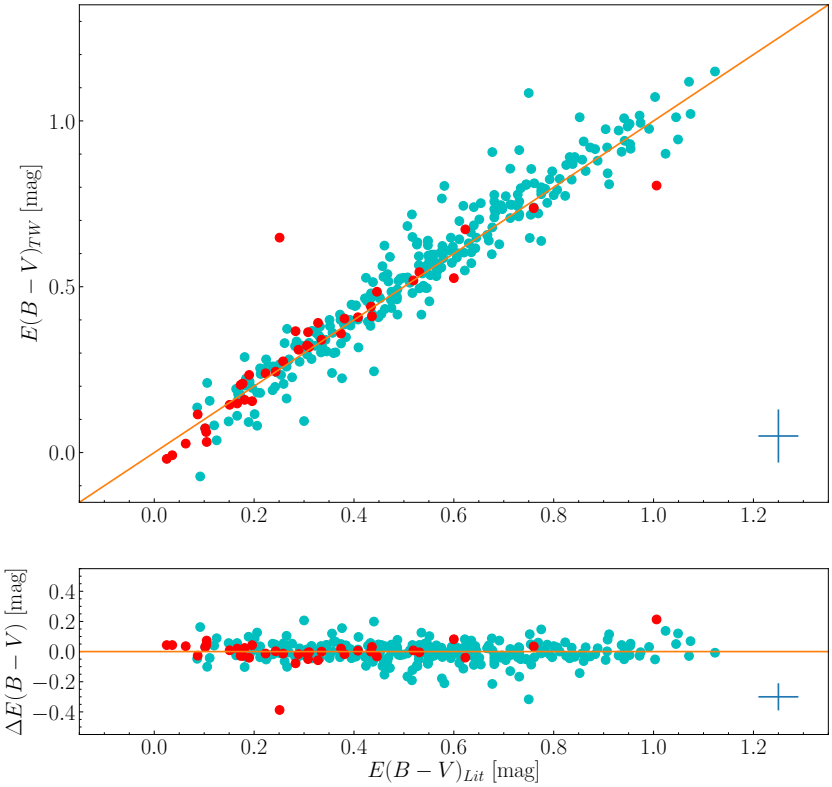

FIGURE 6.8: Comparison between the reddening values estimated from the period-$(V-I)_0$ relation E(B-V)$_{TW}$ and the literature E(B-V)$_{Lit}$ for a sample of 320 GCCs (see text for more detail). *Top panel* shows the 1:1 diagram; whilst the *bottom panel* displays the difference between the two reddening estimates. In both panels, green and red filled circles represent F and FO pulsators, respectively.

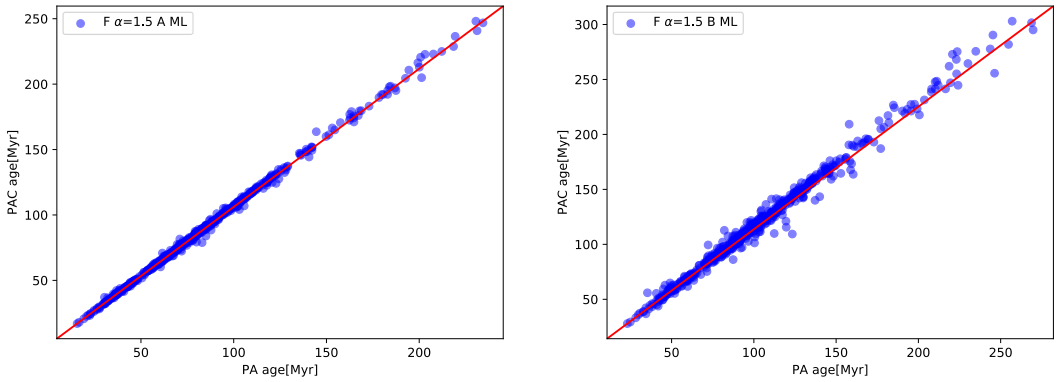

FIGURE 6.9: Comparison between the age estimates obtained by applying the PA and the PAC relations, for the two selected ML cases, (case A in the *left panel* and case B in the *right panel*) to the selected sub-sample of F-mode GCCs. In both panels, the solid line represents the 1:1 line.

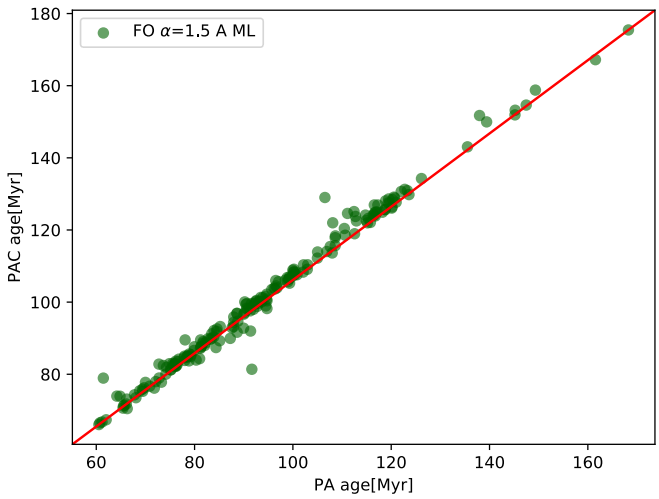

FIGURE 6.10: Comparison between the individual ages obtained by applying the PA and the PAC relations to the selected sub-sample of FO-mode GCC. The solid line represents the 1:1 line.

It was worth checking the level of consistency between the reddening estimates obtained by using the PC relation with those retrieved from the literature for the CC in the compilation by M. A. T. Groenewegen (2018). Fig.6.8 shows a comparison between the E(B-V) values obtained with the two methods for both F and FO pulsators. The lack of any systematic trend in both the 1:1 (top panel) and the residuals (bottom panel) diagrams, supports the reliability of the approach used for estimating the extinction from the PC relation (Ripepi et al., in preparation).

We noted that the reddening error affects the age measurements with an uncertainty of $\Delta(logt)$ ∼0.009 dex and $\Delta(logt)$ ∼ 0.022 dex for F-mode pulsators in cases A and B, respectively. For FO-mode GCCs the uncertainty is $\Delta(logt)$ ∼0.020 dex. As a result, the typical uncertainty of the GCC ages obtained from the PAC relationship, associated with the error of the reddening estimate, is of the order of 1-2%.

The GCC sample age estimates obtained by using the PA and PAC relationships are listed in Tables 6.5 to 6.7.

In order to assess the accuracy of our age estimates, in Figs. 6.9 and 6.10, we compared the individual age estimates obtained by applying the PA and the PAC relationships derived in the previous section, for the selected F and FO-mode GCCs. In Fig. 6.9, the two panels refer to *cases A* (left) and *B* (right). It is worth noting that a good agreement does exist between the age measurements on the whole age range obtained using the two relationships, as proven by the distribution of points with respect to the 1:1 line.

The histogram of the derived age distribution based on the application of the PAC relation, is shown in Fig. 6.11, for both F (left panel) and FO (right panel) pulsators. Inspection of this plot confirms that the predicted ages depend on the assumed ML relation. Thus, providing systematically older ages for brighter ML relations, in agreement with independent evaluations in literature (Anderson et al., 2016; Bono et al., 2005; Senchyna et al., 2015). For F-mode GCCs, the left panel of Fig. 6.11 suggested that the age distribution peaked around ∼ 90 Myr in the assumption of a canonical ML relation (*case A*) and got older by about ∼ 35 Myr in the non-canonical

assumption (*case B*). In the case of FO-mode GCCs (right panel of Fig. 6.11), the estimated age distribution is, as expected, concentrated towards older ages with a peak between $(80 - 85)$ Myr. On the other hand, the age estimates obtained by means of both the PA and PAC relations are almost insensitive to variations in the mixing length parameter. This result was expected because a variation in the efficiency of superadiabatic convection can modify the pulsation amplitude and the boundary of the IS (see e.g. De Somma et al., 2020a; Fiorentino et al., 2007), and references therein), but does not affect the relation between period, color and luminosity at all. Thus, the relation between period, color and age is also unaffected.

The possibility of deriving accurate and reliable age estimates of a large sample of GCCs by using the PA and/or the PAC relations provides the opportunity to perform an age tomography of the Galaxy. Therefore, the opportunity to properly trace the Star Formation history of the various portions of the Milky Way, in particular, the regime of young and intermediate ages is also provided.

In order to show the inferred GCC age distribution as a function of the position in the Galactic disk, the selected Gaia DR2 Cepheid sample was represented in the Galactic coordinates with the predicted individual age varying according to the logarithmic color-bar scale and increasing from blue to red.

The maps shown in Fig. 6.12 refer to F and FO-mode GCCs with ages derived from the PAC relations. From left to right, the panels show the age map for: F-mode GCCs by assuming the ML case A, F-mode GCCs by assuming the ML case B and FO-mode GCCs by assuming the ML case A. In all panels, the pulsation predictions were based on an adopted mixing length equal to α_{ml} =1.5. Inspection of these figures suggests that:

- the predicted ages decrease towards the Galactic center, with the oldest Cepheids located at longer Galactocentric distances.
- for the same assumption about the ML relation, FO-mode Cepheids are found to be systematically older than the F ones.

Although a detailed analysis of this topic was out of the aims of the present investigation, both the age and the spatial distributions of the CCs in our sample as a function of their age can be compared with independent studies on the presence of age gradients among the various stellar populations in the Milky Way. For example, Skowron et al. (2019), applied the PA relation by Anderson et al. (2016) to the OGLE database of GCCs, and found an age distribution (see their Fig. 3) very similar to our results based on PA and PAC relations obtained from case B models. Recently, Bossini et al. (2019) computed the age distribution of 269 Galactic open clusters with astrometric and photometric data from Gaia DR2. However, in this case the possibility of realizing a meaningful comparison is hampered by the fact that the open cluster sample adopted by Bossini et al. (2019) spans an age range limited with respect to that of the GCC sample adopted in the present investigation.

A more detailed analysis of the implications that can be obtained for the star formation history of the various portions of our Galaxy at different locations from the study of the age distribution of CCs, needs to be supplemented with an accurate investigation of the metallicity distribution of these pulsators. In order to properly account for the whole metallicity distribution of Galactic Cepheids, in the next chapter we will discuss the preliminary results of the extension of this theoretical investigation to different metallicity regimes.

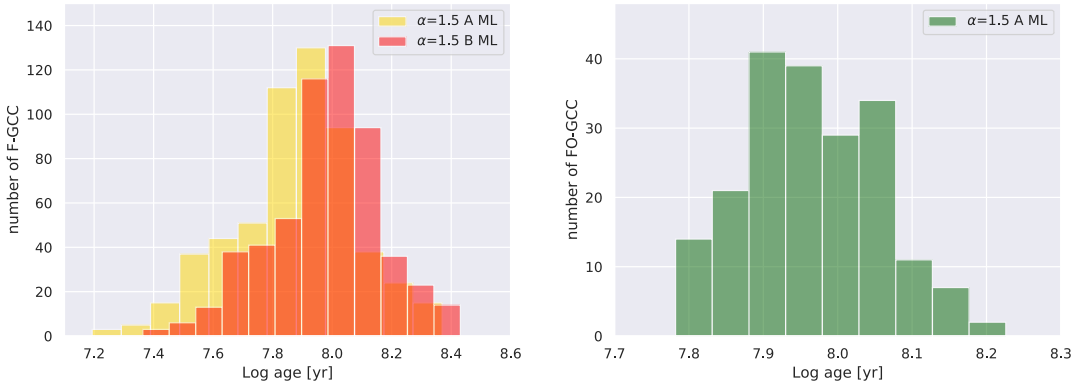

FIGURE 6.11: The predicted age distribution obtained by applying the PAC relation to the selected sample of F *(left panel)* and FO-mode *(right panel)* GCCs, for the labelled assumptions about the efficiency of superadiabatic convection and ML relation.

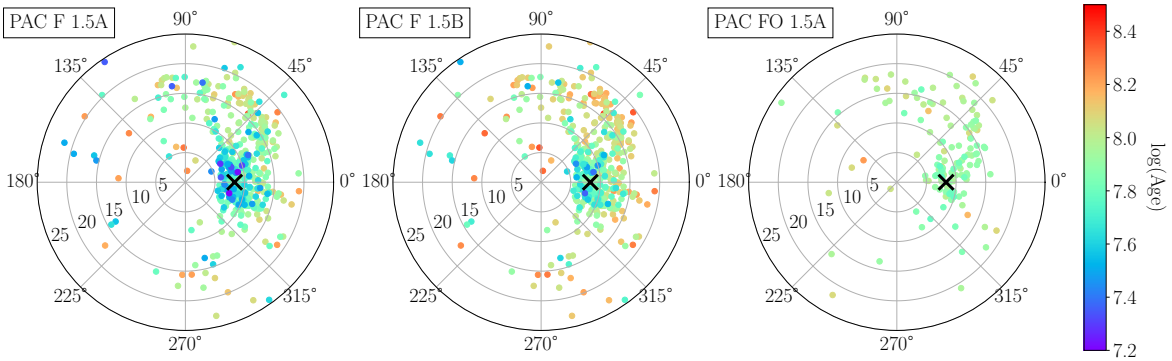

FIGURE 6.12: Distribution of the selected Gaia DR2 Cepheids on the Galactic plane plotted in polar coordinates. The Galactic center is in the middle. The Galactocentric polar coordinate is at 0° in the direction of the Sun, whose position is marked by a black 'X'. Each circle shows Galactocentric distances increasing by 5 kpc, from 0 to 25 kpc. In each panel the colored circles show the predicted individual ages obtained by using the PAC relations, according to the logarithmic color-bar axis. The labels on the top-left of each figure indicate the pulsation mode, while 1.5 A and B refer to the PAC obtained by assuming α_{ml} =1.5 for canonical and noncanonical stellar models, respectively.

TABLE 6.5: Individual ages for the F-mode GCCs in our sample obtained by using both the canonical PA and PAC relations. Columns 1 to 9 show the: Gaia DR2 source id, right ascension in degrees, declination in degrees, period in days, Gaia passband G in mag, Gaia passband G_{BP} in mag and Gaia passband G_{RP} in mag. Columns 8 and 9 show the reddening and the estimated uncertainty in the G_{BP} - G_{RP} color, respectively. Column 10 provides information on the reddening estimate: *L* stands for data from literature, while *O* and *G* refer to the cases for which the extinction was estimated by adopting the PC relation, using the (V-I) color from the OGLE survey and the conversion to the *Gaia* color, respectively (see text for more detail). Columns 11 to 14 list the age and the estimated uncertainty in Myr as obtained by alternately using the PA relation and the PAC one. This table is available in its entirety in Section A.3 in Appendix A.

Gaia DR2 Source Id	RA[deg]	DEC[deg]	P[d]	G[mag]	G_{BP}[mag]	G_{RP}[mag]	E(G_{BP}-G_{RP})[mag]	σE(G_{BP}-G_{RP})[mag]	Note	t_{PA}[Myr]	σ t_{PA}[Myr]	t_{PAC}[Myr]	σ t_{PAC}[Myr]
(1)	(2)	(3)	(4)	(5)	(6)	(7)	(8)	(9)	(10)	(11)	(12)	(13)	(14)
3442172745919329664	82.35887	27.00089	3.34920	11.57	12.21	10.78	0.72	0.12	G	105.55	20.41	98.88	18.9
4704080802304630784	12.82014	-68.98430	0.99469	18.24	18.45	17.79	0.18	0.11	G	248.10	47.99	230.53	44.06
5521400228203695232	123.35129	-42.27568	1.00189	16.05	16.93	15.15	1.23	0.15	G	246.84	47.74	234.34	44.79
6379351625245757568	359.99997	-75.19496	1.03777	17.68	17.98	17.36	0.02	0.11	G	240.80	46.58	231.16	44.18
4711142067840447360	21.61608	-64.87535	1.06447	17.86	18.05	17.41	0.16	0.11	G	236.54	45.75	219.39	41.93
4639539705975935360	50.85364	-74.96868	1.11640	17.83	18.12	17.50	0.02	0.11	G	228.74	44.24	218.50	41.76
4690768156035338624	18.95551	-70.54573	1.14292	17.53	17.82	17.09	0.18	0.11	G	224.99	43.52	212.14	40.54
4703965697180635136	9.31520	-67.04117	1.15729	17.89	18.12	17.43	0.17	0.11	G	223.02	43.14	207.66	39.69
4666616485480394368	60.40851	-69.47789	1.15905	16.29	16.45	15.90	0.12	0.08	O	222.78	43.09	203.12	38.82
4691081375113472256	20.83822	-70.57775	1.17564	17.33	17.45	17.02	0.0	0.11	G	220.56	42.66	200.73	38.36
4637614151878607232	20.74650	-76.24745	1.20857	17.80	17.95	17.36	0.1	0.11	G	216.31	41.84	199.28	38.09
5834840099568788864	241.98124	-58.78225	1.23577	13.71	14.05	13.19	0.31	0.11	G	212.95	41.19	200.06	38.23
4636112425153243904	16.19343	-76.86050	1.25457	17.34	17.55	16.84	0.21	0.11	G	210.70	40.75	194.40	37.15
4690721839108141568	19.01385	-70.91305	1.30481	17.25	17.73	17.00	-0.0	0.11	G	204.95	39.64	201.29	38.47
4698739817197286912	23.24870	-66.49795	1.30920	17.05	17.30	16.67	0.05	0.11	G	204.47	39.55	192.58	36.8
5298606801235832064	140.10591	-62.22648	1.36601	18.36	18.60	17.89	0.18	0.11	G	198.45	38.38	184.56	35.27
...	...	...	...	...	...	...	...	...	...	...	...	...	...

TABLE 6.6: As Table 6.5, but in this case the PA and PAC relations for the noncanonical stellar models have been adopted. This table is available in its entirety in Section A.3 in Appendix A.

Gaia DR2 Source Id	RA[deg]	DEC[deg]	P[d]	G[mag]	G_{BP}[mag]	G_{RP}[mag]	E(G_{BP}-G_{RP})[mag]	σE(G_{BP}-G_{RP})[mag]	Note	t_{PA}[Myr]	σ t_{PA}[Myr]	t_{PAC}[Myr]	σ t_{PAC}[Myr]
(1)	(2)	(3)	(4)	(5)	(6)	(7)	(8)	(9)	(10)	(11)	(12)	(13)	(14)
3442172745919329664	82.35887	27.00089	3.34920	11.57	12.21	10.78	0.72	0.12	G	141.71	26.10	122.49	21.72
4704080802304630784	12.82014	-68.98430	0.99469	18.24	18.45	17.79	0.18	0.11	G	303.00	55.82	257.01	45.57
5521400228203695232	123.35129	-42.27568	1.00189	16.05	16.93	15.15	1.23	0.15	G	301.64	55.56	268.78	47.65
6379351625245757568	359.99997	-75.19496	1.03777	17.68	17.98	17.36	0.02	0.11	G	295.07	54.35	269.73	47.82
4711142067840447360	21.61608	-64.87535	1.06447	17.86	18.05	17.41	0.16	0.11	G	290.41	53.50	245.31	43.49
4639539705975935360	50.85364	-74.96868	1.11640	17.83	18.12	17.50	0.02	0.11	G	281.88	51.92	254.78	45.17
4690768156035338624	18.95551	-70.54573	1.14292	17.53	17.82	17.09	0.18	0.11	G	277.77	51.17	243.67	43.20
4703965697180635136	9.31520	-67.04117	1.15729	17.89	18.12	17.43	0.17	0.11	G	275.60	50.77	234.88	41.64
4666616485480394368	60.40851	-69.47789	1.15905	16.29	16.45	15.90	0.12	0.08	O	275.34	50.72	223.60	39.64
4691081375113472256	20.83822	-70.57775	1.17564	17.33	17.45	17.02	0.0	0.11	G	272.90	50.27	220.70	39.13
4637614151878607232	20.74650	-76.24745	1.20857	17.80	17.95	17.36	0.1	0.11	G	268.22	49.41	223.07	39.55
5834840099568788864	241.98124	-58.78225	1.23577	13.71	14.05	13.19	0.31	0.11	G	264.51	48.73	230.11	40.80
4636112425153243904	16.19343	-76.86050	1.25457	17.34	17.55	16.84	0.21	0.11	G	262.02	48.27	218.67	38.77
4690721839108141568	19.01385	-70.91305	1.30481	17.25	17.73	17.00	-0.0	0.11	G	255.66	47.09	246.30	43.67
4698739817197286912	23.24870	-66.49795	1.30920	17.05	17.30	16.67	0.05	0.11	G	255.13	47.00	223.23	39.58
5298606801235832064	140.10591	-62.22648	1.36601	18.36	18.60	17.89	0.18	0.11	G	248.43	45.76	211.15	37.44
...	...	...	...	...	...	...	...	...	...	...	...	...	...

TABLE 6.7: As Table 6.5, but for the FO-mode GCCs in the selected sample. This table is available in its entirety in Section A.3 in Appendix A.

Gaia DR2 Source Id	RA[deg]	DEC[deg]	P[d]	G[mag]	G_{BP}[mag]	G_{RP}[mag]	E(G_{BP}-G_{RP})[mag]	σE(G_{BP}-G_{RP})[mag]	Note	t_{PA}[Myr]	σ t_{PA}[Myr]	t_{PAC}[Myr]	σ t_{PAC}[Myr]
(1)	(2)	(3)	(4)	(5)	(6)	(7)	(8)	(9)	(10)	(11)	(12)	(13)	(14)
5958267083020200448	263.74736	-44.83491	0.48582	15.31	15.67	14.78	0.48	0.11	G	175.45	21.01	168.26	17.82
4652801401061740800	72.89387	-73.52919	0.54856	17.88	18.20	17.42	0.32	0.11	G	167.21	20.02	161.55	17.11
4649684869708905600	78.33946	-73.18860	0.62515	17.60	17.85	17.14	0.28	0.11	G	158.78	19.01	149.33	15.82
4757521942202075904	84.00743	-62.92647	0.66840	17.23	17.49	16.81	0.21	0.11	G	154.63	18.51	147.46	15.62
4648894973678313600	78.74744	-76.16060	0.68428	17.58	17.85	17.13	0.26	0.11	G	153.20	18.34	145.22	15.38
4260977655080185600	13.85755	59.72753	0.69910	13.67	14.18	12.99	0.72	0.12	G	151.90	18.19	145.17	15.38
5255955821811454592	150.19748	-61.57770	0.70107	14.74	15.09	14.05	0.65	0.12	G	151.73	18.17	137.97	14.61
6380124062227694208	357.83150	-72.69153	0.72213	17.86	18.07	17.44	0.19	0.11	G	149.96	17.96	139.41	14.77
4648520761770393088	85.76598	-75.18605	0.81359	17.25	17.54	16.80	0.25	0.11	G	143.05	17.13	135.51	14.35
4652889258915055488	72.48404	-73.00018	0.95488	17.24	17.54	16.77	0.27	0.11	G	134.26	16.08	126.16	13.36
5542032357742851712	125.44982	-37.46816	1.01087	16.30	17.08	15.38	1.19	0.12	O	131.26	15.72	122.76	13.00
4652312599416423040	68.88711	-74.56297	1.01787	17.03	17.30	16.59	0.18	0.11	G	130.90	15.67	123.28	13.06
4649732762885142272	77.24295	-73.85941	1.02268	17.06	17.35	16.58	0.26	0.11	G	130.66	15.64	122.03	12.92
5860021737714232576	190.95445	-65.86875	1.03985	15.64	16.14	14.78	0.82	0.1	O	129.80	15.54	123.61	13.09
4690203483799384832	12.47494	-70.52511	1.05413	16.86	17.06	16.51	0.03	0.11	G	129.10	15.46	120.55	12.77
5879216457587855872	220.33866	-58.95261	1.05620	17.35	19.40	15.97	3.13	0.28	G	129.00	15.45	106.51	11.28
...	...	...	...	...	...	...	...	...	...	...	...	...	...

Chapter 7

The metal-dependent pulsational scenario

In order to investigate the metallicity effect on the relations adopted for using CCs as distance and age indicators, as well as to pave the way for future investigations of extragalactic Cepheids, the theoretical analysis of CC pulsation models was extended to chemical compositions different from the solar one.
In particular, we considered the following chemical compositions: $Z = 0.004, Y = 0.25$; $Z = 0.008, Y = 0.25$; and $Z = 0.03 - Y = 0.28$, representative of CCs observed in the Small Magellanic Cloud, the Large Magellanic Cloud and M31, respectively. For each chemical composition, a wide range of masses ($3<M/M_{\odot}<11$) and effective temperatures ($3600<T_{eff}[K]<7200$) as well as three assumptions about the ML relation were considered (see Tables 7.17.2 and 7.3 for $Z = 0.004, Y = 0.25$; all chemical composition tables are available in their entirety in Appendix A).

As for the solar chemical composition case, models with a canonical luminosity level were labeled as 'case A', while those with the two noncanonical luminosity levels obtained by increasing the canonical luminosity level by $\Delta \log(L/L_{\odot}) = 0.2$ *dex* and $\Delta \log(L/L_{\odot}) = 0.4$ *dex* were labeled as 'case B' and 'case C', respectively. Moreover, three different values α_{ml}=1.5, α_{ml}=1.7 and α_{ml}=1.9 for the efficiency of superadiabatic convection were chosen. For $Z = 0.03, Y = 0.28$, only the pulsation models for the standard convective efficiency (α_{ml}=1.5) were found to reach a stable limit cycle and only cases A and B ML relations were computed. For each selected model and pulsation mode, the system of nonlinear dynamical and convective equations was integrated until a stable limit cycle was achieved.

In the case of $Z = 0.004$ and $Z = 0.008$, second overtone mode stable pulsation models were also found. For each pulsation model and investigated mode, all the relevant pulsation observables were produced.

In this Chapter the main relations derived from pulsation models with the aforementioned chemical compositions are reported.

7.1 The extended set of pulsation models

As a result of the nonlinear convective model computations, 696 F-mode, 110 FO-mode and 3 SO-mode stable Cepheid pulsation models for $Z = 0.004$, 639 F-mode, 126 FO-mode and 6 SO-mode stable Cepheid pulsation models for $Z = 0.008$, and 127 F-mode and 4 stable FO-mode Cepheid pulsation models for $Z = 0.03$ were produced.

The intrinsic stellar parameters, namely the stellar mass, the luminosity level and the effective temperature, as well as the adopted mixing length parameter, the ML identification defined above, the pulsation period and the mean radius obtained by

TABLE 7.1: The intrinsic stellar parameters for $Z = 0.004, Y = 0.25$ F-mode pulsation models. This table is available in its entirety in A.5 in Appendix A.

		Z=0.004	Y= 0.25			
$M/M_{\odot}$	log(L/$L_{\odot}$)	T_{eff}[K]	α_{ml}	ML	P[d]	log($\overline{R}/R_{\odot}$)
3.0	2.49	5900	1.5	A	1.46027	1.23
3.0	2.49	6000	1.5	A	1.38159	1.217
...						
4.0	2.91	5600	1.5	A	3.23075	1.483
4.0	2.91	5700	1.5	A	3.05052	1.47
...						
5.0	3.24	5300	1.5	A	6.31282	1.687
5.0	3.24	5400	1.5	A	5.94985	1.675
...						
6.0	3.50	5200	1.5	A	10.08817	1.836
6.0	3.50	5300	1.5	A	9.41852	1.822
...						
7.0	3.73	4900	1.5	A	17.46979	2.0
7.0	3.73	5000	1.5	A	16.45231	1.993
...						
8.0	3.92	4800	1.5	A	25.39572	2.115
8.0	3.92	4900	1.5	A	23.85683	2.101
...						
9.0	4.09	4600	1.5	A	37.79583	2.229
9.0	4.09	4700	1.5	A	35.82419	2.22
..						
10.0	4.25	4400	1.5	A	55.45613	2.333
10.0	4.25	4500	1.5	A	51.67512	2.321
...						
11.0	4.39	4300	1.5	A	74.08461	2.418
11.0	4.39	4400	1.5	A	69.86262	2.407
...						

averaging the radius curves (see Section 7.5) are reported in the various columns of Tables 7.1, 7.2 and 7.3 for $Z = 0.004$. Tables 7.4, 7.5 and 7.6 list the same parameters for $Z = 0.008$. Finally, Tables 7.7 and 7.8 report the F and FO-mode parameters for $Z = 0.03$.

7.2 The topology of the instability strip as a function of the chemical composition

The topology of the instability strips for the aforementioned chemical compositions was derived. The inferred F, FO and when available, SO boundary effective temperatures are reported in Tables 7.9, 7.10 and 7.11, for $Z = 0.004$, $Z = 0.008$ and $Z = 0.03$ Cepheid models, respectively. In each table, the mass, the luminosity level, the adopted mixing length parameter, the ML label and the effective temperatures for the SOBE (if present) FOBE, FBE, SORE (if present), FORE and FRE are reported.

TABLE 7.2: The same as in Table 7.2 but for FO-mode pulsation models. This table is available in its entirety in A.5 in A.

		Z=0.004	Y= 0.25			
$M/M_{\odot}$	$\log(L/L_{\odot})$	T_{eff}[K]	α_{ml}	ML	P[d]	$\log(\overline{R}/R_{\odot})$
3.0	2.49	6100	1.5	A	0.96086	1.202
3.0	2.49	6200	1.5	A	0.91345	1.19
...						
4.0	2.91	6000	1.5	A	1.844	1.425
4.0	2.91	6100	1.5	A	1.75159	1.411
...						
5.0	3.24	5600	1.5	A	3.76641	1.646
5.0	3.24	5700	1.5	A	3.56603	1.631
...						
6.0	3.50	5600	1.5	A	5.60191	1.782
6.0	3.50	5700	1.5	A	5.28456	1.768
...						

TABLE 7.3: The same as in Table 7.1 but for SO-mode pulsation models. This table is available in its entirety in A.5 in A.

		Z=0.004	Y= 0.25			
$M/M_{\odot}$	$\log(L/L_{\odot})$	T_{eff}[K]	α_{ml}	ML	P[d]	$\log(\overline{R}/R_{\odot})$
3.0	2.49	6600	1.5	A	0.60227	1.135
3.0	2.49	6700	1.5	A	0.5745	1.121
...						

TABLE 7.4: The intrinsic stellar parameters for $Z = 0.008, Y = 0.25$ F-mode pulsation models. This table is available in its entirety in A.5 in A.

		Z=0.008	Y= 0.25			
$M/M_\odot$	$\log(L/L_\odot)$	T_{eff}[K]	α_{ml}	ML	P[d]	$\log(\overline{R}/R_\odot)$
3.0	2.39	6000	1.5	A	1.15407	1.166
3.0	2.59	5700	1.5	B	2.00247	1.307
...						
4.0	2.81	5600	1.5	A	2.67853	1.431
4.0	2.81	5700	1.5	A	2.52578	1.419
...						
5.0	3.14	5300	1.5	A	5.22834	1.637
5.0	3.14	5400	1.5	A	4.91119	1.624
...						
6.0	3.40	5200	1.5	A	8.3325	1.787
6.0	3.40	5300	1.5	A	7.83128	1.774
...						
7.0	3.63	4900	1.5	A	14.39537	1.955
7.0	3.63	5000	1.5	A	13.5206	1.938
...						
8.0	3.82	4700	1.5	A	22.12951	2.08
8.0	3.82	4800	1.5	A	20.89769	2.071
...						
9.0	3.99	4500	1.5	A	33.33507	2.196
9.0	3.99	4600	1.5	A	31.42639	2.187
...						
10.0	4.14	4400	1.5	A	46.19803	2.294
10.0	4.14	4500	1.5	A	42.75625	2.28
...						
11.0	4.28	4200	1.5	A	65.83958	2.389
11.0	4.28	4300	1.5	A	62.01632	2.378
...						

TABLE 7.5: The same as in Table 7.4 but for FO-mode pulsation models. This table is available in its entirety in A.5 in A.

		Z=0.008	Y= 0.25			
$M/M_\odot$	$\log(L/L_\odot)$	T_{eff}[K]	α_{ml}	ML	P[d]	$\log(\overline{R}/R_\odot)$
3.0	2.39	6100	1.5	A	0.79791	1.151
3.0	2.39	6200	1.5	A	0.75783	1.138
...						
4.0	2.81	5900	1.5	A	1.62559	1.388
4.0	2.81	6000	1.5	A	1.53301	1.375
...						
5.0	3.14	5900	1.5	A	2.60887	1.552
5.0	3.14	6000	1.5	A	2.47821	1.537
...						
6.0	3.40	5500	1.5	A	4.87884	1.746
6.0	3.40	5600	1.5	A	4.61845	1.73
...						

TABLE 7.6: The same as in Table 7.4 but for SO-mode pulsation models. This table is available in its entirety in A.5 in A.

		Z=0.008	Y= 0.25			
$M/M_\odot$	$\log(L/L_\odot)$	T_{eff}[K]	α_{ml}	ML	P[d]	$\log(\overline{R}/R_\odot)$
3.0	2.39	6500	1.5	A	0.52047	1.096
3.0	2.39	6600	1.5	A	0.50097	1.083
...						

TABLE 7.7: The intrinsic stellar parameters for $Z = 0.03, Y = 0.28$ F-mode pulsation models. This table is available in its entirety in Appendix A.

		Z=0.03	Y= 0.28			
$M/M_\odot$	$\log(L/L_\odot)$	T_{eff}[K]	α_{ml}	ML	P[d]	$\log(\overline{R}/R_\odot)$
4.0	2.68	5600	1.5	A	2.14887	1.367
4.0	2.68	5700	1.5	A	2.02639	1.352
...						
5.0	3.01	5300	1.5	A	4.2556	1.581
5.0	3.01	5400	1.5	A	4.00248	1.565
...						
6.0	3.27	5100	1.5	A	7.18299	1.743
6.0	3.27	5200	1.5	A	6.72238	1.727
...						
7.0	3.50	4800	1.5	A	12.63542	1.917
7.0	3.50	4900	1.5	A	11.7897	1.902
...						
8.0	3.69	4600	1.5	A	19.54225	2.045
8.0	3.69	4700	1.5	A	18.00428	2.03
...						
9.0	3.86	4400	1.5	A	29.55613	2.163
9.0	3.86	4500	1.5	A	27.46898	2.148
...						
10.0	4.02	4200	1.5	A	44.51377	2.277
10.0	4.02	4300	1.5	A	41.39259	2.264
...						
11.0	4.15	4100	1.5	A	59.2919	2.36
11.0	4.15	4200	1.5	A	55.14583	2.347
...						

TABLE 7.8: The same as in Table 7.7 but for FO-mode pulsation models. This table is available in its entirety in A.5 in A.

		Z=0.03	Y= 0.28			
$M/M_\odot$	$\log(L/L_\odot)$	T_{eff}[K]	α_{ml}	ML	P[d]	$\log(\overline{R}/R_\odot)$
4.0	2.68	6000	1.5	A	1.21353	1.309
4.0	2.68	6100	1.5	A	1.15266	1.296
...						

By performing a linear fit of the inferred boundary effective temperature values, as a function of the luminosity level, for different assumptions of the α_{ml} parameter, the relations reported in Tables 7.12, 7.14, 7.16, for F and FO-mode $Z = 0.004$, $Z = 0.008$ and $Z = 0.03$ pulsators, respectively, were derived. The quadratic fit coefficients of the boundary values for only the fundamental mode pulsators are shown in Tables 7.13, 7.15 and 7.17.

The linear relations for the boundaries obtained for the canonical ML relation and the standard convective efficiency are plotted in Fig. 7.1 and compared with the boundaries at solar chemical composition ($Z = 0.02$, $Y = 0.28$). These plots show that, in agreement with previous investigations (Bono et al., 1999a; Bono et al., 1997), a change in the chemical composition does significantly affect the topology of the instability strip. In fact, as the metallicity increases from $Z = 0.004$ to $Z = 0.03$ at a fixed mixing length parameter and ML relation, the strip gets redder. This is due to both the decreased Hydrogen abundance that makes pulsation less efficient at the blue edge, delaying the onset of pulsation to lower effective temperatures; and the increased contribution of iron bump opacity to pulsation at the red edge of the instability strip, thus also delaying the quenching of pulsation due to convection.

TABLE 7.9: Predicted Effective Temperatures of the Instability Strip Boundaries for $Z = 0.004$. The assumed error on the boundary predictions is $T_{eff} = \pm 50$ K, based on the adopted effective temperature step in the pulsational model computations.

$M/M_{\odot}$	$\log(L/L_{\odot})$	α_{ml}	ML	SOBE	FOBE	FBE	SORE	FORE	FRE
(1)	(2)	(3)	(4)	(5)	(6)	(7)	(8)	(9)	(10)
3.0	2.49	1.5	A	6850	6750	6050	6550	6050	5850
3.0	2.49	1.7	A		6850	6150		6150	5950
3.0	2.49	1.9	A		6750	6250		6250	6050
3.0	2.69	1.5	B		6650	6050		6050	5650
3.0	2.69	1.7	B		6650	6150		6150	5750
3.0	2.69	1.9	B		6550	6250		6150	5850
3.0	2.89	1.5	C		6450	6150		6150	5450
3.0	2.89	1.7	C		6450	6250		6150	5550
3.0	2.89	1.9	C		6350	6350		6250	5650
4.0	2.91	1.5	A		6550.0	5950		5950.0	5550
4.0	2.91	1.7	A		6550.0	6050		6050.0	5650
4.0	2.91	1.9	A		6450	6150		6150	5750
4.0	3.11	1.5	B		6350	6050		5550	5350
4.0	3.11	1.7	B		6350	6150		5650	5450
4.0	3.11	1.9	B		6250	6250		6150	5550
4.0	3.31	1.5	C		6150	6050		5850	5050
4.0	3.31	1.7	C		6050	6150		5950	5250
4.0	3.31	1.9	C			6050			5350
5.0	3.24	1.5	A		6350	6050		5550	5250
5.0	3.24	1.7	A		6250	6050		6050	5450
5.0	3.24	1.9	A		6250	6150		6050	5550
5.0	3.44	1.5	B		6150	5950		5650	5050
5.0	3.44	1.7	B		6050	6050		5750	5150
5.0	3.44	1.9	B		5950	6050		5850	5350
5.0	3.64	1.5	C			5950			4750
5.0	3.64	1.7	C			5950			4950
5.0	3.64	1.9	C			5950			5150

TABLE 7.9: continued.

$M/M_\odot$	$\log(L/L_\odot)$	α_{ml}	ML	SOBE	FOBE	FBE	SORE	FORE	FRE
(1)	(2)	(3)	(4)	(5)	(6)	(7)	(8)	(9)	(10)
6.0	3.5	1.5	A		6150	5850		5550	5150
6.0	3.5	1.7	A		6050	5950		5650	5250
6.0	3.5	1.9	A		5950	6050		5750	5350
6.0	3.7	1.5	B			5950			4850
6.0	3.7	1.7	B			5950			5050
6.0	3.7	1.9	B			5950			5150
6.0	3.9	1.5	C			5850			4450
6.0	3.9	1.7	C			5850			4750
6.0	3.9	1.9	C			5750			4950
7.0	3.73	1.5	A		5950	5950		5750	4850
7.0	3.73	1.7	A			5950			5050
7.0	3.73	1.9	A			5950			5250
7.0	3.93	1.5	B			5850			4550
7.0	3.93	1.7	B			5850			4850
7.0	3.93	1.9	B			5750			5050
7.0	4.13	1.5	C			5750			4350
7.0	4.13	1.7	C			5650			4450
7.0	4.13	1.9	C			5650			4650
8.0	3.92	1.5	A			5850			4750
8.0	3.92	1.7	A			5850			4950
8.0	3.92	1.9	A			5850			5150
8.0	4.12	1.5	B			5750			4250
8.0	4.12	1.7	B			5750			4550
8.0	4.12	1.9	B			5650			4850
8.0	4.32	1.5	C			5550			4450
8.0	4.32	1.7	C			5550			4250
8.0	4.32	1.9	C			5550			4350
9.0	4.09	1.5	A			5750			4550
9.0	4.09	1.7	A			5750			4750
9.0	4.09	1.9	A			5650			4950
9.0	4.29	1.5	B			5650			4250
9.0	4.29	1.7	B			5650			4450
9.0	4.29	1.9	B			5650			4650
9.0	4.49	1.5	C			5550			4650
9.0	4.49	1.7	C			5450			4550
9.0	4.49	1.9	C			5450			4450
10.0	4.25	1.5	A			5650			4350
10.0	4.25	1.7	A			5650			4650
10.0	4.25	1.9	A			5650			4850
10.0	4.45	1.5	B			5550			4250
10.0	4.45	1.7	B			5550			4350
10.0	4.45	1.9	B			5550			4550
10.0	4.65	1.5	C			5450			4850
10.0	4.65	1.7	C			5450			4850
10.0	4.65	1.9	C			5350			4850
11.0	4.39	1.5	A			5650			4250

TABLE 7.9: continued.

$M/M_\odot$	$\log(L/L_\odot)$	α_{ml}	ML	SOBE	FOBE	FBE	SORE	FORE	FRE
(1)	(2)	(3)	(4)	(5)	(6)	(7)	(8)	(9)	(10)
11.0	4.39	1.7	A			5650			4450
11.0	4.39	1.9	A			5550			4750
11.0	4.59	1.5	B			5550			4450
11.0	4.59	1.7	B			5450			4350
11.0	4.59	1.9	B			5450			4350
11.0	4.79	1.5	C			5350			5150
11.0	4.79	1.7	C			5350			5050
11.0	4.79	1.9	C			5250			5050

TABLE 7.10: Predicted Effective Temperatures of the Instability Strip Boundaries for $Z = 0.008$. The assumed error on the boundary predictions is $T_{eff} = \pm 50\ K$, based on the adopted effective temperature step in the pulsational model computations.

$M/M_\odot$	$\log(L/L_\odot)$	α_{ml}	ML	SOBE	FOBE	FBE	SORE	FORE	FRE
(1)	(2)	(3)	(4)	(5)	(6)	(7)	(8)	(9)	(10)
3.0	2.39	1.5	A	6950	6650	6050	6450	6050	5950
3.0	2.39	1.7	A	6750	6750		6650	6150	
3.0	2.39	1.9	A		6750			6350	
3.0	2.59	1.5	B		6750	6050		5950	5650
3.0	2.59	1.7	B		6650	6150		6050	5750
3.0	2.59	1.9	B		6650	6250		6150	5950
3.0	2.79	1.5	C		6550	6150		6050	5450
3.0	2.79	1.7	C		6550	6150		6150	5650
3.0	2.79	1.9	C		6450	6250		6150	5750
4.0	2.81	1.5	A		6550	5950		5850	5550
4.0	2.81	1.7	A		6550	6050		5950	5750
4.0	2.81	1.9	A		6550	6150		6050	5850
4.0	3.01	1.5	B		6450	6050		5950	5350
4.0	3.01	1.7	B		6350	6050		6050	5450
4.0	3.01	1.9	B		6250	6150		6050	5650
4.0	3.21	1.5	C		6250	5950		5650	5150
4.0	3.21	1.7	C		6150	6150		5750	5250
4.0	3.21	1.9	C			6150			5450
5.0	3.14	1.5	A		6350	5950		5850	5250
5.0	3.14	1.7	A		6350	5950		5950	5450
5.0	3.14	1.9	A		6250	6050		6050	5650
5.0	3.34	1.5	B		6150	5850		5550	5150
5.0	3.34	1.7	B		6050	6050		5650	5350
5.0	3.34	1.9	B			6050			5450
5.0	3.54	1.5	C			5850			4750
5.0	3.54	1.7	C			5850			4950
5.0	3.54	1.9	C			5850			5150
6.0	3.4	1.5	A		6250	5950		5450	5150
6.0	3.4	1.7	A		6150	5950		5550	5250
6.0	3.4	1.9	A			6050			5450
6.0	3.6	1.5	B			5950			4750

TABLE 7.10: continued.

$M/M_\odot$	$\log(L/L_\odot)$	α_{ml}	ML	SOBE	FOBE	FBE	SORE	FORE	FRE
(1)	(2)	(3)	(4)	(5)	(6)	(7)	(8)	(9)	(10)
6.0	3.6	1.7	B			5950			5050
6.0	3.6	1.9	B			5850			5150
6.0	3.8	1.5	C			5750			4450
6.0	3.8	1.7	C			5750			4750
6.0	3.8	1.9	C			5650			4950
7.0	3.63	1.5	A		5950	5850		5550	4850
7.0	3.63	1.7	A		5850	5850		5650	5050
7.0	3.63	1.9	A			5850			5250
7.0	3.83	1.5	B			5850			4550
7.0	3.83	1.7	B			5750			4850
7.0	3.83	1.9	B			5650			5050
7.0	4.03	1.5	C			5650			4250
7.0	4.03	1.7	C			5550			4450
7.0	4.03	1.9	C			5450			4750
8.0	3.82	1.5	A			5750			4650
8.0	3.82	1.7	A			5750			4950
8.0	3.82	1.9	A			5750			5150
8.0	4.02	1.5	B			5650			4250
8.0	4.02	1.7	B			5650			4550
8.0	4.02	1.9	B			5550			4850
8.0	4.22	1.5	C			5550			4150
8.0	4.22	1.7	C			5450			4150
8.0	4.22	1.9	C			5250			4450
9.0	3.99	1.5	A			5750			4450
9.0	3.99	1.7	A			5650			4750
9.0	3.99	1.9	A			5550			4950
9.0	4.19	1.5	B			5550			4050
9.0	4.19	1.7	B			5450			4350
9.0	4.19	1.9	B			5350			4750
9.0	4.39	1.5	C			5350			4250
9.0	4.39	1.7	C			5350			4350
9.0	4.39	1.9	C			5150			4250
10.0	4.14	1.5	A			5550			4350
10.0	4.14	1.7	A			5450			4650
10.0	4.14	1.9	A			5350			4950
10.0	4.34	1.5	B			5450			4050
10.0	4.34	1.7	B			5250			4150
10.0	4.34	1.9	B			5150			4550
10.0	4.54	1.5	C			5250			4450
10.0	4.54	1.7	C			5250			4450
10.0	4.54	1.9	C			5050			4350
11.0	4.28	1.5	A			5550			4150
11.0	4.28	1.7	A			5350			4450
11.0	4.28	1.9	A			5250			4850
11.0	4.48	1.5	B			5350			4050
11.0	4.48	1.7	B			5150			4050

TABLE 7.10: continued.

$M/M_{\odot}$	$\log(L/L_{\odot})$	α_{ml}	ML	SOBE	FOBE	FBE	SORE	FORE	FRE
(1)	(2)	(3)	(4)	(5)	(6)	(7)	(8)	(9)	(10)
11.0	4.48	1.9	B			5050			4350
11.0	4.68	1.5	C			5150			4650
11.0	4.68	1.7	C			5150			4650
11.0	4.68	1.9	C			4950			4650

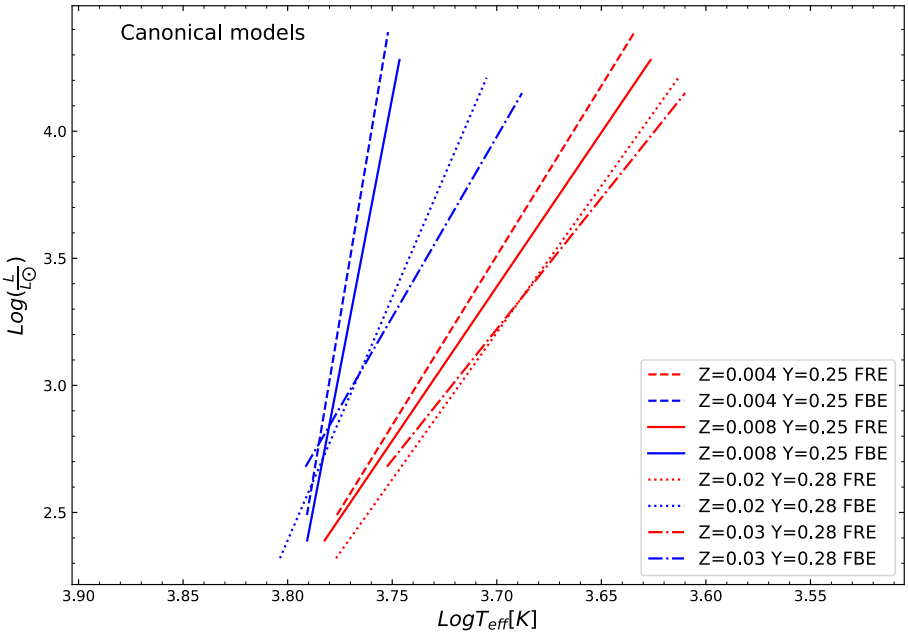

FIGURE 7.1: The F and FO instability strip boundaries for $Z = 0.004$ (dashed lines), $Z = 0.008$ (solid lines), $Z = 0.02$ (dotted lines) and $Z = 0.03$ (dash-dotted lines), as obtained when adopting the canonical ML relation and the standard efficiency for the superadiabatic convection.

TABLE 7.11: Predicted Effective Temperatures of the Instability Strip Boundaries for $Z = 0.03$. The assumed error on the boundary predictions is $T_{eff} = \pm 50$ K, based on the adopted effective temperature step in the pulsational model computations.

$M/M_{\odot}$	$\log(L/L_{\odot})$	α_{ml}	ML	FOBE	FBE	FORE	FRE
(1)	(2)	(3)	(4)	(5)	(6)	(7)	(8)
4.0	2.68	1.5	A	6350	6150	5950	5550
4.0	2.88	1.5	B		5950		5250
5.0	3.01	1.5	A		5850		5250
5.0	3.21	1.5	B		5650		4950
6.0	3.27	1.5	A		5650		5050
6.0	3.47	1.5	B		5450		4650
7.0	3.5	1.5	A		5450		4750
7.0	3.7	1.5	B		5250		4350
8.0	3.69	1.5	A		5250		4550
8.0	3.89	1.5	B		5050		4150
9.0	3.86	1.5	A		5150		4350
9.0	4.06	1.5	B		4950		3950
10.0	4.02	1.5	A		4950		4150
10.0	4.22	1.5	B		4750		3750
11.0	4.15	1.5	A		4850		4050
11.0	4.35	1.5	B		4750		3650

TABLE 7.12: The coefficients of the linear relation $\log T_{eff}$ = a +b $\log(L/L_{\odot})$ for the boundaries of the F and FO-mode IS for $Z = 0.004$ and $Y = 0.25$ varying both the ML relation and the mixing length parameter.

α_{ml}	ML	a	b	σ_a	σ_b	R^2
FBE						
1.5	A	3.825	-0.016	0.012	0.003	0.7696
1.5	B	3.849	-0.022	0.011	0.003	0.8879
1.5	C	3.889	-0.033	0.010	0.003	0.9589
1.7	A	3.842	-0.020	0.009	0.002	0.9075
1.7	B	3.876	-0.029	0.013	0.003	0.9188
1.7	C	3.911	-0.038	0.008	0.002	0.9803
1.9	A	3.873	-0.028	0.013	0.004	0.9009
1.9	B	3.895	-0.034	0.011	0.003	0.9565
1.9	C	3.924	-0.042	0.005	0.001	0.9939
FRE						
1.5	A	3.958	-0.074	0.014	0.004	0.9814
1.5	B	3.937	-0.069	0.033	0.009	0.9031
1.5	C	3.762	-0.021	0.073	0.018	0.1598
1.7	A	3.941	-0.064	0.011	0.003	0.9840
1.7	B	3.949	-0.069	0.014	0.004	0.9819
1.7	C	3.825	-0.035	0.069	0.017	0.3785
1.9	A	3.920	-0.055	0.007	0.002	0.9918
1.9	B	3.950	-0.065	0.015	0.004	0.9758
1.9	C	3.860	-0.042	0.061	0.015	0.5236
FOBE						
1.5	A	3.941	-0.044	0.012	0.004	0.9796
1.5	B	3.945	-0.045	0.005	0.002	0.9988
1.7	A	3.971	-0.054	0.007	0.002	0.9963
1.7	B	3.970	-0.054	0.014	0.005	0.9932
1.9	A	3.961	-0.052	0.017	0.005	0.9791
1.9	B	3.966	-0.055	0.014	0.005	0.9931
FORE						
1.5	A	3.844	-0.026	0.043	0.013	0.5588
1.5	B	3.888	-0.042	0.099	0.032	0.6320
1.7	A	3.870	-0.031	0.046	0.015	0.6807
1.7	B	3.894	-0.041	0.097	0.031	0.6321
1.9	A	3.882	-0.033	0.031	0.010	0.8443
1.9	B	3.867	-0.028	0.058	0.019	0.6879

TABLE 7.13: The coefficients of the the quadratic relation $\log T_{eff}$ = a + b $\log(L/L_\odot)$ +c $(\log(L/L_\odot))^2$ for the boundaries of the F-mode IS for $Z = 0.004$ and $Y = 0.25$ varying both the ML relation and the mixing length parameter.

α_{ml}	ML	a	b	σ_a	σ_b	R^2		
FBE								
1.5	A	3.708	0.054	-0.010	0.057	0.034	0.005	0.8657
1.5	B	3.681	0.072	-0.013	0.033	0.018	0.003	0.9791
1.5	C	3.740	0.047	-0.010	0.040	0.021	0.003	0.9878
1.7	A	3.734	0.045	-0.009	0.033	0.019	0.003	0.9676
1.7	B	3.674	0.084	-0.015	0.010	0.005	0.001	0.9989
1.7	C	3.847	-0.004	-0.004	0.053	0.028	0.004	0.9842
1.9	A	3.702	0.074	-0.015	0.039	0.023	0.003	0.9766
1.9	B	3.788	0.026	-0.008	0.055	0.031	0.004	0.9736
1.9	C	3.885	-0.021	-0.003	0.032	0.017	0.002	0.9951
FRE								
1.5	A	3.776	0.035	-0.016	0.046	0.027	0.004	0.9950
1.5	B	4.157	-0.193	0.017	0.202	0.112	0.015	0.9195
1.5	C	4.917	-0.633	0.079	0.196	0.103	0.013	0.8781
1.7	A	3.789	0.026	-0.013	0.034	0.020	0.003	0.9964
1.7	B	3.880	-0.030	-0.005	0.087	0.048	0.007	0.9836
1.7	C	4.728	-0.515	0.062	0.316	0.166	0.021	0.7406
1.9	A	3.851	-0.014	-0.006	0.033	0.019	0.003	0.9953
1.9	B	3.738	0.053	-0.016	0.050	0.028	0.004	0.9940
1.9	C	4.520	-0.392	0.045	0.339	0.178	0.023	0.7108

7.3 On the dependency of the period-mass-luminosity-temperature relation on the metallicity

As already performed for solar chemical composition models (See Chapter 3), a linear regression analysis of the period as a function of the luminosity, the mass, and the effective temperature (see Tables 3.1 and 3.2) was carried out. The coefficients of the relations for F and FO pulsators, at each chosen chemical composition, are reported in Table 7.18, and an inspection of their values confirms that they are not significantly affected by the choice of mixing length parameter.
Concerning the metallicity effect, we noticed that metallicity has a larger effect on both the zero-point and the coefficient of $\log T_{eff}$ than the other coefficients. In particular, in agreement with previous investigations (see e.g. Bono et al., 2000b), longer periods are expected for higher metal abundance models, when all the other parameters are fixed.

7.4 The light and radial velocity curves

As already shown for the solar metallicity case, the computation of nonlinear pulsation models allowed us to obtain sound predictions about the variation of all relevant quantities such as the luminosity, the radius, the radial velocity, the surface temperature and gravity along a model pulsation cycle.

The bolometric light curves for a sequence of canonical models listed in Tables 7.9, 7.10 and 7.11 are shown in the left panels of Figs 7.2, 7.3 and 7.4, for each labeled

TABLE 7.14: The coefficients of the linear relation $\log T_{eff}$ = a +b $\log(L/L_{\odot})$ for the boundaries of the F and FO-mode IS for $Z = 0.008$ and $Y = 0.25$ varying both the ML relation and the mixing length parameter.

α_{ml}	ML	a	b	σ_a	σ_b	R^2
FBE						
1.5	A	3.833	-0.020	0.012	0.003	0.8362
1.5	B	3.865	-0.029	0.017	0.005	0.8444
1.5	C	3.905	-0.040	0.013	0.003	0.9527
1.7	A	3.888	-0.035	0.020	0.005	0.8745
1.7	B	3.910	-0.041	0.024	0.006	0.8601
1.7	C	3.921	-0.044	0.012	0.003	0.9660
1.9	A	3.934	-0.048	0.025	0.007	0.8960
1.9	B	3.942	-0.051	0.020	0.005	0.9288
1.9	C	3.967	-0.058	0.012	0.003	0.9802
FRE						
1.5	A	3.975	-0.081	0.014	0.004	0.9839
1.5	B	3.987	-0.087	0.022	0.006	0.9692
1.5	C	3.857	-0.050	0.058	0.015	0.6218
1.7	A	3.965	-0.072	0.011	0.003	0.9899
1.7	B	3.993	-0.084	0.026	0.007	0.9540
1.7	C	3.900	-0.058	0.050	0.013	0.7475
1.9	A	3.930	-0.058	0.009	0.002	0.9899
1.9	B	3.962	-0.069	0.015	0.004	0.9778
1.9	C	3.943	-0.066	0.038	0.010	0.8726
FOBE						
1.5	A	3.916	-0.037	0.021	0.007	0.9073
1.5	B	3.969	-0.054	0.013	0.004	0.9932
1.7	A	3.949	-0.048	0.020	0.006	0.9506
1.7	B	3.965	-0.054	0.014	0.005	0.9932
1.9	A	3.936	-0.044	0.024	0.009	0.9626
FORE						
1.5	A	3.864	-0.034	0.029	0.009	0.8122
1.5	B	3.879	-0.039	0.078	0.026	0.6879
1.7	A	3.870	-0.034	0.029	0.009	0.8123
1.7	B	3.885	-0.038	0.076	0.025	0.6879
1.9	A	3.869	-0.029	0.040	0.014	0.8073

TABLE 7.15: The coefficients of the quadratic relation $\log T_{eff}$ = a + b $\log(L/L_\odot)$ +c $(\log(L/L_\odot))^2$ for the boundaries of the F-mode IS for $Z = 0.008$ and $Y = 0.25$ varying both the ML relation and the mixing length parameter.

α_{ml}	ML	a	b	c	σ_a	σ_b	σ_c	R^2
FBE								
1.5	A	3.696	0.065	-0.013	0.044	0.026	0.004	0.9391
1.5	B	3.633	0.106	-0.019	0.061	0.035	0.005	0.9549
1.5	C	3.711	0.066	-0.014	0.046	0.025	0.003	0.9885
1.7	A	3.528	0.171	-0.029	0.066	0.038	0.005	0.9820
1.7	B	3.551	0.166	-0.029	0.044	0.025	0.004	0.9885
1.7	C	3.765	0.041	-0.011	0.056	0.031	0.004	0.9852
1.9	A	3.483	0.211	-0.036	0.069	0.040	0.006	0.9892
1.9	B	3.633	0.128	-0.025	0.030	0.017	0.002	0.9963
1.9	C	3.812	0.027	-0.011	0.056	0.031	0.004	0.9913
FRE								
1.5	A	3.806	0.023	-0.015	0.049	0.030	0.004	0.9947
1.5	B	3.891	-0.031	-0.008	0.139	0.080	0.011	0.9715
1.5	C	4.646	-0.481	0.057	0.237	0.128	0.017	0.8691
1.7	A	3.820	0.011	-0.012	0.071	0.040	0.006	0.9946
1.7	B	3.607	0.139	-0.031	0.062	0.036	0.005	0.9939
1.7	C	4.482	-0.376	0.042	0.253	0.137	0.018	0.8674
1.9	A	3.936	-0.061	0.000	0.076	0.043	0.006	0.9899
1.9	B	3.768	0.043	-0.016	0.055	0.031	0.004	0.9929
1.9	C	4.159	-0.184	0.016	0.247	0.133	0.018	0.8873

TABLE 7.16: The coefficients of the linear relation $\log T_{eff}$ = a +b $\log(L/L_\odot)$ for the boundaries of the F and FO-mode IS for $Z = 0.03$ and $Y = 0.28$ varying both the ML relation and the mixing length parameter.

α	ML	a	b	σ_a	σ_b	R^2
FBE						
1.5	A	3.979	-0.070	0.007	0.002	0.9953
1.5	B	3.976	-0.070	0.009	0.002	0.9937
FRE						
1.5	A	4.009	-0.096	0.015	0.004	0.9892
1.5	B	4.048	-0.111	0.013	0.004	0.9940

TABLE 7.17: The coefficients of the quadratic relation $\log T_{eff}$ = a + b $\log(L/L_\odot)$ +c $(\log(L/L_\odot))^2$ for the boundaries of the F-mode IS for $Z = 0.03$ and $Y = 0.28$ varying both the ML relation and the mixing length parameter.

α_{ml}	ML	a	b	c	σ_a	σ_b	σ_c	R^2
FBE								
1.5	A	3.878	-0.010	-0.009	0.037	0.022	0.003	0.9981
1.5	B	3.957	-0.059	-0.001	0.076	0.042	0.006	0.9937
FRE								
1.5	A	3.764	0.049	-0.021	0.052	0.031	0.004	0.9980
1.5	B	3.822	0.016	-0.017	0.059	0.033	0.005	0.9985

TABLE 7.18: The coefficients of the PMLT relations $\log P$ = a +blog T_{eff} + c log $(M/M_{\odot})$ + d log(L/$L_{\odot}$) for both F and FO pulsators as a function of the assumed α_{ml} parameter for $Z = 0.004$ and $Y = 0.25$, $Z = 0.008$ and $Y = 0.25$, $Z = 0.03$ and $Y = 0.28$. For comparison, the relations for $Z = 0.02$ and $Y = 0.28$ are also reported.

α_{ml}	a	b	c	d	σ_a	σ_b	σ_c	σ_d	R^2
				Z=0.004	Y= 0.25				
F									
1.5	10.711	-3.315	-0.776	0.918	0.109	0.028	0.017	0.005	0.9990
1.7	10.699	-3.312	-0.788	0.921	0.104	0.026	0.014	0.005	0.9995
1.9	10.764	-3.327	-0.791	0.919	0.124	0.031	0.014	0.005	0.9996
FO									
1.5	12.042	-3.636	-0.574	0.799	1.271	0.325	0.112	0.037	0.9867
1.7	11.590	-3.524	-0.677	0.828	1.385	0.352	0.102	0.036	0.9929
1.9	11.182	-3.410	-0.591	0.801	0.434	0.111	0.023	0.009	0.9999
				Z=0.008	Y= 0.25				
F									
1.5	10.482	-3.254	-0.773	0.920	0.103	0.026	0.017	0.005	0.9991
1.7	10.588	-3.283	-0.777	0.922	0.110	0.028	0.015	0.005	0.9995
1.9	11.077	-3.405	-0.770	0.911	0.184	0.046	0.017	0.007	0.9996
FO									
1.5	10.880	-3.337	-0.622	0.816	0.122	0.031	0.009	0.003	0.9999
1.7	10.927	-3.348	-0.622	0.813	0.223	0.057	0.014	0.005	0.9998
1.9	10.774	-3.300	-0.618	0.802	0.302	0.077	0.014	0.006	0.9998
				Z=0.02	Y= 0.28				
F									
1.5	10.268	-3.192	-0.758	0.919	0.001	0.025	0.015	0.005	0.9995
1.7	10.538	-3.258	-0.749	0.911	0.002	0.050	0.019	0.007	0.9996
1.9	11.488	-3.469	-0.695	0.847	0.003	0.089	0.012	0.006	0.9999
FO									
1.5	10.595	-3.253	-0.621	0.804	0.002	0.067	0.014	0.005	0.9996
1.7	10.359	-3.186	-0.576	0.788	0.002	0.056	0.009	0.003	0.9999
				Z=0.03	Y= 0.28				
F									
1.5	10.414	-3.227	-0.765	0.918	0.119	0.029	0.023	0.008	0.9998

mass, luminosity and mixing length parameter (see labeled values at the top of each plot). The radial velocity of these models are represented in the right panels of the same plots. In both panels, dotted lines refer to SO-mode models (if any), dashed lines refer to FO-mode models, whereas solid lines represent F-mode models. The model period, in days, and effective temperature, in kelvin, are also reported in the left and right panels, respectively. The morphology and amplitude of the curves both vary with the position of the model within the instability strip and depend on the adopted chemical composition. They also show a general decrease in the pulsation amplitudes as the metallicity increases, due to the increased contribution of opacity in the ionization regions to convection.

In particular, within the period range of 6 days < P <16 days, CCs show the Hertzsprung progression phenomenon i.e. the evolution of the position in phase of the secondary maximum (bump) in both light and the radial velocity curves as a function of the pulsation period (See Chapter 3). As expected, based on previous theoretical studies for 0.004 < Z < 0.02 (see e.g. Bono et al., 2000c), an analysis of Figs 7.2, 7.3, 7.4 and Fig. 3.5 in Chapter 3 suggests that an increase in the metal content causes a shift of the HP center (defined as the period at which the secondary bump reaches the same brightness as the primary one during its evolution from the decreasing to the rising branch of the curve) toward shorter periods. In fact, passing from $Z = 0.004$ to $Z = 0.008$ and finally to $Z = 0.02$ for a $M/M_{\odot} = 7$ model, the period corresponding to the HP center moves from about 11.4 to about 10.3 days and finally, to about 7.5 days. A detailed investigation of the dependence of the period, corresponding to the HP center, on metallicity will be the subject of a future work (Marconi, De Somma et al. 2021 in preparation).

$M/M_{\odot}$ **=3.0** $\log(\mathbf{L}/L_{\odot})$ **=2.49** $\alpha_{ml} = 1.5$

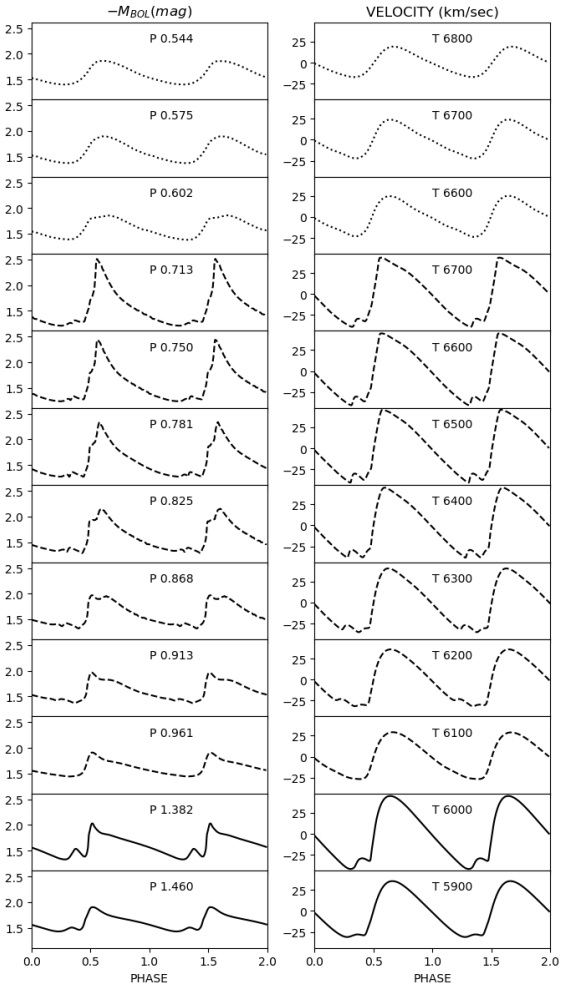

FIGURE 7.2: Bolometric light curves (left panel) and radial velocity curves (right panel) for a sequence of nonlinear F (solid line) and FO-mode models (dashed lines) derived for Z = 0.004 and Y = 0.25 at a fixed mass, luminosity and α_{ml} parameter (see labeled values at the top of the plot), adopting the canonical ML relation.

$M/M_{\odot}$ **=4.0** $\log(\mathbf{L}/L_{\odot})$ **=2.91** $\alpha_{ml} = 1.5$

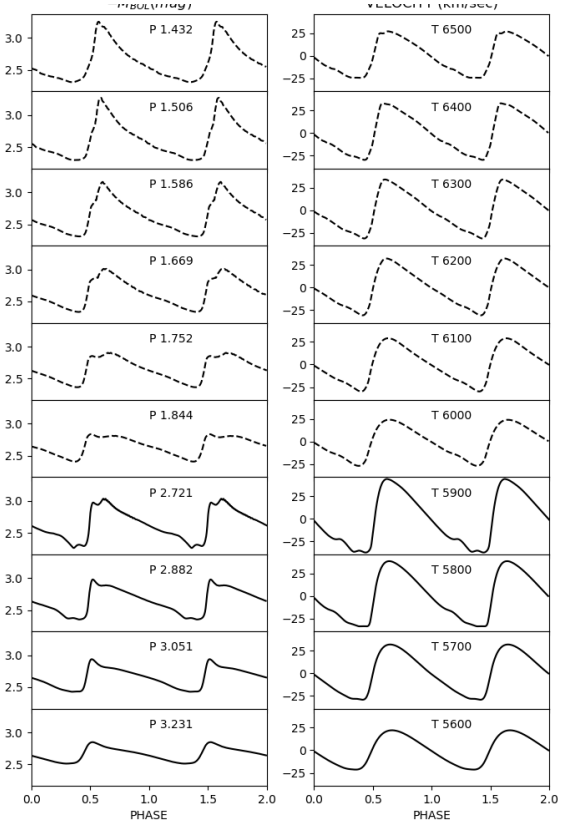

FIG.7.2-Continued.

$M/M_{\odot}$ **=5.0** $\log(\mathbf{L}/L_{\odot})$ **=3.24** $\alpha_{ml} = 1.5$

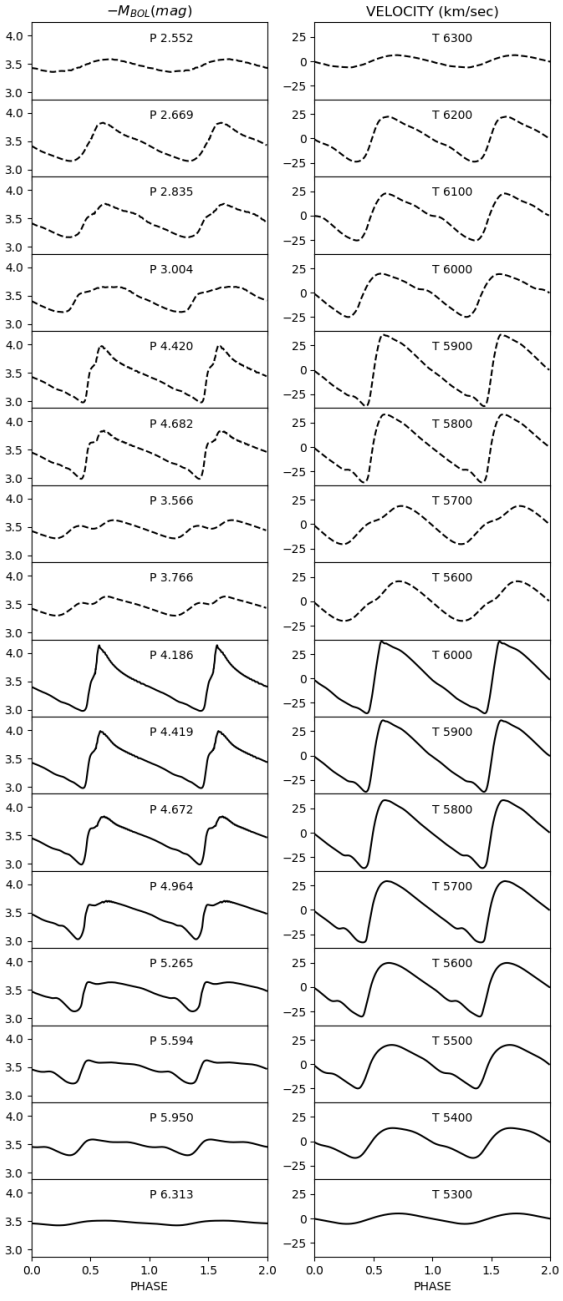

FIG.7.2-Continued.

$M/M_{\odot}$ **=6.0** $\log(\mathbf{L}/L_{\odot})$ **=3.50** $\alpha_{ml} = 1.5$

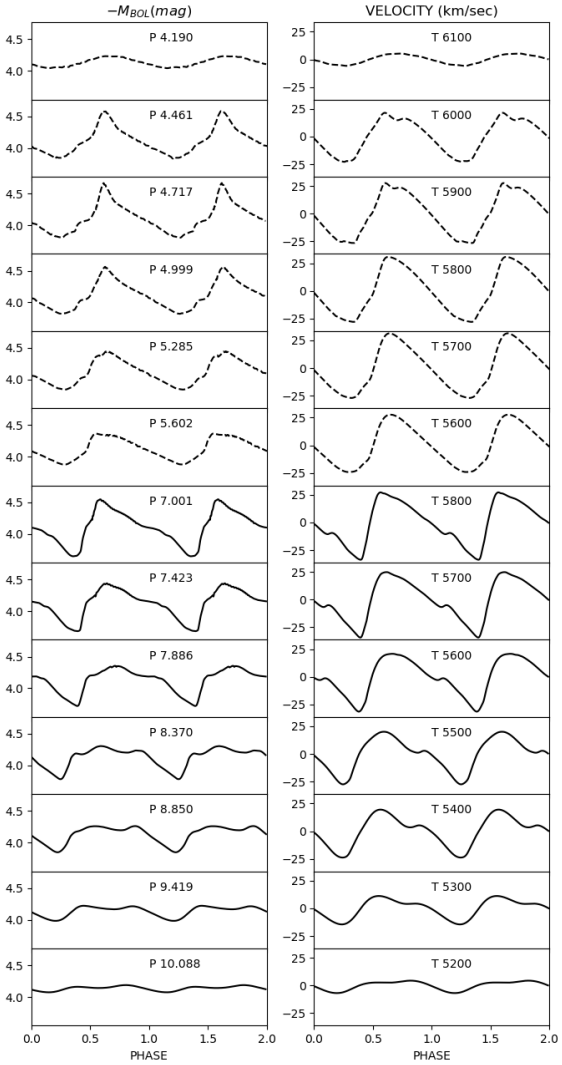

FIG.7.2-Continued.

$M/M_{\odot}$ **=7.0** $\log(\mathbf{L}/L_{\odot})$ **=3.73** $\alpha_{ml} = 1.5$

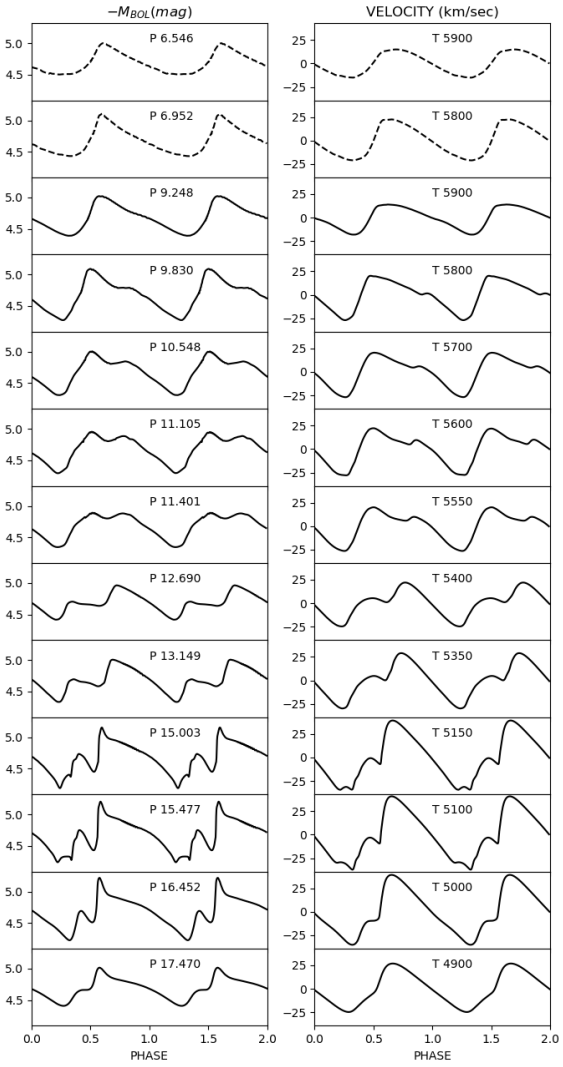

FIG.7.2-Continued.

$M/M_{\odot}$ **=8.0** $\log(\mathbf{L}/L_{\odot})$ **=3.92** $\alpha_{ml} = 1.5$

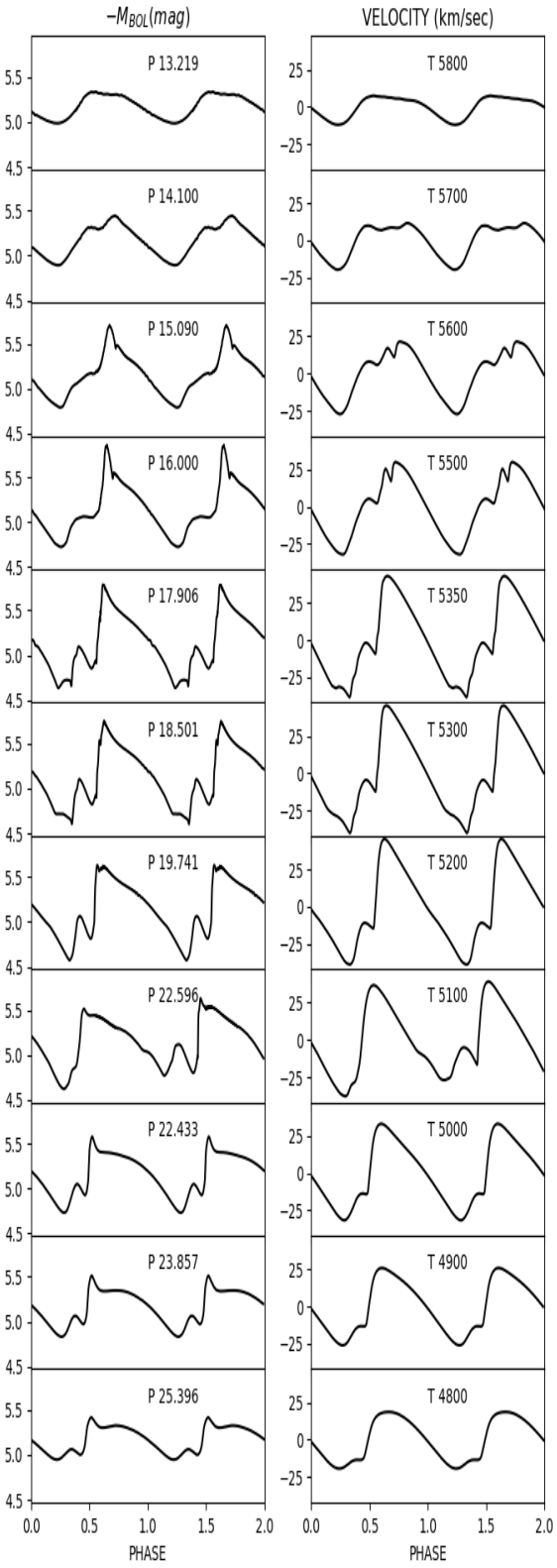

FIG.7.2-Continued.

$M/M_{\odot}$ **=9.0** $\log(\mathbf{L}/L_{\odot})$ **=4.09** $\alpha_{ml} = 1.5$

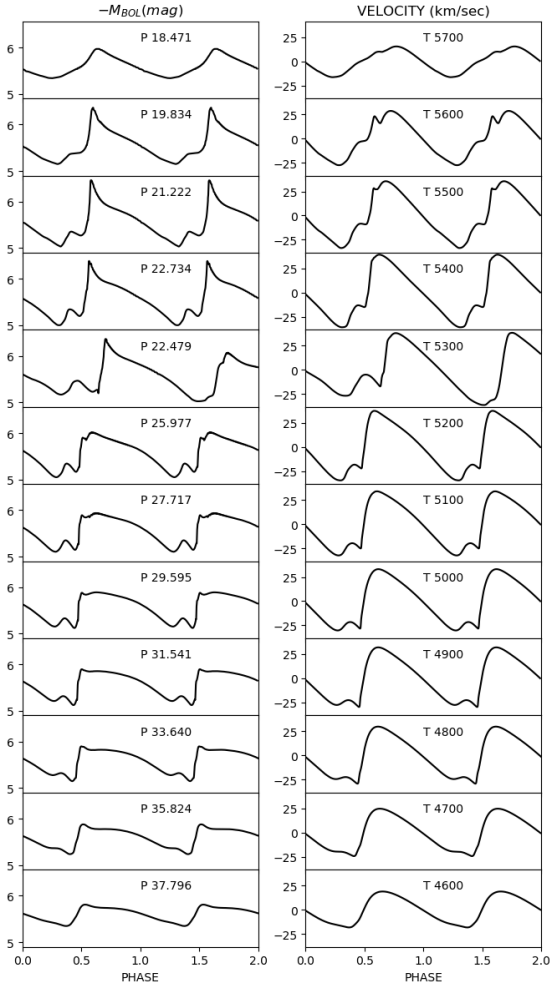

FIG.7.2-Continued.

$M/M_{\odot}$ **=10.0** $\log(\mathbf{L}/L_{\odot})$ **=4.25** $\alpha_{ml} = 1.5$

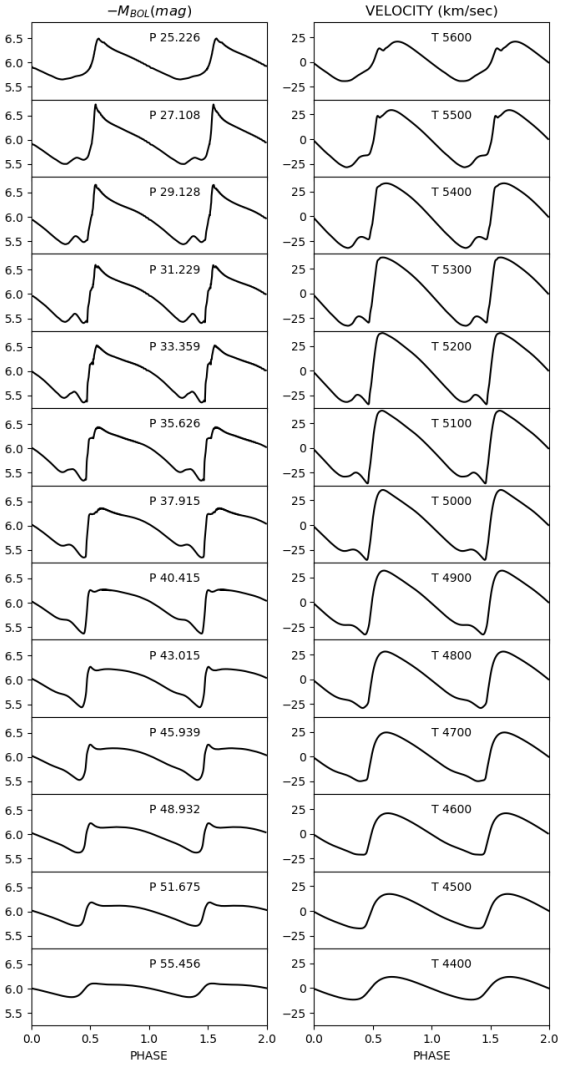

FIG.7.2-Continued.

$M/M_{\odot}$ **=11.0** $\log(\mathbf{L}/L_{\odot})$ **=4.39** $\alpha_{ml} = 1.5$

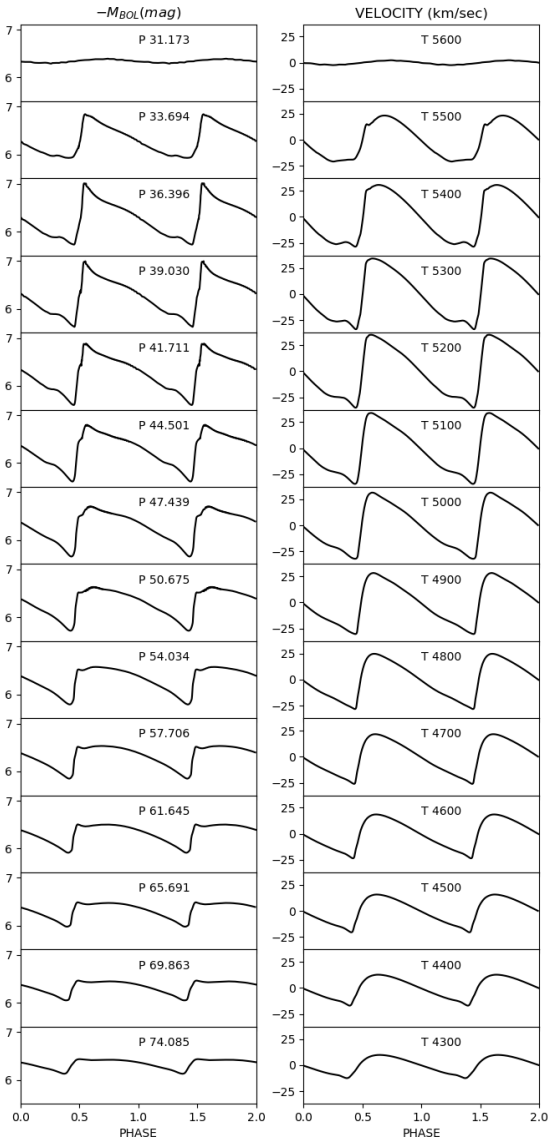

FIG.7.2-Continued.

$M/M_{\odot}$ **=3.0** $\log(\mathbf{L}/L_{\odot})$ **=2.39** $\alpha_{ml} = 1.5$

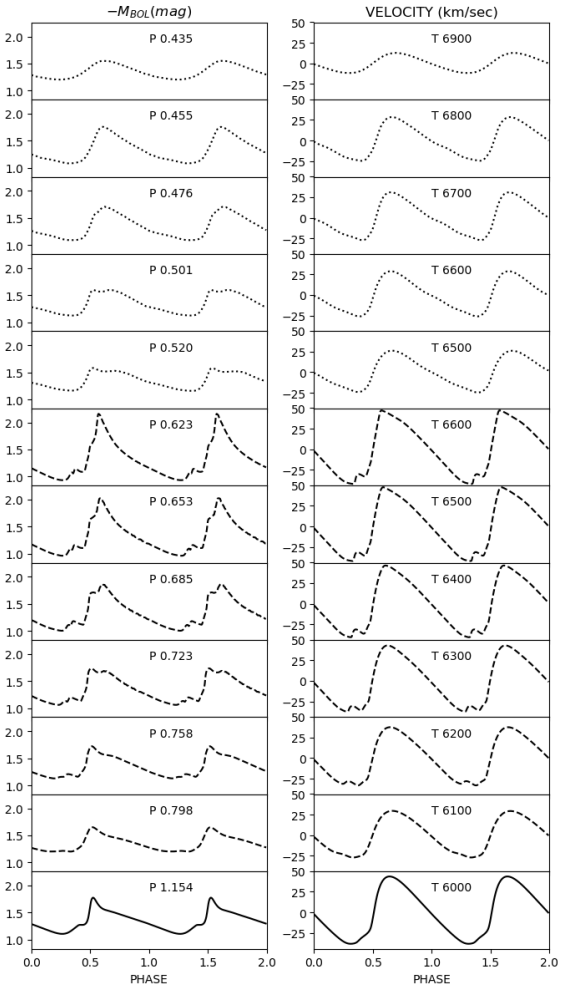

FIGURE 7.3: Bolometric light curves (left panel) and radial velocity curves (right panel) for a sequence of nonlinear F (solid line) and FO-mode models (dashed lines) derived for Z = 0.008 and Y = 0.25 at a fixed mass, luminosity and α_{ml} parameter (see labeled values at the top of the plot), adopting the canonical ML relation.

$M/M_{\odot}$ **=4.0** $\log(\mathbf{L}/L_{\odot})$ **=2.81** $\alpha_{ml} = 1.5$

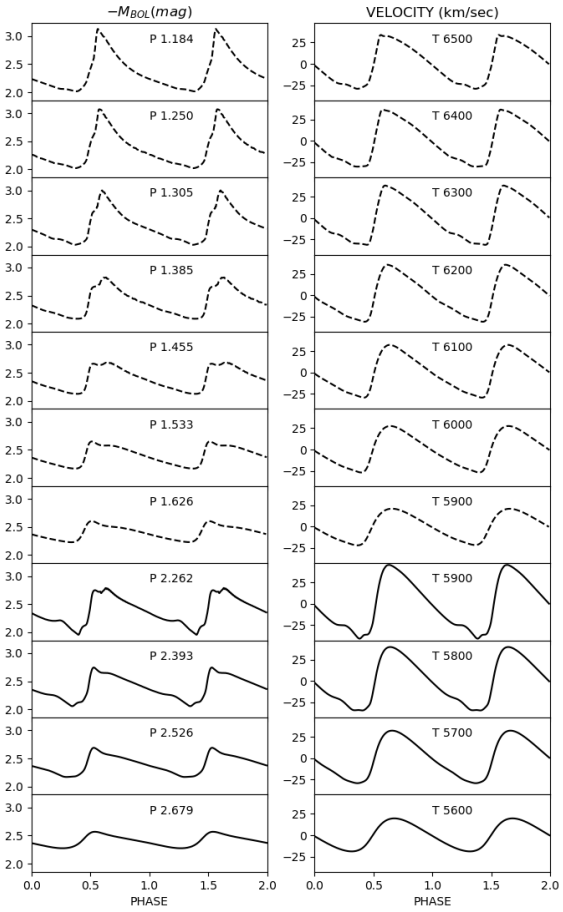

FIG.7.3-Continued.

$M/M_{\odot}$ **=5.0** $\log(\mathbf{L}/L_{\odot})$ **=3.14** $\alpha_{ml} = 1.5$

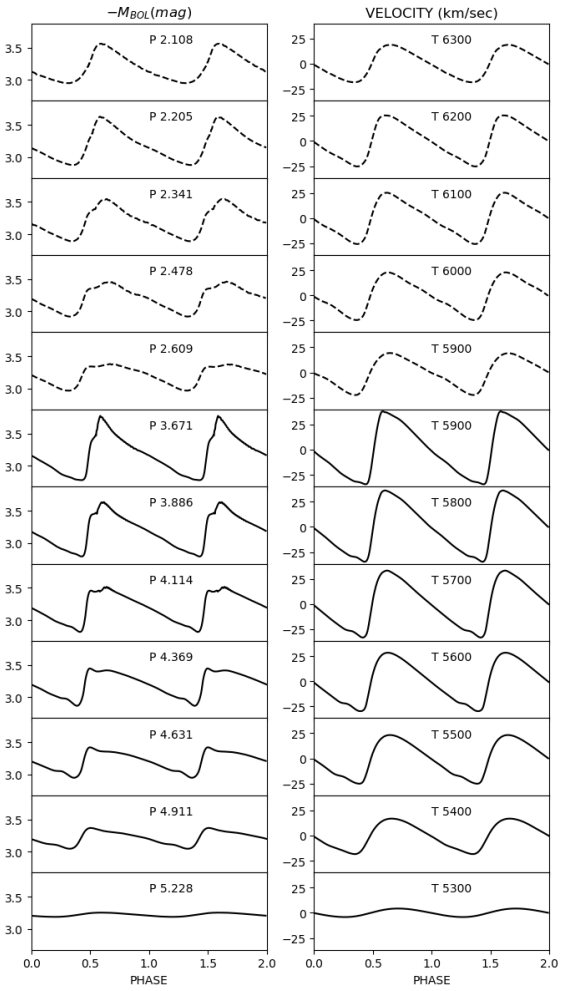

FIG.7.3-Continued.

$M/M_{\odot}$ **=6.0** $\log(\mathbf{L}/L_{\odot})$ **=3.40** $\alpha_{ml} = 1.5$

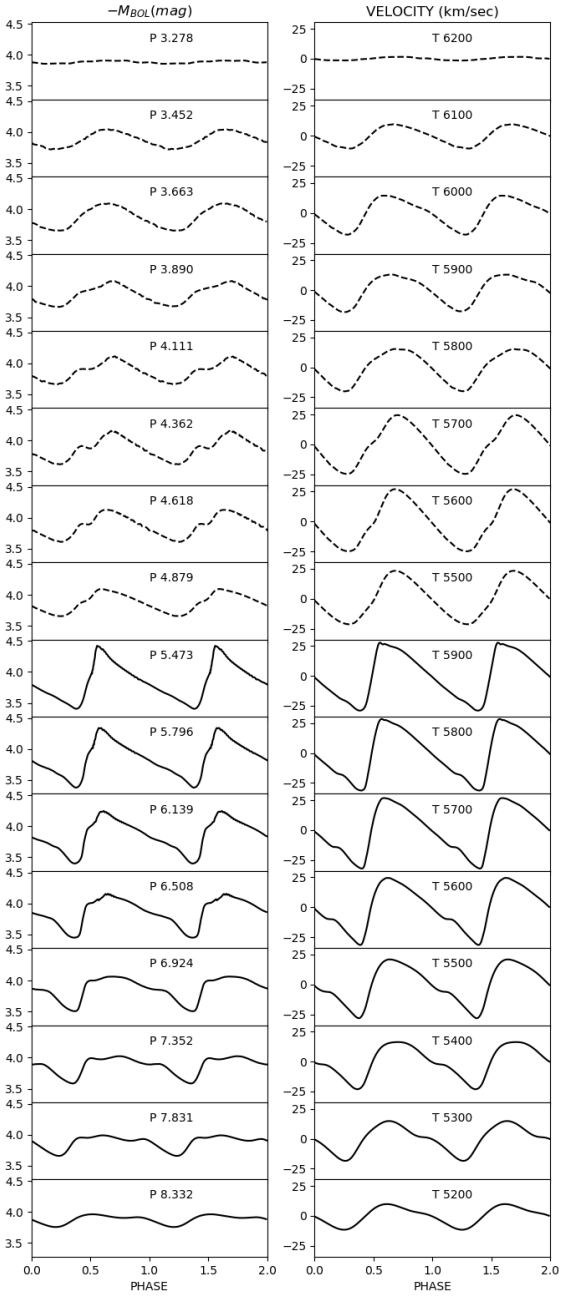

FIG.7.3-Continued.

$M/M_{\odot}$ **=7.0** $\log(\mathbf{L}/L_{\odot})$ **=3.63** $\alpha_{ml} = 1.5$

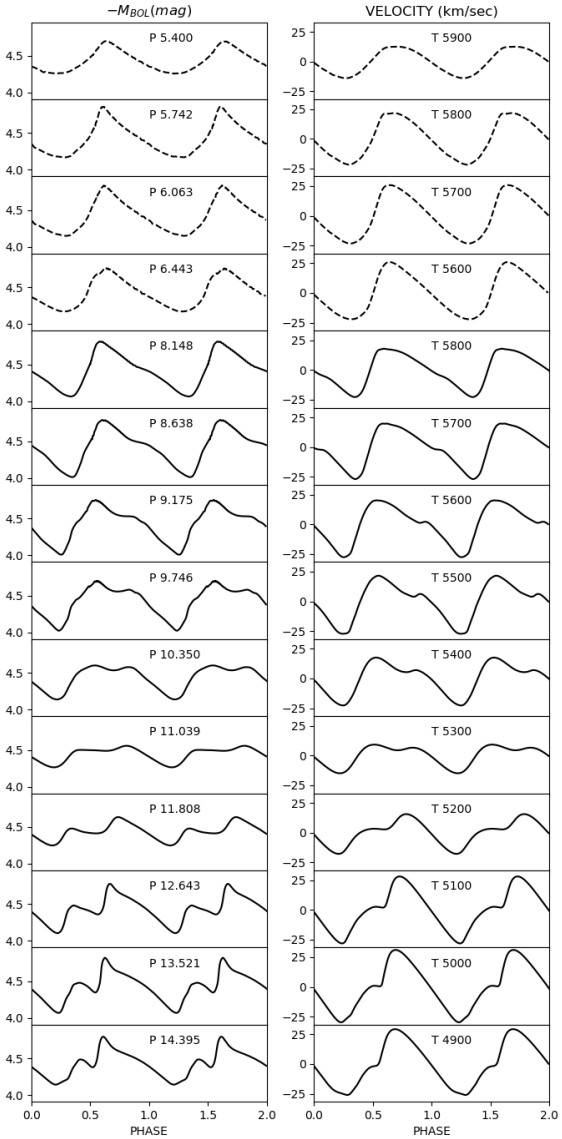

FIG.7.3-Continued.

$M/M_{\odot}$ **=8.0** $\log(\mathbf{L}/L_{\odot})$ **=3.82** $\alpha_{ml} = 1.5$

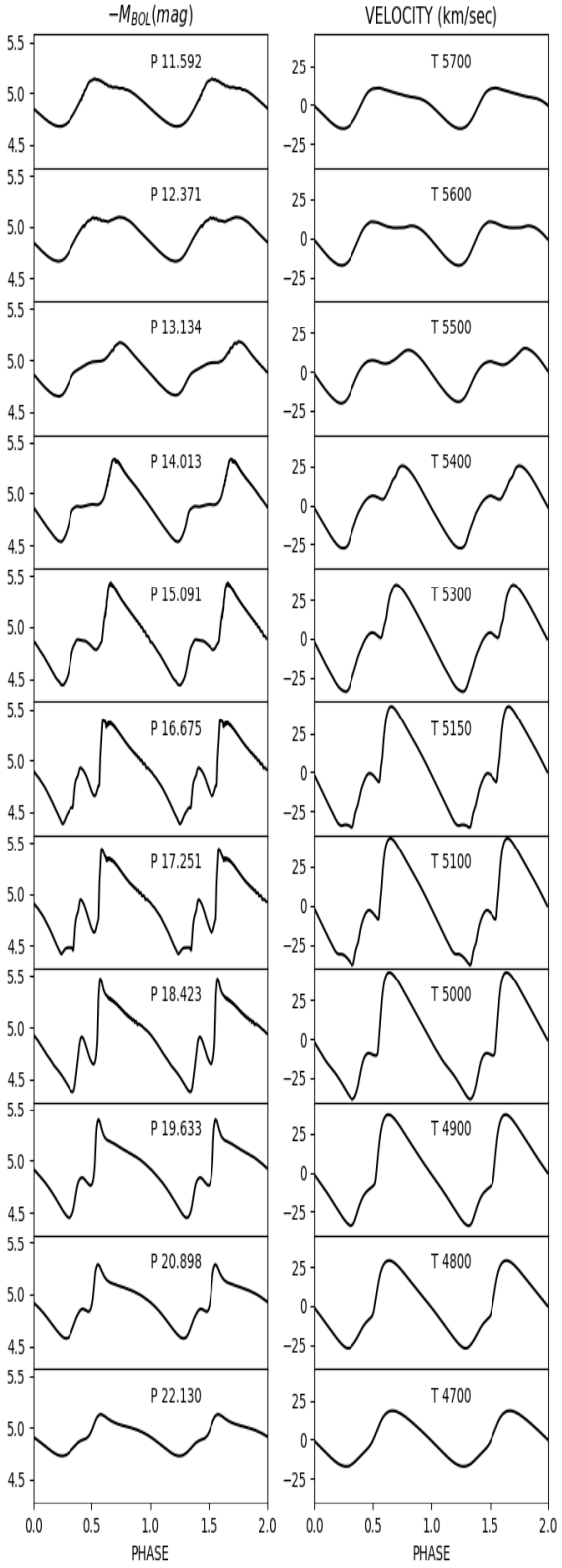

FIG.7.3-Continued.

$M/M_{\odot}$ **=9.0** $\log(\mathbf{L}/L_{\odot})$ **=3.99** $\alpha_{ml} = 1.5$

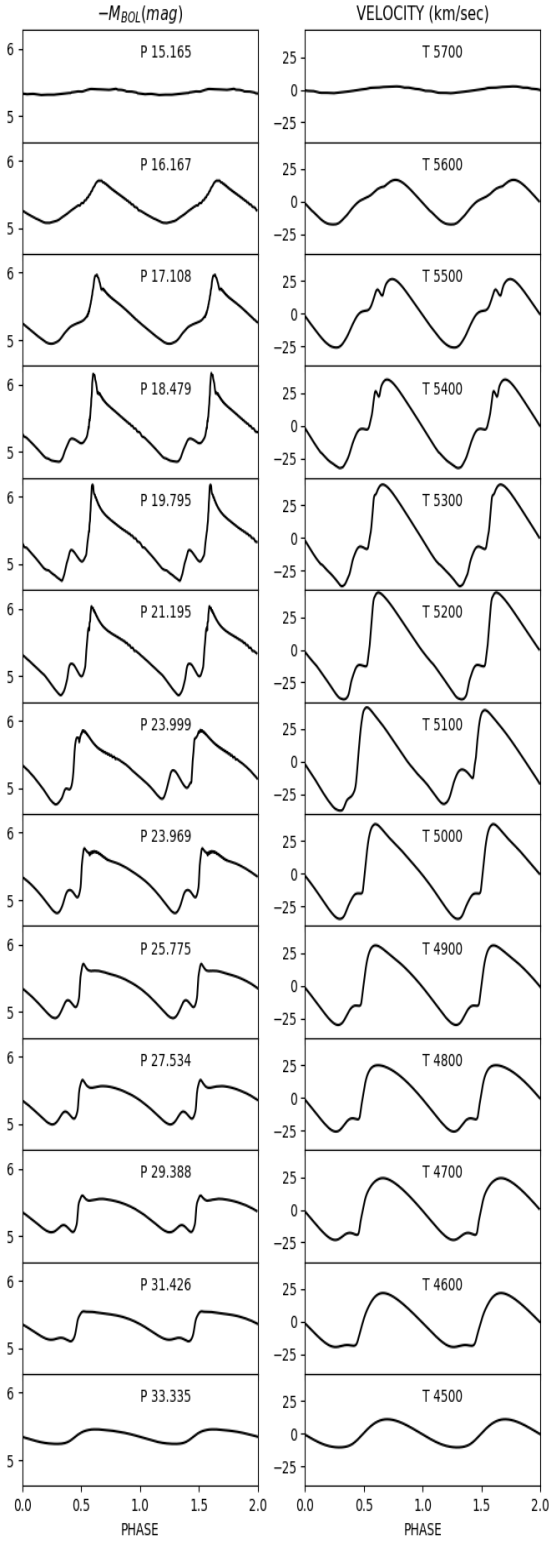

FIG.7.3-Continued.

$M/M_{\odot}$ **=10.0** $\log(\mathbf{L}/L_{\odot})$ **=4.14** $\alpha_{ml} = 1.5$

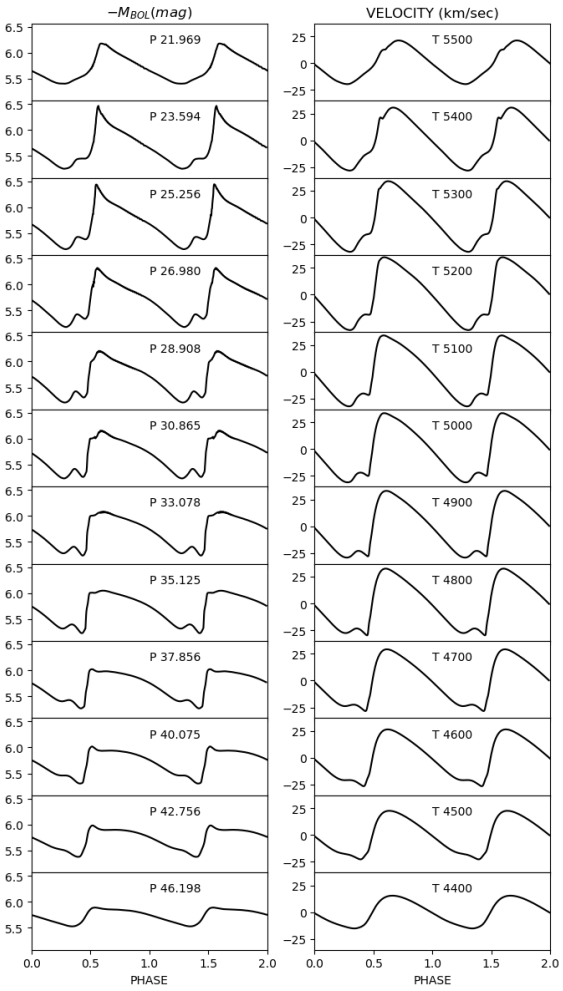

FIG.7.3-Continued.

$M/M_{\odot}$ **=11.0** $\log(\mathbf{L}/L_{\odot})$ **=4.28** $\alpha_{ml} = 1.5$

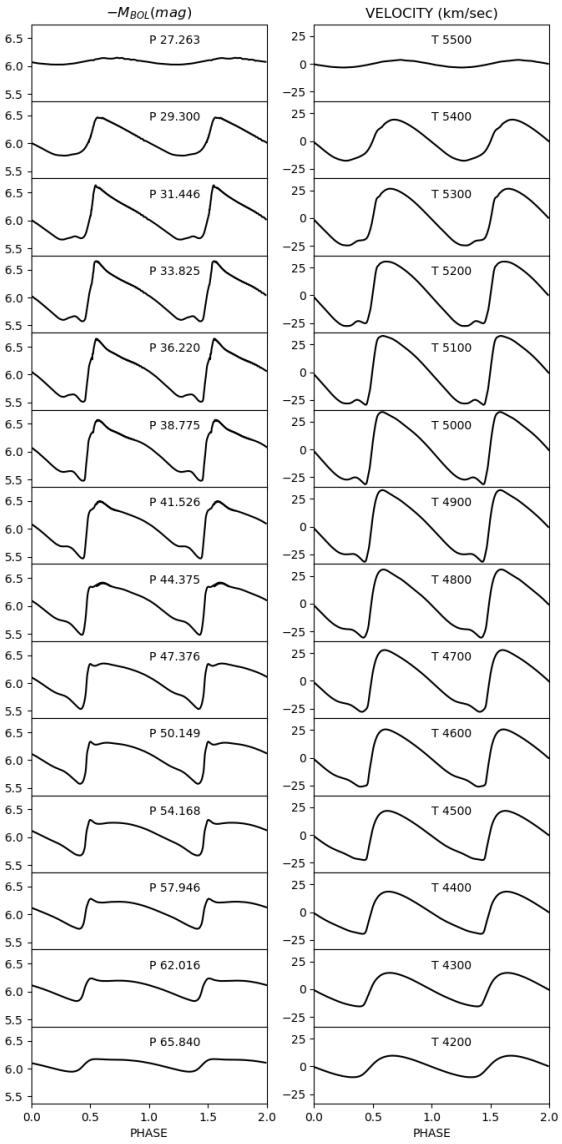

FIG.7.3-Continued.

$M/M_{\odot}$ **=4.0** $\log(\mathbf{L}/L_{\odot})$ **=2.68** $\alpha_{ml} = 1.5$

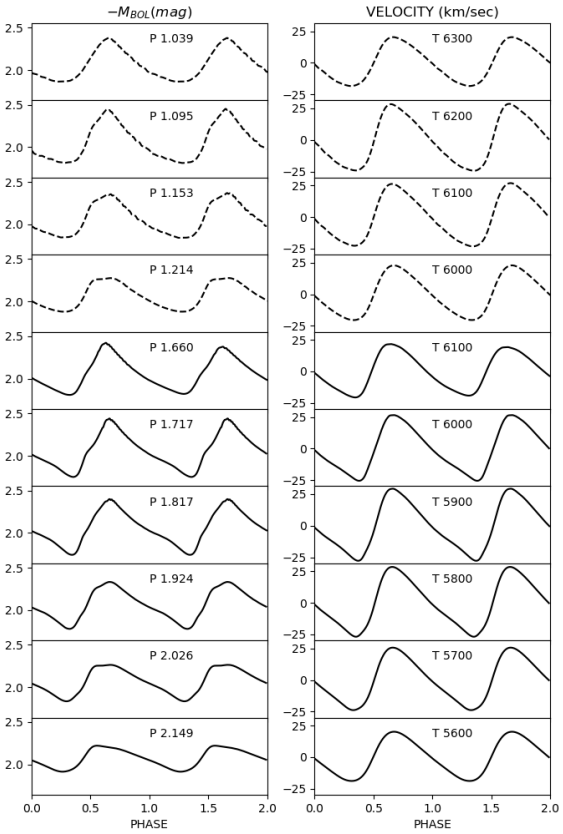

FIGURE 7.4: Bolometric light curves (left panel) and radial velocity curves (right panel) for a sequence of nonlinear F (solid line) and FO-mode models (dashed lines) derived for Z = 0.03 and Y = 0.28 at a fixed mass, luminosity and α_{ml} parameter (see labeled values at the top of the plot), adopting the canonical ML relation.

$M/M_{\odot}$ **=5.0** $\log(\mathbf{L}/L_{\odot})$ **=3.01** $\alpha_{ml} = 1.5$

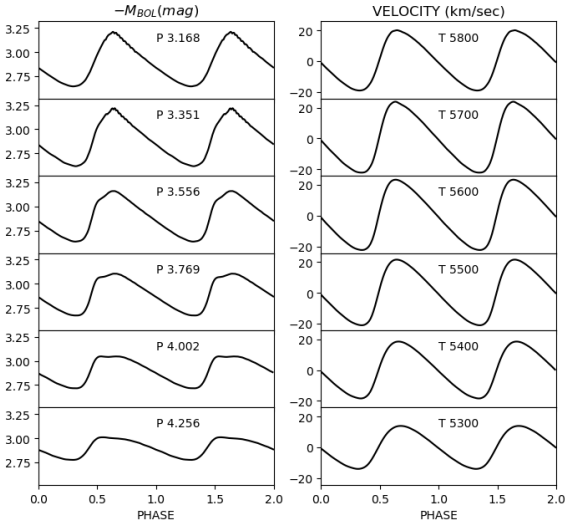

FIG.7.4-Continued.

$M/M_{\odot}$ **=6.0** $\log(\mathbf{L}/L_{\odot})$ **=3.27** $\alpha_{ml} = 1.5$

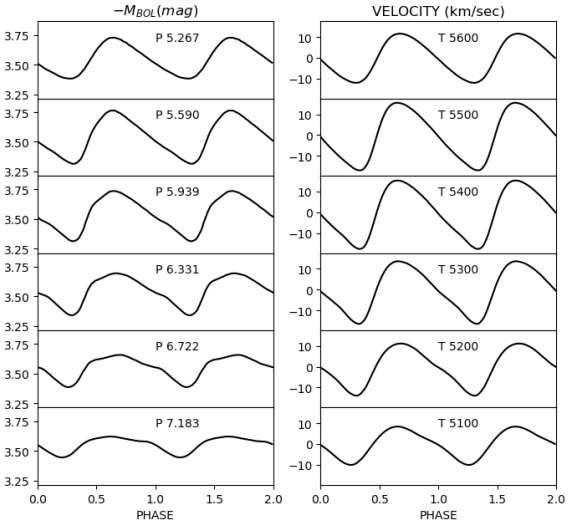

FIG.7.4-Continued.

$M/M_{\odot}$ **=7.0** $\log(\mathbf{L}/L_{\odot})$ **=3.50** $\alpha_{ml} = 1.5$

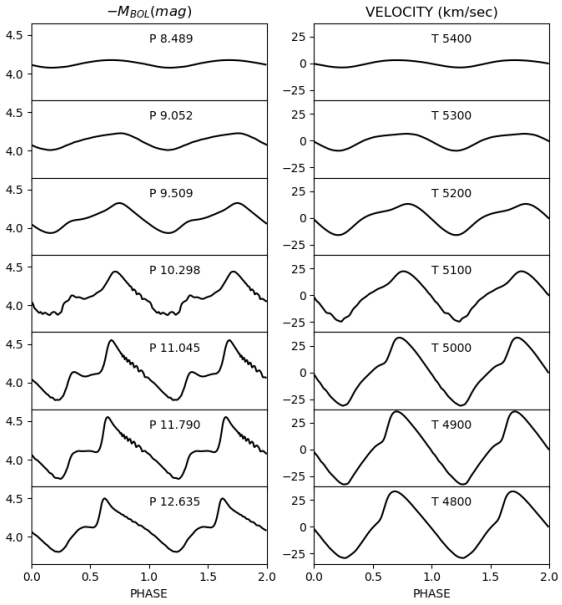

FIG.7.4-Continued.

$M/M_{\odot}$ **=8.0** $\log(\mathbf{L}/L_{\odot})$ **=3.69** $\alpha_{ml} = 1.5$

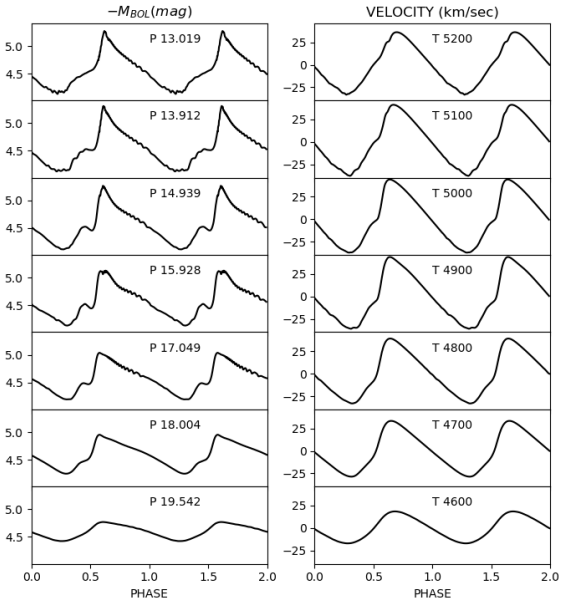

FIG.7.4-Continued.

$M/M_{\odot}$ **=9.0** $\log(\mathbf{L}/L_{\odot})$ **=3.86** $\alpha_{ml} = 1.5$

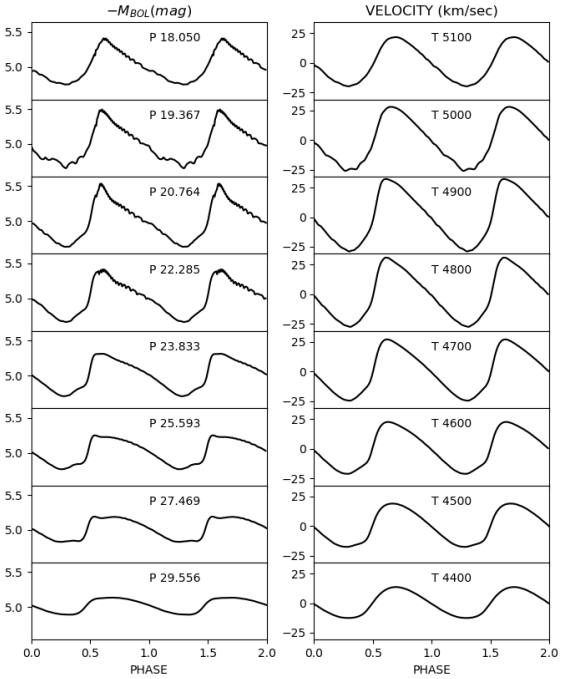

FIG.7.4-Continued.

$M/M_{\odot}$ **=10.0** $\log(\mathbf{L}/L_{\odot})$ **=4.02** $\alpha_{ml} = 1.5$

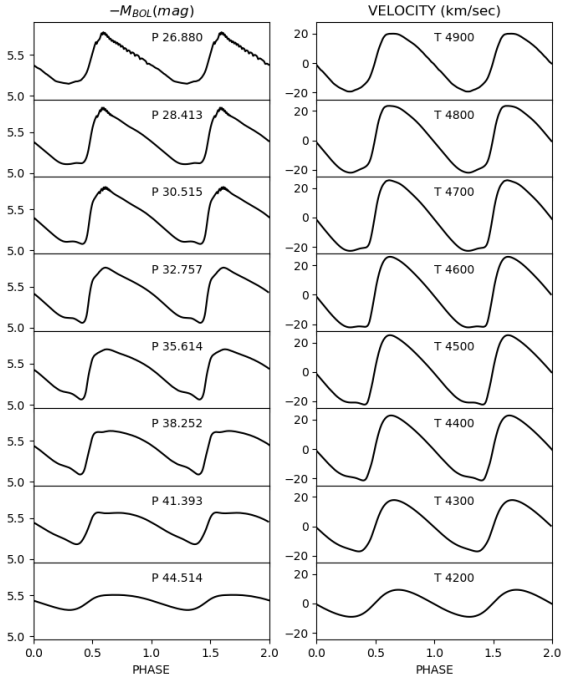

FIG.7.4-Continued.

$M/M_{\odot}$ **=11.0** $\log(\mathbf{L}/L_{\odot})$ **=4.15** $\alpha_{ml} = 1.5$

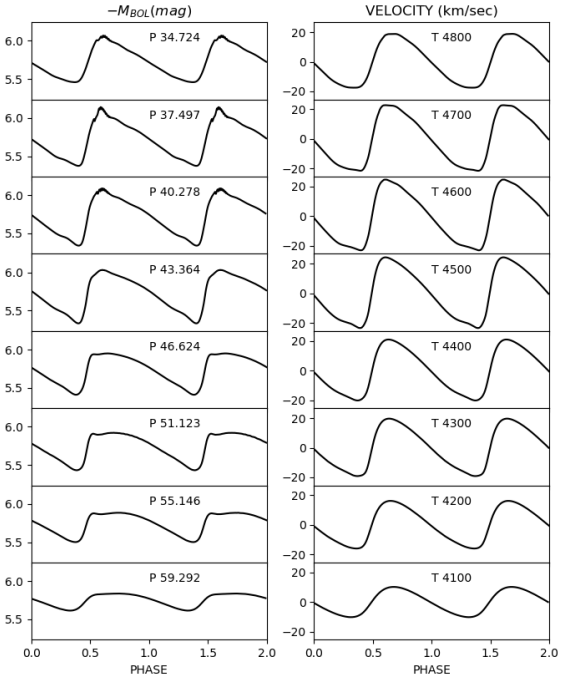

FIG.7.4-Continued.

7.5 The Period-Radius and Period-Mass-Radius relations

From the radius curves, the mean radii were derived and correlated with the pulsation periods. If the width in temperature of the IS is neglected, the pulsation relation connecting the period of a variable, at a fixed chemical composition, on stellar mass, luminosity (radius), and effective temperature becomes a period-mass-radius relation. This means that independent estimates of both period and mean radius provide an independent evaluation of Cepheid masses. Theoretical PR and PMR relation coefficients for both F and FO-mode pulsation models for $Z = 0.004$, $Z = 0.008$, $Z = 0.02$ and $Z = 0.03$ are reported in Tables 7.19 and 7.21, respectively.
These relations depend on the ML relation and, marginally, on the metal content. In particular, for a short period variable ($\log P = 0.3$) with $Z = 0.004$, the predicted mean radius increases by 5.0% from case A to B and by about 10% from case A to C. For a long period variable ($\log P = 1.8$) the variation in the predicted mean radius increases by up to 8% moving from case A to B and by up to 15% moving from case A to C. On the other hand, for canonical radii, an increase in the metal content from $Z = 0.004$ to $Z = 0.008$ and finally to $Z = 0.03$ leads to a variation that ranges from 0.5% to almost 4% for both short and long period variables. Similar results were obtained for noncanonical models. By adding a metallicity coefficient to the PR relation, a period-radius-metallicity (PRZ) relation for both F and FO-mode models of all chemical compositions (including $Z = 0.02$), were derived and reported in Table 7.20. These relations show a negligible metallicity term.

TABLE 7.19: The coefficients of the relation $\log(R/R_\odot)$=a+b $\log P$ for both F and FO Cepheids derived by adopting $Z = 0.004$, $Y = 0.25$; $Z = 0.008$, $Y = 0.25$; and $Z = 0.03$, $Y = 0.28$ as a function of the assumed α_{ml} parameter and A, B, C ML relations. For comparison, the relations for $Z = 0.02$, $Y = 0.28$ are also reported.

α_{ml}	ML	a	b	σ_a	σ_b	R^2
			Z=0.004	Y= 0.25		
F						
1.5	A	1.146	0.703	0.007	0.005	0.9958
1.5	B	1.131	0.690	0.007	0.005	0.9954
1.5	C	1.101	0.690	0.007	0.005	0.9955
1.7	A	1.143	0.708	0.006	0.005	0.9973
1.7	B	1.129	0.692	0.006	0.004	0.9970
1.7	C	1.104	0.687	0.006	0.004	0.9970
1.9	A	1.140	0.714	0.005	0.004	0.9984
1.9	B	1.128	0.694	0.005	0.004	0.9978
1.9	C	1.103	0.687	0.006	0.004	0.9978
FO						
1.5	A	1.229	0.731	0.008	0.017	0.9853
1.5	B	1.206	0.725	0.012	0.025	0.9800
1.5	C	1.182	0.741	0.003	0.006	0.9997
1.7	A	1.231	0.752	0.002	0.005	0.9993
1.7	B	1.209	0.713	0.014	0.032	0.9749
1.7	C	1.178	0.746	0.007	0.017	0.9989
1.9	A	1.229	0.756	0.002	0.005	0.9995
1.9	B	1.203	0.752	0.003	0.008	0.9995
			Z=0.008	Y= 0.25		
F						

TABLE 7.19: continued.

α_{ml}	ML	a	b	σ_a	σ_b	R^2
1.5	A	1.153	0.703	0.006	0.005	0.9966
1.5	B	1.137	0.690	0.006	0.004	0.9961
1.5	C	1.105	0.690	0.006	0.004	0.9972
1.7	A	1.154	0.706	0.005	0.004	0.9979
1.7	B	1.137	0.689	0.006	0.004	0.9973
1.7	C	1.111	0.686	0.005	0.004	0.9978
1.9	A	1.151	0.711	0.004	0.004	0.9990
1.9	B	1.133	0.695	0.005	0.004	0.9986
1.9	C	1.115	0.683	0.005	0.003	0.9987
FO						
1.5	A	1.239	0.756	0.002	0.004	0.9990
1.5	B	1.216	0.747	0.002	0.006	0.9988
1.5	C	1.193	0.736	0.004	0.009	0.9987
1.7	A	1.239	0.755	0.002	0.005	0.9992
1.7	B	1.215	0.747	0.002	0.006	0.9993
1.7	C	1.194	0.732	0.003	0.008	0.9993
1.9	A	1.241	0.768	0.001	0.007	0.9993
1.9	B	1.214	0.748	0.002	0.014	0.9984
1.9	C	1.220	0.573	0.001	0.003	1.0000
			Z=0.02	Y= 0.28		
F						
1.5	A	1.142	0.702	0.004	0.003	0.998
1.5	B	1.128	0.685	0.005	0.003	0.998
1.5	C	1.104	0.680	0.005	0.003	0.998
1.7	A	1.140	0.705	0.004	0.003	0.999
1.7	B	1.126	0.685	0.005	0.003	0.999
1.7	C	1.105	0.678	0.005	0.003	0.999
1.9	A	1.124	0.743	0.003	0.007	0.999
1.9	B	1.101	0.729	0.003	0.008	0.999
1.9	C	1.077	0.715	0.003	0.005	0.999
FO						
1.5	A	1.242	0.768	0.001	0.005	0.999
1.5	B	1.216	0.762	0.003	0.015	0.997
1.5	C	1.193	0.742	0.003	0.009	0.997
1.7	A	1.243	0.773	0.002	0.009	0.840
			Z=0.03	Y= 0.28		
F						
1.5	A	1.151	0.699	0.004	0.003	0.9988
1.5	B	1.145	0.676	0.005	0.004	0.9979
FO						
1.5	A	1.257	0.624	0.001	0.013	0.9992

TABLE 7.20: The coefficients of the PRZ relation (log $R/R_\odot$ =a + b log P + c [Fe/H]) predicted for both F and FO Classical Cepheids of all the considered chemical compositions (including $Z = 0.02$) by varying the assumed α_{ml} parameter and A, B, C ML relations.

α_{ml}	ML	a	b	c	σ_a	σ_b	σ_c	R^2
F								
1.5	A	-1.626	1.420	0.007	0.009	0.005	0.004	0.9972
1.5	B	-1.640	1.453	0.016	0.010	0.005	0.004	0.9965
1.5	C	-1.586	1.450	0.023	0.011	0.005	0.006	0.9967
1.7	A	-1.610	1.411	0.009	0.010	0.005	0.006	0.9978
1.7	B	-1.628	1.449	0.023	0.011	0.005	0.006	0.9974
1.7	C	-1.596	1.453	0.015	0.010	0.005	0.006	0.9977
1.9	A	-1.597	1.394	-0.016	0.010	0.006	0.009	0.9986
1.9	B	-1.615	1.433	-0.007	0.011	0.006	0.011	0.9982
1.9	C	-1.601	1.452	-0.001	0.011	0.005	0.010	0.9983
FO								
1.5	A	-1.653	1.325	-0.044	0.018	0.013	0.011	0.9936
1.5	B	-1.638	1.339	-0.043	0.027	0.020	0.014	0.9919
1.5	C	-1.616	1.351	-0.023	0.016	0.011	0.006	0.9989
1.7	A	-1.644	1.321	-0.025	0.008	0.006	0.006	0.9992
1.7	B	-1.647	1.345	-0.047	0.037	0.029	0.024	0.9901
1.7	C	-1.623	1.353	-0.034	0.020	0.014	0.009	0.9990
1.9	A	-1.655	1.315	-0.057	0.010	0.007	0.009	0.9995
1.9	B	-1.633	1.331	-0.045	0.016	0.012	0.012	0.9992
1.9	C	-2.078	1.713	0.021	0.006	0.005	0.001	1.0000

TABLE 7.21: The coefficients of the relation log P =a+b log M + clog $R/R_\odot$ for both F and FO Cepheids derived by adopting $Z = 0.004, Y = 0.25$, $Z = 0.008, Y = 0.25$ and $Z = 0.03, Y = 0.28$ as a function of the assumed α_{ml} parameter and A, B, C ML relations. The relations for $Z = 0.02$ $Y = 0.28$ are reported for comparison.

α_{ml}	ML	a	b	c	σ_a	σ_b	σ_c	R^2
			Z=0.004	Y= 0.25				
F								
1.5	A	-1.712	-0.998	1.901	0.009	0.047	0.023	0.9994
1.5	B	-1.782	-0.966	1.916	0.014	0.057	0.029	0.9989
1.5	C	-1.813	-0.874	1.889	0.022	0.067	0.035	0.9985
1.7	A	-1.710	-0.994	1.901	0.008	0.047	0.024	0.9996
1.7	B	-1.783	-1.016	1.940	0.013	0.059	0.029	0.9993
1.7	C	-1.808	-0.890	1.896	0.019	0.068	0.034	0.9991
1.9	A	-1.704	-1.016	1.909	0.009	0.062	0.032	0.9997
1.9	B	-1.788	-1.078	1.970	0.015	0.077	0.038	0.9994
1.9	C	-1.811	-0.948	1.922	0.020	0.079	0.040	0.9993
FO								
1.5	A	-1.789	-1.242	1.980	0.068	0.468	0.240	0.9884
1.5	B	-1.732	-0.755	1.722	0.104	0.543	0.270	0.9821
1.5	C	-1.676	-0.435	1.560	0.019	0.091	0.045	1.0000
1.7	A	-1.705	-0.708	1.685	0.006	0.046	0.023	1.0000
1.7	B	-1.771	-0.969	1.835	0.145	0.858	0.420	0.9771
1.7	C	-1.766	-0.947	1.805	0.049	0.238	0.117	0.9999

TABLE 7.21: continued.

α_{ml}	ML	a	b	c	σ_a	σ_b	σ_c	R^2
1.9	A	-1.701	-0.716	1.687	0.012	0.105	0.054	0.9999
1.9	B	-1.708	-0.653	1.662	0.008	0.044	0.022	1.0000
				Z=0.008	Y= 0.25			
F								
1.5	A	-1.671	-0.874	1.830	0.007	0.037	0.018	0.9996
1.5	B	-1.729	-0.910	1.871	0.011	0.052	0.025	0.9991
1.5	C	-1.740	-0.717	1.797	0.016	0.060	0.030	0.9989
1.7	A	-1.672	-0.904	1.845	0.007	0.047	0.022	0.9997
1.7	B	-1.745	-1.085	1.955	0.010	0.061	0.029	0.9995
1.7	C	-1.757	-0.770	1.828	0.016	0.066	0.032	0.9992
1.9	A	-1.665	-0.882	1.834	0.007	0.069	0.034	0.9998
1.9	B	-1.743	-1.116	1.970	0.013	0.101	0.048	0.9996
1.9	C	-1.772	-0.887	1.883	0.020	0.106	0.051	0.9994
FO								
1.5	A	-1.700	-0.687	1.675	0.004	0.033	0.017	0.9999
1.5	B	-1.696	-0.602	1.633	0.006	0.039	0.020	0.9999
1.5	C	-1.696	-0.555	1.617	0.007	0.037	0.017	1.0000
1.7	A	-1.698	-0.710	1.685	0.007	0.067	0.034	0.9999
1.7	B	-1.707	-0.663	1.666	0.006	0.043	0.021	1.0000
1.7	C	-1.713	-0.642	1.662	0.007	0.045	0.021	1.0000
1.9	A	-1.667	-0.632	1.626	0.006	0.055	0.029	1.0000
1.9	B	-1.711	-0.698	1.686	0.015	0.094	0.048	0.9999
				Z=0.02	Y= 0.28			
F								
1.5	A	-1.641	-0.890	1.830	0.007	0.06	0.03	0.999
1.5	B	-1.709	-0.920	1.874	0.01	0.072	0.03	0.998
1.5	C	-1.721	-0.687	1.784	0.01	0.06	0.03	0.998
1.7	A	-1.642	-1.144	1.948	0.008	0.14	0.06	0.999
1.7	B	-1.725	-1.194	2.001	0.01	0.13	0.06	0.999
1.7	C	-1.687	-0.583	1.728	0.02	0.11	0.05	0.999
1.9	A	-1.570	-0.778	1.737	0.02	0.3	0.1	0.999
1.9	B	-1.573	-0.720	1.709	0.01	0.09	0.05	0.999
1.9	C	-1.587	-0.547	1.654	0.01	0.06	0.03	0.999
FO								
1.5	A	-1.659	-0.564	1.590	0.005	0.06	0.03	0.999
1.5	B	-1.695	-0.779	1.707	0.02	0.1007	0.05	0.999
1.5	C	-1.738	-0.698	1.704	0.01	0.06	0.03	0.999
1.7	A	-1.644	-0.589	1.591	0.01	0.1	0.05	0.902
				Z=0.03	Y= 0.28			
F								
1.5	A	-1.629	-0.826	1.795	0.008	0.081	0.036	0.9996
1.5	B	-1.718	-0.890	1.865	0.011	0.083	0.037	0.9992

7.6 The period-age and period-age-color relations

In this section, the analysis performed in Chapter 6 is extended to the derivation of PA and multi-filter PAC relations for all the investigated chemical compositions. By combining our pulsation model results for the aforementioned chemical compositions with the corresponding stellar evolution model predictions, and adopting the PMLT relations derived in this Chapter, the period for each combination of mass, luminosity and effective temperature, along the portions of the evolutionary tracks within the predicted instability strip boundaries, was derived.

A linear regression between the periods estimated from pulsation models and the age and mean colors derived from the evolutionary models, allowed for the derivation of accurate PA and the first PAC relations in the Gaia bands. The coefficients of the PA and PAC relations are reported in Tables 7.22 and 7.23. Fig. 7.5 shows the canonical (left panel) and noncanonical (right panel) PA relations obtained for the standard convective efficiency for $Z = 0.004$ (dashed blue line), $Z = 0.008$ (solid green line), $Z = 0.02$ (dotted cyan line) and $Z = 0.03$ (dash-dotted magenta line). Noncanonical stellar models account for core overshooting. This means that, during the hydrogen burning phase, these models have a bigger convective core and live longer in the Main Sequence phase of the HR diagram than models that do not take overshooting into account, thus entering the IS with older ages. Then, as already verified in Chapter 6, the brighter ML relations (right panel in Fig. 7.5) provide systematically older ages than canonical ones, for all chemical compositions.

Fig. 7.6 shows the same comparison as Fig. 7.5 but for FO-mode models. In this case, due to the reduced number of available models, only the canonical case for $Z = 0.004$, $Z = 0.008$ and $Z = 0.02$ is represented. As FO pulsators have masses and periods smaller than the F pulsators, their ages are systematically older than the F ones for each chemical composition. Again we note a non-negligible metallicity effect on both the slope and the zero point of the plotted relations.

As already mentioned in Chapter 6, like the PL relation, the PA relation is affected by the intrinsic dispersion, due to the finite width of the instability strip. This implies that the use of PA relations provides individual CC ages affected by systematic errors related to the position within the instability strip. As such, in order to derive accurate age estimates for CCs in the early Gaia data release 3 (EGDR3), we took into account magnitudes and colors in the corresponding photometric system (for the stellar models in the BASTI library) and derived the first theoretical PAC relations in the Gaia bands for $Z = 0.004$, 0.008 and 0.03, following the same approach adopted for $Z = 0.02$ models in Chapter 6. The coefficients of these relations are reported in Table 7.23.

Although these results are still preliminary, it appears evident that the metallicity effect cannot be neglected in the use of CCs as age and distance indicators. Therefore, we plan to quantify the impact of metallicity variations on current determinations of H_0, based on the CC extragalactic distance scale calibration.
Indeed, the results presented in the present Chapter will be included and further expanded and discussed in two forthcoming papers (De Somma 2021 (a) and De Somma 2021 (b) in preparation).

TABLE 7.22: The coefficients of the F and FO-mode PA relations in the form $\log t = a + b \log P$, for $Z = 0.004, Y = 0.25$, $Z = 0.008; Y = 0.25$ and $Z = 0.03, Y = 0.28$ derived by assuming linear IS boundaries and adopting both *case A* and *B* ML relations and α_{ml} =1.5 . The last column represents the root-mean-square deviation (σ) coefficient.

	Z=0.004	Y= 0.25			
Fundamental mode					
ML	a	b	σ_a	σ_b	σ
A	8.455	-0.800	0.013	0.013	0.126
B	8.570	-0.692	0.019	0.014	0.105
First overtone mode					
A	8.342	-0.891	0.024	0.063	0.090
	Z=0.008	Y= 0.25			
Fundamental mode					
A	8.398	-0.776	0.016	0.013	0.132
B	8.503	-0.688	0.010	0.007	0.121
First overtone mode					
A	8.139	-0.552	0.033	0.058	0.065
	Z=0.02	Y= 0.28			
Fundamental mode					
A	8.393	-0.704	0.008	0.009	0.084
B	8.480	-0.626	0.010	0.009	0.080
First overtone mode					
A	8.120	-0.396	0.020	0.057	0.052
	Z=0.03	Y= 0.28			
Fundamental mode					
A	8.336	-0.673	0.009	0.010	0.076
B	8.356	-0.555	0.012	0.009	0.082

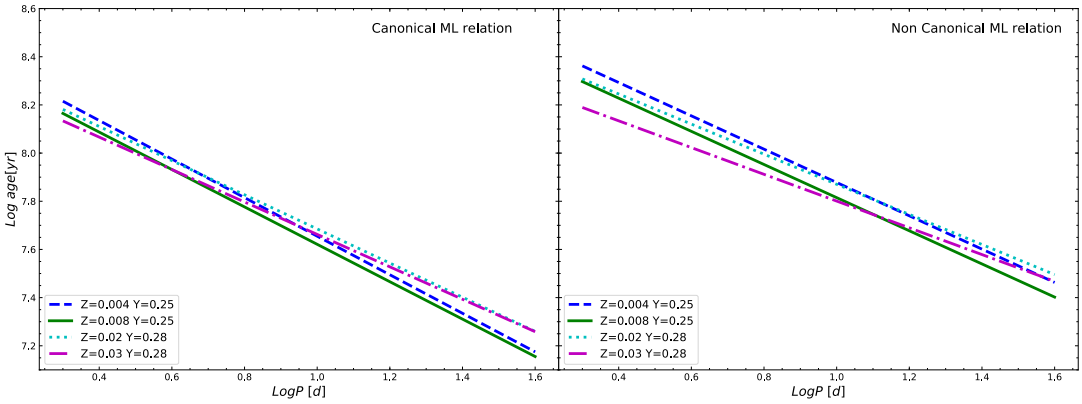

FIGURE 7.5: Fundamental PA relations for $Z = 0.004$ (dashed lines), $Z = 0.008$ (solid lines), $Z = 0.02$ (dotted lines) and $Z = 0.03$ (dash-dotted lines), as obtained when adopting the canonical ML relation (left panel) and noncanonical ML relation (right panel) and the standard efficiency for the superadiabatic convection.

TABLE 7.23: The coefficients of the F and FO PA relations $\log t = a + b \log P + c$ ($< G_{BP} >$ - $< G_{RP} >$), for $Z = 0.004, Y = 0.25$; $Z = 0.008, Y = 0.25$ and $Z = 0.03, Y = 0.28$ derived by adopting both *case A* and *B* ML relations and α_{ml} =1.5 . The last column represents the root-mean-square deviation (σ) coefficient.

		Z=0.004	Y= 0.25				
Fundamental mode							
ML	a	b	c	σ_a	σ_b	σ_c	σ
A	8.794	-0.571	-0.543	0.036	0.026	0.055	0.118
B	8.517	-0.758	0.135	0.024	0.024	0.038	0.104
First overtone mode							
A	8.002	-1.097	0.668	0.107	0.088	0.206	0.087
		Z=0.008	Y= 0.25				
Fundamental mode							
A	8.772	-0.313	-0.769	0.026	0.030	0.045	0.121
B	8.783	-0.401	-0.533	0.030	0.030	0.054	0.118
First overtone mode							
A	8.044	-0.601	0.180	0.100	0.076	0.179	0.064
		Z=0.02	Y= 0.28				
Fundamental mode							
1.5	A	8.303	-0.751	0.121	0.045	0.025	0.083
1.5	B	8.275	-0.734	0.278	0.029	0.017	0.077
First overtone mode							
1.5	A	7.961	-0.508	0.255	0.137	0.064	0.046
		Z=0.03	Y= 0.28				
Fundamental mode							
A	8.211	-0.752	0.181	0.036	0.024	0.050	0.076
B	8.369	-0.539	-0.027	0.021	0.023	0.035	0.082

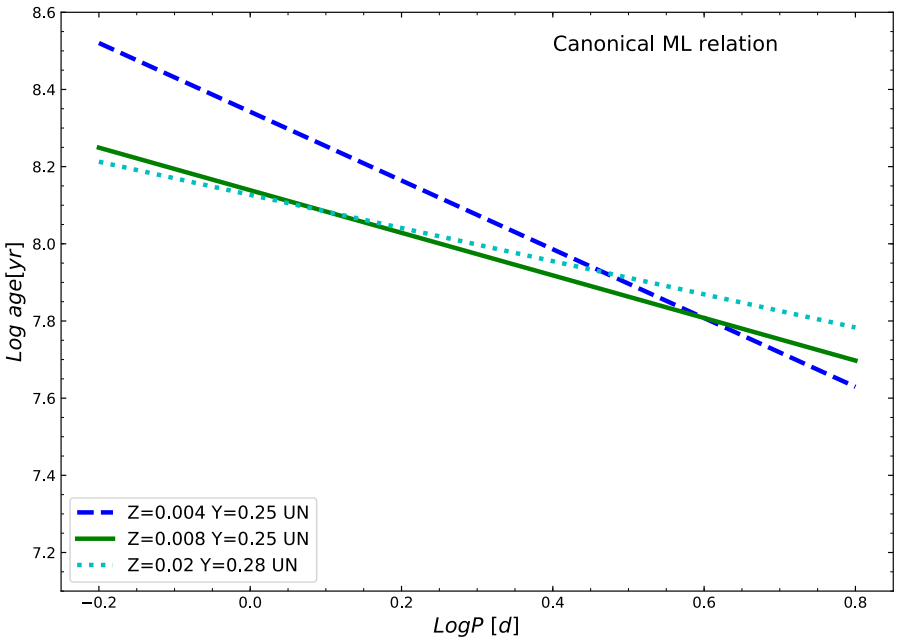

FIGURE 7.6: First overtone PA relations for $Z = 0.004$ (dashed lines), $Z = 0.008$ (solid lines), $Z = 0.02$ (dotted lines) and $Z = 0.03$, as obtained when adopting the canonical ML relation and the standard efficiency for the superadiabatic convection.

Chapter 8

The conclusions and future perspectives

The main aim of my PhD project was to investigate, from a theoretical point of view the residual systematic uncertainties in the relations that make reliable CCs distance and age indicators. To this purpose, we started the computation of an extensive and detailed set of nonlinear convective pulsation models to investigate CCs in various galactic and extra-galactic environments. As a first step, we computed a new, updated model set, at solar chemical composition (Z=0.02 Y=0.28), for a wide range of stellar masses, varying both the ML and the efficiency of super-adiabatic convection. All the predicted pulsation observables for the F and FO-mode models were discussed in detail and the following main results were drawn:

- As expected on the basis of previous investigations, while the predicted instability strip gets narrower as the efficiency of superadiabatic convection increases, it does not significantly depend on the assumed ML relation, apart from a small, but non-negligible effect, at the brightest luminosity levels.
- Analytical relations connecting the pulsation period of the F and FO-mode models to the intrinsic stellar properties, M, L, and T_{eff}, were derived for each assumed mixing length parameter value, and they showed a mild dependence on the adopted value.
- From the predicted radius curves and mean radii, the theoretical PR and PMR relations were derived. The PR relations were compared with similar relations in the literature, and showed a good agreement. In addition, the PR and PMR relations were found to be only slightly dependent on the assumed ML relation, in agreement with previous results in literature.
- The obtained bolometric light curves were found to be sensitive to the assumed value of the mixing length parameter with the amplitude decreasing as the efficiency of superadiabatic convection increases, whereas the dependence on the ML relation was found to be much less evident.
- From this set of models, the first atlas of theoretical light curves, transferred into the Gaia filters, for F and FO Galactic Cepheids, was derived.
- The obtained mean magnitudes and colors were used to derive the first theoretical Cepheid PLC and PW relations in the Gaia photometric passbands.

The derived PLC and PW relations were applied to the Galactic Cepheid data in the Gaia DR2 database to derive theoretical individual parallaxes that were compared with the Gaia DR2 ones. In particular, the mean offset of the Gaia parallaxes,

that was expected on the basis of several investigations in the most recent literature (see, e.g. Riess et al., 2021) was derived. A quantitative analysis of this offset and its dependence on the physical and numerical assumptions is mandatory in order to understand and to try to reduce the Hubble constant tension. Indeed, a variation in the parallax of the order of $< \Delta\varpi > = \pm$ 0.02 mas for a typical parallax of the order of ϖ = 0.5 mas implies a relative parallax error and, in turn, a relative error on H_0 of 4%. The mean offset derived by Riess et al. (2018a) by comparing Gaia results with the HST-WFC3 spatial scanning mode measurements corresponding to $< \Delta\varpi >$=0.046$\pm$0.013 mas (observations with the WFC3 spatial scanning mode in the optical and near-infrared allow to mitigate saturation and reduce pixel-to-pixel calibration errors to reach a mean photometric error of 5 mmag per observation. Spatial scans offer the additional advantage of varying the position of the source on the detector, which averages down pixel-to-pixel errors in the flat fields, and can also be used to vary the pixel phase, reducing the uncertainty from undersampled pointspread-function photometry), was successfully reproduced within the errors by our model predictions, apart from the cases at the brightest luminosity levels (full efficiency of overshooting and/or mass loss and/or rotation). Moreover, in order to exploit Gaia parallax information for Galactic Cepheids, so as to constrain their intrinsic stellar parameters, we also derived theoretical mass-dependent PW (PWM) relations for both the F and FO-mode pulsators.

These relations were found to be almost insensitive to the adopted efficiency of superadiabatic convection.
Their inversion and application to a subset of Gaia DR2 GCCs with positive parallax and relative parallax error below 10%, allowed us to constrain the individual stellar masses and, in turn, the stellar mass distribution for GCCs.
The inferred mass histograms peaked around $5.6M_{\odot}$ and $5.4M_{\odot}$ for the F and FO-mode pulsators, respectively. When Gaia DR2 GCC parallaxes were corrected for the offset ($< \Delta\varpi >$=0.046$\pm$ 0.013 mas) derived by Riess et al. (2018a), the inferred mass distributions moved slightly towards smaller masses, with the peak of the F and FO mass histograms occurring around $5.2M_{\odot}$ and $5.1M_{\odot}$, respectively.
In addition, a comparison with independent mass evaluations for a number of Cepheids in binary systems in common with our sample, supported the predictive capabilities of our theoretical scenario.

The most recently updated evolutionary predictions for the assumed solar chemical composition based on the BASTI stellar evolution database were combined with the updated dataset of nonlinear convective Cepheid models in order to constrain individual ages, using CCs as age indicators.
This was done to derive updated and accurate PA relations, as well as the first PAC relations in the Gaia DR2 photometric passbands, for various assumptions about the ML relations and the efficiency of superadiabatic convection in pulsation models.
The coefficients of these relations and hence, the corresponding age predictions, were found to significantly depend on the assumed ML relations, with the non-canonical ML relation providing ages older than the canonical ML relation.
In particular, for the case of PA relations, the predicted percentage age differences between the values obtained in the canonical and the noncanonical case, range from $\sim$ 36% to $\sim$ 60%. This trend was confirmed by the behaviour of the PAC relations.
The application of the new PA and Gaia-band PAC relations to the selected sample of Gaia DR2 GCC, produced individual ages which systematically increased as the ML relation changed from canonical to noncanonical models.
When adopting canonical ML models, the inferred age distribution of F-mode GCCs

in our sample peaked at around 90 Myr, while for the noncanonical case the peak shifted upwards by $\sim$ 35 Myr. This occurrence held when adopting both the PA and the PAC relations.
On the other hand, the age estimates obtained by means of both the PA and PAC relations were almost insensitive to variations in the mixing length parameter.
This result was expected because a variation in the efficiency of superadiabatic convection can modify the pulsation amplitude and the boundary of the IS but does not affect the relation between period, color and luminosity at all, and hence, the relation between period, color and age.
The FO-mode GCCs in the selected sample were found to be significantly older than the average F-mode pulsator age distribution. This is due to the smaller masses and shorter periods that characterize FO-mode pulsators.
A preliminary comparison between the age map distribution obtained in this work with other similar analyses in literature was performed. In general, we found that older Cepheids were located at further Galactocentric distance than younger pulsators, an occurrence in fine agreement with previous results for the age distribution of Milky Way CCs.

Finally, a first step to investigate the metallicity effect on the theoretical relations adopted for using CCs as distance indicators and age tracers was taken. The PMLT relation, topology of the instability strip, atlas of light and radial velocity curves, as well as the PR, PRZ, PMR, PA and PAC relations were provided suggesting a significant effect of metallicity on almost all these relations. The expansion and refinement of this investigation will allow us to quantify the metallicity effect on the Hubble constant estimate based on the calibration of the extragalactic distance scale.

In the future I plan to apply the same theoretical relations to the next coming Gaia data releases as well as to extend the theoretical scenario to other photometric systems. These updates will allow us to provide a new theoretical calibration of the extragalactic distance scale, reduce the error in mass determinations to just a few % and constrain the mass distributions of Cepheid samples in the Local Group for which accurate distances, e.g. LSST astrometric distances, will become available.

Appendix A

In the following sections the tables partially shown in Chapters 3, 4, 5, 6 and 7 are present in their entirety.

A.1 The intrinsic stellar parameters for computed F and FO-mode models at solar chemical composition

TABLE A.1: The intrinsic stellar parameters for computed F-mode models.

		Z=0.02	Y= 0.28			
$M/M_\odot$	$\log(L/L_\odot)$	T_{eff}[K]	α_{ml}	ML	P[d]	$\log(\overline{R}/R_\odot)$
(1)	(2)	(3)	(4)	(5)	(6)	(7)
3.0	2.32	5900	1.5	A	1.07716	1.142
3.0	2.32	6000	1.5	A	1.03611	1.129
3.0	2.32	6100	1.5	A	0.97997	1.115
3.0	2.32	6100	1.7	A	0.98004	1.114
3.0	2.32	6200	1.7	A	0.93202	1.101
3.0	2.32	6200	1.9	A	0.93319	1.100
3.0	2.52	5600	1.5	B	1.90853	1.287
3.0	2.52	5700	1.5	B	1.80054	1.273
3.0	2.52	5800	1.5	B	1.70066	1.261
3.0	2.52	5900	1.5	B	1.60999	1.247
3.0	2.52	6000	1.5	B	1.52707	1.233
3.0	2.52	5800	1.7	B	1.70066	1.257
3.0	2.52	5900	1.7	B	1.60796	1.244
3.0	2.52	6000	1.7	B	1.52758	1.231
3.0	2.52	6100	1.7	B	1.44264	1.217
3.0	2.52	6000	1.9	B	1.52569	1.228
3.0	2.52	6100	1.9	B	1.44454	1.215
3.0	2.72	5400	1.5	C	3.17345	1.418
3.0	2.72	5500	1.5	C	2.99834	1.405
3.0	2.72	5600	1.5	C	2.82583	1.391
3.0	2.72	5700	1.5	C	2.67191	1.375
3.0	2.72	5800	1.5	C	2.51664	1.362
3.0	2.72	5900	1.5	C	2.37806	1.347
3.0	2.72	6000	1.5	C	2.25267	1.333
3.0	2.72	5600	1.7	C	2.82583	1.389
3.0	2.72	5700	1.7	C	2.66525	1.375
3.0	2.72	5800	1.7	C	2.52294	1.360
3.0	2.72	5900	1.7	C	2.38103	1.345
3.0	2.72	6000	1.7	C	2.25267	1.332

TABLE A.1: continued.

$M/M_{\odot}$	$\log(L/L_{\odot})$	T_{eff}[K]	α_{ml}	ML	P[d]	$\log(\overline{R}/R_{\odot})$
(1)	(2)	(3)	(4)	(5)	(6)	(7)
3.0	2.72	6100	1.7	C	2.1306	1.317
3.0	2.72	5800	1.9	C	2.51664	1.359
3.0	2.72	5900	1.9	C	2.37806	1.345
3.0	2.72	6000	1.9	C	2.24986	1.330
3.0	2.72	6100	1.9	C	2.13066	1.315
4.0	2.74	5500	1.5	A	2.56311	1.412
4.0	2.74	5600	1.5	A	2.42218	1.399
4.0	2.74	5700	1.5	A	2.27149	1.383
4.0	2.74	5800	1.5	A	2.15572	1.370
4.0	2.74	5900	1.5	A	2.03155	1.356
4.0	2.74	5800	1.7	A	2.15839	1.367
4.0	2.74	5900	1.7	A	2.03171	1.354
4.0	2.74	6000	1.7	A	1.92779	1.339
4.0	2.74	5900	1.9	A	2.02664	1.351
4.0	2.74	6000	1.9	A	1.92536	1.339
4.0	2.94	5300	1.5	B	4.29863	1.545
4.0	2.94	5400	1.5	B	4.03965	1.530
4.0	2.94	5500	1.5	B	3.80242	1.515
4.0	2.94	5600	1.5	B	3.56453	1.499
4.0	2.94	5700	1.5	B	3.37987	1.486
4.0	2.94	5800	1.5	B	3.19837	1.471
4.0	2.94	5900	1.5	B	3.01509	1.456
4.0	2.94	5500	1.7	B	3.80242	1.513
4.0	2.94	5600	1.7	B	3.56009	1.497
4.0	2.94	5700	1.7	B	3.37987	1.485
4.0	2.94	5800	1.7	B	3.19039	1.470
4.0	2.94	5900	1.7	B	3.01885	1.455
4.0	2.94	5700	1.9	B	3.37987	1.483
4.0	2.94	5800	1.9	B	3.19039	1.469
4.0	2.94	5900	1.9	B	3.00755	1.453
4.0	3.14	5000	1.5	C	7.81065	1.699
4.0	3.14	5100	1.5	C	7.33711	1.684
4.0	3.14	5200	1.5	C	6.87354	1.667
4.0	3.14	5300	1.5	C	6.44196	1.649
4.0	3.14	5400	1.5	C	5.99093	1.630
4.0	3.14	5500	1.5	C	5.66752	1.616
4.0	3.14	5600	1.5	C	5.35073	1.600
4.0	3.14	5700	1.5	C	5.04389	1.586
4.0	3.14	5800	1.5	C	4.74944	1.571
4.0	3.14	5200	1.7	C	6.83095	1.661
4.0	3.14	5300	1.7	C	6.42601	1.647
4.0	3.14	5400	1.7	C	5.99093	1.629
4.0	3.14	5500	1.7	C	5.66752	1.615
4.0	3.14	5600	1.7	C	5.33742	1.599
4.0	3.14	5700	1.7	C	5.03133	1.584
4.0	3.14	5800	1.7	C	4.74944	1.570

TABLE A.1: continued.

$M/M_{\odot}$	$\log(L/L_{\odot})$	T_{eff}[K]	α_{ml}	ML	P[d]	$\log(\overline{R}/R_{\odot})$
(1)	(2)	(3)	(4)	(5)	(6)	(7)
4.0	3.14	5500	1.9	C	5.66752	1.614
4.0	3.14	5600	1.9	C	5.33742	1.599
4.0	3.14	5700	1.9	C	5.03133	1.583
5.0	3.07	5300	1.5	A	4.73277	1.608
5.0	3.07	5400	1.5	A	4.44069	1.592
5.0	3.07	5500	1.5	A	4.19743	1.578
5.0	3.07	5600	1.5	A	3.93086	1.563
5.0	3.07	5700	1.5	A	3.7214	1.549
5.0	3.07	5800	1.5	A	3.52146	1.533
5.0	3.07	5500	1.7	A	4.18693	1.575
5.0	3.07	5600	1.7	A	3.92593	1.561
5.0	3.07	5700	1.7	A	3.7214	1.547
5.0	3.07	5800	1.7	A	3.5039	1.531
5.0	3.07	5900	1.7	A	3.31139	1.516
5.0	3.07	5700	1.9	A	3.72138	1.546
5.0	3.07	5800	1.9	A	3.50385	1.530
5.0	3.27	5000	1.5	B	8.55037	1.761
5.0	3.27	5100	1.5	B	8.03633	1.745
5.0	3.27	5200	1.5	B	7.54078	1.725
5.0	3.27	5300	1.5	B	7.05991	1.708
5.0	3.27	5400	1.5	B	6.65715	1.694
5.0	3.27	5500	1.5	B	6.24377	1.678
5.0	3.27	5600	1.5	B	5.87984	1.663
5.0	3.27	5700	1.5	B	5.54353	1.648
5.0	3.27	5800	1.5	B	5.22027	1.631
5.0	3.27	5200	1.7	B	7.50321	1.722
5.0	3.27	5300	1.7	B	7.0423	1.708
5.0	3.27	5400	1.7	B	6.64059	1.692
5.0	3.27	5500	1.7	B	6.24377	1.676
5.0	3.27	5600	1.7	B	5.87984	1.662
5.0	3.27	5700	1.7	B	5.54353	1.647
5.0	3.47	4600	1.5	C	16.97743	1.922
5.0	3.47	4700	1.5	C	15.73981	1.908
5.0	3.47	4800	1.5	C	14.85544	1.897
5.0	3.47	4900	1.5	C	13.7875	1.881
5.0	3.47	5000	1.5	C	12.97535	1.868
5.0	3.47	5100	1.5	C	12.22245	1.854
5.0	3.47	5200	1.5	C	11.4762	1.840
5.0	3.47	5300	1.5	C	10.72549	1.823
5.0	3.47	5400	1.5	C	9.94997	1.802
5.0	3.47	5500	1.5	C	9.42263	1.786
5.0	3.47	5600	1.5	C	8.8056	1.763
5.0	3.47	5700	1.5	C	8.30213	1.748
5.0	3.47	4900	1.7	C	13.68194	1.872
5.0	3.47	5000	1.7	C	12.86181	1.860
5.0	3.47	5100	1.7	C	12.13183	1.849

TABLE A.1: continued.

$M/M_\odot$	$\log(L/L_\odot)$	T_{eff}[K]	α_{ml}	ML	P[d]	$\log(\overline{R}/R_\odot)$
(1)	(2)	(3)	(4)	(5)	(6)	(7)
5.0	3.47	5200	1.7	C	11.37788	1.835
5.0	3.47	5300	1.7	C	10.69957	1.819
5.0	3.47	5400	1.7	C	9.94997	1.800
5.0	3.47	5500	1.7	C	9.41113	1.783
5.0	3.47	5300	1.9	C	10.59377	1.809
6.0	3.33	5000	1.5	A	8.6011	1.789
6.0	3.33	5100	1.5	A	8.0714	1.772
6.0	3.33	5200	1.5	A	7.54675	1.756
6.0	3.33	5300	1.5	A	7.09067	1.742
6.0	3.33	5400	1.5	A	6.65862	1.727
6.0	3.33	5500	1.5	A	6.23545	1.710
6.0	3.33	5600	1.5	A	5.91682	1.696
6.0	3.33	5700	1.5	A	5.5647	1.680
6.0	3.33	5800	1.5	A	5.25316	1.664
6.0	3.33	5300	1.7	A	7.07294	1.740
6.0	3.33	5400	1.7	A	6.65862	1.725
6.0	3.33	5500	1.7	A	6.23545	1.709
6.0	3.33	5600	1.7	A	5.91682	1.695
6.0	3.53	4700	1.5	B	15.92523	1.942
6.0	3.53	4800	1.5	B	14.90301	1.931
6.0	3.53	4900	1.5	B	13.84606	1.916
6.0	3.53	5000	1.5	B	13.09375	1.904
6.0	3.53	5100	1.5	B	12.24931	1.889
6.0	3.53	5200	1.5	B	11.37476	1.869
6.0	3.53	5300	1.5	B	10.75712	1.854
6.0	3.53	5400	1.5	B	9.98642	1.832
6.0	3.53	5500	1.5	B	9.48668	1.816
6.0	3.53	5600	1.5	B	8.87017	1.796
6.0	3.53	5000	1.7	B	12.94873	1.892
6.0	3.53	5100	1.7	B	12.18877	1.882
6.0	3.53	5200	1.7	B	11.34625	1.865
6.0	3.53	5300	1.7	B	10.71737	1.850
6.0	3.53	5400	1.7	B	9.97385	1.830
6.0	3.73	4300	1.5	C	32.13056	2.105
6.0	3.73	4400	1.5	C	29.89931	2.094
6.0	3.73	4500	1.5	C	27.9581	2.082
6.0	3.73	4600	1.5	C	26.07593	2.068
6.0	3.73	4700	1.5	C	24.21215	2.050
6.0	3.73	4800	1.5	C	22.77338	2.037
6.0	3.73	4900	1.5	C	21.31181	2.021
6.0	3.73	5000	1.5	C	19.88333	2.003
6.0	3.73	5100	1.5	C	18.58507	1.986
6.0	3.73	5200	1.5	C	17.39873	1.969
6.0	3.73	5300	1.5	C	16.1463	1.948
6.0	3.73	4600	1.7	C	25.81701	2.055
6.0	3.73	4700	1.7	C	23.96562	2.041

TABLE A.1: continued.

$M/M_{\odot}$	$\log(L/L_{\odot})$	T_{eff}[K]	α_{ml}	ML	P[d]	$\log(\overline{R}/R_{\odot})$
(1)	(2)	(3)	(4)	(5)	(6)	(7)
6.0	3.73	4800	1.7	C	22.60556	2.029
6.0	3.73	4900	1.7	C	21.10231	2.014
6.0	3.73	5000	1.7	C	19.7375	1.998
6.0	3.73	5100	1.7	C	18.44884	1.981
6.0	3.73	5200	1.7	C	17.27164	1.963
7.0	3.56	4800	1.5	A	14.00799	1.942
7.0	3.56	4900	1.5	A	13.0515	1.928
7.0	3.56	5000	1.5	A	12.20012	1.912
7.0	3.56	5100	1.5	A	11.5374	1.897
7.0	3.56	5200	1.5	A	10.77847	1.879
7.0	3.56	5300	1.5	A	10.07762	1.858
7.0	3.56	5400	1.5	A	9.41961	1.840
7.0	3.56	5500	1.5	A	8.79075	1.820
7.0	3.56	5200	1.7	A	10.73846	1.876
7.0	3.56	5300	1.7	A	10.06517	1.858
7.0	3.56	5400	1.7	A	9.41961	1.839
7.0	3.76	4400	1.5	B	28.03657	2.103
7.0	3.76	4500	1.5	B	25.95567	2.090
7.0	3.76	4600	1.5	B	24.42963	2.077
7.0	3.76	4700	1.5	B	22.79803	2.061
7.0	3.76	4800	1.5	B	21.25822	2.045
7.0	3.76	4900	1.5	B	19.70081	2.028
7.0	3.76	5000	1.5	B	18.58623	2.014
7.0	3.76	5100	1.5	B	17.42477	1.998
7.0	3.76	5200	1.5	B	16.22245	1.980
7.0	3.76	5300	1.5	B	15.2397	1.963
7.0	3.76	4800	1.7	B	21.10035	2.037
7.0	3.76	4900	1.7	B	19.55046	2.021
7.0	3.76	5000	1.7	B	18.49456	2.007
7.0	3.76	5100	1.7	B	17.2963	1.992
7.0	3.76	5200	1.7	B	16.10139	1.973
7.0	3.96	4000	1.5	C	56.62106	2.263
7.0	3.96	4100	1.5	C	53.09965	2.252
7.0	3.96	4200	1.5	C	49.73993	2.240
7.0	3.96	4300	1.5	C	46.45938	2.227
7.0	3.96	4400	1.5	C	43.28206	2.212
7.0	3.96	4500	1.5	C	40.07975	2.195
7.0	3.96	4600	1.5	C	37.65683	2.182
7.0	3.96	4700	1.5	C	34.70845	2.164
7.0	3.96	4800	1.5	C	32.26574	2.146
7.0	3.96	4900	1.5	C	30.1684	2.129
7.0	3.96	5000	1.5	C	28.45787	2.115
7.0	3.96	5100	1.5	C	26.56725	2.096
7.0	3.96	4400	1.7	C	42.95417	2.205
7.0	3.96	4500	1.7	C	39.76979	2.190
7.0	3.96	4600	1.7	C	37.3765	2.176

TABLE A.1: continued.

$M/M_\odot$	$\log(L/L_\odot)$	T_{eff}[K]	α_{ml}	ML	P[d]	$\log(\overline{R}/R_\odot)$
(1)	(2)	(3)	(4)	(5)	(6)	(7)
7.0	3.96	4700	1.7	C	34.43796	2.157
7.0	3.96	4800	1.7	C	32.09583	2.141
7.0	3.96	4900	1.7	C	29.93333	2.124
7.0	3.96	5000	1.7	C	28.25093	2.106
8.0	3.75	4600	1.5	A	21.7684	2.070
8.0	3.75	4700	1.5	A	20.2235	2.056
8.0	3.75	4800	1.5	A	19.02442	2.042
8.0	3.75	4900	1.5	A	17.78229	2.028
8.0	3.75	5000	1.5	A	16.67326	2.014
8.0	3.75	5100	1.5	A	15.62037	1.999
8.0	3.75	5200	1.5	A	14.61829	1.980
8.0	3.75	5300	1.5	A	13.60255	1.960
8.0	3.75	5400	1.5	A	12.73484	1.936
8.0	3.75	4900	1.7	A	17.65023	2.016
8.0	3.75	5000	1.7	A	16.52905	2.003
8.0	3.75	5100	1.7	A	15.50498	1.990
8.0	3.75	5200	1.7	A	14.54618	1.975
8.0	3.95	4200	1.5	B	44.34745	2.233
8.0	3.95	4300	1.5	B	41.37778	2.222
8.0	3.95	4400	1.5	B	38.50035	2.208
8.0	3.95	4500	1.5	B	35.54873	2.192
8.0	3.95	4600	1.5	B	33.50579	2.179
8.0	3.95	4700	1.5	B	31.31042	2.162
8.0	3.95	4800	1.5	B	29.17894	2.145
8.0	3.95	4900	1.5	B	26.89711	2.127
8.0	3.95	5000	1.5	B	25.39363	2.112
8.0	3.95	5100	1.5	B	23.70243	2.093
8.0	3.95	5200	1.5	B	21.87049	2.066
8.0	3.95	4500	1.7	B	35.26505	2.181
8.0	3.95	4600	1.7	B	33.25637	2.170
8.0	3.95	4700	1.7	B	31.00197	2.155
8.0	3.95	4800	1.7	B	28.96389	2.138
8.0	3.95	4900	1.7	B	26.69074	2.119
8.0	3.95	5000	1.7	B	25.17616	2.104
8.0	4.15	3800	1.5	C	89.05428	2.387
8.0	4.15	3900	1.5	C	84.07951	2.378
8.0	4.15	4000	1.5	C	77.92523	2.363
8.0	4.15	4100	1.5	C	73.9287	2.354
8.0	4.15	4200	1.5	C	68.98287	2.341
8.0	4.15	4300	1.5	C	64.35625	2.325
8.0	4.15	4400	1.5	C	59.88495	2.311
8.0	4.15	4500	1.5	C	55.76725	2.296
8.0	4.15	4600	1.5	C	51.98958	2.280
8.0	4.15	4700	1.5	C	47.74074	2.260
8.0	4.15	4800	1.5	C	45.10938	2.246
8.0	4.15	4900	1.5	C	42.05208	2.228

TABLE A.1: continued.

$M/M_{\odot}$	$\log(L/L_{\odot})$	T_{eff}[K]	α_{ml}	ML	P[d]	$\log(\overline{R}/R_{\odot})$
(1)	(2)	(3)	(4)	(5)	(6)	(7)
8.0	4.15	5000	1.5	C	39.06678	2.207
8.0	4.15	5100	1.5	C	36.35463	2.187
8.0	4.15	4100	1.7	C	72.36817	2.346
8.0	4.15	4200	1.7	C	68.26227	2.334
8.0	4.15	4300	1.7	C	63.5419	2.320
8.0	4.15	4400	1.7	C	59.2831	2.306
8.0	4.15	4500	1.7	C	55.35012	2.290
8.0	4.15	4600	1.7	C	51.60544	2.275
8.0	4.15	4700	1.7	C	47.61713	2.256
8.0	4.15	4800	1.7	C	44.77928	2.239
8.0	4.15	4900	1.7	C	41.64282	2.219
9.0	3.92	4400	1.5	A	33.08715	2.190
9.0	3.92	4500	1.5	A	30.575	2.174
9.0	3.92	4600	1.5	A	28.78553	2.162
9.0	3.92	4700	1.5	A	26.87187	2.146
9.0	3.92	4800	1.5	A	24.79722	2.126
9.0	3.92	4900	1.5	A	23.15984	2.111
9.0	3.92	5000	1.5	A	21.87396	2.097
9.0	3.92	5100	1.5	A	20.43495	2.079
9.0	3.92	5200	1.5	A	19.06655	2.060
9.0	3.92	4800	1.7	A	24.67141	2.119
9.0	3.92	4900	1.7	A	22.98391	2.104
9.0	3.92	5000	1.7	A	21.65845	2.088
9.0	3.92	5100	1.7	A	20.25856	2.069
9.0	4.12	4000	1.5	B	67.38669	2.349
9.0	4.12	4100	1.5	B	62.4765	2.336
9.0	4.12	4200	1.5	B	58.91562	2.326
9.0	4.12	4300	1.5	B	54.91088	2.312
9.0	4.12	4400	1.5	B	51.04931	2.296
9.0	4.12	4500	1.5	B	47.14572	2.279
9.0	4.12	4600	1.5	B	44.45972	2.266
9.0	4.12	4700	1.5	B	41.41632	2.249
9.0	4.12	4800	1.5	B	38.48032	2.231
9.0	4.12	4900	1.5	B	35.91817	2.213
9.0	4.12	5000	1.5	B	33.49745	2.195
9.0	4.12	4300	1.7	B	54.48785	2.303
9.0	4.12	4400	1.7	B	50.79213	2.290
9.0	4.12	4500	1.7	B	46.76956	2.273
9.0	4.12	4600	1.7	B	44.13044	2.259
9.0	4.12	4700	1.7	B	41.00833	2.241
9.0	4.12	4800	1.7	B	38.29306	2.225
9.0	4.32	4200	1.5	C	92.98669	2.428
9.0	4.32	4300	1.5	C	86.47917	2.412
9.0	4.32	4400	1.5	C	80.4375	2.398
9.0	4.32	4500	1.5	C	74.82546	2.381
9.0	4.32	4600	1.5	C	69.79248	2.365

TABLE A.1: continued.

$M/M_{\odot}$	$\log(L/L_{\odot})$	T_{eff}[K]	α_{ml}	ML	P[d]	$\log(\overline{R}/R_{\odot})$
(1)	(2)	(3)	(4)	(5)	(6)	(7)
9.0	4.32	4700	1.5	C	64.83843	2.347
9.0	4.32	4800	1.5	C	59.09155	2.324
9.0	4.32	4900	1.5	C	54.87859	2.301
9.0	4.32	4300	1.7	C	85.61273	2.408
9.0	4.32	4400	1.7	C	79.63912	2.392
9.0	4.32	4500	1.7	C	74.27384	2.377
9.0	4.32	4600	1.7	C	69.28299	2.360
9.0	4.32	4700	1.7	C	64.2838	2.343
10.0	4.08	4200	1.5	A	48.711	2.297
10.0	4.08	4300	1.5	A	45.74965	2.285
10.0	4.08	4400	1.5	A	42.62315	2.271
10.0	4.08	4500	1.5	A	39.69306	2.256
10.0	4.08	4600	1.5	A	36.95729	2.241
10.0	4.08	4700	1.5	A	34.13333	2.223
10.0	4.08	4800	1.5	A	31.76424	2.204
10.0	4.08	4900	1.5	A	29.59248	2.186
10.0	4.08	5000	1.5	A	27.67373	2.169
10.0	4.08	5100	1.5	A	26.04653	2.150
10.0	4.08	4600	1.7	A	36.68287	2.232
10.0	4.08	4700	1.7	A	33.95961	2.215
10.0	4.08	4800	1.7	A	31.43843	2.196
10.0	4.08	4900	1.7	A	29.36551	2.178
10.0	4.28	3800	1.5	B	98.87824	2.453
10.0	4.28	3900	1.5	B	93.31562	2.442
10.0	4.28	4000	1.5	B	87.64282	2.430
10.0	4.28	4100	1.5	B	81.94595	2.418
10.0	4.28	4200	1.5	B	76.55775	2.405
10.0	4.28	4300	1.5	B	71.32859	2.390
10.0	4.28	4400	1.5	B	66.28681	2.375
10.0	4.28	4500	1.5	B	60.83507	2.355
10.0	4.28	4600	1.5	B	57.40752	2.343
10.0	4.28	4700	1.5	B	53.46933	2.325
10.0	4.28	4800	1.5	B	49.78507	2.308
10.0	4.28	4900	1.5	B	46.33831	2.288
10.0	4.28	4100	1.7	B	80.86771	2.410
10.0	4.28	4200	1.7	B	75.38981	2.396
10.0	4.28	4300	1.7	B	70.60984	2.384
10.0	4.28	4400	1.7	B	65.79097	2.368
10.0	4.28	4500	1.7	B	60.3603	2.349
10.0	4.28	4600	1.7	B	57.12546	2.336
10.0	4.28	4700	1.7	B	53.07488	2.319
10.0	4.48	4500	1.5	C	95.22049	2.453
10.0	4.48	4600	1.5	C	88.37836	2.435
10.0	4.48	4700	1.5	C	84.08704	2.422
10.0	4.48	4800	1.5	C	78.33912	2.403
10.0	4.48	4500	1.7	C	94.68854	2.447

TABLE A.1: continued.

$M/M_\odot$	$\log(L/L_\odot)$	T_{eff}[K]	α_{ml}	ML	P[d]	$\log(\overline{R}/R_\odot)$
(1)	(2)	(3)	(4)	(5)	(6)	(7)
10.0	4.48	4600	1.7	C	87.89931	2.430
10.0	4.48	4700	1.7	C	83.88345	2.418
11.0	4.21	4100	1.5	A	66.40289	2.386
11.0	4.21	4200	1.5	A	61.14294	2.371
11.0	4.21	4300	1.5	A	57.56181	2.358
11.0	4.21	4400	1.5	A	52.97674	2.340
11.0	4.21	4500	1.5	A	49.99711	2.328
11.0	4.21	4600	1.5	A	46.41921	2.312
11.0	4.21	4700	1.5	A	43.30313	2.295
11.0	4.21	4800	1.5	A	40.2625	2.276
11.0	4.21	4900	1.5	A	37.10914	2.254
11.0	4.21	4400	1.7	A	52.41921	2.333
11.0	4.21	4500	1.7	A	49.62488	2.319
11.0	4.21	4600	1.7	A	46.19167	2.303
11.0	4.21	4700	1.7	A	42.98391	2.286
11.0	4.41	4000	1.5	B	111.85729	2.501
11.0	4.41	4100	1.5	B	104.26343	2.489
11.0	4.41	4200	1.5	B	97.0691	2.474
11.0	4.41	4300	1.5	B	90.36539	2.459
11.0	4.41	4400	1.5	B	84.11829	2.444
11.0	4.41	4500	1.5	B	78.32581	2.427
11.0	4.41	4600	1.5	B	72.75984	2.411
11.0	4.41	4700	1.5	B	67.6765	2.393
11.0	4.41	4800	1.5	B	61.67766	2.368
11.0	4.41	3900	1.7	B	115.91435	2.504
11.0	4.41	4000	1.7	B	109.23148	2.494
11.0	4.41	4100	1.7	B	102.62917	2.482
11.0	4.41	4200	1.7	B	96.07859	2.469
11.0	4.41	4300	1.7	B	89.45718	2.455
11.0	4.41	4400	1.7	B	83.28333	2.440
11.0	4.41	4500	1.7	B	77.7456	2.423
11.0	4.41	4600	1.7	B	72.22616	2.406
11.0	4.41	4700	1.7	B	67.01262	2.386
11.0	4.61	4600	1.5	C	116.01968	2.508
11.0	4.61	4700	1.5	C	107.81019	2.491
11.0	4.61	4800	1.5	C	100.91389	2.472
11.0	4.61	4600	1.7	C	115.46007	2.504

TABLE A.2: The intrinsic stellar parameters for computed FO-mode models.

		Z=0.02	Y= 0.28			
$M/M_\odot$	$\log(L/L_\odot)$	T_{eff}[K]	α_{ml}	ML	P[d]	$\log(\overline{R}/R_\odot)$
(1)	(2)	(3)	(4)	(5)	(6)	(7)
3.0	2.32	6200	1.5	A	0.6715	1.103
3.0	2.32	6300	1.5	A	0.6403	1.090
3.0	2.32	6400	1.5	A	0.6090	1.076

TABLE A.2: continued.

$M/M_\odot$	$\log(L/L_\odot)$	T_{eff}[K]	α_{ml}	ML	P[d]	$\log(\overline{R}/R_\odot)$
(1)	(2)	(3)	(4)	(5)	(6)	(7)
3.0	2.32	6500	1.5	A	0.5802	1.062
3.0	2.32	6300	1.7	A	0.6402	1.088
3.0	2.32	6400	1.7	A	0.6080	1.075
3.0	2.32	6500	1.7	A	0.5783	1.062
3.0	2.52	6000	1.5	B	1.0990	1.231
3.0	2.52	6100	1.5	B	1.0169	1.217
3.0	2.52	6200	1.5	B	0.9600	1.202
3.0	2.52	6300	1.5	B	0.9164	1.190
3.0	2.52	6400	1.5	B	0.8719	1.176
3.0	2.52	6500	1.5	B	0.8333	1.163
3.0	2.52	6200	1.7	B	0.9615	1.202
3.0	2.52	6300	1.7	B	0.9179	1.189
3.0	2.52	6400	1.7	B	0.8705	1.175
3.0	2.52	6500	1.7	B	0.8319	1.160
3.0	2.72	6000	1.5	C	1.5693	1.330
3.0	2.72	6100	1.5	C	1.4787	1.316
3.0	2.72	6200	1.5	C	1.3980	1.302
3.0	2.72	6300	1.5	C	1.3275	1.289
3.0	2.72	6400	1.5	C	1.2609	1.274
3.0	2.72	6200	1.7	C	1.3933	1.301
4.0	2.74	5900	1.5	A	1.4240	1.354
4.0	2.74	6000	1.5	A	1.3551	1.341
4.0	2.74	6100	1.5	A	1.2861	1.326
4.0	2.74	6200	1.5	A	1.2217	1.312
4.0	2.74	6300	1.5	A	1.1565	1.298
4.0	2.74	6400	1.5	A	1.1038	1.285
4.0	2.74	6100	1.7	A	1.2860	1.324
4.0	2.74	6200	1.7	A	1.2197	1.311
4.0	2.74	6300	1.7	A	1.1584	1.297
4.0	2.94	5900	1.5	B	2.0801	1.455
4.0	2.94	6000	1.5	B	1.9678	1.441
4.0	2.94	6100	1.5	B	1.8634	1.425
4.0	2.94	6200	1.5	B	1.7665	1.412
4.0	3.14	6000	1.5	C	2.9045	1.539
5.0	3.07	5800	1.5	A	2.3904	1.530
5.0	3.07	5900	1.5	A	2.2912	1.517
5.0	3.07	6000	1.5	A	2.1616	1.502
5.0	3.07	6100	1.5	A	2.0550	1.487
6.0	3.33	5800	1.5	A	3.5712	1.664

A.2 Mean magnitudes in the *Gaia* filters for F and FO-mode models at varying assumptions of ML relations and values of the mixing length parameters

TABLE A.3: Mean magnitudes in the *Gaia* filters for F-mode models at varying assumptions of the ML relation and values of α_{ml} parameter.

		Z=0.02	Y= 0.28				
$M/M_\odot$	$\log(L/L_\odot)$	T_{eff}[K]	α_{ml}	ML	G	G_{BP}	G_{RP}
(1)	(2)	(3)	(4)	(5)	(6)	(7)	(8)
3.0	2.32	5900	1.5	A	1.31	-1.03	-1.75
3.0	2.32	6000	1.5	A	1.31	-1.05	-1.73
3.0	2.32	6100	1.5	A	1.32	-1.07	-1.72
3.0	2.32	6100	1.7	A	1.32	-1.07	-1.72
3.0	2.32	6200	1.7	A	1.32	-1.08	-1.70
3.0	2.32	6200	1.9	A	1.32	-1.09	-1.70
3.0	2.52	5600	1.5	B	1.80	-1.47	-2.29
3.0	2.52	5700	1.5	B	1.80	-1.49	-2.28
3.0	2.52	5800	1.5	B	1.81	-1.51	-2.26
3.0	2.52	5800	1.7	B	1.81	-1.51	-2.26
3.0	2.52	5900	1.5	B	1.81	-1.53	-2.25
3.0	2.52	5900	1.7	B	1.81	-1.53	-2.25
3.0	2.52	6000	1.5	B	1.82	-1.55	-2.23
3.0	2.52	6000	1.7	B	1.82	-1.55	-2.23
3.0	2.52	6000	1.9	B	1.82	-1.55	-2.24
3.0	2.52	6100	1.7	B	1.82	-1.57	-2.22
3.0	2.52	6100	1.9	B	1.82	-1.57	-2.22
3.0	2.72	5400	1.5	C	2.28	-1.91	-2.81
3.0	2.72	5500	1.5	C	2.29	-1.94	-2.80
3.0	2.72	5600	1.5	C	2.30	-1.97	-2.79
3.0	2.72	5600	1.7	C	2.30	-1.97	-2.79
3.0	2.72	5700	1.5	C	2.30	-1.99	-2.78
3.0	2.72	5700	1.7	C	2.31	-1.99	-2.78
3.0	2.72	5800	1.5	C	2.31	-2.02	-2.76
3.0	2.72	5800	1.7	C	2.31	-2.01	-2.76
3.0	2.72	5800	1.9	C	2.31	-2.02	-2.77
3.0	2.72	5900	1.5	C	2.32	-2.04	-2.75
3.0	2.72	5900	1.7	C	2.32	-2.04	-2.75
3.0	2.72	5900	1.9	C	2.32	-2.04	-2.75
3.0	2.72	6000	1.5	C	2.32	-2.06	-2.73
3.0	2.72	6000	1.7	C	2.32	-2.06	-2.73
3.0	2.72	6000	1.9	C	2.32	-2.06	-2.74
3.0	2.72	6100	1.7	C	2.32	-2.08	-2.72
3.0	2.72	6100	1.9	C	2.33	-2.08	-2.72
4.0	2.74	5500	1.5	A	2.34	-1.99	-2.85
4.0	2.74	5600	1.5	A	2.34	-2.01	-2.83
4.0	2.74	5700	1.5	A	2.35	-2.04	-2.82
4.0	2.74	5800	1.5	A	2.36	-2.06	-2.81
4.0	2.74	5800	1.7	A	2.36	-2.06	-2.81
4.0	2.74	5900	1.5	A	2.36	-2.08	-2.79
4.0	2.74	5900	1.7	A	2.36	-2.08	-2.79
4.0	2.74	5900	1.9	A	2.36	-2.08	-2.80
4.0	2.74	6000	1.7	A	2.37	-2.10	-2.78
4.0	2.74	6000	1.9	A	2.37	-2.10	-2.78

TABLE A.3: continued.

$M/M_{\odot}$	$\log(L/L_{\odot})$	T_{eff}[K]	α_{ml}	ML	G	G_{BP}	G_{RP}
(1)	(2)	(3)	(4)	(5)	(6)	(7)	(8)
4.0	2.94	5300	1.5	B	2.82	-2.43	-3.37
4.0	2.94	5400	1.5	B	2.83	-2.46	-3.36
4.0	2.94	5500	1.5	B	2.84	-2.49	-3.35
4.0	2.94	5500	1.7	B	2.84	-2.49	-3.35
4.0	2.94	5600	1.5	B	2.84	-2.52	-3.33
4.0	2.94	5600	1.7	B	2.85	-2.52	-3.34
4.0	2.94	5700	1.5	B	2.85	-2.54	-3.32
4.0	2.94	5700	1.7	B	2.85	-2.54	-3.32
4.0	2.94	5700	1.9	B	2.86	-2.54	-3.33
4.0	2.94	5800	1.5	B	2.86	-2.56	-3.31
4.0	2.94	5800	1.7	B	2.86	-2.56	-3.31
4.0	2.94	5800	1.9	B	2.86	-2.56	-3.31
4.0	2.94	5900	1.5	B	2.86	-2.59	-3.29
4.0	2.94	5900	1.7	B	2.86	-2.59	-3.30
4.0	2.94	5900	1.9	B	2.87	-2.59	-3.30
4.0	3.14	5000	1.5	C	3.27	-2.82	-3.87
4.0	3.14	5100	1.5	C	3.28	-2.85	-3.87
4.0	3.14	5200	1.5	C	3.30	-2.89	-3.87
4.0	3.14	5200	1.7	C	3.30	-2.90	-3.88
4.0	3.14	5300	1.5	C	3.31	-2.93	-3.87
4.0	3.14	5300	1.7	C	3.32	-2.93	-3.87
4.0	3.14	5400	1.5	C	3.33	-2.96	-3.86
4.0	3.14	5400	1.7	C	3.33	-2.96	-3.86
4.0	3.14	5500	1.5	C	3.34	-2.99	-3.85
4.0	3.14	5500	1.7	C	3.34	-2.99	-3.85
4.0	3.14	5500	1.9	C	3.34	-2.99	-3.85
4.0	3.14	5600	1.5	C	3.35	-3.02	-3.84
4.0	3.14	5600	1.7	C	3.35	-3.02	-3.84
4.0	3.14	5600	1.9	C	3.35	-3.02	-3.84
4.0	3.14	5700	1.5	C	3.36	-3.04	-3.83
4.0	3.14	5700	1.7	C	3.36	-3.04	-3.83
4.0	3.14	5700	1.9	C	3.36	-3.04	-3.83
4.0	3.14	5800	1.5	C	3.36	-3.07	-3.81
4.0	3.14	5800	1.7	C	3.36	-3.07	-3.82
5.0	3.07	5300	1.5	A	3.13	-2.74	-3.68
5.0	3.07	5400	1.5	A	3.14	-2.77	-3.67
5.0	3.07	5500	1.5	A	3.15	-2.80	-3.66
5.0	3.07	5500	1.7	A	3.15	-2.80	-3.66
5.0	3.07	5600	1.5	A	3.16	-2.83	-3.64
5.0	3.07	5600	1.7	A	3.16	-2.83	-3.65
5.0	3.07	5700	1.5	A	3.16	-2.85	-3.63
5.0	3.07	5700	1.7	A	3.17	-2.85	-3.64
5.0	3.07	5700	1.9	A	3.17	-2.85	-3.64
5.0	3.07	5800	1.5	A	3.17	-2.88	-3.62
5.0	3.07	5800	1.7	A	3.17	-2.88	-3.62
5.0	3.07	5800	1.9	A	3.17	-2.88	-3.63

TABLE A.3: continued.

$M/M_\odot$	$\log(L/L_\odot)$	T_{eff}[K]	α_{ml}	ML	G	G_{BP}	G_{RP}
(1)	(2)	(3)	(4)	(5)	(6)	(7)	(8)
5.0	3.07	5900	1.7	A	3.18	-2.90	-3.61
5.0	3.27	5000	1.5	B	3.58	-3.13	-4.19
5.0	3.27	5100	1.5	B	3.60	-3.17	-4.19
5.0	3.27	5200	1.5	B	3.61	-3.21	-4.19
5.0	3.27	5200	1.7	B	3.62	-3.21	-4.19
5.0	3.27	5300	1.5	B	3.63	-3.24	-4.18
5.0	3.27	5300	1.7	B	3.63	-3.24	-4.18
5.0	3.27	5400	1.5	B	3.64	-3.27	-4.17
5.0	3.27	5400	1.7	B	3.64	-3.27	-4.17
5.0	3.27	5500	1.5	B	3.65	-3.30	-4.16
5.0	3.27	5500	1.7	B	3.65	-3.30	-4.16
5.0	3.27	5600	1.5	B	3.66	-3.33	-4.15
5.0	3.27	5600	1.7	B	3.66	-3.33	-4.15
5.0	3.27	5700	1.5	B	3.67	-3.36	-4.14
5.0	3.27	5700	1.7	B	3.67	-3.36	-4.14
5.0	3.27	5800	1.5	B	3.68	-3.38	-4.13
5.0	3.47	4600	1.5	C	4.00	-3.46	-4.68
5.0	3.47	4700	1.5	C	4.02	-3.51	-4.68
5.0	3.47	4800	1.5	C	4.04	-3.54	-4.69
5.0	3.47	4900	1.5	C	4.06	-3.59	-4.68
5.0	3.47	4900	1.7	C	4.07	-3.60	-4.70
5.0	3.47	5000	1.5	C	4.07	-3.62	-4.68
5.0	3.47	5000	1.7	C	4.08	-3.63	-4.69
5.0	3.47	5100	1.5	C	4.09	-3.66	-4.67
5.0	3.47	5100	1.7	C	4.09	-3.67	-4.68
5.0	3.47	5200	1.5	C	4.10	-3.70	-4.67
5.0	3.47	5200	1.7	C	4.11	-3.70	-4.68
5.0	3.47	5300	1.5	C	4.11	-3.74	-4.66
5.0	3.47	5300	1.7	C	4.12	-3.74	-4.67
5.0	3.47	5300	1.9	C	4.13	-3.74	-4.69
5.0	3.47	5400	1.5	C	4.13	-3.78	-4.65
5.0	3.47	5400	1.7	C	4.13	-3.78	-4.66
5.0	3.47	5500	1.5	C	4.14	-3.81	-4.65
5.0	3.47	5500	1.7	C	4.15	-3.80	-4.66
5.0	3.47	5600	1.5	C	4.16	-3.83	-4.66
5.0	3.47	5700	1.5	C	4.17	-3.86	-4.65
6.0	3.33	5000	1.5	A	3.75	-3.30	-4.36
6.0	3.33	5100	1.5	A	3.76	-3.33	-4.36
6.0	3.33	5200	1.5	A	3.78	-3.37	-4.35
6.0	3.33	5300	1.5	A	3.79	-3.40	-4.34
6.0	3.33	5300	1.7	A	3.79	-3.40	-4.34
6.0	3.33	5400	1.5	A	3.80	-3.43	-4.33
6.0	3.33	5400	1.7	A	3.81	-3.44	-4.34
6.0	3.33	5500	1.5	A	3.81	-3.47	-4.32
6.0	3.33	5500	1.7	A	3.82	-3.47	-4.33
6.0	3.33	5600	1.5	A	3.82	-3.49	-4.31

TABLE A.3: continued.

$M/M_\odot$	$\log(L/L_\odot)$	T_{eff}[K]	α_{ml}	ML	G	G_{BP}	G_{RP}
(1)	(2)	(3)	(4)	(5)	(6)	(7)	(8)
6.0	3.33	5600	1.7	A	3.82	-3.49	-4.32
6.0	3.33	5700	1.5	A	3.83	-3.52	-4.30
6.0	3.33	5800	1.5	A	3.84	-3.54	-4.29
6.0	3.53	4700	1.5	B	4.18	-3.67	-4.85
6.0	3.53	4800	1.5	B	4.20	-3.70	-4.85
6.0	3.53	4900	1.5	B	4.22	-3.75	-4.84
6.0	3.53	5000	1.5	B	4.23	-3.78	-4.84
6.0	3.53	5000	1.7	B	4.25	-3.79	-4.86
6.0	3.53	5100	1.5	B	4.25	-3.82	-4.83
6.0	3.53	5100	1.7	B	4.26	-3.83	-4.84
6.0	3.53	5200	1.5	B	4.27	-3.87	-4.83
6.0	3.53	5200	1.7	B	4.27	-3.87	-4.84
6.0	3.53	5300	1.5	B	4.28	-3.90	-4.82
6.0	3.53	5300	1.7	B	4.28	-3.90	-4.83
6.0	3.53	5400	1.5	B	4.30	-3.94	-4.82
6.0	3.53	5400	1.7	B	4.30	-3.94	-4.82
6.0	3.53	5500	1.5	B	4.31	-3.97	-4.82
6.0	3.53	5600	1.5	B	4.33	-3.99	-4.82
6.0	3.73	4300	1.5	C	4.57	-3.96	-5.31
6.0	3.73	4400	1.5	C	4.59	-4.01	-5.32
6.0	3.73	4500	1.5	C	4.62	-4.05	-5.33
6.0	3.73	4600	1.5	C	4.64	-4.10	-5.33
6.0	3.73	4600	1.7	C	4.66	-4.12	-5.35
6.0	3.73	4700	1.5	C	4.67	-4.15	-5.34
6.0	3.73	4700	1.7	C	4.68	-4.17	-5.35
6.0	3.73	4800	1.5	C	4.69	-4.19	-5.34
6.0	3.73	4800	1.7	C	4.70	-4.20	-5.35
6.0	3.73	4900	1.5	C	4.71	-4.24	-5.34
6.0	3.73	4900	1.7	C	4.72	-4.25	-5.35
6.0	3.73	5000	1.5	C	4.73	-4.28	-5.34
6.0	3.73	5000	1.7	C	4.74	-4.29	-5.35
6.0	3.73	5100	1.5	C	4.75	-4.33	-5.34
6.0	3.73	5100	1.7	C	4.76	-4.33	-5.35
6.0	3.73	5200	1.5	C	4.77	-4.37	-5.34
6.0	3.73	5200	1.7	C	4.78	-4.37	-5.35
6.0	3.73	5300	1.5	C	4.79	-4.41	-5.34
7.0	3.56	4800	1.5	A	4.26	-3.77	-4.91
7.0	3.56	4900	1.5	A	4.28	-3.81	-4.90
7.0	3.56	5000	1.5	A	4.30	-3.85	-4.90
7.0	3.56	5100	1.5	A	4.31	-3.89	-4.90
7.0	3.56	5200	1.5	A	4.33	-3.93	-4.90
7.0	3.56	5200	1.7	A	4.33	-3.93	-4.90
7.0	3.56	5300	1.5	A	4.35	-3.96	-4.90
7.0	3.56	5300	1.7	A	4.35	-3.96	-4.90
7.0	3.56	5400	1.5	A	4.37	-4.00	-4.90
7.0	3.56	5400	1.7	A	4.37	-4.00	-4.90

TABLE A.3: continued.

$M/M_\odot$	$\log(L/L_\odot)$	T_{eff}[K]	α_{ml}	ML	G	G_{BP}	G_{RP}
(1)	(2)	(3)	(4)	(5)	(6)	(7)	(8)
7.0	3.56	5500	1.5	A	4.38	-4.03	-4.89
7.0	3.76	4400	1.5	B	4.66	-4.08	-5.38
7.0	3.76	4500	1.5	B	4.68	-4.12	-5.39
7.0	3.76	4600	1.5	B	4.71	-4.16	-5.40
7.0	3.76	4700	1.5	B	4.73	-4.21	-5.40
7.0	3.76	4800	1.5	B	4.75	-4.26	-5.41
7.0	3.76	4800	1.7	B	4.77	-4.27	-5.42
7.0	3.76	4900	1.5	B	4.78	-4.31	-5.41
7.0	3.76	4900	1.7	B	4.79	-4.32	-5.42
7.0	3.76	5000	1.5	B	4.80	-4.35	-5.40
7.0	3.76	5000	1.7	B	4.80	-4.35	-5.42
7.0	3.76	5100	1.5	B	4.81	-4.39	-5.40
7.0	3.76	5100	1.7	B	4.82	-4.39	-5.41
7.0	3.76	5200	1.5	B	4.83	-4.43	-5.39
7.0	3.76	5200	1.7	B	4.84	-4.43	-5.41
7.0	3.76	5300	1.5	B	4.85	-4.47	-5.39
7.0	3.96	4000	1.5	C	5.02	-4.35	-5.82
7.0	3.96	4100	1.5	C	5.05	-4.39	-5.83
7.0	3.96	4200	1.5	C	5.08	-4.44	-5.85
7.0	3.96	4300	1.5	C	5.11	-4.50	-5.86
7.0	3.96	4400	1.5	C	5.14	-4.55	-5.87
7.0	3.96	4400	1.7	C	5.16	-4.57	-5.88
7.0	3.96	4500	1.5	C	5.17	-4.61	-5.89
7.0	3.96	4500	1.7	C	5.18	-4.62	-5.89
7.0	3.96	4600	1.5	C	5.20	-4.65	-5.89
7.0	3.96	4600	1.7	C	5.21	-4.67	-5.90
7.0	3.96	4700	1.5	C	5.23	-4.71	-5.90
7.0	3.96	4700	1.7	C	5.24	-4.72	-5.91
7.0	3.96	4800	1.5	C	5.25	-4.76	-5.90
7.0	3.96	4800	1.7	C	5.26	-4.77	-5.91
7.0	3.96	4900	1.5	C	5.28	-4.81	-5.91
7.0	3.96	4900	1.7	C	5.29	-4.81	-5.92
7.0	3.96	5000	1.5	C	5.30	-4.85	-5.91
7.0	3.96	5000	1.7	C	5.31	-4.85	-5.92
7.0	3.96	5100	1.5	C	5.32	-4.89	-5.91
8.0	3.75	4600	1.5	A	4.70	-4.16	-5.39
8.0	3.75	4700	1.5	A	4.72	-4.21	-5.39
8.0	3.75	4800	1.5	A	4.74	-4.25	-5.39
8.0	3.75	4900	1.5	A	4.76	-4.29	-5.39
8.0	3.75	4900	1.7	A	4.78	-4.30	-5.41
8.0	3.75	5000	1.5	A	4.78	-4.33	-5.38
8.0	3.75	5000	1.7	A	4.79	-4.34	-5.40
8.0	3.75	5100	1.5	A	4.79	-4.37	-5.38
8.0	3.75	5100	1.7	A	4.81	-4.38	-5.39
8.0	3.75	5200	1.5	A	4.81	-4.41	-5.37
8.0	3.75	5200	1.7	A	4.82	-4.42	-5.39

TABLE A.3: continued.

$M/M_{\odot}$	$\log(L/L_{\odot})$	T_{eff}[K]	α_{ml}	ML	G	G_{BP}	G_{RP}
(1)	(2)	(3)	(4)	(5)	(6)	(7)	(8)
8.0	3.75	5300	1.5	A	4.83	-4.46	-5.37
8.0	3.75	5400	1.5	A	4.85	-4.48	-5.39
8.0	3.95	4200	1.5	B	5.07	-4.44	-5.84
8.0	3.95	4300	1.5	B	5.10	-4.49	-5.85
8.0	3.95	4400	1.5	B	5.13	-4.54	-5.86
8.0	3.95	4500	1.5	B	5.16	-4.60	-5.87
8.0	3.95	4500	1.7	B	5.18	-4.62	-5.88
8.0	3.95	4600	1.5	B	5.19	-4.64	-5.88
8.0	3.95	4600	1.7	B	5.20	-4.66	-5.89
8.0	3.95	4700	1.5	B	5.21	-4.69	-5.88
8.0	3.95	4700	1.7	B	5.22	-4.70	-5.90
8.0	3.95	4800	1.5	B	5.24	-4.74	-5.89
8.0	3.95	4800	1.7	B	5.25	-4.75	-5.90
8.0	3.95	4900	1.5	B	5.26	-4.80	-5.89
8.0	3.95	4900	1.7	B	5.27	-4.80	-5.90
8.0	3.95	5000	1.5	B	5.28	-4.83	-5.89
8.0	3.95	5000	1.7	B	5.29	-4.84	-5.91
8.0	3.95	5100	1.5	B	5.30	-4.88	-5.89
8.0	3.95	5200	1.5	B	5.33	-4.92	-5.91
8.0	4.15	3800	1.5	C	5.43	-4.71	-6.27
8.0	4.15	3900	1.5	C	5.46	-4.76	-6.28
8.0	4.15	4000	1.5	C	5.50	-4.82	-6.30
8.0	4.15	4100	1.5	C	5.53	-4.86	-6.31
8.0	4.15	4100	1.7	C	5.55	-4.89	-6.33
8.0	4.15	4200	1.5	C	5.56	-4.92	-6.33
8.0	4.15	4200	1.7	C	5.58	-4.94	-6.34
8.0	4.15	4300	1.5	C	5.59	-4.97	-6.35
8.0	4.15	4300	1.7	C	5.61	-4.99	-6.35
8.0	4.15	4400	1.5	C	5.63	-5.03	-6.36
8.0	4.15	4400	1.7	C	5.64	-5.05	-6.37
8.0	4.15	4500	1.5	C	5.66	-5.08	-6.37
8.0	4.15	4500	1.7	C	5.67	-5.10	-6.38
8.0	4.15	4600	1.5	C	5.69	-5.14	-6.38
8.0	4.15	4600	1.7	C	5.69	-5.15	-6.39
8.0	4.15	4700	1.5	C	5.72	-5.20	-6.39
8.0	4.15	4700	1.7	C	5.73	-5.20	-6.40
8.0	4.15	4800	1.5	C	5.74	-5.24	-6.39
8.0	4.15	4800	1.7	C	5.75	-5.24	-6.40
8.0	4.15	4900	1.5	C	5.76	-5.29	-6.40
8.0	4.15	4900	1.7	C	5.78	-5.29	-6.41
8.0	4.15	5000	1.5	C	5.79	-5.33	-6.41
8.0	4.15	5100	1.5	C	5.81	-5.37	-6.41
9.0	3.92	4400	1.5	A	5.07	-4.48	-5.79
9.0	3.92	4500	1.5	A	5.09	-4.53	-5.80
9.0	3.92	4600	1.5	A	5.12	-4.58	-5.81
9.0	3.92	4700	1.5	A	5.14	-4.62	-5.82

TABLE A.3: continued.

$M/M_\odot$	$\log(L/L_\odot)$	T_{eff}[K]	α_{ml}	ML	G	G_{BP}	G_{RP}
(1)	(2)	(3)	(4)	(5)	(6)	(7)	(8)
9.0	3.92	4800	1.5	A	5.17	-4.68	-5.82
9.0	3.92	4800	1.7	A	5.18	-4.69	-5.83
9.0	3.92	4900	1.5	A	5.19	-4.73	-5.82
9.0	3.92	4900	1.7	A	5.20	-4.73	-5.83
9.0	3.92	5000	1.5	A	5.21	-4.76	-5.82
9.0	3.92	5000	1.7	A	5.22	-4.77	-5.84
9.0	3.92	5100	1.5	A	5.23	-4.81	-5.82
9.0	3.92	5100	1.7	A	5.24	-4.80	-5.84
9.0	3.92	5200	1.5	A	5.25	-4.85	-5.82
9.0	4.12	4000	1.5	B	5.43	-4.75	-6.23
9.0	4.12	4100	1.5	B	5.46	-4.80	-6.25
9.0	4.12	4200	1.5	B	5.49	-4.85	-6.26
9.0	4.12	4300	1.5	B	5.52	-4.90	-6.27
9.0	4.12	4300	1.7	B	5.54	-4.93	-6.28
9.0	4.12	4400	1.5	B	5.55	-4.96	-6.29
9.0	4.12	4400	1.7	B	5.57	-4.98	-6.30
9.0	4.12	4500	1.5	B	5.59	-5.02	-6.30
9.0	4.12	4500	1.7	B	5.60	-5.04	-6.31
9.0	4.12	4600	1.5	B	5.61	-5.07	-6.31
9.0	4.12	4600	1.7	B	5.62	-5.08	-6.32
9.0	4.12	4700	1.5	B	5.64	-5.12	-6.31
9.0	4.12	4700	1.7	B	5.65	-5.13	-6.33
9.0	4.12	4800	1.5	B	5.67	-5.17	-6.32
9.0	4.12	4800	1.7	B	5.68	-5.18	-6.33
9.0	4.12	4900	1.5	B	5.69	-5.22	-6.32
9.0	4.12	5000	1.5	B	5.72	-5.26	-6.33
9.0	4.32	4200	1.5	C	5.99	-5.34	-6.76
9.0	4.32	4300	1.5	C	6.02	-5.40	-6.78
9.0	4.32	4300	1.7	C	6.03	-5.41	-6.78
9.0	4.32	4400	1.5	C	6.05	-5.45	-6.79
9.0	4.32	4400	1.7	C	6.06	-5.47	-6.80
9.0	4.32	4500	1.5	C	6.08	-5.51	-6.80
9.0	4.32	4500	1.7	C	6.09	-5.52	-6.81
9.0	4.32	4600	1.5	C	6.11	-5.56	-6.81
9.0	4.32	4600	1.7	C	6.12	-5.57	-6.82
9.0	4.32	4700	1.5	C	6.14	-5.62	-6.82
9.0	4.32	4700	1.7	C	6.15	-5.62	-6.83
9.0	4.32	4800	1.5	C	6.18	-5.68	-6.83
9.0	4.32	4900	1.5	C	6.21	-5.73	-6.85
10.0	4.08	4200	1.5	A	5.38	-4.75	-6.15
10.0	4.08	4300	1.5	A	5.41	-4.80	-6.16
10.0	4.08	4400	1.5	A	5.44	-4.85	-6.17
10.0	4.08	4500	1.5	A	5.47	-4.90	-6.18
10.0	4.08	4600	1.5	A	5.50	-4.95	-6.19
10.0	4.08	4600	1.7	A	5.51	-4.97	-6.20
10.0	4.08	4700	1.5	A	5.53	-5.01	-6.20

TABLE A.3: continued.

$M/M_\odot$	$\log(L/L_\odot)$	T_{eff}[K]	α_{ml}	ML	G	G_{BP}	G_{RP}
(1)	(2)	(3)	(4)	(5)	(6)	(7)	(8)
10.0	4.08	4700	1.7	A	5.54	-5.02	-6.21
10.0	4.08	4800	1.5	A	5.55	-5.06	-6.20
10.0	4.08	4800	1.7	A	5.57	-5.07	-6.22
10.0	4.08	4900	1.5	A	5.58	-5.11	-6.21
10.0	4.08	4900	1.7	A	5.59	-5.11	-6.22
10.0	4.08	5000	1.5	A	5.60	-5.15	-6.21
10.0	4.08	5100	1.5	A	5.62	-5.19	-6.22
10.0	4.28	3800	1.5	B	5.74	-5.01	-6.58
10.0	4.28	3900	1.5	B	5.77	-5.06	-6.59
10.0	4.28	4000	1.5	B	5.80	-5.11	-6.61
10.0	4.28	4100	1.5	B	5.83	-5.17	-6.62
10.0	4.28	4100	1.7	B	5.85	-5.20	-6.64
10.0	4.28	4200	1.5	B	5.87	-5.22	-6.64
10.0	4.28	4200	1.7	B	5.88	-5.25	-6.65
10.0	4.28	4300	1.5	B	5.90	-5.28	-6.66
10.0	4.28	4300	1.7	B	5.92	-5.30	-6.66
10.0	4.28	4400	1.5	B	5.94	-5.34	-6.67
10.0	4.28	4400	1.7	B	5.95	-5.35	-6.68
10.0	4.28	4500	1.5	B	5.97	-5.40	-6.69
10.0	4.28	4500	1.7	B	5.98	-5.42	-6.69
10.0	4.28	4600	1.5	B	6.00	-5.45	-6.69
10.0	4.28	4600	1.7	B	6.01	-5.46	-6.70
10.0	4.28	4700	1.5	B	6.02	-5.50	-6.70
10.0	4.28	4700	1.7	B	6.04	-5.51	-6.71
10.0	4.28	4800	1.5	B	6.05	-5.55	-6.71
10.0	4.28	4900	1.5	B	6.08	-5.60	-6.72
10.0	4.48	4500	1.5	C	6.48	-5.91	-7.19
10.0	4.48	4500	1.7	C	6.49	-5.92	-7.20
10.0	4.48	4600	1.5	C	6.51	-5.97	-7.21
10.0	4.48	4600	1.7	C	6.52	-5.97	-7.21
10.0	4.48	4700	1.5	C	6.53	-6.00	-7.21
10.0	4.48	4700	1.7	C	6.54	-6.01	-7.22
10.0	4.48	4800	1.5	C	6.56	-6.05	-7.22
11.0	4.21	4100	1.5	A	5.68	-5.02	-6.47
11.0	4.21	4200	1.5	A	5.72	-5.08	-6.49
11.0	4.21	4300	1.5	A	5.75	-5.13	-6.50
11.0	4.21	4400	1.5	A	5.79	-5.20	-6.52
11.0	4.21	4400	1.7	A	5.80	-5.21	-6.53
11.0	4.21	4500	1.5	A	5.81	-5.24	-6.53
11.0	4.21	4500	1.7	A	5.83	-5.26	-6.54
11.0	4.21	4600	1.5	A	5.84	-5.30	-6.54
11.0	4.21	4600	1.7	A	5.86	-5.31	-6.55
11.0	4.21	4700	1.5	A	5.87	-5.35	-6.54
11.0	4.21	4700	1.7	A	5.88	-5.36	-6.56
11.0	4.21	4800	1.5	A	5.90	-5.40	-6.55
11.0	4.21	4900	1.5	A	5.93	-5.46	-6.56

TABLE A.3: continued.

$M/M_\odot$	$\log(L/L_\odot)$	T_{eff}[K]	α_{ml}	ML	G	G_{BP}	G_{RP}
(1)	(2)	(3)	(4)	(5)	(6)	(7)	(8)
11.0	4.41	3900	1.7	B	6.13	-5.43	-6.95
11.0	4.41	4000	1.5	B	6.14	-5.45	-6.95
11.0	4.41	4000	1.7	B	6.16	-5.48	-6.96
11.0	4.41	4100	1.5	B	6.18	-5.51	-6.97
11.0	4.41	4100	1.7	B	6.19	-5.53	-6.98
11.0	4.41	4200	1.5	B	6.21	-5.57	-6.99
11.0	4.41	4200	1.7	B	6.23	-5.59	-7.00
11.0	4.41	4300	1.5	B	6.25	-5.62	-7.00
11.0	4.41	4300	1.7	B	6.26	-5.64	-7.01
11.0	4.41	4400	1.5	B	6.28	-5.68	-7.02
11.0	4.41	4400	1.7	B	6.29	-5.70	-7.03
11.0	4.41	4500	1.5	B	6.31	-5.74	-7.03
11.0	4.41	4500	1.7	B	6.32	-5.75	-7.04
11.0	4.41	4600	1.5	B	6.34	-5.79	-7.04
11.0	4.41	4600	1.7	B	6.35	-5.80	-7.05
11.0	4.41	4700	1.5	B	6.37	-5.85	-7.05
11.0	4.41	4700	1.7	B	6.39	-5.86	-7.07
11.0	4.41	4800	1.5	B	6.41	-5.91	-7.07
11.0	4.61	4600	1.5	C	6.85	-6.29	-7.55
11.0	4.61	4600	1.7	C	6.86	-6.30	-7.56
11.0	4.61	4700	1.5	C	6.88	-6.35	-7.56
11.0	4.61	4800	1.5	C	6.91	-6.39	-7.57

TABLE A.4: Mean magnitudes in the *Gaia* filters for FO-mode models at varying assumptions of the ML relation and values of α_{ml} parameter.

		Z=0.02	Y= 0.28				
$M/M_\odot$	$\log(L/L_\odot)$	T_{eff}[K]	α_{ml}	ML	G	G_{BP}	G_{RP}
(1)	(2)	(3)	(4)	(5)	(6)	(7)	(8)
3.0	2.32	6200	1.5	A	-1.32	-1.08	-1.70
3.0	2.32	6300	1.5	A	-1.32	-1.10	-1.68
3.0	2.32	6300	1.7	A	-1.32	-1.10	-1.69
3.0	2.32	6400	1.5	A	-1.32	-1.11	-1.66
3.0	2.32	6400	1.7	A	-1.32	-1.11	-1.67
3.0	2.32	6500	1.5	A	-1.32	-1.13	-1.64
3.0	2.32	6500	1.7	A	-1.32	-1.13	-1.65
3.0	2.52	6000	1.5	B	-1.82	-1.55	-2.24
3.0	2.52	6100	1.5	B	-1.82	-1.57	-2.22
3.0	2.52	6200	1.5	B	-1.82	-1.59	-2.20
3.0	2.52	6200	1.7	B	-1.83	-1.59	-2.20
3.0	2.52	6300	1.5	B	-1.82	-1.61	-2.18
3.0	2.52	6300	1.7	B	-1.83	-1.61	-2.19
3.0	2.52	6400	1.5	B	-1.82	-1.62	-2.16
3.0	2.52	6400	1.7	B	-1.83	-1.62	-2.17
3.0	2.52	6500	1.5	B	-1.82	-1.63	-2.14
3.0	2.52	6500	1.7	B	-1.83	-1.64	-2.16

TABLE A.4: continued.

$M/M_{\odot}$	$\log(L/L_{\odot})$	T_{eff}[K]	α_{ml}	ML	G	G_{BP}	G_{RP}
(1)	(2)	(3)	(4)	(5)	(6)	(7)	(8)
3.0	2.72	6000	1.5	C	-2.32	-2.06	-2.74
3.0	2.72	6100	1.5	C	-2.33	-2.08	-2.72
3.0	2.72	6200	1.5	C	-2.33	-2.10	-2.70
3.0	2.72	6200	1.7	C	-2.33	-2.10	-2.71
3.0	2.72	6300	1.5	C	-2.33	-2.11	-2.69
3.0	2.72	6400	1.5	C	-2.33	-2.13	-2.67
4.0	2.74	5900	1.5	A	-2.36	-2.08	-2.80
4.0	2.74	6000	1.5	A	-2.37	-2.10	-2.78
4.0	2.74	6100	1.5	A	-2.37	-2.12	-2.76
4.0	2.74	6100	1.7	A	-2.37	-2.12	-2.77
4.0	2.74	6200	1.5	A	-2.37	-2.14	-2.75
4.0	2.74	6200	1.7	A	-2.37	-2.14	-2.75
4.0	2.74	6300	1.5	A	-2.37	-2.16	-2.73
4.0	2.74	6300	1.7	A	-2.38	-2.16	-2.73
4.0	2.74	6400	1.5	A	-2.37	-2.17	-2.71
4.0	2.94	5900	1.5	B	-2.87	-2.59	-3.30
4.0	2.94	6000	1.5	B	-2.87	-2.61	-3.28
4.0	2.94	6100	1.5	B	-2.87	-2.63	-3.27
4.0	2.94	6200	1.5	B	-2.88	-2.64	-3.25
4.0	3.14	6000	1.5	C	-3.38	-3.11	-3.79
5.0	3.07	5800	1.5	A	-3.17	-2.88	-3.63
5.0	3.07	5900	1.5	A	-3.18	-2.90	-3.61
5.0	3.07	6000	1.5	A	-3.18	-2.92	-3.60
5.0	3.07	6100	1.5	A	-3.19	-2.94	-3.58
6.0	3.33	5800	1.5	A	-3.84	-3.54	-4.29

A.3 Individual mass estimates derived from the theoretical PWM relations combined with Gaia DR2 parallaxes, for the selected F and FO-mode GCCs

TABLE A.5: The individual masses estimated from the theoretical PWM relations combined with Gaia DR2 parallaxes, for the F and FO-mode GCCs selected from the sample by Ripepi et al. (2019).

Gaia DR2 Source Id	Mode	P[d]	G[mag]	G_{BP}[mag]	G_{RP}[mag]	ϖ[mas]	$\sigma\,\varpi$[mas]	$M/M_{\odot}$	$\sigma M/M_{\odot}$	$M/M_{\odot}$ corr	$\sigma M/M_{\odot}$ corr
(1)	(2)	(3)	(4)	(5)	(6)	(7)	(8)	(9)	(10)	(11)	
1857884212378132096	F	4.43546	5.46	5.77	5.07	1.674	0.089	4.2	0.5	4.0	0.5
4066429066901946368	F	5.05787	6.82	7.37	6.23	1.119	0.053	5.2	0.6	4.8	0.5
5235910694044165760	F	3.08613	8.70	9.22	8.06	0.681	0.032	4.1	0.5	3.6	0.4
279382060625871360	F	3.29487	7.19	7.81	6.48	1.272	0.035	6.2	0.5	5.7	0.4
5824464493705913472	F	3.38932	6.44	6.86	5.91	1.475	0.037	4.5	0.3	4.3	0.3
5932997939411720960	F	3.45291	9.79	10.63	8.92	0.547	0.036	5.5	0.8	4.7	0.7
5351721738384434048	F	3.68221	8.08	8.45	7.59	0.561	0.037	5.4	0.8	4.6	0.7
465719182408723072	F	3.83288	10.43	11.14	9.64	0.307	0.028	6.1	1.2	4.6	0.9
6059635702888301952	F	3.83834	7.99	8.43	7.42	0.621	0.038	6.1	0.8	5.3	0.7
2166861170366710272	F	4.04921	10.29	11.11	9.41	0.528	0.028	3.1	0.4	2.6	0.3
422923956470923008	F	4.07117	9.54	10.14	8.83	0.399	0.030	5.6	0.9	4.5	0.7
3027940437469882880	F	4.25689	9.32	9.95	8.59	0.492	0.040	4.7	0.8	3.9	0.7
5338024572321721216	F	4.26618	9.44	9.99	8.79	0.374	0.027	5.5	0.9	4.3	0.7
2014609252631258496	F	4.27863	11.57	12.60	10.58	0.390	0.027	2.9	0.4	2.3	0.4
1977074811892425600	F	4.32355	8.96	9.40	8.39	0.403	0.034	5.2	0.9	4.2	0.8
2060021625508894592	F	4.36470	9.49	10.10	8.77	0.399	0.028	5.6	0.9	4.5	0.7
6055722403534963840	F	4.42452	9.46	10.21	8.65	0.446	0.031	6.9	1.1	5.7	0.9
426881614218441600	F	4.50162	9.55	10.21	8.79	0.403	0.030	6.0	1.0	4.8	0.8
4054440301294394624	F	4.52781	7.55	8.14	6.92	0.920	0.047	5.1	0.6	4.6	0.5
5521459979795304320	F	4.63985	7.71	8.26	7.05	0.852	0.035	4.9	0.5	4.4	0.4
5338438297925480320	F	4.67767	9.41	9.97	8.73	0.375	0.026	5.6	0.9	4.4	0.7
3046774762417915136	F	4.67830	7.83	8.33	7.20	0.616	0.047	7.3	1.2	6.3	1.0
6060173364061645696	F	4.68971	6.36	6.80	5.79	1.021	0.045	8.5	0.9	7.7	0.8
1960750328384177408	F	4.86438	8.67	9.19	8.03	0.435	0.028	6.8	1.0	5.5	0.8
2078709577944648192	F	4.92549	8.90	9.42	8.26	0.413	0.023	6.1	0.8	4.9	0.6
5258574068220187648	F	4.93255	10.24	10.94	9.46	0.365	0.032	3.9	0.7	3.1	0.6
2055122987639665664	F	4.95045	12.27	13.38	11.21	0.339	0.033	2.3	0.5	1.7	0.4
270272675510149504	F	4.97249	9.12	9.99	8.23	0.521	0.038	8.9	1.4	7.5	1.2
2003938801532007808	F	4.98330	8.61	9.15	7.94	0.437	0.035	7.7	1.3	6.2	1.1

TABLE A.5: continued.

Gaia DR2 Source Id	Mode	P[d]	G[mag]	G_{BP}[mag]	G_{RP}[mag]	ϖ[mas]	$\sigma\,\varpi$[mas]	$M/M_\odot$	$\sigma M/M_\odot$	$M/M_\odot$ corr	$\sigma M/M_\odot$ corr
(1)	(2)	(3)	(4)	(5)	(6)	(7)	(8)	(9)	(10)	(11)	
2011315528113463808	F	4.99754	10.50	11.42	9.58	0.355	0.026	6.1	1.0	4.8	0.8
473293889810320128	F	5.06643	10.00	11.16	8.95	0.716	0.031	4.5	0.5	3.9	0.4
5871738271033526016	F	5.07890	7.43	7.89	6.85	0.841	0.034	4.4	0.4	4.0	0.4
2166303099490547072	F	5.09955	10.53	11.69	9.46	0.528	0.027	5.2	0.6	4.4	0.5
4080122796947250176	F	5.15424	7.25	7.83	6.58	0.986	0.047	5.3	0.6	4.9	0.5
4085919765884068736	F	6.63703	6.63	7.21	5.93	1.248	0.041	5.0	0.4	4.6	0.4
1827869808377481216	F	5.19725	10.03	10.96	9.09	0.419	0.034	6.8	1.2	5.5	1.0
5254295559276699392	F	5.20456	9.06	9.56	8.44	0.374	0.028	5.6	0.9	4.4	0.7
1968971582984827136	F	5.25760	8.88	9.91	7.90	0.896	0.027	5.4	0.4	4.9	0.4
6053622679932061056	F	5.26567	9.01	9.91	8.12	0.783	0.045	4.2	0.5	3.8	0.5
4147381366335558784	F	5.30141	9.96	11.03	8.94	0.670	0.040	4.1	0.5	3.6	0.5
5334506135119058304	F	5.30996	8.49	9.08	7.79	0.549	0.032	5.8	0.8	4.9	0.6
1960981328902089088	F	5.33166	8.57	9.13	7.90	0.509	0.031	5.7	0.8	4.7	0.6
458239995077788544	F	5.36511	10.46	11.49	9.51	0.366	0.035	7.1	1.4	5.6	1.1
4190143160245024256	F	5.37668	7.54	8.03	6.92	0.738	0.052	5.6	0.9	4.9	0.8
2010285491880986112	F	5.44090	9.28	9.96	8.51	0.413	0.032	6.5	1.1	5.2	0.9
5891675303053080704	F	5.49457	6.55	7.11	5.93	1.340	0.045	4.6	0.4	4.3	0.4
459035766618689280	F	5.53070	10.37	11.47	9.37	0.394	0.035	8.1	1.5	6.4	1.2
5539107450645759232	F	5.56408	10.59	11.47	9.75	0.258	0.025	7.8	1.6	5.6	1.1
422226488141991296	F	5.80901	8.78	9.37	8.08	0.359	0.033	9.7	1.9	7.5	1.5
5327836325732931840	F	5.85935	9.21	9.96	8.39	0.407	0.029	8.2	1.3	6.6	1.0
5436296928693979392	F	5.89839	9.12	9.52	8.58	0.292	0.029	5.7	1.2	4.2	0.9
2055014277739104896	F	5.95590	8.91	9.76	8.02	0.697	0.039	4.8	0.6	4.2	0.5
4092905375639902464	F	6.74522	6.35	7.01	5.62	1.460	0.045	5.6	0.5	5.2	0.4
4312361436842603520	F	6.11423	7.66	8.44	6.84	0.930	0.057	6.6	0.9	5.9	0.8
6059764002146656128	F	6.22040	8.07	8.64	7.38	0.524	0.046	7.8	1.5	6.5	1.2
2008504454839717120	F	6.23397	9.00	9.92	8.08	0.679	0.030	5.4	0.6	4.7	0.5
525136962570940160	F	6.27279	10.23	11.24	9.28	0.374	0.028	6.9	1.1	5.5	0.9
2015820463470505600	F	6.29664	9.24	10.22	8.28	0.588	0.032	6.8	0.8	5.8	0.7

TABLE A.5: continued.

Gaia DR2 Source Id	Mode	P[d]	G[mag]	G_{BP}[mag]	G_{RP}[mag]	ϖ[mas]	$\sigma\,\varpi$[mas]	$M/M_{\odot}$	$\sigma M/M_{\odot}$	$M/M_{\odot}$ corr	$\sigma M/M_{\odot}$ corr
(1)	(2)	(3)	(4)	(5)	(6)	(7)	(8)	(9)	(10)	(11)	
5823134325151372032	F	6.31663	6.22	6.59	5.63	1.075	0.030	5.8	0.4	5.4	0.4
2027263738130844288	F	6.32059	8.23	9.14	7.30	0.841	0.039	7.1	0.8	6.4	0.7
4096979650282842112	F	6.42429	8.41	9.08	7.59	0.702	0.059	4.5	0.8	3.9	0.7
5312196047720402048	F	6.45380	11.06	12.07	10.08	0.275	0.026	6.2	1.2	4.5	0.9
5868480143187802240	F	6.45975	8.08	8.71	7.34	0.557	0.039	7.9	1.2	6.7	1.0
174489098011145216	F	6.46466	7.05	7.73	6.27	1.042	0.064	6.8	0.9	6.2	0.9
5541507237862358912	F	6.66423	7.71	8.14	7.16	0.568	0.030	5.3	0.6	4.5	0.5
5302258008774271488	F	6.69695	7.11	7.60	6.50	0.760	0.023	6.2	0.5	5.5	0.4
6054829806275577216	F	6.73287	6.30	6.81	5.68	1.140	0.028	6.2	0.4	5.7	0.4
4204653587029046400	F	6.80601	7.34	8.02	6.57	0.944	0.048	5.9	0.7	5.3	0.6
5324034867356093056	F	6.92436	7.22	7.93	6.44	1.007	0.037	6.1	0.6	5.5	0.5
4057701830728920064	F	7.01753	4.21	4.75	3.70	3.431	0.202	3.8	0.5	3.7	0.5
5877533315817003648	F	7.06626	6.42	6.96	5.77	1.015	0.032	7.4	0.6	6.7	0.6
5309174967720762496	F	7.13431	9.69	10.51	8.83	0.312	0.029	8.9	1.8	6.7	1.3
5257664497238811776	F	7.19619	8.95	9.58	8.22	0.355	0.030	7.8	1.4	6.1	1.1
4307944836090489600	F	7.23996	9.35	10.33	8.39	0.554	0.055	5.9	1.3	5.0	1.1
2165771172070496512	F	7.25140	9.95	10.88	9.00	0.387	0.028	6.4	1.0	5.1	0.8
5855468247702904704	F	7.51028	6.10	6.55	5.55	1.000	0.029	6.9	0.5	6.3	0.5
5337191279923824384	F	7.53200	7.80	8.35	7.14	0.704	0.030	4.0	0.4	3.5	0.4
5339394082770287232	F	7.72081	6.61	7.08	6.01	0.796	0.035	7.5	0.8	6.7	0.7
2016028168089215488	F	7.80112	10.08	11.04	9.12	0.383	0.031	5.7	1.0	4.5	0.8
2030063919381336832	F	7.81823	9.37	10.16	8.51	0.400	0.032	6.3	1.1	5.1	0.9
1873112207907294848	F	7.85582	9.05	9.82	8.20	0.446	0.028	6.4	0.9	5.2	0.7
470361114339849472	F	7.91561	7.16	7.92	6.32	0.782	0.040	11.6	1.4	10.3	1.2
1825621002188696448	F	7.99014	6.58	7.41	5.72	1.053	0.039	12.8	1.2	11.8	1.1
428620663657823232	F	8.00066	8.51	9.23	7.71	0.422	0.034	10.0	1.7	8.1	1.4
512524361613040640	F	8.37701	6.64	7.46	5.78	1.296	0.031	7.5	0.5	6.9	0.5
5254097093074642944	F	9.19783	8.80	9.39	8.12	0.328	0.029	7.0	1.3	5.4	1.0
4056026175045038464	F	9.31686	8.24	9.08	7.43	0.697	0.064	4.9	1.0	4.3	0.8

TABLE A.5: continued.

Gaia DR2 Source Id	Mode	P[d]	G[mag]	G_{BP}[mag]	G_{RP}[mag]	ϖ[mas]	$\sigma\,\varpi$[mas]	$M/M_\odot$	$\sigma M/M_\odot$	$M/M_\odot$ corr	$\sigma M/M_\odot$ corr
(1)	(2)	(3)	(4)	(5)	(6)	(7)	(8)	(9)	(10)	(11)	
5854560115494081024	F	9.46519	8.26	8.97	7.47	0.496	0.031	7.3	1.0	6.1	0.8
4269036830424588800	F	9.48055	7.90	8.67	7.12	0.690	0.050	5.7	0.9	5.0	0.8
5835124087174043136	F	9.75376	6.15	6.70	5.52	1.062	0.042	6.1	0.6	5.6	0.5
2070224337474904064	F	10.14797	9.42	10.48	8.42	0.447	0.029	7.8	1.1	6.4	0.9
506779550797525760	F	10.87727	8.84	9.58	8.04	0.330	0.031	9.1	1.8	6.9	1.4
2007201567928631296	F	10.88439	8.04	8.70	7.29	0.458	0.038	7.9	1.4	6.5	1.2
5871922507947292032	F	10.94947	7.47	8.03	6.79	0.537	0.042	7.1	1.2	6.0	1.0
5313887130948758016	F	11.20064	8.88	9.83	7.95	0.391	0.032	11.3	2.0	9.0	1.6
200708636406382720	F	11.62570	7.34	7.94	6.68	0.543	0.051	7.7	1.5	6.5	1.3
5332375453374624640	F	11.63735	9.33	10.09	8.59	0.264	0.026	7.8	1.6	5.6	1.2
5240441472232302848	F	12.43802	8.85	9.60	8.06	0.330	0.027	7.9	1.4	6.0	1.1
5884729035255064064	F	12.63346	8.96	9.87	8.03	0.400	0.035	8.0	1.5	6.4	1.2
4267397694768545920	F	13.75460	6.61	7.39	5.85	0.888	0.054	7.9	1.1	7.2	1.0
5351331755370445056	F	14.10712	8.07	8.99	7.51	0.406	0.037	8.6	1.7	6.9	1.3
6026412893938675712	F	6.06133	6.67	7.17	5.95	1.131	0.055	5.7	0.6	5.3	0.6
2161786374436607616	F	14.71797	8.39	9.71	7.28	0.781	0.037	8.8	1.0	7.9	0.9
2071433765909167232	F	15.11946	8.82	9.73	7.91	0.362	0.026	9.2	1.4	7.2	1.1
1870258975238302208	F	16.39062	6.07	6.69	5.36	0.898	0.027	7.3	0.6	6.6	0.5
5338036117182452096	F	16.65998	8.19	8.90	7.38	0.424	0.035	6.4	1.1	5.2	0.9
2058374144759464064	F	17.07369	8.46	9.24	7.61	0.381	0.033	7.4	1.4	5.8	1.1
4175017625462647168	F	17.12484	5.52	6.41	4.64	1.361	0.083	11.1	1.5	10.4	1.4
5255254711361371520	F	18.17758	8.30	8.97	7.52	0.320	0.031	8.4	1.7	6.4	1.3
5351161399785606016	F	18.87302	7.15	7.82	6.43	0.512	0.041	8.2	1.4	6.8	1.2
1873250780732545920	F	20.14034	9.27	10.36	8.28	0.350	0.028	7.7	1.3	6.0	1.0
5523162573544337408	F	20.49764	6.66	7.31	5.90	0.547	0.032	10.9	1.4	9.2	1.2
5964193485048327808	F	28.86509	8.85	10.11	7.76	0.504	0.045	6.1	1.2	5.1	1.0
5546476927338700416	F	41.46411	6.46	7.30	5.58	0.584	0.026	9.9	1.0	8.4	0.9
5351436724362450304	FO	1.11936	11.09	11.62	10.41	0.389	0.030	3.3	0.7	2.4	0.5
2164475809937299584	FO	1.76585	10.18	10.74	9.49	0.343	0.027	7.6	1.7	5.4	1.2

TABLE A.5: continued.

Gaia DR2 Source Id	Mode	P[d]	G[mag]	G_{BP}[mag]	G_{RP}[mag]	ϖ[mas]	$\sigma\,\varpi$[mas]	$M/M_{\odot}$	$\sigma M/M_{\odot}$	$M/M_{\odot}$ corr	$\sigma M/M_{\odot}$ corr
(1)	(2)	(3)	(4)	(5)	(6)	(7)	(8)	(9)	(10)	(11)	
5245796334347122944	FO	2.06344	8.09	8.53	7.54	0.858	0.026	3.5	0.4	3.0	0.3
3398383973788673024	FO	2.10240	7.88	8.29	7.35	0.805	0.053	4.7	0.9	4.0	0.8
2203988169026743936	FO	2.11413	7.51	8.05	6.84	1.133	0.033	5.6	0.6	5.0	0.5
6057943520139661184	FO	2.30569	9.77	10.32	9.10	0.396	0.033	5.1	1.2	3.8	0.9
5877460679352962048	FO	2.39812	7.29	7.73	6.70	0.995	0.040	5.7	0.7	5.0	0.6
5824226655600824704	FO	2.42829	7.58	8.02	7.02	0.889	0.032	4.7	0.6	4.1	0.5
1853025642297186688	FO	2.49930	5.62	5.93	5.20	1.706	0.055	4.7	0.5	4.4	0.5
2007654601080023040	FO	2.80533	9.12	9.68	8.43	0.496	0.039	4.9	1.1	3.8	0.9
429182376660681984	FO	2.84185	9.90	10.50	9.18	0.385	0.028	4.2	0.9	3.1	0.6
4319599865468760832	FO	2.97303	10.15	11.24	9.14	0.571	0.038	6.2	1.2	5.0	1.0
5258420858142702208	FO	3.03785	9.12	9.61	8.50	0.365	0.026	7.0	1.4	5.0	1.0
2200929331984972672	FO	3.05313	10.87	11.74	9.96	0.317	0.027	5.5	1.4	3.8	0.9
5848500161483878400	FO	3.06525	7.10	7.64	6.44	1.016	0.036	6.6	0.8	5.9	0.7
5613541295473114496	FO	3.12653	8.99	9.63	8.26	0.515	0.031	5.6	1.0	4.5	0.8
3409635486731094400	FO	3.14835	6.23	6.75	5.59	1.428	0.061	6.6	0.9	6.1	0.8
5334449269746243328	FO	3.21183	8.42	8.81	7.89	0.425	0.032	6.5	1.4	4.9	1.1
511226491206912128	FO	3.22284	9.83	10.65	8.96	0.481	0.037	5.0	1.1	3.9	0.9
1971722045688053248	FO	3.28391	8.67	9.33	7.92	0.561	0.032	7.0	1.2	5.6	1.0
1964855904803120640	FO	3.33233	5.72	6.03	5.32	1.151	0.066	7.1	1.2	6.4	1.1
6058439910929477120	FO	3.34248	5.26	5.65	4.81	1.778	0.087	5.3	0.8	4.9	0.7
429635993926502912	FO	3.65163	10.44	11.33	9.53	0.327	0.028	6.9	1.7	4.8	1.2
5932565900081831040	FO	3.78678	8.58	9.10	7.93	0.474	0.038	5.3	1.2	4.1	1.0
5519380077440172672	FO	4.22646	5.53	5.89	5.11	1.217	0.057	6.3	0.9	5.7	0.8
428839329030983040	FO	4.30649	8.68	9.37	7.90	0.509	0.030	6.5	1.1	5.1	0.9
5881995546318024704	FO	4.37292	8.65	9.30	7.92	0.463	0.038	6.8	1.6	5.2	1.2
4514145288240593408	FO	4.47115	5.11	5.59	4.57	1.810	0.107	5.7	1.0	5.3	0.9
2004036486267748352	FO	5.44565	8.09	8.63	7.41	0.496	0.038	5.5	1.2	4.3	0.9
5506374096132016512	FO	5.69296	5.44	5.85	4.96	1.261	0.064	4.9	0.8	4.5	0.7
5337634589276921856	FO	5.72548	8.82	9.39	8.13	0.355	0.029	5.4	1.3	3.9	0.9

A.4 Individual ages for the selected F and FO-mode GCCs obtained by using both the canonical PA and PAC relations

TABLE A.6: Individual ages for the F-mode GCCs in our sample, obtained by using both the canonical PA and PAC relations.

Gaia DR2 Source Id	RA	DEC	P	G	G_{BP}	G_{RP}	E(G_{BP}-G_{RP})	σE(G_{BP}-G_{RP})	Note	t_{PA}	$\sigma\, t_{PA}$	t_{PAC}	$\sigma\, t_{PAC}$
(1)	(2)	(3)	(4)	(5)	(6)	(7)	(8)	(9)	(10)	(11)	(12)	(13)	(14)
3442172745919329664	82.35887	27.00089	3.34920	11.57	12.21	10.78	0.72	0.12	G	105.55	20.41	98.88	18.9
4704080802304630784	12.82014	-68.98430	0.99469	18.24	18.45	17.79	0.18	0.11	G	248.10	47.99	230.53	44.06
5521400228203695232	123.35129	-42.27568	1.00189	16.05	16.93	15.15	1.23	0.15	G	246.84	47.74	234.34	44.79
6379351625245757568	359.99997	-75.19496	1.03777	17.68	17.98	17.36	0.02	0.11	G	240.80	46.58	231.16	44.18
4711142067840447360	21.61608	-64.87535	1.06447	17.86	18.05	17.41	0.16	0.11	G	236.54	45.75	219.39	41.93
4639539705975935360	50.85364	-74.96868	1.11640	17.83	18.12	17.50	0.02	0.11	G	228.74	44.24	218.50	41.76
4690768156035338624	18.95551	-70.54573	1.14292	17.53	17.82	17.09	0.18	0.11	G	224.99	43.52	212.14	40.54
4703965697180635136	9.31520	-67.04117	1.15729	17.89	18.12	17.43	0.17	0.11	G	223.02	43.14	207.66	39.69
4666616485480394368	60.40851	-69.47789	1.15905	16.29	16.45	15.90	0.12	0.08	O	222.78	43.09	203.12	38.82
4691081375113472256	20.83822	-70.57775	1.17564	17.33	17.45	17.02	0.0	0.11	G	220.56	42.66	200.73	38.36
4637614151878607232	20.74650	-76.24745	1.20857	17.80	17.95	17.36	0.1	0.11	G	216.31	41.84	199.28	38.09
5834840099568788864	241.98124	-58.78225	1.23577	13.71	14.05	13.19	0.31	0.11	G	212.95	41.19	200.06	38.23
4636112425153243904	16.19343	-76.86050	1.25457	17.34	17.55	16.84	0.21	0.11	G	210.70	40.75	194.40	37.15
4690721839108141568	19.01385	-70.91305	1.30481	17.25	17.73	17.00	-0.0	0.11	G	204.95	39.64	201.29	38.47
4698739817197286912	23.24870	-66.49795	1.30920	17.05	17.30	16.67	0.05	0.11	G	204.47	39.55	192.58	36.8
5298606801235832064	140.10591	-62.22648	1.36601	18.36	18.60	17.89	0.18	0.11	G	198.45	38.38	184.56	35.27
5850083595712857472	220.66054	-64.27433	1.37135	17.67	18.47	16.71	1.23	0.15	G	197.90	38.28	183.88	35.14
4690414800484275840	12.25946	-70.13797	1.37867	17.09	17.39	16.78	-0.0	0.11	G	197.16	38.13	186.94	35.73
5935901715187592704	255.13630	-53.09007	1.39879	15.45	15.92	14.78	0.58	0.12	G	195.16	37.75	183.01	34.98
5615958881027868544	115.24714	-22.49207	1.39928	15.46	16.23	14.69	0.89	0.11	O	195.11	37.74	187.45	35.82
4627114812265929856	55.76893	-76.93405	1.42992	17.95	18.31	17.50	0.18	0.11	G	192.16	37.17	182.94	34.96
4690838421706602624	15.93439	-70.90033	1.43044	17.33	17.58	16.94	0.06	0.11	G	192.11	37.16	180.59	34.51
4637822960304562560	24.11091	-75.12545	1.43113	17.25	17.49	16.82	0.11	0.11	G	192.04	37.14	179.71	34.35
6027070573648725632	251.47116	-33.16585	1.45594	13.89	14.47	13.13	0.75	0.12	G	189.73	36.70	178.32	34.08
5321579073778197888	130.00710	-52.33019	1.53045	15.25	15.90	14.48	0.81	0.12	G	183.18	35.43	172.97	33.06
6008381624727734784	237.76802	-39.75981	1.57244	17.10	17.91	16.20	1.12	0.14	G	179.73	34.76	168.77	32.26
4649187405119614848	75.03872	-75.15255	1.57491	16.97	17.25	16.49	0.18	0.11	G	179.53	34.72	167.82	32.07
4108167833903339520	259.75244	-27.43467	1.58118	16.78	17.65	15.71	1.45	0.16	G	179.03	34.63	163.50	31.25
4691023998645738368	17.49608	-69.93794	1.60821	16.70	16.83	16.30	0.0	0.11	G	176.90	34.22	162.54	31.06
4650261219962135424	85.33831	-74.16668	1.62049	16.91	17.29	16.43	0.22	0.11	G	175.96	34.03	167.16	31.95

TABLE A.6: continued.

Gaia DR2 Source Id	RA	DEC	P	G	G_{BP}	G_{RP}	E(G_{BP}-G_{RP})	σE(G_{BP}-G_{RP})	Note	t_{PA}	$\sigma\, t_{PA}$	t_{PAC}	$\sigma\, t_{PAC}$
(1)	(2)	(3)	(4)	(5)	(6)	(7)	(8)	(9)	(10)	(11)	(12)	(13)	(14)
426580107514101376	15.41660	60.59426	1.62477	14.87	15.52	14.07	0.85	0.13	G	175.63	33.97	164.77	31.49
4684195339947360512	6.98869	-76.24706	1.64272	17.58	17.86	17.10	0.17	0.11	G	174.28	33.71	162.87	31.13
2031982665929461504	296.05399	29.68730	1.64410	16.22	17.13	15.31	1.2	0.14	G	174.18	33.69	164.77	31.49
181620805307496192	76.98162	33.05659	1.66805	14.61	15.30	13.80	0.88	0.13	G	172.41	33.35	162.36	31.03
4702506576531479424	12.34403	-69.50825	1.68632	17.24	17.63	16.86	0.08	0.11	G	171.09	33.09	164.81	31.5
2021540814501736320	293.71912	25.61797	1.69319	17.40	18.66	16.25	1.87	0.19	G	170.60	33.00	157.51	30.1
4684369749977673472	13.14590	-75.95877	1.75282	17.35	17.52	16.89	0.09	0.11	G	166.50	32.20	153.11	29.26
4392367984521092608	254.76077	4.79169	1.77576	14.89	15.22	14.38	0.23	0.11	G	164.98	31.91	154.50	29.53
4652327614621999872	70.43479	-74.41493	1.79655	16.84	16.86	16.26	0.21	0.11	G	163.63	31.65	144.51	27.62
5516409029527928064	125.97858	-47.25490	1.83399	15.20	15.90	14.37	0.91	0.13	G	161.28	31.19	151.29	28.91
5814577169727787392	254.58683	-67.66312	1.85575	13.93	14.19	13.51	0.06	0.11	G	159.94	30.94	149.78	28.63
4189050211325803008	299.56897	-12.07101	1.99398	17.75	18.07	17.21	0.24	0.11	G	152.05	29.41	141.93	27.12
252595410453952384	67.62787	43.65313	1.99947	13.06	14.01	12.09	1.29	0.15	G	151.76	29.35	142.30	27.2
5928285810456681344	247.54255	-57.33140	2.00665	13.64	14.08	13.01	0.44	0.11	G	151.38	29.28	142.10	27.16
5851830444814064512	206.04645	-65.60886	2.02729	15.84	16.51	14.95	0.97	0.13	G	150.29	29.07	139.10	26.58
2928096226097916160	109.16266	-22.18043	2.04402	14.73	15.46	13.87	0.96	0.13	G	149.42	28.90	140.17	26.79
5322875157471168768	129.59122	-49.81203	2.04472	15.13	15.93	14.31	0.92	0.13	G	149.39	28.89	142.17	27.17
5859972946880769408	189.52856	-66.38308	2.06540	15.01	15.58	14.31	0.63	0.09	O	148.33	28.69	139.25	26.61
4636099402811865344	19.45728	-76.56544	2.06770	16.80	17.11	16.32	0.16	0.11	G	148.22	28.67	138.81	26.53
6379917835078618752	359.03700	-73.64989	2.08819	17.15	17.32	16.70	0.05	0.11	G	147.19	28.47	135.36	25.87
5211831178906807040	93.60903	-79.18168	2.09182	16.74	16.98	16.24	0.15	0.11	G	147.01	28.43	136.03	26.0
2162679246615275264	315.66755	45.09280	2.11305	16.28	17.23	15.27	1.34	0.15	G	145.97	28.23	135.76	25.95
200016111582079744	73.82548	39.97972	2.12061	13.35	13.95	12.58	0.73	0.08	L	145.60	28.16	136.31	26.05
5613411827982576768	112.81549	-25.90739	2.14810	11.58	12.04	10.97	0.29	0.08	O	144.29	27.91	140.62	26.88
5256605839340504576	149.84616	-60.33354	2.30293	14.62	15.23	13.86	0.71	0.12	G	137.39	26.57	129.19	24.69
228673477705878400	63.37936	41.31878	2.31244	14.04	14.74	13.23	0.85	0.13	G	136.99	26.50	128.88	24.63
6377896696484508544	355.61170	-75.25641	2.33045	17.06	17.34	16.70	-0.0	0.11	G	136.25	26.35	127.20	24.31
5521137101325930624	122.45845	-43.97272	2.34215	14.33	14.88	13.65	0.56	0.11	G	135.77	26.26	128.02	24.47
5521712145909463680	128.16223	-46.79047	2.36600	15.36	16.18	14.36	1.23	0.15	G	134.80	26.07	124.09	23.72

TABLE A.6: continued.

Gaia DR2 Source Id	RA	DEC	P	G	G_{BP}	G_{RP}	E(G_{BP}-G_{RP})	σE(G_{BP}-G_{RP})	Note	t_{PA}	$\sigma\ t_{PA}$	t_{PAC}	$\sigma\ t_{PAC}$
(1)	(2)	(3)	(4)	(5)	(6)	(7)	(8)	(9)	(10)	(11)	(12)	(13)	(14)
5534744416711687424	119.86019	-40.02830	2.36819	14.81	15.55	13.92	0.99	0.13	G	134.71	26.06	125.47	23.98
4688062360997085440	21.38773	-70.75956	2.37759	16.60	17.05	16.33	0.0	0.11	G	134.34	25.98	128.20	24.5
5310255272261039488	138.08441	-55.23391	2.39764	14.44	15.10	13.65	0.79	0.12	G	133.55	25.83	125.42	23.97
3134002107923090944	101.39057	7.81629	2.42684	12.82	13.74	12.10	0.88	0.11	O	132.41	25.61	127.43	24.35
4445130042844217216	249.98383	7.67920	2.44837	15.83	16.15	15.32	0.18	0.11	G	131.59	25.45	122.86	23.48
1865228537734352896	317.06710	32.74552	2.45861	14.11	14.56	13.50	0.39	0.11	G	131.21	25.38	123.36	23.58
4650211741937480192	86.25630	-73.56541	2.47100	16.37	16.64	15.80	0.23	0.11	G	130.74	25.29	120.43	23.02
207722317998325632	80.88983	44.76008	2.47685	12.75	13.46	11.93	0.85	0.13	G	130.53	25.25	122.64	23.44
523700107035878272	14.38545	63.15643	2.48837	13.96	14.89	13.01	1.22	0.14	G	130.10	25.16	122.04	23.32
5596920115637629184	119.15388	-30.95279	2.49448	13.91	14.77	12.99	1.15	0.12	O	129.88	25.12	120.27	22.99
4757183606166564864	83.55789	-63.16699	2.50146	16.10	16.40	15.61	0.14	0.11	G	129.62	25.07	121.19	23.16
5329778887909167232	131.65005	-46.52931	2.52412	15.66	16.74	14.60	1.51	0.16	G	128.80	24.91	119.65	22.87
5520935444020919296	122.93820	-44.17210	2.54078	14.99	15.78	14.08	1.05	0.14	G	128.20	24.80	119.35	22.81
5613111347760892672	110.69908	-26.71455	2.54548	12.91	13.38	12.29	0.4	0.11	G	128.04	24.76	120.37	23.0
2934255449716149760	107.39410	-18.56329	2.54653	13.25	14.02	12.37	0.99	0.13	G	128.00	24.76	119.57	22.85
5520440663787736192	122.44604	-45.35460	2.55121	15.84	16.42	15.08	0.69	0.12	G	127.84	24.73	119.47	22.83
2932101334643047680	105.10347	-20.43170	2.55778	12.65	13.15	11.98	0.36	0.05	L	127.60	24.68	124.36	23.77
470144751068871808	61.63394	58.11309	2.57812	16.51	16.97	15.88	0.42	0.11	G	126.89	24.54	119.01	22.74
5597352047599988352	119.45786	-29.38405	2.58612	11.59	12.21	10.84	0.73	0.1	O	126.62	24.49	117.57	22.47
5404862853352596736	149.21983	-51.60892	2.60474	13.30	14.09	12.41	1.0	0.11	O	125.98	24.37	118.31	22.61
5599566983722741248	114.47706	-29.43804	2.62004	14.18	14.88	13.38	0.81	0.12	G	125.46	24.27	118.10	22.57
5617745003304609536	109.88037	-23.80181	2.63003	14.53	15.53	13.52	1.35	0.15	G	125.13	24.20	116.71	22.3
2004103831357741696	332.32734	51.40539	2.63200	14.84	15.40	14.13	0.59	0.12	G	125.06	24.19	117.42	22.44
3425576270732293632	93.99953	23.74749	2.63501	11.57	12.24	10.79	0.75	0.1	L	124.96	24.17	118.22	22.59
4690127037676227840	13.29901	-70.85695	2.63769	16.20	16.67	15.89	0.0	0.11	G	124.87	24.15	120.72	23.07
5254994264542210560	153.53708	-59.85044	2.64145	15.11	15.96	14.18	1.08	0.12	O	124.74	24.13	117.65	22.48
5932284528150696704	245.22589	-53.55461	2.64407	11.70	11.99	11.25	0.03	0.08	O	124.66	24.11	118.10	22.57
5857845872913577856	199.32909	-66.11714	2.65755	15.60	16.34	14.72	0.96	0.13	G	124.21	24.02	115.98	22.17
1986816867172796 16	72.85353	38.18855	2.65963	13.15	13.88	12.23	0.78	0.07	L	124.14	24.01	122.82	23.47

TABLE A.6: continued.

Gaia DR2 Source Id	RA	DEC	P	G	G_{BP}	G_{RP}	E(G_{BP}-G_{RP})	σE(G_{BP}-G_{RP})	Note	t_{PA}	$\sigma\ t_{PA}$	t_{PAC}	$\sigma\ t_{PAC}$
(1)	(2)	(3)	(4)	(5)	(6)	(7)	(8)	(9)	(10)	(11)	(12)	(13)	(14)
5322962499927658880	129.02740	-49.26527	2.66635	14.82	15.62	13.88	1.1	0.14	G	123.92	23.97	114.90	21.96
3330259852538068608	91.85611	11.15198	3.88939	11.07	11.64	10.37	0.5	0.06	L	95.00	18.37	89.84	17.17
5611563995612988928	112.16780	-29.34422	2.70160	12.72	13.13	12.17	0.27	0.11	G	122.78	23.75	115.58	22.09
3133819112256378368	100.02326	7.60583	2.70467	10.13	10.86	9.35	0.74	0.08	L	122.69	23.73	117.87	22.53
5515778734493663232	127.31510	-46.74924	2.71653	14.80	15.48	13.93	0.9	0.13	G	122.31	23.66	113.59	21.71
4688033735040263168	23.36268	-70.67097	2.74408	16.45	16.67	16.04	-0.0	0.11	G	121.44	23.49	112.23	21.45
5280590173638560128	104.74084	-68.31085	2.75554	15.96	16.28	15.44	0.17	0.11	G	121.09	23.42	112.95	21.59
355488086540394112	35.70997	50.07193	2.75989	14.54	14.96	13.95	0.32	0.11	G	120.95	23.39	113.44	21.68
5520506531407532928	121.80022	-45.06591	2.77254	14.02	14.57	13.29	0.6	0.12	G	120.56	23.32	112.83	21.56
5545066700588440832	119.73893	-36.89733	2.77514	15.07	16.06	14.05	1.35	0.15	G	120.48	23.30	112.11	21.43
4637956099996538752	18.33566	-75.37716	2.77979	16.46	16.76	15.98	0.11	0.11	G	120.34	23.28	112.29	21.46
2948568273607650560	105.01213	-14.16082	2.78195	13.90	14.80	13.11	0.91	0.13	G	120.28	23.26	115.97	22.16
4066429066901946368	273.26040	-23.11729	5.05787	6.82	7.37	6.23	0.25	0.03	L	78.96	15.27	76.16	14.56
460909093912435072	42.02334	57.93448	2.79873	14.03	15.07	13.01	1.39	0.15	G	119.77	23.17	111.65	21.34
430052537038350976	0.60589	62.84717	2.81345	14.41	15.25	13.49	1.08	0.14	G	119.33	23.08	111.62	21.33
1873298884367855872	314.17890	40.25849	2.82245	16.21	17.13	15.23	1.25	0.15	G	119.06	23.03	110.80	21.18
5616130129962210048	110.43814	-26.53341	2.82545	12.91	13.38	12.30	0.37	0.11	G	118.97	23.01	112.02	21.41
3117307814859500416	97.77268	-2.14679	3.13523	13.29	14.09	12.47	0.9	0.12	L	110.57	21.39	104.02	19.88
5293246995583678336	109.08524	-60.30341	2.84929	15.52	16.19	14.69	0.83	0.13	G	118.27	22.87	110.27	21.07
5544259212380322560	120.85675	-37.19998	2.85529	14.09	14.84	13.23	0.93	0.11	O	118.09	22.84	110.08	21.04
2928335747830554240	108.43497	-21.72421	2.86166	14.22	14.98	13.36	0.94	0.13	G	117.91	22.81	110.57	21.13
4757607983288353024	83.76190	-62.33990	2.86849	16.03	16.25	15.52	0.12	0.11	G	117.71	22.77	108.11	20.66
513074186146353536	24.74994	64.98924	2.87151	11.01	11.84	10.14	1.03	0.11	L	117.62	22.75	109.72	20.97
4688114725237948672	24.52435	-70.61840	2.88021	16.38	16.64	15.99	-0.0	0.11	G	117.37	22.70	108.80	20.79
261927068718088832	81.89283	50.86737	2.88526	13.17	13.81	12.41	0.7	0.12	G	117.23	22.67	110.22	21.06
4682206533865906944	65.11048	-57.85114	2.89258	15.71	16.00	15.30	-0.0	0.11	G	117.02	22.63	110.03	21.03
5253289093802878592	152.85139	-61.48616	2.91146	14.11	14.59	13.44	0.46	0.11	G	116.48	22.53	109.01	20.83
2947842664653933824	104.19146	-15.63763	3.69400	13.25	13.97	12.43	0.81	0.12	G	98.51	19.05	92.36	17.65
5310969267622303872	136.56210	-54.93719	2.92762	14.52	15.11	13.78	0.63	0.12	G	116.03	22.44	108.96	20.82

TABLE A.6: continued.

Gaia DR2 Source Id	RA	DEC	P	G	G_{BP}	G_{RP}	E(G_{BP}-G_{RP})	σE(G_{BP}-G_{RP})	Note	t_{PA}	$\sigma\ t_{PA}$	t_{PAC}	$\sigma\ t_{PAC}$
(1)	(2)	(3)	(4)	(5)	(6)	(7)	(8)	(9)	(10)	(11)	(12)	(13)	(14)
4642866828161408512	52.89342	-70.99389	2.92900	16.29	16.60	15.82	0.08	0.11	G	115.99	22.43	108.83	20.8
5533064637824258816	119.78798	-43.17517	2.92921	13.49	13.98	12.84	0.45	0.11	G	115.99	22.43	108.97	20.82
5598642947280233984	116.71718	-30.66590	2.96840	14.15	14.95	13.28	0.97	0.11	O	114.91	22.22	107.76	20.59
5856662557855409280	187.47093	-68.27871	2.98190	14.44	14.92	13.79	0.44	0.11	G	114.54	22.15	107.43	20.53
5318708901756763520	131.02834	-51.91945	2.98495	15.08	15.82	14.23	0.89	0.13	G	114.46	22.14	107.38	20.52
4265371574109405824	284.35111	-0.73024	2.98806	10.56	11.32	9.69	0.99	0.14	L	114.37	22.12	105.79	20.22
5519861423017907840	124.43265	-45.18550	3.00610	14.46	15.24	13.61	0.93	0.13	G	113.89	22.03	107.23	20.49
5241937353463150848	162.59092	-62.19142	3.02574	15.21	16.09	14.26	1.16	0.12	O	113.37	21.93	105.26	20.12
466906311366699520	48.44587	63.34948	3.03268	13.18	14.11	12.24	1.17	0.14	G	113.19	21.89	106.22	20.3
5252269709082759936	156.40361	-62.55651	3.04556	15.10	15.67	14.35	0.64	0.12	G	112.85	21.83	105.32	20.13
5310863370918375552	140.55281	-53.06412	3.05163	13.60	14.46	12.66	1.11	0.12	O	112.69	21.80	105.41	20.14
5863815636949490048	202.86552	-65.32720	3.06221	15.68	16.55	14.75	1.08	0.12	O	112.42	21.74	106.26	20.31
2930525287803260288	109.84202	-19.54033	3.07149	12.79	13.35	12.07	0.57	0.09	O	112.18	21.70	105.38	20.14
5858259014403682304	195.97407	-66.33292	3.08394	15.37	16.09	14.47	0.95	0.11	O	111.86	21.64	103.91	19.86
5235910694044165760	176.13694	-67.30525	3.08613	8.70	9.22	8.06	0.43	0.06	L	111.80	21.62	105.46	20.16
5237406545247540608	171.64645	-65.58218	3.11677	14.99	15.84	14.04	1.12	0.14	G	111.03	21.47	103.25	19.73
5335753015664095104	173.80588	-60.91465	3.12750	14.19	14.98	13.30	1.0	0.11	O	110.76	21.42	103.37	19.76
5594991812757424768	115.97856	-32.50378	3.14920	14.81	15.79	13.80	1.33	0.15	G	110.22	21.32	102.23	19.54
2932737092877188352	105.22172	-19.45929	3.15504	12.36	12.85	11.73	0.4	0.11	G	110.08	21.29	103.74	19.83
2059517087110475392	299.88745	36.02152	3.16632	15.16	16.04	14.20	1.16	0.14	G	109.80	21.24	102.08	19.51
5329323277776517120	130.36480	-47.64966	3.17573	14.05	14.90	13.10	1.13	0.14	G	109.57	21.19	101.81	19.46
5239658688657671680	160.70962	-65.55805	3.18304	16.74	17.37	16.02	0.6	0.12	G	109.40	21.16	103.55	19.79
5322878146768508800	129.73194	-49.77016	3.18474	14.62	15.39	13.75	0.94	0.13	G	109.35	21.15	102.37	19.56
5612661716228387200	111.62263	-27.92502	3.18518	12.78	13.26	12.14	0.41	0.11	G	109.34	21.15	102.75	19.64
377753613615880832	14.89365	45.40672	3.20017	11.48	11.87	10.98	0.16	0.11	G	108.98	21.08	102.94	19.67
5875602191067578752	230.82679	-61.21710	3.23038	15.66	16.48	14.71	1.1	0.14	G	108.26	20.94	100.28	19.17
512491028363231616	24.35667	63.69136	3.23980	13.13	14.16	12.13	1.33	0.15	G	108.04	20.90	100.93	19.29
4513100717859042176	286.49619	16.09800	3.26984	13.47	14.24	12.60	0.93	0.13	G	107.34	20.76	100.65	19.23
5617316606087829888	109.16777	-24.50300	3.27499	12.80	13.31	12.13	0.47	0.11	G	107.22	20.74	100.60	19.23

TABLE A.6: continued.

Gaia DR2 Source Id	RA	DEC	P	G	G_{BP}	G_{RP}	E(G_{BP}-G_{RP})	σE(G_{BP}-G_{RP})	Note	t_{PA}	$\sigma\ t_{PA}$	t_{PAC}	$\sigma\ t_{PAC}$
(1)	(2)	(3)	(4)	(5)	(6)	(7)	(8)	(9)	(10)	(11)	(12)	(13)	(14)
5520505328816739584	121.80935	-45.12830	3.28292	13.45	14.07	12.67	0.69	0.12	G	107.04	20.70	100.13	19.14
5241803217391469568	165.52136	-62.28989	3.28899	14.54	15.40	13.59	1.1	0.12	O	106.90	20.68	100.11	19.13
279382060625871360	76.63188	55.35352	3.29487	7.19	7.81	6.48	0.55	0.07	L	106.77	20.65	102.22	19.54
5405496240766414464	148.01595	-51.99247	3.29644	13.56	14.38	12.67	1.01	0.11	O	106.73	20.64	99.63	19.04
505178760644698880	31.25913	57.14294	3.29700	12.34	12.82	11.68	0.35	0.05	L	106.72	20.64	102.14	19.52
5306043592977093504	145.89770	-57.23830	3.00860	15.29	16.16	14.31	1.23	0.13	O	113.82	22.02	104.31	19.93
505368121464666112	29.62897	57.81985	3.32910	13.78	14.44	12.98	0.74	0.12	G	105.99	20.50	99.42	19.0
5600862070985787136	119.26547	-28.16158	3.33098	11.61	12.25	10.88	0.58	0.09	O	105.95	20.49	101.70	19.44
5605736961940589568	110.81312	-29.72244	3.33617	12.87	13.38	12.30	0.3	0.11	G	105.84	20.47	100.86	19.28
5313250548085699712	139.88405	-51.62042	3.35503	12.70	13.62	11.69	1.34	0.13	O	105.42	20.39	95.64	18.28
5516452460238707968	125.52706	-47.30395	3.36831	14.28	14.93	13.46	0.77	0.12	G	105.12	20.33	98.08	18.75
2073935223599391872	300.89457	39.15963	3.37031	13.22	13.96	12.38	1.02	0.13	L	105.08	20.32	94.39	18.04
5592331544376193792	113.82822	-31.66418	3.38307	13.77	14.53	12.93	0.87	0.13	G	104.80	20.27	98.67	18.86
5824464493705913472	229.94041	-66.49608	3.38932	6.44	6.86	5.91	0.23	0.04	L	104.66	20.24	98.41	18.81
5598852026287511424	116.00045	-30.14146	3.39082	13.12	13.66	12.45	0.58	0.09	O	104.63	20.24	95.93	18.33
2025217890612425344	293.14591	26.80479	3.39154	15.51	16.38	14.54	1.15	0.14	G	104.62	20.23	96.98	18.53
5857294605251013760	193.30159	-67.96426	3.40117	14.41	14.91	13.73	0.48	0.11	G	104.41	20.19	97.69	18.67
206211859601169792	74.06344	44.78185	3.40680	12.54	13.43	11.62	1.1	0.14	G	104.29	20.17	97.74	18.68
189739251272296192	85.62191	37.64633	3.41272	12.05	12.93	11.18	0.84	0.11	L	104.16	20.15	103.05	19.69
4690436069162376576	10.68389	-70.27426	3.42463	16.23	16.48	15.74	0.07	0.11	G	103.90	20.10	96.22	18.39
5932997939411720960	243.72813	-53.33844	3.45291	9.79	10.63	8.92	0.92	0.08	L	103.30	19.98	98.50	18.82
3051144427784813824	103.54766	-7.66438	3.45403	13.28	13.98	12.44	0.85	0.11	L	103.28	19.98	96.08	18.36
5547358117187868288	122.79503	-33.51586	3.48218	10.44	11.05	9.72	0.58	0.06	L	102.69	19.86	97.06	18.55
5310265099146146816	138.32401	-54.93121	3.50424	14.23	15.01	13.34	0.96	0.13	G	102.24	19.77	95.53	18.26
515527570241664512	34.14985	65.17655	3.52190	12.69	13.52	11.78	1.02	0.13	G	101.88	19.70	95.22	18.2
2936165984303583360	105.87696	-15.54334	3.52281	13.45	14.09	12.65	0.73	0.12	G	101.86	19.70	95.12	18.18
5268616973048513664	107.46385	-68.48372	3.52627	15.80	16.25	15.26	0.23	0.11	G	101.79	19.69	96.40	18.42
5618354751226656640	112.51063	-23.67398	3.54416	13.26	14.12	12.36	1.08	0.14	L	101.42	19.62	93.94	17.95
5612495762995320576	113.72248	-26.85579	3.55250	13.56	14.36	12.63	1.03	0.13	G	101.26	19.58	94.15	17.99

TABLE A.6: continued.

Gaia DR2 Source Id	RA	DEC	P	G	G_{BP}	G_{RP}	E(G_{BP}-G_{RP})	σE(G_{BP}-G_{RP})	Note	t_{PA}	$\sigma\ t_{PA}$	t_{PAC}	$\sigma\ t_{PAC}$
(1)	(2)	(3)	(4)	(5)	(6)	(7)	(8)	(9)	(10)	(11)	(12)	(13)	(14)
5547421437881152256	122.36346	-33.26212	3.56310	11.82	12.44	11.06	0.8	0.1	O	101.04	19.54	90.90	17.37
2162640763705905920	316.08941	45.23937	3.56914	13.70	14.61	12.76	1.13	0.14	G	100.92	19.52	94.55	18.07
5311139245252191616	137.38339	-53.98770	3.59050	11.68	12.22	11.02	0.44	0.11	G	100.50	19.44	94.79	18.12
5599370549100412544	114.32029	-29.60773	3.59160	14.17	15.06	13.23	1.12	0.14	G	100.48	19.43	93.92	17.95
2952257272558933248	101.92934	-13.66668	4.85729	11.71	12.23	10.93	0.57	0.12	G	81.24	15.71	74.92	14.32
3441484760885586176	86.43715	27.06790	3.62280	11.67	12.56	10.71	1.13	0.15	L	99.87	19.32	93.43	17.86
429562773322439296	3.51343	60.98626	3.63045	11.91	12.73	11.01	0.99	0.13	L	99.72	19.29	93.81	17.93
457807268533229056	38.46902	57.02750	3.64942	11.13	11.84	10.31	0.84	0.08	L	99.36	19.22	92.23	17.63
5329405672431387648	130.00864	-47.19842	3.67080	13.98	14.88	13.03	1.14	0.14	G	98.95	19.14	92.32	17.64
5351721738384434048	157.29679	-57.61339	3.68221	8.08	8.45	7.59	0.14	0.03	L	98.73	19.10	92.16	17.61
5542528959037609984	127.24360	-36.23207	3.70536	11.33	12.03	10.52	0.77	0.12	G	98.30	19.01	92.19	17.62
5539023922122441728	118.71081	-37.62246	3.70789	12.47	13.45	11.50	1.23	0.15	G	98.25	19.00	91.87	17.56
4707044742055169152	9.21974	-66.59323	3.72828	16.74	17.10	16.23	0.14	0.11	G	97.87	18.93	91.92	17.57
2202500843341252736	328.64443	59.12168	3.75817	13.83	14.85	12.81	1.34	0.15	G	97.32	18.82	90.48	17.29
2200018111723748224	335.91092	57.68078	3.76750	11.66	12.55	10.75	1.06	0.14	L	97.15	18.79	91.18	17.43
3445039825569144192	86.71173	31.59791	3.04664	11.88	12.55	11.09	0.76	0.1	L	112.82	21.82	105.89	20.24
3378049163365268608	100.78130	20.93911	3.78798	9.70	10.10	9.22	0.28	0.07	L	96.78	18.72	87.53	16.73
5856994365517642112	194.75148	-68.57855	3.79741	13.12	13.58	12.60	0.19	0.11	G	96.61	18.69	91.94	17.57
5311409896910828800	137.14651	-53.19702	3.80582	13.72	14.48	12.86	0.89	0.13	G	96.46	18.66	90.39	17.28
430647231080076416	5.01280	63.17979	3.81071	11.68	12.53	10.74	1.01	0.13	L	96.38	18.64	91.53	17.49
465719182408723072	41.18048	61.46470	3.83288	10.43	11.14	9.64	0.76	0.09	L	95.98	18.56	89.88	17.18
6059635702888301952	190.35842	-59.79419	3.83834	7.99	8.43	7.42	0.33	0.04	L	95.89	18.55	88.63	16.94
509629965971797376	25.81989	59.99762	3.84314	12.33	13.18	11.42	1.02	0.13	G	95.80	18.53	89.65	17.13
2031776202613700480	296.20306	29.26468	3.84599	6.69	7.01	6.22	0.17	0.04	L	95.75	18.52	86.84	16.6
2012494342018730496	353.33454	61.11907	3.87118	12.21	13.18	11.23	1.22	0.14	G	95.31	18.44	88.94	17.0
5619369359933924992	111.25618	-23.15791	3.89113	13.75	14.75	12.76	1.26	0.15	G	94.97	18.37	88.60	16.93
2072235820984829312	299.71473	37.64725	3.89187	14.29	14.88	13.51	0.67	0.12	G	94.96	18.37	88.26	16.87
2072329902270080128	299.38702	38.09177	3.89671	13.59	14.22	12.81	0.68	0.12	G	94.87	18.35	88.62	16.94
5335934297643679360	172.92831	-60.73455	3.89770	13.14	13.88	12.32	0.78	0.1	O	94.86	18.35	89.85	17.17

TABLE A.6: continued.

Gaia DR2 Source Id	RA	DEC	P	G	G_{BP}	G_{RP}	E(G_{BP}-G_{RP})	σE(G_{BP}-G_{RP})	Note	t_{PA}	$\sigma\ t_{PA}$	t_{PAC}	$\sigma\ t_{PAC}$
(1)	(2)	(3)	(4)	(5)	(6)	(7)	(8)	(9)	(10)	(11)	(12)	(13)	(14)
4253603501158148736	280.61175	-5.34085	3.91771	10.51	11.41	9.60	1.05	0.1	L	94.52	18.28	89.21	17.05
5615233993628681216	112.66125	-24.68752	3.91882	13.09	13.87	12.21	0.91	0.11	O	94.50	18.28	88.92	16.99
2010134274671099264	345.33801	57.86702	3.91921	11.49	12.30	10.62	0.92	0.12	L	94.49	18.28	89.18	17.04
3052092481686246016	107.65830	-7.12290	3.28782	12.52	13.23	11.64	0.68	0.09	L	106.93	20.68	105.65	20.19
5540422122959807232	125.36087	-38.42170	3.96098	12.55	13.54	11.57	1.22	0.13	O	93.79	18.14	87.96	16.81
5606739884038472704	109.26954	-28.82351	3.96993	12.72	13.24	12.05	0.45	0.11	G	93.64	18.11	87.83	16.79
486834100624652800	54.08395	62.28723	3.99690	12.74	13.79	11.72	1.31	0.17	L	93.19	18.03	87.73	16.77
2015458213056909184	351.49362	61.26683	4.00024	12.51	13.36	11.59	0.92	0.12	L	93.14	18.01	89.90	17.18
506923449381427968	32.69322	59.25369	4.00720	12.24	13.07	11.35	0.94	0.12	L	93.03	17.99	88.11	16.84
5238994102591371776	162.35781	-66.62534	4.01417	14.04	14.61	13.31	0.56	0.11	G	92.91	17.97	87.01	16.63
514674933331699584	32.62154	63.29753	4.03790	10.27	10.96	9.49	0.76	0.1	L	92.53	17.90	85.70	16.38
2166861170366710272	313.73970	47.53379	4.04921	10.29	11.11	9.41	1.02	0.13	L	92.34	17.86	84.95	16.23
5242076514741190272	162.97536	-61.46728	4.05483	12.23	12.91	11.45	0.68	0.1	O	92.25	17.84	87.54	16.73
5530071831587999232	129.78343	-37.37551	4.06392	12.24	12.87	11.48	0.66	0.09	O	92.11	17.82	85.87	16.41
422923956470923008	3.79087	58.42428	4.07117	9.54	10.14	8.83	0.61	0.06	L	91.99	17.79	85.09	16.26
5545837900614099584	121.29597	-34.36027	4.08860	11.73	12.56	10.84	0.9	0.11	O	91.72	17.74	87.57	16.74
5254281334339678208	160.11285	-60.07640	4.08916	13.97	14.91	12.96	1.25	0.15	G	91.71	17.74	84.80	16.21
5241961409628951296	162.73299	-62.09798	4.09530	14.32	15.12	13.43	0.99	0.11	O	91.61	17.72	84.80	16.21
5861648327739540736	193.74820	-65.20062	4.10167	14.64	15.63	13.62	1.28	0.13	O	91.51	17.70	85.32	16.31
511706805997227648	25.25207	63.05553	4.13309	12.66	13.61	11.69	1.19	0.14	G	91.02	17.61	84.93	16.23
3127458403130026112	101.78917	3.96710	4.13423	10.21	10.72	9.53	0.42	0.04	L	91.00	17.60	85.67	16.37
462252662762965120	50.94951	59.35567	4.15636	11.84	12.87	10.84	1.22	0.16	L	90.66	17.54	86.38	16.51
5321257604065975040	128.76428	-52.47757	4.15812	14.51	15.28	13.68	0.83	0.13	G	90.64	17.53	85.35	16.31
2031590552598614784	295.87018	29.23810	4.15973	14.49	15.30	13.56	1.02	0.13	G	90.61	17.53	84.17	16.09
5852389305960163328	208.75541	-64.03195	4.16962	11.28	12.18	10.36	1.06	0.14	G	90.46	17.50	84.93	16.23
5614191175568405376	115.20408	-25.45771	4.17117	12.42	13.36	11.45	1.15	0.12	O	90.44	17.49	84.94	16.23
5619786177922254336	110.28102	-21.51060	4.17560	12.51	13.26	11.67	0.82	0.1	O	90.37	17.48	85.12	16.27
2934506447605426944	105.97944	-17.87991	4.20487	11.59	12.31	10.79	0.75	0.12	G	89.92	17.39	84.59	16.17
4690834328595493760	16.04228	-70.95614	4.20529	15.60	15.92	15.22	0.0	0.11	G	89.92	17.39	83.12	15.89

TABLE A.6: continued.

Gaia DR2 Source Id	RA	DEC	P	G	G_{BP}	G_{RP}	E(G_{BP}-G_{RP})	σE(G_{BP}-G_{RP})	Note	t_{PA}	$\sigma\ t_{PA}$	t_{PAC}	$\sigma\ t_{PAC}$
(1)	(2)	(3)	(4)	(5)	(6)	(7)	(8)	(9)	(10)	(11)	(12)	(13)	(14)
5253875717619475200	158.46303	-61.80622	4.23097	14.74	15.57	13.80	1.07	0.12	O	89.53	17.32	82.66	15.8
1981367545804985088	329.05685	52.98601	4.23698	11.95	12.85	11.02	1.07	0.14	G	89.44	17.30	83.66	15.99
515832929535462016	41.08082	64.76592	4.23841	10.96	11.83	10.06	1.01	0.13	G	89.42	17.30	84.02	16.06
5254653759541047424	155.20707	-61.25195	4.23925	13.98	14.57	13.25	0.57	0.12	G	89.41	17.29	83.80	16.02
5587972801102905984	113.75856	-35.91299	4.24340	12.16	12.74	11.47	0.5	0.11	G	89.35	17.28	84.07	16.07
5521352536886237952	123.41069	-42.69920	4.24935	13.62	14.40	12.76	0.89	0.13	G	89.26	17.26	83.56	15.97
3027940437469882880	110.38690	-16.68722	4.25689	9.32	9.95	8.59	0.64	0.06	L	89.15	17.24	82.66	15.8
522468168674975616	18.17150	61.21335	4.25925	10.96	11.64	10.19	0.63	0.07	L	89.11	17.24	84.98	16.24
5338024572321721216	164.46108	-60.74208	4.26618	9.44	9.99	8.79	0.55	0.07	L	89.01	17.22	80.98	15.48
510584788742165760	19.00502	61.62071	4.27770	11.35	12.36	10.37	1.16	0.15	L	88.84	17.18	85.04	16.25
2014609252631258496	342.09618	60.40476	4.27863	11.57	12.60	10.58	1.27	0.15	G	88.83	17.18	83.18	15.9
5620400182140135168	112.95453	-20.14966	4.28543	10.96	11.65	10.18	0.67	0.06	L	88.73	17.16	84.16	16.08
2033008274099620480	296.26534	31.33077	4.28897	12.25	13.01	11.39	0.87	0.11	L	88.68	17.15	82.87	15.84
228741784865956224	64.27528	41.73183	4.29045	10.67	11.41	9.90	0.72	0.09	L	88.66	17.15	83.80	16.01
429890595286480384	0.67404	61.86107	4.30528	12.11	13.08	11.13	0.99	0.13	L	88.44	17.11	87.78	16.78
1977074811892425600	332.26210	51.04585	4.32355	8.96	9.40	8.39	0.29	0.04	L	88.18	17.06	81.86	15.64
2074102933481447808	301.83830	40.17809	4.32699	13.77	14.52	12.91	0.82	0.08	L	88.13	17.05	83.22	15.9
5311298983669288832	136.84989	-54.09276	4.35093	13.37	13.93	12.65	0.52	0.11	G	87.79	16.98	82.20	15.71
2060021625508894592	302.28232	37.15195	4.36470	9.49	10.10	8.77	0.61	0.1	L	87.59	16.94	80.98	15.48
429385923752386944	0.24680	60.95900	4.36516	10.86	11.53	9.96	0.9	0.07	L	87.59	16.94	79.87	15.27
2006033847910275584	335.02002	56.06090	4.36625	12.13	12.97	11.21	1.01	0.13	G	87.57	16.94	81.70	15.61
204588190167650048	71.39513	43.57284	4.37214	13.22	14.18	12.25	1.19	0.14	G	87.49	16.92	81.57	15.59
4693901042617667584	27.66874	-70.50366	4.37264	15.68	15.92	15.29	0.0	0.11	G	87.48	16.92	79.18	15.13
5594091823824942464	119.66611	-33.50405	4.40279	11.64	12.44	10.78	0.84	0.1	O	87.06	16.84	83.08	15.88
197337185858157440	84.11148	44.59136	4.40345	11.82	12.43	11.25	0.48	0.06	L	87.05	16.84	80.17	15.32
6055722403534963840	195.79449	-60.87747	4.42452	9.46	10.21	8.65	0.78	0.08	L	86.76	16.78	81.66	15.61
3397212822106196992	81.77704	16.93643	4.43840	12.75	13.32	12.06	0.48	0.11	G	86.57	16.74	81.58	15.59
2936110669428633216	106.65835	-15.80206	4.46484	12.42	13.21	11.56	0.82	0.1	O	86.21	16.67	82.22	15.71
5881952871520184960	234.52125	-58.69441	4.47575	15.24	16.25	14.22	1.32	0.13	O	86.06	16.65	79.55	15.2

TABLE A.6: continued.

Gaia DR2 Source Id	RA	DEC	P	G	G_{BP}	G_{RP}	E(G_{BP}-G_{RP})	σE(G_{BP}-G_{RP})	Note	t_{PA}	$\sigma\ t_{PA}$	t_{PAC}	$\sigma\ t_{PAC}$
(1)	(2)	(3)	(4)	(5)	(6)	(7)	(8)	(9)	(10)	(11)	(12)	(13)	(14)
2011892320749270912	359.53791	61.21363	4.47861	10.57	11.12	9.66	0.74	0.07	L	86.02	16.64	79.71	15.23
2005011237689458688	335.31995	54.53204	4.47944	11.44	12.16	10.63	0.76	0.07	L	86.01	16.64	80.52	15.39
5254078504458244352	160.72436	-61.02361	4.48366	12.84	13.68	11.94	0.97	0.11	O	85.95	16.62	80.57	15.4
426881614218441600	12.47192	60.12738	4.50162	9.55	10.21	8.79	0.7	0.08	L	85.71	16.58	79.42	15.18
5254000340399606016	157.26590	-60.78069	4.50519	14.48	15.29	13.56	1.03	0.11	O	85.66	16.57	78.97	15.09
5594382644652353664	119.05201	-32.60264	4.51675	11.53	12.38	10.70	0.87	0.13	G	85.51	16.54	81.13	15.51
5850308411442294400	206.85370	-68.24990	4.52474	13.65	14.14	13.00	0.37	0.11	G	85.40	16.52	80.01	15.29
4054440301294394624	262.70159	-33.60992	4.52781	7.55	8.14	6.92	0.48	0.05	L	85.36	16.51	79.41	15.18
5534012004528220160	119.94883	-42.02838	4.54706	13.90	14.74	12.98	1.01	0.13	G	85.11	16.46	79.32	15.16
506699870563323264	33.28119	58.07995	4.56524	11.27	11.94	10.55	0.62	0.06	L	84.87	16.41	79.45	15.18
2012787293154800896	358.60238	62.14947	4.56615	11.45	12.28	10.57	0.96	0.12	L	84.85	16.41	79.13	15.12
5338148473537341312	165.30989	-60.11656	4.58610	11.08	11.81	10.25	0.76	0.07	L	84.59	16.36	79.99	15.29
4690829659971892480	16.84515	-70.88734	4.59426	15.88	16.22	15.37	0.09	0.11	G	84.49	16.34	78.98	15.09
5253884788591163648	158.53969	-61.59759	4.61631	13.91	14.75	12.99	1.01	0.11	O	84.20	16.29	78.52	15.01
5253661725170126720	159.49855	-62.20590	4.63195	14.41	15.35	13.63	0.9	0.11	O	84.00	16.25	79.82	15.25
1981006115714214912	327.39800	52.39523	4.63908	11.46	12.45	10.48	0.91	0.23	L	83.91	16.23	85.05	16.25
5521459979795304320	129.42007	-47.36195	4.63985	7.71	8.26	7.05	0.38	0.04	L	83.90	16.23	80.08	15.3
2170880813073764352	322.34628	49.11002	4.64071	11.77	12.62	10.87	0.99	0.13	G	83.89	16.23	78.47	15.0
3044483895581000192	107.31421	-13.78609	4.67003	10.09	10.85	9.26	0.77	0.07	L	83.52	16.15	79.29	15.15
5338207327417387520	163.13667	-60.52675	4.67416	10.94	11.55	10.19	0.54	0.08	L	83.47	16.14	79.15	15.13
5338438297925480320	162.89899	-59.38499	4.67767	9.41	9.97	8.73	0.52	0.04	L	83.43	16.14	77.28	14.77
3046774762417915136	109.15680	-11.48730	4.67830	7.83	8.33	7.20	0.32	0.03	L	83.42	16.13	78.98	15.09
6060173364061645696	193.59158	-58.43063	4.68971	6.36	6.80	5.79	0.23	0.03	L	83.27	16.11	78.33	14.97
5861196531541297664	187.06483	-65.04976	4.72838	14.52	15.34	13.58	1.06	0.12	O	82.79	16.01	76.02	14.53
1998384927774603520	359.11116	58.02686	4.73481	11.71	12.60	10.79	1.03	0.13	G	82.72	16.00	77.45	14.8
5242088403212116864	163.61189	-61.34710	4.75984	11.54	12.32	10.69	0.85	0.13	G	82.41	15.94	77.35	14.78
5533407170051636608	122.95171	-42.05164	4.76441	14.79	15.90	13.77	1.36	0.15	G	82.35	15.93	77.05	14.72
5541229748611783296	123.70107	-37.65190	4.78070	13.80	14.82	12.79	1.24	0.13	O	82.16	15.89	77.20	14.75
3051692843568009600	106.78562	-7.79513	4.49659	12.54	13.27	11.70	0.87	0.11	L	85.78	16.59	79.04	15.11

TABLE A.6: continued.

Gaia DR2 Source Id	RA	DEC	P	G	G_{BP}	G_{RP}	E(G_{BP}-G_{RP})	σE(G_{BP}-G_{RP})	Note	t_{PA}	$\sigma\ t_{PA}$	t_{PAC}	$\sigma\ t_{PAC}$
(1)	(2)	(3)	(4)	(5)	(6)	(7)	(8)	(9)	(10)	(11)	(12)	(13)	(14)
2011303326105008768	353.74839	59.35815	4.78948	12.14	13.26	11.08	1.45	0.16	G	82.05	15.87	75.96	14.52
3099066951319051008	102.70284	-7.98073	4.80971	12.57	13.26	11.77	0.62	0.08	L	81.81	15.82	78.58	15.02
5864184488751391744	203.61003	-64.37098	4.82483	14.71	15.56	13.75	1.31	0.13	O	81.63	15.79	70.95	13.56
5329338700985814656	130.05832	-47.55156	4.82751	13.24	14.15	12.28	1.12	0.14	G	81.59	15.78	75.92	14.51
2928116120387181824	108.72647	-22.23586	4.84478	12.81	13.54	11.97	0.8	0.12	G	81.39	15.74	76.09	14.54
5306782361701536128	140.15436	-56.85401	4.86219	13.91	14.60	13.11	0.72	0.12	G	81.18	15.70	75.90	14.51
1960750328384177408	327.92260	43.13402	4.86438	8.67	9.19	8.03	0.39	0.04	L	81.16	15.70	75.77	14.48
2011892703004353792	359.57487	61.22105	4.87514	10.66	11.41	9.83	0.75	0.07	L	81.03	15.67	77.01	14.72
3344297935963515008	91.43635	13.23999	4.90958	11.89	12.64	11.03	0.71	0.06	L	80.63	15.60	78.05	14.92
2078709577944648192	297.06443	43.12692	4.92549	8.90	9.42	8.26	0.43	0.05	L	80.45	15.56	74.51	14.24
5258574068220187648	153.88689	-58.17444	4.93255	10.24	10.94	9.46	0.59	0.08	L	80.37	15.54	77.63	14.84
2060460704279873536	304.19788	36.54994	4.94524	11.57	12.65	10.54	1.45	0.19	L	80.22	15.52	72.74	13.9
2055122987639665664	301.33609	32.65909	4.95045	12.27	13.38	11.21	1.35	0.18	L	80.16	15.50	75.78	14.48
270272675510149504	64.94524	48.95326	4.97249	9.12	9.99	8.23	0.92	0.09	L	79.91	15.46	76.03	14.53
5333640230992516480	173.32410	-63.24240	4.97458	11.78	12.80	10.78	1.26	0.15	G	79.89	15.45	74.40	14.22
3351921532976862336	100.15651	11.72748	4.97853	11.77	12.69	10.82	1.1	0.14	G	79.84	15.44	74.52	14.24
2003938801532007808	342.15829	56.32153	4.98330	8.61	9.15	7.94	0.4	0.06	L	79.79	15.43	75.42	14.41
6057402526059795072	181.66763	-62.59685	4.98851	12.06	13.02	11.10	1.14	0.12	O	79.73	15.42	74.80	14.29
2011315528113463808	354.70162	59.39182	4.99754	10.50	11.42	9.58	1.09	0.1	L	79.63	15.40	73.99	14.14
5699042480743325312	120.09545	-23.70317	5.02730	10.08	10.53	9.49	0.26	0.04	L	79.30	15.34	74.28	14.2
515599111517099136	33.60315	65.59945	5.02942	11.90	12.75	11.01	0.7	0.12	L	79.27	15.33	79.92	15.27
2164359918864249728	316.94415	46.73698	5.05758	11.90	12.74	11.01	0.99	0.13	L	78.96	15.27	73.22	13.99
3390186156826555136	79.69992	13.98667	5.06607	11.52	12.19	10.67	0.78	0.12	G	78.87	15.25	73.13	13.98
473293889810320128	57.10698	59.44227	5.06643	10.00	11.16	8.95	1.01	0.1	L	78.87	15.25	82.97	15.86
5595650351503904896	118.45324	-30.46031	5.07756	10.55	11.29	9.73	0.74	0.07	L	78.74	15.23	74.52	14.24
5871738271033526016	207.68449	-57.58051	5.07890	7.43	7.89	6.85	0.28	0.03	L	78.73	15.23	73.31	14.01
2166303099490547072	311.55230	45.47861	5.09955	10.53	11.69	9.46	1.45	0.19	L	78.51	15.18	73.66	14.08
5241157421762533248	162.23993	-64.17420	5.10249	13.62	14.29	12.82	0.7	0.12	G	78.47	15.18	73.31	14.01
5307006215391311360	142.54990	-56.80824	5.13704	14.57	15.64	13.51	1.39	0.14	O	78.10	15.11	72.19	13.8

TABLE A.6: continued.

Gaia DR2 Source Id	RA	DEC	P	G	G_{BP}	G_{RP}	E(G_{BP}-G_{RP})	σE(G_{BP}-G_{RP})	Note	t_{PA}	$\sigma\ t_{PA}$	t_{PAC}	$\sigma\ t_{PAC}$
(1)	(2)	(3)	(4)	(5)	(6)	(7)	(8)	(9)	(10)	(11)	(12)	(13)	(14)
2011892325047232256	359.53933	61.21370	5.14077	10.49	11.07	9.62	0.75	0.1	L	78.06	15.10	71.37	13.64
4080122796947250176	281.32290	-20.64739	5.15424	7.25	7.83	6.58	0.42	0.04	L	77.92	15.07	73.83	14.11
4085919765884068736	282.74947	-20.29525	6.63703	6.63	7.21	5.93	0.38	0.03	L	65.21	12.61	62.29	11.9
1827869808377481216	296.64660	22.88975	5.19725	10.03	10.96	9.09	1.23	0.12	L	77.46	14.98	69.51	13.28
4690377382729299328	10.34143	-70.61853	5.20108	15.23	15.52	14.77	-0.0	0.11	G	77.42	14.97	71.93	13.75
5254295559276699392	159.07421	-61.01256	5.20456	9.06	9.56	8.44	0.29	0.05	L	77.39	14.97	73.40	14.03
5853170268450896768	219.37630	-63.62524	5.21445	14.44	15.27	13.50	1.08	0.12	O	77.28	14.95	70.47	13.47
5257939993613539456	147.08272	-57.81045	5.21666	12.34	13.28	11.37	1.15	0.12	O	77.26	14.94	71.94	13.75
513830684503187840	34.09382	62.55776	5.23993	12.62	13.62	11.62	1.23	0.15	G	77.02	14.90	71.77	13.72
5698636279917579520	119.52141	-24.04176	5.25024	10.34	10.80	9.73	0.35	0.05	L	76.91	14.88	70.68	13.51
1968971582984827136	318.66850	41.71634	5.25760	8.88	9.91	7.90	1.22	0.11	L	76.84	14.86	71.92	13.75
189726984845700480	86.05833	37.58687	5.25943	11.56	12.33	10.81	0.74	0.1	L	76.82	14.86	71.81	13.72
6053622679932061056	188.32775	-63.50637	5.26567	9.01	9.91	8.12	0.86	0.09	L	76.75	14.85	74.66	14.27
5594100246268225280	119.84298	-33.35713	5.28196	13.39	14.27	12.46	1.01	0.11	O	76.59	14.81	72.08	13.78
4147381366335558784	272.50888	-13.54596	5.30141	9.96	11.03	8.94	1.31	0.11	L	76.39	14.77	71.29	13.62
5334506135119058304	171.27392	-60.73461	5.30996	8.49	9.08	7.79	0.48	0.1	L	76.30	14.76	71.74	13.71
5307761545524640256	147.17283	-55.51953	5.32402	9.79	10.57	8.95	0.79	0.1	L	76.16	14.73	71.90	13.74
1960981328902089088	330.10480	43.44535	5.33166	8.57	9.13	7.90	0.45	0.05	L	76.08	14.72	71.00	13.57
5338215200143652992	163.78784	-60.54772	5.33671	11.44	12.27	10.56	0.92	0.13	G	76.03	14.71	71.19	13.61
5255220656517219840	156.71194	-59.66953	5.34632	9.03	9.64	8.31	0.58	0.05	L	75.94	14.69	70.43	13.46
458239995077788544	38.63042	58.83162	5.36511	10.46	11.49	9.51	1.2	0.1	L	75.75	14.65	70.75	13.52
4190143160245024256	298.08750	-11.36692	5.37668	7.54	8.03	6.92	0.25	0.03	L	75.63	14.63	72.20	13.8
2010285491880986112	346.79198	58.55419	5.44090	9.28	9.96	8.51	0.64	0.06	L	75.00	14.51	70.57	13.49
5547742052903182080	122.60782	-32.52136	5.46460	10.99	11.72	10.18	0.74	0.12	G	74.78	14.46	70.24	13.42
5312211543950752128	142.56597	-53.05868	5.48394	11.19	12.09	10.25	1.06	0.14	G	74.59	14.43	69.67	13.31
5338131529834231680	164.77043	-60.27884	5.49457	11.65	12.46	10.76	0.91	0.13	G	74.49	14.41	69.62	13.31
5891675303053080704	218.13779	-56.88775	5.49457	6.55	7.11	5.93	0.36	0.04	L	74.49	14.41	70.33	13.44
523887951723531648	11.62454	63.54327	5.51273	11.17	12.21	10.18	1.29	0.17	L	74.32	14.37	68.58	13.11
5715183929918131968	115.47870	-21.13306	5.51615	10.27	10.82	9.61	0.45	0.04	L	74.28	14.37	69.00	13.19

TABLE A.6: continued.

Gaia DR2 Source Id	RA	DEC	P	G	G_{BP}	G_{RP}	E(G_{BP}-G_{RP})	σE(G_{BP}-G_{RP})	Note	t_{PA}	$\sigma\ t_{PA}$	t_{PAC}	$\sigma\ t_{PAC}$
(1)	(2)	(3)	(4)	(5)	(6)	(7)	(8)	(9)	(10)	(11)	(12)	(13)	(14)
459035766618689280	36.89776	58.91715	5.53070	10.37	11.47	9.37	1.28	0.11	L	74.15	14.34	69.95	13.37
5253795384546671104	158.01837	-61.78262	5.54225	8.70	9.18	8.09	0.25	0.03	L	74.04	14.32	70.07	13.39
4103989346187406464	276.80604	-15.11799	5.54693	10.07	10.94	9.18	0.95	0.13	G	73.99	14.31	69.51	13.28
5539107450645759232	118.43778	-36.97038	5.56408	10.59	11.47	9.75	0.88	0.13	G	73.83	14.28	70.02	13.38
5254512193075687168	158.63079	-59.80854	5.57332	11.84	12.94	10.79	1.31	0.13	O	73.75	14.26	69.99	13.38
5525918495131126912	126.02410	-44.85228	5.59210	13.08	14.24	12.02	1.45	0.16	G	73.57	14.23	68.31	13.05
506602976101284736	26.76131	59.60626	5.60412	13.19	13.92	12.35	0.64	0.15	L	73.46	14.21	71.43	13.65
5283779135317992448	98.37366	-65.99373	5.63702	15.67	16.06	15.11	0.16	0.11	G	73.16	14.15	68.38	13.07
2005753545481718912	331.89771	55.36274	5.65812	12.18	13.11	11.22	1.23	0.12	L	72.97	14.11	65.86	12.59
5242185808733501696	162.09637	-60.65394	5.66418	12.16	12.99	11.26	0.93	0.11	O	72.91	14.10	68.37	13.07
2015622212085282048	354.86371	62.37214	5.66617	11.06	12.01	10.12	1.03	0.09	L	72.89	14.10	69.29	13.24
2202863166783787520	330.67041	59.45248	5.68839	13.10	14.14	12.10	1.26	0.15	G	72.69	14.06	67.76	12.95
5261561063335550208	95.02971	-75.36110	5.70035	15.26	15.65	14.69	0.17	0.11	G	72.58	14.04	67.70	12.94
2931247014102560000	108.29864	-18.73074	5.72861	10.60	11.39	9.75	0.62	0.12	L	72.33	13.99	71.94	13.75
2034428980559814400	299.89044	33.74604	5.78290	11.05	11.99	10.12	0.99	0.13	L	71.85	13.90	68.67	13.12
5600471160241231616	118.49014	-28.36762	5.80047	12.61	13.41	11.73	0.91	0.11	O	71.70	13.87	66.46	12.7
422226488141991296	3.61766	56.25293	5.80901	8.78	9.37	8.08	0.44	0.08	L	71.63	13.85	67.82	12.96
5613165915335320192	111.16913	-26.18849	5.81585	11.45	12.33	10.54	0.94	0.12	L	71.57	13.84	67.94	12.98
5327836325732931840	131.23286	-50.56002	5.85935	9.21	9.96	8.39	0.72	0.07	L	71.19	13.77	67.59	12.92
5595072420703114624	116.96477	-32.17133	5.86387	13.12	14.08	12.16	1.13	0.14	G	71.15	13.76	66.27	12.66
5544213926244557184	120.20160	-37.82794	5.88476	10.63	11.53	9.71	1.02	0.13	G	70.98	13.73	66.36	12.68
5436296928693979392	143.46188	-36.61574	5.89839	9.12	9.52	8.58	0.41	0.05	L	70.86	13.71	61.54	11.76
467560314629168640	41.46454	63.30457	5.90466	11.96	12.78	11.08	0.91	0.12	L	70.81	13.70	65.96	12.61
5308893149150949248	145.29272	-53.81604	5.90482	11.10	11.98	10.19	0.97	0.09	L	70.81	13.70	66.62	12.73
2055014277739104896	303.09511	32.87160	5.95590	8.91	9.76	8.02	0.88	0.09	L	70.38	13.61	66.83	12.77
5927687916632523264	250.53743	-57.31247	5.95730	12.82	13.38	12.12	0.46	0.11	G	70.37	13.61	65.85	12.58
5544001136384668288	121.32198	-37.58019	6.02134	13.52	14.50	12.51	1.23	0.13	O	69.84	13.51	64.30	12.29
4092905375639902464	277.97221	-19.12510	6.74522	6.35	7.01	5.62	0.55	0.05	L	64.47	12.47	60.53	11.57
1808020329279916288	300.29090	15.80350	6.10820	9.90	10.44	9.26	0.31	0.04	L	69.14	13.37	65.87	12.59

TABLE A.6: continued.

Gaia DR2 Source Id	RA	DEC	P	G	G_{BP}	G_{RP}	E(G_{BP}-G_{RP})	σE(G_{BP}-G_{RP})	Note	t_{PA}	$\sigma\ t_{PA}$	t_{PAC}	$\sigma\ t_{PAC}$
(1)	(2)	(3)	(4)	(5)	(6)	(7)	(8)	(9)	(10)	(11)	(12)	(13)	(14)
4312361436842603520	287.31663	10.55247	6.11423	7.66	8.44	6.84	0.86	0.07	L	69.09	13.36	63.38	12.11
6053428684887800320	185.88240	-64.47089	6.12121	11.32	12.29	10.35	0.96	0.09	L	69.03	13.35	67.57	12.91
4303770918113986304	299.38759	11.04366	6.17926	9.72	10.21	9.10	0.14	0.02	L	68.58	13.26	67.01	12.81
4093976334264606976	273.85944	-20.62955	6.17945	10.19	11.07	9.25	1.11	0.14	L	68.58	13.26	62.31	11.91
5932812431123862016	241.29147	-53.91943	6.19933	9.48	10.30	8.64	0.78	0.08	L	68.42	13.23	65.23	12.47
506581226385580288	27.77925	59.88821	6.20627	10.30	11.02	9.50	0.66	0.06	L	68.37	13.22	64.66	12.36
6059764002146656128	191.59278	-59.12473	6.22040	8.07	8.64	7.38	0.4	0.04	L	68.26	13.20	64.79	12.38
2059598687167348352	299.44206	35.63605	6.22543	12.68	13.69	11.69	1.26	0.16	L	68.22	13.19	62.54	11.95
2008504454839717120	341.60318	59.44219	6.23397	9.00	9.92	8.08	0.95	0.08	L	68.15	13.18	65.22	12.46
430670222050230912	9.18544	62.27424	6.24022	11.73	12.72	10.75	1.16	0.15	L	68.11	13.17	63.72	12.18
525136962570940160	18.75456	65.59940	6.27279	10.23	11.24	9.28	1.17	0.1	L	67.86	13.12	63.08	12.06
2015820463470505600	354.31691	62.42899	6.29664	9.24	10.22	8.28	1.08	0.09	L	67.67	13.09	64.22	12.27
4512950187838606464	286.51934	15.74941	6.30024	14.61	15.49	13.67	1.03	0.13	G	67.65	13.08	62.94	12.03
5823134325151372032	240.29463	-63.77655	6.31663	6.22	6.59	5.63	0.12	0.02	L	67.52	13.06	63.71	12.18
2027263738130844288	299.36918	26.55645	6.32059	8.23	9.14	7.30	1.05	0.09	L	67.49	13.05	62.86	12.01
1994462866719961216	354.40810	54.84718	6.33647	9.03	9.72	8.26	0.63	0.12	G	67.38	13.03	63.32	12.1
5339149677605627264	169.58945	-59.23796	6.39427	12.57	13.31	11.72	0.77	0.1	O	66.95	12.95	62.66	11.98
6057514092119497472	183.24857	-62.09682	6.39726	10.47	11.36	9.60	0.86	0.07	L	66.92	12.94	63.99	12.23
2006989121667184384	340.36050	56.43277	6.41896	8.55	9.09	7.89	0.36	0.04	L	66.76	12.91	62.90	12.02
4096979650282842112	276.18542	-16.79717	6.42429	8.41	9.08	7.59	0.67	0.06	L	66.73	12.91	62.53	11.95
3291491450496573824	74.97904	10.28845	6.44163	14.32	14.74	13.69	0.27	0.11	G	66.60	12.88	61.69	11.79
5254071873026676864	160.70349	-61.12298	6.45365	11.21	11.96	10.38	0.75	0.12	G	66.51	12.86	62.36	11.92
5312196047720402048	143.34884	-52.75585	6.45380	11.06	12.07	10.08	1.14	0.1	L	66.51	12.86	62.85	12.01
5868480143187802240	199.74280	-62.38235	6.45975	8.08	8.71	7.34	0.5	0.08	L	66.47	12.86	63.00	12.04
174489098011145216	71.94298	36.72278	6.46466	7.05	7.73	6.27	0.65	0.06	L	66.43	12.85	62.04	11.86
513282131279401728	23.91530	65.33050	6.55713	12.49	13.65	11.42	1.45	0.16	G	65.77	12.72	60.90	11.64
4096140001386430080	275.82979	-18.57477	6.56959	9.80	10.83	8.83	1.13	0.09	L	65.68	12.70	62.19	11.88
272444829450300160	67.57792	53.94018	6.56983	11.86	12.74	10.95	0.96	0.13	G	65.68	12.70	61.52	11.76
5541507237862358912	123.09332	-36.94374	6.66423	7.71	8.14	7.16	0.22	0.02	L	65.02	12.58	59.83	11.43

TABLE A.6: continued.

Gaia DR2 Source Id	RA	DEC	P	G	G_{BP}	G_{RP}	E(G_{BP}-G_{RP})	σE(G_{BP}-G_{RP})	Note	t_{PA}	$\sigma\ t_{PA}$	t_{PAC}	$\sigma\ t_{PAC}$
(1)	(2)	(3)	(4)	(5)	(6)	(7)	(8)	(9)	(10)	(11)	(12)	(13)	(14)
5302258008774271488	127.18202	-60.12256	6.69695	7.11	7.60	6.50	0.22	0.03	L	64.80	12.53	61.49	11.75
5338072980840100608	165.93830	-60.64226	6.69721	9.84	10.49	9.10	0.59	0.06	L	64.80	12.53	60.23	11.51
4314923363333177984	293.01969	11.54976	6.69729	12.54	13.22	11.75	0.65	0.12	G	64.80	12.53	60.62	11.58
2177714415280658944	323.72762	55.94226	6.71632	12.85	13.93	11.82	1.31	0.15	G	64.67	12.51	60.06	11.48
6054829806275577216	185.33793	-62.28164	6.73287	6.30	6.81	5.68	0.26	0.04	L	64.56	12.49	61.26	11.71
429544700100302080	4.26041	60.80280	6.79828	13.65	14.60	12.67	1.02	0.13	L	64.12	12.40	61.45	11.74
4204653587029046400	287.08654	-7.43777	6.80601	7.34	8.02	6.57	0.58	0.05	L	64.07	12.39	60.67	11.6
5935042378098601856	243.98144	-51.12073	6.81248	10.33	11.31	9.38	1.1	0.14	G	64.03	12.38	59.99	11.47
4505300988492333312	281.47541	12.33610	7.50794	9.75	10.36	9.00	0.53	0.07	L	59.79	11.56	55.75	10.65
430766016998901376	8.31747	62.90726	6.84634	10.97	11.87	10.07	1.04	0.09	L	63.80	12.34	58.53	11.19
5324034867356093056	137.06555	-51.43625	6.92436	7.22	7.93	6.44	0.59	0.05	L	63.30	12.24	60.37	11.54
2030848897634605440	300.19314	30.90759	6.96110	12.11	13.21	11.06	1.41	0.18	L	63.06	12.20	57.36	10.96
5352181712213705856	159.03578	-56.04323	6.98477	10.22	10.83	9.31	0.72	0.06	L	62.91	12.17	58.40	11.16
3031875585286182144	110.50990	-14.31818	6.99483	9.24	9.82	8.54	0.5	0.06	L	62.85	12.16	57.89	11.06
5334563996911649408	179.47384	-62.64613	7.00373	11.44	12.37	10.49	1.06	0.14	G	62.79	12.14	58.58	11.2
5903821951590649600	228.74274	-46.87257	7.05894	13.89	14.42	13.21	0.37	0.11	G	62.44	12.08	58.39	11.16
5877533315817003648	219.29985	-62.01092	7.06626	6.42	6.96	5.77	0.31	0.04	L	62.40	12.07	59.21	11.32
3113441691460573312	102.63473	0.00700	7.09748	11.97	12.83	11.03	0.88	0.11	L	62.20	12.03	59.52	11.38
5240438203718296192	165.36850	-64.29067	7.12163	13.71	14.51	12.82	0.87	0.13	G	62.06	12.00	57.78	11.04
5309174967720762496	144.21441	-53.03278	7.13431	9.69	10.51	8.83	0.93	0.11	L	61.98	11.99	56.52	10.8
5860785795219397376	184.39009	-65.75399	7.13451	13.83	14.46	12.97	0.58	0.09	O	61.98	11.99	59.27	11.33
5257664497238811776	148.85895	-58.42969	7.19619	8.95	9.58	8.22	0.51	0.04	L	61.60	11.92	57.85	11.06
5600628115523816320	117.51301	-28.25514	7.19862	10.32	11.10	9.50	0.78	0.1	L	61.59	11.91	57.38	10.97
5626365410677889792	131.05061	-35.47371	7.21689	9.94	10.60	9.17	0.59	0.12	G	61.48	11.89	57.65	11.02
2174677564161400064	326.32669	54.49638	7.23099	11.38	12.40	10.39	1.19	0.14	G	61.39	11.87	57.12	10.92
2007997408188526336	337.20867	58.21093	7.23213	10.62	11.46	9.74	0.86	0.07	L	61.39	11.87	57.81	11.05
4307944836090489600	290.25978	8.51633	7.23996	9.35	10.33	8.39	1.1	0.09	L	61.34	11.86	57.39	10.97
2165771172070496512	317.72654	49.14204	7.25140	9.95	10.88	9.00	1.05	0.09	L	61.27	11.85	57.23	10.94
5335963189825411072	172.84735	-60.58341	7.34403	13.08	13.96	12.13	1.04	0.12	O	60.73	11.75	56.08	10.72

TABLE A.6: continued.

Gaia DR2 Source Id	RA	DEC	P	G	G_{BP}	G_{RP}	E(G_{BP}-G_{RP})	σE(G_{BP}-G_{RP})	Note	t_{PA}	$\sigma\ t_{PA}$	t_{PAC}	$\sigma\ t_{PAC}$
(1)	(2)	(3)	(4)	(5)	(6)	(7)	(8)	(9)	(10)	(11)	(12)	(13)	(14)
5613564621430610560	111.82868	-25.78535	7.41934	12.70	13.62	11.73	0.78	0.23	L	60.29	11.66	60.57	11.58
3112475495616980992	104.50389	-0.37596	7.42462	10.35	11.04	9.57	0.59	0.06	L	60.26	11.66	57.05	10.9
5855468247702904704	190.52089	-69.40756	7.51028	6.10	6.55	5.55	0.2	0.04	L	59.78	11.56	55.20	10.55
2934712880912798464	108.42673	-17.62026	7.51211	12.39	13.36	11.42	1.11	0.14	G	59.77	11.56	55.63	10.63
5337191279923824384	168.04213	-61.75487	7.53200	7.80	8.35	7.14	0.29	0.03	L	59.66	11.54	56.89	10.87
3368698813404804352	95.55497	14.67813	7.56688	8.12	8.76	7.42	0.45	0.04	L	59.46	11.50	56.28	10.76
5337958876494096256	165.10434	-60.99319	7.63695	12.31	13.20	11.37	0.99	0.11	O	59.08	11.43	55.10	10.53
5339394082770287232	167.42135	-58.83772	7.72081	6.61	7.08	6.01	0.15	0.02	L	58.63	11.34	55.95	10.69
5415098722470316544	152.59186	-44.15874	7.77785	13.69	14.15	13.08	0.23	0.11	G	58.32	11.28	54.51	10.42
2016028168089215488	356.26093	63.00385	7.80112	10.08	11.04	9.12	1.01	0.08	L	58.20	11.26	55.38	10.58
2030063919381336832	299.79498	29.45072	7.81823	9.37	10.16	8.51	0.82	0.07	L	58.11	11.24	54.04	10.33
1873112207907294848	316.06930	39.97223	7.85582	9.05	9.82	8.20	0.8	0.07	L	57.91	11.20	53.55	10.23
470361114339849472	61.24359	58.65978	7.91561	7.16	7.92	6.32	0.74	0.06	L	57.61	11.14	54.02	10.32
5614916921960857088	114.04436	-25.36403	7.96016	14.49	15.58	13.45	1.29	0.13	O	57.38	11.10	53.35	10.2
2170785842762144512	322.18718	48.97821	7.96686	10.10	10.90	9.24	0.8	0.12	G	57.34	11.09	53.70	10.26
1825621002188696448	294.15720	20.33293	7.99014	6.58	7.41	5.72	0.81	0.07	L	57.23	11.07	53.96	10.31
428620663657823232	7.49410	60.21196	8.00066	8.51	9.23	7.71	0.66	0.05	L	57.17	11.06	53.61	10.25
261548119462093568	77.66762	49.68760	8.00263	9.06	9.69	8.32	0.53	0.06	L	57.16	11.06	53.29	10.18
5236551193933797888	174.75935	-65.20662	8.00290	14.65	15.67	13.62	1.18	0.12	O	57.16	11.06	53.56	10.24
3050050207554658048	105.24924	-8.70898	8.01127	9.62	10.32	8.79	0.68	0.07	L	57.12	11.05	53.30	10.19
5852880955104044800	214.51090	-64.42147	8.19958	14.15	15.00	13.17	1.04	0.12	O	56.19	10.87	51.58	9.86
5887482762148283008	228.20632	-54.75528	8.22041	9.02	9.90	8.19	0.91	0.1	L	56.09	10.85	51.56	9.85
512524361613040640	23.18010	63.59380	8.37701	6.64	7.46	5.78	0.8	0.11	L	55.35	10.71	52.09	9.96
3329849043206545920	92.80659	9.61249	8.61488	8.67	9.24	7.99	0.3	0.03	L	54.27	10.50	51.93	9.92
202939854734748032	70.99117	40.83478	8.63925	11.13	11.87	10.29	0.72	0.06	L	54.17	10.48	50.60	9.67
5613972681993587200	115.49584	-25.87617	8.93422	8.74	9.31	8.04	0.41	0.04	L	52.90	10.23	49.24	9.41
5254097093074642944	159.83465	-61.15243	9.19783	8.80	9.39	8.12	0.24	0.03	L	51.83	10.02	50.58	9.67
4056026175045038464	267.15626	-30.47597	9.31686	8.24	9.08	7.43	0.77	0.07	L	51.36	9.93	48.08	9.19
5854560115494081024	215.45224	-61.54966	9.46519	8.26	8.97	7.47	0.58	0.05	L	50.79	9.82	48.09	9.19

TABLE A.6: continued.

Gaia DR2 Source Id	RA	DEC	P	G	G_{BP}	G_{RP}	E(G_{BP}-G_{RP})	σE(G_{BP}-G_{RP})	Note	t_{PA}	$\sigma\ t_{PA}$	t_{PAC}	$\sigma\ t_{PAC}$
(1)	(2)	(3)	(4)	(5)	(6)	(7)	(8)	(9)	(10)	(11)	(12)	(13)	(14)
4269036830424588800	288.19714	3.55740	9.48055	7.90	8.67	7.12	0.66	0.05	L	50.74	9.81	47.54	9.09
5329838158460391296	131.22276	-46.34296	9.56113	7.97	8.53	7.36	0.32	0.03	L	50.43	9.75	46.73	8.93
5835124087174043136	244.71595	-57.89980	9.75376	6.15	6.70	5.52	0.25	0.02	L	49.73	9.62	47.09	9.0
5351423049186195328	158.22527	-58.52100	9.75912	11.01	11.86	10.14	0.71	0.07	L	49.71	9.62	48.18	9.21
5993655659352495616	243.61906	-40.79315	9.76457	12.20	12.89	11.39	0.62	0.12	G	49.69	9.61	46.24	8.84
5254662177677566464	155.34567	-61.07408	9.76811	8.59	9.09	7.96	0.23	0.03	L	49.68	9.61	46.62	8.91
2013029941628292352	359.39565	62.71824	9.80569	9.44	10.16	8.65	0.66	0.06	L	49.54	9.58	45.95	8.78
5241804518715438336	165.39269	-62.21022	9.84085	12.20	13.06	11.27	0.92	0.11	O	49.42	9.56	45.97	8.79
5328248672646357120	132.04364	-48.65915	9.84168	11.91	13.00	10.91	1.19	0.11	L	49.42	9.56	46.36	8.86
5328949100222702848	130.67412	-48.68614	10.02929	14.30	15.33	13.28	1.19	0.14	G	48.76	9.43	45.15	8.63
4685261526923834496	2.60032	-75.17706	10.09004	14.71	15.03	14.23	0.0	0.11	G	48.56	9.39	44.31	8.47
2070224337474904064	311.49913	45.30694	10.14797	9.42	10.48	8.42	1.12	0.09	L	48.36	9.35	45.81	8.75
5337257834740652160	167.55357	-60.84747	10.27245	11.09	12.12	10.09	1.11	0.11	L	47.95	9.27	45.07	8.61
201574982848108416	74.92307	40.83603	10.30573	9.92	10.67	9.10	0.73	0.08	L	47.84	9.25	43.93	8.4
4156450099578283776	279.51377	-8.36895	10.34150	8.88	9.93	7.92	1.07	0.09	L	47.72	9.23	45.11	8.62
5241780677399802624	165.37783	-62.29079	10.35488	10.31	11.08	9.47	0.63	0.06	L	47.68	9.22	45.65	8.72
5859119760248045312	198.50696	-64.32488	10.35635	10.85	11.83	9.89	1.06	0.13	L	47.68	9.22	44.47	8.5
5538569613358406144	117.35518	-38.23935	10.50594	12.62	13.34	11.79	0.67	0.12	G	47.20	9.13	43.95	8.4
4267549637851481344	286.16423	1.30614	17.13794	7.88	8.66	7.00	0.75	0.07	L	33.44	6.47	30.68	5.86
5337764640889249536	168.58836	-60.05292	10.70960	9.27	9.92	8.51	0.45	0.05	L	46.56	9.01	44.25	8.46
506779550797525760	31.95200	58.44353	10.87727	8.84	9.58	8.04	0.65	0.06	L	46.06	8.91	42.87	8.19
2007201567928631296	340.21724	56.82946	10.88439	8.04	8.70	7.29	0.48	0.04	L	46.04	8.90	43.43	8.3
5871922507947292032	205.07765	-57.61318	10.94947	7.47	8.03	6.79	0.33	0.03	L	45.84	8.87	42.87	8.19
3027495856819349248	113.41167	-16.31710	10.98248	11.04	11.89	10.16	0.82	0.12	G	45.75	8.85	42.75	8.17
4256744187345732224	280.53297	-4.29349	11.05302	9.92	11.04	8.88	1.26	0.1	L	45.54	8.81	42.59	8.14
203496585576324224	72.44976	42.28970	11.11731	8.60	9.23	7.85	0.44	0.06	L	45.35	8.77	42.91	8.2
5611465073923671424	106.94491	-24.91952	11.18235	11.25	11.81	10.56	0.35	0.11	G	45.17	8.74	42.18	8.06
5313887130948758016	142.92069	-49.65499	11.20064	8.88	9.83	7.95	0.92	0.08	L	45.12	8.73	42.85	8.19
462407693902385792	52.35821	60.44647	11.27625	11.76	12.88	10.76	1.18	0.1	L	44.90	8.69	42.43	8.11

TABLE A.6: continued.

Gaia DR2 Source Id	RA	DEC	P	G	G_{BP}	G_{RP}	E(G_{BP}-G_{RP})	σE(G_{BP}-G_{RP})	Note	t_{PA}	$\sigma\ t_{PA}$	t_{PAC}	$\sigma\ t_{PAC}$
(1)	(2)	(3)	(4)	(5)	(6)	(7)	(8)	(9)	(10)	(11)	(12)	(13)	(14)
5932569709575669504	243.32248	-54.23490	11.28752	7.98	8.65	7.24	0.43	0.04	L	44.87	8.68	42.80	8.18
3430067092837622272	91.64561	26.32922	11.30513	9.34	9.97	8.64	0.47	0.06	L	44.82	8.67	41.46	7.92
2002637323358768000	343.65706	54.26545	11.31916	13.43	14.15	12.54	0.74	0.1	L	44.78	8.66	41.37	7.91
200708636406382720	75.34662	39.96038	11.62570	7.34	7.94	6.68	0.34	0.04	L	43.95	8.50	41.10	7.85
5332375453374624640	178.07378	-65.40418	11.63735	9.33	10.09	8.59	0.58	0.07	L	43.92	8.49	41.00	7.84
2030427789026783488	299.45419	30.26590	11.66304	10.42	11.28	9.52	1.05	0.13	L	43.85	8.48	38.75	7.41
2073922579215436288	301.01866	39.10421	11.92821	12.97	13.86	12.03	0.93	0.13	G	43.16	8.35	40.05	7.65
1999252442448732288	358.02928	58.74172	12.14061	9.32	10.20	8.46	0.86	0.08	L	42.63	8.24	39.46	7.54
5336389564126521728	175.70084	-58.99339	12.18311	10.90	11.71	10.02	0.75	0.08	L	42.52	8.22	39.90	7.62
6054992602724692608	188.59725	-61.23762	12.21766	11.13	12.23	10.11	1.29	0.12	L	42.44	8.21	38.68	7.39
4066375912402666624	274.06943	-23.30591	12.27464	15.32	16.30	14.35	1.29	0.13	O	42.30	8.18	36.85	7.04
5616601820448126336	111.52996	-25.25730	12.35350	9.39	10.15	8.59	0.74	0.06	L	42.11	8.14	38.10	7.28
5240441472232302848	165.56688	-64.26289	12.43802	8.85	9.60	8.06	0.53	0.05	L	41.91	8.11	40.02	7.65
5884729035255064064	238.67837	-54.56644	12.63346	8.96	9.87	8.03	0.82	0.1	L	41.45	8.02	39.63	7.57
470386952863752576	61.53736	58.80875	12.65005	10.26	11.19	9.37	0.7	0.09	L	41.41	8.01	40.77	7.79
5865206961464617088	201.62523	-63.16263	12.88787	11.05	12.22	10.01	1.34	0.21	L	40.87	7.91	37.51	7.17
4253435825622331392	280.73864	-5.82091	12.91058	9.10	9.92	8.35	0.72	0.08	L	40.82	7.90	37.22	7.11
5310669788148987520	139.59222	-54.41226	13.12071	13.73	14.71	12.75	1.06	0.14	G	40.36	7.81	37.37	7.14
5311616398935271168	140.00627	-52.85618	13.23958	10.85	11.86	9.89	0.98	0.11	L	40.11	7.76	37.96	7.25
4313179507891570304	287.50172	12.53654	13.43999	10.08	11.20	9.07	1.38	0.18	L	39.68	7.68	35.09	6.71
5350852677538959104	162.75755	-58.59059	13.45493	10.91	11.91	9.97	0.94	0.08	L	39.65	7.67	37.75	7.22
5600915775257809152	119.42569	-27.60189	13.45979	11.49	12.36	10.66	0.84	0.1	L	39.64	7.67	36.28	6.93
5614312705966204288	117.01604	-25.57777	13.59892	9.50	10.14	8.79	0.49	0.05	L	39.36	7.61	36.03	6.89
459263743483634304	36.80736	59.46060	13.63864	9.14	10.11	8.19	0.96	0.11	L	39.28	7.60	36.90	7.05
5596601154188852352	121.58947	-30.09687	13.67010	9.49	10.23	8.67	0.57	0.05	L	39.21	7.58	37.12	7.09
6030635804488868480	249.53582	-31.47765	13.68681	12.78	13.33	12.09	0.32	0.11	G	39.18	7.58	36.48	6.97
4267397694768545920	287.05729	1.29863	13.75460	6.61	7.39	5.85	0.66	0.06	L	39.04	7.55	35.95	6.87
5586922973654572416	116.29911	-36.97475	13.76670	12.17	12.95	11.27	0.78	0.12	G	39.02	7.55	36.05	6.89
4087335043492541696	286.51307	-18.42825	13.77231	12.49	13.06	11.81	0.31	0.11	G	39.01	7.54	36.44	6.96

TABLE A.6: continued.

Gaia DR2 Source Id	RA	DEC	P	G	G_{BP}	G_{RP}	E(G_{BP}-G_{RP})	σE(G_{BP}-G_{RP})	Note	t_{PA}	$\sigma\ t_{PA}$	t_{PAC}	$\sigma\ t_{PAC}$
(1)	(2)	(3)	(4)	(5)	(6)	(7)	(8)	(9)	(10)	(11)	(12)	(13)	(14)
2065772109994415 36	74.41700	46.09253	13.84765	11.03	12.01	10.07	1.06	0.09	L	38.86	7.52	35.59	6.8
2243309938950947200	304.41505	62.75205	13.98367	14.12	14.63	13.61	0.02	0.11	G	38.59	7.46	36.68	7.01
5351331755370445056	161.23472	-56.28954	14.10712	8.07	8.99	7.51	0.51	0.05	L	38.35	7.42	36.08	6.9
5597327141100381568	119.74674	-29.30786	14.15735	9.98	10.74	9.17	0.61	0.05	L	38.26	7.40	35.87	6.86
2016626856473497344	352.30314	63.37430	14.37514	10.78	11.94	9.72	1.29	0.11	L	37.85	7.32	35.28	6.74
6026412893938675712	254.58229	-33.60913	6.06133	6.67	7.17	5.95	0.46	0.04	L	69.51	13.45	64.16	12.26
2161786374436607616	315.02658	42.59755	14.71797	8.39	9.71	7.28	1.52	0.12	L	37.23	7.20	34.44	6.58
508915489570374272	24.30841	57.75922	14.79237	8.81	9.08	8.01	0.59	0.06	L	37.09	7.17	30.31	5.79
2034684200359279488	297.82201	32.67553	15.00336	13.12	14.18	12.05	1.42	0.18	L	36.73	7.10	32.06	6.13
5864955727424819200	203.49590	-64.05556	15.04436	9.72	10.54	8.88	0.57	0.06	L	36.65	7.09	35.56	6.8
2016581673416790656	350.61846	62.75714	15.09343	10.12	11.35	9.12	1.27	0.11	L	36.57	7.07	34.13	6.52
2071433765909167232	308.22621	46.60125	15.11946	8.82	9.73	7.91	0.8	0.07	L	36.53	7.06	34.69	6.63
3324153371114695680	95.35961	6.47015	15.23122	8.02	8.65	7.32	0.36	0.04	L	36.34	7.03	34.08	6.51
5537860123428416640	119.69307	-38.99433	15.55821	11.46	12.34	10.55	0.9	0.12	L	35.80	6.92	32.75	6.26
6704330080883057536	281.53600	-48.63307	16.09459	12.59	13.03	11.97	0.12	0.11	G	34.95	6.76	32.33	6.18
1870258975238302208	310.85080	35.58778	16.39062	6.07	6.69	5.36	0.34	0.03	L	34.51	6.67	32.41	6.19
6026305309220584576	253.41732	-33.34511	16.40369	12.99	13.59	12.25	0.39	0.11	G	34.49	6.67	32.03	6.12
4638315266636230400	30.74872	-74.05691	16.48065	14.19	14.70	13.59	0.13	0.11	G	34.38	6.65	32.24	6.16
5338036117182452096	166.05607	-60.97991	16.65998	8.19	8.90	7.38	0.5	0.05	L	34.11	6.60	32.24	6.16
2058374144759464064	301.11066	34.11225	17.07369	8.46	9.24	7.61	0.69	0.06	L	33.53	6.49	31.04	5.93
5878388529664102016	218.79935	-60.99798	17.11025	9.85	10.96	8.74	1.27	0.12	L	33.48	6.48	31.01	5.93
2198162651491732608	329.46952	56.16389	17.87198	9.83	10.85	8.87	0.92	0.1	L	32.47	6.28	30.98	5.92
5253717937706836480	159.23233	-61.58131	18.05246	11.66	12.47	10.73	0.76	0.1	O	32.24	6.24	30.06	5.75
6026596989041710336	254.88447	-32.95258	18.13188	12.53	13.10	11.76	0.4	0.11	G	32.14	6.22	29.64	5.66
5255254711361371520	157.07013	-59.35018	18.17758	8.30	8.97	7.52	0.44	0.06	L	32.08	6.21	30.21	5.77
188724234539584256	78.84160	40.07802	18.19076	9.78	10.66	8.85	0.74	0.1	L	32.07	6.20	30.62	5.85
5351161399785606016	161.13616	-57.56536	18.87302	7.15	7.82	6.43	0.36	0.04	L	31.25	6.04	29.46	5.63
1873250780732545920	314.33680	40.17749	20.14034	9.27	10.36	8.28	1.13	0.11	L	29.85	5.77	27.46	5.25
5523162573544337408	129.25540	-44.11465	20.49764	6.66	7.31	5.90	0.41	0.04	L	29.48	5.70	27.52	5.26

TABLE A.6: continued.

Gaia DR2 Source Id	RA	DEC	P	G	G_{BP}	G_{RP}	E(G_{BP}-G_{RP})	σE(G_{BP}-G_{RP})	Note	t_{PA}	$\sigma\ t_{PA}$	t_{PAC}	$\sigma\ t_{PAC}$
(1)	(2)	(3)	(4)	(5)	(6)	(7)	(8)	(9)	(10)	(11)	(12)	(13)	(14)
5937099633141128448	251.32962	-51.34264	20.85306	9.60	10.51	8.67	0.74	0.06	L	29.13	5.63	27.90	5.33
4644478166748030976	35.20622	-73.08565	21.36729	13.63	14.02	13.06	0.0	0.11	G	28.63	5.54	26.33	5.03
4094784475310672128	274.24882	-19.07583	21.83410	7.48	8.43	6.62	0.62	0.06	L	28.20	5.45	27.59	5.27
4103564728516764032	280.45457	-14.50543	11.03608	13.65	14.58	12.94	0.58	0.12	G	45.59	8.82	44.40	8.49
6350220751862829952	358.65290	-83.28872	22.44150	14.31	15.01	13.60	0.34	0.11	G	27.66	5.35	26.14	5.0
5600052040150252800	114.64682	-28.49960	23.17284	9.22	9.95	8.42	0.58	0.05	L	27.04	5.23	24.68	4.72
5253571526514498176	159.11275	-62.19251	24.21976	12.41	13.32	11.49	0.76	0.1	O	26.21	5.07	24.73	4.73
5858474003300201856	193.43279	-65.89971	26.46392	11.93	12.63	11.09	0.51	0.09	O	24.63	4.76	22.91	4.38
6096564686351860992	213.33208	-44.89374	26.68846	12.41	13.00	11.69	0.28	0.11	G	24.48	4.74	22.71	4.34
5355057622305532928	155.17091	-55.32138	28.16616	7.82	8.68	6.96	0.73	0.06	L	23.57	4.56	21.60	4.13
5964193485048327808	252.91061	-45.42671	28.86509	8.85	10.11	7.76	1.15	0.11	L	23.17	4.48	22.46	4.29
5597379741549105280	119.59202	-29.13008	30.09021	8.12	9.00	7.26	0.72	0.06	L	22.50	4.35	20.69	3.95
5238808628736339584	164.28834	-65.13474	15.71624	8.66	9.31	7.85	0.47	0.04	L	35.54	6.87	33.41	6.38
5864135319959353600	204.15366	-64.55832	34.05097	9.10	10.18	8.12	0.98	0.1	L	20.62	3.99	19.18	3.67
5546476927338700416	123.26755	-34.57851	41.46411	6.46	7.30	5.58	0.61	0.05	L	17.95	3.47	16.69	3.19
2027951173435143680	297.87876	27.46021	44.87621	6.66	7.50	5.78	0.64	0.06	L	16.98	3.28	15.61	2.98

TABLE A.7: Individual ages for the selected F-mode GCCs obtained by using both the noncanonical PA and PAC relations.

Gaia DR2 Source Id	RA	DEC	P	G	G_{BP}	G_{RP}	E(G_{BP}-G_{RP})	σE(G_{BP}-G_{RP})	Note	t_{PA}	$\sigma\, t_{PA}$	t_{PAC}	$\sigma\, t_{PAC}$
(1)	(2)	(3)	(4)	(5)	(6)	(7)	(8)	(9)	(10)	(11)	(12)	(13)	(14)
3442172745919329664	82.35887	27.00089	3.34920	11.57	12.21	10.78	0.72	0.12	G	141.71	26.10	122.49	21.72
4704080802304630784	12.82014	-68.98430	0.99469	18.24	18.45	17.79	0.18	0.11	G	303.00	55.82	257.01	45.57
5521400228203695232	123.35129	-42.27568	1.00189	16.05	16.93	15.15	1.23	0.15	G	301.64	55.56	268.78	47.65
6379351625245757568	359.99997	-75.19496	1.03777	17.68	17.98	17.36	0.02	0.11	G	295.07	54.35	269.73	47.82
4711142067840447360	21.61608	-64.87535	1.06447	17.86	18.05	17.41	0.16	0.11	G	290.41	53.50	245.31	43.49
4639539705975935360	50.85364	-74.96868	1.11640	17.83	18.12	17.50	0.02	0.11	G	281.88	51.92	254.78	45.17
4690768156035338624	18.95551	-70.54573	1.14292	17.53	17.82	17.09	0.18	0.11	G	277.77	51.17	243.67	43.20
4703965697180635136	9.31520	-67.04117	1.15729	17.89	18.12	17.43	0.17	0.11	G	275.60	50.77	234.88	41.64
4666616485480394368	60.40851	-69.47789	1.15905	16.29	16.45	15.90	0.12	0.08	O	275.34	50.72	223.60	39.64
4691081375113472256	20.83822	-70.57775	1.17564	17.33	17.45	17.02	0.0	0.11	G	272.90	50.27	220.70	39.13
4637614151878607232	20.74650	-76.24745	1.20857	17.80	17.95	17.36	0.1	0.11	G	268.22	49.41	223.07	39.55
5834840099568788864	241.98124	-58.78225	1.23577	13.71	14.05	13.19	0.31	0.11	G	264.51	48.73	230.11	40.80
4636112425153243904	16.19343	-76.86050	1.25457	17.34	17.55	16.84	0.21	0.11	G	262.02	48.27	218.67	38.77
4690721839108141568	19.01385	-70.91305	1.30481	17.25	17.73	17.00	-0.0	0.11	G	255.66	47.09	246.30	43.67
4698739817197286912	23.24870	-66.49795	1.30920	17.05	17.30	16.67	0.05	0.11	G	255.13	47.00	223.23	39.58
5298606801235832064	140.10591	-62.22648	1.36601	18.36	18.60	17.89	0.18	0.11	G	248.43	45.76	211.15	37.44
5850083595712857472	220.66054	-64.27433	1.37135	17.67	18.47	16.71	1.23	0.15	G	247.83	45.65	210.17	37.26
4690414800484275840	12.25946	-70.13797	1.37867	17.09	17.39	16.78	-0.0	0.11	G	247.00	45.50	219.47	38.91
5935901715187592704	255.13630	-53.09007	1.39879	15.45	15.92	14.78	0.58	0.12	G	244.77	45.09	212.04	37.59
5615958881027868544	115.24714	-22.49207	1.39928	15.46	16.23	14.69	0.89	0.11	O	244.72	45.08	224.10	39.73
4627114812265929856	55.76893	-76.93405	1.42992	17.95	18.31	17.50	0.18	0.11	G	241.42	44.47	216.52	38.39
4690838421706602624	15.93439	-70.90033	1.43044	17.33	17.58	16.94	0.06	0.11	G	241.37	44.46	210.25	37.28
4637822960304562560	24.11091	-75.12545	1.43113	17.25	17.49	16.82	0.11	0.11	G	241.29	44.45	208.02	36.88
6027070573648725632	251.47116	-33.16585	1.45594	13.89	14.47	13.13	0.75	0.12	G	238.71	43.97	207.84	36.85
5321579073778197888	130.00710	-52.33019	1.53045	15.25	15.90	14.48	0.81	0.12	G	231.37	42.62	203.63	36.10
6008381624727734784	237.76802	-39.75981	1.57244	17.10	17.91	16.20	1.12	0.14	G	227.48	41.90	197.69	35.05
4649187405119614848	75.03872	-75.15255	1.57491	16.97	17.25	16.49	0.18	0.11	G	227.26	41.86	195.43	34.65
4108167833903339520	259.75244	-27.43467	1.58118	16.78	17.65	15.71	1.45	0.16	G	226.69	41.76	184.78	32.76
4691023998645738368	17.49608	-69.93794	1.60821	16.70	16.83	16.30	0.0	0.11	G	224.30	41.32	185.40	32.87
4650261219962135424	85.33831	-74.16668	1.62049	16.91	17.29	16.43	0.22	0.11	G	223.23	41.12	199.23	35.32

TABLE A.7: continued.

Gaia DR2 Source Id	RA	DEC	P	G	G_{BP}	G_{RP}	E(G_{BP}-G_{RP})	σE(G_{BP}-G_{RP})	Note	t_{PA}	$\sigma\, t_{PA}$	t_{PAC}	$\sigma\, t_{PAC}$
(1)	(2)	(3)	(4)	(5)	(6)	(7)	(8)	(9)	(10)	(11)	(12)	(13)	(14)
426580107514101376	15.41660	60.59426	1.62477	14.87	15.52	14.07	0.85	0.13	G	222.87	41.05	193.24	34.26
4684195339947360512	6.98869	-76.24706	1.64272	17.58	17.86	17.10	0.17	0.11	G	221.34	40.77	190.24	33.73
2031982665929461504	296.05399	29.68730	1.64410	16.22	17.13	15.31	1.2	0.14	G	221.22	40.75	195.53	34.67
181620805307496192	76.98162	33.05659	1.66805	14.61	15.30	13.80	0.88	0.13	G	219.23	40.38	191.76	34.00
4702506576531479424	12.34403	-69.50825	1.68632	17.24	17.63	16.86	0.08	0.11	G	217.74	40.11	200.62	35.57
2021540814501736320	293.71912	25.61797	1.69319	17.40	18.66	16.25	1.87	0.19	G	217.19	40.01	181.51	32.18
4684369749977673472	13.14590	-75.95877	1.75282	17.35	17.52	16.89	0.09	0.11	G	212.53	39.15	176.02	31.21
4392367984521092608	254.76077	4.79169	1.77576	14.89	15.22	14.38	0.23	0.11	G	210.81	38.83	182.05	32.28
4652327614621999872	70.43479	-74.41493	1.79655	16.84	16.86	16.26	0.21	0.11	G	209.28	38.55	157.93	28.00
5516409029527928064	125.97858	-47.25490	1.83399	15.20	15.90	14.37	0.91	0.13	G	206.59	38.06	179.11	31.76
5814577169727787392	254.58683	-67.66312	1.85575	13.93	14.19	13.51	0.06	0.11	G	205.07	37.78	177.09	31.40
4189050211325803008	299.56897	-12.07101	1.99398	17.75	18.07	17.21	0.24	0.11	G	196.05	36.11	168.03	29.79
252595410453952384	67.62787	43.65313	1.99947	13.06	14.01	12.09	1.29	0.15	G	195.72	36.05	169.51	30.05
5928285810456681344	247.54255	-57.33140	2.00665	13.64	14.08	13.01	0.44	0.11	G	195.28	35.97	169.56	30.06
5851830444814064512	206.04645	-65.60886	2.02729	15.84	16.51	14.95	0.97	0.13	G	194.03	35.74	163.09	28.92
2928096226097916160	109.16266	-22.18043	2.04402	14.73	15.46	13.87	0.96	0.13	G	193.04	35.56	167.34	29.67
5322875157471168768	129.59122	-49.81203	2.04472	15.13	15.93	14.31	0.92	0.13	G	192.99	35.55	172.95	30.66
5859972946880769408	189.52856	-66.38308	2.06540	15.01	15.58	14.31	0.63	0.09	O	191.78	35.33	166.54	29.53
4636099402811865344	19.45728	-76.56544	2.06770	16.80	17.11	16.32	0.16	0.11	G	191.65	35.30	165.51	29.35
6379917835078618752	359.03700	-73.64989	2.08819	17.15	17.32	16.70	0.05	0.11	G	190.47	35.09	157.75	27.97
5211831178906807040	93.60903	-79.18168	2.09182	16.74	16.98	16.24	0.15	0.11	G	190.26	35.05	159.82	28.34
2162679246615275264	315.66755	45.09280	2.11305	16.28	17.23	15.27	1.34	0.15	G	189.06	34.83	160.69	28.49
200016111582079744	73.82548	39.97972	2.12061	13.35	13.95	12.58	0.73	0.08	L	188.64	34.75	162.79	28.86
5613411827982576768	112.81549	-25.90739	2.14810	11.58	12.04	10.97	0.29	0.08	O	187.13	34.47	177.10	31.40
5256605839340504576	149.84616	-60.33354	2.30293	14.62	15.23	13.86	0.71	0.12	G	179.15	33.00	156.16	27.69
228673477705878400	63.37936	41.31878	2.31244	14.04	14.74	13.23	0.85	0.13	G	178.69	32.92	155.94	27.65
6377896696484508544	355.61170	-75.25641	2.33045	17.06	17.34	16.70	-0.0	0.11	G	177.82	32.76	152.48	27.03
5521137101325930624	122.45845	-43.97272	2.34215	14.33	14.88	13.65	0.56	0.11	G	177.26	32.65	155.50	27.57
5521712145909463680	128.16223	-46.79047	2.36600	15.36	16.18	14.36	1.23	0.15	G	176.14	32.45	146.23	25.93

TABLE A.7: continued.

Gaia DR2 Source Id	RA	DEC	P	G	G_{BP}	G_{RP}	E(G_{BP}-G_{RP})	σE(G_{BP}-G_{RP})	Note	t_{PA}	$\sigma\ t_{PA}$	t_{PAC}	$\sigma\ t_{PAC}$
(1)	(2)	(3)	(4)	(5)	(6)	(7)	(8)	(9)	(10)	(11)	(12)	(13)	(14)
5534744416711687424	119.86019	-40.02830	2.36819	14.81	15.55	13.92	0.99	0.13	G	176.04	32.43	150.12	26.62
4688062360997085440	21.38773	-70.75956	2.37759	16.60	17.05	16.33	0.0	0.11	G	175.61	32.35	158.35	28.08
5310255272261039488	138.08441	-55.23391	2.39764	14.44	15.10	13.65	0.79	0.12	G	174.68	32.18	151.83	26.92
3134002107923090944	101.39057	7.81629	2.42684	12.82	13.74	12.10	0.88	0.11	O	173.37	31.94	159.38	28.26
4445130042844217216	249.98383	7.67920	2.44837	15.83	16.15	15.32	0.18	0.11	G	172.41	31.76	147.84	26.21
1865228537734352896	317.06710	32.74552	2.45861	14.11	14.56	13.50	0.39	0.11	G	171.96	31.68	149.84	26.57
4650211741937480192	86.25630	-73.56541	2.47100	16.37	16.64	15.80	0.23	0.11	G	171.42	31.58	142.51	25.27
207722317998325632	80.88983	44.76008	2.47685	12.75	13.46	11.93	0.85	0.13	G	171.17	31.53	148.94	26.41
523700107035878272	14.38545	63.15643	2.48837	13.96	14.89	13.01	1.22	0.14	G	170.67	31.44	147.96	26.23
5596920115637629184	119.15388	-30.95279	2.49448	13.91	14.77	12.99	1.15	0.12	O	170.41	31.39	143.42	25.43
4757183606166564864	83.55789	-63.16699	2.50146	16.10	16.40	15.61	0.14	0.11	G	170.11	31.34	146.36	25.95
5329778887909167232	131.65005	-46.52931	2.52412	15.66	16.74	14.60	1.51	0.16	G	169.15	31.16	143.40	25.42
5520935444020919296	122.93820	-44.17210	2.54078	14.99	15.78	14.08	1.05	0.14	G	168.46	31.03	143.50	25.44
5613111347760892672	110.69908	-26.71455	2.54548	12.91	13.38	12.29	0.4	0.11	G	168.26	31.00	146.61	25.99
2934255449716149760	107.39410	-18.56329	2.54653	13.25	14.02	12.37	0.99	0.13	G	168.22	30.99	144.44	25.61
5520440663787736192	122.44604	-45.35460	2.55121	15.84	16.42	15.08	0.69	0.12	G	168.03	30.95	144.42	25.61
2932101334643047680	105.10347	-20.43170	2.55778	12.65	13.15	11.98	0.36	0.05	L	167.76	30.90	158.77	28.15
470144751068871808	61.63394	58.11309	2.57812	16.51	16.97	15.88	0.42	0.11	G	166.93	30.75	144.63	25.64
5597352047599988352	119.45786	-29.38405	2.58612	11.59	12.21	10.84	0.73	0.1	O	166.60	30.69	141.09	25.02
5404862853352596736	149.21983	-51.60892	2.60474	13.30	14.09	12.41	1.0	0.11	O	165.86	30.55	144.14	25.56
5599566983722741248	114.47706	-29.43804	2.62004	14.18	14.88	13.38	0.81	0.12	G	165.25	30.44	144.41	25.60
5617745003304609536	109.88037	-23.80181	2.63003	14.53	15.53	13.52	1.35	0.15	G	164.86	30.37	141.06	25.01
2004103831357741696	332.32734	51.40539	2.63200	14.84	15.40	14.13	0.59	0.12	G	164.78	30.35	143.15	25.38
3425576270732293632	93.99953	23.74749	2.63501	11.57	12.24	10.79	0.75	0.1	L	164.66	30.33	145.55	25.81
4690127037676227840	13.29901	-70.85695	2.63769	16.20	16.67	15.89	0.0	0.11	G	164.56	30.31	152.87	27.10
5254994264542210560	153.53708	-59.85044	2.64145	15.11	15.96	14.18	1.08	0.12	O	164.41	30.29	144.29	25.58
5932284528150696704	245.22589	-53.55461	2.64407	11.70	11.99	11.25	0.03	0.08	O	164.31	30.27	145.71	25.83
5857845872913577856	199.32909	-66.11714	2.65755	15.60	16.34	14.72	0.96	0.13	G	163.79	30.17	140.48	24.91
1986816867172796 16	72.85353	38.18855	2.65963	13.15	13.88	12.23	0.78	0.07	L	163.70	30.16	160.38	28.44

TABLE A.7: continued.

Gaia DR2 Source Id	RA	DEC	P	G	G_{BP}	G_{RP}	E(G_{BP}-G_{RP})	σE(G_{BP}-G_{RP})	Note	t_{PA}	$\sigma\ t_{PA}$	t_{PAC}	$\sigma\ t_{PAC}$
(1)	(2)	(3)	(4)	(5)	(6)	(7)	(8)	(9)	(10)	(11)	(12)	(13)	(14)
5322962499927658880	129.02740	-49.26527	2.66635	14.82	15.62	13.88	1.1	0.14	G	163.45	30.11	137.93	24.46
3330259852538068608	91.85611	11.15198	3.88939	11.07	11.64	10.37	0.5	0.06	L	129.04	23.77	113.96	20.21
5611563995612988928	112.16780	-29.34422	2.70160	12.72	13.13	12.17	0.27	0.11	G	162.11	29.86	141.65	25.11
3133819112256378368	100.02326	7.60583	2.70467	10.13	10.86	9.35	0.74	0.08	L	161.99	29.84	148.35	26.30
5515778734493663232	127.31510	-46.74924	2.71653	14.80	15.48	13.93	0.9	0.13	G	161.55	29.76	136.87	24.27
4688033735040263168	23.36268	-70.67097	2.74408	16.45	16.67	16.04	-0.0	0.11	G	160.53	29.57	134.47	23.84
5280590173638560128	104.74084	-68.31085	2.75554	15.96	16.28	15.44	0.17	0.11	G	160.11	29.49	137.01	24.29
355488086540394112	35.70997	50.07193	2.75989	14.54	14.96	13.95	0.32	0.11	G	159.96	29.47	138.60	24.57
5520506531407532928	121.80022	-45.06591	2.77254	14.02	14.57	13.29	0.6	0.12	G	159.50	29.38	137.53	24.38
5545066700588440832	119.73893	-36.89733	2.77514	15.07	16.06	14.05	1.35	0.15	G	159.41	29.36	135.63	24.05
4637956099996538752	18.33566	-75.37716	2.77979	16.46	16.76	15.98	0.11	0.11	G	159.24	29.33	136.37	24.18
2948568273607650560	105.01213	-14.16082	2.78195	13.90	14.80	13.11	0.91	0.13	G	159.16	29.32	146.98	26.06
4066429066901946368	273.26040	-23.11729	5.05787	6.82	7.37	6.23	0.25	0.03	L	109.48	20.17	101.17	17.94
460909093912435072	42.02334	57.93448	2.79873	14.03	15.07	13.01	1.39	0.15	G	158.56	29.21	135.50	24.02
430052537038350976	0.60589	62.84717	2.81345	14.41	15.25	13.49	1.08	0.14	G	158.04	29.11	136.12	24.13
1873298884367855872	314.17890	40.25849	2.82245	16.21	17.13	15.23	1.25	0.15	G	157.73	29.05	134.27	23.81
5616130129962210048	110.43814	-26.53341	2.82545	12.91	13.38	12.30	0.37	0.11	G	157.62	29.04	137.83	24.44
3117307814859500416	97.77268	-2.14679	3.13523	13.29	14.09	12.47	0.9	0.12	L	147.68	27.20	128.89	22.85
5293246995583678336	109.08524	-60.30341	2.84929	15.52	16.19	14.69	0.83	0.13	G	156.80	28.88	134.04	23.76
5544259212380322560	120.85675	-37.19998	2.85529	14.09	14.84	13.23	0.93	0.11	O	156.59	28.84	133.78	23.72
2928335747830554240	108.43497	-21.72421	2.86166	14.22	14.98	13.36	0.94	0.13	G	156.37	28.80	135.46	24.02
4757607983288353024	83.76190	-62.33990	2.86849	16.03	16.25	15.52	0.12	0.11	G	156.14	28.76	128.93	22.86
513074186146353536	24.74994	64.98924	2.87151	11.01	11.84	10.14	1.03	0.11	L	156.04	28.74	133.53	23.67
4688114725237948672	24.52435	-70.61840	2.88021	16.38	16.64	15.99	-0.0	0.11	G	155.74	28.69	131.37	23.29
261927068718088832	81.89283	50.86737	2.88526	13.17	13.81	12.41	0.7	0.12	G	155.57	28.66	135.57	24.04
4682206533865906944	65.11048	-57.85114	2.89258	15.71	16.00	15.30	-0.0	0.11	G	155.32	28.61	135.39	24.00
5253289093802878592	152.85139	-61.48616	2.91146	14.11	14.59	13.44	0.46	0.11	G	154.69	28.50	133.37	23.65
2947842664653933824	104.19146	-15.63763	3.69400	13.25	13.97	12.43	0.81	0.12	G	133.27	24.55	115.38	20.46
5310969267622303872	136.56210	-54.93719	2.92762	14.52	15.11	13.78	0.63	0.12	G	154.16	28.40	133.96	23.75

TABLE A.7: continued.

Gaia DR2 Source Id	RA	DEC	P	G	G_{BP}	G_{RP}	E(G_{BP}-G_{RP})	σE(G_{BP}-G_{RP})	Note	t_{PA}	$\sigma\ t_{PA}$	t_{PAC}	$\sigma\ t_{PAC}$
(1)	(2)	(3)	(4)	(5)	(6)	(7)	(8)	(9)	(10)	(11)	(12)	(13)	(14)
4642866828161408512	52.89342	-70.99389	2.92900	16.29	16.60	15.82	0.08	0.11	G	154.11	28.39	133.66	23.70
5533064637824258816	119.78798	-43.17517	2.92921	13.49	13.98	12.84	0.45	0.11	G	154.10	28.39	134.05	23.77
5598642947280233984	116.71718	-30.66590	2.96840	14.15	14.95	13.28	0.97	0.11	O	152.83	28.15	132.41	23.48
5856662557855409280	187.47093	-68.27871	2.98190	14.44	14.92	13.79	0.44	0.11	G	152.39	28.07	132.05	23.41
5318708901756763520	131.02834	-51.91945	2.98495	15.08	15.82	14.23	0.89	0.13	G	152.30	28.05	132.07	23.42
4265371574109405824	284.35111	-0.73024	2.98806	10.56	11.32	9.69	0.99	0.14	L	152.20	28.04	127.75	22.65
5519861423017907840	124.43265	-45.18550	3.00610	14.46	15.24	13.61	0.93	0.13	G	151.62	27.93	132.55	23.50
5241937353463150848	162.59092	-62.19142	3.02574	15.21	16.09	14.26	1.16	0.12	O	151.01	27.82	127.86	22.67
466906311366699520	48.44587	63.34948	3.03268	13.18	14.11	12.24	1.17	0.14	G	150.79	27.78	130.85	23.20
5252269709082759936	156.40361	-62.55651	3.04556	15.10	15.67	14.35	0.64	0.12	G	150.39	27.70	128.84	22.84
5310863370918375552	140.55281	-53.06412	3.05163	13.60	14.46	12.66	1.11	0.12	O	150.20	27.67	129.35	22.93
5863815636949490048	202.86552	-65.32720	3.06221	15.68	16.55	14.75	1.08	0.12	O	149.88	27.61	132.22	23.44
2930525287803260288	109.84202	-19.54033	3.07149	12.79	13.35	12.07	0.57	0.09	O	149.60	27.56	130.12	23.07
5858259014403682304	195.97407	-66.33292	3.08394	15.37	16.09	14.47	0.95	0.11	O	149.22	27.49	126.48	22.43
5235910694044165760	176.13694	-67.30525	3.08613	8.70	9.22	8.06	0.43	0.06	L	149.15	27.47	130.96	23.22
5237406545247540608	171.64645	-65.58218	3.11677	14.99	15.84	14.04	1.12	0.14	G	148.23	27.31	125.96	22.33
5335753015664095104	173.80588	-60.91465	3.12750	14.19	14.98	13.30	1.0	0.11	O	147.91	27.25	126.73	22.47
5594991812757424768	115.97856	-32.50378	3.14920	14.81	15.79	13.80	1.33	0.15	G	147.27	27.13	124.40	22.06
2932737092877188352	105.22172	-19.45929	3.15504	12.36	12.85	11.73	0.4	0.11	G	147.10	27.10	128.89	22.85
2059517087110475392	299.88745	36.02152	3.16632	15.16	16.04	14.20	1.16	0.14	G	146.78	27.04	124.65	22.10
5329323277776517120	130.36480	-47.64966	3.17573	14.05	14.90	13.10	1.13	0.14	G	146.50	26.99	124.24	22.03
5239658688657671680	160.70962	-65.55805	3.18304	16.74	17.37	16.02	0.6	0.12	G	146.29	26.95	129.47	22.95
5322878146768508800	129.73194	-49.77016	3.18474	14.62	15.39	13.75	0.94	0.13	G	146.24	26.94	126.17	22.37
5612661716228387200	111.62263	-27.92502	3.18518	12.78	13.26	12.14	0.41	0.11	G	146.23	26.94	127.26	22.56
377753613615880832	14.89365	45.40672	3.20017	11.48	11.87	10.98	0.16	0.11	G	145.80	26.86	128.41	22.77
5875602191067578752	230.82679	-61.21710	3.23038	15.66	16.48	14.71	1.1	0.14	G	144.95	26.70	122.06	21.64
512491028363231616	24.35667	63.69136	3.23980	13.13	14.16	12.13	1.33	0.15	G	144.68	26.65	124.23	22.03
4513100717859042176	286.49619	16.09800	3.26984	13.47	14.24	12.60	0.93	0.13	G	143.85	26.50	124.57	22.09
5617316606087829888	109.16777	-24.50300	3.27499	12.80	13.31	12.13	0.47	0.11	G	143.71	26.47	124.63	22.10

TABLE A.7: continued.

Gaia DR2 Source Id	RA	DEC	P	G	G_{BP}	G_{RP}	E(G_{BP}-G_{RP})	σE(G_{BP}-G_{RP})	Note	t_{PA}	$\sigma\ t_{PA}$	t_{PAC}	$\sigma\ t_{PAC}$
(1)	(2)	(3)	(4)	(5)	(6)	(7)	(8)	(9)	(10)	(11)	(12)	(13)	(14)
5520505328816739584	121.80935	-45.12830	3.28292	13.45	14.07	12.67	0.69	0.12	G	143.49	26.43	123.60	21.91
5241803217391469568	165.52136	-62.28989	3.28899	14.54	15.40	13.59	1.1	0.12	O	143.32	26.40	123.77	21.94
279382060625871360	76.63188	55.35352	3.29487	7.19	7.81	6.48	0.55	0.07	L	143.16	26.37	130.06	23.06
5405496240766414464	148.01595	-51.99247	3.29644	13.56	14.38	12.67	1.01	0.11	O	143.12	26.36	122.67	21.75
505178760644698880	31.25913	57.14294	3.29700	12.34	12.82	11.68	0.35	0.05	L	143.11	26.36	129.92	23.03
5306043592977093504	145.89770	-57.23830	3.00860	15.29	16.16	14.31	1.23	0.13	O	151.55	27.92	124.51	22.07
505368121464666112	29.62897	57.81985	3.32910	13.78	14.44	12.98	0.74	0.12	G	142.24	26.20	123.27	21.86
5600862070985787136	119.26547	-28.16158	3.33098	11.61	12.25	10.88	0.58	0.09	O	142.19	26.19	129.95	23.04
5605736961940589568	110.81312	-29.72244	3.33617	12.87	13.38	12.30	0.3	0.11	G	142.05	26.17	127.69	22.64
5313250548085699712	139.88405	-51.62042	3.35503	12.70	13.62	11.69	1.34	0.13	O	141.55	26.07	113.65	20.15
5516452460238707968	125.52706	-47.30395	3.36831	14.28	14.93	13.46	0.77	0.12	G	141.20	26.01	120.90	21.44
2073935223599391872	300.89457	39.15963	3.37031	13.22	13.96	12.38	1.02	0.13	L	141.15	26.00	110.77	19.64
5592331544376193792	113.82822	-31.66418	3.38307	13.77	14.53	12.93	0.87	0.13	G	140.82	25.94	123.09	21.82
5824464493705913472	229.94041	-66.49608	3.38932	6.44	6.86	5.91	0.23	0.04	L	140.65	25.91	122.58	21.73
5598852026287511424	116.00045	-30.14146	3.39082	13.12	13.66	12.45	0.58	0.09	O	140.61	25.90	115.65	20.51
2025217890612425344	293.14591	26.80479	3.39154	15.51	16.38	14.54	1.15	0.14	G	140.60	25.90	118.60	21.03
5857294605251013760	193.30159	-67.96426	3.40117	14.41	14.91	13.73	0.48	0.11	G	140.35	25.85	120.94	21.44
206211859601169792	74.06344	44.78185	3.40680	12.54	13.43	11.62	1.1	0.14	G	140.20	25.83	121.28	21.50
189739251272296192	85.62191	37.64633	3.41272	12.05	12.93	11.18	0.84	0.11	L	140.05	25.80	137.19	24.32
4690436069162376576	10.68389	-70.27426	3.42463	16.23	16.48	15.74	0.07	0.11	G	139.74	25.74	117.60	20.85
5932997939411720960	243.72813	-53.33844	3.45291	9.79	10.63	8.92	0.92	0.08	L	139.03	25.61	125.13	22.19
3051144427784813824	103.54766	-7.66438	3.45403	13.28	13.98	12.44	0.85	0.11	L	139.00	25.60	118.21	20.96
5547358117187868288	122.79503	-33.51586	3.48218	10.44	11.05	9.72	0.58	0.06	L	138.29	25.47	121.98	21.63
5310265099146146816	138.32401	-54.93121	3.50424	14.23	15.01	13.34	0.96	0.13	G	137.75	25.37	118.35	20.98
515527570241664512	34.14985	65.17655	3.52190	12.69	13.52	11.78	1.02	0.13	G	137.31	25.29	118.06	20.93
2936165984303583360	105.87696	-15.54334	3.52281	13.45	14.09	12.65	0.73	0.12	G	137.29	25.29	117.81	20.89
5268616973048513664	107.46385	-68.48372	3.52627	15.80	16.25	15.26	0.23	0.11	G	137.21	25.27	121.59	21.56
5618354751226656640	112.51063	-23.67398	3.54416	13.26	14.12	12.36	1.08	0.14	L	136.77	25.19	115.15	20.42
5612495762995320576	113.72248	-26.85579	3.55250	13.56	14.36	12.63	1.03	0.13	G	136.57	25.16	116.02	20.57

TABLE A.7: continued.

Gaia DR2 Source Id	RA	DEC	P	G	G_{BP}	G_{RP}	E(G_{BP}-G_{RP})	σE(G_{BP}-G_{RP})	Note	t_{PA}	$\sigma\ t_{PA}$	t_{PAC}	$\sigma\ t_{PAC}$
(1)	(2)	(3)	(4)	(5)	(6)	(7)	(8)	(9)	(10)	(11)	(12)	(13)	(14)
5547421437881152256	122.36346	-33.26212	3.56310	11.82	12.44	11.06	0.8	0.1	O	136.32	25.11	107.33	19.03
2162640763705905920	316.08941	45.23937	3.56914	13.70	14.61	12.76	1.13	0.14	G	136.17	25.08	117.69	20.87
5311139245252191616	137.38339	-53.98770	3.59050	11.68	12.22	11.02	0.44	0.11	G	135.67	24.99	119.08	21.11
5599370549100412544	114.32029	-29.60773	3.59160	14.17	15.06	13.23	1.12	0.14	G	135.64	24.99	116.62	20.68
2952257272558933248	101.92934	-13.66668	4.85729	11.71	12.23	10.93	0.57	0.12	G	112.28	20.68	93.58	16.59
3441484760885586176	86.43715	27.06790	3.62280	11.67	12.56	10.71	1.13	0.15	L	134.91	24.85	116.22	20.61
429562773322439296	3.51343	60.98626	3.63045	11.91	12.73	11.01	0.99	0.13	L	134.73	24.82	117.57	20.85
457807268533229056	38.46902	57.02750	3.64942	11.13	11.84	10.31	0.84	0.08	L	134.29	24.74	113.64	20.15
5329405672431387648	130.00864	-47.19842	3.67080	13.98	14.88	13.03	1.14	0.14	G	133.80	24.65	114.56	20.31
5351721738384434048	157.29679	-57.61339	3.68221	8.08	8.45	7.59	0.14	0.03	L	133.54	24.60	114.45	20.29
5542528959037609984	127.24360	-36.23207	3.70536	11.33	12.03	10.52	0.77	0.12	G	133.02	24.50	115.26	20.44
5539023922122441728	118.71081	-37.62246	3.70789	12.47	13.45	11.50	1.23	0.15	G	132.96	24.49	114.42	20.29
4707044742055169152	9.21974	-66.59323	3.72828	16.74	17.10	16.23	0.14	0.11	G	132.51	24.41	115.18	20.42
2202500843341252736	328.64443	59.12168	3.75817	13.83	14.85	12.81	1.34	0.15	G	131.85	24.29	111.95	19.85
2200018111723748224	335.91092	57.68078	3.76750	11.66	12.55	10.75	1.06	0.14	L	131.64	24.25	114.26	20.26
3445039825569144192	86.71173	31.59791	3.04664	11.88	12.55	11.09	0.76	0.1	L	150.36	27.70	130.52	23.14
3378049163365268608	100.78130	20.93911	3.78798	9.70	10.10	9.22	0.28	0.07	L	131.19	24.17	104.58	18.54
5856994365517642112	194.75148	-68.57855	3.79741	13.12	13.58	12.60	0.19	0.11	G	130.99	24.13	117.37	20.81
5311409896910828800	137.14651	-53.19702	3.80582	13.72	14.48	12.86	0.89	0.13	G	130.81	24.10	113.12	20.06
430647231080076416	5.01280	63.17979	3.81071	11.68	12.53	10.74	1.01	0.13	L	130.70	24.08	116.56	20.67
465719182408723072	41.18048	61.46470	3.83288	10.43	11.14	9.64	0.76	0.09	L	130.23	23.99	112.44	19.94
6059635702888301952	190.35842	-59.79419	3.83834	7.99	8.43	7.42	0.33	0.04	L	130.11	23.97	109.04	19.33
509629965971797376	25.81989	59.99762	3.84314	12.33	13.18	11.42	1.02	0.13	G	130.01	23.95	112.09	19.87
2031776202613700480	296.20306	29.26468	3.84599	6.69	7.01	6.22	0.17	0.04	L	129.95	23.94	104.24	18.48
2012494342018730496	353.33454	61.11907	3.87118	12.21	13.18	11.23	1.22	0.14	G	129.42	23.84	110.86	19.65
5619369359933924992	111.25618	-23.15791	3.89113	13.75	14.75	12.76	1.26	0.15	G	129.01	23.76	110.43	19.58
2072235820984829312	299.71473	37.64725	3.89187	14.29	14.88	13.51	0.67	0.12	G	128.99	23.76	109.48	19.41
2072329902270080128	299.38702	38.09177	3.89671	13.59	14.22	12.81	0.68	0.12	G	128.89	23.74	110.65	19.62
5335934297643679360	172.92831	-60.73455	3.89770	13.14	13.88	12.32	0.78	0.1	O	128.87	23.74	114.23	20.25

TABLE A.7: continued.

Gaia DR2 Source Id	RA	DEC	P	G	G_{BP}	G_{RP}	E(G_{BP}-G_{RP})	σE(G_{BP}-G_{RP})	Note	t_{PA}	$\sigma\ t_{PA}$	t_{PAC}	$\sigma\ t_{PAC}$
(1)	(2)	(3)	(4)	(5)	(6)	(7)	(8)	(9)	(10)	(11)	(12)	(13)	(14)
4253603501158148736	280.61175	-5.34085	3.91771	10.51	11.41	9.60	1.05	0.1	L	128.46	23.66	112.95	20.03
5615233993628681216	112.66125	-24.68752	3.91882	13.09	13.87	12.21	0.91	0.11	O	128.44	23.66	112.15	19.88
2010134274671099264	345.33801	57.86702	3.91921	11.49	12.30	10.62	0.92	0.12	L	128.43	23.66	112.91	20.02
3052092481686246016	107.65830	-7.12290	3.28782	12.52	13.23	11.64	0.68	0.09	L	143.36	26.41	140.03	24.83
5540422122959807232	125.36087	-38.42170	3.96098	12.55	13.54	11.57	1.22	0.13	O	127.58	23.50	110.53	19.60
5606739884038472704	109.26954	-28.82351	3.96993	12.72	13.24	12.05	0.45	0.11	G	127.40	23.47	110.42	19.58
486834100624652800	54.08395	62.28723	3.99690	12.74	13.79	11.72	1.31	0.17	L	126.86	23.37	110.88	19.66
2015458213056909184	351.49362	61.26683	4.00024	12.51	13.36	11.59	0.92	0.12	L	126.79	23.36	117.37	20.81
506923449381427968	32.69322	59.25369	4.00720	12.24	13.07	11.35	0.94	0.12	L	126.65	23.33	112.25	19.90
5238994102591371776	162.35781	-66.62534	4.01417	14.04	14.61	13.31	0.56	0.11	G	126.52	23.31	109.25	19.37
514674933331699584	32.62154	63.29753	4.03790	10.27	10.96	9.49	0.76	0.1	L	126.05	23.22	106.14	18.82
2166861170366710272	313.73970	47.53379	4.04921	10.29	11.11	9.41	1.02	0.13	L	125.83	23.18	104.29	18.49
5242076514741190272	162.97536	-61.46728	4.05483	12.23	12.91	11.45	0.68	0.1	O	125.72	23.16	111.91	19.84
5530071831587999232	129.78343	-37.37551	4.06392	12.24	12.87	11.48	0.66	0.09	O	125.55	23.13	107.31	19.03
422923956470923008	3.79087	58.42428	4.07117	9.54	10.14	8.83	0.61	0.06	L	125.41	23.10	105.27	18.66
5545837900614099584	121.29597	-34.36027	4.08860	11.73	12.56	10.84	0.9	0.11	O	125.07	23.04	112.92	20.02
5254281334339678208	160.11285	-60.07640	4.08916	13.97	14.91	12.96	1.25	0.15	G	125.06	23.04	104.89	18.60
5241961409628951296	162.73299	-62.09798	4.09530	14.32	15.12	13.43	0.99	0.11	O	124.94	23.02	105.05	18.62
5861648327739540736	193.74820	-65.20062	4.10167	14.64	15.63	13.62	1.28	0.13	O	124.82	22.99	106.69	18.92
511706805997227648	25.25207	63.05553	4.13309	12.66	13.61	11.69	1.19	0.14	G	124.23	22.88	106.37	18.86
3127458403130026112	101.78917	3.96710	4.13423	10.21	10.72	9.53	0.42	0.04	L	124.20	22.88	108.56	19.25
462252662762965120	50.94951	59.35567	4.15636	11.84	12.87	10.84	1.22	0.16	L	123.79	22.80	111.23	19.72
5321257604065975040	128.76428	-52.47757	4.15812	14.51	15.28	13.68	0.83	0.13	G	123.76	22.80	108.25	19.19
2031590552598614784	295.87018	29.23810	4.15973	14.49	15.30	13.56	1.02	0.13	G	123.73	22.79	104.88	18.60
5852389305960163328	208.75541	-64.03195	4.16962	11.28	12.18	10.36	1.06	0.14	G	123.54	22.76	107.31	19.03
5614191175568405376	115.20408	-25.45771	4.17117	12.42	13.36	11.45	1.15	0.12	O	123.51	22.75	107.37	19.04
5619786177922254336	110.28102	-21.51060	4.17560	12.51	13.26	11.67	0.82	0.1	O	123.43	22.74	108.01	19.15
2934506447605426944	105.97944	-17.87991	4.20487	11.59	12.31	10.79	0.75	0.12	G	122.89	22.64	107.23	19.01
4690834328595493760	16.04228	-70.95614	4.20529	15.60	15.92	15.22	0.0	0.11	G	122.89	22.64	103.00	18.26

TABLE A.7: continued.

Gaia DR2 Source Id	RA	DEC	P	G	G_{BP}	G_{RP}	E(G_{BP}-G_{RP})	σE(G_{BP}-G_{RP})	Note	t_{PA}	$\sigma\ t_{PA}$	t_{PAC}	$\sigma\ t_{PAC}$
(1)	(2)	(3)	(4)	(5)	(6)	(7)	(8)	(9)	(10)	(11)	(12)	(13)	(14)
5253875717619475200	158.46303	-61.80622	4.23097	14.74	15.57	13.80	1.07	0.12	O	122.42	22.55	102.30	18.14
1981367545804985088	329.05685	52.98601	4.23698	11.95	12.85	11.02	1.07	0.14	G	122.31	22.53	105.32	18.67
515832929535462016	41.08082	64.76592	4.23841	10.96	11.83	10.06	1.01	0.13	G	122.28	22.53	106.40	18.87
5254653759541047424	155.20707	-61.25195	4.23925	13.98	14.57	13.25	0.57	0.12	G	122.27	22.52	105.78	18.75
5587972801102905984	113.75856	-35.91299	4.24340	12.16	12.74	11.47	0.5	0.11	G	122.19	22.51	106.66	18.91
5521352536886237952	123.41069	-42.69920	4.24935	13.62	14.40	12.76	0.89	0.13	G	122.09	22.49	105.34	18.68
3027940437469882880	110.38690	-16.68722	4.25689	9.32	9.95	8.59	0.64	0.06	L	121.95	22.46	102.92	18.25
522468168674975616	18.17150	61.21335	4.25925	10.96	11.64	10.19	0.63	0.07	L	121.91	22.46	109.76	19.46
5338024572321721216	164.46108	-60.74208	4.26618	9.44	9.99	8.79	0.55	0.07	L	121.79	22.43	98.39	17.44
510584788742165760	19.00502	61.62071	4.27770	11.35	12.36	10.37	1.16	0.15	L	121.58	22.40	110.40	19.57
2014609252631258496	342.09618	60.40476	4.27863	11.57	12.60	10.58	1.27	0.15	G	121.56	22.39	104.95	18.61
5620400182140135168	112.95453	-20.14966	4.28543	10.96	11.65	10.18	0.67	0.06	L	121.44	22.37	107.98	19.14
2033008274099620480	296.26534	31.33077	4.28897	12.25	13.01	11.39	0.87	0.11	L	121.38	22.36	104.31	18.49
228741784865956224	64.27528	41.73183	4.29045	10.67	11.41	9.90	0.72	0.09	L	121.35	22.35	107.04	18.98
429890595286480384	0.67404	61.86107	4.30528	12.11	13.08	11.13	0.99	0.13	L	121.09	22.31	119.51	21.19
1977074811892425600	332.26210	51.04585	4.32355	8.96	9.40	8.39	0.29	0.04	L	120.77	22.25	102.21	18.12
2074102933481447808	301.83830	40.17809	4.32699	13.77	14.52	12.91	0.82	0.08	L	120.71	22.24	106.25	18.84
5311298983669288832	136.84989	-54.09276	4.35093	13.37	13.93	12.65	0.52	0.11	G	120.30	22.16	103.83	18.41
2060021625508894592	302.28232	37.15195	4.36470	9.49	10.10	8.77	0.61	0.1	L	120.06	22.12	100.66	17.85
429385923752386944	0.24680	60.95900	4.36516	10.86	11.53	9.96	0.9	0.07	L	120.05	22.11	97.53	17.29
2006033847910275584	335.02002	56.06090	4.36625	12.13	12.97	11.21	1.01	0.13	G	120.03	22.11	102.76	18.22
204588190167650048	71.39513	43.57284	4.37214	13.22	14.18	12.25	1.19	0.14	G	119.93	22.09	102.51	18.17
4693901042617667584	27.66874	-70.50366	4.37264	15.68	15.92	15.29	0.0	0.11	G	119.92	22.09	95.77	16.98
5594091823824942464	119.66611	-33.50405	4.40279	11.64	12.44	10.78	0.84	0.1	O	119.41	22.00	107.69	19.09
197337185858157440	84.11148	44.59136	4.40345	11.82	12.43	11.25	0.48	0.06	L	119.39	21.99	99.22	17.59
6055722403534963840	195.79449	-60.87747	4.42452	9.46	10.21	8.65	0.78	0.08	L	119.04	21.93	104.00	18.44
3397212822106196992	81.77704	16.93643	4.43840	12.75	13.32	12.06	0.48	0.11	G	118.81	21.88	104.10	18.46
2936110669428633216	106.65835	-15.80206	4.46484	12.42	13.21	11.56	0.82	0.1	O	118.36	21.80	106.60	18.90
5881952871520184960	234.52125	-58.69441	4.47575	15.24	16.25	14.22	1.32	0.13	O	118.18	21.77	99.06	17.56

TABLE A.7: continued.

Gaia DR2 Source Id	RA	DEC	P	G	G_{BP}	G_{RP}	E(G_{BP}-G_{RP})	σE(G_{BP}-G_{RP})	Note	t_{PA}	$\sigma\ t_{PA}$	t_{PAC}	$\sigma\ t_{PAC}$
(1)	(2)	(3)	(4)	(5)	(6)	(7)	(8)	(9)	(10)	(11)	(12)	(13)	(14)
2011892320749270912	359.53791	61.21363	4.47861	10.57	11.12	9.66	0.74	0.07	L	118.14	21.76	99.57	17.65
2005011237689458688	335.31995	54.53204	4.47944	11.44	12.16	10.63	0.76	0.07	L	118.12	21.76	101.92	18.07
5254078504458244352	160.72436	-61.02361	4.48366	12.84	13.68	11.94	0.97	0.11	O	118.05	21.75	102.18	18.12
426881614218441600	12.47192	60.12738	4.50162	9.55	10.21	8.79	0.7	0.08	L	117.76	21.69	99.25	17.60
5254000340399606016	157.26590	-60.78069	4.50519	14.48	15.29	13.56	1.03	0.11	O	117.70	21.68	98.04	17.38
5594382644652353664	119.05201	-32.60264	4.51675	11.53	12.38	10.70	0.87	0.13	G	117.51	21.65	104.57	18.54
5850308411442294400	206.85370	-68.24990	4.52474	13.65	14.14	13.00	0.37	0.11	G	117.38	21.62	101.46	17.99
4054440301294394624	262.70159	-33.60992	4.52781	7.55	8.14	6.92	0.48	0.05	L	117.33	21.61	99.80	17.69
5534012004528220160	119.94883	-42.02838	4.54706	13.90	14.74	12.98	1.01	0.13	G	117.02	21.56	99.94	17.72
506699870563323264	33.28119	58.07995	4.56524	11.27	11.94	10.55	0.62	0.06	L	116.73	21.50	100.73	17.86
2012787293154800896	358.60238	62.14947	4.56615	11.45	12.28	10.57	0.96	0.12	L	116.71	21.50	99.82	17.70
5338148473537341312	165.30989	-60.11656	4.58610	11.08	11.81	10.25	0.76	0.07	L	116.40	21.44	102.76	18.22
4690829659971892480	16.84515	-70.88734	4.59426	15.88	16.22	15.37	0.09	0.11	G	116.27	21.42	99.99	17.73
5253884788591163648	158.53969	-61.59759	4.61631	13.91	14.75	12.99	1.01	0.11	O	115.92	21.35	99.13	17.58
5253661725170126720	159.49855	-62.20590	4.63195	14.41	15.35	13.63	0.9	0.11	O	115.67	21.31	103.28	18.31
1981006115714214912	327.39800	52.39523	4.63908	11.46	12.45	10.48	0.91	0.23	L	115.56	21.29	119.68	21.22
5521459979795304320	129.42007	-47.36195	4.63985	7.71	8.26	7.05	0.38	0.04	L	115.55	21.29	104.23	18.48
2170880813073764352	322.34628	49.11002	4.64071	11.77	12.62	10.87	0.99	0.13	G	115.54	21.28	99.48	17.64
3044483895581000192	107.31421	-13.78609	4.67003	10.09	10.85	9.26	0.77	0.07	L	115.08	21.20	102.54	18.18
5338207327417387520	163.13667	-60.52675	4.67416	10.94	11.55	10.19	0.54	0.08	L	115.02	21.19	102.22	18.12
5338438297925480320	162.89899	-59.38499	4.67767	9.41	9.97	8.73	0.52	0.04	L	114.96	21.18	96.83	17.17
3046774762417915136	109.15680	-11.48730	4.67830	7.83	8.33	7.20	0.32	0.03	L	114.95	21.18	101.79	18.05
6060173364061645696	193.59158	-58.43063	4.68971	6.36	6.80	5.79	0.23	0.03	L	114.78	21.14	100.13	17.75
5861196531541297664	187.06483	-65.04976	4.72838	14.52	15.34	13.58	1.06	0.12	O	114.19	21.03	94.22	16.71
1998384927774603520	359.11116	58.02686	4.73481	11.71	12.60	10.79	1.03	0.13	G	114.09	21.02	98.50	17.46
5242088403212116864	163.61189	-61.34710	4.75984	11.54	12.32	10.69	0.85	0.13	G	113.72	20.95	98.71	17.50
5533407170051636608	122.95171	-42.05164	4.76441	14.79	15.90	13.77	1.36	0.15	G	113.65	20.93	97.92	17.36
5541229748611783296	123.70107	-37.65190	4.78070	13.80	14.82	12.79	1.24	0.13	O	113.41	20.89	98.71	17.50
3051692843568009600	106.78562	-7.79513	4.49659	12.54	13.27	11.70	0.87	0.11	L	117.84	21.71	98.06	17.39

TABLE A.7: continued.

Gaia DR2 Source Id	RA	DEC	P	G	G_{BP}	G_{RP}	E(G_{BP}-G_{RP})	σE(G_{BP}-G_{RP})	Note	t_{PA}	$\sigma\ t_{PA}$	t_{PAC}	$\sigma\ t_{PAC}$
(1)	(2)	(3)	(4)	(5)	(6)	(7)	(8)	(9)	(10)	(11)	(12)	(13)	(14)
2011303326105008768	353.74839	59.35815	4.78948	12.14	13.26	11.08	1.45	0.16	G	113.28	20.87	95.28	16.89
3099066951319051008	102.70284	-7.98073	4.80971	12.57	13.26	11.77	0.62	0.08	L	112.98	20.81	103.42	18.34
5864184488751391744	203.61003	-64.37098	4.82483	14.71	15.56	13.75	1.31	0.13	O	112.76	20.77	82.04	14.55
5329338700985814656	130.05832	-47.55156	4.82751	13.24	14.15	12.28	1.12	0.14	G	112.72	20.76	95.89	17.00
2928116120387181824	108.72647	-22.23586	4.84478	12.81	13.54	11.97	0.8	0.12	G	112.47	20.72	96.74	17.15
5306782361701536128	140.15436	-56.85401	4.86219	13.91	14.60	13.11	0.72	0.12	G	112.21	20.67	96.53	17.11
1960750328384177408	327.92260	43.13402	4.86438	8.67	9.19	8.03	0.39	0.04	L	112.18	20.66	96.20	17.06
2011892703004353792	359.57487	61.22105	4.87514	10.66	11.41	9.83	0.75	0.07	L	112.03	20.64	100.07	17.74
3344297935963515008	91.43635	13.23999	4.90958	11.89	12.64	11.03	0.71	0.06	L	111.53	20.55	103.93	18.43
2078709577944648192	297.06443	43.12692	4.92549	8.90	9.42	8.26	0.43	0.05	L	111.31	20.50	93.72	16.62
5258574068220187648	153.88689	-58.17444	4.93255	10.24	10.94	9.46	0.59	0.08	L	111.21	20.49	103.12	18.28
2060460704279873536	304.19788	36.54994	4.94524	11.57	12.65	10.54	1.45	0.19	L	111.03	20.45	89.03	15.78
2055122987639665664	301.33609	32.65909	4.95045	12.27	13.38	11.21	1.35	0.18	L	110.96	20.44	97.92	17.36
270272675510149504	64.94524	48.95326	4.97249	9.12	9.99	8.23	0.92	0.09	L	110.65	20.38	99.09	17.57
5333640230992516480	173.32410	-63.24240	4.97458	11.78	12.80	10.78	1.26	0.15	G	110.62	20.38	94.32	16.72
3351921532976862336	100.15651	11.72748	4.97853	11.77	12.69	10.82	1.1	0.14	G	110.56	20.37	94.75	16.80
2003938801532007808	342.15829	56.32153	4.98330	8.61	9.15	7.94	0.4	0.06	L	110.50	20.35	97.47	17.28
6057402526059795072	181.66763	-62.59685	4.98851	12.06	13.02	11.10	1.14	0.12	O	110.43	20.34	95.74	16.97
2011315528113463808	354.70162	59.39182	4.99754	10.50	11.42	9.58	1.09	0.1	L	110.30	20.32	93.55	16.59
5699042480743325312	120.09545	-23.70317	5.02730	10.08	10.53	9.49	0.26	0.04	L	109.89	20.24	94.94	16.83
515599111517099136	33.60315	65.59945	5.02942	11.90	12.75	11.01	0.7	0.12	L	109.86	20.24	112.38	19.93
2164359918864249728	316.94415	46.73698	5.05758	11.90	12.74	11.01	0.99	0.13	L	109.48	20.17	92.41	16.38
3390186156826555136	79.69992	13.98667	5.06607	11.52	12.19	10.67	0.78	0.12	G	109.36	20.15	92.30	16.37
473293889810320128	57.10698	59.44227	5.06643	10.00	11.16	8.95	1.01	0.1	L	109.36	20.14	123.37	21.87
5595650351503904896	118.45324	-30.46031	5.07756	10.55	11.29	9.73	0.74	0.07	L	109.21	20.12	96.62	17.13
5871738271033526016	207.68449	-57.58051	5.07890	7.43	7.89	6.85	0.28	0.03	L	109.19	20.11	93.06	16.50
2166303099490547072	311.55230	45.47861	5.09955	10.53	11.69	9.46	1.45	0.19	L	108.91	20.06	94.48	16.75
5241157421762533248	162.23993	-64.17420	5.10249	13.62	14.29	12.82	0.7	0.12	G	108.88	20.06	93.48	16.57
5307006215391311360	142.54990	-56.80824	5.13704	14.57	15.64	13.51	1.39	0.14	O	108.42	19.97	90.86	16.11

TABLE A.7: continued.

Gaia DR2 Source Id	RA	DEC	P	G	G_{BP}	G_{RP}	E(G_{BP}-G_{RP})	σE(G_{BP}-G_{RP})	Note	t_{PA}	$\sigma\ t_{PA}$	t_{PAC}	$\sigma\ t_{PAC}$
(1)	(2)	(3)	(4)	(5)	(6)	(7)	(8)	(9)	(10)	(11)	(12)	(13)	(14)
2011892325047232256	359.53933	61.21370	5.14077	10.49	11.07	9.62	0.75	0.1	L	108.37	19.96	88.56	15.70
4080122796947250176	281.32290	-20.64739	5.15424	7.25	7.83	6.58	0.42	0.04	L	108.19	19.93	95.99	17.02
4085919765884068736	282.74947	-20.29525	6.63703	6.63	7.21	5.93	0.38	0.03	L	92.35	17.01	83.44	14.79
1827869808377481216	296.64660	22.88975	5.19725	10.03	10.96	9.09	1.23	0.12	L	107.63	19.83	84.26	14.94
4690377382729299328	10.34143	-70.61853	5.20108	15.23	15.52	14.77	-0.0	0.11	G	107.58	19.82	91.22	16.17
5254295559276699392	159.07421	-61.01256	5.20456	9.06	9.56	8.44	0.29	0.05	L	107.53	19.81	95.63	16.96
5853170268450896768	219.37630	-63.62524	5.21445	14.44	15.27	13.50	1.08	0.12	O	107.41	19.78	87.23	15.47
5257939993613539456	147.08272	-57.81045	5.21666	12.34	13.28	11.37	1.15	0.12	O	107.38	19.78	91.51	16.22
513830684503187840	34.09382	62.55776	5.23993	12.62	13.62	11.62	1.23	0.15	G	107.08	19.72	91.42	16.21
5698636279917579520	119.52141	-24.04176	5.25024	10.34	10.80	9.73	0.35	0.05	L	106.95	19.70	88.44	15.68
1968971582984827136	318.66850	41.71634	5.25760	8.88	9.91	7.90	1.22	0.11	L	106.85	19.68	92.17	16.34
189726984845700480	86.05833	37.58687	5.25943	11.56	12.33	10.81	0.74	0.1	L	106.83	19.68	91.88	16.29
6053622679932061056	188.32775	-63.50637	5.26567	9.01	9.91	8.12	0.86	0.09	L	106.75	19.66	100.60	17.84
5594100246268225280	119.84298	-33.35713	5.28196	13.39	14.27	12.46	1.01	0.11	O	106.54	19.63	93.08	16.50
4147381366335558784	272.50888	-13.54596	5.30141	9.96	11.03	8.94	1.31	0.11	L	106.30	19.58	91.06	16.14
5334506135119058304	171.27392	-60.73461	5.30996	8.49	9.08	7.79	0.48	0.1	L	106.19	19.56	92.54	16.41
5307761545524640256	147.17283	-55.51953	5.32402	9.79	10.57	8.95	0.79	0.1	L	106.02	19.53	93.26	16.53
1960981328902089088	330.10480	43.44535	5.33166	8.57	9.13	7.90	0.45	0.05	L	105.92	19.51	90.74	16.09
5338215200143652992	163.78784	-60.54772	5.33671	11.44	12.27	10.56	0.92	0.13	G	105.86	19.50	91.37	16.20
5255220656517219840	156.71194	-59.66953	5.34632	9.03	9.64	8.31	0.58	0.05	L	105.74	19.48	89.30	15.83
458239995077788544	38.63042	58.83162	5.36511	10.46	11.49	9.51	1.2	0.1	L	105.51	19.44	90.56	16.06
4190143160245024256	298.08750	-11.36692	5.37668	7.54	8.03	6.92	0.25	0.03	L	105.37	19.41	95.07	16.86
2010285491880986112	346.79198	58.55419	5.44090	9.28	9.96	8.51	0.64	0.06	L	104.59	19.27	91.29	16.18
5547742052903182080	122.60782	-32.52136	5.46460	10.99	11.72	10.18	0.74	0.12	G	104.30	19.21	90.70	16.08
5312211543950752128	142.56597	-53.05868	5.48394	11.19	12.09	10.25	1.06	0.14	G	104.07	19.17	89.33	15.84
5338131529834231680	164.77043	-60.27884	5.49457	11.65	12.46	10.76	0.91	0.13	G	103.94	19.15	89.36	15.84
5891675303053080704	218.13779	-56.88775	5.49457	6.55	7.11	5.93	0.36	0.04	L	103.94	19.15	91.48	16.22
523887951723531648	11.62454	63.54327	5.51273	11.17	12.21	10.18	1.29	0.17	L	103.73	19.11	86.60	15.35
5715183929918131968	115.47870	-21.13306	5.51615	10.27	10.82	9.61	0.45	0.04	L	103.69	19.10	87.88	15.58

TABLE A.7: continued.

Gaia DR2 Source Id	RA	DEC	P	G	G_{BP}	G_{RP}	E(G_{BP}-G_{RP})	σE(G_{BP}-G_{RP})	Note	t_{PA}	$\sigma\ t_{PA}$	t_{PAC}	$\sigma\ t_{PAC}$
(1)	(2)	(3)	(4)	(5)	(6)	(7)	(8)	(9)	(10)	(11)	(12)	(13)	(14)
459035766618689280	36.89776	58.91715	5.53070	10.37	11.47	9.37	1.28	0.11	L	103.52	19.07	90.92	16.12
5253795384546671104	158.01837	-61.78262	5.54225	8.70	9.18	8.09	0.25	0.03	L	103.38	19.04	91.48	16.22
4103989346187406464	276.80604	-15.11799	5.54693	10.07	10.94	9.18	0.95	0.13	G	103.33	19.03	89.87	15.93
5539107450645759232	118.43778	-36.97038	5.56408	10.59	11.47	9.75	0.88	0.13	G	103.13	19.00	91.69	16.26
5254512193075687168	158.63079	-59.80854	5.57332	11.84	12.94	10.79	1.31	0.13	O	103.02	18.98	91.75	16.27
5525918495131126912	126.02410	-44.85228	5.59210	13.08	14.24	12.02	1.45	0.16	G	102.81	18.94	87.04	15.43
506602976101284736	26.76131	59.60626	5.60412	13.19	13.92	12.35	0.64	0.15	L	102.67	18.91	96.65	17.14
5283779135317992448	98.37366	-65.99373	5.63702	15.67	16.06	15.11	0.16	0.11	G	102.29	18.84	87.95	15.59
2005753545481718912	331.89771	55.36274	5.65812	12.18	13.11	11.22	1.23	0.12	L	102.05	18.80	80.97	14.36
5242185808733501696	162.09637	-60.65394	5.66418	12.16	12.99	11.26	0.93	0.11	O	101.98	18.79	88.35	15.66
2015622212085282048	354.86371	62.37214	5.66617	11.06	12.01	10.12	1.03	0.09	L	101.96	18.78	91.13	16.16
2202863166783787520	330.67041	59.45248	5.68839	13.10	14.14	12.10	1.26	0.15	G	101.71	18.74	86.89	15.41
5261561063335550208	95.02971	-75.36110	5.70035	15.26	15.65	14.69	0.17	0.11	G	101.58	18.71	86.90	15.41
2931247014102560000	108.29864	-18.73074	5.72861	10.60	11.39	9.75	0.62	0.12	L	101.27	18.65	100.41	17.80
2034428980559814400	299.89044	33.74604	5.78290	11.05	11.99	10.12	0.99	0.13	L	100.67	18.54	91.08	16.15
5600471160241231616	118.49014	-28.36762	5.80047	12.61	13.41	11.73	0.91	0.11	O	100.48	18.51	84.75	15.03
422226488141991296	3.61766	56.25293	5.80901	8.78	9.37	8.08	0.44	0.08	L	100.39	18.49	88.92	15.77
5613165915335320192	111.16913	-26.18849	5.81585	11.45	12.33	10.54	0.94	0.12	L	100.31	18.48	89.37	15.85
5327836325732931840	131.23286	-50.56002	5.85935	9.21	9.96	8.39	0.72	0.07	L	99.84	18.39	88.97	15.77
5595072420703114624	116.96477	-32.17133	5.86387	13.12	14.08	12.16	1.13	0.14	G	99.80	18.38	85.09	15.09
5544213926244557184	120.20160	-37.82794	5.88476	10.63	11.53	9.71	1.02	0.13	G	99.57	18.34	85.67	15.19
5436296928693979392	143.46188	-36.61574	5.89839	9.12	9.52	8.58	0.41	0.05	L	99.43	18.32	72.21	12.80
467560314629168640	41.46454	63.30457	5.90466	11.96	12.78	11.08	0.91	0.12	L	99.36	18.30	84.78	15.03
5308893149150949248	145.29272	-53.81604	5.90482	11.10	11.98	10.19	0.97	0.09	L	99.36	18.30	86.72	15.38
2055014277739104896	303.09511	32.87160	5.95590	8.91	9.76	8.02	0.88	0.09	L	98.83	18.20	88.11	15.62
5927687916632523264	250.53743	-57.31247	5.95730	12.82	13.38	12.12	0.46	0.11	G	98.81	18.20	85.19	15.10
5544001136384668288	121.32198	-37.58019	6.02134	13.52	14.50	12.51	1.23	0.13	O	98.15	18.08	81.50	14.45
4092905375639902464	277.97221	-19.12510	6.74522	6.35	7.01	5.62	0.55	0.05	L	91.42	16.84	79.40	14.08
1808020329279916288	300.29090	15.80350	6.10820	9.90	10.44	9.26	0.31	0.04	L	97.28	17.92	87.39	15.49

TABLE A.7: continued.

Gaia DR2 Source Id	RA	DEC	P	G	G_{BP}	G_{RP}	E(G_{BP}-G_{RP})	σE(G_{BP}-G_{RP})	Note	t_{PA}	$\sigma\ t_{PA}$	t_{PAC}	$\sigma\ t_{PAC}$
(1)	(2)	(3)	(4)	(5)	(6)	(7)	(8)	(9)	(10)	(11)	(12)	(13)	(14)
4312361436842603520	287.31663	10.55247	6.11423	7.66	8.44	6.84	0.86	0.07	L	97.22	17.91	80.07	14.20
6053428684887800320	185.88240	-64.47089	6.12121	11.32	12.29	10.35	0.96	0.09	L	97.15	17.90	92.85	16.46
4303770918113986304	299.38759	11.04366	6.17926	9.72	10.21	9.10	0.14	0.02	L	96.58	17.79	91.95	16.30
4093976334264606976	273.85944	-20.62955	6.17945	10.19	11.07	9.25	1.11	0.14	L	96.58	17.79	77.80	13.79
5932812431123862016	241.29147	-53.91943	6.19933	9.48	10.30	8.64	0.78	0.08	L	96.38	17.75	86.71	15.37
506581226385580288	27.77925	59.88821	6.20627	10.30	11.02	9.50	0.66	0.06	L	96.31	17.74	85.09	15.09
6059764002146656128	191.59278	-59.12473	6.22040	8.07	8.64	7.38	0.4	0.04	L	96.18	17.72	85.67	15.19
2059598687167348352	299.44206	35.63605	6.22543	12.68	13.69	11.69	1.26	0.16	L	96.13	17.71	79.05	14.02
2008504454839717120	341.60318	59.44219	6.23397	9.00	9.92	8.08	0.95	0.08	L	96.05	17.69	87.16	15.45
430670222050230912	9.18544	62.27424	6.24022	11.73	12.72	10.75	1.16	0.15	L	95.99	17.68	82.72	14.67
525136962570940160	18.75456	65.59940	6.27279	10.23	11.24	9.28	1.17	0.1	L	95.67	17.62	81.23	14.40
2015820463470505600	354.31691	62.42899	6.29664	9.24	10.22	8.28	1.08	0.09	L	95.45	17.58	84.96	15.06
4512950187838606464	286.51934	15.74941	6.30024	14.61	15.49	13.67	1.03	0.13	G	95.41	17.58	81.17	14.39
5823134325151372032	240.29463	-63.77655	6.31663	6.22	6.59	5.63	0.12	0.02	L	95.26	17.55	83.68	14.84
2027263738130844288	299.36918	26.55645	6.32059	8.23	9.14	7.30	1.05	0.09	L	95.22	17.54	81.20	14.40
1994462866719961216	354.40810	54.84718	6.33647	9.03	9.72	8.26	0.63	0.12	G	95.07	17.51	82.76	14.67
5339149677605627264	169.58945	-59.23796	6.39427	12.57	13.31	11.72	0.77	0.1	O	94.53	17.41	81.54	14.46
6057514092119497472	183.24857	-62.09682	6.39726	10.47	11.36	9.60	0.86	0.07	L	94.50	17.41	85.60	15.18
2006989121667184384	340.36050	56.43277	6.41896	8.55	9.09	7.89	0.36	0.04	L	94.30	17.37	82.57	14.64
4096979650282842112	276.18542	-16.79717	6.42429	8.41	9.08	7.59	0.67	0.06	L	94.25	17.36	81.52	14.45
3291491450496573824	74.97904	10.28845	6.44163	14.32	14.74	13.69	0.27	0.11	G	94.10	17.33	79.23	14.05
5254071873026676864	160.70349	-61.12298	6.45365	11.21	11.96	10.38	0.75	0.12	G	93.99	17.31	81.37	14.43
5312196047720402048	143.34884	-52.75585	6.45380	11.06	12.07	10.08	1.14	0.1	L	93.98	17.31	82.86	14.69
5868480143187802240	199.74280	-62.38235	6.45975	8.08	8.71	7.34	0.5	0.08	L	93.93	17.30	83.38	14.78
174489098011145216	71.94298	36.72278	6.46466	7.05	7.73	6.27	0.65	0.06	L	93.89	17.29	80.57	14.28
513282131279401728	23.91530	65.33050	6.55713	12.49	13.65	11.42	1.45	0.16	G	93.05	17.14	78.29	13.88
4096140001386430080	275.82979	-18.57477	6.56959	9.80	10.83	8.83	1.13	0.09	L	92.94	17.12	82.30	14.59
272444829450300160	67.57792	53.94018	6.56983	11.86	12.74	10.95	0.96	0.13	G	92.94	17.12	80.28	14.23
5541507237862358912	123.09332	-36.94374	6.66423	7.71	8.14	7.16	0.22	0.02	L	92.12	16.97	76.39	13.54

TABLE A.7: continued.

Gaia DR2 Source Id	RA	DEC	P	G	G_{BP}	G_{RP}	E(G_{BP}-G_{RP})	σE(G_{BP}-G_{RP})	Note	t_{PA}	$\sigma\ t_{PA}$	t_{PAC}	$\sigma\ t_{PAC}$
(1)	(2)	(3)	(4)	(5)	(6)	(7)	(8)	(9)	(10)	(11)	(12)	(13)	(14)
5302258008774271488	127.18202	-60.12256	6.69695	7.11	7.60	6.50	0.22	0.03	L	91.83	16.92	81.75	14.49
5338072980840100608	165.93830	-60.64226	6.69721	9.84	10.49	9.10	0.59	0.06	L	91.83	16.92	77.94	13.82
4314923363333177984	293.01969	11.54976	6.69729	12.54	13.22	11.75	0.65	0.12	G	91.83	16.92	79.10	14.02
2177714415280658944	323.72762	55.94226	6.71632	12.85	13.93	11.82	1.31	0.15	G	91.67	16.89	77.65	13.77
6054829806275577216	185.33793	-62.28164	6.73287	6.30	6.81	5.68	0.26	0.04	L	91.53	16.86	81.46	14.44
429544700100302080	4.26041	60.80280	6.79828	13.65	14.60	12.67	1.02	0.13	L	90.97	16.76	82.86	14.69
4204653587029046400	287.08654	-7.43777	6.80601	7.34	8.02	6.57	0.58	0.05	L	90.91	16.75	80.55	14.28
5935042378098601856	243.98144	-51.12073	6.81248	10.33	11.31	9.38	1.1	0.14	G	90.86	16.74	78.57	13.93
4505300988492333312	281.47541	12.33610	7.50794	9.75	10.36	9.00	0.53	0.07	L	85.49	15.75	73.09	12.96
430766016998901376	8.31747	62.90726	6.84634	10.97	11.87	10.07	1.04	0.09	L	90.57	16.68	74.60	13.23
5324034867356093056	137.06555	-51.43625	6.92436	7.22	7.93	6.44	0.59	0.05	L	89.93	16.57	80.98	14.36
2030848897634605440	300.19314	30.90759	6.96110	12.11	13.21	11.06	1.41	0.18	L	89.64	16.51	72.40	12.84
5352181712213705856	159.03578	-56.04323	6.98477	10.22	10.83	9.31	0.72	0.06	L	89.45	16.48	75.69	13.42
3031875585286182144	110.50990	-14.31818	6.99483	9.24	9.82	8.54	0.5	0.06	L	89.37	16.46	74.30	13.17
5334563996911649408	179.47384	-62.64613	7.00373	11.44	12.37	10.49	1.06	0.14	G	89.29	16.45	76.45	13.56
5903821951590649600	228.74274	-46.87257	7.05894	13.89	14.42	13.21	0.37	0.11	G	88.86	16.37	76.47	13.56
5877533315817003648	219.29985	-62.01092	7.06626	6.42	6.96	5.77	0.31	0.04	L	88.80	16.36	79.05	14.01
3113441691460573312	102.63473	0.00700	7.09748	11.97	12.83	11.03	0.88	0.11	L	88.55	16.31	80.35	14.25
5240438203718296192	165.36850	-64.29067	7.12163	13.71	14.51	12.82	0.87	0.13	G	88.37	16.28	75.29	13.35
5309174967720762496	144.21441	-53.03278	7.13431	9.69	10.51	8.83	0.93	0.11	L	88.27	16.26	71.70	12.71
5860785795219397376	184.39009	-65.75399	7.13451	13.83	14.46	12.97	0.58	0.09	O	88.27	16.26	79.97	14.18
5257664497238811776	148.85895	-58.42969	7.19619	8.95	9.58	8.22	0.51	0.04	L	87.79	16.17	76.29	13.53
5600628115523816320	117.51301	-28.25514	7.19862	10.32	11.10	9.50	0.78	0.1	L	87.77	16.17	74.90	13.28
5626365410677889792	131.05061	-35.47371	7.21689	9.94	10.60	9.17	0.59	0.12	G	87.63	16.14	75.89	13.46
2174677564161400064	326.32669	54.49638	7.23099	11.38	12.40	10.39	1.19	0.14	G	87.53	16.12	74.47	13.20
2007997408188526336	337.20867	58.21093	7.23213	10.62	11.46	9.74	0.86	0.07	L	87.52	16.12	76.55	13.57
4307944836090489600	290.25978	8.51633	7.23996	9.35	10.33	8.39	1.1	0.09	L	87.46	16.11	75.36	13.36
2165771172070496512	317.72654	49.14204	7.25140	9.95	10.88	9.00	1.05	0.09	L	87.37	16.09	74.98	13.29
5335963189825411072	172.84735	-60.58341	7.34403	13.08	13.96	12.13	1.04	0.12	O	86.68	15.97	72.48	12.85

TABLE A.7: continued.

Gaia DR2 Source Id	RA	DEC	P	G	G_{BP}	G_{RP}	E(G_{BP}-G_{RP})	σE(G_{BP}-G_{RP})	Note	t_{PA}	$\sigma\ t_{PA}$	t_{PAC}	$\sigma\ t_{PAC}$
(1)	(2)	(3)	(4)	(5)	(6)	(7)	(8)	(9)	(10)	(11)	(12)	(13)	(14)
5613564621430610560	111.82868	-25.78535	7.41934	12.70	13.62	11.73	0.78	0.23	L	86.13	15.87	87.41	15.50
3112475495616980992	104.50389	-0.37596	7.42462	10.35	11.04	9.57	0.59	0.06	L	86.09	15.86	76.20	13.51
5855468247702904704	190.52089	-69.40756	7.51028	6.10	6.55	5.55	0.2	0.04	L	85.48	15.75	71.46	12.67
2934712880912798464	108.42673	-17.62026	7.51211	12.39	13.36	11.42	1.11	0.14	G	85.46	15.74	72.77	12.90
5337191279923824384	168.04213	-61.75487	7.53200	7.80	8.35	7.14	0.29	0.03	L	85.32	15.72	76.80	13.62
3368698813404804352	95.55497	14.67813	7.56688	8.12	8.76	7.42	0.45	0.04	L	85.07	15.67	75.28	13.35
5337958876494096256	165.10434	-60.99319	7.63695	12.31	13.20	11.37	0.99	0.11	O	84.58	15.58	72.35	12.83
5339394082770287232	167.42135	-58.83772	7.72081	6.61	7.08	6.01	0.15	0.02	L	84.01	15.47	75.78	13.44
5415098722470316544	152.59186	-44.15874	7.77785	13.69	14.15	13.08	0.23	0.11	G	83.62	15.40	71.88	12.74
2016028168089215488	356.26093	63.00385	7.80112	10.08	11.04	9.12	1.01	0.08	L	83.47	15.38	74.78	13.26
2030063919381336832	299.79498	29.45072	7.81823	9.37	10.16	8.51	0.82	0.07	L	83.35	15.35	70.84	12.56
1873112207907294848	316.06930	39.97223	7.85582	9.05	9.82	8.20	0.8	0.07	L	83.10	15.31	69.70	12.36
470361114339849472	61.24359	58.65978	7.91561	7.16	7.92	6.32	0.74	0.06	L	82.71	15.24	71.63	12.70
5614916921960857088	114.04436	-25.36403	7.96016	14.49	15.58	13.45	1.29	0.13	O	82.42	15.18	69.99	12.41
2170785842762144512	322.18718	48.97821	7.96686	10.10	10.90	9.24	0.8	0.12	G	82.37	15.17	71.12	12.61
1825621002188696448	294.15720	20.33293	7.99014	6.58	7.41	5.72	0.81	0.07	L	82.22	15.15	72.14	12.79
428620663657823232	7.49410	60.21196	8.00066	8.51	9.23	7.71	0.66	0.05	L	82.16	15.13	71.15	12.61
261548119462093568	77.66762	49.68760	8.00263	9.06	9.69	8.32	0.53	0.06	L	82.14	15.13	70.18	12.44
5236551193933797888	174.75935	-65.20662	8.00290	14.65	15.67	13.62	1.18	0.12	O	82.14	15.13	71.02	12.59
3050050207554658048	105.24924	-8.70898	8.01127	9.62	10.32	8.79	0.68	0.07	L	82.09	15.12	70.31	12.47
5852880955104044800	214.51090	-64.42147	8.19958	14.15	15.00	13.17	1.04	0.12	O	80.90	14.90	66.73	11.83
5887482762148283008	228.20632	-54.75528	8.22041	9.02	9.90	8.19	0.91	0.1	L	80.77	14.88	66.81	11.85
512524361613040640	23.18010	63.59380	8.37701	6.64	7.46	5.78	0.8	0.11	L	79.83	14.70	69.72	12.36
3329849043206545920	92.80659	9.61249	8.61488	8.67	9.24	7.99	0.3	0.03	L	78.44	14.45	71.16	12.62
202939854734748032	70.99117	40.83478	8.63925	11.13	11.87	10.29	0.72	0.06	L	78.30	14.42	67.23	11.92
5613972681993587200	115.49584	-25.87617	8.93422	8.74	9.31	8.04	0.41	0.04	L	76.67	14.12	65.29	11.58
5254097093074642944	159.83465	-61.15243	9.19783	8.80	9.39	8.12	0.24	0.03	L	75.29	13.87	71.48	12.67
4056026175045038464	267.15626	-30.47597	9.31686	8.24	9.08	7.43	0.77	0.07	L	74.69	13.76	64.44	11.43
5854560115494081024	215.45224	-61.54966	9.46519	8.26	8.97	7.47	0.58	0.05	L	73.95	13.62	65.49	11.61

TABLE A.7: continued.

Gaia DR2 Source Id	RA	DEC	P	G	G_{BP}	G_{RP}	E(G_{BP}-G_{RP})	σE(G_{BP}-G_{RP})	Note	t_{PA}	$\sigma\ t_{PA}$	t_{PAC}	$\sigma\ t_{PAC}$
(1)	(2)	(3)	(4)	(5)	(6)	(7)	(8)	(9)	(10)	(11)	(12)	(13)	(14)
4269036830424588800	288.19714	3.55740	9.48055	7.90	8.67	7.12	0.66	0.05	L	73.88	13.61	63.88	11.33
5329838158460391296	131.22276	-46.34296	9.56113	7.97	8.53	7.36	0.32	0.03	L	73.49	13.54	61.93	10.98
5835124087174043136	244.71595	-57.89980	9.75376	6.15	6.70	5.52	0.25	0.02	L	72.57	13.37	64.29	11.40
5351423049186195328	158.22527	-58.52100	9.75912	11.01	11.86	10.14	0.71	0.07	L	72.55	13.36	67.79	12.02
5993655659352495616	243.61906	-40.79315	9.76457	12.20	12.89	11.39	0.62	0.12	G	72.52	13.36	61.72	10.94
5254662177677566464	155.34567	-61.07408	9.76811	8.59	9.09	7.96	0.23	0.03	L	72.51	13.36	62.91	11.15
2013029941628292352	359.39565	62.71824	9.80569	9.44	10.16	8.65	0.66	0.06	L	72.33	13.32	61.10	10.83
5241804518715438336	165.39269	-62.21022	9.84085	12.20	13.06	11.27	0.92	0.11	O	72.17	13.29	61.36	10.88
5328248672646357120	132.04364	-48.65915	9.84168	11.91	13.00	10.91	1.19	0.11	L	72.17	13.29	62.56	11.09
5328949100222702848	130.67412	-48.68614	10.02929	14.30	15.33	13.28	1.19	0.14	G	71.32	13.14	60.00	10.64
4685261526923834496	2.60032	-75.17706	10.09004	14.71	15.03	14.23	0.0	0.11	G	71.05	13.09	57.80	10.25
2070224337474904064	311.49913	45.30694	10.14797	9.42	10.48	8.42	1.12	0.09	L	70.80	13.04	62.75	11.12
5337257834740652160	167.55357	-60.84747	10.27245	11.09	12.12	10.09	1.11	0.11	L	70.26	12.94	61.18	10.85
201574982848108416	74.92307	40.83603	10.30573	9.92	10.67	9.10	0.73	0.08	L	70.12	12.92	57.88	10.26
4156450099578283776	279.51377	-8.36895	10.34150	8.88	9.93	7.92	1.07	0.09	L	69.96	12.89	61.72	10.94
5241780677399802624	165.37783	-62.29079	10.35488	10.31	11.08	9.47	0.63	0.06	L	69.91	12.88	63.50	11.26
5859119760248045312	198.50696	-64.32488	10.35635	10.85	11.83	9.89	1.06	0.13	L	69.90	12.88	59.81	10.60
5538569613358406144	117.35518	-38.23935	10.50594	12.62	13.34	11.79	0.67	0.12	G	69.28	12.76	59.07	10.47
4267549637851481344	286.16423	1.30614	17.13794	7.88	8.66	7.00	0.75	0.07	L	51.00	9.39	42.00	7.45
5337764640889249536	168.58836	-60.05292	10.70960	9.27	9.92	8.51	0.45	0.05	L	68.45	12.61	61.13	10.84
506779550797525760	31.95200	58.44353	10.87727	8.84	9.58	8.04	0.65	0.06	L	67.79	12.49	57.71	10.23
2007201567928631296	340.21724	56.82946	10.88439	8.04	8.70	7.29	0.48	0.04	L	67.76	12.48	59.52	10.55
5871922507947292032	205.07765	-57.61318	10.94947	7.47	8.03	6.79	0.33	0.03	L	67.51	12.43	58.12	10.30
3027495856819349248	113.41167	-16.31710	10.98248	11.04	11.89	10.16	0.82	0.12	G	67.38	12.41	57.92	10.27
4256744187345732224	280.53297	-4.29349	11.05302	9.92	11.04	8.88	1.26	0.1	L	67.11	12.36	57.76	10.24
203496585576324224	72.44976	42.28970	11.11731	8.60	9.23	7.85	0.44	0.06	L	66.87	12.32	59.13	10.48
5611465073923671424	106.94491	-24.91952	11.18235	11.25	11.81	10.56	0.35	0.11	G	66.62	12.27	57.15	10.13
5313887130948758016	142.92069	-49.65499	11.20064	8.88	9.83	7.95	0.92	0.08	L	66.55	12.26	59.37	10.53
462407693902385792	52.35821	60.44647	11.27625	11.76	12.88	10.76	1.18	0.1	L	66.27	12.21	58.43	10.36

TABLE A.7: continued.

Gaia DR2 Source Id	RA	DEC	P	G	G_{BP}	G_{RP}	E(G_{BP}-G_{RP})	σE(G_{BP}-G_{RP})	Note	t_{PA}	$\sigma\ t_{PA}$	t_{PAC}	$\sigma\ t_{PAC}$
(1)	(2)	(3)	(4)	(5)	(6)	(7)	(8)	(9)	(10)	(11)	(12)	(13)	(14)
5932569709575669504	243.32248	-54.23490	11.28752	7.98	8.65	7.24	0.43	0.04	L	66.23	12.20	59.67	10.58
3430067092837622272	91.64561	26.32922	11.30513	9.34	9.97	8.64	0.47	0.06	L	66.17	12.19	55.55	9.85
2002637323358768000	343.65706	54.26545	11.31916	13.43	14.15	12.54	0.74	0.1	L	66.12	12.18	55.33	9.81
200708636406382720	75.34662	39.96038	11.62570	7.34	7.94	6.68	0.34	0.04	L	65.02	11.98	55.97	9.92
5332375453374624640	178.07378	-65.40418	11.63735	9.33	10.09	8.59	0.58	0.07	L	64.98	11.97	55.71	9.88
2030427789026783488	299.45419	30.26590	11.66304	10.42	11.28	9.52	1.05	0.13	L	64.89	11.95	49.05	8.70
2073922579215436288	301.01866	39.10421	11.92821	12.97	13.86	12.03	0.93	0.13	G	63.98	11.79	54.10	9.59
1999252442448732288	358.02928	58.74172	12.14061	9.32	10.20	8.46	0.86	0.08	L	63.28	11.66	53.21	9.43
5336389564126521728	175.70084	-58.99339	12.18311	10.90	11.71	10.02	0.75	0.08	L	63.14	11.63	54.76	9.71
6054992602724692608	188.59725	-61.23762	12.21766	11.13	12.23	10.11	1.29	0.12	L	63.03	11.61	51.14	9.07
4066375912402666624	274.06943	-23.30591	12.27464	15.32	16.30	14.35	1.29	0.13	O	62.85	11.58	45.96	8.15
5616601820448126336	111.52996	-25.25730	12.35350	9.39	10.15	8.59	0.74	0.06	L	62.59	11.53	49.95	8.86
5240441472232302848	165.56688	-64.26289	12.43802	8.85	9.60	8.06	0.53	0.05	L	62.33	11.48	56.30	9.98
5884729035255064064	238.67837	-54.56644	12.63346	8.96	9.87	8.03	0.82	0.1	L	61.72	11.37	55.89	9.91
470386952863752576	61.53736	58.80875	12.65005	10.26	11.19	9.37	0.7	0.09	L	61.67	11.36	59.75	10.59
5865206961464617088	201.62523	-63.16263	12.88787	11.05	12.22	10.01	1.34	0.21	L	60.96	11.23	50.26	8.91
4253435825622331392	280.73864	-5.82091	12.91058	9.10	9.92	8.35	0.72	0.08	L	60.89	11.22	49.45	8.77
5310669788148987520	139.59222	-54.41226	13.12071	13.73	14.71	12.75	1.06	0.14	G	60.28	11.10	50.71	8.99
5311616398935271168	140.00627	-52.85618	13.23958	10.85	11.86	9.89	0.98	0.11	L	59.94	11.04	53.04	9.40
4313179507891570304	287.50172	12.53654	13.43999	10.08	11.20	9.07	1.38	0.18	L	59.38	10.94	44.94	7.97
5350852677538959104	162.75755	-58.59059	13.45493	10.91	11.91	9.97	0.94	0.08	L	59.34	10.93	53.22	9.44
5600915775257809152	119.42569	-27.60189	13.45979	11.49	12.36	10.66	0.84	0.1	L	59.32	10.93	48.59	8.62
5614312705966204288	117.01604	-25.57777	13.59892	9.50	10.14	8.79	0.49	0.05	L	58.94	10.86	48.31	8.56
459263743483634304	36.80736	59.46060	13.63864	9.14	10.11	8.19	0.96	0.11	L	58.83	10.84	51.18	9.07
5596601154188852352	121.58947	-30.09687	13.67010	9.49	10.23	8.67	0.57	0.05	L	58.75	10.82	52.01	9.22
6030635804488868480	249.53582	-31.47765	13.68681	12.78	13.33	12.09	0.32	0.11	G	58.70	10.81	50.02	8.87
4267397694768545920	287.05729	1.29863	13.75460	6.61	7.39	5.85	0.66	0.06	L	58.52	10.78	48.60	8.62
5586922973654572416	116.29911	-36.97475	13.76670	12.17	12.95	11.27	0.78	0.12	G	58.49	10.77	48.96	8.68
4087335043492541696	286.51307	-18.42825	13.77231	12.49	13.06	11.81	0.31	0.11	G	58.48	10.77	50.22	8.90

TABLE A.7: continued.

Gaia DR2 Source Id	RA	DEC	P	G	G_{BP}	G_{RP}	E(G_{BP}-G_{RP})	σE(G_{BP}-G_{RP})	Note	t_{PA}	$\sigma\ t_{PA}$	t_{PAC}	$\sigma\ t_{PAC}$
(1)	(2)	(3)	(4)	(5)	(6)	(7)	(8)	(9)	(10)	(11)	(12)	(13)	(14)
2065772109994415 36	74.41700	46.09253	13.84765	11.03	12.01	10.07	1.06	0.09	L	58.28	10.74	47.81	8.48
2243309938950947200	304.41505	62.75205	13.98367	14.12	14.63	13.61	0.02	0.11	G	57.92	10.67	51.76	9.18
5351331755370445056	161.23472	-56.28954	14.10712	8.07	8.99	7.51	0.51	0.05	L	57.60	10.61	50.28	8.91
5597327141100381568	119.74674	-29.30786	14.15735	9.98	10.74	9.17	0.61	0.05	L	57.48	10.59	49.77	8.82
2016626856473497344	352.30314	63.37430	14.37514	10.78	11.94	9.72	1.29	0.11	L	56.93	10.49	48.62	8.62
6026412893938675712	254.58229	-33.60913	6.06133	6.67	7.17	5.95	0.46	0.04	L	97.75	18.01	81.63	14.47
2161786374436607616	315.02658	42.59755	14.71797	8.39	9.71	7.28	1.52	0.12	L	56.10	10.33	47.10	8.35
508915489570374272	24.30841	57.75922	14.79237	8.81	9.08	8.01	0.59	0.06	L	55.92	10.30	35.32	6.26
2034684200359279488	297.82201	32.67553	15.00336	13.12	14.18	12.05	1.42	0.18	L	55.43	10.21	40.72	7.22
5864955727424819200	203.49590	-64.05556	15.04436	9.72	10.54	8.88	0.57	0.06	L	55.33	10.19	51.83	9.19
2016581673416790656	350.61846	62.75714	15.09343	10.12	11.35	9.12	1.27	0.11	L	55.22	10.17	47.29	8.38
2071433765909167232	308.22621	46.60125	15.11946	8.82	9.73	7.91	0.8	0.07	L	55.16	10.16	49.20	8.72
3324153371114695680	95.35961	6.47015	15.23122	8.02	8.65	7.32	0.36	0.04	L	54.90	10.11	47.56	8.43
5537860123428416640	119.69307	-38.99433	15.55821	11.46	12.34	10.55	0.9	0.12	L	54.18	9.98	44.34	7.86
6704330080883057536	281.53600	-48.63307	16.09459	12.59	13.03	11.97	0.12	0.11	G	53.04	9.77	44.53	7.89
1870258975238302208	310.85080	35.58778	16.39062	6.07	6.69	5.36	0.34	0.03	L	52.44	9.66	45.58	8.08
6026305309220584576	253.41732	-33.34511	16.40369	12.99	13.59	12.25	0.39	0.11	G	52.41	9.65	44.42	7.88
4638315266636230400	30.74872	-74.05691	16.48065	14.19	14.70	13.59	0.13	0.11	G	52.26	9.63	45.30	8.03
5338036117182452096	166.05607	-60.97991	16.65998	8.19	8.90	7.38	0.5	0.05	L	51.91	9.56	45.78	8.12
2058374144759464064	301.11066	34.11225	17.07369	8.46	9.24	7.61	0.69	0.06	L	51.12	9.42	42.99	7.62
5878388529664102016	218.79935	-60.99798	17.11025	9.85	10.96	8.74	1.27	0.12	L	51.05	9.40	42.98	7.62
2198162651491732608	329.46952	56.16389	17.87198	9.83	10.85	8.87	0.92	0.1	L	49.68	9.15	44.78	7.94
5253717937706836480	159.23233	-61.58131	18.05246	11.66	12.47	10.73	0.76	0.1	O	49.36	9.09	42.21	7.48
6026596989041710336	254.88447	-32.95258	18.13188	12.53	13.10	11.76	0.4	0.11	G	49.23	9.07	41.02	7.27
5255254711361371520	157.07013	-59.35018	18.17758	8.30	8.97	7.52	0.44	0.06	L	49.15	9.05	42.99	7.62
188724234539584256	78.84160	40.07802	18.19076	9.78	10.66	8.85	0.74	0.1	L	49.13	9.05	44.36	7.86
5351161399785606016	161.13616	-57.56536	18.87302	7.15	7.82	6.43	0.36	0.04	L	48.01	8.84	42.09	7.46
1873250780732545920	314.33680	40.17749	20.14034	9.27	10.36	8.28	1.13	0.11	L	46.10	8.49	38.20	6.77
5523162573544337408	129.25540	-44.11465	20.49764	6.66	7.31	5.90	0.41	0.04	L	45.59	8.40	39.09	6.93

TABLE A.7: continued.

Gaia DR2 Source Id	RA	DEC	P	G	G_{BP}	G_{RP}	E(G_{BP}-G_{RP})	σE(G_{BP}-G_{RP})	Note	t_{PA}	$\sigma\ t_{PA}$	t_{PAC}	$\sigma\ t_{PAC}$
(1)	(2)	(3)	(4)	(5)	(6)	(7)	(8)	(9)	(10)	(11)	(12)	(13)	(14)
5937099633141128448	251.32962	-51.34264	20.85306	9.60	10.51	8.67	0.74	0.06	L	45.10	8.31	41.03	7.28
4644478166748030976	35.20622	-73.08565	21.36729	13.63	14.02	13.06	0.0	0.11	G	44.42	8.18	36.80	6.52
4094784475310672128	274.24882	-19.07583	21.83410	7.48	8.43	6.62	0.62	0.06	L	43.82	8.07	41.83	7.42
4103564728516764032	280.45457	-14.50543	11.03608	13.65	14.58	12.94	0.58	0.12	G	67.17	12.37	63.48	11.25
6350220751862829952	358.65290	-83.28872	22.44150	14.31	15.01	13.60	0.34	0.11	G	43.08	7.94	37.97	6.73
5600052040150252800	114.64682	-28.49960	23.17284	9.22	9.95	8.42	0.58	0.05	L	42.22	7.78	34.35	6.09
5253571526514498176	159.11275	-62.19251	24.21976	12.41	13.32	11.49	0.76	0.1	O	41.07	7.57	36.05	6.39
5858474003300201856	193.43279	-65.89971	26.46392	11.93	12.63	11.09	0.51	0.09	O	38.85	7.16	33.03	5.86
6096564686351860992	213.33208	-44.89374	26.68846	12.41	13.00	11.69	0.28	0.11	G	38.65	7.12	32.65	5.79
5355057622305532928	155.17091	-55.32138	28.16616	7.82	8.68	6.96	0.73	0.06	L	37.37	6.88	30.69	5.44
5964193485048327808	252.91061	-45.42671	28.86509	8.85	10.11	7.76	1.15	0.11	L	36.80	6.78	34.38	6.10
5597379741549105280	119.59202	-29.13008	30.09021	8.12	9.00	7.26	0.72	0.06	L	35.85	6.60	29.69	5.26
5238808628736339584	164.28834	-65.13474	15.71624	8.66	9.31	7.85	0.47	0.04	L	53.84	9.92	46.88	8.31
5864135319959353600	204.15366	-64.55832	34.05097	9.10	10.18	8.12	0.98	0.1	L	33.18	6.11	28.19	5.00
5546476927338700416	123.26755	-34.57851	41.46411	6.46	7.30	5.58	0.61	0.05	L	29.33	5.40	24.90	4.42
2027951173435143680	297.87876	27.46021	44.87621	6.66	7.50	5.78	0.64	0.06	L	27.92	5.14	23.10	4.09

TABLE A.8: Individual ages for the selected FO-mode GCCs obtained by using both the canonical PA and PAC relations.

Gaia DR2 Source Id	RA	DEC	P	G	G_{BP}	G_{RP}	E(G_{BP}-G_{RP})	σE(G_{BP}-G_{RP})	Note	t_{PA}	$\sigma\, t_{PA}$	t_{PAC}	$\sigma\, t_{PAC}$
(1)	(2)	(3)	(4)	(5)	(6)	(7)	(8)	(9)	(10)	(11)	(12)	(13)	(14)
5958267083020200448	263.74736	-44.83491	0.48582	15.31	15.67	14.78	0.48	0.11	G	175.45	21.01	168.26	17.82
4652801401061740800	72.89387	-73.52919	0.54856	17.88	18.20	17.42	0.32	0.11	G	167.21	20.02	161.55	17.11
4649684869708905600	78.33946	-73.18860	0.62515	17.60	17.85	17.14	0.28	0.11	G	158.78	19.01	149.33	15.82
4757521942202075904	84.00743	-62.92647	0.66840	17.23	17.49	16.81	0.21	0.11	G	154.63	18.51	147.46	15.62
4648894973678313600	78.74744	-76.16060	0.68428	17.58	17.85	17.13	0.26	0.11	G	153.20	18.34	145.22	15.38
426097765508018560	13.85755	59.72753	0.69910	13.67	14.18	12.99	0.72	0.12	G	151.90	18.19	145.17	15.38
5255955821811454592	150.19748	-61.57770	0.70107	14.74	15.09	14.05	0.65	0.12	G	151.73	18.17	137.97	14.61
6380124062227694208	357.83150	-72.69153	0.72213	17.86	18.07	17.44	0.19	0.11	G	149.96	17.96	139.41	14.77
4648520761770393088	85.76598	-75.18605	0.81359	17.25	17.54	16.80	0.25	0.11	G	143.05	17.13	135.51	14.35
4652889258915055488	72.48404	-73.00018	0.95488	17.24	17.54	16.77	0.27	0.11	G	134.26	16.08	126.16	13.36
5542032357742851712	125.44982	-37.46816	1.01087	16.30	17.08	15.38	1.19	0.12	O	131.26	15.72	122.76	13.00
4652312599416423040	68.88711	-74.56297	1.01787	17.03	17.30	16.59	0.18	0.11	G	130.90	15.67	123.28	13.06
4649732762885142272	77.24295	-73.85941	1.02268	17.06	17.35	16.58	0.26	0.11	G	130.66	15.64	122.03	12.92
5860021737714232576	190.95445	-65.86875	1.03985	15.64	16.14	14.78	0.82	0.1	O	129.80	15.54	123.61	13.09
4690203483799384832	12.47494	-70.52511	1.05413	16.86	17.06	16.51	0.03	0.11	G	129.10	15.46	120.55	12.77
5879216457587855872	220.33866	-58.95261	1.05620	17.35	19.40	15.97	3.13	0.28	G	129.00	15.45	106.51	11.28
4650448854192694144	84.54695	-73.04031	1.05937	17.06	17.37	16.55	0.29	0.11	G	128.85	15.43	120.72	12.79
5264781017499895936	90.70098	-74.81688	1.06456	17.00	17.31	16.47	0.33	0.11	G	128.60	15.40	119.49	12.66
5262612604471337344	112.55193	-74.18419	1.06846	16.96	17.27	16.47	0.28	0.11	G	128.41	15.38	120.29	12.74
4636454029673286400	17.74748	-75.46487	1.07579	16.93	17.12	16.56	0.06	0.11	G	128.07	15.33	118.85	12.59
457599392117044224	37.51571	56.69572	1.08362	14.26	14.77	13.58	0.64	0.12	G	127.70	15.29	121.01	12.82
4649292305396315904	75.79134	-74.77767	1.08725	16.91	17.17	16.47	0.17	0.11	G	127.53	15.27	119.38	12.64
4757456147604475392	81.34978	-62.60265	1.09098	16.36	16.57	16.01	0.03	0.11	G	127.36	15.25	119.56	12.66
5984686633766186752	239.21288	-47.24860	1.10006	17.53	18.72	16.43	1.79	0.18	G	126.94	15.20	116.56	12.35
5978153915467156992	257.17120	-34.22662	1.10037	16.06	16.91	15.10	1.29	0.15	G	126.93	15.20	117.28	12.42
5280952256562534784	106.38399	-67.14481	1.11229	16.67	17.24	15.96	0.72	0.12	G	126.39	15.13	120.18	12.73
5351436724362450304	157.99176	-58.24496	1.11936	11.09	11.62	10.41	0.65	0.12	G	126.07	15.09	120.10	12.72
4296034376370310144	292.98705	8.05287	1.12815	15.60	16.01	15.02	0.44	0.11	G	125.68	15.05	118.71	12.57
4649121747955000448	77.26192	-74.66745	1.12938	16.84	17.13	16.41	0.17	0.11	G	125.62	15.04	118.78	12.58
6388401494999249280	359.61640	-68.76654	1.14138	17.31	17.49	17.02	0.0	0.11	G	125.10	14.98	112.44	11.91

TABLE A.8: continued.

Gaia DR2 Source Id	RA	DEC	P	G	G_{BP}	G_{RP}	E(G_{BP}-G_{RP})	σE(G_{BP}-G_{RP})	Note	t_{PA}	$\sigma\ t_{PA}$	t_{PAC}	$\sigma\ t_{PAC}$
(1)	(2)	(3)	(4)	(5)	(6)	(7)	(8)	(9)	(10)	(11)	(12)	(13)	(14)
4691907009561849088	13.52583	-70.09840	1.14422	17.39	17.61	17.00	0.07	0.11	G	124.98	14.96	116.83	12.37
5610147893350949504	107.91737	-26.97786	1.14435	13.22	13.56	12.71	0.31	0.11	G	124.97	14.96	117.13	12.41
4757580426778468480	83.23229	-62.74256	1.14539	16.58	16.85	16.19	0.1	0.11	G	124.93	14.96	118.22	12.52
4757352209396545664	82.53930	-63.27145	1.15017	16.74	17.03	16.28	0.21	0.11	G	124.72	14.93	116.62	12.35
4117130567344719232	266.37656	-21.56332	1.15336	15.57	16.66	14.46	1.74	0.16	O	124.58	14.92	111.12	11.77
5604731630351388928	109.71092	-32.64398	1.16324	12.74	13.02	12.29	0.19	0.11	G	124.16	14.87	116.31	12.32
4693976423589147648	27.99098	-69.98706	1.16412	17.18	17.36	16.80	0.04	0.11	G	124.13	14.86	114.76	12.16
5237294738660182912	173.70859	-65.08935	1.16453	16.56	17.60	15.48	1.57	0.15	O	124.11	14.86	116.51	12.34
5265006108149270016	91.76627	-74.14746	1.16991	16.91	17.27	16.39	0.33	0.11	G	123.88	14.83	116.76	12.37
4703737747608086272	5.59416	-68.47642	1.17306	17.24	17.38	16.89	0.0	0.11	G	123.75	14.82	112.73	11.94
4652373209998248832	72.57003	-74.23271	1.18622	16.94	17.25	16.45	0.25	0.11	G	123.21	14.75	115.34	12.22
4650275547972932608	84.58900	-74.11395	1.20074	16.63	16.91	16.17	0.19	0.11	G	122.61	14.68	114.90	12.17
4685118349894560128	7.25192	-75.20856	1.20327	17.11	17.30	16.78	-0.0	0.11	G	122.51	14.67	112.92	11.96
4649352954637972224	73.46156	-74.63390	1.21391	16.75	17.07	16.29	0.22	0.11	G	122.08	14.62	115.76	12.26
4705063044144940416	21.21681	-65.43852	1.21627	17.07	17.22	16.77	0.0	0.11	G	121.99	14.61	108.10	11.45
5612678213207148032	111.30775	-27.79913	1.21642	13.14	13.59	12.52	0.5	0.11	G	121.99	14.61	115.17	12.20
5311837740049326848	137.44370	-52.56716	1.25693	17.96	19.08	16.88	1.68	0.17	G	120.41	14.42	110.47	11.70
5311347637061714304	137.25223	-53.59880	1.29623	12.22	12.74	11.55	0.61	0.12	G	118.95	14.24	112.54	11.92
5613275454180075264	112.04712	-26.49072	1.30756	15.45	16.20	14.57	1.07	0.14	G	118.54	14.19	110.63	11.72
5857396447520828288	196.47891	-67.30630	1.31275	15.12	15.57	14.43	0.61	0.12	G	118.36	14.17	108.65	11.51
4134649262221615104	258.39633	-18.09767	1.32706	14.44	14.76	13.89	0.33	0.11	G	117.85	14.11	108.60	11.50
5851370058646053120	205.56594	-66.97277	1.39185	15.25	15.76	14.57	0.61	0.12	G	115.65	13.85	108.61	11.50
4637883330365589376	19.13912	-75.74839	1.39916	16.91	17.17	16.48	0.12	0.11	G	115.41	13.82	107.60	11.40
4650280594551796864	83.97161	-74.03424	1.44214	16.55	16.86	16.09	0.19	0.11	G	114.03	13.65	106.89	11.32
4688096922599486336	22.41111	-70.44117	1.44633	16.55	16.77	16.14	0.08	0.11	G	113.90	13.64	105.02	11.12
4649981772207548672	89.03492	-74.93384	1.45533	16.50	16.86	16.02	0.23	0.11	G	113.62	13.60	108.00	11.44
5533237604747205120	122.05543	-43.25773	1.50255	13.94	14.37	13.32	0.46	0.11	G	112.20	13.43	104.99	11.12
6715705353307835776	286.24834	-41.24300	1.56682	11.93	12.75	11.03	1.13	0.14	G	110.35	13.21	103.01	10.91
5279103771359717760	98.49359	-69.58687	1.56734	15.91	16.13	15.52	0.04	0.11	G	110.34	13.21	102.17	10.82

TABLE A.8: continued.

Gaia DR2 Source Id	RA	DEC	P	G	G_{BP}	G_{RP}	E(G_{BP}-G_{RP})	σE(G_{BP}-G_{RP})	Note	t_{PA}	$\sigma\, t_{PA}$	t_{PAC}	$\sigma\, t_{PAC}$
(1)	(2)	(3)	(4)	(5)	(6)	(7)	(8)	(9)	(10)	(11)	(12)	(13)	(14)
5236253535532145792	178.47741	-66.15551	1.61221	15.41	16.07	14.58	0.92	0.11	O	109.11	13.06	100.22	10.61
4652839746530357120	72.51981	-73.13928	1.61261	16.33	16.63	15.91	0.11	0.11	G	109.10	13.06	102.93	10.90
4690389954099065984	11.18371	-70.34446	1.62180	17.50	17.73	17.09	0.07	0.11	G	108.85	13.03	99.98	10.59
4633993842341089152	31.03923	-77.07734	1.64148	17.45	17.73	17.00	0.14	0.11	G	108.33	12.97	100.19	10.61
4684545126380271488	15.02763	-75.21117	1.64178	16.00	16.23	15.64	0.0	0.11	G	108.33	12.97	100.18	10.61
4650241016434474624	86.69286	-73.38162	1.64223	16.14	16.45	15.72	0.11	0.11	G	108.31	12.97	102.08	10.81
5238583980437740416	165.04708	-66.57781	1.64338	14.57	15.07	13.89	0.59	0.12	G	108.28	12.97	100.68	10.66
5317494559886504704	133.34151	-54.05494	1.66917	13.41	13.79	12.85	0.33	0.11	G	107.62	12.89	100.38	10.63
5253058471238877312	155.13635	-62.12037	1.67042	13.72	14.18	13.10	0.48	0.11	G	107.59	12.88	100.83	10.68
4649714659602296448	76.35029	-74.03501	1.68909	16.17	16.44	15.76	0.08	0.11	G	107.11	12.83	99.84	10.57
4650425115918541312	85.71464	-73.43898	1.69512	16.15	16.44	15.69	0.15	0.11	G	106.96	12.81	99.32	10.52
5324781367038315648	132.52689	-50.88632	1.70128	14.58	15.45	13.63	1.22	0.14	G	106.81	12.79	98.87	10.47
5587628692622346624	116.43209	-35.40995	1.71526	14.35	15.03	13.54	0.89	0.13	G	106.46	12.75	99.18	10.50
5850702517654588928	207.15791	-66.88149	1.72076	14.78	15.24	14.13	0.51	0.11	G	106.33	12.73	99.15	10.50
5306502089316773248	141.31930	-57.56125	1.73125	14.64	15.27	13.86	0.81	0.12	G	106.07	12.70	98.44	10.43
5306051873674535680	146.31100	-57.27895	1.73470	15.00	15.87	14.05	1.24	0.13	O	105.99	12.69	96.51	10.22
4649467368264365312	79.98448	-74.44347	1.74813	16.25	16.55	15.75	0.22	0.11	G	105.67	12.65	97.09	10.28
5599120204043561600	113.85342	-31.07499	1.74843	13.57	14.07	12.92	0.53	0.11	G	105.66	12.65	98.95	10.48
2164475809937299584	317.78601	47.16828	1.76585	10.18	10.74	9.49	0.62	0.12	G	105.25	12.60	99.33	10.52
5607793392275328640	106.26306	-29.86583	1.79788	15.08	15.37	14.61	0.16	0.11	G	104.50	12.51	96.59	10.23
4650394089074151168	85.29071	-73.67826	1.82035	16.16	16.48	15.68	0.18	0.11	G	103.99	12.45	96.78	10.25
4649470739818783104	79.60945	-74.44693	1.82744	16.16	16.47	15.67	0.19	0.11	G	103.83	12.43	96.16	10.18
5609883112903185152	108.15032	-27.83878	1.83506	12.62	12.95	12.13	0.2	0.11	G	103.66	12.41	96.39	10.21
4688179115387628544	24.10374	-70.41784	1.84246	16.42	16.70	15.97	0.12	0.11	G	103.49	12.39	95.70	10.14
5516544028942005120	126.74790	-46.55246	1.90177	14.41	14.99	13.65	0.73	0.12	G	102.20	12.24	94.69	10.03
5857773580024503552	201.67066	-65.86683	1.93030	15.32	16.06	14.43	1.0	0.11	O	101.60	12.16	94.47	10.01
5533667238912747648	122.49124	-41.54244	1.94450	15.04	15.96	14.08	1.26	0.15	G	101.31	12.13	93.48	9.90
508824711142351488	30.47766	62.70521	1.94936	13.87	14.63	12.99	1.02	0.13	G	101.21	12.12	93.86	9.94
5329861901039268736	131.14422	-46.08450	1.96760	14.26	15.19	13.29	1.26	0.13	O	100.83	12.07	94.66	10.03

TABLE A.8: continued.

Gaia DR2 Source Id	RA	DEC	P	G	G_{BP}	G_{RP}	E(G_{BP}-G_{RP})	σE(G_{BP}-G_{RP})	Note	t_{PA}	$\sigma\ t_{PA}$	t_{PAC}	$\sigma\ t_{PAC}$
(1)	(2)	(3)	(4)	(5)	(6)	(7)	(8)	(9)	(10)	(11)	(12)	(13)	(14)
4650327358155154176	83.68263	-74.01122	1.98597	15.82	16.08	15.39	0.07	0.11	G	100.46	12.03	92.62	9.81
5241983434223208192	161.77131	-62.17635	1.99082	14.89	15.70	13.97	1.07	0.12	O	100.37	12.02	94.73	10.03
6723719246886877440	277.60780	-39.85986	1.99883	12.26	13.26	11.26	1.38	0.15	G	100.21	12.00	92.44	9.79
5606634988063582848	109.96244	-28.79174	1.99937	12.52	12.89	11.97	0.29	0.11	G	100.20	12.00	93.13	9.86
5864085979393757824	203.27370	-64.58181	2.00621	15.53	16.47	14.52	1.37	0.14	O	100.06	11.98	90.21	9.55
5406720409514852352	152.68706	-50.15948	2.00631	11.89	12.35	11.28	0.42	0.11	G	100.06	11.98	93.63	9.92
5858749121746467456	197.53034	-65.31814	2.02235	14.71	15.40	13.88	0.9	0.11	O	99.74	11.94	92.35	9.78
5251623535508264064	156.10874	-64.71312	2.02842	12.49	12.95	11.87	0.44	0.11	G	99.62	11.93	92.97	9.85
5322072960659445760	129.57544	-50.47626	2.03043	15.39	16.23	14.43	1.2	0.14	G	99.59	11.92	90.63	9.60
4640289096166011392	40.62046	-74.72156	2.03078	16.16	16.41	15.73	0.06	0.11	G	99.58	11.92	91.56	9.70
5543722994310379136	125.64924	-34.40031	2.03970	14.33	14.88	13.60	0.69	0.1	O	99.41	11.90	90.45	9.58
4190528813947695232	298.45948	-9.93928	2.04003	14.23	14.62	13.67	0.32	0.11	G	99.40	11.90	92.15	9.76
5245796334347122944	150.01533	-66.27623	2.06344	8.09	8.53	7.54	0.3	0.06	L	98.95	11.85	94.48	10.01
3054600330268450560	111.10215	-7.85545	2.07131	10.15	10.57	9.59	0.33	0.11	G	98.80	11.83	92.71	9.82
2195158098523149312	310.87509	61.75625	2.09946	14.31	14.85	13.59	0.63	0.12	G	98.28	11.77	90.60	9.60
3398383973788673024	86.41888	18.65688	2.10240	7.88	8.29	7.35	0.23	0.02	L	98.22	11.76	94.72	10.03
2203988169026743936	329.46631	61.01885	2.11413	7.51	8.05	6.84	0.55	0.07	L	98.00	11.73	91.98	9.74
524799786155513984	18.62522	64.65289	2.11885	12.54	13.45	11.59	1.22	0.14	G	97.92	11.72	90.79	9.62
3425495186047291136	92.58065	24.02085	2.13754	10.49	11.00	9.85	0.49	0.11	G	97.58	11.68	91.32	9.67
4767484964954044544	87.95841	-55.74149	2.16924	15.36	15.65	14.92	0.08	0.11	G	97.01	11.62	90.14	9.55
4690719846243518208	18.54532	-70.98892	2.17640	15.99	16.23	15.61	-0.0	0.11	G	96.88	11.60	88.62	9.39
2930223059544294912	111.42332	-19.89666	2.17773	11.21	11.76	10.53	0.61	0.09	O	96.86	11.60	88.63	9.39
5611675694812770176	113.56309	-28.62465	2.18938	12.97	13.51	12.28	0.58	0.12	G	96.66	11.57	90.02	9.54
5251882921501101312	158.02003	-63.67476	2.23584	15.84	16.21	15.26	0.32	0.11	G	95.86	11.48	87.96	9.32
6057943520139661184	186.29705	-61.34817	2.30569	9.77	10.32	9.10	0.55	0.11	G	94.70	11.34	88.80	9.41
2949440564287527552	104.71105	-13.73667	2.32596	11.92	12.50	11.21	0.63	0.12	G	94.37	11.30	87.94	9.31
5877460679352962048	221.67487	-61.46196	2.39812	7.29	7.73	6.70	0.35	0.06	L	93.23	11.16	87.93	9.31
3157950918582624256	104.70966	9.62273	2.39815	9.23	9.55	8.78	0.14	0.03	L	93.23	11.16	85.22	9.03
4650132886338231296	88.06762	-74.12767	2.42105	15.93	16.28	15.49	0.09	0.11	G	92.88	11.12	87.62	9.28

TABLE A.8: continued.

Gaia DR2 Source Id	RA	DEC	P	G	G_{BP}	G_{RP}	E(G_{BP}-G_{RP})	σE(G_{BP}-G_{RP})	Note	t_{PA}	$\sigma\, t_{PA}$	t_{PAC}	$\sigma\, t_{PAC}$
(1)	(2)	(3)	(4)	(5)	(6)	(7)	(8)	(9)	(10)	(11)	(12)	(13)	(14)
5824226655600824704	232.70754	-65.59936	2.42829	7.58	8.02	7.02	0.26	0.1	L	92.77	11.11	89.97	9.53
5257722221591844480	147.63941	-58.85915	2.44212	14.62	15.51	13.66	1.21	0.14	G	92.56	11.08	84.57	8.96
5241536688894529408	162.42510	-62.63364	2.47137	14.52	15.25	13.62	1.0	0.11	O	92.13	11.03	83.95	8.89
5311598634949142400	139.31963	-53.08485	2.48165	10.41	10.92	9.76	0.38	0.05	L	91.98	11.01	91.39	9.68
5546003793739552896	119.74495	-34.07069	2.48812	14.64	15.52	13.68	1.18	0.12	O	91.88	11.00	84.50	8.95
3028237786647550464	112.35338	-15.97682	2.50363	12.77	13.68	11.82	1.11	0.12	O	91.66	10.97	88.66	9.39
5930952980798060032	250.81165	-52.27422	2.53380	15.74	16.44	14.89	0.9	0.13	G	91.22	10.92	83.49	8.84
3027132189042054400	114.83954	-17.34696	2.59875	10.76	11.24	10.12	0.45	0.11	G	90.31	10.81	83.88	8.88
5614274807174596864	115.45717	-25.04177	2.62584	10.35	10.87	9.70	0.42	0.05	L	89.94	10.77	87.27	9.24
5718755624717348096	116.00252	-17.12887	2.62974	11.30	11.69	10.76	0.25	0.11	G	89.89	10.76	83.45	8.84
5525825109665030528	132.70396	-39.44449	2.63045	12.64	13.53	11.71	1.16	0.14	G	89.88	10.76	82.77	8.77
3350719221309022720	101.47216	10.06146	2.64460	10.41	10.92	9.75	0.5	0.11	G	89.69	10.74	83.13	8.80
5594180167020044544	120.11432	-33.31980	2.65696	12.94	13.58	12.16	0.84	0.1	O	89.52	10.72	78.08	8.27
4684364458577939328	12.41486	-76.07638	2.65759	15.75	15.99	15.31	0.03	0.11	G	89.52	10.72	81.23	8.60
3112550812164329856	105.47340	-1.13095	2.67492	8.43	8.79	7.94	0.12	0.02	L	89.29	10.69	85.11	9.01
5598174486604978176	116.20151	-31.36252	2.69267	13.83	14.71	12.89	1.14	0.14	G	89.05	10.66	81.75	8.66
5547538196579026816	122.56082	-32.89204	2.71935	12.80	13.69	11.86	1.14	0.12	O	88.71	10.62	82.23	8.71
4513544886184515584	286.95604	16.95625	2.72920	14.44	15.17	13.60	0.9	0.13	G	88.58	10.61	81.69	8.65
3105345570728492416	101.18311	-3.95240	2.77475	11.39	12.04	10.62	0.72	0.09	L	88.00	10.54	82.06	8.69
3107234707804768384	100.46536	-1.33498	2.79810	11.82	12.42	11.08	0.65	0.12	G	87.71	10.50	81.31	8.61
2007654601080023040	338.42226	57.31830	2.80533	9.12	9.68	8.43	0.59	0.08	L	87.62	10.49	79.96	8.47
3398143803515552768	88.22807	18.01082	2.81521	12.22	12.85	11.47	0.69	0.12	G	87.50	10.48	81.31	8.61
425324052915862912	10.09664	58.61852	2.82322	13.03	13.55	12.34	0.44	0.06	L	87.40	10.46	84.36	8.94
429182376660681984	3.16670	60.22643	2.84185	9.90	10.50	9.18	0.62	0.12	G	87.17	10.44	81.18	8.60
5598479085688742656	115.17910	-30.71466	2.89019	12.54	13.01	11.89	0.43	0.11	G	86.59	10.37	79.89	8.46
4319599865468760832	290.79264	13.85664	2.97303	10.15	11.24	9.14	1.41	0.16	G	85.63	10.25	78.91	8.36
468646563398354176	61.61184	56.38261	2.99120	10.78	11.50	9.96	0.83	0.13	G	85.42	10.23	79.27	8.40
6703004658279987200	272.40289	-50.27762	3.01343	11.87	12.90	10.88	1.32	0.15	G	85.17	10.20	78.61	8.33
2008577744163053696	341.59050	59.95872	3.02796	11.06	11.96	10.12	1.16	0.14	G	85.01	10.18	77.94	8.26

TABLE A.8: continued.

Gaia DR2 Source Id	RA	DEC	P	G	G_{BP}	G_{RP}	E(G_{BP}-G_{RP})	σE(G_{BP}-G_{RP})	Note	t_{PA}	$\sigma\ t_{PA}$	t_{PAC}	$\sigma\ t_{PAC}$
(1)	(2)	(3)	(4)	(5)	(6)	(7)	(8)	(9)	(10)	(11)	(12)	(13)	(14)
5258420858142702208	152.56700	-58.18688	3.03785	9.12	9.61	8.50	0.39	0.11	G	84.90	10.17	79.19	8.39
3121755094578376832	95.20696	0.04161	3.03825	11.65	12.29	10.88	0.71	0.12	G	84.89	10.16	78.51	8.32
2200929331984972672	337.77214	60.26569	3.05313	10.87	11.74	9.96	1.07	0.14	G	84.73	10.15	78.46	8.31
5848500161483878400	222.62620	-67.49763	3.06525	7.10	7.64	6.44	0.5	0.04	L	84.60	10.13	77.87	8.25
4156512638614879104	279.16501	-8.18483	3.09090	9.62	10.40	8.79	0.84	0.07	L	84.32	10.10	81.03	8.58
3050824676059815168	104.89544	-8.37710	3.10304	13.30	14.21	12.34	1.18	0.14	G	84.19	10.08	76.80	8.13
5613541295473114496	111.61767	-25.92677	3.12653	8.99	9.63	8.26	0.6	0.05	L	83.94	10.05	80.32	8.51
3356119713188276096	98.47754	14.47138	3.13632	10.38	10.98	9.67	0.59	0.05	L	83.83	10.04	78.02	8.26
3409635486731094400	69.31155	18.54301	3.14835	6.23	6.75	5.59	0.41	0.04	L	83.71	10.02	78.87	8.35
2953155500537706752	102.77785	-11.33744	3.15452	13.27	14.17	12.31	1.17	0.14	G	83.64	10.01	76.21	8.07
1833295112309561344	300.69070	23.27608	3.16429	13.11	13.99	12.19	1.1	0.14	G	83.54	10.00	76.66	8.12
5334449269746243328	171.30404	-61.36915	3.21183	8.42	8.81	7.89	0.22	0.02	L	83.05	9.94	76.08	8.06
4628830428362208512	61.12043	-75.07970	3.21459	15.15	15.43	14.70	0.04	0.11	G	83.02	9.94	75.60	8.01
511226491206912128	26.79965	61.42249	3.22284	9.83	10.65	8.96	1.03	0.09	L	82.93	9.93	74.89	7.93
6387986571094721280	353.32270	-67.76696	3.23536	15.51	15.74	15.11	0.0	0.11	G	82.81	9.91	72.75	7.71
4650239813843637248	86.77105	-73.41004	3.24359	15.50	15.85	14.98	0.17	0.11	G	82.72	9.90	75.99	8.05
3049261303661303552	103.66285	-10.91295	3.25924	12.36	13.14	11.49	0.95	0.13	G	82.57	9.89	75.67	8.01
2952531635068093952	100.53995	-12.66113	3.26141	11.41	11.92	10.75	0.46	0.11	G	82.55	9.88	76.42	8.09
5614701001056464384	116.11513	-24.28858	3.27320	12.50	13.21	11.69	0.86	0.11	O	82.43	9.87	73.65	7.80
1971722045688053248	320.13710	45.46749	3.28391	8.67	9.33	7.92	0.7	0.06	L	82.32	9.86	76.18	8.07
514736269771300224	33.88110	63.51778	3.29886	10.32	11.00	9.53	0.75	0.12	G	82.17	9.84	76.18	8.07
5593427031607304704	112.12402	-30.65555	3.30515	12.05	12.45	11.51	0.22	0.11	G	82.11	9.83	75.79	8.03
5336579363014965376	171.69650	-58.81950	3.32711	12.88	13.51	12.10	0.72	0.1	O	81.90	9.81	74.29	7.87
5960623272099513856	264.40651	-40.81355	3.38020	7.05	7.51	6.12	0.34	0.04	L	81.38	9.74	91.65	9.71
5255209665741407744	156.49253	-59.94550	3.39566	10.75	11.38	9.99	0.66	0.12	G	81.24	9.73	75.17	7.96
3027746854704868608	111.98560	-16.83151	3.39628	10.85	11.65	9.98	0.95	0.13	G	81.23	9.73	75.14	7.96
5347071319596612864	167.83483	-54.55701	3.52731	7.78	8.12	7.32	0.07	0.11	G	80.02	9.58	74.16	7.85
2935055065243490048	107.71609	-16.73962	3.64877	11.94	12.55	11.19	0.63	0.12	G	78.96	9.45	72.78	7.71
429635993926502912	2.46412	61.51404	3.65163	10.44	11.33	9.53	1.36	0.18	L	78.93	9.45	61.44	6.51

TABLE A.8: continued.

Gaia DR2 Source Id	RA	DEC	P	G	G_{BP}	G_{RP}	E(G_{BP}-G_{RP})	σE(G_{BP}-G_{RP})	Note	t_{PA}	$\sigma\, t_{PA}$	t_{PAC}	$\sigma\, t_{PAC}$
(1)	(2)	(3)	(4)	(5)	(6)	(7)	(8)	(9)	(10)	(11)	(12)	(13)	(14)
4237423603350413568	300.63619	0.71388	3.76719	10.95	11.38	10.38	0.25	0.11	G	77.96	9.34	72.10	7.64
5932565900081831040	242.83526	-54.35413	3.78678	8.58	9.10	7.93	0.39	0.04	L	77.80	9.32	73.25	7.76
5836231845180574592	240.40305	-56.18477	3.79369	15.02	15.94	14.05	1.19	0.12	O	77.75	9.31	70.01	7.41
2246124001521354368	310.79959	67.24650	3.92667	12.35	12.87	11.70	0.42	0.11	G	76.69	9.18	70.87	7.51
2006085421882734336	333.44753	55.41078	3.98692	12.18	12.95	11.32	0.89	0.13	G	76.23	9.13	69.73	7.39
5334591003669216000	178.38968	-62.85220	3.99765	9.72	10.32	9.02	0.51	0.07	L	76.15	9.12	71.80	7.61
4664274255137737984	77.76935	-63.43402	4.03938	15.80	16.14	15.30	0.1	0.11	G	75.84	9.08	69.39	7.35
4649907692617316480	76.13718	-73.15621	4.09895	15.02	15.35	14.54	0.06	0.11	G	75.40	9.03	68.84	7.29
5310680130430560768	139.02433	-54.30973	4.11692	11.01	11.52	10.36	0.4	0.11	G	75.27	9.01	69.45	7.36
6060761362259462528	189.78014	-58.28456	4.25428	12.83	13.44	12.07	0.62	0.12	G	74.30	8.90	67.77	7.18
428839329030983040	6.64980	60.79817	4.30649	8.68	9.37	7.90	0.81	0.1	L	73.94	8.85	64.18	6.80
5254916611530412672	154.36075	-60.33320	4.31079	13.77	14.52	12.85	0.99	0.11	O	73.91	8.85	64.84	6.87
5881995546318024704	232.96911	-59.24980	4.37292	8.65	9.30	7.92	0.61	0.12	G	73.49	8.80	68.07	7.21
5339554336583678464	168.50011	-57.91090	4.43091	8.09	8.52	7.54	0.24	0.02	L	73.11	8.75	66.21	7.01
5715901567412202496	117.25952	-19.11357	4.64442	9.52	10.00	8.90	0.32	0.11	G	71.76	8.59	66.11	7.00
5718760258978008320	116.04965	-17.08099	4.70117	10.04	10.50	9.45	0.28	0.11	G	71.42	8.55	65.71	6.96
1965135696153566336	319.08500	38.92738	4.74035	9.51	9.95	8.93	0.25	0.11	G	71.18	8.52	65.53	6.94
3345254098763568768	92.59262	14.64450	4.83734	9.53	10.18	8.79	0.59	0.12	G	70.61	8.46	65.45	6.93
5711201189563596416	119.24042	-22.82542	4.86103	8.46	8.92	7.86	0.24	0.04	L	70.48	8.44	66.30	7.02
2004036486267748352	342.26323	56.42820	5.44565	8.09	8.63	7.41	0.42	0.05	L	67.38	8.07	62.01	6.57
2045359534871088384	294.54825	32.48955	5.57148	10.45	10.95	9.82	0.33	0.04	L	66.77	7.99	61.17	6.48
5868451040512196224	202.88916	-61.58237	5.62283	6.39	6.83	5.83	0.2	0.05	L	66.53	7.97	60.75	6.43
5337634589276921856	167.68575	-60.75027	5.72548	8.82	9.39	8.13	0.45	0.07	L	66.06	7.91	60.54	6.41

A.5 The intrinsic stellar parameters for computed $Z = 0.004, Y = 0.25$; $Z = 0.008, Y = 0.25$ and $Z = 0.03, Y = 0.28$ F, FO and SO-mode (if any) models

TABLE A.9: The intrinsic stellar parameters for computed F-mode models.

		Z=0.004	Y= 0.25			
$M/M_\odot$	$\log(L/L_\odot)$	T_{eff}[K]	α_{ml}	ML	P[d]	$\log(\overline{R}/R_\odot)$
(1)	(2)	(3)	(4)	(5)	(6)	(7)
3.0	2.49	5900	1.5	A	1.46027	1.23
3.0	2.49	6000	1.5	A	1.38159	1.217
3.0	2.49	6000	1.7	A	1.38248	1.215
3.0	2.49	6100	1.7	A	1.31251	1.204
3.0	2.49	6100	1.9	A	1.31104	1.201
3.0	2.49	6200	1.9	A	1.24545	1.19
3.0	2.69	5700	1.5	B	2.40817	1.357
3.0	2.69	5800	1.5	B	2.27668	1.345
3.0	2.69	5900	1.5	B	2.14295	1.332
3.0	2.69	6000	1.5	B	2.03485	1.321
3.0	2.69	5800	1.7	B	2.271	1.343
3.0	2.69	5900	1.7	B	2.14295	1.33
3.0	2.69	6000	1.7	B	2.0323	1.319
3.0	2.69	6100	1.7	B	1.92534	1.306
3.0	2.69	5900	1.9	B	2.14025	1.328
3.0	2.69	6000	1.9	B	2.0323	1.317
3.0	2.69	6100	1.9	B	1.92294	1.304
3.0	2.69	6200	1.9	B	1.81248	1.289
3.0	2.89	5500	1.5	C	4.02464	1.485
3.0	2.89	5600	1.5	C	3.78218	1.473
3.0	2.89	5700	1.5	C	3.56681	1.46
3.0	2.89	5800	1.5	C	3.36907	1.447
3.0	2.89	5900	1.5	C	3.17749	1.433
3.0	2.89	6000	1.5	C	3.00397	1.42
3.0	2.89	6100	1.5	C	2.81626	1.405
3.0	2.89	5600	1.7	C	3.78218	1.47
3.0	2.89	5700	1.7	C	3.56681	1.459
3.0	2.89	5800	1.7	C	3.36068	1.446
3.0	2.89	5900	1.7	C	3.18542	1.433
3.0	2.89	6000	1.7	C	3.00397	1.419
3.0	2.89	6100	1.7	C	2.8198	1.404
3.0	2.89	6200	1.7	C	2.68855	1.391
3.0	2.89	5700	1.9	C	3.55789	1.456
3.0	2.89	5800	1.9	C	3.36907	1.445
3.0	2.89	5900	1.9	C	3.18145	1.432
3.0	2.89	6000	1.9	C	3.00397	1.418
3.0	2.89	6100	1.9	C	2.82334	1.403
3.0	2.89	6200	1.9	C	2.6852	1.391
3.0	2.89	6300	1.9	C	2.54758	1.377
4.0	2.91	5600	1.5	A	3.23075	1.483

TABLE A.9: continued.

$M/M_{\odot}$	$\log(L/L_{\odot})$	T_{eff}[K]	α_{ml}	ML	P[d]	$\log(\overline{R}/R_{\odot})$
(1)	(2)	(3)	(4)	(5)	(6)	(7)
4.0	2.91	5700	1.5	A	3.05052	1.47
4.0	2.91	5800	1.5	A	2.88156	1.457
4.0	2.91	5900	1.5	A	2.72058	1.444
4.0	2.91	5700	1.7	A	3.04288	1.467
4.0	2.91	5800	1.7	A	2.87796	1.455
4.0	2.91	5900	1.7	A	2.72058	1.442
4.0	2.91	6000	1.7	A	2.55775	1.428
4.0	2.91	5800	1.9	A	2.87793	1.452
4.0	2.91	5900	1.9	A	2.71718	1.44
4.0	2.91	6000	1.9	A	2.56096	1.426
4.0	2.91	6100	1.9	A	2.42479	1.412
4.0	3.11	5400	1.5	B	5.40816	1.611
4.0	3.11	5500	1.5	B	5.08933	1.597
4.0	3.11	5600	1.5	B	4.78719	1.584
4.0	3.11	5700	1.5	B	4.51712	1.571
4.0	3.11	5800	1.5	B	4.25959	1.557
4.0	3.11	5900	1.5	B	4.01811	1.544
4.0	3.11	6000	1.5	B	3.80476	1.53
4.0	3.11	5500	1.7	B	5.07657	1.594
4.0	3.11	5600	1.7	B	4.78119	1.582
4.0	3.11	5700	1.7	B	4.52275	1.57
4.0	3.11	5800	1.7	B	4.25959	1.556
4.0	3.11	5900	1.7	B	4.01811	1.543
4.0	3.11	6000	1.7	B	3.80002	1.528
4.0	3.11	6100	1.7	B	3.58771	1.515
4.0	3.11	5600	1.9	B	4.78119	1.579
4.0	3.11	5700	1.9	B	4.51147	1.568
4.0	3.11	5800	1.9	B	4.25959	1.555
4.0	3.11	5900	1.9	B	4.01811	1.542
4.0	3.11	6000	1.9	B	3.79529	1.528
4.0	3.11	6100	1.9	B	3.58771	1.513
4.0	3.11	6200	1.9	B	3.39611	1.498
4.0	3.31	5100	1.5	C	9.90397	1.765
4.0	3.31	5200	1.5	C	9.30613	1.752
4.0	3.31	5250	1.5	C	8.97425	1.743
4.0	3.31	5450	1.5	C	7.94531	1.71
4.0	3.31	5500	1.5	C	7.6598	1.699
4.0	3.31	5600	1.5	C	6.66287	1.685
4.0	3.31	5700	1.5	C	6.75932	1.672
4.0	3.31	5750	1.5	C	6.54106	1.666
4.0	3.31	5900	1.5	C	5.26096	1.644
4.0	3.31	6000	1.5	C	5.64735	1.629
4.0	3.31	5300	1.7	C	8.68992	1.732
4.0	3.31	5400	1.7	C	8.10073	1.715
4.0	3.31	5500	1.7	C	7.6598	1.698
4.0	3.31	5600	1.7	C	7.16303	1.683

TABLE A.9: continued.

$M/M_{\odot}$	$\log(L/L_{\odot})$	T_{eff}[K]	α_{ml}	ML	P[d]	$\log(\overline{R}/R_{\odot})$
(1)	(2)	(3)	(4)	(5)	(6)	(7)
4.0	3.31	5700	1.7	C	6.74253	1.672
4.0	3.31	5800	1.7	C	6.2887	1.656
4.0	3.31	5900	1.7	C	5.37985	1.642
4.0	3.31	6000	1.7	C	5.63333	1.629
4.0	3.31	6100	1.7	C	5.33456	1.613
4.0	3.31	5400	1.9	C	8.04873	1.71
4.0	3.31	5500	1.9	C	7.62169	1.697
4.0	3.31	5600	1.9	C	7.16303	1.682
4.0	3.31	5700	1.9	C	6.72576	1.669
4.0	3.31	5800	1.9	C	6.28073	1.655
4.0	3.31	5900	1.9	C	5.98917	1.643
4.0	3.31	6000	1.9	C	5.63333	1.628
5.0	3.24	5300	1.5	A	6.31282	1.687
5.0	3.24	5400	1.5	A	5.94985	1.675
5.0	3.24	5500	1.5	A	5.59429	1.661
5.0	3.24	5600	1.5	A	5.26516	1.648
5.0	3.24	5700	1.5	A	4.96355	1.634
5.0	3.24	5800	1.5	A	4.67157	1.62
5.0	3.24	5900	1.5	A	4.41861	1.607
5.0	3.24	6000	1.5	A	4.18582	1.592
5.0	3.24	5500	1.7	A	5.57329	1.658
5.0	3.24	5600	1.7	A	5.26516	1.646
5.0	3.24	5700	1.7	A	4.95116	1.633
5.0	3.24	5800	1.7	A	4.67157	1.618
5.0	3.24	5900	1.7	A	4.4131	1.606
5.0	3.24	6000	1.7	A	4.17541	1.59
5.0	3.24	5600	1.9	A	5.25199	1.644
5.0	3.24	5700	1.9	A	4.95735	1.631
5.0	3.24	5800	1.9	A	4.67742	1.617
5.0	3.24	5900	1.9	A	4.42412	1.605
5.0	3.24	6000	1.9	A	4.17541	1.589
5.0	3.24	6100	1.9	A	3.94328	1.575
5.0	3.44	5100	1.5	B	10.84407	1.828
5.0	3.44	5300	1.5	B	9.47963	1.793
5.0	3.44	5400	1.5	B	9.40481	1.774
5.0	3.44	5500	1.5	B	8.29811	1.761
5.0	3.44	5600	1.5	B	7.81729	1.749
5.0	3.44	5700	1.5	B	6.57405	1.734
5.0	3.44	5800	1.5	B	6.23935	1.72
5.0	3.44	5900	1.5	B	6.57487	1.707
5.0	3.44	5200	1.7	B	10.05332	1.806
5.0	3.44	5300	1.7	B	9.44313	1.788
5.0	3.44	5400	1.7	B	8.85924	1.774
5.0	3.44	5500	1.7	B	8.29811	1.759
5.0	3.44	5600	1.7	B	7.79735	1.747
5.0	3.44	5700	1.7	B	7.39351	1.733

TABLE A.9: continued.

$M/M_{\odot}$	$\log(L/L_{\odot})$	T_{eff}[K]	α_{ml}	ML	P[d]	$\log(\overline{R}/R_{\odot})$
(1)	(2)	(3)	(4)	(5)	(6)	(7)
5.0	3.44	5800	1.7	B	6.94995	1.72
5.0	3.44	5900	1.7	B	6.56671	1.706
5.0	3.44	6000	1.7	B	6.1945	1.69
5.0	3.44	5400	1.9	B	8.83669	1.772
5.0	3.44	5500	1.9	B	8.29811	1.758
5.0	3.44	5600	1.9	B	7.77741	1.745
5.0	3.44	5700	1.9	B	7.38429	1.732
5.0	3.44	5800	1.9	B	6.94995	1.719
5.0	3.44	5900	1.9	B	6.56671	1.705
5.0	3.44	6000	1.9	B	6.17909	1.69
5.0	3.64	4800	1.5	C	19.78553	1.969
5.0	3.64	4900	1.5	C	18.68576	1.958
5.0	3.64	5000	1.5	C	17.59907	1.946
5.0	3.64	5100	1.5	C	16.50486	1.931
5.0	3.64	5200	1.5	C	15.43391	1.918
5.0	3.64	5300	1.5	C	13.30463	1.908
5.0	3.64	5400	1.5	C	13.73079	1.893
5.0	3.64	5500	1.5	C	12.87917	1.877
5.0	3.64	5600	1.5	C	12.00023	1.859
5.0	3.64	5700	1.5	C	11.23178	1.84
5.0	3.64	5800	1.5	C	10.4824	1.822
5.0	3.64	5900	1.5	C	9.83338	1.804
5.0	3.64	5200	1.9	C	15.17234	1.907
5.0	3.64	5300	1.9	C	14.41539	1.897
5.0	3.64	5400	1.9	C	13.56308	1.886
5.0	3.64	5500	1.9	C	12.78507	1.873
5.0	3.64	5600	1.9	C	11.95625	1.856
5.0	3.64	5700	1.9	C	11.19044	1.839
5.0	3.64	5800	1.9	C	10.4824	1.821
5.0	3.64	5900	1.9	C	9.80904	1.804
6.0	3.50	5200	1.5	A	10.08817	1.836
6.0	3.50	5300	1.5	A	9.41852	1.822
6.0	3.50	5400	1.5	A	8.8495	1.809
6.0	3.50	5500	1.5	A	8.3703	1.795
6.0	3.50	5600	1.5	A	7.88559	1.781
6.0	3.50	5700	1.5	A	7.42312	1.768
6.0	3.50	5800	1.5	A	7.00052	1.753
6.0	3.50	5300	1.7	A	9.41852	1.82
6.0	3.50	5400	1.7	A	8.83821	1.806
6.0	3.50	5500	1.7	A	8.3703	1.793
6.0	3.50	5600	1.7	A	7.87576	1.78
6.0	3.50	5700	1.7	A	7.41388	1.767
6.0	3.50	5800	1.7	A	6.9831	1.752
6.0	3.50	5900	1.7	A	6.59345	1.737
6.0	3.50	5400	1.9	A	8.83821	1.804
6.0	3.50	5500	1.9	A	8.3703	1.792

TABLE A.9: continued.

$M/M_{\odot}$	$\log(L/L_{\odot})$	T_{eff}[K]	α_{ml}	ML	P[d]	$\log(\overline{R}/R_{\odot})$
(1)	(2)	(3)	(4)	(5)	(6)	(7)
6.0	3.50	5600	1.9	A	7.86593	1.78
6.0	3.50	5700	1.9	A	7.41388	1.765
6.0	3.50	5800	1.9	A	6.9831	1.751
6.0	3.50	5900	1.9	A	6.59345	1.737
6.0	3.50	6000	1.9	A	6.21539	1.722
6.0	3.70	4900	1.5	B	18.59074	1.988
6.0	3.70	5000	1.5	B	17.53461	1.977
6.0	3.70	5100	1.5	B	16.13542	1.967
6.0	3.70	5200	1.5	B	15.44676	1.952
6.0	3.70	5300	1.5	B	14.60648	1.939
6.0	3.70	5400	1.5	B	13.65324	1.922
6.0	3.70	5550	1.5	B	12.33287	1.895
6.0	3.70	5600	1.5	B	11.88218	1.884
6.0	3.70	5700	1.5	B	11.13161	1.867
6.0	3.70	5800	1.5	B	10.43983	1.852
6.0	3.70	5900	1.5	B	9.82302	1.836
6.0	3.70	5100	1.7	B	16.31597	1.96
6.0	3.70	5200	1.7	B	15.30752	1.948
6.0	3.70	5300	1.7	B	14.49896	1.936
6.0	3.70	5400	1.7	B	13.60301	1.919
6.0	3.70	5550	1.7	B	12.31771	1.894
6.0	3.70	5600	1.7	B	11.91157	1.884
6.0	3.70	5700	1.7	B	11.15922	1.868
6.0	3.70	5800	1.7	B	10.4658	1.852
6.0	3.70	5900	1.7	B	9.82302	1.835
6.0	3.70	5200	1.9	B	15.18831	1.94
6.0	3.70	5300	1.9	B	14.4272	1.932
6.0	3.70	5400	1.9	B	13.536	1.917
6.0	3.70	5450	1.9	B	13.14549	1.91
6.0	3.70	5550	1.9	B	12.31771	1.893
6.0	3.70	5600	1.9	B	11.89687	1.884
6.0	3.70	5700	1.9	B	11.13161	1.866
6.0	3.70	5800	1.9	B	10.4658	1.852
6.0	3.70	5900	1.9	B	9.84747	1.837
6.0	3.90	4500	1.5	C	36.60231	2.142
6.0	3.90	4600	1.5	C	34.48819	2.133
6.0	3.90	4700	1.5	C	32.40613	2.121
6.0	3.90	4800	1.5	C	30.35116	2.108
6.0	3.90	4900	1.5	C	28.62569	2.097
6.0	3.90	5000	1.5	C	26.99664	2.085
6.0	3.90	5100	1.5	C	25.15428	2.071
6.0	3.90	5200	1.5	C	23.84109	2.059
6.0	3.90	5300	1.5	C	22.34977	2.045
6.0	3.90	5400	1.5	C	20.75266	2.026
6.0	3.90	5500	1.5	C	19.55625	2.012
6.0	3.90	5600	1.5	C	18.29468	1.994

TABLE A.9: continued.

$M/M_{\odot}$	$\log(L/L_{\odot})$	T_{eff}[K]	α_{ml}	ML	P[d]	$\log(\overline{R}/R_{\odot})$
(1)	(2)	(3)	(4)	(5)	(6)	(7)
6.0	3.90	5700	1.5	C	17.0265	1.973
6.0	3.90	5800	1.5	C	14.725	1.951
6.0	3.90	4800	1.7	C	30.06829	2.1
6.0	3.90	4900	1.7	C	28.40637	2.09
6.0	3.90	5000	1.7	C	26.76157	2.078
6.0	3.90	5100	1.7	C	24.98275	2.066
6.0	3.90	5200	1.7	C	23.65486	2.055
6.0	3.90	5300	1.7	C	22.1934	2.041
6.0	3.90	5400	1.7	C	20.61933	2.023
6.0	3.90	5500	1.7	C	19.5088	2.01
6.0	3.90	5600	1.7	C	18.27245	1.991
6.0	3.90	5700	1.7	C	16.96424	1.972
6.0	3.90	5800	1.7	C	15.85475	1.951
6.0	3.90	5000	1.9	C	26.45938	2.071
6.0	3.90	5100	1.9	C	24.77037	2.059
6.0	3.90	5200	1.9	C	23.47963	2.048
6.0	3.90	5300	1.9	C	22.03021	2.035
6.0	3.90	5400	1.9	C	20.45926	2.019
6.0	3.90	5500	1.9	C	19.414	2.007
6.0	3.90	5600	1.9	C	18.13935	1.989
6.0	3.90	5700	1.9	C	16.92269	1.97
7.0	3.73	4900	1.5	A	17.46979	2.0
7.0	3.73	5000	1.5	A	16.45231	1.993
7.0	3.73	5100	1.5	A	15.47731	1.978
7.0	3.73	5150	1.5	A	15.00301	1.97
7.0	3.73	5350	1.5	A	13.14873	1.935
7.0	3.73	5400	1.5	A	12.68993	1.925
7.0	3.73	5550	1.5	A	11.40065	1.9
7.0	3.73	5600	1.5	A	11.10537	1.895
7.0	3.73	5700	1.5	A	10.54833	1.88
7.0	3.73	5800	1.5	A	9.8301	1.865
7.0	3.73	5900	1.5	A	9.24826	1.849
7.0	3.73	5100	1.7	A	15.34225	1.972
7.0	3.73	5200	1.7	A	14.43854	1.958
7.0	3.73	5350	1.7	A	13.08368	1.932
7.0	3.73	5400	1.7	A	12.65845	1.923
7.0	3.73	5500	1.7	A	11.71019	1.906
7.0	3.73	5600	1.7	A	11.10537	1.894
7.0	3.73	5700	1.7	A	10.49624	1.88
7.0	3.73	5800	1.7	A	9.84234	1.865
7.0	3.73	5900	1.7	A	9.24826	1.849
7.0	3.73	5300	1.9	A	13.38287	1.938
7.0	3.73	5400	1.9	A	12.62697	1.921
7.0	3.73	5500	1.9	A	11.71019	1.905
7.0	3.73	5600	1.9	A	11.07767	1.891
7.0	3.73	5700	1.9	A	10.49624	1.879

TABLE A.9: continued.

$M/M_{\odot}$	$\log(L/L_{\odot})$	T_{eff}[K]	α_{ml}	ML	P[d]	$\log(\overline{R}/R_{\odot})$
(1)	(2)	(3)	(4)	(5)	(6)	(7)
7.0	3.73	5800	1.9	A	9.84234	1.864
7.0	3.73	5900	1.9	A	9.27132	1.848
7.0	3.93	4600	1.5	B	32.25174	2.143
7.0	3.93	4700	1.5	B	30.13947	2.132
7.0	3.93	4800	1.5	B	28.55012	2.123
7.0	3.93	4900	1.5	B	26.82697	2.111
7.0	3.93	5000	1.5	B	25.19687	2.097
7.0	3.93	5100	1.5	B	23.71644	2.083
7.0	3.93	5200	1.5	B	22.16759	2.067
7.0	3.93	5300	1.5	B	21.08345	2.051
7.0	3.93	5400	1.5	B	20.71134	2.037
7.0	3.93	5500	1.5	B	18.19514	2.021
7.0	3.93	5600	1.5	B	16.975	2.002
7.0	3.93	5700	1.5	B	15.85405	1.983
7.0	3.93	5800	1.5	B	14.77373	1.964
7.0	3.93	4900	1.7	B	26.46887	2.102
7.0	3.93	5000	1.7	B	24.97546	2.09
7.0	3.93	5100	1.7	B	23.45949	2.077
7.0	3.93	5200	1.7	B	22.02407	2.064
7.0	3.93	5300	1.7	B	20.68542	2.05
7.0	3.93	5400	1.7	B	20.40648	2.036
7.0	3.93	5500	1.7	B	18.1728	2.019
7.0	3.93	5600	1.7	B	16.975	2.001
7.0	3.93	5700	1.7	B	15.81505	1.982
7.0	3.93	5800	1.7	B	14.77373	1.964
7.0	3.93	5100	1.9	B	23.25394	2.071
7.0	3.93	5200	1.9	B	21.86019	2.057
7.0	3.93	5300	1.9	B	20.55799	2.046
7.0	3.93	5400	1.9	B	19.33623	2.032
7.0	3.93	5500	1.9	B	18.10613	2.018
7.0	3.93	5600	1.9	B	16.93333	2.0
7.0	3.93	5700	1.9	B	15.79549	1.98
7.0	4.13	4400	1.5	C	56.51343	2.272
7.0	4.13	4500	1.5	C	53.09942	2.259
7.0	4.13	4600	1.5	C	50.12616	2.248
7.0	4.13	4700	1.5	C	46.98715	2.235
7.0	4.13	4800	1.5	C	43.93854	2.223
7.0	4.13	4900	1.5	C	41.13773	2.209
7.0	4.13	5000	1.5	C	38.71829	2.197
7.0	4.13	5100	1.5	C	36.18472	2.183
7.0	4.13	5200	1.5	C	34.01887	2.17
7.0	4.13	5300	1.5	C	31.87755	2.155
7.0	4.13	5400	1.5	C	29.97465	2.141
7.0	4.13	5500	1.5	C	27.93819	2.123
7.0	4.13	5600	1.5	C	25.94954	2.103
7.0	4.13	5700	1.5	C	21.90463	2.08

TABLE A.9: continued.

$M/M_{\odot}$	$\log(L/L_{\odot})$	T_{eff}[K]	α_{ml}	ML	P[d]	$\log(\overline{R}/R_{\odot})$
(1)	(2)	(3)	(4)	(5)	(6)	(7)
7.0	4.13	4500	1.7	C	52.03437	2.252
7.0	4.13	4600	1.7	C	49.31771	2.242
7.0	4.13	4700	1.7	C	46.36736	2.229
7.0	4.13	4800	1.7	C	43.53854	2.217
7.0	4.13	4900	1.7	C	40.87442	2.206
7.0	4.13	5000	1.7	C	38.52373	2.192
7.0	4.13	5100	1.7	C	35.95949	2.18
7.0	4.13	5200	1.7	C	33.87257	2.167
7.0	4.13	5300	1.7	C	31.70255	2.152
7.0	4.13	5400	1.7	C	29.75729	2.137
7.0	4.13	5500	1.7	C	27.81979	2.121
7.0	4.13	5600	1.7	C	25.79167	2.099
7.0	4.13	4700	1.9	C	45.87141	2.221
7.0	4.13	4800	1.9	C	43.19572	2.211
7.0	4.13	4900	1.9	C	40.66377	2.199
7.0	4.13	5000	1.9	C	38.23183	2.188
7.0	4.13	5100	1.9	C	35.82431	2.174
7.0	4.13	5200	1.9	C	33.66343	2.163
7.0	4.13	5300	1.9	C	31.50799	2.148
7.0	4.13	5400	1.9	C	29.57604	2.133
7.0	4.13	5500	1.9	C	27.61701	2.116
7.0	4.13	5600	1.9	C	25.57072	2.095
8.0	3.92	4800	1.5	A	25.39572	2.115
8.0	3.92	4900	1.5	A	23.85683	2.101
8.0	3.92	5000	1.5	A	22.43333	2.091
8.0	3.92	5100	1.5	A	22.59572	2.079
8.0	3.92	5200	1.5	A	19.7412	2.064
8.0	3.92	5300	1.5	A	18.50081	2.049
8.0	3.92	5350	1.5	A	17.90613	2.041
8.0	3.92	5500	1.5	A	16.00012	2.009
8.0	3.92	5600	1.5	A	15.09005	1.994
8.0	3.92	5700	1.5	A	14.09954	1.975
8.0	3.92	5800	1.5	A	13.2191	1.961
8.0	3.92	5000	1.7	A	22.1522	2.084
8.0	3.92	5100	1.7	A	20.86968	2.072
8.0	3.92	5200	1.7	A	19.64375	2.061
8.0	3.92	5300	1.7	A	18.43252	2.047
8.0	3.92	5400	1.7	A	17.27303	2.029
8.0	3.92	5500	1.7	A	15.97975	2.009
8.0	3.92	5600	1.7	A	15.0713	1.992
8.0	3.92	5700	1.7	A	14.09954	1.975
8.0	3.92	5800	1.7	A	13.2191	1.96
8.0	3.92	5200	1.9	A	19.49745	2.055
8.0	3.92	5300	1.9	A	18.36435	2.043
8.0	3.92	5400	1.9	A	17.20914	2.028
8.0	3.92	5500	1.9	A	15.97975	2.009

TABLE A.9: continued.

$M/M_{\odot}$	$\log(L/L_{\odot})$	T_{eff}[K]	α_{ml}	ML	P[d]	$\log(\overline{R}/R_{\odot})$
(1)	(2)	(3)	(4)	(5)	(6)	(7)
8.0	3.92	5600	1.9	A	15.05266	1.992
8.0	3.92	5700	1.9	A	14.06447	1.976
8.0	3.92	5800	1.9	A	13.2191	1.96
8.0	4.12	4300	1.5	B	53.10579	2.278
8.0	4.12	4400	1.5	B	49.98657	2.269
8.0	4.12	4500	1.5	B	47.22581	2.257
8.0	4.12	4600	1.5	B	44.06829	2.246
8.0	4.12	4700	1.5	B	41.7235	2.235
8.0	4.12	4800	1.5	B	39.036	2.222
8.0	4.12	4900	1.5	B	36.66921	2.209
8.0	4.12	5000	1.5	B	34.44954	2.197
8.0	4.12	5100	1.5	B	32.28183	2.183
8.0	4.12	5200	1.5	B	30.40683	2.169
8.0	4.12	5300	1.5	B	28.4985	2.154
8.0	4.12	5400	1.5	B	26.57234	2.137
8.0	4.12	5500	1.5	B	24.83264	2.119
8.0	4.12	5600	1.5	B	23.11597	2.099
8.0	4.12	5700	1.5	B	21.3603	2.076
8.0	4.12	4600	1.7	B	43.42407	2.235
8.0	4.12	4700	1.7	B	41.28657	2.226
8.0	4.12	4800	1.7	B	38.73333	2.216
8.0	4.12	4900	1.7	B	36.29653	2.204
8.0	4.12	5000	1.7	B	34.1478	2.192
8.0	4.12	5100	1.7	B	32.12176	2.178
8.0	4.12	5200	1.7	B	30.17442	2.164
8.0	4.12	5300	1.7	B	28.29074	2.15
8.0	4.12	5400	1.7	B	26.49155	2.134
8.0	4.12	5500	1.7	B	24.71192	2.117
8.0	4.12	5600	1.7	B	22.97488	2.096
8.0	4.12	5700	1.7	B	21.3603	2.077
8.0	4.12	4900	1.9	B	36.06354	2.194
8.0	4.12	5000	1.9	B	33.97535	2.185
8.0	4.12	5100	1.9	B	31.84178	2.173
8.0	4.12	5200	1.9	B	29.93264	2.16
8.0	4.12	5300	1.9	B	28.08287	2.145
8.0	4.12	5400	1.9	B	26.29769	2.13
8.0	4.12	5500	1.9	B	24.5309	2.113
8.0	4.12	5600	1.9	B	22.89016	2.093
8.0	4.32	4500	1.5	C	74.15637	2.358
8.0	4.32	4600	1.5	C	69.30556	2.347
8.0	4.32	4700	1.5	C	65.01042	2.334
8.0	4.32	4800	1.5	C	60.82674	2.32
8.0	4.32	4900	1.5	C	56.99699	2.306
8.0	4.32	5000	1.5	C	53.25336	2.294
8.0	4.32	5100	1.5	C	49.8059	2.28
8.0	4.32	5200	1.5	C	46.68241	2.266

TABLE A.9: continued.

$M/M_\odot$	$\log(L/L_\odot)$	T_{eff}[K]	α_{ml}	ML	P[d]	$\log(\overline{R}/R_\odot)$
(1)	(2)	(3)	(4)	(5)	(6)	(7)
8.0	4.32	5300	1.5	C	43.5603	2.249
8.0	4.32	5400	1.5	C	40.59942	2.232
8.0	4.32	5500	1.5	C	37.69329	2.213
8.0	4.32	4300	1.7	C	80.85405	2.374
8.0	4.32	4400	1.7	C	76.94074	2.364
8.0	4.32	4500	1.7	C	72.74583	2.353
8.0	4.32	4600	1.7	C	68.16632	2.341
8.0	4.32	4700	1.7	C	64.15058	2.328
8.0	4.32	4800	1.7	C	60.19803	2.316
8.0	4.32	4900	1.7	C	56.63576	2.304
8.0	4.32	5000	1.7	C	52.85347	2.29
8.0	4.32	5100	1.7	C	49.55938	2.276
8.0	4.32	5200	1.7	C	46.511	2.261
8.0	4.32	5300	1.7	C	43.34792	2.247
8.0	4.32	5400	1.7	C	40.50046	2.231
8.0	4.32	5500	1.7	C	37.41678	2.208
8.0	4.32	4400	1.9	C	75.11968	2.358
8.0	4.32	4500	1.9	C	71.3353	2.346
8.0	4.32	4600	1.9	C	67.2169	2.337
8.0	4.32	4700	1.9	C	63.46262	2.323
8.0	4.32	4800	1.9	C	59.7265	2.311
8.0	4.32	4900	1.9	C	56.05787	2.299
8.0	4.32	5000	1.9	C	52.52014	2.287
8.0	4.32	5100	1.9	C	49.18947	2.272
8.0	4.32	5200	1.9	C	46.16817	2.258
8.0	4.32	5300	1.9	C	43.13542	2.243
8.0	4.32	5400	1.9	C	40.3522	2.227
8.0	4.32	5500	1.9	C	37.50903	2.208
9.0	4.09	4600	1.5	A	37.79583	2.229
9.0	4.09	4700	1.5	A	35.82419	2.22
9.0	4.09	4800	1.5	A	33.6397	2.208
9.0	4.09	4900	1.5	A	31.54051	2.195
9.0	4.09	5000	1.5	A	29.59549	2.181
9.0	4.09	5100	1.5	A	27.71678	2.166
9.0	4.09	5200	1.5	A	25.97674	2.151
9.0	4.09	5300	1.5	A	22.47917	2.136
9.0	4.09	5400	1.5	A	22.73368	2.12
9.0	4.09	5500	1.5	A	21.22188	2.101
9.0	4.09	5600	1.5	A	19.83391	2.082
9.0	4.09	5700	1.5	A	18.47072	2.062
9.0	4.09	4800	1.7	A	33.08125	2.196
9.0	4.09	4900	1.7	A	31.18345	2.186
9.0	4.09	5000	1.7	A	29.37465	2.175
9.0	4.09	5100	1.7	A	27.51146	2.161
9.0	4.09	5200	1.7	A	25.81736	2.146
9.0	4.09	5300	1.7	A	24.56019	2.132

TABLE A.9: continued.

$M/M_{\odot}$	$\log(L/L_{\odot})$	T_{eff}[K]	α_{ml}	ML	P[d]	$\log(\overline{R}/R_{\odot})$
(1)	(2)	(3)	(4)	(5)	(6)	(7)
9.0	4.09	5400	1.7	A	22.67813	2.117
9.0	4.09	5500	1.7	A	21.19583	2.101
9.0	4.09	5600	1.7	A	19.80949	2.081
9.0	4.09	5700	1.7	A	18.425	2.063
9.0	4.09	5000	1.9	A	28.93299	2.164
9.0	4.09	5100	1.9	A	27.23773	2.153
9.0	4.09	5200	1.9	A	25.62616	2.142
9.0	4.09	5300	1.9	A	24.02535	2.129
9.0	4.09	5400	1.9	A	22.59479	2.115
9.0	4.09	5500	1.9	A	21.14387	2.099
9.0	4.09	5600	1.9	A	19.73634	2.08
9.0	4.29	4300	1.5	B	70.97176	2.369
9.0	4.29	4400	1.5	B	66.69699	2.358
9.0	4.29	4500	1.5	B	62.86979	2.345
9.0	4.29	4600	1.5	B	59.11759	2.333
9.0	4.29	4700	1.5	B	55.4331	2.321
9.0	4.29	4800	1.5	B	51.86782	2.307
9.0	4.29	4900	1.5	B	48.59537	2.294
9.0	4.29	5000	1.5	B	45.50556	2.281
9.0	4.29	5100	1.5	B	42.67269	2.267
9.0	4.29	5200	1.5	B	39.91597	2.253
9.0	4.29	5300	1.5	B	37.43368	2.239
9.0	4.29	5400	1.5	B	35.07674	2.222
9.0	4.29	5500	1.5	B	32.6272	2.202
9.0	4.29	5600	1.5	B	30.0184	2.177
9.0	4.29	4500	1.7	B	61.84757	2.337
9.0	4.29	4600	1.7	B	58.33565	2.328
9.0	4.29	4700	1.7	B	54.71319	2.314
9.0	4.29	4800	1.7	B	51.40289	2.302
9.0	4.29	4900	1.7	B	48.289	2.289
9.0	4.29	5000	1.7	B	45.22222	2.276
9.0	4.29	5100	1.7	B	42.3838	2.262
9.0	4.29	5200	1.7	B	39.8184	2.249
9.0	4.29	5300	1.7	B	37.25197	2.234
9.0	4.29	5400	1.7	B	34.86493	2.218
9.0	4.29	5500	1.7	B	32.35035	2.198
9.0	4.29	5600	1.7	B	30.0184	2.177
9.0	4.29	4700	1.9	B	54.13727	2.306
9.0	4.29	4800	1.9	B	50.87164	2.296
9.0	4.29	4900	1.9	B	47.9213	2.284
9.0	4.29	5000	1.9	B	44.9956	2.271
9.0	4.29	5100	1.9	B	42.06863	2.259
9.0	4.29	5200	1.9	B	39.42801	2.245
9.0	4.29	5300	1.9	B	37.02488	2.23
9.0	4.29	5400	1.9	B	34.5684	2.214
9.0	4.29	5500	1.9	B	32.15266	2.194

TABLE A.9: continued.

$M/M_{\odot}$	$\log(L/L_{\odot})$	T_{eff}[K]	α_{ml}	ML	P[d]	$\log(\overline{R}/R_{\odot})$
(1)	(2)	(3)	(4)	(5)	(6)	(7)
9.0	4.29	5600	1.9	B	30.09236	2.178
9.0	4.49	4700	1.5	C	87.42882	2.418
9.0	4.49	4800	1.5	C	81.44815	2.405
9.0	4.49	4900	1.5	C	76.14514	2.392
9.0	4.49	5000	1.5	C	70.95197	2.377
9.0	4.49	5100	1.5	C	66.29421	2.364
9.0	4.49	5200	1.5	C	61.86609	2.348
9.0	4.49	5300	1.5	C	57.58576	2.331
9.0	4.49	5400	1.5	C	53.58924	2.313
9.0	4.49	5500	1.5	C	49.79954	2.294
9.0	4.49	4600	1.7	C	92.26887	2.428
9.0	4.49	4700	1.7	C	86.29931	2.414
9.0	4.49	4800	1.7	C	80.6191	2.401
9.0	4.49	4900	1.7	C	75.38368	2.387
9.0	4.49	5000	1.7	C	70.51343	2.375
9.0	4.49	5100	1.7	C	65.97002	2.36
9.0	4.49	5200	1.7	C	61.49028	2.346
9.0	4.49	5300	1.7	C	57.30613	2.329
9.0	4.49	5400	1.7	C	53.45926	2.312
9.0	4.49	4500	1.9	C	96.44606	2.435
9.0	4.49	4600	1.9	C	90.78472	2.424
9.0	4.49	4700	1.9	C	85.16968	2.411
9.0	4.49	4800	1.9	C	79.99745	2.398
9.0	4.49	4900	1.9	C	74.81262	2.384
9.0	4.49	5000	1.9	C	69.98715	2.372
9.0	4.49	5100	1.9	C	65.64583	2.359
9.0	4.49	5200	1.9	C	61.18958	2.343
9.0	4.49	5300	1.9	C	57.16644	2.327
9.0	4.49	5400	1.9	C	53.32917	2.309
10.0	4.25	4400	1.5	A	55.45613	2.333
10.0	4.25	4500	1.5	A	51.67512	2.321
10.0	4.25	4600	1.5	A	48.93171	2.311
10.0	4.25	4700	1.5	A	45.93854	2.3
10.0	4.25	4800	1.5	A	43.0147	2.286
10.0	4.25	4900	1.5	A	40.41481	2.274
10.0	4.25	5000	1.5	A	37.91505	2.261
10.0	4.25	5100	1.5	A	35.62593	2.246
10.0	4.25	5200	1.5	A	33.35938	2.231
10.0	4.25	5300	1.5	A	31.22905	2.214
10.0	4.25	5400	1.5	A	29.12801	2.197
10.0	4.25	5500	1.5	A	27.10833	2.177
10.0	4.25	5600	1.5	A	25.22558	2.158
10.0	4.25	4700	1.7	A	45.46366	2.289
10.0	4.25	4800	1.7	A	42.68542	2.278
10.0	4.25	4900	1.7	A	40.05938	2.267
10.0	4.25	5000	1.7	A	37.67986	2.255

TABLE A.9: continued.

$M/M_{\odot}$	$\log(L/L_{\odot})$	T_{eff}[K]	α_{ml}	ML	P[d]	$\log(\overline{R}/R_{\odot})$
(1)	(2)	(3)	(4)	(5)	(6)	(7)
10.0	4.25	5100	1.7	A	35.32014	2.241
10.0	4.25	5200	1.7	A	33.11539	2.226
10.0	4.25	5300	1.7	A	31.00174	2.21
10.0	4.25	5400	1.7	A	28.95104	2.194
10.0	4.25	5500	1.7	A	27.04213	2.176
10.0	4.25	5600	1.7	A	25.10162	2.156
10.0	4.25	4900	1.9	A	39.60243	2.256
10.0	4.25	5000	1.9	A	37.25648	2.246
10.0	4.25	5100	1.9	A	35.03623	2.234
10.0	4.25	5200	1.9	A	32.89178	2.221
10.0	4.25	5300	1.9	A	30.73646	2.206
10.0	4.25	5400	1.9	A	28.80949	2.19
10.0	4.25	5500	1.9	A	26.87662	2.172
10.0	4.25	5600	1.9	A	25.03958	2.153
10.0	4.45	4300	1.5	B	92.68715	2.447
10.0	4.45	4400	1.5	B	87.08472	2.436
10.0	4.45	4500	1.5	B	81.69421	2.423
10.0	4.45	4600	1.5	B	76.51204	2.41
10.0	4.45	4700	1.5	B	71.5272	2.398
10.0	4.45	4800	1.5	B	66.90382	2.385
10.0	4.45	4900	1.5	B	62.60127	2.371
10.0	4.45	5000	1.5	B	58.62488	2.357
10.0	4.45	5100	1.5	B	54.93796	2.343
10.0	4.45	5200	1.5	B	51.31933	2.327
10.0	4.45	5300	1.5	B	47.98542	2.311
10.0	4.45	5400	1.5	B	44.65926	2.294
10.0	4.45	5500	1.5	B	41.14931	2.269
10.0	4.45	4400	1.7	B	85.16019	2.429
10.0	4.45	4500	1.7	B	80.15278	2.418
10.0	4.45	4600	1.7	B	75.50255	2.406
10.0	4.45	4700	1.7	B	70.59826	2.392
10.0	4.45	4800	1.7	B	66.38924	2.379
10.0	4.45	4900	1.7	B	62.20752	2.367
10.0	4.45	5000	1.7	B	58.11574	2.352
10.0	4.45	5100	1.7	B	54.60127	2.339
10.0	4.45	5200	1.7	B	50.94433	2.324
10.0	4.45	5300	1.7	B	47.66551	2.309
10.0	4.45	5400	1.7	B	44.44248	2.291
10.0	4.45	5500	1.7	B	41.25046	2.269
10.0	4.45	4600	1.9	B	74.69502	2.399
10.0	4.45	4700	1.9	B	70.04097	2.387
10.0	4.45	4800	1.9	B	65.87454	2.375
10.0	4.45	4900	1.9	B	61.89248	2.363
10.0	4.45	5000	1.9	B	57.89757	2.348
10.0	4.45	5100	1.9	B	54.2647	2.336
10.0	4.45	5200	1.9	B	50.75683	2.32

TABLE A.9: continued.

$M/M_{\odot}$	$\log(L/L_{\odot})$	T_{eff}[K]	α_{ml}	ML	P[d]	$\log(\overline{R}/R_{\odot})$
(1)	(2)	(3)	(4)	(5)	(6)	(7)
10.0	4.45	5300	1.9	B	47.3456	2.305
10.0	4.45	5400	1.9	B	44.11736	2.288
10.0	4.45	5500	1.9	B	41.25046	2.269
10.0	4.65	4900	1.5	C	98.98391	2.465
10.0	4.65	5000	1.5	C	92.22037	2.452
10.0	4.65	5100	1.5	C	85.61192	2.438
10.0	4.65	5200	1.5	C	79.77488	2.421
10.0	4.65	5300	1.5	C	73.96898	2.404
10.0	4.65	5400	1.5	C	68.95405	2.388
10.0	4.65	4900	1.7	C	97.99896	2.463
10.0	4.65	5000	1.7	C	91.54398	2.449
10.0	4.65	5100	1.7	C	85.19525	2.436
10.0	4.65	5200	1.7	C	79.29201	2.42
10.0	4.65	5300	1.7	C	73.78947	2.402
10.0	4.65	5400	1.7	C	68.95405	2.388
10.0	4.65	4900	1.9	C	97.014	2.461
10.0	4.65	5000	1.9	C	90.64201	2.447
10.0	4.65	5100	1.9	C	84.7787	2.433
10.0	4.65	5200	1.9	C	79.19549	2.419
10.0	4.65	5300	1.9	C	73.96898	2.401
11.0	4.39	4300	1.5	A	74.08461	2.418
11.0	4.39	4400	1.5	A	69.86262	2.407
11.0	4.39	4500	1.5	A	65.69109	2.394
11.0	4.39	4600	1.5	A	61.64514	2.383
11.0	4.39	4700	1.5	A	57.70637	2.368
11.0	4.39	4800	1.5	A	54.03403	2.356
11.0	4.39	4900	1.5	A	50.67512	2.343
11.0	4.39	5000	1.5	A	47.43912	2.328
11.0	4.39	5100	1.5	A	44.50127	2.315
11.0	4.39	5200	1.5	A	41.711	2.3
11.0	4.39	5300	1.5	A	39.02951	2.285
11.0	4.39	5400	1.5	A	36.3963	2.267
11.0	4.39	5500	1.5	A	33.69363	2.245
11.0	4.39	5600	1.5	A	31.17338	2.223
11.0	4.39	4500	1.7	A	64.63449	2.384
11.0	4.39	4600	1.7	A	60.99792	2.374
11.0	4.39	4700	1.7	A	57.10995	2.363
11.0	4.39	4800	1.7	A	53.5522	2.35
11.0	4.39	4900	1.7	A	50.29363	2.337
11.0	4.39	5000	1.7	A	47.086	2.324
11.0	4.39	5100	1.7	A	44.17373	2.31
11.0	4.39	5200	1.7	A	41.3809	2.296
11.0	4.39	5300	1.7	A	38.79306	2.28
11.0	4.39	5400	1.7	A	36.15359	2.263
11.0	4.39	5500	1.7	A	33.61111	2.242
11.0	4.39	5600	1.7	A	31.25046	2.222

TABLE A.9: continued.

$M/M_{\odot}$	$\log(L/L_{\odot})$	T_{eff}[K]	α_{ml}	ML	P[d]	$\log(\overline{R}/R_{\odot})$
(1)	(2)	(3)	(4)	(5)	(6)	(7)
11.0	4.39	4800	1.9	A	53.13924	2.342
11.0	4.39	4900	1.9	A	49.84861	2.33
11.0	4.39	5000	1.9	A	46.73287	2.318
11.0	4.39	5100	1.9	A	43.79144	2.304
11.0	4.39	5200	1.9	A	41.02546	2.291
11.0	4.39	5300	1.9	A	38.46181	2.275
11.0	4.39	5400	1.9	A	35.88866	2.258
11.0	4.39	5500	1.9	A	33.32245	2.238
11.0	4.59	4500	1.5	B	102.3044	2.49
11.0	4.59	4600	1.5	B	86.23414	2.477
11.0	4.59	4700	1.5	B	90.51215	2.465
11.0	4.59	4800	1.5	B	84.61435	2.452
11.0	4.59	4900	1.5	B	79.21852	2.439
11.0	4.59	5000	1.5	B	73.82697	2.424
11.0	4.59	5100	1.5	B	69.08762	2.41
11.0	4.59	5200	1.5	B	64.4265	2.394
11.0	4.59	5300	1.5	B	60.00012	2.378
11.0	4.59	5400	1.5	B	55.79884	2.358
11.0	4.59	5500	1.5	B	52.01076	2.34
11.0	4.59	4400	1.7	B	108.47986	2.5
11.0	4.59	4500	1.7	B	100.79988	2.485
11.0	4.59	4600	1.7	B	95.67396	2.474
11.0	4.59	4700	1.7	B	89.57419	2.461
11.0	4.59	4800	1.7	B	83.75312	2.449
11.0	4.59	4900	1.7	B	78.42627	2.435
11.0	4.59	5000	1.7	B	73.32477	2.422
11.0	4.59	5100	1.7	B	68.58079	2.407
11.0	4.59	5200	1.7	B	64.07384	2.391
11.0	4.59	5300	1.7	B	59.70856	2.374
11.0	4.59	5400	1.7	B	55.52731	2.356
11.0	4.59	4400	1.9	B	105.7375	2.494
11.0	4.59	4500	1.9	B	98.99456	2.479
11.0	4.59	4600	1.9	B	94.39826	2.471
11.0	4.59	4700	1.9	B	88.40174	2.457
11.0	4.59	4800	1.9	B	83.10718	2.445
11.0	4.59	4900	1.9	B	77.83218	2.432
11.0	4.59	5000	1.9	B	72.86817	2.418
11.0	4.59	5100	1.9	B	68.32743	2.404
11.0	4.59	5200	1.9	B	63.79954	2.388
11.0	4.59	5300	1.9	B	59.48981	2.372
11.0	4.59	5400	1.9	B	55.52731	2.356
11.0	4.79	5200	1.5	C	101.36227	2.489
11.0	4.79	5300	1.5	C	93.37998	2.472
11.0	4.79	5100	1.7	C	112.16956	2.508
11.0	4.79	5200	1.7	C	100.87674	2.489
11.0	4.79	5300	1.7	C	93.1544	2.471

TABLE A.9: continued.

$M/M_\odot$	$\log(L/L_\odot)$	T_{eff}[K]	α_{ml}	ML	P[d]	$\log(\overline{R}/R_\odot)$
(1)	(2)	(3)	(4)	(5)	(6)	(7)
11.0	4.79	5100	1.9	C	109.55185	2.504
11.0	4.79	5200	1.9	C	100.63391	2.487

TABLE A.10: The intrinsic stellar parameters for computed FO-mode models.

Z=0.004 Y= 0.25						
$M/M_\odot$	$\log(L/L_\odot)$	T_{eff}[K]	α_{ml}	ML	P[d]	$\log(\overline{R}/R_\odot)$
(1)	(2)	(3)	(4)	(5)	(6)	(7)
3.0	2.49	6100	1.5	A	0.96086	1.202
3.0	2.49	6200	1.5	A	0.91345	1.19
3.0	2.49	6300	1.5	A	0.86753	1.176
3.0	2.49	6400	1.5	A	0.82503	1.164
3.0	2.49	6500	1.5	A	0.78114	1.149
3.0	2.49	6600	1.5	A	0.74973	1.137
3.0	2.49	6700	1.5	A	0.71273	1.123
3.0	2.49	6200	1.7	A	0.91041	1.188
3.0	2.49	6300	1.7	A	0.86609	1.175
3.0	2.49	6400	1.7	A	0.82229	1.162
3.0	2.49	6500	1.7	A	0.78114	1.148
3.0	2.49	6600	1.7	A	0.74973	1.137
3.0	2.49	6700	1.7	A	0.71155	1.122
3.0	2.49	6800	1.7	A	0.66206	1.106
3.0	2.49	6300	1.9	A	0.86897	1.174
3.0	2.49	6400	1.9	A	0.82503	1.161
3.0	2.49	6500	1.9	A	0.78114	1.147
3.0	2.49	6600	1.9	A	0.74848	1.135
3.0	2.49	6700	1.9	A	0.71392	1.121
3.0	2.69	6100	1.5	B	1.39567	1.303
3.0	2.69	6200	1.5	B	1.31759	1.289
3.0	2.69	6300	1.5	B	1.25825	1.276
3.0	2.69	6400	1.5	B	1.19487	1.263
3.0	2.69	6500	1.5	B	1.1293	1.248
3.0	2.69	6600	1.5	B	1.07942	1.236
3.0	2.69	6200	1.7	B	1.31538	1.287
3.0	2.69	6300	1.7	B	1.25618	1.276
3.0	2.69	6400	1.7	B	1.19094	1.262
3.0	2.69	6500	1.7	B	1.12551	1.247
3.0	2.69	6600	1.7	B	1.08123	1.236
3.0	2.69	6200	1.9	B	1.31759	1.287
3.0	2.69	6300	1.9	B	1.25618	1.275
3.0	2.69	6400	1.9	B	1.19291	1.261
3.0	2.69	6500	1.9	B	1.12456	1.246
3.0	2.89	6200	1.5	C	1.93149	1.39
3.0	2.89	6300	1.5	C	1.83572	1.377
3.0	2.89	6400	1.5	C	1.74108	1.363
3.0	2.89	6200	1.7	C	1.95705	1.39

TABLE A.10: continued.

$M/M_\odot$	$\log(L/L_\odot)$	T_{eff}[K]	α_{ml}	ML	P[d]	$\log(\overline{R}/R_\odot)$
(1)	(2)	(3)	(4)	(5)	(6)	(7)
3.0	2.89	6300	1.7	C	1.83572	1.376
3.0	2.89	6400	1.7	C	1.74108	1.362
3.0	2.89	6300	1.9	C	1.82318	1.374
4.0	2.91	6000	1.5	A	1.844	1.425
4.0	2.91	6100	1.5	A	1.75159	1.411
4.0	2.91	6200	1.5	A	1.66859	1.399
4.0	2.91	6300	1.5	A	1.58554	1.386
4.0	2.91	6400	1.5	A	1.50613	1.372
4.0	2.91	6500	1.5	A	1.43211	1.358
4.0	2.91	6100	1.7	A	1.75159	1.41
4.0	2.91	6200	1.7	A	1.66582	1.398
4.0	2.91	6300	1.7	A	1.58292	1.385
4.0	2.91	6400	1.7	A	1.50613	1.371
4.0	2.91	6500	1.7	A	1.42735	1.357
4.0	2.91	6200	1.9	A	1.67135	1.398
4.0	2.91	6300	1.9	A	1.58029	1.385
4.0	2.91	6400	1.9	A	1.50613	1.371
4.0	3.11	5600	1.5	B	3.41301	1.583
4.0	3.11	5700	1.5	B	3.23049	1.572
4.0	3.11	5800	1.5	B	3.06166	1.557
4.0	3.11	5900	1.5	B	2.90478	1.542
4.0	3.11	6000	1.5	B	3.80135	1.53
4.0	3.11	6100	1.5	B	2.58971	1.514
4.0	3.11	6200	1.5	B	2.44197	1.499
4.0	3.11	6300	1.5	B	2.31318	1.484
4.0	3.11	5700	1.7	B	3.21976	1.568
4.0	3.11	5800	1.7	B	3.05155	1.555
4.0	3.11	5900	1.7	B	2.83811	1.539
4.0	3.11	6000	1.7	B	3.79237	1.529
4.0	3.11	6100	1.7	B	2.57692	1.513
4.0	3.11	6200	1.7	B	2.44598	1.498
4.0	3.11	6300	1.7	B	2.31318	1.483
4.0	3.11	6200	1.9	B	2.44197	1.498
4.0	3.31	5900	1.5	C	4.2399	1.645
4.0	3.31	6000	1.5	C	4.01713	1.629
4.0	3.31	6100	1.5	C	3.79794	1.613
4.0	3.31	6000	1.7	C	4.01058	1.629
5.0	3.24	5600	1.5	A	3.76641	1.646
5.0	3.24	5700	1.5	A	3.56603	1.631
5.0	3.24	5800	1.5	A	4.68204	1.62
5.0	3.24	5900	1.5	A	4.41984	1.607
5.0	3.24	6000	1.5	A	3.00411	1.59
5.0	3.24	6100	1.5	A	2.83514	1.575
5.0	3.24	6200	1.5	A	2.66922	1.56
5.0	3.24	6300	1.5	A	2.55204	1.545
5.0	3.24	6100	1.7	A	2.83981	1.575

TABLE A.10: continued.

$M/M_\odot$	$\log(L/L_\odot)$	T_{eff}[K]	α_{ml}	ML	P[d]	$\log(\overline{R}/R_\odot)$
(1)	(2)	(3)	(4)	(5)	(6)	(7)
5.0	3.24	6200	1.7	A	2.66468	1.559
5.0	3.24	6100	1.9	A	2.8445	1.573
5.0	3.24	6200	1.9	A	2.66014	1.557
5.0	3.44	5700	1.5	B	5.21976	1.736
5.0	3.44	5800	1.5	B	4.94384	1.721
5.0	3.44	5900	1.5	B	4.67175	1.707
5.0	3.44	6000	1.5	B	4.41993	1.691
5.0	3.44	6100	1.5	B	4.15936	1.674
5.0	3.44	5800	1.7	B	4.94384	1.719
5.0	3.44	5900	1.7	B	4.65644	1.706
5.0	3.44	6000	1.7	B	4.40549	1.691
5.0	3.44	5900	1.9	B	4.65644	1.704
6.0	3.50	5600	1.5	A	5.60191	1.782
6.0	3.50	5700	1.5	A	5.28456	1.768
6.0	3.50	5800	1.5	A	4.99863	1.755
6.0	3.50	5900	1.5	A	4.71741	1.738
6.0	3.50	6000	1.5	A	4.4609	1.722
6.0	3.50	6100	1.5	A	4.19019	1.707
6.0	3.50	5700	1.7	A	5.25839	1.766
6.0	3.50	5800	1.7	A	4.99863	1.753
6.0	3.50	5900	1.7	A	4.70193	1.737
6.0	3.50	6000	1.7	A	4.44995	1.721
6.0	3.50	5800	1.9	A	4.974	1.75
6.0	3.50	5900	1.9	A	4.70193	1.735
7.0	3.73	5800	1.5	A	6.95219	1.866
7.0	3.73	5900	1.5	A	6.54584	1.85

TABLE A.11: The intrinsic stellar parameters for computed SO-mode models.

		Z=0.004 Y= 0.25				
$M/M_\odot$	$\log(L/L_\odot)$	T_{eff}[K]	α_{ml}	ML	P[d]	$\log(\overline{R}/R_\odot)$
(1)	(2)	(3)	(4)	(5)	(6)	(7)
3.0	2.49	6600	1.5	A	0.60227	1.135
3.0	2.49	6700	1.5	A	0.5745	1.121
3.0	2.49	6800	1.5	A	0.54392	1.106

TABLE A.12: The intrinsic stellar parameters for computed F-mode models.

		Z=0.008 Y= 0.25				
$M/M_\odot$	$\log(L/L_\odot)$	T_{eff}[K]	α_{ml}	ML	P[d]	$\log(\overline{R}/R_\odot)$
(1)	(2)	(3)	(4)	(5)	(6)	(7)
3.0	2.39	6000	1.5	A	1.15407	1.166
3.0	2.59	5700	1.5	B	2.00247	1.307
3.0	2.59	5800	1.5	B	1.88759	1.295
3.0	2.59	5900	1.5	B	1.79074	1.282

TABLE A.12: continued.

$M/M_\odot$	$\log(L/L_\odot)$	T_{eff}[K]	α_{ml}	ML	P[d]	$\log(\overline{R}/R_\odot)$
(1)	(2)	(3)	(4)	(5)	(6)	(7)
3.0	2.59	6000	1.5	B	1.69168	1.269
3.0	2.59	5800	1.7	B	1.88992	1.289
3.0	2.59	5900	1.7	B	1.7885	1.278
3.0	2.59	6000	1.7	B	1.68956	1.267
3.0	2.59	6100	1.7	B	1.59998	1.254
3.0	2.59	6000	1.9	B	1.68535	1.264
3.0	2.59	6100	1.9	B	1.59799	1.252
3.0	2.59	6200	1.9	B	1.51815	1.238
3.0	2.79	5500	1.5	C	3.31913	1.435
3.0	2.79	5600	1.5	C	3.11795	1.422
3.0	2.79	5700	1.5	C	2.954	1.409
3.0	2.79	5800	1.5	C	2.79053	1.396
3.0	2.79	5900	1.5	C	2.62019	1.381
3.0	2.79	6000	1.5	C	2.49095	1.369
3.0	2.79	6100	1.5	C	2.3567	1.355
3.0	2.79	5700	1.7	C	2.94294	1.408
3.0	2.79	5800	1.7	C	2.78705	1.395
3.0	2.79	5900	1.7	C	2.61689	1.379
3.0	2.79	6000	1.7	C	2.49095	1.368
3.0	2.79	6100	1.7	C	2.35376	1.354
3.0	2.79	5800	1.9	C	2.78358	1.392
3.0	2.79	5900	1.9	C	2.6136	1.379
3.0	2.79	6000	1.9	C	2.48784	1.367
3.0	2.79	6100	1.9	C	2.35082	1.353
3.0	2.79	6200	1.9	C	2.23005	1.339
4.0	2.81	5600	1.5	A	2.67853	1.431
4.0	2.81	5700	1.5	A	2.52578	1.419
4.0	2.81	5800	1.5	A	2.39326	1.406
4.0	2.81	5900	1.5	A	2.26223	1.392
4.0	2.81	5800	1.7	A	2.39027	1.403
4.0	2.81	5900	1.7	A	2.25941	1.39
4.0	2.81	6000	1.7	A	2.13177	1.376
4.0	2.81	5900	1.9	A	2.2594	1.387
4.0	2.81	6000	1.9	A	2.1291	1.374
4.0	2.81	6100	1.9	A	2.01936	1.361
4.0	3.01	5400	1.5	B	4.46676	1.56
4.0	3.01	5500	1.5	B	4.21606	1.547
4.0	3.01	5600	1.5	B	3.9624	1.534
4.0	3.01	5700	1.5	B	3.7244	1.52
4.0	3.01	5800	1.5	B	3.50106	1.506
4.0	3.01	5900	1.5	B	3.31791	1.491
4.0	3.01	6000	1.5	B	3.1531	1.478
4.0	3.01	5500	1.7	B	4.20028	1.545
4.0	3.01	5600	1.7	B	3.9624	1.531
4.0	3.01	5700	1.7	B	3.71972	1.518
4.0	3.01	5800	1.7	B	3.50549	1.503

TABLE A.12: continued.

$M/M_{\odot}$	$\log(L/L_{\odot})$	T_{eff}[K]	α_{ml}	ML	P[d]	$\log(\overline{R}/R_{\odot})$
(1)	(2)	(3)	(4)	(5)	(6)	(7)
4.0	3.01	5900	1.7	B	3.31374	1.489
4.0	3.01	6000	1.7	B	3.14918	1.477
4.0	3.01	5700	1.9	B	3.71503	1.516
4.0	3.01	5800	1.9	B	3.5099	1.503
4.0	3.01	5900	1.9	B	3.31374	1.489
4.0	3.01	6000	1.9	B	3.14918	1.475
4.0	3.01	6100	1.9	B	2.97587	1.462
4.0	3.21	5200	1.5	C	7.60684	1.694
4.0	3.21	5300	1.5	C	7.10568	1.678
4.0	3.21	5400	1.5	C	6.64074	1.662
4.0	3.21	5500	1.5	C	6.2713	1.65
4.0	3.21	5600	1.5	C	5.90389	1.636
4.0	3.21	5650	1.5	C	5.74234	1.629
4.0	3.21	5800	1.5	C	5.23689	1.607
4.0	3.21	5900	1.5	C	4.94839	1.593
4.0	3.21	5300	1.7	C	7.08793	1.676
4.0	3.21	5400	1.7	C	6.62389	1.66
4.0	3.21	5500	1.7	C	6.2713	1.648
4.0	3.21	5600	1.7	C	5.89653	1.633
4.0	3.21	5700	1.7	C	5.55831	1.62
4.0	3.21	5800	1.7	C	5.23689	1.606
4.0	3.21	5900	1.7	C	4.94839	1.591
4.0	3.21	6000	1.7	C	4.6726	1.577
4.0	3.21	6100	1.7	C	4.40766	1.56
4.0	3.21	5500	1.9	C	6.25566	1.645
4.0	3.21	5600	1.9	C	5.89653	1.632
4.0	3.21	5700	1.9	C	5.55138	1.619
4.0	3.21	5800	1.9	C	5.23037	1.604
4.0	3.21	5900	1.9	C	4.94223	1.59
4.0	3.21	6000	1.9	C	4.6726	1.576
4.0	3.21	6100	1.9	C	4.40769	1.56
5.0	3.14	5300	1.5	A	5.22834	1.637
5.0	3.14	5400	1.5	A	4.91119	1.624
5.0	3.14	5500	1.5	A	4.63084	1.611
5.0	3.14	5600	1.5	A	4.36931	1.598
5.0	3.14	5700	1.5	A	4.11382	1.584
5.0	3.14	5800	1.5	A	3.88644	1.569
5.0	3.14	5900	1.5	A	3.67065	1.555
5.0	3.14	5500	1.7	A	4.63082	1.608
5.0	3.14	5600	1.7	A	4.35841	1.594
5.0	3.14	5700	1.7	A	4.10868	1.581
5.0	3.14	5800	1.7	A	3.8816	1.568
5.0	3.14	5900	1.7	A	3.66609	1.553
5.0	3.14	5700	1.9	A	4.10868	1.579
5.0	3.14	5800	1.9	A	3.87675	1.565
5.0	3.14	5900	1.9	A	3.67067	1.552

TABLE A.12: continued.

$M/M_{\odot}$	$\log(L/L_{\odot})$	T_{eff}[K]	α_{ml}	ML	P[d]	$\log(\overline{R}/R_{\odot})$
(1)	(2)	(3)	(4)	(5)	(6)	(7)
5.0	3.14	6000	1.9	A	3.46652	1.539
5.0	3.34	5200	1.5	B	8.30534	1.755
5.0	3.34	5300	1.5	B	7.78196	1.74
5.0	3.34	5400	1.5	B	7.33834	1.727
5.0	3.34	5500	1.5	B	6.8994	1.713
5.0	3.34	5600	1.5	B	6.48208	1.698
5.0	3.34	5700	1.5	B	6.07112	1.681
5.0	3.34	5800	1.5	B	5.76083	1.669
5.0	3.34	5400	1.7	B	7.32003	1.725
5.0	3.34	5500	1.7	B	6.87362	1.71
5.0	3.34	5600	1.7	B	6.48208	1.696
5.0	3.34	5700	1.7	B	6.06347	1.681
5.0	3.34	5800	1.7	B	5.75366	1.668
5.0	3.34	5900	1.7	B	5.43752	1.654
5.0	3.34	6000	1.7	B	5.13038	1.639
5.0	3.34	5500	1.9	B	6.87362	1.708
5.0	3.34	5600	1.9	B	6.46591	1.696
5.0	3.34	5700	1.9	B	6.05581	1.679
5.0	3.34	5800	1.9	B	5.75366	1.667
5.0	3.34	5900	1.9	B	5.43075	1.652
5.0	3.34	6000	1.9	B	5.13038	1.638
5.0	3.54	4800	1.5	C	16.36157	1.921
5.0	3.54	4900	1.5	C	15.35637	1.91
5.0	3.54	5000	1.5	C	14.40382	1.897
5.0	3.54	5100	1.5	C	13.5588	1.885
5.0	3.54	5200	1.5	C	12.72338	1.871
5.0	3.54	5300	1.5	C	11.95868	1.856
5.0	3.54	5350	1.5	C	11.5414	1.847
5.0	3.54	5500	1.5	C	10.45433	1.82
5.0	3.54	5600	1.5	C	9.77182	1.802
5.0	3.54	5700	1.5	C	9.07709	1.781
5.0	3.54	5800	1.5	C	8.61109	1.768
5.0	3.54	5000	1.7	C	14.25938	1.888
5.0	3.54	5100	1.7	C	13.45833	1.879
5.0	3.54	5200	1.7	C	12.64525	1.867
5.0	3.54	5300	1.7	C	11.90012	1.853
5.0	3.54	5400	1.7	C	11.14299	1.837
5.0	3.54	5500	1.7	C	10.44149	1.82
5.0	3.54	5600	1.7	C	9.77182	1.801
5.0	3.54	5700	1.7	C	9.07709	1.78
5.0	3.54	5800	1.7	C	8.61109	1.768
5.0	3.54	5200	1.9	C	12.53576	1.859
5.0	3.54	5300	1.9	C	11.82708	1.849
5.0	3.54	5400	1.9	C	11.11561	1.834
5.0	3.54	5550	1.9	C	10.11973	1.809
5.0	3.54	5600	1.9	C	9.77182	1.801

TABLE A.12: continued.

$M/M_{\odot}$	$\log(L/L_{\odot})$	T_{eff}[K]	α_{ml}	ML	P[d]	$\log(\overline{R}/R_{\odot})$
(1)	(2)	(3)	(4)	(5)	(6)	(7)
5.0	3.54	5700	1.9	C	9.07709	1.78
5.0	3.54	5800	1.9	C	8.61109	1.768
6.0	3.40	5200	1.5	A	8.3325	1.787
6.0	3.40	5300	1.5	A	7.83128	1.774
6.0	3.40	5400	1.5	A	7.3519	1.76
6.0	3.40	5500	1.5	A	6.92432	1.746
6.0	3.40	5600	1.5	A	6.5085	1.731
6.0	3.40	5700	1.5	A	6.13917	1.717
6.0	3.40	5800	1.5	A	5.79627	1.701
6.0	3.40	5900	1.5	A	5.47296	1.686
6.0	3.40	5300	1.7	A	7.81171	1.772
6.0	3.40	5400	1.7	A	7.3519	1.758
6.0	3.40	5500	1.7	A	6.90705	1.744
6.0	3.40	5600	1.7	A	6.51662	1.729
6.0	3.40	5700	1.7	A	6.14682	1.715
6.0	3.40	5800	1.7	A	5.77462	1.7
6.0	3.40	5900	1.7	A	5.47296	1.686
6.0	3.40	5500	1.9	A	6.90705	1.742
6.0	3.40	5600	1.9	A	6.50037	1.727
6.0	3.40	5700	1.9	A	6.1315	1.713
6.0	3.40	5800	1.9	A	5.77462	1.699
6.0	3.40	5900	1.9	A	5.45934	1.684
6.0	3.40	6000	1.9	A	5.15275	1.67
6.0	3.60	4800	1.5	B	16.31991	1.953
6.0	3.60	4900	1.5	B	15.36944	1.944
6.0	3.60	5000	1.5	B	14.47685	1.933
6.0	3.60	5100	1.5	B	13.52431	1.918
6.0	3.60	5150	1.5	B	13.13738	1.91
6.0	3.60	5350	1.5	B	11.38587	1.872
6.0	3.60	5400	1.5	B	10.99512	1.862
6.0	3.60	5500	1.5	B	10.3836	1.845
6.0	3.60	5600	1.5	B	9.73574	1.831
6.0	3.60	5700	1.5	B	9.14086	1.814
6.0	3.60	5800	1.5	B	8.56646	1.798
6.0	3.60	5900	1.5	B	7.63124	1.784
6.0	3.60	5100	1.7	B	13.47407	1.913
6.0	3.60	5200	1.7	B	12.6412	1.898
6.0	3.60	5250	1.7	B	12.25914	1.889
6.0	3.60	5350	1.7	B	11.38226	1.87
6.0	3.60	5400	1.7	B	10.99512	1.861
6.0	3.60	5500	1.7	B	10.35784	1.844
6.0	3.60	5600	1.7	B	9.73574	1.83
6.0	3.60	5700	1.7	B	9.09492	1.813
6.0	3.60	5800	1.7	B	8.54477	1.798
6.0	3.60	5900	1.7	B	8.13859	1.784
6.0	3.60	5200	1.9	B	12.48484	1.886

TABLE A.12: continued.

$M/M_\odot$	$\log(L/L_\odot)$	T_{eff}[K]	α_{ml}	ML	P[d]	$\log(\overline{R}/R_\odot)$
(1)	(2)	(3)	(4)	(5)	(6)	(7)
6.0	3.60	5300	1.9	B	11.81817	1.878
6.0	3.60	5400	1.9	B	10.96714	1.86
6.0	3.60	5500	1.9	B	10.3836	1.844
6.0	3.60	5600	1.9	B	9.73574	1.829
6.0	3.60	5700	1.9	B	9.09492	1.813
6.0	3.60	5800	1.9	B	8.5444	1.797
6.0	3.80	4500	1.5	C	30.37731	2.102
6.0	3.80	4600	1.5	C	28.32431	2.09
6.0	3.80	4700	1.5	C	26.84525	2.078
6.0	3.80	4800	1.5	C	25.11597	2.066
6.0	3.80	4900	1.5	C	23.5412	2.052
6.0	3.80	5000	1.5	C	22.10995	2.037
6.0	3.80	5100	1.5	C	20.71146	2.022
6.0	3.80	5200	1.5	C	19.39722	2.007
6.0	3.80	5300	1.5	C	18.18681	1.99
6.0	3.80	5400	1.5	C	16.9331	1.971
6.0	3.80	5500	1.5	C	15.85544	1.956
6.0	3.80	5600	1.5	C	14.80347	1.937
6.0	3.80	5700	1.5	C	13.79549	1.915
6.0	3.80	4800	1.7	C	24.86354	2.055
6.0	3.80	4900	1.7	C	23.30694	2.043
6.0	3.80	5000	1.7	C	21.8787	2.031
6.0	3.80	5100	1.7	C	20.54676	2.016
6.0	3.80	5200	1.7	C	19.25544	2.003
6.0	3.80	5300	1.7	C	18.07407	1.987
6.0	3.80	5400	1.7	C	16.72882	1.97
6.0	3.80	5500	1.7	C	15.83611	1.955
6.0	3.80	5600	1.7	C	14.7853	1.935
6.0	3.80	5700	1.7	C	13.79549	1.914
6.0	3.80	5000	1.9	C	21.661	2.022
6.0	3.80	5100	1.9	C	20.36944	2.011
6.0	3.80	5200	1.9	C	19.13727	1.997
6.0	3.80	5300	1.9	C	17.96377	1.983
6.0	3.80	5400	1.9	C	16.6647	1.966
6.0	3.80	5500	1.9	C	15.75868	1.951
6.0	3.80	5600	1.9	C	14.73079	1.934
7.0	3.63	4900	1.5	A	14.39537	1.955
7.0	3.63	5000	1.5	A	13.5206	1.938
7.0	3.63	5100	1.5	A	12.64294	1.921
7.0	3.63	5200	1.5	A	11.80799	1.903
7.0	3.63	5300	1.5	A	11.0391	1.887
7.0	3.63	5400	1.5	A	10.3502	1.872
7.0	3.63	5500	1.5	A	9.74608	1.859
7.0	3.63	5600	1.5	A	9.17502	1.843
7.0	3.63	5700	1.5	A	8.6378	1.829
7.0	3.63	5800	1.5	A	8.14832	1.812

TABLE A.12: continued.

$M/M_{\odot}$	$\log(L/L_{\odot})$	T_{eff}[K]	α_{ml}	ML	P[d]	$\log(\overline{R}/R_{\odot})$
(1)	(2)	(3)	(4)	(5)	(6)	(7)
7.0	3.63	5100	1.7	A	12.53264	1.915
7.0	3.63	5200	1.7	A	11.77859	1.901
7.0	3.63	5300	1.7	A	11.01149	1.886
7.0	3.63	5400	1.7	A	10.3502	1.87
7.0	3.63	5500	1.7	A	9.72177	1.857
7.0	3.63	5600	1.7	A	9.1636	1.842
7.0	3.63	5700	1.7	A	8.62705	1.828
7.0	3.63	5800	1.7	A	8.12806	1.811
7.0	3.63	5300	1.9	A	11.01149	1.885
7.0	3.63	5400	1.9	A	10.3502	1.869
7.0	3.63	5500	1.9	A	9.72177	1.856
7.0	3.63	5600	1.9	A	9.1636	1.84
7.0	3.63	5700	1.9	A	8.62705	1.827
7.0	3.63	5800	1.9	A	8.12806	1.811
7.0	3.83	4600	1.5	B	26.69977	2.101
7.0	3.83	4700	1.5	B	25.08565	2.088
7.0	3.83	4800	1.5	B	23.49363	2.075
7.0	3.83	4900	1.5	B	21.9581	2.059
7.0	3.83	5000	1.5	B	20.41377	2.044
7.0	3.83	5100	1.5	B	18.00174	2.032
7.0	3.83	5200	1.5	B	18.10069	2.018
7.0	3.83	5300	1.5	B	16.94167	2.002
7.0	3.83	5400	1.5	B	15.84641	1.984
7.0	3.83	5500	1.5	B	14.79178	1.965
7.0	3.83	5600	1.5	B	13.85509	1.947
7.0	3.83	5700	1.5	B	12.96377	1.927
7.0	3.83	5800	1.5	B	12.10729	1.911
7.0	3.83	4900	1.7	B	21.7662	2.052
7.0	3.83	5000	1.7	B	20.28102	2.038
7.0	3.83	5100	1.7	B	19.04213	2.027
7.0	3.83	5200	1.7	B	18.01192	2.014
7.0	3.83	5300	1.7	B	16.8794	2.0
7.0	3.83	5400	1.7	B	15.84641	1.982
7.0	3.83	5500	1.7	B	14.81007	1.964
7.0	3.83	5600	1.7	B	13.82095	1.945
7.0	3.83	5700	1.7	B	12.96377	1.927
7.0	3.83	5100	1.9	B	18.92118	2.019
7.0	3.83	5200	1.9	B	17.87882	2.008
7.0	3.83	5300	1.9	B	16.79653	1.996
7.0	3.83	5400	1.9	B	15.74931	1.98
7.0	3.83	5500	1.9	B	14.81007	1.964
7.0	3.83	5600	1.9	B	13.80382	1.945
7.0	4.03	4300	1.5	C	49.91412	2.244
7.0	4.03	4400	1.5	C	46.92569	2.233
7.0	4.03	4500	1.5	C	43.39745	2.217
7.0	4.03	4600	1.5	C	41.09965	2.206

TABLE A.12: continued.

$M/M_\odot$	$\log(L/L_\odot)$	T_{eff}[K]	α_{ml}	ML	P[d]	$\log(\overline{R}/R_\odot)$
(1)	(2)	(3)	(4)	(5)	(6)	(7)
7.0	4.03	4700	1.5	C	38.51609	2.192
7.0	4.03	4800	1.5	C	36.06528	2.179
7.0	4.03	4900	1.5	C	33.5566	2.164
7.0	4.03	5000	1.5	C	31.39016	2.149
7.0	4.03	5100	1.5	C	29.62708	2.136
7.0	4.03	5200	1.5	C	27.75012	2.12
7.0	4.03	5300	1.5	C	25.93796	2.104
7.0	4.03	5400	1.5	C	24.21296	2.087
7.0	4.03	5500	1.5	C	22.50532	2.066
7.0	4.03	5600	1.5	C	20.90266	2.043
7.0	4.03	4500	1.7	C	43.01898	2.21
7.0	4.03	4600	1.7	C	40.78113	2.199
7.0	4.03	4700	1.7	C	38.12407	2.186
7.0	4.03	4800	1.7	C	35.88403	2.174
7.0	4.03	4900	1.7	C	33.32049	2.159
7.0	4.03	5000	1.7	C	31.1088	2.145
7.0	4.03	5100	1.7	C	29.41007	2.132
7.0	4.03	5200	1.7	C	27.54815	2.117
7.0	4.03	5300	1.7	C	25.76516	2.1
7.0	4.03	5400	1.7	C	24.06597	2.082
7.0	4.03	5500	1.7	C	22.39525	2.061
7.0	4.03	4800	1.9	C	35.52153	2.166
7.0	4.03	4900	1.9	C	33.06285	2.153
7.0	4.03	5000	1.9	C	31.02836	2.138
7.0	4.03	5100	1.9	C	29.22917	2.125
7.0	4.03	5200	1.9	C	27.41343	2.112
7.0	4.03	5300	1.9	C	25.63947	2.094
7.0	4.03	5400	1.9	C	23.9191	2.078
8.0	3.82	4700	1.5	A	22.12951	2.08
8.0	3.82	4800	1.5	A	20.89769	2.071
8.0	3.82	4900	1.5	A	19.63345	2.059
8.0	3.82	5000	1.5	A	18.4228	2.046
8.0	3.82	5100	1.5	A	17.25127	2.029
8.0	3.82	5150	1.5	A	16.67477	2.02
8.0	3.82	5300	1.5	A	15.09109	1.992
8.0	3.82	5400	1.5	A	14.01343	1.971
8.0	3.82	5500	1.5	A	13.13368	1.955
8.0	3.82	5600	1.5	A	12.37118	1.94
8.0	3.82	5700	1.5	A	11.59236	1.923
8.0	3.82	5000	1.7	A	18.26319	2.038
8.0	3.82	5100	1.7	A	17.14491	2.024
8.0	3.82	5200	1.7	A	16.08414	2.009
8.0	3.82	5300	1.7	A	15.05382	1.991
8.0	3.82	5400	1.7	A	13.99583	1.971
8.0	3.82	5500	1.7	A	13.16644	1.954
8.0	3.82	5600	1.7	A	12.37118	1.939

TABLE A.12: continued.

$M/M_{\odot}$	$\log(L/L_{\odot})$	T_{eff}[K]	α_{ml}	ML	P[d]	$\log(\overline{R}/R_{\odot})$
(1)	(2)	(3)	(4)	(5)	(6)	(7)
8.0	3.82	5700	1.7	A	11.59236	1.923
8.0	3.82	5200	1.9	A	16.00451	2.003
8.0	3.82	5300	1.9	A	15.01667	1.988
8.0	3.82	5400	1.9	A	13.94282	1.97
8.0	3.82	5500	1.9	A	13.13368	1.954
8.0	3.82	5600	1.9	A	12.34051	1.937
8.0	3.82	5700	1.9	A	11.59236	1.922
8.0	4.02	4300	1.5	B	44.03889	2.238
8.0	4.02	4400	1.5	B	41.3919	2.228
8.0	4.02	4500	1.5	B	38.81065	2.216
8.0	4.02	4600	1.5	B	36.56076	2.204
8.0	4.02	4700	1.5	B	34.086	2.19
8.0	4.02	4800	1.5	B	32.17708	2.178
8.0	4.02	4900	1.5	B	30.11088	2.164
8.0	4.02	5000	1.5	B	28.18519	2.149
8.0	4.02	5100	1.5	B	26.38067	2.132
8.0	4.02	5200	1.5	B	24.67315	2.116
8.0	4.02	5300	1.5	B	23.04537	2.099
8.0	4.02	5400	1.5	B	21.54641	2.082
8.0	4.02	5500	1.5	B	20.09259	2.062
8.0	4.02	5600	1.5	B	18.70197	2.041
8.0	4.02	4600	1.7	B	36.09444	2.191
8.0	4.02	4700	1.7	B	33.72141	2.181
8.0	4.02	4800	1.7	B	31.85532	2.171
8.0	4.02	4900	1.7	B	29.84965	2.156
8.0	4.02	5000	1.7	B	27.97708	2.142
8.0	4.02	5100	1.7	B	26.20313	2.127
8.0	4.02	5200	1.7	B	24.52269	2.112
8.0	4.02	5300	1.7	B	22.961	2.096
8.0	4.02	5400	1.7	B	21.4412	2.078
8.0	4.02	5500	1.7	B	20.01863	2.059
8.0	4.02	5600	1.7	B	18.65567	2.039
8.0	4.02	4900	1.9	B	29.55116	2.146
8.0	4.02	5000	1.9	B	27.73449	2.134
8.0	4.02	5100	1.9	B	26.00949	2.122
8.0	4.02	5200	1.9	B	24.34213	2.107
8.0	4.02	5300	1.9	B	22.79236	2.091
8.0	4.02	5400	1.9	B	21.30972	2.074
8.0	4.02	5500	1.9	B	19.92037	2.055
8.0	4.22	4200	1.5	C	73.9066	2.357
8.0	4.22	4300	1.5	C	69.56262	2.344
8.0	4.22	4400	1.5	C	64.59433	2.33
8.0	4.22	4500	1.5	C	59.96481	2.317
8.0	4.22	4600	1.5	C	56.78044	2.305
8.0	4.22	4700	1.5	C	53.12824	2.29
8.0	4.22	4800	1.5	C	49.19144	2.275

TABLE A.12: continued.

$M/M_{\odot}$	$\log(L/L_{\odot})$	T_{eff}[K]	α_{ml}	ML	P[d]	$\log(\overline{R}/R_{\odot})$
(1)	(2)	(3)	(4)	(5)	(6)	(7)
8.0	4.22	4900	1.5	C	46.28785	2.261
8.0	4.22	5000	1.5	C	43.33924	2.246
8.0	4.22	5100	1.5	C	40.55359	2.231
8.0	4.22	5200	1.5	C	37.80405	2.214
8.0	4.22	5300	1.5	C	35.29769	2.196
8.0	4.22	5400	1.5	C	32.54329	2.171
8.0	4.22	5500	1.5	C	30.61632	2.156
8.0	4.22	4200	1.7	C	71.83056	2.347
8.0	4.22	4300	1.7	C	68.05035	2.337
8.0	4.22	4400	1.7	C	63.68715	2.325
8.0	4.22	4500	1.7	C	59.43414	2.31
8.0	4.22	4600	1.7	C	56.19653	2.299
8.0	4.22	4700	1.7	C	52.72477	2.287
8.0	4.22	4800	1.7	C	48.93056	2.27
8.0	4.22	4900	1.7	C	46.0581	2.258
8.0	4.22	5000	1.7	C	43.1265	2.243
8.0	4.22	5100	1.7	C	40.25764	2.228
8.0	4.22	5200	1.7	C	37.62049	2.21
8.0	4.22	5300	1.7	C	35.04097	2.192
8.0	4.22	5400	1.7	C	32.62326	2.172
8.0	4.22	4500	1.9	C	58.54965	2.304
8.0	4.22	4600	1.9	C	55.75868	2.294
8.0	4.22	4700	1.9	C	52.3213	2.28
8.0	4.22	4800	1.9	C	48.53912	2.265
8.0	4.22	4900	1.9	C	45.71354	2.253
8.0	4.22	5000	1.9	C	42.86065	2.237
8.0	4.22	5100	1.9	C	40.0603	2.223
8.0	4.22	5200	1.9	C	37.34525	2.205
9.0	3.99	4500	1.5	A	33.33507	2.196
9.0	3.99	4600	1.5	A	31.42639	2.187
9.0	3.99	4700	1.5	A	29.38773	2.172
9.0	3.99	4800	1.5	A	27.53414	2.159
9.0	3.99	4900	1.5	A	25.77488	2.143
9.0	3.99	5000	1.5	A	23.96852	2.129
9.0	3.99	5100	1.5	A	23.99884	2.116
9.0	3.99	5200	1.5	A	21.19549	2.101
9.0	3.99	5300	1.5	A	19.79468	2.083
9.0	3.99	5400	1.5	A	18.47917	2.065
9.0	3.99	5500	1.5	A	17.10752	2.043
9.0	3.99	5600	1.5	A	16.16725	2.026
9.0	3.99	5700	1.5	A	15.16481	2.009
9.0	3.99	4800	1.7	A	27.2581	2.149
9.0	3.99	4900	1.7	A	25.5184	2.138
9.0	3.99	5000	1.7	A	23.81505	2.123
9.0	3.99	5100	1.7	A	22.52789	2.112
9.0	3.99	5200	1.7	A	21.09155	2.097

TABLE A.12: continued.

$M/M_{\odot}$	$\log(L/L_{\odot})$	T_{eff}[K]	α_{ml}	ML	P[d]	$\log(\overline{R}/R_{\odot})$
(1)	(2)	(3)	(4)	(5)	(6)	(7)
9.0	3.99	5300	1.7	A	19.74606	2.082
9.0	3.99	5400	1.7	A	18.45648	2.064
9.0	3.99	5500	1.7	A	17.10752	2.043
9.0	3.99	5600	1.7	A	16.16725	2.025
9.0	3.99	5000	1.9	A	23.5081	2.113
9.0	3.99	5100	1.9	A	22.30532	2.105
9.0	3.99	5200	1.9	A	21.01366	2.092
9.0	3.99	5300	1.9	A	19.67315	2.077
9.0	3.99	5400	1.9	A	18.43368	2.061
9.0	3.99	5500	1.9	A	17.08576	2.04
9.0	4.19	4100	1.5	B	66.62998	2.351
9.0	4.19	4200	1.5	B	62.82049	2.343
9.0	4.19	4300	1.5	B	59.07766	2.332
9.0	4.19	4400	1.5	B	55.41435	2.32
9.0	4.19	4500	1.5	B	51.71991	2.306
9.0	4.19	4600	1.5	B	48.42975	2.292
9.0	4.19	4700	1.5	B	45.39664	2.279
9.0	4.19	4800	1.5	B	42.41655	2.264
9.0	4.19	4900	1.5	B	39.6941	2.249
9.0	4.19	5000	1.5	B	37.10938	2.234
9.0	4.19	5100	1.5	B	34.79688	2.219
9.0	4.19	5200	1.5	B	32.44653	2.202
9.0	4.19	5300	1.5	B	30.36586	2.185
9.0	4.19	5400	1.5	B	28.19896	2.163
9.0	4.19	5500	1.5	B	26.1588	2.14
9.0	4.19	4400	1.7	B	54.68137	2.308
9.0	4.19	4500	1.7	B	51.17836	2.298
9.0	4.19	4600	1.7	B	48.05718	2.286
9.0	4.19	4700	1.7	B	45.05278	2.271
9.0	4.19	4800	1.7	B	42.09838	2.257
9.0	4.19	4900	1.7	B	39.4485	2.244
9.0	4.19	5000	1.7	B	36.88148	2.229
9.0	4.19	5100	1.7	B	34.54259	2.215
9.0	4.19	5200	1.7	B	32.20972	2.197
9.0	4.19	5300	1.7	B	30.07095	2.18
9.0	4.19	5400	1.7	B	28.06111	2.159
9.0	4.19	4800	1.9	B	41.78032	2.251
9.0	4.19	4900	1.9	B	39.00637	2.237
9.0	4.19	5000	1.9	B	36.56227	2.222
9.0	4.19	5100	1.9	B	34.24595	2.208
9.0	4.19	5200	1.9	B	31.9728	2.192
9.0	4.19	5300	1.9	B	29.84988	2.174
9.0	4.39	4300	1.5	C	78.56262	2.433
9.0	4.39	4400	1.5	C	86.98947	2.418
9.0	4.39	4500	1.5	C	81.15845	2.405
9.0	4.39	4600	1.5	C	75.62176	2.391

TABLE A.12: continued.

$M/M_{\odot}$	$\log(L/L_{\odot})$	T_{eff}[K]	α_{ml}	ML	P[d]	$\log(\overline{R}/R_{\odot})$
(1)	(2)	(3)	(4)	(5)	(6)	(7)
9.0	4.39	4700	1.5	C	70.49086	2.376
9.0	4.39	4800	1.5	C	65.99352	2.361
9.0	4.39	4900	1.5	C	61.51296	2.347
9.0	4.39	5000	1.5	C	57.42199	2.331
9.0	4.39	5100	1.5	C	53.46852	2.313
9.0	4.39	5200	1.5	C	49.6816	2.293
9.0	4.39	5300	1.5	C	46.20579	2.273
9.0	4.39	4400	1.7	C	85.59769	2.414
9.0	4.39	4500	1.7	C	80.09618	2.4
9.0	4.39	4600	1.7	C	75.03704	2.386
9.0	4.39	4700	1.7	C	69.95278	2.372
9.0	4.39	4800	1.7	C	65.49977	2.358
9.0	4.39	4900	1.7	C	61.05729	2.342
9.0	4.39	5000	1.7	C	57.1412	2.328
9.0	4.39	5100	1.7	C	53.33843	2.31
9.0	4.39	5200	1.7	C	49.56076	2.291
9.0	4.39	5300	1.7	C	46.37477	2.274
9.0	4.39	4300	1.9	C	89.6419	2.419
9.0	4.39	4400	1.9	C	84.43773	2.407
9.0	4.39	4500	1.9	C	79.24641	2.396
9.0	4.39	4600	1.9	C	74.25752	2.383
9.0	4.39	4700	1.9	C	69.4147	2.368
9.0	4.39	4800	1.9	C	65.00602	2.354
9.0	4.39	4900	1.9	C	60.75347	2.338
9.0	4.39	5000	1.9	C	56.86042	2.322
9.0	4.39	5100	1.9	C	52.81806	2.305
10.0	4.14	4400	1.5	A	46.19803	2.294
10.0	4.14	4500	1.5	A	42.75625	2.28
10.0	4.14	4600	1.5	A	40.07512	2.266
10.0	4.14	4700	1.5	A	37.85613	2.254
10.0	4.14	4800	1.5	A	35.12454	2.238
10.0	4.14	4900	1.5	A	33.07789	2.225
10.0	4.14	5000	1.5	A	30.86539	2.209
10.0	4.14	5100	1.5	A	28.9081	2.193
10.0	4.14	5200	1.5	A	26.97963	2.177
10.0	4.14	5300	1.5	A	25.25625	2.159
10.0	4.14	5400	1.5	A	23.59444	2.141
10.0	4.14	5500	1.5	A	21.96898	2.12
10.0	4.14	4700	1.7	A	37.47662	2.245
10.0	4.14	4800	1.7	A	34.75382	2.231
10.0	4.14	4900	1.7	A	32.83287	2.219
10.0	4.14	5000	1.7	A	30.55822	2.203
10.0	4.14	5100	1.7	A	28.76655	2.189
10.0	4.14	5200	1.7	A	26.91354	2.173
10.0	4.14	5300	1.7	A	25.16354	2.156
10.0	4.14	5400	1.7	A	23.50775	2.138

TABLE A.12: continued.

$M/M_{\odot}$	$\log(L/L_{\odot})$	T_{eff}[K]	α_{ml}	ML	P[d]	$\log(\overline{R}/R_{\odot})$
(1)	(2)	(3)	(4)	(5)	(6)	(7)
10.0	4.14	5000	1.9	A	30.32789	2.196
10.0	4.14	5100	1.9	A	28.44815	2.181
10.0	4.14	5200	1.9	A	26.68241	2.167
10.0	4.14	5300	1.9	A	25.00914	2.152
10.0	4.34	4100	1.5	B	86.76181	2.433
10.0	4.34	4200	1.5	B	81.93044	2.421
10.0	4.34	4300	1.5	B	76.79005	2.409
10.0	4.34	4400	1.5	B	71.77199	2.397
10.0	4.34	4500	1.5	B	67.04086	2.382
10.0	4.34	4600	1.5	B	62.68299	2.37
10.0	4.34	4700	1.5	B	58.12685	2.354
10.0	4.34	4800	1.5	B	54.63495	2.339
10.0	4.34	4900	1.5	B	51.01319	2.325
10.0	4.34	5000	1.5	B	47.70139	2.31
10.0	4.34	5100	1.5	B	44.57905	2.294
10.0	4.34	5200	1.5	B	41.60741	2.276
10.0	4.34	5300	1.5	B	38.68218	2.255
10.0	4.34	5400	1.5	B	35.88032	2.233
10.0	4.34	4200	1.7	B	79.67963	2.413
10.0	4.34	4300	1.7	B	75.35278	2.403
10.0	4.34	4400	1.7	B	70.63877	2.39
10.0	4.34	4500	1.7	B	66.34977	2.377
10.0	4.34	4600	1.7	B	62.20567	2.363
10.0	4.34	4700	1.7	B	57.67037	2.348
10.0	4.34	4800	1.7	B	54.15984	2.335
10.0	4.34	4900	1.7	B	50.63623	2.321
10.0	4.34	5000	1.7	B	47.29375	2.305
10.0	4.34	5100	1.7	B	44.2544	2.289
10.0	4.34	5200	1.7	B	41.25486	2.271
10.0	4.34	4600	1.9	B	61.56933	2.357
10.0	4.34	4700	1.9	B	57.21389	2.343
10.0	4.34	4800	1.9	B	53.88843	2.328
10.0	4.34	4900	1.9	B	50.38495	2.314
10.0	4.34	5000	1.9	B	46.94421	2.299
10.0	4.34	5100	1.9	B	43.82164	2.28
10.0	4.54	4500	1.5	C	106.6522	2.481
10.0	4.54	4600	1.5	C	98.71921	2.466
10.0	4.54	4700	1.5	C	91.72465	2.452
10.0	4.54	4800	1.5	C	85.49826	2.436
10.0	4.54	4900	1.5	C	79.61713	2.42
10.0	4.54	5000	1.5	C	74.06875	2.403
10.0	4.54	5100	1.5	C	69.26296	2.387
10.0	4.54	5200	1.5	C	64.36238	2.367
10.0	4.54	4500	1.7	C	105.02384	2.476
10.0	4.54	4600	1.7	C	97.72211	2.463
10.0	4.54	4700	1.7	C	90.80741	2.447

TABLE A.12: continued.

$M/M_{\odot}$	$\log(L/L_{\odot})$	T_{eff}[K]	α_{ml}	ML	P[d]	$\log(\overline{R}/R_{\odot})$
(1)	(2)	(3)	(4)	(5)	(6)	(7)
10.0	4.54	4800	1.7	C	84.86505	2.433
10.0	4.54	4900	1.7	C	79.0331	2.418
10.0	4.54	5000	1.7	C	73.70914	2.402
10.0	4.54	5100	1.7	C	68.76343	2.385
10.0	4.54	5200	1.7	C	64.20764	2.366
10.0	4.54	4400	1.9	C	110.52778	2.485
10.0	4.54	4500	1.9	C	103.3956	2.473
10.0	4.54	4600	1.9	C	96.72488	2.458
10.0	4.54	4700	1.9	C	90.34873	2.445
10.0	4.54	4800	1.9	C	84.23171	2.429
10.0	4.54	4900	1.9	C	78.64375	2.414
10.0	4.54	5000	1.9	C	73.16979	2.396
11.0	4.28	4200	1.5	A	65.83958	2.389
11.0	4.28	4300	1.5	A	62.01632	2.378
11.0	4.28	4400	1.5	A	57.94641	2.367
11.0	4.28	4500	1.5	A	54.16829	2.354
11.0	4.28	4600	1.5	A	50.14884	2.338
11.0	4.28	4700	1.5	A	47.37627	2.325
11.0	4.28	4800	1.5	A	44.37546	2.312
11.0	4.28	4900	1.5	A	41.52593	2.296
11.0	4.28	5000	1.5	A	38.77465	2.28
11.0	4.28	5100	1.5	A	36.22014	2.264
11.0	4.28	5200	1.5	A	33.825	2.246
11.0	4.28	5300	1.5	A	31.44583	2.227
11.0	4.28	5400	1.5	A	29.30023	2.206
11.0	4.28	5500	1.5	A	27.26296	2.186
11.0	4.28	4500	1.7	A	53.47199	2.344
11.0	4.28	4600	1.7	A	49.67894	2.329
11.0	4.28	4700	1.7	A	47.02014	2.318
11.0	4.28	4800	1.7	A	43.99051	2.305
11.0	4.28	4900	1.7	A	41.11782	2.29
11.0	4.28	5000	1.7	A	38.49016	2.276
11.0	4.28	5100	1.7	A	35.95544	2.258
11.0	4.28	5200	1.7	A	33.57801	2.241
11.0	4.28	5300	1.7	A	31.29201	2.223
11.0	4.28	4900	1.9	A	40.70972	2.281
11.0	4.28	5000	1.9	A	38.111	2.266
11.0	4.28	5100	1.9	A	35.55845	2.251
11.0	4.28	5200	1.9	A	33.24942	2.234
11.0	4.48	4100	1.5	B	91.42037	2.503
11.0	4.48	4200	1.5	B	103.83912	2.493
11.0	4.48	4300	1.5	B	97.45984	2.481
11.0	4.48	4400	1.5	B	90.91516	2.466
11.0	4.48	4500	1.5	B	84.94676	2.453
11.0	4.48	4600	1.5	B	78.0169	2.436
11.0	4.48	4700	1.5	B	73.72361	2.424

TABLE A.12: continued.

$M/M_\odot$	$\log(L/L_\odot)$	T_{eff}[K]	α_{ml}	ML	P[d]	$\log(\overline{R}/R_\odot)$
(1)	(2)	(3)	(4)	(5)	(6)	(7)
11.0	4.48	4800	1.5	B	68.73125	2.408
11.0	4.48	4900	1.5	B	64.16759	2.394
11.0	4.48	5000	1.5	B	59.85035	2.376
11.0	4.48	5100	1.5	B	55.87581	2.36
11.0	4.48	5200	1.5	B	51.98183	2.34
11.0	4.48	5300	1.5	B	48.20567	2.319
11.0	4.48	4100	1.7	B	106.38588	2.495
11.0	4.48	4200	1.7	B	101.2787	2.486
11.0	4.48	4300	1.7	B	95.38623	2.474
11.0	4.48	4400	1.7	B	89.49086	2.461
11.0	4.48	4500	1.7	B	83.85764	2.447
11.0	4.48	4600	1.7	B	77.37384	2.431
11.0	4.48	4700	1.7	B	73.16921	2.418
11.0	4.48	4800	1.7	B	68.39016	2.405
11.0	4.48	4900	1.7	B	63.8522	2.39
11.0	4.48	5000	1.7	B	59.55833	2.372
11.0	4.48	5100	1.7	B	55.53715	2.356
11.0	4.48	4400	1.9	B	88.30394	2.455
11.0	4.48	4500	1.9	B	82.98646	2.442
11.0	4.48	4600	1.9	B	76.7309	2.427
11.0	4.48	4700	1.9	B	72.61493	2.413
11.0	4.48	4800	1.9	B	67.87859	2.398
11.0	4.48	4900	1.9	B	63.37928	2.383
11.0	4.48	5000	1.9	B	58.97442	2.365
11.0	4.68	4700	1.5	C	119.7963	2.519
11.0	4.68	4800	1.5	C	108.17558	2.502
11.0	4.68	4900	1.5	C	100.6772	2.487
11.0	4.68	5000	1.5	C	93.77315	2.471
11.0	4.68	5100	1.5	C	87.64039	2.454
11.0	4.68	4700	1.7	C	116.32407	2.515
11.0	4.68	4800	1.7	C	107.64132	2.501
11.0	4.68	4900	1.7	C	99.94236	2.484
11.0	4.68	5000	1.7	C	93.54722	2.469
11.0	4.68	5100	1.7	C	87.43125	2.452
11.0	4.68	4700	1.9	C	114.87685	2.514
11.0	4.68	4800	1.9	C	106.84005	2.499
11.0	4.68	4900	1.9	C	99.45243	2.482

TABLE A.13: The intrinsic stellar parameters for computed FO-mode models.

		Z=0.008	Y= 0.25			
$M/M_\odot$	$\log(L/L_\odot)$	T_{eff}[K]	α_{ml}	ML	P[d]	$\log(\overline{R}/R_\odot)$
(1)	(2)	(3)	(4)	(5)	(6)	(7)
3.0	2.39	6100	1.5	A	0.79791	1.151
3.0	2.39	6200	1.5	A	0.75783	1.138
3.0	2.39	6300	1.5	A	0.72289	1.126

TABLE A.13: continued.

$M/M_\odot$	$\log(L/L_\odot)$	T_{eff}[K]	α_{ml}	ML	P[d]	$\log(\overline{R}/R_\odot)$
(1)	(2)	(3)	(4)	(5)	(6)	(7)
3.0	2.39	6400	1.5	A	0.68463	1.112
3.0	2.39	6500	1.5	A	0.65323	1.098
3.0	2.39	6600	1.5	A	0.62295	1.086
3.0	2.39	6200	1.7	A	0.75783	1.136
3.0	2.39	6300	1.7	A	0.72169	1.123
3.0	2.39	6400	1.7	A	0.68577	1.111
3.0	2.39	6500	1.7	A	0.65323	1.097
3.0	2.39	6600	1.7	A	0.62295	1.085
3.0	2.39	6700	1.7	A	0.59454	1.071
3.0	2.39	6400	1.9	A	0.68463	1.11
3.0	2.39	6500	1.9	A	0.65214	1.096
3.0	2.39	6600	1.9	A	0.62243	1.084
3.0	2.39	6700	1.9	A	0.59553	1.071
3.0	2.59	6000	1.5	B	1.2134	1.264
3.0	2.59	6100	1.5	B	1.15121	1.251
3.0	2.59	6200	1.5	B	1.09342	1.239
3.0	2.59	6300	1.5	B	1.03929	1.225
3.0	2.59	6400	1.5	B	0.98816	1.212
3.0	2.59	6500	1.5	B	0.93431	1.197
3.0	2.59	6600	1.5	B	0.88963	1.184
3.0	2.59	6700	1.5	B	0.85217	1.168
3.0	2.59	6100	1.7	B	1.15696	1.251
3.0	2.59	6200	1.7	B	1.09342	1.238
3.0	2.59	6300	1.7	B	1.03929	1.224
3.0	2.59	6400	1.7	B	0.98816	1.21
3.0	2.59	6500	1.7	B	0.93431	1.197
3.0	2.59	6600	1.7	B	0.89112	1.183
3.0	2.59	6200	1.9	B	1.09705	1.236
3.0	2.59	6300	1.9	B	1.03757	1.222
3.0	2.59	6400	1.9	B	0.9898	1.21
3.0	2.59	6500	1.9	B	0.93273	1.195
3.0	2.59	6600	1.9	B	0.89037	1.181
3.0	2.79	6100	1.5	C	1.67913	1.351
3.0	2.79	6200	1.5	C	1.59503	1.338
3.0	2.79	6300	1.5	C	1.51167	1.325
3.0	2.79	6400	1.5	C	1.43685	1.31
3.0	2.79	6500	1.5	C	1.3627	1.295
3.0	2.79	6200	1.7	C	1.6003	1.338
3.0	2.79	6300	1.7	C	1.51666	1.325
3.0	2.79	6400	1.7	C	1.43927	1.311
3.0	2.79	6500	1.7	C	1.3672	1.296
3.0	2.79	6200	1.9	C	1.59241	1.336
3.0	2.79	6300	1.9	C	1.51666	1.324
3.0	2.79	6400	1.9	C	1.43451	1.31
4.0	2.81	5900	1.5	A	1.62559	1.388
4.0	2.81	6000	1.5	A	1.53301	1.375

TABLE A.13: continued.

$M/M_{\odot}$	$\log(L/L_{\odot})$	T_{eff}[K]	α_{ml}	ML	P[d]	$\log(\overline{R}/R_{\odot})$
(1)	(2)	(3)	(4)	(5)	(6)	(7)
4.0	2.81	6100	1.5	A	1.45461	1.362
4.0	2.81	6200	1.5	A	1.38473	1.348
4.0	2.81	6300	1.5	A	1.30512	1.333
4.0	2.81	6400	1.5	A	1.25025	1.32
4.0	2.81	6500	1.5	A	1.18449	1.305
4.0	2.81	6000	1.7	A	1.52784	1.372
4.0	2.81	6100	1.7	A	1.45218	1.36
4.0	2.81	6200	1.7	A	1.38704	1.346
4.0	2.81	6300	1.7	A	1.30731	1.333
4.0	2.81	6400	1.7	A	1.24818	1.32
4.0	2.81	6500	1.7	A	1.18449	1.305
4.0	2.81	6100	1.9	A	1.45704	1.358
4.0	2.81	6200	1.9	A	1.38244	1.347
4.0	2.81	6300	1.9	A	1.30731	1.332
4.0	2.81	6400	1.9	A	1.24818	1.319
4.0	2.81	6500	1.9	A	1.18052	1.304
4.0	3.01	6000	1.5	B	2.24179	1.475
4.0	3.01	6100	1.5	B	2.12035	1.462
4.0	3.01	6200	1.5	B	1.99541	1.446
4.0	3.01	6300	1.5	B	1.90983	1.433
4.0	3.01	6400	1.5	B	1.81256	1.418
4.0	3.01	6100	1.7	B	2.12035	1.461
4.0	3.01	6200	1.7	B	2.00221	1.445
4.0	3.01	6300	1.7	B	1.90983	1.432
4.0	3.01	6100	1.9	B	2.14843	1.46
4.0	3.01	6200	1.9	B	2.00221	1.444
4.0	3.21	5700	1.5	C	3.91602	1.622
4.0	3.21	5800	1.5	C	3.70924	1.607
4.0	3.21	5900	1.5	C	3.50234	1.593
4.0	3.21	6000	1.5	C	3.30535	1.578
4.0	3.21	6100	1.5	C	3.13284	1.563
4.0	3.21	6200	1.5	C	2.94538	1.545
4.0	3.21	5800	1.7	C	3.70266	1.605
4.0	3.21	5900	1.7	C	3.50234	1.591
4.0	3.21	6000	1.7	C	3.29973	1.576
4.0	3.21	6100	1.7	C	3.12273	1.561
5.0	3.14	5900	1.5	A	2.60887	1.552
5.0	3.14	6000	1.5	A	2.47821	1.537
5.0	3.14	6100	1.5	A	2.34137	1.524
5.0	3.14	6200	1.5	A	2.20483	1.509
5.0	3.14	6300	1.5	A	2.10826	1.496
5.0	3.14	6000	1.7	A	2.46184	1.536
5.0	3.14	6100	1.7	A	2.33363	1.523
5.0	3.14	6200	1.7	A	2.20483	1.508
5.0	3.14	6300	1.7	A	2.10131	1.495
5.0	3.14	6100	1.9	A	2.33363	1.522

TABLE A.13: continued.

$M/M_\odot$	log(L/$L_\odot$)	T_{eff}[K]	α_{ml}	ML	P[d]	log($\overline{R}/R_\odot$)
(1)	(2)	(3)	(4)	(5)	(6)	(7)
5.0	3.14	6200	1.9	A	2.20483	1.507
5.0	3.34	5600	1.5	B	4.56631	1.698
5.0	3.34	5700	1.5	B	4.28316	1.684
5.0	3.34	5800	1.5	B	4.08241	1.671
5.0	3.34	5900	1.5	B	3.85576	1.655
5.0	3.34	6000	1.5	B	3.63963	1.638
5.0	3.34	6100	1.5	B	3.43774	1.624
5.0	3.34	5700	1.7	B	4.28316	1.681
5.0	3.34	5800	1.7	B	4.07571	1.668
5.0	3.34	5900	1.7	B	3.85576	1.653
5.0	3.34	6000	1.7	B	3.6277	1.637
6.0	3.40	5500	1.5	A	4.87884	1.746
6.0	3.40	5600	1.5	A	4.61845	1.73
6.0	3.40	5700	1.5	A	4.36213	1.715
6.0	3.40	5800	1.5	A	4.11089	1.699
6.0	3.40	5900	1.5	A	3.89044	1.684
6.0	3.40	6000	1.5	A	3.66273	1.671
6.0	3.40	6100	1.5	A	3.45172	1.655
6.0	3.40	6200	1.5	A	3.27817	1.642
6.0	3.40	5600	1.7	A	4.58796	1.728
6.0	3.40	5700	1.7	A	4.34778	1.714
6.0	3.40	5800	1.7	A	4.13793	1.698
6.0	3.40	5900	1.7	A	3.95421	1.685
6.0	3.40	6000	1.7	A	3.65076	1.67
6.0	3.40	6100	1.7	A	3.46311	1.654
7.0	3.63	5600	1.5	A	6.44336	1.843
7.0	3.63	5700	1.5	A	6.06308	1.83
7.0	3.63	5800	1.5	A	5.74236	1.813
7.0	3.63	5900	1.5	A	5.40022	1.798
7.0	3.63	5700	1.7	A	6.06308	1.827
7.0	3.63	5800	1.7	A	5.7236	1.811

TABLE A.14: The intrinsic stellar parameters for computed SO-mode models.

		Z=0.008	Y= 0.25			
$M/M_\odot$	log(L/$L_\odot$)	T_{eff}[K]	α_{ml}	ML	P[d]	log($\overline{R}/R_\odot$)
(1)	(2)	(3)	(4)	(5)	(6)	(7)
3.0	2.39	6500	1.5	A	0.52047	1.096
3.0	2.39	6600	1.5	A	0.50097	1.083
3.0	2.39	6700	1.5	A	0.47628	1.071
3.0	2.39	6800	1.5	A	0.45485	1.058
3.0	2.39	6900	1.5	A	0.43455	1.043
3.0	2.39	6700	1.7	A	0.47628	1.07

TABLE A.15: The intrinsic stellar parameters for computed F-mode models.

		Z=0.03	Y= 0.28			
$M/M_\odot$	log(L/$L_\odot$)	T_{eff}[K]	α_{ml}	ML	P[d]	log($\overline{R}/R_\odot$)
(1)	(2)	(3)	(4)	(5)	(6)	(7)
4.0	2.68	5600	1.5	A	2.14887	1.367
4.0	2.68	5700	1.5	A	2.02639	1.352
4.0	2.68	5800	1.5	A	1.92388	1.339
4.0	2.68	5900	1.5	A	1.81678	1.325
4.0	2.68	6000	1.5	A	1.71735	1.309
4.0	2.68	6100	1.5	A	1.66045	1.296
4.0	2.88	5300	1.5	B	3.82169	1.516
4.0	2.88	5400	1.5	B	3.6036	1.501
4.0	2.88	5500	1.5	B	3.39337	1.486
4.0	2.88	5600	1.5	B	3.16762	1.468
4.0	2.88	5700	1.5	B	3.01821	1.455
4.0	2.88	5800	1.5	B	2.84645	1.441
4.0	2.88	5900	1.5	B	2.68406	1.426
5.0	3.01	5300	1.5	A	4.2556	1.581
5.0	3.01	5400	1.5	A	4.00248	1.565
5.0	3.01	5500	1.5	A	3.76854	1.551
5.0	3.01	5600	1.5	A	3.55648	1.536
5.0	3.01	5700	1.5	A	3.35089	1.521
5.0	3.01	5800	1.5	A	3.16791	1.505
5.0	3.21	5000	1.5	B	7.72772	1.73
5.0	3.21	5100	1.5	B	7.22242	1.713
5.0	3.21	5200	1.5	B	6.6902	1.695
5.0	3.21	5300	1.5	B	6.3661	1.682
5.0	3.21	5400	1.5	B	5.97267	1.666
5.0	3.21	5500	1.5	B	5.62288	1.652
5.0	3.21	5600	1.5	B	5.29789	1.636
6.0	3.27	5100	1.5	A	7.18299	1.743
6.0	3.27	5200	1.5	A	6.72238	1.727
6.0	3.27	5300	1.5	A	6.33052	1.712
6.0	3.27	5400	1.5	A	5.93872	1.697
6.0	3.27	5500	1.5	A	5.59045	1.681
6.0	3.27	5600	1.5	A	5.26714	1.664
6.0	3.47	4700	1.5	B	14.23299	1.917
6.0	3.47	4800	1.5	B	13.27014	1.906
6.0	3.47	4900	1.5	B	12.42743	1.89
6.0	3.47	5000	1.5	B	11.61412	1.875
6.0	3.47	5100	1.5	B	10.89613	1.857
6.0	3.47	5200	1.5	B	10.19829	1.839
6.0	3.47	5300	1.5	B	9.53266	1.819
6.0	3.47	5400	1.5	B	8.93985	1.8
7.0	3.50	4800	1.5	A	12.63542	1.917
7.0	3.50	4900	1.5	A	11.7897	1.902
7.0	3.50	5000	1.5	A	11.0448	1.883
7.0	3.50	5100	1.5	A	10.29799	1.864
7.0	3.50	5200	1.5	A	9.50878	1.842

TABLE A.15: continued.

$M/M_\odot$	$\log(L/L_\odot)$	T_{eff}[K]	α_{ml}	ML	P[d]	$\log(\overline{R}/R_\odot)$
(1)	(2)	(3)	(4)	(5)	(6)	(7)
7.0	3.50	5300	1.5	A	9.05206	1.827
7.0	3.50	5400	1.5	A	8.48928	1.811
7.0	3.70	4400	1.5	B	25.42894	2.082
7.0	3.70	4500	1.5	B	23.68877	2.067
7.0	3.70	4600	1.5	B	22.07037	2.052
7.0	3.70	4700	1.5	B	20.53785	2.037
7.0	3.70	4800	1.5	B	19.20683	2.022
7.0	3.70	4900	1.5	B	17.94248	2.006
7.0	3.70	5000	1.5	B	16.46713	1.986
7.0	3.70	5100	1.5	B	15.68924	1.972
7.0	3.70	5200	1.5	B	14.64676	1.952
8.0	3.69	4600	1.5	A	19.54225	2.045
8.0	3.69	4700	1.5	A	18.00428	2.03
8.0	3.69	4800	1.5	A	17.0485	2.018
8.0	3.69	4900	1.5	A	15.92789	2.003
8.0	3.69	5000	1.5	A	14.93935	1.986
8.0	3.69	5100	1.5	A	13.9125	1.968
8.0	3.69	5200	1.5	A	13.01944	1.949
8.0	3.89	4200	1.5	B	39.97477	2.212
8.0	3.89	4300	1.5	B	37.13171	2.199
8.0	3.89	4400	1.5	B	34.6235	2.183
8.0	3.89	4500	1.5	B	32.27025	2.169
8.0	3.89	4600	1.5	B	29.96794	2.151
8.0	3.89	4700	1.5	B	27.91157	2.136
8.0	3.89	4800	1.5	B	26.0309	2.118
8.0	3.89	4900	1.5	B	23.73611	2.094
8.0	3.89	5000	1.5	B	22.63889	2.079
9.0	3.86	4400	1.5	A	29.55613	2.163
9.0	3.86	4500	1.5	A	27.46898	2.148
9.0	3.86	4600	1.5	A	25.59271	2.132
9.0	3.86	4700	1.5	A	23.83264	2.118
9.0	3.86	4800	1.5	A	22.28519	2.101
9.0	3.86	4900	1.5	A	20.76447	2.085
9.0	3.86	5000	1.5	A	19.36678	2.066
9.0	3.86	5100	1.5	A	18.05012	2.045
9.0	4.06	4000	1.5	B	61.02986	2.328
9.0	4.06	4100	1.5	B	56.79468	2.316
9.0	4.06	4200	1.5	B	52.82894	2.302
9.0	4.06	4300	1.5	B	49.23194	2.288
9.0	4.06	4400	1.5	B	45.72095	2.272
9.0	4.06	4500	1.5	B	42.4816	2.255
9.0	4.06	4600	1.5	B	39.56435	2.239
9.0	4.06	4700	1.5	B	36.47222	2.219
9.0	4.06	4800	1.5	B	33.89363	2.198
9.0	4.06	4900	1.5	B	31.47951	2.178
10.0	4.02	4200	1.5	A	44.51377	2.277

TABLE A.15: continued.

$M/M_{\odot}$	$\log(L/L_{\odot})$	T_{eff}[K]	α_{ml}	ML	P[d]	$\log(\overline{R}/R_{\odot})$
(1)	(2)	(3)	(4)	(5)	(6)	(7)
10.0	4.02	4300	1.5	A	41.39259	2.264
10.0	4.02	4400	1.5	A	38.25243	2.248
10.0	4.02	4500	1.5	A	35.61354	2.233
10.0	4.02	4600	1.5	A	32.75683	2.212
10.0	4.02	4700	1.5	A	30.51528	2.194
10.0	4.02	4800	1.5	A	28.41331	2.177
10.0	4.02	4900	1.5	A	26.87986	2.162
10.0	4.22	3800	1.5	B	89.77025	2.436
10.0	4.22	3900	1.5	B	83.71551	2.422
10.0	4.22	4000	1.5	B	78.63102	2.41
10.0	4.22	4100	1.5	B	72.96586	2.395
10.0	4.22	4200	1.5	B	67.83021	2.381
10.0	4.22	4300	1.5	B	63.01493	2.364
10.0	4.22	4400	1.5	B	58.52998	2.347
10.0	4.22	4500	1.5	B	54.38437	2.33
10.0	4.22	4600	1.5	B	54.38437	2.33
10.0	4.22	4700	1.5	B	46.81053	2.293
11.0	4.15	4100	1.5	A	59.2919	2.36
11.0	4.15	4200	1.5	A	55.14583	2.347
11.0	4.15	4300	1.5	A	51.12257	2.333
11.0	4.15	4400	1.5	A	46.62419	2.31
11.0	4.15	4500	1.5	A	43.36424	2.296
11.0	4.15	4600	1.5	A	40.27836	2.277
11.0	4.15	4700	1.5	A	37.49688	2.26
11.0	4.15	4800	1.5	A	34.72396	2.24
11.0	4.35	3700	1.5	B	121.7419	2.519
11.0	4.35	3800	1.5	B	114.62465	2.507
11.0	4.35	3900	1.5	B	104.71933	2.491
11.0	4.35	4000	1.5	B	100.10856	2.481
11.0	4.35	4100	1.5	B	93.03681	2.467
11.0	4.35	4200	1.5	B	86.1934	2.451
11.0	4.35	4300	1.5	B	80.15718	2.434
11.0	4.35	4400	1.5	B	74.41308	2.419
11.0	4.35	4500	1.5	B	69.25856	2.401
11.0	4.35	4600	1.5	B	64.2853	2.382
11.0	4.35	4700	1.5	B	59.46493	2.36

TABLE A.16: The intrinsic stellar parameters for computed FO-mode models.

		Z=0.03	Y= 0.28			
$M/M_{\odot}$	$\log(L/L_{\odot})$	T_{eff}[K]	α_{ml}	ML	P[d]	$\log(\overline{R}/R_{\odot})$
(1)	(2)	(3)	(4)	(5)	(6)	(7)
4.0	2.68	6000	1.5	A	1.21353	1.309
4.0	2.68	6100	1.5	A	1.15266	1.296
4.0	2.68	6200	1.5	A	1.09496	1.282
4.0	2.68	6300	1.5	A	1.03927	1.267

TABLE A.16: continued.

$M/M_{\odot}$	$\log(L/L_{\odot})$	T_{eff}[K]	α_{ml}	ML	P[d]	$\log(\overline{R}/R_{\odot})$
(1)	(2)	(3)	(4)	(5)	(6)	(7)

Whole bibliography

Anderson, R. I., H. Saio, S. Ekström, C. Georgy, and G. Meynet (June 2016). "On the effect of rotation on populations of classical Cepheids. II. Pulsation analysis for metallicities 0.014, 0.006, and 0.002". In: *aap* 591, A8, A8. DOI: 10.1051/0004-6361/201528031. arXiv: 1604.05691 [astro-ph.SR].

Bailey, J. E. et al. (Jan. 2015). "A higher-than-predicted measurement of iron opacity at solar interior temperatures". In: *nat* 517.7532, pp. 56–59. DOI: 10.1038/nature14048.

Baker, N. and R. Kippenhahn (Oct. 1965). "The Pulsations of Models of Delta Cephei Stars. II." In: *apj* 142, p. 868. DOI: 10.1086/148359.

Bergemann, M. and A. Serenelli (2014). "Solar Abundance Problem". In: *Determination of Atmospheric Parameters of B*, pp. 245–258. DOI: 10.1007/978-3-319-06956-2_21.

Bhardwaj, A., S. M. Kanbur, M. Marconi, M. Rejkuba, H. P. Singh, and C. Ngeow (Sept. 2017). "Multiwavelength light curve parameters of Cepheid variables". In: *European Physical Journal Web of Conferences*. Vol. 152. European Physical Journal Web of Conferences, p. 01010. DOI: 10.1051/epjconf/201715201010. arXiv: 1704.02098 [astro-ph.SR].

Bird, J. C., K.Z. Stanek, and José L. Prieto (Apr. 2009). "Using Ultra Long Period Cepheids to Extend the Cosmic Distance Ladder to 100 Mpc and Beyond". In: *apj* 695.2, pp. 874–882. DOI: 10.1088/0004-637X/695/2/874. arXiv: 0807.4933 [astro-ph].

Böhm-Vitense, E. (Jan. 1958). "Über die Wasserstoffkonvektionszone in Sternen verschiedener Effektivtemperaturen und Leuchtkräfte. Mit 5 Textabbildungen". In: *zap* 46, p. 108.

Bono, G., F. Caputo, S. Cassisi, V. Castellani, and M. Marconi (Nov. 1997). "Evolutionary and Pulsational Constraints for Super-Metal-rich Stars with Z = 0.04". In: *apj* 489.2, pp. 822–847. DOI: 10.1086/304807.

Bono, G., F. Caputo, S. Cassisi, M. Marconi, L. Piersanti, and A. Tornambè (Nov. 2000a). "Intermediate-Mass Star Models with Different Helium and Metal Contents". In: *apj* 543.2, pp. 955–971. DOI: 10.1086/317156. arXiv: astro-ph/0006251 [astro-ph].

Bono, G., F. Caputo, V. Castellani, and M. Marconi (Feb. 1999a). "Theoretical Models for Classical Cepheids. II. Period-Luminosity, Period-Color, and Period-Luminosity-Color Relations". In: *apj* 512.2, pp. 711–723. DOI: 10.1086/306815. arXiv: astro-ph/9809127 [astro-ph].

Bono, G., F. Caputo, V. Castellani, M. Marconi, J. Storm, and S. Degl'Innocenti (Oct. 2003). "A pulsational approach to near-infrared and visual magnitudes of RR Lyr stars". In: *mnras* 344.4, pp. 1097–1106. DOI: 10.1046/j.1365-8711.2003.06878.x. arXiv: astro-ph/0306142 [astro-ph].

Bono, G., F. Caputo, and M. Marconi (Apr. 1998). "On the Theoretical Period-Radius Relation of Classical Cepheids". In: *apjl* 497.1, pp. L43–L46. DOI: 10.1086/311270.

Bono, G., F. Caputo, M. Marconi, and I. Musella (May 2010). "Insights into the Cepheid Distance Scale". In: *apj* 715.1, pp. 277–291. DOI: 10.1088/0004-637X/715/1/277. arXiv: 1004.0363 [astro-ph.SR].

Bono, G., V. Castellani, and M. Marconi (Jan. 2000b). "Classical Cepheid Pulsation Models. III. The Predictable Scenario". In: *apj* 529.1, pp. 293–317. DOI: 10.1086/308263. arXiv: astro-ph/9908014 [astro-ph].

Bono, G., W.P. Gieren, M. Marconi, P. Fouqué, and F. Caputo (Dec. 2001). "Improving the Mass Determination of Galactic Cepheids". In: *apj* 563.1, pp. 319–324. DOI: 10.1086/323834. arXiv: astro-ph/0108271 [astro-ph].

Bono, G., M Marconi, and R. F. Stellingwerf (May 1999b). "Classical Cepheid Pulsation Models. I. Physical Structure". In: *apjs* 122.1, pp. 167–205. DOI: 10.1086/313207.

Bono, G., M. Marconi, S. Cassisi, F. Caputo, W. Gieren, and G. Pietrzynski (Mar. 2005). "Classical Cepheid Pulsation Models. X. The Period-Age Relation". In: *apj* 621.2, pp. 966–977. DOI: 10.1086/427744. arXiv: astro-ph/0411756 [astro-ph].

Bono, G., M. Marconi, and R.F. Stellingwerf (Aug. 2000c). "Classical Cepheid pulsation models — VI. The Hertzsprung progression". In: *aap* 360, pp. 245–262. arXiv: astro-ph/0006229 [astro-ph].

Bono, G. and R. ~ F. Stellingwerf (July 1994). "Pulsation and Stability of RR Lyrae Stars. I. Instability Strip". In: *apjs* 93, p. 233. DOI: 10.1086/192054.

Bono, G. and R.F. Stellingwerf (Jan. 1992). "RR Lyrae convective models". In: *memsai* 63.2, pp. 357–384.

Bossini, D. et al. (Mar. 2019). "Age determination for 269 Gaia DR2 open clusters". In: *aap* 623, A108, A108. DOI: 10.1051/0004-6361/201834693. arXiv: 1901.04733 [astro-ph.SR].

Braga, V.F. et al. (Mar. 2018). "On the RR Lyrae Stars in Globulars. V. The Complete Near-infrared (JHK $_s$) Census of ω Centauri RR Lyrae Variables". In: *aj* 155.3, 137, p. 137. DOI: 10.3847/1538-3881/aaadab. arXiv: 1802.03578 [astro-ph.SR].

Caffau, E., H. -G. Ludwig, M. Steffen, B. Freytag, and P. Bonifacio (Feb. 2011). "Solar Chemical Abundances Determined with a CO5BOLD 3D Model Atmosphere". In: *solphys* 268.2, pp. 255–269. DOI: 10.1007/s11207-010-9541-4. arXiv: 1003.1190 [astro-ph.SR].

Caputo, F., G. Bono, G. Fiorentino, M. Marconi, and I. Musella (Aug. 2005a). "Pulsation and Evolutionary Masses of Classical Cepheids. I. Milky Way Variables". In: *apj* 629.2, pp. 1021–1033. DOI: 10.1086/431641. arXiv: astro-ph/0505149 [astro-ph].

— (Aug. 2005b). "Pulsation and Evolutionary Masses of Classical Cepheids. I. Milky Way Variables". In: *apj* 629.2, pp. 1021–1033. DOI: 10.1086/431641. arXiv: astro-ph/0505149 [astro-ph].

Caputo, F., V. Castellani, S. Degl'Innocenti, G. Fiorentino, and M. Marconi (Sept. 2004). "Bright metal-poor variables: Why "Anomalous" Cepheids?" In: *aap* 424, pp. 927–934. DOI: 10.1051/0004-6361:20040307. arXiv: astro-ph/0405395 [astro-ph].

Caputo, F., V. Castellani, M. Marconi, and V. Ripepi (Aug. 2000a). "Pulsational M_V versus [Fe/H] relation(s) for globular cluster RR Lyrae variables". In: *mnras* 316.4, pp. 819–826. DOI: 10.1046/j.1365-8711.2000.03591.x. arXiv: astro-ph/0003473 [astro-ph].

Caputo, F., M. Marconi, and I. Musella (Feb. 2000b). "Theoretical models for classical Cepheids. V. Multiwavelength relations". In: *aap* 354, pp. 610–620. arXiv: astro-ph/9911441 [astro-ph].

Caputo, F., M. Marconi, I. Musella, and P. Santolamazza (July 2000c). "Theoretical models for classical Cepheids. VII. Metallicity effects on the Cepheid distance scale". In: *aap* 359, pp. 1059–1067. arXiv: astro-ph/0006228 [astro-ph].

Cassisi, S. and M. Salaris (2013). *Old Stellar Populations: How to Study the Fossil Record of Galaxy Formation*.

Castelli, F. and R.L. Kurucz (Jan. 2003). "New Grids of ATLAS9 Model Atmospheres". In: *Modelling of Stellar Atmospheres*. Ed. by N. Piskunov, W.W. Weiss, and D.F. Gray. Vol. 210, A20. arXiv: astro-ph/0405087 [astro-ph].

Catelan, M., B. J. Pritzl, and H. A. Smith (Oct. 2004). "The RR Lyrae Period-Luminosity Relation. I. Theoretical Calibration". In: *apjs* 154.2, pp. 633–649. DOI: 10.1086/422916. arXiv: astro-ph/0406067 [astro-ph].

Catelan, M. and H. A. Smith (2015a). *Pulsating Stars*.

Catelan, M. and H.Ã. Smith (2015b). *Pulsating Stars*.

Chiosi, C., P. ~ R. Wood, and N. Capitanio (June 1993). "Theoretical Models of Cepheid Variables and Their BVI C Colors and Magnitudes". In: *apjs* 86, p. 541. DOI: 10.1086/191790.

Clement, C. M. et al. (Nov. 2001). "Variable Stars in Galactic Globular Clusters". In: *aj* 122.5, pp. 2587–2599. DOI: 10.1086/323719. arXiv: astro-ph/0108024 [astro-ph].

Clementini, G. et al. (Feb. 2019). "Gaia Data Release 2. Specific characterisation and validation of all-sky Cepheids and RR Lyrae stars". In: *aap* 622, A60, A60. DOI: 10.1051/0004-6361/201833374. arXiv: 1805.02079 [astro-ph.SR].

Coppola, G., M. Dall'Ora, V. Ripepi, M. Marconi, I. Musella, G. Bono, A.M. Piersimoni, P.B. Stetson, and J. Storm (Sept. 2011). "Distance to Galactic globulars using the near-infrared magnitudes of RR Lyrae stars - IV. The case of M5 (NGC 5904)". In: *mnras* 416.2, pp. 1056–1066. DOI: 10.1111/j.1365-2966.2011.19102.x. arXiv: 1105.4031 [astro-ph.GA].

Cox, A.Ñ. (Jan. 1980). "The masses of Cepheids". In: *araa* 18, pp. 15–41. DOI: 10.1146/annurev.aa.18.090180.000311.

Cox, J. P. (1980). *Theory of stellar pulsation*.

Cox, J. P. and R. T. Giuli (1968). *Principles of stellar structure*.

De Somma, G., M. Marconi, S. Cassisi, V. Ripepi, S. Leccia, R. Molinaro, and I. Musella (June 2020a). "Updated theoretical period-age and period-age-colour relations for Galactic Classical Cepheids: an application to the Gaia DR2 sample". In: *mnras* 496.4, pp. 5039–5051. DOI: 10.1093/mnras/staa1834. arXiv: 2006.12861 [astro-ph.SR].

De Somma, G., M. Marconi, R. Molinaro, M. Cignoni, I. Musella, and V. Ripepi (Mar. 2020b). "An Extended Theoretical Scenario for Classical Cepheids. I. Modeling Galactic Cepheids in the Gaia Photometric System". In: *apjs* 247.1, 30, p. 30. DOI: 10.3847/1538-4365/ab7204. arXiv: 2001.11065 [astro-ph.SR].

Demarque, P. and A. ~ W. Hirshfeld (Dec. 1975). "On the nature of the bright variables in dwarf spheroidal galaxies." In: *apj* 202, pp. 346–352. DOI: 10.1086/153982.

Di Criscienzo, M., F. Caputo, M. Marconi, and S. Cassisi (Sept. 2007). "Synthetic properties of bright metal-poor variables. II. BL Hercules stars". In: *aap* 471.3, pp. 893–900. DOI: 10.1051/0004-6361:20066541. arXiv: 0705.2679 [astro-ph].

Di Criscienzo, M., M. Marconi, and F. Caputo (Sept. 2004). "RR Lyrae Stars in Galactic Globular Clusters. III. Pulsational Predictions for Metal Content Z=0.0001 to Z=0.006". In: *apj* 612.2, pp. 1092–1106. DOI: 10.1086/422742. arXiv: astro-ph/0405415 [astro-ph].

Di Criscienzo, M., M. Marconi, I. Musella, M. Cignoni, and V. Ripepi (Jan. 2013). "Predicted properties of galactic and magellanic classical Cepheids in the SDSS filters". In: *mnras* 428.1, pp. 212–219. DOI: 10.1093/mnras/sts023. arXiv: 1209.4090 [astro-ph.SR].

Efremov, Iu. N. (Apr. 1978). "The period-age relation for Cepheids". In: *sovast* 22, p. 161.

Efremov, Y. N. and B. G. Elmegreen (Sept. 1998). "Hierarchical star formation from the time-space distribution of star clusters in the Large Magellanic Cloud". In: *mnras* 299.2, pp. 588–594. DOI: 10.1046/j.1365-8711.1998.01819.x. arXiv: astro-ph/9805259 [astro-ph].

Efremov, Yu. N. (Dec. 2003). "Cepheids in LMC Clusters and the Period-Age Relation". In: *Astronomy Reports* 47.12, pp. 1000–1012. DOI: 10.1134/1.1633613.

Evans, N. R., L. Berdnikov, N. Gorynya, A. Rastorguev, and J. Eaton (Sept. 2011). "The Orbit of the Cepheid V350 Sgr Revisited". In: *aj* 142.3, 87, p. 87. DOI: 10.1088/0004-6256/142/3/87.

Evans, N. R., C. Proffitt, K. G. Carpenter, E. M. Winston, G. V. Kober, H. M. Günther, N. Gorynya, A. Rastorguev, and L. Inno (Oct. 2018). "The Mass of the Cepheid V350 Sgr". In: *apj* 866.1, 30, p. 30. DOI: 10.3847/1538-4357/aade03. arXiv: 1808.10472 [astro-ph.SR].

Fiorentino, G., F. Caputo, M. Marconi, and I. Musella (Sept. 2002). "Theoretical Models for Classical Cepheids. VIII. Effects of Helium and Heavy-Element Abundance on the Cepheid Distance Scale". In: *apj* 576.1, pp. 402–412. DOI: 10.1086/341731. arXiv: astro-ph/0205147 [astro-ph].

Fiorentino, G., M. Limongi, F. Caputo, and M. Marconi (Dec. 2006). "Synthetic properties of bright metal-poor variables. I. "Anomalous" Cepheids". In: *aap* 460.1, pp. 155–166. DOI: 10.1051/0004-6361:20065349. arXiv: astro-ph/0609029 [astro-ph].

Fiorentino, G., M. Marconi, I. Musella, and F. Caputo (Dec. 2007). "Classical Cepheid pulsation models. XI. Effects of convection and chemical composition on the period-luminosity and period-Wesenheit relations". In: *aap* 476.2, pp. 863–879. DOI: 10.1051/0004-6361:20077587. arXiv: 0707.0959 [astro-ph].

Fiorentino, G. and M. Monelli (Apr. 2012a). "Anomalous Cepheids in the Large Magellanic Cloud. Insight into their origin and connection with the star formation history". In: *aap* 540, A102, A102. DOI: 10.1051/0004-6361/201118621. arXiv: 1202.2752 [astro-ph.SR].

Fiorentino, G., I. Musella, and M. Marconi (Oct. 2013). "Cepheid theoretical models and observations in HST/WFC3 filters: the effect on the Hubble constant H_0". In: *mnras* 434.4, pp. 2866–2876. DOI: 10.1093/mnras/stt1193. arXiv: 1306.6276 [astro-ph.CO].

Fiorentino, G. et al. (Sept. 2012b). "Ultra long period Cepheids: a primary standard candle out to the Hubble flow". In: *apss* 341.1, pp. 143–150. DOI: 10.1007/s10509-012-1043-4. arXiv: 1203.0026 [astro-ph.CO].

Freedman, W. L. and B. F. Madore (June 2011). "Two New Tests of the Metallicity Sensitivity of the Cepheid Period-luminosity Relation (the Leavitt Law)". In: *apj* 734.1, 46, p. 46. DOI: 10.1088/0004-637X/734/1/46. arXiv: 1103.6235 [astro-ph.SR].

Gaia Collaboration, Brown, and Vallenari (Nov. 2016a). "Gaia Data Release 1. Summary of the astrometric, photometric, and survey properties". In: *aap* 595, A2, A2. DOI: 10.1051/0004-6361/201629512. arXiv: 1609.04172 [astro-ph.IM].

— (Aug. 2018). "Gaia Data Release 2. Summary of the contents and survey properties". In: *aap* 616, A1, A1. DOI: 10.1051/0004-6361/201833051. arXiv: 1804.09365 [astro-ph.GA].

Gaia Collaboration, Prusti, and de Bruijne (Nov. 2016b). "The Gaia mission". In: *aap* 595, A1, A1. DOI: 10.1051/0004-6361/201629272. arXiv: 1609.04153 [astro-ph.IM].

Gallenne, A., P. Kervella, A. Mérand, G. Pietrzyński, W. Gieren, N. Nardetto, and B. Trahin (Dec. 2017). "Observational calibration of the projection factor of Cepheids. IV. Period-projection factor relation of Galactic and Magellanic Cloud Cepheids". In: *aap* 608, A18, A18. DOI: 10.1051/0004-6361/201731589. arXiv: 1708.09851 [astro-ph.SR].

Gallenne, A. et al. (Nov. 2018). "A Geometrical 1% Distance to the Short-period Binary Cepheid V1334 Cygni". In: *apj* 867.2, 121, p. 121. DOI: 10.3847/1538-4357/aae373. arXiv: 1809.07486 [astro-ph.SR].

Grebel, E. K. and W. Brandner (Dec. 1998). "The Recent Star Formation History of the Large Magellanic Cloud". In: *Magellanic Clouds and Other Dwarf Galaxies*, pp. 151–154.

Grevesse, N. and A. J. Sauval (May 1998). "Standard Solar Composition". In: *ssr* 85, pp. 161–174. DOI: 10.1023/A:1005161325181.

Groenewegen, M. A. T. (Nov. 2018). "The Cepheid period-luminosity-metallicity relation based on Gaia DR2 data". In: *aap* 619, A8, A8. DOI: 10.1051/0004-6361/201833478. arXiv: 1808.05796 [astro-ph.SR].

Groenewegen, M.Ã.T. (Feb. 2013). "Baade-Wesselink distances to Galactic and Magellanic Cloud Cepheids and the effect of metallicity". In: *aap* 550, A70, A70. DOI: 10.1051/0004-6361/201220446. arXiv: 1212.5478 [astro-ph.GA].

Hidalgo, S. L., A. Pietrinferni, S. Cassisi, M. Salaris, A. Mucciarelli, A. Savino, A. Aparicio, V. Silva Aguirre, and K. Verma (Apr. 2018). "The Updated BaSTI Stellar Evolution Models and Isochrones. I. Solar-scaled Calculations". In: *apj* 856.2, 125, p. 125. DOI: 10.3847/1538-4357/aab158. arXiv: 1802.07319 [astro-ph.GA].

Hirshfeld, A. ~ W. (Oct. 1980). "The stellar content of dwarf spheroidal galaxies." In: *apj* 241, pp. 111–124. DOI: 10.1086/158322.

Inno, L., G. Bono, M. Romaniello, N. Matsunaga, A. Pietrinferni, K. Genovali, B. Lemasle, M. Marconi, and F. Primas (May 2015). "The Recent Star Formation History of the Magellanic Clouds Traced by Classical Cepheids". In: *Fifty Years of Wide Field Studies in the Southern Hemisphere: Resolved Stellar Populations of the Galactic Bulge and Magellanic Clouds*. Ed. by S. Points and A. Kunder. Vol. 491. Astronomical Society of the Pacific Conference Series, p. 265.

Keller, S. C. and P. R. Wood (May 2006). "Bump Cepheids in the Magellanic Clouds: Metallicities, the Distances to the LMC and SMC, and the Pulsation-Evolution Mass Discrepancy". In: *apj* 642.2, pp. 834–841. DOI: 10.1086/501115. arXiv: astro-ph/0601225 [astro-ph].

Kervella, P., A. Gallenne, N. R. Evans, L. Szabados, F. Arenou, A. Mérand, N. Nardetto, W. Gieren, and G. Pietrzynski (Mar. 2019). "Multiplicity of Galactic Cepheids and RR Lyrae stars from Gaia DR2. II. Resolved common proper motion pairs". In: *aap* 623, A117, A117. DOI: 10.1051/0004-6361/201834211. arXiv: 1908.00545 [astro-ph.SR].

Lindegren, L. et al. (Aug. 2018). "Gaia Data Release 2. The astrometric solution". In: *aap* 616, A2, A2. DOI: 10.1051/0004-6361/201832727. arXiv: 1804.09366 [astro-ph.IM].

Lodders, K. (Jan. 2010). "Solar System Abundances of the Elements". In: *Astrophysics and Space Science Proceedings* 16, p. 379. DOI: 10.1007/978-3-642-10352-0_8. arXiv: 1010.2746 [astro-ph.SR].

Macri, L.M., K.Z. Stanek, D. Bersier, L.J. Greenhill, and M.J. Reid (Dec. 2006). "A New Cepheid Distance to the Maser-Host Galaxy NGC 4258 and Its Implications for the Hubble Constant". In: *apj* 652.2, pp. 1133–1149. DOI: 10.1086/508530. arXiv: astro-ph/0608211 [astro-ph].

Magnier, E. A., T. Augusteijn, S. Prins, J. van Paradijs, and W. H. G. Lewin (Dec. 1997). "Cepheids as tracers of star formation in M 31. I. Observations and identifications". In: *aaps* 126, pp. 401–406. DOI: 10.1051/aas:1997394.

Marconi, M., G. Bono, F. Caputo, S. Cassisi, P. Pietrukowicz, G. Pietrzynski, and W. Gieren (Jan. 2006). "Classical Cepheids as age indicators ." In: *memsai* 77, p. 67. arXiv: astro-ph/0510033 [astro-ph].

Marconi, M., G. De Somma, V. Ripepi, R. Molinaro, I. Musella, S. Leccia, and M. I. Moretti (July 2020). "Predicted Masses of Galactic Cepheids in the Gaia Data Release 2". In: *apjl* 898.1, L7, p. L7. DOI: 10.3847/2041-8213/aba12b. arXiv: 2006.16610 [astro-ph.SR].

Marconi, M., G. Fiorentino, and F. Caputo (Apr. 2004). "Updated pulsation models for anomalous Cepheids". In: *aap* 417, pp. 1101–1114. DOI: 10.1051/0004-6361:20040020. arXiv: astro-ph/0401332 [astro-ph].

Marconi, M. and D. Minniti (Feb. 2018). "Gauging the Helium Abundance of the Galactic Bulge RR Lyrae Stars". In: *apjl* 853.2, L20, p. L20. DOI: 10.3847/2041-8213/aaa8e3. arXiv: 1801.05883 [astro-ph.SR].

Marconi, M., R. Molinaro, V. Ripepi, S. Leccia, I. Musella, G. De Somma, M. Gatto, and M. I. Moretti (Jan. 2021). "A theoretical scenario for Galactic RR Lyrae in the Gaia data base: constraints on the parallax offset". In: *mnras* 500.4, pp. 5009–5023. DOI: 10.1093/mnras/staa3558. arXiv: 2011.06675 [astro-ph.SR].

Marconi, M., R. Molinaro, V. Ripepi, I. Musella, and E. Brocato (Jan. 2013a). "Theoretical fit of Cepheid light a radial velocity curves in the Large Magellanic Cloud cluster NGC 1866". In: *mnras* 428.3, pp. 2185–2197. DOI: 10.1093/mnras/sts197. arXiv: 1210.4343 [astro-ph.SR].

Marconi, M., I. Musella, and G. Fiorentino (Oct. 2005). "Cepheid Pulsation Models at Varying Metallicity and $\Delta Y/\Delta Z$". In: *apj* 632.1, pp. 590–610. DOI: 10.1086/432790. arXiv: astro-ph/0506207 [astro-ph].

Marconi, M. et al. (May 2013b). "The Eclipsing Binary Cepheid OGLE-LMC-CEP-0227 in the Large Magellanic Cloud: Pulsation Modeling of Light and Radial Velocity Curves". In: *apjl* 768.1, L6, p. L6. DOI: 10.1088/2041-8205/768/1/L6. arXiv: 1304.0860 [astro-ph.SR].

Marconi, M. et al. (Apr. 2017). "The VMC survey - XXIII. Model fitting of light and radial velocity curves of Small Magellanic Cloud classical Cepheids". In: *mnras* 466.3, pp. 3206–3216. DOI: 10.1093/mnras/stw3289. arXiv: 1612.04650 [astro-ph.SR].

Molinaro, R., V. Ripepi, M. Marconi, G. Bono, J. Lub, S. Pedicelli, and J.W. Pel (May 2011). "CORS Baade-Wesselink method in the Walraven photometric system: the period-radius and the period-luminosity relation of classical Cepheids". In: *mnras* 413.2, pp. 942–956. DOI: 10.1111/j.1365-2966.2010.18183.x. arXiv: 1012.4376 [astro-ph.SR].

Moskalik, P., J.R. Buchler, and A. Marom (Feb. 1992a). "Toward a Resolution of the Bump and Beat Cepheid Mass Discrepancies". In: *apj* 385, p. 685. DOI: 10.1086/170975.

Moskalik, P. and W.Ã. Dziembowski (Mar. 1992b). "New opacities and the origin of the β Cephei pulsation." In: *aap* 256, pp. L5–L8.

Musella, I. et al. (Sept. 2012). "Stellar Archeology in the Galactic Halo with Ultra-faint Dwarfs. VII. Hercules". In: *apj* 756.2, 121, p. 121. DOI: 10.1088/0004-637X/756/2/121. arXiv: 1206.4031 [astro-ph.GA].

Natale, G., M. Marconi, and G. Bono (Feb. 2008). "Theoretical Fits of the δ Cephei Light, Radius, and Radial Velocity Curves". In: *apjl* 674.2, p. L93. DOI: 10.1086/526518. arXiv: 0711.2857 [astro-ph].

Neilson, H. R. and N. Langer (Jan. 2012). "Is there a mass discrepancy in the Cepheid binary OGLE-LMC-CEP0227?" In: *aap* 537, A26, A26. DOI: 10.1051/0004-6361/201117829. arXiv: 1110.6657 [astro-ph.SR].

Ngeow, C., S. M. Kanbur, S. Nikolaev, J. Buonaccorsi, K. H. Cook, and D. L. Welch (Nov. 2005). "Further empirical evidence for the non-linearity of the period-luminosity relations as seen in the Large Magellanic Cloud Cepheids". In: *mnras* 363.3, pp. 831–846. DOI: 10.1111/j.1365-2966.2005.09477.x. arXiv: astro-ph/0507601 [astro-ph].

Pietrinferni, A., S. Cassisi, M. Salaris, and F. Castelli (Sept. 2004). "A Large Stellar Evolution Database for Population Synthesis Studies. I. Scaled Solar Models and Isochrones". In: *apj* 612.1, pp. 168–190. DOI: 10.1086/422498. arXiv: astro-ph/0405193 [astro-ph].

Pietrzyński, G., I. B. Thompson, W. Gieren, D. Graczyk, G. Bono, A. Udalski, I. Soszyński, D. Minniti, and B. Pilecki (Nov. 2010). "The dynamical mass of a classical Cepheid variable star in an eclipsing binary system". In: *nat* 468.7323, pp. 542–544. DOI: 10.1038/nature09598. arXiv: 1012.0231 [astro-ph.GA].

Pietrzyński, Grzegorz et al. (Dec. 2011). "The Araucaria Project: Accurate Determination of the Dynamical Mass of the Classical Cepheid in the Eclipsing System OGLE-LMC-CEP-1812". In: *apjl* 742.2, L20, p. L20. DOI: 10.1088/2041-8205/742/2/L20. arXiv: 1109.5414 [astro-ph.SR].

Planck Collaboration, Ade, and Aghanim (Sept. 2016). "Planck collaboration". In: *aap* 594, A13, A13. DOI: 10.1051/0004-6361/201525830. arXiv: 1502.01589 [astro-ph.CO].

Prada Moroni, P.G., M. Gennaro, G. Bono, G. Pietrzyński, W. Gieren, B. Pilecki, D. Graczyk, and I.B. Thompson (Apr. 2012). "On the Evolutionary and Pulsation Mass of Classical Cepheids. III. The Case of the Eclipsing Binary Cepheid CEP0227 in the Large Magellanic Cloud". In: *apj* 749.2, 108, p. 108. DOI: 10.1088/0004-637X/749/2/108. arXiv: 1202.2855 [astro-ph.SR].

Ragosta, F. et al. (Dec. 2019). "The VMC survey - XXXV. model fitting of LMC Cepheid light curves". In: *mnras* 490.4, pp. 4975–4984. DOI: 10.1093/mnras/stz2881. arXiv: 1910.05052 [astro-ph.SR].

Reimers, D. (Jan. 1975). "Circumstellar absorption lines and mass loss from red giants." In: *Memoires of the Societe Royale des Sciences de Liege* 8, pp. 369–382.

Renzini, A., L. Greggio, C. Ritossa, and L. Ferrario (Nov. 1992). "Why Stars Inflate to and Deflate from Red Giant Dimensions". In: *apj* 400, p. 280. DOI: 10.1086/171995.

Riess, A. G., S. Casertano, W. Yuan, J. B. Bowers, L. Macri, J. C. Zinn, and D. Scolnic (Feb. 2021). "Cosmic Distances Calibrated to 1% Precision with Gaia EDR3 Parallaxes and Hubble Space Telescope Photometry of 75 Milky Way Cepheids Confirm Tension with ΛCDM". In: *apjl* 908.1, L6, p. L6. DOI: 10.3847/2041-8213/abdbaf. arXiv: 2012.08534 [astro-ph.CO].

Riess, A. G. et al. (July 2016a). "A 2.4% Determination of the Local Value of the Hubble Constant". In: *apj* 826.1, 56, p. 56. DOI: 10.3847/0004-637X/826/1/56. arXiv: 1604.01424 [astro-ph.CO].

— (July 2016b). "A 2.4% Determination of the Local Value of the Hubble Constant". In: *apj* 826.1, 56, p. 56. DOI: 10.3847/0004-637X/826/1/56. arXiv: 1604.01424 [astro-ph.CO].

Riess, A. G. et al. (July 2018a). "Milky Way Cepheid Standards for Measuring Cosmic Distances and Application to Gaia DR2: Implications for the Hubble Constant". In: *apj* 861.2, 126, p. 126. DOI: 10.3847/1538-4357/aac82e. arXiv: 1804.10655 [astro-ph.CO].

Riess, A. G. et al. (Mar. 2018b). "New Parallaxes of Galactic Cepheids from Spatially Scanning the Hubble Space Telescope: Implications for the Hubble Constant". In: *apj* 855.2, 136, p. 136. DOI: 10.3847/1538-4357/aaadb7. arXiv: 1801.01120 [astro-ph.SR].

Ripepi, V., R. Molinaro, I. Musella, M. Marconi, S. Leccia, and L. Eyer (May 2019). "Reclassification of Cepheids in the Gaia Data Release 2. Period-luminosity and period-Wesenheit relations in the Gaia passbands". In: *aap* 625, A14, A14. DOI: 10.1051/0004-6361/201834506. arXiv: 1810.10486 [astro-ph.SR].

Ripepi, V. et al. (Jan. 2014). "The VMC Survey - VIII. First results for anomalous Cepheids". In: *mnras* 437.3, pp. 2307–2319. DOI: 10.1093/mnras/stt2047. arXiv: 1310.5967 [astro-ph.SR].

Ripepi, V. et al. (Oct. 2020). "Period-luminosity-metallicity relation of classical Cepheids". In: *aap* 642, A230, A230. DOI: 10.1051/0004-6361/202038714. arXiv: 2008.04608 [astro-ph.SR].

Romaniello, M., F. Primas, M. Mottini, S. Pedicelli, B. Lemasle, G. Bono, P. François, M.Ã.T. Groenewegen, and C.D. Laney (Sept. 2008). "The influence of chemical composition on the properties of Cepheid stars. II. The iron content". In: *aap* 488.2, pp. 731–747. DOI: 10.1051/0004-6361:20065661. arXiv: 0807.1196 [astro-ph].

Salaris, M. and S. Cassisi (2005). *Evolution of Stars and Stellar Populations*.

— (2006). *Evolution of Stars and Stellar Populations*.

Senchyna, P., L. C. Johnson, J. J. Dalcanton, L. C. Beerman, M. Fouesneau, A. Dolphin, B. F. Williams, P. Rosenfield, and S. S. Larsen (Nov. 2015). "Panchromatic Hubble Andromeda Treasury. XIV. The Period-Age Relationship of Cepheid Variables in M31 Star Clusters". In: *apj* 813.1, 31, p. 31. DOI: 10.1088/0004-637X/813/1/31. arXiv: 1509.04791 [astro-ph.SR].

Skowron, D. M. et al. (Aug. 2019). "A three-dimensional map of the Milky Way using classical Cepheid variable stars". In: *Science* 365.6452, pp. 478–482. DOI: 10.1126/science.aau3181. arXiv: 1806.10653 [astro-ph.GA].

Soszyński, I., A. Udalski, M.K. Szymański, M. Kubiak, G. Pietrzyński, Ł. Wyrzykowski, O. Szewczyk, K. Ulaczyk, and R. Poleski (Dec. 2008). "The Optical Gravitational Lensing Experiment. The OGLE-III Catalog of Variable Stars. II.Type II Cepheids and Anomalous Cepheids in the Large Magellanic Cloud". In: *actaa* 58, p. 293. arXiv: 0811.3636 [astro-ph].

Stellingwerf, R. ~ F. (Nov. 1982). "Convection in pulsating stars. I. Non linear hydrodynamics." In: *apj* 262, pp. 330–338. DOI: 10.1086/160425.

Szabó, R., Z. Kolláth, and J.R. Buchler (Oct. 2004). "Automated nonlinear stellar pulsation calculations: Applications to RR Lyrae stars. The slope of the fundamental blue edge and the first RRd model survey". In: *aap* 425, pp. 627–639. DOI: 10.1051/0004-6361:20035698. arXiv: astro-ph/0406373 [astro-ph].

Tammann, G. A., A. Sandage, and B. Reindl (June 2003). "New Period-Luminosity and Period-Color relations of classical Cepheids: I. Cepheids in the Galaxy". In: *aap* 404, pp. 423–448. DOI: 10.1051/0004-6361:20030354. arXiv: astro-ph/0303378 [astro-ph].

Tsvetkov, T. G. (Dec. 1980). "On the Period - Age Relation for Cepheids". In: *Pisma v Astronomicheskii Zhurnal* 6, p. 756.

Udalski, A. et al. (Dec. 2018). "OGLE Collection of Galactic Cepheids". In: *actaa* 68.4, pp. 315–339. DOI: 10.32023/0001-5237/68.4.1. arXiv: 1810.09489 [astro-ph.SR].

Ulaczyk, K. et al. (June 2013). "Variable Stars from the OGLE-III Shallow Survey in the Large Magellanic Cloud". In: *actaa* 63.2, pp. 159–179. arXiv: 1306.4802 [astro-ph.SR].

Zhevakin, S.Ã. (Jan. 1963). "Physical Basis of the Pulsation Theory of Variable Stars". In: *araa* 1, p. 367. DOI: 10.1146/annurev.aa.01.090163.002055.